Damping Behaviour of Slender Telecommunications Structures

by

Jose Alfonso Jimenez Capilla

Submitted by Jose Alfonso Jimenez Capilla to the University of Exeter

as a thesis for the degree of

Doctor of Philosophy in Vibration Engineering

Nov 2020

I certify that all material in this thesis which is not my own work has been identified and that no material has previously been submitted and approved for the award of a degree by this or any other University.

Signature: 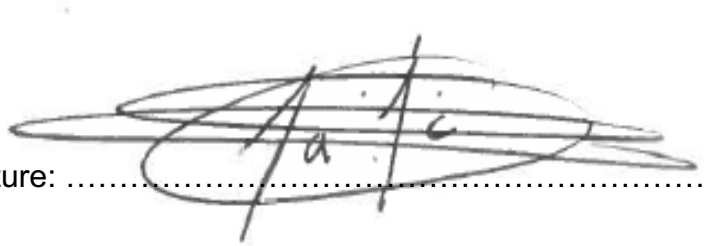

A quien estuvo ahí.

ABSTRACT

During the last two decades, the development of mobile telecommunications ('telecoms') technologies has resulted in an increased number of antennas to be accommodated around us on different kinds of structures. From new, short monopoles to old high guyed masts, all are considered sensitive flexible structures under wind, many of which are required to hold more equipment than their initial design loading capacity. The dynamic analysis of these structures has been neglected for years, in part as it is clearly a field that requires further investigations with new modern methodologies and knowledge. Within the industry, damping is the topic that provides the most uncertainty between existing expert consultants. The complex nature of damping arises from the high deviation between similar structures and the number of involved sources that modify this behaviour, from boundary conditions to aerodynamic effect, or nonlinear amplitude and frequency dependence relationship.

In this PhD research, several projects related to response-data acquisition were used to determine how damping behaves for each selected typology structure (monopoles, lattice towers and high guyed masts). Old and new estimation techniques have been applied after human and wind-ambient excitation to provide reliable data to verify current approaches of assessing damping and provide new clues and perspective about understanding damping in this kind of structures. The research counts on a study of the generic structural damping component on short structures compounded by soil-foundation component and material-connection defined by free decaying responses. A study of non-linearities exist on the response that help to determine sources of damping, and finally, diverse studies of monitoring systems under wind excitation were carried out to allow the research to study actual service response to extract aerodynamic damping, and the accuracy of current drag factors for different wind effects.

This new perspective provides essential knowledge to structural engineers when designing current and future structures, advising on the effectiveness and feasibility of external damping providers, not just as an option to minimise aeroelastic vortex

shedding effects, but also to reduce the buffeting response with the consequential structural capacity improvement. Results also show the deficiency of current standards and recommendations in the estimation of dynamic properties, especially on damping matter.

ACKNOWLEDGMENTS

Firstly, the author would like to thank his supervisor, Prof James M.W. Brownjohn for his guidance and support during the studies at University of Exeter, at all times. Thanks also for providing help and opportunities to carry out all the ideas raised during the research.

To Ki Young Koo, Ivan Au and Julian Londono for deciding to work on the research, spending valuable hours to extract the best from each proposed study. In addition, to all people included within the Vibration Engineering Section of University of Exeter for their support.

Thanks to Arqiva for an unusual and invaluable collaborative effort that has helped make possible an advanced research under long distance travelling conditions.

The author wishes to express his distinct gratitude to Mr Mike Thompson and Mr Duncan Gould for their guidance and support from the beginning of this journey and dealing with daily work in Winchester. Working with such respected and inspirational individuals has been a privilege and has confirmed a thankfulness for the chances given.

To the structural engineering team, the author would like to express his appreciation to the colleagues who collaborated as climbers during field surveys, Mr Christos Panayi, Mr James Harrison-Furse, Mr John Lohoar, Mr Darius Sikorski, Mr David Howell, Mr Joel Buggins, Mr Eyal Ortner, and managers who counted on the author for important projects incorporated to the research: Mr Matt Smith, Mr Sean Deeley, Mr Mike Elliott and Mr Martin Southgate.

More thanks must go to Mr John Rees of COWI for supplying unique consultant help about some matters discussed for the duration of my research.

To all people who shared their lives with the author during the programme, some of them helped to continue on difficult moments, Mr Alejandro Huerta, Mr Jose Marti, Mr Alberto Lopez and Mrs Andreea Stefan.

Finally, the author is deeply grateful to his family. Thanks for your love and support throughout all the years away from home, and for your patience and understanding.

LIST OF CONTENTS

LIST OF FIGURES

LIST OF TABLES

NOMENCLATURE

δ	Generic damping expressed as logarithmic decrement [-]
δ_{Total}	Total damping on the structure expressed as logarithmic decrement [-]
δ_s	Structural damping expressed as logarithmic decrement [-]
δ_a	Aerodynamic damping expressed as logarithmic decrement [-]
δ_T	Structural damping values given by [24] expressed as logarithmic decrement [-]
δ_d	External damping expressed as logarithmic decrement [-]
K_δ	Soil-Foundation factor given by [24] [-]
ζ	Generic damping expressed as critical damping coefficient [%]
ζ_{Total}	Total damping on the structure expressed as critical damping coefficient [%]
ζ_s	Structural damping expressed as critical damping coefficient [%]
ζ_{s0}	Structural damping at low deflections expressed as critical damping coefficient [%]
ζ'_s	Structural damping expressed at very large deflections as critical damping coefficient [%]
ζ_a	Aerodynamic damping expressed as critical damping coefficient [%]
ζ_T	Structural damping values given by [24] expressed as critical damping coefficient [%]
ζ_{mat}	Material damping [%]
ζ_{frict}	Friction/coulomb damping [%]
ζ_{foun}	Foundation damping [%]
$\zeta_{foun,j}$	Radiation damping of foundation [%]
$\zeta_{foun,mat}$	Material damping of foundation [%]
ρ_a	Mass density of air [kg/m^3]

ρ_s	Mass density of the material of the tower structure [kg/m^3]
j	Modal property
m	Generic mass
m_H	Mass per unit length [kg/m]
m_T	Total mass analysed [kg]
m_e	Effective mass [kg]
m_a	Added air mas [kg]
D	Cross wind dimension of the structure [m]
ε	Equivalent roughness height of cylinder surface [m]
H	Height of the structure [m]
h_T	Total height analysed [m]
b	Base of the structure [m]
W	Width of the structure [m]
R_{WT}	Total wind resistances analysed [m^2]
τ_o	Ratio volume/resistance constant given by [24] [m]
dB	Depth of the structure along wind direction given by [24] [m]
x_o	Initial deflection or gap of structure [m]
a, h	Sizes of TLD [m]
$c_s c_d$	Structural factor given by [26] [-]
$I_v(z_s)$	Turbulence intensity at each reference height by [26]
B^2	Background factor by [26] [-]
R^2	Resonance response factor by [26] [-]
β	Dynamic augmentation factor given by [31] [-]
$R_h R_b$	Aerodynamic admittance function of the structure [-]
f	Generic natural frequency of the structure [Hz]
$T(s)$	Time period of vibration [s]
T_{fr}	Analysed data frame [min]

n_o	Main natural frequency of the structure given by [31] [Hz]
f_w	Fundamental frequency of liquid sloshing motion in TLD [Hz]
V, v	Generic wind-flow speed [m/s]
V_m	Mean basic wind speed [m/s]
V_{crit}	Critical vortex shedding wind speed [m/s]
V_H	Hourly mean wind speed [m/s]
Re	Reynolds number [-]
St	Strouhal number [-]
S_c	Scruton number [-]
$\Delta\dot{Q}$	Change in structural velocity [-]
ΔF	Change in wind loading [-]
k	Generic stiffness [-]
k_s	Generic structural stiffness [-]
k_f	Generic foundation stiffness [-]
$\overline{k_J}$	Dynamic complex stiffness function [-]
c	Generic damping expressed as coefficient [-]
c_s	Generic coefficient of structural damping [-]
c_f	Generic coefficient of foundation damping [-]
x, y	Displacement of the structure [m]
$\dot{x}, \dot{y}$	Velocity of the structure [m/s]
$\ddot{x}, \ddot{y}$	Acceleration of the structure [m/s^2]
f_d	Function of damping forces [-]
f_{nl}	Nonlinear function of damping forces [-]
ω	Generic (circular) natural frequency [rad/sec]
ω_n	Undamped (circular) natural frequency [rad/sec]
ω_d	Damped (circular) natural frequency [rad/sec]
ϕ	Phase angle between damped oscillations [°]

μ	Generic mode shape [-]
C_D	Generic drag coefficient [-]
C_{Dm}	Mean drag coefficient [-]
C_{Dr}	Local drag factor at each level of the structure [-]
C_{Du}	Step drag factor of model recommended for tapered structures [-]
B_p	Soils resistant stress [MPa]
a_o	Dimensionless frequency [-]
$\overline{\omega_x}, \overline{\omega_{yy}}$	Fictional natural frequencies for each form of oscillations [rad/sec]
ξ	Non dimensional factor of first translation mode shape given by [26] [-]
U, θ	Deflections [m] and overturning [rad]
F, M	Horizontal forcing [kN] and moment [kNm]
r	Foundation radius [m]
υ	Soil Poisson ratio [-]

ABREVIATIONS AND ACRONYMOUS

AC	Alternating current
BAYOMA	Fast Bayesian operational modal analysis
CF	Curve fitting method
CVA	Canonical variate analysis
DAQ	Data acquisition system
DC	Direct current
DTT	Digital terrestrial television
DVA	Dynamic vibration absorber
EMA	Experimental modal analysis
ERA	Eigensystem realization algorithm method
ESDU	Engineering Sciences Data Unit
FEM	Finit element method
FFT	Fast Fourier transform
FRF	Frequency response function
GPS	Global positioning system
GRP	Glass fibre reinforced polymer
GOM	GPS/OCXO/ Arduino Mega2560 board
HCD	Hanging chains damper
HGM	High guyed mast
IASS	International Association of Shell and Spatial Structures
LT	Lattice tower
MLE	Maximum likelihood estimator
MP	Modal property

MPV	Most probable value
NA	National Annex
NLLF	Negative log of likelihood function
OMA	Operational modal analysis
PC	Principal component
PSD	Power spectrum density
RFI	Radio frequency interference
RMS	Root mean square
SDOF	Single degree of freedom
SHM	Structural health monitoring
SPT	Standard penetration test
SSI	Soil-Structure interaction
SSI	Stochastic subspace identification
SV	Singular value decomposition
TLD	Tuned liquid damper
TMD	Tuned mass damper
UHF	Ultra high frequency
ULS	Ultimate limit state
UPC	Unweighted principal component
VHF	Very high frequency
VS	Vortex shedding

Chapter 1 Introduction

Unlike the simplest static structures which are dominated by dead weight and adding time-invariant loading, slender and flexible structures must be defined in a dynamic context. Loads induce motion responses which modify future loads and resistances which augment the danger under ultimate limit cases and presence of dynamic issues like fatigue on those structure.

Currently, among others properties, damping, as the capacity to absorb energy of the system, is the main cause of uncertainty in dynamic structural response. There are dependences on material, internal connections, boundary conditions or external loading, both inherent structural sources and the aerodynamic damping forces.

On the other hand, with fast-moving technology development we currently are experiencing, the level of upgrading of certain engineering like telecommunications has increased. Consequently, there is need for a redevelopment or optimization of the infrastructure.

This thesis aims to provide a comprehensive view of damping behaviour during service life of telecom structures working essentially under fluctuating wind loading. The new load/wind-resistance requirements based on heavier and larger payloads with different shape represent a challenge requiring a damping optimization which has been not considered since the introduction of current standards on late 80s.

ARQIVA is a telecommunication company that provides infrastructure and broadcast transmission facilities throughout the United Kingdom and the Republic of Ireland; in addition, it also provides commercial meter facilities throughout Scotland and the north of England. As a site owner, Arqiva manages more than 10,000 sites, having structural responsibility of slender towers, rooftops and other specific structures. As an owner, the investigation and development of structural engineering knowledge in dynamics becomes an important topic with potentially large financial consequences, as an increase in the improved understanding of the structural integrity creates an

opportunity to increase capacities for further customers, and also to extend the lifetime of structures with these new developments.

Figure 1-1 Picture of Emley Moor transmitting station. Arqiva portfolio. Arqiva.

1.1 Background of Telecommunications Structures

Arqiva counts on an extensive portfolio of infrastructures. It does not only provide services enabling population to connect through TV, radio, mobile and machine-to-machine data services. It also takes huge importance during national catastrophes to maintain continual telecommunications services in post-disaster conditions. Three different structure types are considered for the research.

1.1.1 High Guyed Masts

High guyed masts (HGMs), Figure 1-2, are considered unique structures defined by high flexibility, slenderness and light weight. As a result of these characteristics, they also present a high degree of dynamic sensitivity to several aerodynamic effects.

Built to accommodate the growth in radio and television broadcasting, the majority of UK HGMs were designed in the 60s and 70s. In this era, there was little consideration of dynamics, materials performance or non-linear behaviour. Surprisingly, not too many issues appeared over the years, due to safety factors taken in the design, but lately with new generations of broadcasting, digital radio, telecoms and others, extra

capacity is required from these structures and safety factors may no longer be adequate.

Figure 1-2 Belmont HGM. Martin Brown May 2015. www.mb21.co.uk.

Currently, there are more than 100 HGMs which are used to host all radio and the majority of television broadcasting over the UK. The typologies are very varied, most are based on square and triangular steel lattice, but there are also masts with tubular columns (Figure 1-2) of different sizes while in some masts, the main body of the mast is based on a combination between different types. In addition, HGMs vary according to the distribution of cables, the number of levels or geometry and the different types of foundation including fixings for guys.

The structural complexity and flexible nature of HGMs point to the need for advanced dynamic assessments in order to determine their structural capacities. Such analysis is difficult, as the understanding of dynamic behaviour of these structures is limited, due to several factors:

- There has been a lack of technical development through the years with very little research published, particularly since code development decades ago, with some key knowledge not available in public domain.
- HGMs have a very large number of natural modes in a narrow frequency band. In the range 0 - 5 Hz, more than 20 modes can be easily found, with consequent difficulty in isolating them for analysis. That issue increases highly the challenge of modal analysis and superposition, along with understanding of the structural response.
- Acting mainly under fluctuating wind loading, the causes of dangerous responses are difficult to differentiate, between cases of turbulent buffeting of the structure, vortex shedding effects over bluff elements of the main structure and galloping issues with each set of stays, elements behaving as if randomly in modes that could involve the total behaviour of the mast.
- The confidence in existing theories to estimate mean wind speed over a range of heights and season of the year is not high. Sometimes site-specific analyses are required for a better understanding and correct load application.
- There is high variance of stiffness with the amplitude of the motion which can also change in different vibration modes, leading to a nonlinear complexity difficult to consider in normal engineering design. This fact together with the non-linear

material behaviour or other effects such as P-delta deflection terms, requires a highly technical understanding to properly manage such structures.

- A significant ignorance of damping on both structural damping, difficult to define according to material and connections and a likely amplitude response dependency, and aerodynamic damping which becomes important due to the influence of stays, make more difficult the estimation process.

At present all these uncertainties force designers to adopt very conservative approaches in engineering judgement. The key consultants dealing with HGM agree that for structural assessments carried out to check the integrity of some of the masts the existing design code(s) appears be based on incorrect methods of assessing damping which lead on hazardous results in dynamics.

1.1.2 Lattice Towers

Lattice towers (LTs) have been an economic solution for the communication industry over many years. Their origin comes from the evolution of transmission line towers which were designed for maximum efficiency, using the lowest weight of steel. They tend to be a good option for heights between 10 m and 150 m, above which HGMs are a more cost-effective solution. Lattice towers are fabricated predominately of galvanized steel angles, tubes or solid round members, and generally have bolted, riveted or welded connections.

LTs are the most common structure type with more than 4000 lattice towers over the UK. Normally, LTs are lower than 60 m tall but there are some special cases such as Crystal Palace or Croydon up to almost 200 m tall. Those tall LTs still provide mainly broadcast and radio as Figure 1-3. However, short types have been extensively used for the last two decades as telecoms are now the main customer (for LTs), requiring space to hold ancillary equipment for several customers. With recent evolution in telecoms requirements, LTs tend to be heavily loaded near to the top of the structure. This has meant that the mass distribution over the tower is very irregular resulting in having significant dynamic response under adverse weather conditions, not only because of the antennas and the wind impact, but also due to the necessary steelworks and cabling.

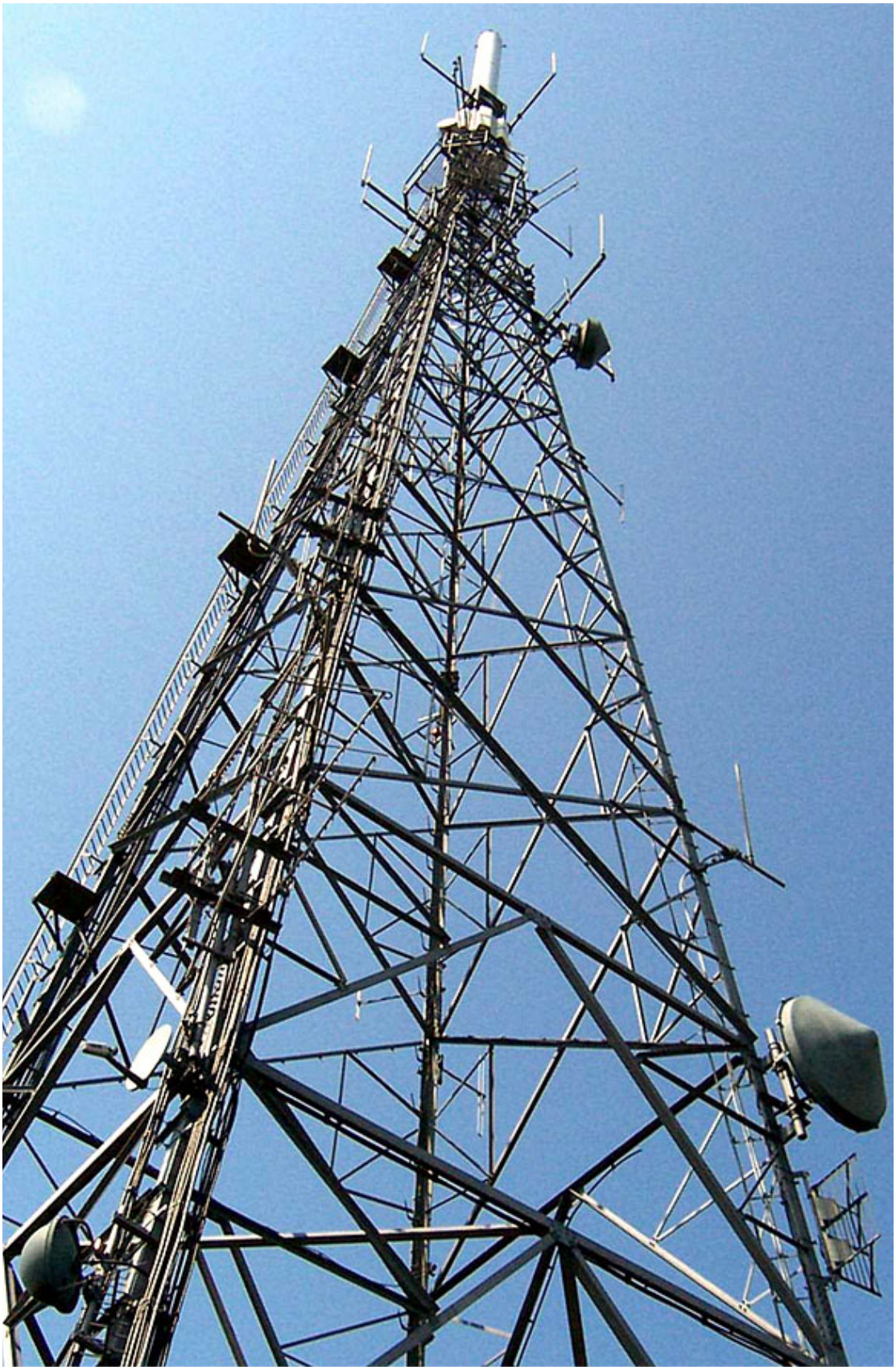

Figure 1-3 Cambret Hill transmitting lattice tower. David Neale 2014. www.mb21.co.uk.

Clearly, with lower slenderness ratios than HGMs, LTs are designed with a focus on static behaviour. Not more than three natural frequencies can appear in the frequency band of wind energy; usually the first mode appears between 0.6 - 2.5 Hz. This value is common in the sector which takes lower values for tallest structures. They depend on geometry and connections, but the main factor which will define any kind of dynamic response will be the mass distribution.

In terms of dynamic structural engineering, firstly, under serviceability limits, it is important to limit the number of hours any antenna is out of operation due to different climatic condition, due to heavy financial penalties. Hence the design of a LT must look for a solution in which damping is optimised to avoid unserviceable deflections under certain conditions.

Second, in the design of LTs, some codes (e.g. British Standard 8100) use a “Static Number” to verify the need for dynamic or spectral assessment or at least consider whether a dynamic augmentation factor is appropriate (usually multiplying by 120% the wind impact). This number, which is approached by a combination of geometry, mass and wind loading shows the wind excitability of the structure.

Lastly, there have been some challenging problems because of vortex shedding effects on bluff radio and TV broadcast antennas (cylinder and slender antennas placed at the top of the structures, Figure 1-3). That has been a source of dangerous across-wind vibrational events with fatigue issues.

1.1.3 Monopoles

Monopoles are the common solution for telecoms providers to serve customers in population centres, hence they tend to be as unobtrusive as possible, not very high and very simple. Most types are based on a steel tubular mast between 5 and 40 m height. Any equipment is usually at or very close to the top, with cabling running inside the mast or outside close to an access ladder if it is necessary.

The weakest part is often the connections at the foundation level. All the stresses are concentrated there, where almost all structures issues occur, i.e. fatigue problems, plate and bolt failures.

Figure 1-4 Mizens Farm monopole. J. A. Jimenez Capilla. July 2017. Arqiva.

Dynamic response of monopoles is defined by a pair of cantilevered first flexural mode shapes between 0.5 and 2 Hz working under turbulent buffeting loading plus secondary modes between 3 – 5 Hz. Vortex shedding is rarely susceptible to appear under first vibration mode.

Monopoles are a crucial structural type as it is expected that their numbers will grow significantly in the future. New generations of telecoms technology require to have a shorter distance between antenna and final customer, meaning that the supporting structures must be in urban areas to be efficient. The new requirements are more relevant to monopoles which become more wind sensitive and reduce their 25-years design life, shorter than for other civil engineering structures.

Structural assessments on monopoles are based on simplistic static approaches of the first vibration mode with augmentation dynamic factor applied to wind loading due to dynamics under turbulent buffeting similar to the approach applied to LTs. Again, damping has a prime importance in determining these factors. However, being shorter structures under more turbulent wind flow, less aerodynamic damping is expected in those structures.

Three sources of damping should be considered to determine the total damping for design:

- Structural damping, generally defined by a pre-set value defined in the literature based on material, connections and construction method not specifically defined according to type of structure. In addition, some recommendations agree to factor this value by foundation coefficient to take into account possible effects of soil-foundation interaction.
- Aerodynamic damping defined from the aerodynamic forces modifying the response of the structure to turbulent wind buffeting. The relevant parameters are the wind conditions and the drag factor (due to structure geometry). The issue has been well studied for tall structures with relatively low turbulence intensity, unlike monopoles which tend to operate in highly turbulent winds dependent on the roughness of the terrain profile.
- External damping provided by dampers which until now have predominately been used to mitigate aeroelastic issues like vortex shedding, but which can increase

highly the capacity of the structure as effectively as (but more efficiently than) strengthening.

1.2 Motivation of the Study

The need for a more realistic treatment of damping in the design of guyed masts, lattice towers and monopoles has been recognised by engineering specialists for years. The uncertainty and associated complexity have forced designers to adopt conservative approaches. As a consequence:

- Static approaches based on augmentation factors due to dynamics are dependent on historical damping measurement approaches extracted from building or bridge engineering fields, which may be inappropriate for telecoms towers.
- To assess possible vortex shedding effect on communications structures, there is need to have an exhaustive knowledge of the aeroelasticity phenomena defined by the structural damping behaviour.

On the other hand, the requirements of coming telecom technologies are driving new structural developments assisted by improvements in methods for assessing dynamic performance in terms of acquisition of data, monitoring or estimation techniques.

- New loading based on heavier and larger antennae will change stiffness and damping properties of structures. The main impact of those changes is in deterioration of dynamic performance: the structures become more wind sensitive and the risk of dynamic failure increases. New developments are necessary to provide more realistic structural assessments.
- The current standards have been proven to not represent properly the dynamics of discussed structures. An upgrade or reformulation of the guidance is required.
- During the last decade, the development of new sensing solutions based on digital acquisition has led to affordable instrumentation for telecoms structural engineering.
- New structural identification methods are able to provide more reliable estimation of dynamic properties, with high degree of accuracy, providing acceptable precision for damping estimation.

- In a few occasions liquid and mass dampers were found to be suitable for vibration mitigation in problematic structures with important aeroelastic issues. To apply this approach to mitigating buffeting effects requires better understanding of structural response and current damping behaviour.

Given the positive response received from owners, manufacturers, consultants and academics, the research was designed as a practical and analytical research into dynamic performance of existing telecommunications structures in the Arqiva Portfolio.

1.3 Aims and Objectives

Of the previous challenges of current perspective of analyse communications structures, damping, from different sides, appears to have received less attention. The goals of the research have been to:

- Increase current knowledge of structural damping including a verification of the proposed values in the literature, introduce new methodologies to study amplitude dependencies, and study likely contributions of soil-foundation in damping.
- Study and verify existing methods of assessing total damping including aerodynamic contributions.
- Study the capability of different typology of dampers to prevent aeroelastic events. This includes investigations of the loading/response phenomena on different type of communications structures.

1.4 Outline of Report

The wide range of research studies in dealing with several sources of damping (structural, aerodynamic and external damping) in such different structures (HGM, LT and monopoles) under several response events (turbulent buffeting, VS or galloping) requires careful organisation of the dissertation. The criteria chosen to arrange this text shows initially the studies related to structural damping (Chapter 3, Chapter 4 and Chapter 5) later aerodynamic damping (Chapter 6 and Chapter 7) and finally projects related to existing damping providers (Chapter 8 and Chapter 9). That way the thesis will be organised as follows:

Chapter 1 states an introduction to the current research, definition of the issued structures and the motivation of the study.

Chapter 2 provides a literature review of generic damping properties and particularities applied to each source on each chosen structure. A background of the current standards related to damping points to necessary improvements and future applications.

Chapter 3 presents results of a campaign of modal surveys on monopoles. With the goal of obtaining reliable values of structural damping, numerous monopole types were tested under human external excitation. Accelerometers captured the response then traditional curve fitting methods and eigensystem realization algorithm were used for the dynamic property estimation.

Chapter 4 describes the estimation of non-linearities in free decay responses obtained during few monopole surveys. Backbone curve methodology helps to understand the real behaviour of stiffness and damping along the amplitude. The exercise provides clues on the sources of damping, with a significant component from dry-friction.

Charter 5 presents the application of a soil-structure interaction formulation to find the influence of the group soil-foundation interface as main boundary condition influencing structural damping. Three sites with known and different soil stiffness conditions were tested under two main modes of oscillation: horizontal translation and rocking.

So far, the current research has been concerned with the complete structural damping system. More focus will now be made to extend verified results over the design point of view.

Chapter 6 describes a monitoring system created to measure the response of short telecoms structures. This system correlates wind loading with responses of the structure for the desire time frame. Fast Bayesian modal analysis (BAYOMA) has been implemented and analysed as structural identification method to examine further implications for further acquisition projects.

Chapter 7 summarises all results obtained from two monopoles equal to the work described in Chapter 6 to build the aerodynamic and total components of damping. Discrepancies and concerns about current recommendations are settled and a new

perspective is recommended. Generic analytical models are validated by correlating with results developing new drag coefficients.

Chapter 8 investigates the performance of additional damping solutions to mitigate strong vortex shedding events on high lattice towers induced from large bluff broadcasting antennae. Two specific cases are studied: mechanical dampers acting on antennae behaviour at Salisbury, and chain-hanging dampers at Brougher Mountain.

Chapter 9 outlines the analysis carried out using data acquired using an innovative structural health monitoring system installed on Moel-y-Parc high guyed mast. This is a unique project providing valuable knowledge of response of an HGM acting under buffeting, vortex shedding and galloping effect, including the effect of a pair of tuned liquid dampers.

Chapter 10 provides the most important conclusions, along with recommendations for further works.

References and Appendixes are found as last section providing supplementary information about each part of the research.

Preface to Chapter 2

This chapter is a literature review addressing the existing experimental and analytical characterisation of damping in telecommunications structures. The chapter includes an exhaustive and diverse summary of recommendations given by national authorities and representative studies and models from various fields of civil engineering such as building or bridges.

The literature survey indicated a low number of researches on the area with remarkable lack of knowledge on fundamental matters. Therefore, in order to maintain a good balance in presentation and not neglect significant issues, the research develops important investigations on most important source of damping for each structure type.

Chapter 2 Literature Review

2.1 Introduction

The dynamic behaviour of modern communication structures – masts and towers – is a serious challenge for structural engineers around the world. New technologies, which use completely new equipment with special requirements in terms of deflections and mass distribution, are pushing the limits of current structural capacities and static analysis methods, necessitating knowledge from lesser-known engineering fields. The clear impact of new technology arrival on the continued structural availability and financial performance of existing structures has recently encouraged studies that revisit the 30-year-old regulations of this field.

Damping is one of the most uncertain and important factors governing dynamic response of flexible structures under wind loading [1]. The number of simultaneously acting energy dissipation sources and mechanisms and the performance of each mechanism depending on the amplitude of the response and the variance of results between similar structures challenge engineers' ability to identify or estimate appropriate values of damping. Furthermore, this factor is essential to dissipate vibrations from serviceability limitations to prevent structural collapse from fatigue failure; consequently, optimal solutions for dynamics issues should be based on adding supplemental damping thorough various mechanisms. However, new identification methodologies [2] and new response acquisition methods may also help to clarify the correct estimation of damping.

The structures discussed in this work present a particular challenge to wind engineering. They are characterised [3] by their requirement to hold high masses with high wind-impact at required heights, by their limited visual intrusion, and by their cost-effectiveness and efficiency. These structures also count on a slenderness atypical to civil engineering and with complex dynamic behaviour excited mainly under wind loading.

Important to these structure's dynamic sensitivity are the low range of natural frequencies, mainly less than 2 Hz. This range is determined by the geometry and design (i.e., mass and stiffness) of a solution. Damping also strongly depends on parameters such as material: structures are made predominately of galvanised steel angles, tubes, or round members and tend to have bolted, riveted, or welded connections. Furthermore, the geotechnical nature of the site and the foundation solution implemented are a demonstrated source of damping that must be considered for towers. Finally, the aerodynamic component of damping becomes increasingly important the taller the structure.

As introduced in [4], several ambient environmental excitations cause (or result from) substantial dynamic effects that depend on the type of communication structure:

- Monopoles. Due to their low height, the main response of these structures arises from along- and across-wind loading that is determined by buffeting under atmospheric turbulence [5]. The cylindrical geometry of monopole shafts and special antennas can also generate across-flow dynamic loading and oscillations due to vortex shedding; these are sometimes enhanced by interference effects from other nearby structures [6].
- Lattice towers (LTs). Oscillations of these structures are caused predominately by along-wind buffeting on the first cantilevered bending mode shape [7], with serviceability issues caused by excessive deflection occurring appearing at the upper level of the structure. Due to their geometry, empty lattice tower structures exhibit no evidence of across-wind aeroelastic events, but bluff bodies or high wind can impact installed ancillaries and generate the phenomenon to excite secondary modes.
- High guyed masts (HGMs). The characteristics of a slender column structure in conjunction with different sets of stays result in a complex structure subject to a high number of possible issues that one must consider. Besides the previously mentioned buffeting and vortex shedding, which have similar effects in these structures and monopoles, several types of galloping can induce oscillations. The density of frequencies is high on a low range.

As damping opposes structural motion with a force proportional to velocity [8], it becomes an essential property when estimating each phenomena outlined in the list above.

The following sections provide a background on damping; the behaviour of its components; current and old approaches to damping; and a description of diverse dynamic monitoring, field tests and identification methods employed in this study.

2.2 Background

Measuring damping and modelling slender structures under wind loading have historically been more important in other fields of civil engineering. Work related to understanding the real dynamic behaviour of towers and masts has drawn from the work of these other fields.

The best studies of slender structures are from the field of building engineering. A summary of the values of several existing studies that indicate linear behaviour of structural damping between low and high amplitude responses is provided by Engineering Sciences Data Unit (ESDU) [9]. Studies have also indicated that tuned and absorber dampers and friction dampers are excellent options to reduce unacceptable defections to occupants.

Because Japan experiences high seismic activity, researchers there have become the main providers of investigations on the dynamics of slender structures. Databases of building damping [10, 11] have indicated that damping depends on height, foundation type, building usage and vibration amplitude; this information is used for several types of vibration test and various evaluation methods. In addition, dominant response frequency (stiffness behaviour) does not take a constant and monotonic values.

Other experiments [12] have suggested also that damping and frequency do not keep constant with the amplitude of vibration, even for relatively small amplitudes. Some empirical approaches [13] have been able to predict this amplitude dependency by considering a confirmed soil-foundation influence. Freestanding communication structures are more significantly subject to all of these concerns than buildings due to their high wind-sensitivity.

Although previous work has identified sources of damping, tolerance bounds of damping values in the literature vary severely providing high uncertainty [14]. To reduce this variance, and to avoid any detrimental impacts of excessively conservative damping estimations, newly manufactured damping devices have been introduced to assure structural integrity.

Another class of slender structure that is exposed to high wind impact is the suspended span (suspension, cable-stayed) bridge. In such dynamic structures, damping works differently for each mode. Higher values of damping are found in torsional, vertical, and high frequency modes that are governed by the effects at joints [15], and contributions from suspension, hanger and stay cables. Work related to these structures is highly applicable to high guyed masts at low modes, as both these structure and suspension bridges have complex mode shapes and high level of mass mobilisation.

Transmission lattice towers are likely the most similar in structure to communications structures. Similarly to HGM with guys, the dynamic behaviour of transmission lattice towers tend to be determined by conductors [16] in different ways. Considerable complexity arises from the interaction between structures and conductors, which cannot always be decoupled, resulting in closely spaced frequencies; the modelling of conductors with nonlinear behaviour and their high-impact aerodynamic damping.

Unlike the previously discussed structures, the existing databases of damping measurements for lattice towers is extremely limited. Only a few examples have been introduced in [17] that confirm the existence of nonlinearity and average measured values of structural damping. It also confirms the agreement of aerodynamic damping to mean wind speed, mean deflection and natural frequency.

All of the referenced literature supports the existence of three main sources of damping: structural damping; aerodynamic damping and external damping providers:

- Structural damping might be related to the energy dissipating effect, which is a result of material damping, friction damping, and soil-foundation damping. The difficulty of distinguishing between sources has led to the use of equivalent viscous models to form simplistic solutions that avoid amplitude-dependent nonlinearities.

- Aerodynamic or fluid damping arises from the relative motion between a body and a fluid and contributes significantly to damping in many cases. This contribution, which may be positive or negative, is estimated from fluid force terms and response levels. Tall and complex structures like HGM experience high values of aerodynamic damping, or negative values in the case of vortex shedding or ice loading in guys. This form of damping may not be possible to simplify to viscous damping due to non-linearities and cross-coupling between degrees of freedom.
- Additional damping with auxiliary dampers to increase the inherent damping is one of the best strengthening methods to limit the motion of structures during dangerous wind events. Among several solutions used in civil engineering, the passive category has proven to be the most effective for masts and towers. Due to limited site access under considerable heavy weather conditions with possible power restrictions, structural engineers rely on systems which require simple mechanisms. Tuned mass dampers (TMDs), which are based on chain motions [18], and tuned liquid dampers (TLDs) [19], which use water tanks, have proven highly effective in decreasing response in several installations of Arqiva's portfolio. These methods incorporate large lumped masses which modify stiffness and dynamics of superstructures. This form of damping may not be possible to simplify to viscous damping since requirements for representation as proportional damping may be invalidated.

The following section summarises the recommendations and standards of different countries and organisations for addressing damping for structural dynamic assessment during initial design or review.

2.2.1 Standards for Damping in Masts and Towers

The damping in structures is usually represented in a highly theoretical manner, normally by a linear viscous dashpot [20]. The damping coefficient, c, represents dissipation of energy in the system and via damping forces related to the velocity of the structure. Several means are present in the literature to describe damping coefficient. The most used in national codes is the logarithmic decrement (log-dec, δ), which gives the ratio between successive peaks during a decay motion. In academia, dimensionless damping ratio extracted form critical damping coefficient (ζ) dependent

on the mass and stiffness of the structure, is more widely used. The relationship between them follows:

Eq. 2-1

$$\delta = \frac{2\pi\zeta}{\sqrt{1-\zeta^2}}$$

The first standards to include damping as an important property in the definition of structural response in guyed masts were the recommendations [21] developed by The International Association of Shell and Spatial Structures (IASS). Globally, the IASS Group 4 is one of the leading organisations focused on the development of this civil engineering field. The organisation defined the following three main components of damping:

- The inherent structural damping, δ_s (log dec), whose values in the absence of better information are suggested in Table 2-1:

Table 2-1. Structural damping values [21]. Section 3.3.6.1.

Construction	Logarithmic decrement, δ_s	Critical damping [%], ζ_s
Fully welded steelwork	0.012	0.191
High strength friction bolted steelwork; glass reinforced plastic	0.020	0.318
Normal bolted and riveted steelwork	0.030	0.477

- The aerodynamic damping, δ_a, reflects contributions that arise from guys for each vibration mode chosen during the dynamic analysis.
- Artificial damping is provided by dampers for very sensitive masts with low structural and aerodynamic damping.

Members of IASS have collaborated on and supported this present research to improve current knowledge and consequently modify current restrictive national codes. They have provided relevant results from unpublished full-scale and directed the current author to important literature.

American codes [22], which use a 3-second gust as the basic design wind speed due to the existence of hurricanes and high wind events do not consider dynamic response

due to dynamic excitations. Dynamics are only considered in the case of seismic design.

Canadian codes [23] do not consider damping in the equivalent dynamic response of all structures. However, for specific load cases like wind turbulence in high guyed masts, earthquake-resistant design, and fatigue issues due to aeroelastic effects like vortex shedding (VS), the structural damping ratio ζ_s ranges between 0.5 – 0.7 % of the critical value recommended for metallic poles with friction fit or bolted connections; however, damping ratios for all-welded poles with few ancillary attachments can be as low as 0.2 – 0.3 %. Considered negative aerodynamic damping due to VS is defined as follows:

Eq. 2-2

$$\zeta_a = -S_c \frac{\rho_a D^2}{m_H}$$

where ρ_a is the air density (approximately 1.29 kg/m3), D is the size of the structure (in m), and m_H is the mass per unit length (in kg/m) averaged over the top one-third of the structure. Finally, the factor S_c is the 'Scruton Number' defined more in deep in 2.3.2.1 and Eq. 2-19 .

In 1986, the United Kingdom produced the Standard for Loading of Lattice Towers [24]. It includes the dynamic response of the structure in the definition of the gust factor. The dynamic response has been obtained by comparing several example structures of different geometries, heights, and widths, assuming typical values of damping. The code also recommends an advanced methodology to calculate total damping with no specific application except for spectral analyses of natural frequencies less than 2 Hz. This approach, detailed in Appendix E determines structural damping using the nature of structural connections of the superstructure and an influence factor dependant on the foundations-soils influence (see Table 2-2 and Table 2-3). This allowance includes three foundation categories: shallow slab on soft soil, which absorbs significant energy during vibration (K_δ = 3); a shallow slab on medium stiff soil (K_δ = 1.5); and a rock soil or piled foundation with no damping enhancement (K_δ = 1).

Eq. 2-3

$$\delta_S = K_\delta \delta_T$$

Table 2-2. Structural Damping Values. Log Dec. [24].

Structural connections	Surface finish at connections	log-dec, δ_T	Critical damping [%], ζ_T
All welded or all friction grip or fitted bolted	All finishes	0.015	0.239
Welded bracings: bolted flange plate connection to legs	All finishes	0.015	0.239
Welded bracings: black bolted gusset connection to legs	Cleaned, unpainted	0.060	0.955
	Grit-blasted, metal-sprayed	0.045	0.716
	Galvanised	0.030	0.477
Black bolted bracing: bolted flange plate connection to legs	Cleaned, unpainted	0.040	0.637
	Grit-blasted, metal-sprayed	0.030	0.477
	Galvanised	0.020	0.318
Black bolted bracing: black bolted gusset connection to legs	Cleaned, unpainted	0.080	1.273
	Grit-blasted, metal-sprayed	0.060	0.955
	Galvanised	0.040	0.637

Table 2-3. Augmentation Factor. [24].

Type of foundations	Factor, K_δ
Piled foundation or footing on stiff soil or rock	1
Spread footing on medium stiff soil	1.5
Spread footing on soft soil	3

British Standards [24] also produced the so-called static number, with which one can consider a dynamically sensitive structure and apply spectral analysis. This number, which is discussed in section 5.1.1., relies only on geometric parameters, as an empirical approach to determining the wind-sensitivity of the LTs, defined in Eq. 2-4:

Eq. 2-4

$$Static\ number = \frac{7m_T}{\rho_s R_{WT}\sqrt{d_B \tau_o}}\left(\frac{5}{6} - \frac{h_T}{H}\right)^2 < 1$$

The variables in Eq. 2-4 indicate the following:

R_{WT} is the sum of the panel resistances in the top portion of the tower, such that R_{WT} is just less than one-third of the overall summation ΣR_{WT} of the whole tower (in m^2);

ρ_s is the density of the material of the tower structure (in kg/m^3);

m_T is the total mass of the panels comprising R_{WT} (in kg);

H is the height of the tower (in m);

h_T is the total height of the panels comprising RWT but is less than H/3 (in m);

τ_o is a volume/resistance constant taken as 0.001 m;

d_B is the depth in the direction of the wind and is equal to the product of the base, d, for rectangular towers (in m); 0.75 × base width for triangular towers (in m).

Australian and New Zealand code [25] have started to introduce the dynamic response factor for buildings and freestanding towers with fundamental natural frequency less than 1 Hz. The dynamic factor counts on background and resonance parts for along-wind response dependant on a variable critical damping which assumes different values depending on each of the following limit states:

- Ultimate limit states have the following values:
    - Steel structures: 2 % of critical damping.
    - Reinforced-concrete structures: 3 % of critical damping.
- For serviceability limit states
    - Steel structures: 1.2 % of critical for deflection calculations and 1 % of critical for accelerations calculations.
    - Reinforced-concrete structures: 0.015 of critical for deflection calculations and 0.01 for accelerations.

Finally, [25] also recommends that users should seek other more trustworthy sources of damping data due to uncertainty caused by the type of construction, building sizes and amplitude of vibration.

To limit discrepancies among the criteria expressed in European standards [26] and [27], the national annex (NA) for application in the UK established the current structural integrity criteria [28]. The structural factor C_sC_d includes both the simultaneous occurrence of peak wind pressure on a structure's surface and the effect of the vibrations of the structure due to turbulence. This factor depends on the resonant response of the structure, which uses the following total damping estimation:

Eq. 2-5

$$\delta_{Total} = \delta_s + \delta_a + \delta_d$$

As indicated in previous Eq. 2-5, damping provided from special devices is grouped with typical aerodynamic and structural damping, neither of which consider the soil interaction of Table 2-4. This approach is also used to define cross wind aeroelastic instabilities in its Appendix E.

Furthermore, previous building codes [29, 30] implement damping as a specific property to describe the susceptibility to dynamic excitation. By defining the type of building by its connections and materials, these codes define dynamic augmentation as a function of the height of building under consideration.

Monopole codes [31 – 33] have a more consistent structural engineering methodology based on a quasi-static approach where dynamics under turbulent buffeting are included as an important determinant of wind loading design. Normally, charts like Figure 2-1 are created to define the so-called augmentation or dynamic factor, β. Some codes require a method of assessing damping, and others predefine curves for recommended values.

Table 2-4. Approximate values of the logarithmic decrement of structural damping in the fundamental mode, δ_s. [26]

Structure Type		Structural damping, δs	Structural damping [%], ζ_s
reinforced concrete buildings		0.1	1.591
steel buildings		0.05	0.796
mixed structures concrete + steel		0.08	1.273
reinforced concrete towers and chimneys		0.03	0.478
unlined welded steel stacks without external thermal insulation		0.012	0.191
unlined welded steel stack with external thermal insulation		0.02	0.318
steel stack with one liner with external thermal insulation	H/b < 18	0.02	0.318
	20 <H/b < 24	0.04	0.637
	H/b > 26	0.014	0.229
steel stack with two or more liners with external thermal insulation	H/b < 18	0.02	0.318
	20 <H/b < 24	0.04	0.637
	H/b > 26	0.025	0.398
steel stack with internal brick liner		0.07	1.114
steel stack with internal gunite		0.03	0.478
coupled steel stack without liner		0.015	0.239
guyed steel stack without liner		0.04	0.637
steel bridges + lattice steel towers	welded	0.02	0.318
	high resistance bolts	0.03	0.478
	ordinary bolts	0.05	0.796
composite bridges		0.04	0.637
concrete bridges	prestressed without cracks	0.04	0.637
	with cracks	0.1	1.591
timer bridges		0.06 - 0.012	0.955 – 0.191
bridges, aluminium alloys		0.02	0.318
bridges, glass or fibre reinforced plastic		0.04 - 0.08	0.637 - 1.273
cables	parallel cables	0.006	0.096
	spiral cables	0.02	0.318
For intermediate values of H/b, linear interpolation may be used			

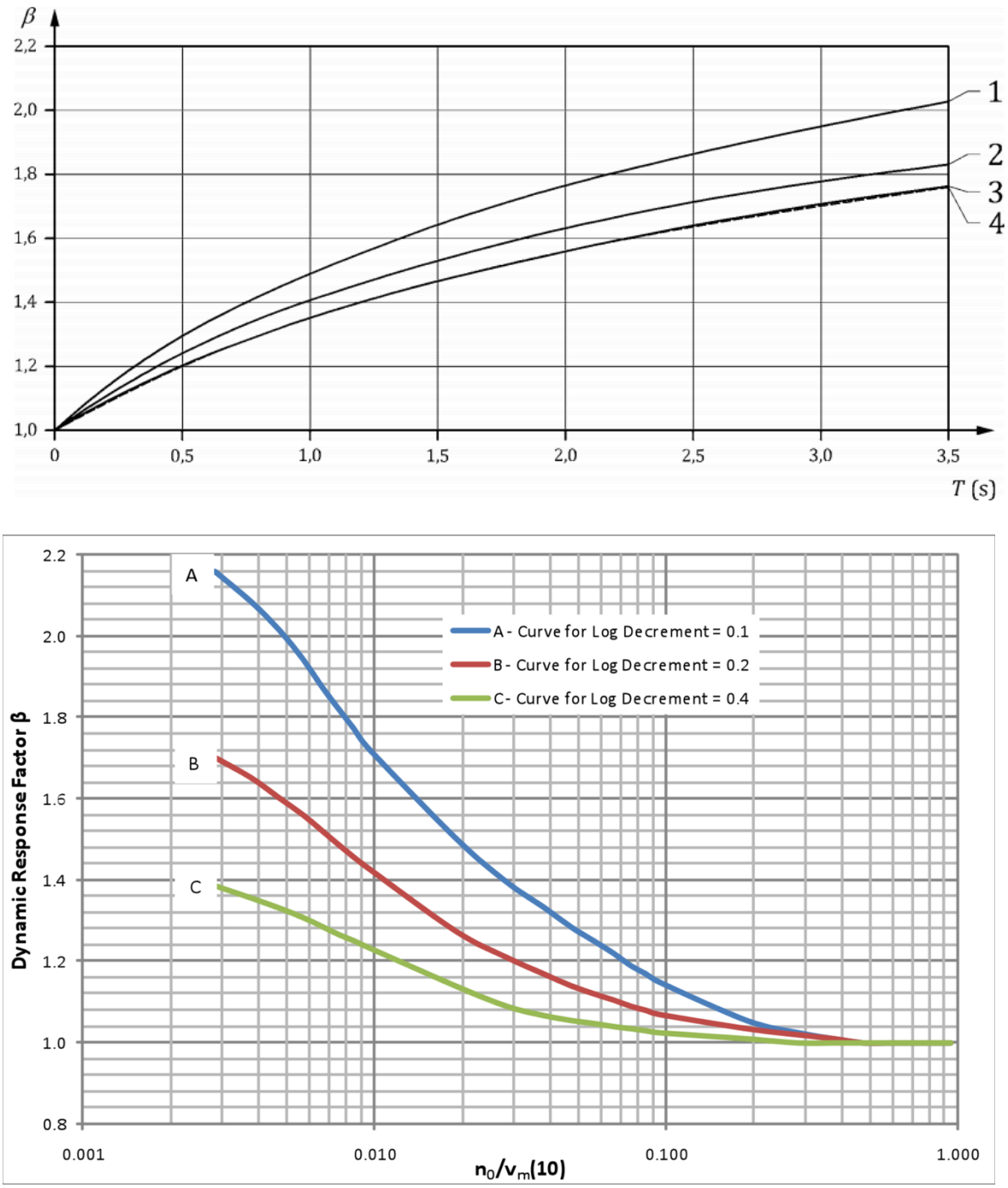

Figure 2-1. (Top) Coefficient β for the dynamic behaviour of columns. 1 metal; 2 prestressed concrete; 3 reinforced concrete; 4 fibre reinforced polymer composite [32]*. (Bottom) Dynamic factor β versus ratio n_o/V_m* [31]*.*

The variables in Figure 2-1 indicate the following:

β, is the dynamic augmentation factor applied to the static wind pressure.

n_o, is the fundamental translational frequency in Hz.

V_m, is the mean basic wind speed dependant on the location of the structure.

Sources [31] and [34] consider in more detail the influence of three different foundation categories (soft, medium and rocks/piles); the findings are similar to British Standards for lattice towers.

In similar fields like chimney design [35], specific values of structural damping are showed to explain the existence of vortex shedding events thorough the Scruton number. Those values can be increased by 0.5 % in case of soft conditions of the soils, if the rotation of foundation decreases the first natural frequency more than about 10 %.

It is clear that due to the effects of along-wind buffeting or across-wind vortex shedding, damping must be a key property when one is defining dynamic responses in slender structures. The complexity of understanding and resolving the uncertainty of damping mechanisms has led standards authorities around the world to avoid the topic of damping as much as possible; instead they recommend first searching for better expertise or carrying out experiments based on field tests and, if such evaluations are not available, using conservative values to address damping. In fact, some standards decided to neglect the issue altogether by incorporating damping assumptions into code formulations. The considerable discrepancy in methodologies concerning wind loading formulation and structural response have led to different predicted-response results for the same cases in different countries [36, 37]. Formulating a single criterion has become a goal of consultants, manufacturers, and owners around world in terms of understanding of damping and its implementation on structural assessments.

2.3 Modelling and Estimating Damping

As was previously introduced, damping is considered a critical concern in the design of telecoms structures. Each structure must have sufficient damping to mitigate effects of dynamic loads provided by the wind in order to maintain structural integrity under acceptable serviceability levels. Current guidelines are basic and recommend a good prior-to-construction estimation of damping; however, this estimation could lead to considerable dynamic issues including fatigue damages. Including a damping control device is a feasible mitigation option.

The modelling of damping forces in a vibrating structure has been an active area of research in structural dynamics for many years. While damping and stiffness can be modelled in finite element simulations with specific mass and stiffness matrices derived using first principles, there exists no such approach for damping, and other than discrete damping elements, there is no first-principles damping matrix [2], i.e. damping does not relate to a unique phenomenon. There is much uncertainty in quantifying damping that arises from working nonlinearly with the amplitude and from unknown complex mechanisms of along- and across-wind response within the structure [38].

The sections below discuss the types of damping sources that are available to communications structures.

2.3.1 Structural Damping

Structural damping is a measure of the energy dissipation in a vibrating structure that returns the structure to a quiescent state. Damping capacity is defined as the ratio of the energy dissipated during one oscillation cycle to the maximum amount of energy accumulated in the structure during that cycle. The considered effects/contributions to overall damping, which are analogous to converting mechanical energy into heat, are material damping (ζ_{mat}), friction/coulomb damping (ζ_{frict}), and soil-foundation interaction damping (ζ_{foun}).

As is typical in structural engineering, the most common approach is an equivalent viscous damping model because it leads to a linear equation of motion. Dissipation in this model is due to various mechanisms (Figure 2-2) such as cracking, nonlinearity in the elastic phase of response, interaction with non-structural elements, soil-structure interaction, et cetera. As it is very difficult and unpractical to estimate each mechanism individually, the elastic viscous damping represents the combined effect of all of the dissipation mechanisms [39].

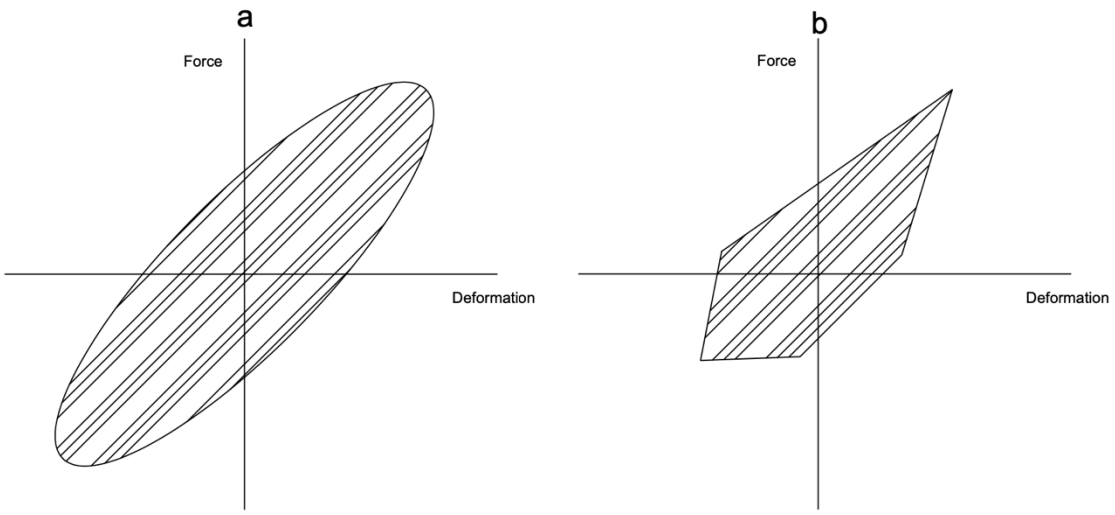

Figure 2-2 Dissipated and stored force for (a) viscous damping and (b) hysteretic cycles [39].

There is no direct relationship between such damping and real physical phenomena. However, the adoption of the viscous damping concept simplifies the solution of the following scalar differential equation of motion response proportional to the velocity of a body in the case of a single degree of freedom:

Eq. 2-6

$$m\ddot{x} + f_d(x, \dot{x})\dot{x} + kx = f_{tot}$$

Where the damping forces can be summarised as linear viscous damping with the coefficient, c:

Eq. 2-7

$$f_d(x, \dot{x}) = c\dot{x} = 2m\zeta\omega_n\dot{x}$$

Where ζ is defined by Eq. 2-8 as:

Eq. 2-8

$$\zeta = \frac{c}{2m\omega_n}$$

and x is the displacement, ω_n is the natural vibration frequency (rad/s) of the system, and ζ is the damping ratio or fraction of critical damping as Figure 2-3. For $\zeta < 1$, the solution for the motion equation is:

Eq. 2-9

$$x(t) = xe^{-\zeta\omega_n t}\sin(\omega_d t + \phi)$$

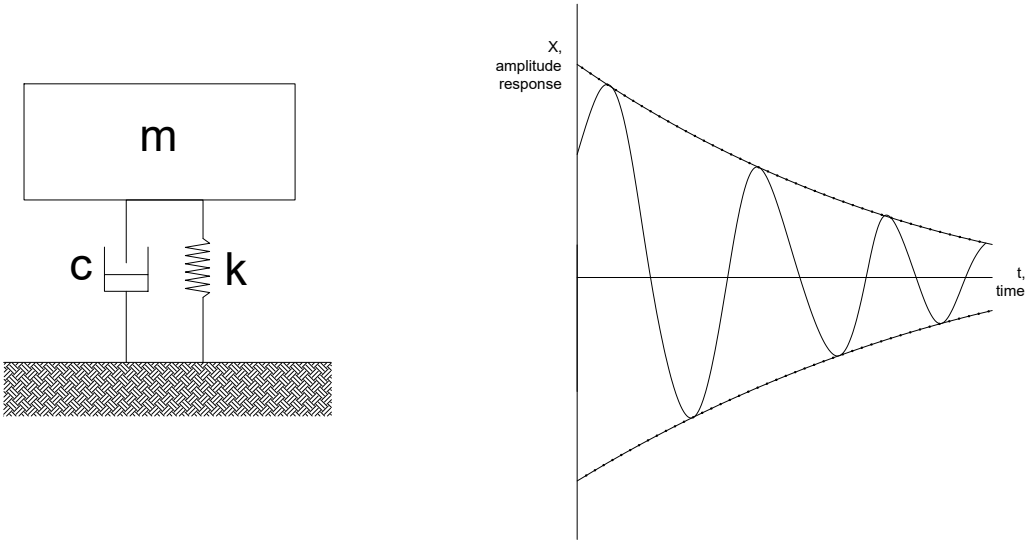

Figure 2-3 Viscous model and vibration decay of a system with viscous damping, [40].

Where $\omega_d = \sqrt{1-\zeta^2}\omega_n$ is the damped (circular) natural frequency (which is always lower than the undamped natural frequency ω_n in the presence of damping) and ϕ is the phase angle of the damped oscillations.

The first advances in understanding and quantifying structural damping arose from research conducted in nuclear structural buildings [41, 42]. The results of these studies were used extensively in the US and Japan for seismic analysis in the 60s and 70s. Further researches, [43, 44] classified damping by materials, stress levels, connection types or soil-foundations influence, firstly applied to communications structures in [45].

The most important mechanisms considered in structural damping are material damping and friction/coulomb interfacial damping. In actual slender structures, material damping is based on energy losses due to internal hysteresis in materials that comprise the structure [46]. This damping stems from molecular interactions within the structure material. As evidenced in the literature, the typology, treatment and construction processes of a material define its final characteristics. Laboratory tests of materials with the same properties have identified several discrepancies in microscopic and macroscopic behaviour. These discrepancies render modelling and

prediction of material damping a highly complex endeavour. Researchers have therefore sought phenomenological theories to represent structural damping.

On the other hand, there is evidence that a high percentage of structural damping is caused by connection friction (Coulomb friction) of the structural response. These friction forces occur when relative motion occurs between adjacent members. In communication towers and masts, these members include the joints between leg bracings and horizontal members of lattice towers and the joints between the foundation and superstructure or between steelwork installed to hold equipment. Those forces are independent of the amplitude, frequency, and velocity of tower motion and constantly oppose the normal motion of the structure. Welded connections tend to reduce the contribution of interfacial damping compared to bolted connections.

The forces involved in the motion of such a system are visualised in Figure 2-4, and the corresponding equations are as follows:

Eq. 2-10

$$m\ddot{x} = -kx - f_d \quad if\ \ddot{x} > 0$$

$$m\ddot{x} = kx - f_d \quad if\ \ddot{x} < 0$$

The general solution is then:

Eq. 2-11

$$x(t) = A\sin\omega t + B\cos\omega t + \frac{f_d}{k} \quad (\dot{x} < 0)$$

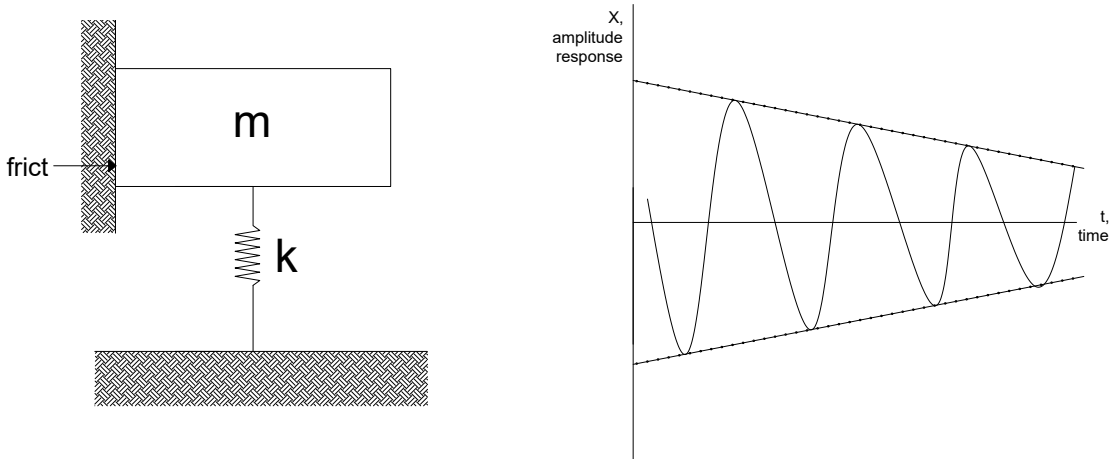

Figure 2-4 Free response with dry friction damping.

The final contribution to structural damping is the soil-foundations interaction [47, 48], which can be also divided into two components, as first introduced in [49]: the energy loss through propagation of waves from the footing and the internal energy loss due to hysteretic and viscous effects. The literature defines representative damping ratios for each component source: radiation damping and soils-material damping.

Two main forms of oscillation, horizontal translation and rocking, are investigated in the present research to determine their impact during freely decaying response.

To conclude, the equivalent viscous damping values are a longstanding subject [50]. Thousands of field and labs tests have been conducted in an effort to determine optimal approaches, but expert consultants are concerned that issues remain. The wide range of values is described in Table 2-5.

Table 2-5. Typical values of structural damping ratio from literature review [51].

Structure	ζ_s [%]	
	Min	Max
Building	0.5	5
Steel tower, unlined, welded construction	0.4	0.7
Steel tower, unlined, bolted construction	0.6	1
Steel tower, unlined, welded, elevated in steel support structure	0.3	0.5
With lining (at least 50 mm thick)	+0.2 to the above values	
Concrete tower	0.5	1.2
Concrete tower with internal partitions	1.2	2.5
Steel bridges	0.3	1
Reinforced concrete bridges	0.5	2
Pre-stressed concrete bridges	0.3	1

The current amount of research on masts and towers is insufficient to establish a suitable knowledge of damping in different structures. The present work assesses and improves existing recommendations.

Further, use of the equivalent viscous damping model obscures the more realistic behaviour of damping with amplitude dependency. In reality, damping depends on several structural systems which further complicate the estimation of damping levels. Nonlinearity effects and loading may affect the accuracy of conventional damping

estimation procedures [52]. Furthermore, complex dynamic responses with closely spaced vibrational modes might appear to transfer damping between modes, increasing the difficulty in estimating damping, or possibly approach adjacent irregularities in foundation-soils interaction in terms of damping. The research studies this issue in Chapter 4 and Chapter 5 with tools like backbone curves to provide more light to the advanced analysis of amplitude dependency in damping.

The following sections develop the main topics that are the object of this research.

2.3.1.1 Nonlinearities

Reviews of dynamic responses in several civil engineering structures have found that current approaches to address stiffness and overall damping behaviour are essentially primary approximations of real behaviours, and these behaviours are very difficult to detail and model with sufficient accuracy for analyses. In damping, the equivalent viscous approach assumes correlated values of energy dissipation for particular systems and ignores essential variables which create dependencies.

Such assumptions are fundamentally incorrect, as real behaviour is defined by several types of nonlinearity that are encountered during dynamic testing. These manifest in various forms such as polynomial behaviour of hysteric material damping, nonlinear behaviour of friction at connections, asymmetries of boundary conditions due to soil-foundations interaction, clearance, impact and friction of loose cabling.

These nonlinearities usually depend on amplitude, velocity and frequency [53], and these dependencies add nonlinear components (Figure 2-5) to the typical equivalent viscous damping approach of dynamic motion as :

Eq. 2-12

$$m\ddot{x} + c\dot{x} + kx + f_{nl,1}(x) + f_{nl,2}(\dot{x}) = f_{tot}$$

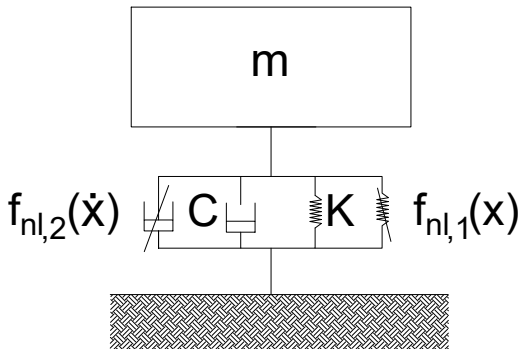

Figure 2-5. Model of nonlinearities in communication structures.

The ESDU [54] has developed a theory of structural damping for fundamental natural modes of vibration. In the field of building design, the damping relevant to the resonant component of the response amplitude adheres to the relation defined in the following equation, Eq. 2-13.

Eq. 2-13

$$(\zeta_s)_j = (\zeta_{s0})_j + (\zeta'_s)_j \frac{x_H}{H}$$

The method defined in [54] identifies three regions as indicated in Figure 2-6. Region A comprises small amplitudes of responses with small values of structural damping, $(\zeta_{s0})_j$. The friction interaction between structural and non-structural elements of the building and material hysteresis creates region B, and damping from wind excitation falls within this region. Finally, a constant region C with an upper limit defined by measurements for the very large deflections associated with earthquake excitation; both limits describe $(\zeta'_s)_j$, which is the rate of increase of the structural damping with x_H/H. Each type of communication structure has a unique curve that is similar to Figure 2-6. The present research aims to determine this curvature using suitable response data acquired with no wind influence.

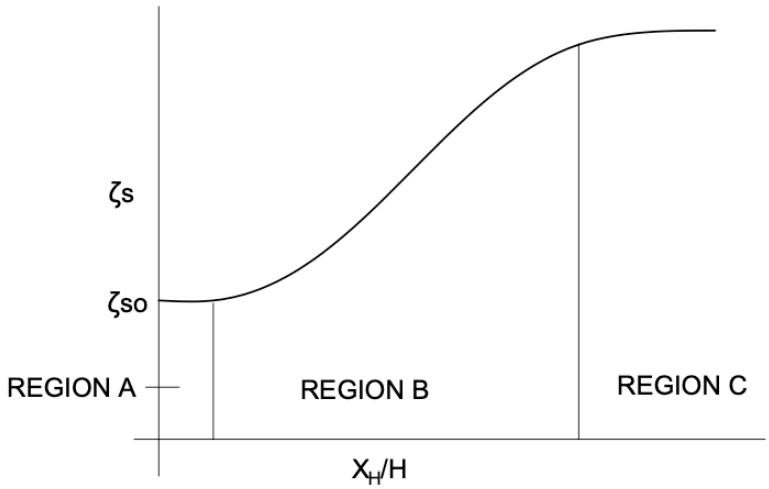

Figure 2-6. Sketch of typical variation of structural damping with the approximate amplitude of a building [54].

Of currently available tools, the analysis of constructed frequency response functions (FRFs) in the frequency domain and the extraction of backbone curves from free decaying response in the time domain are proven methodologies to detect nonlinearities.

Given access to free decaying response data, the backbone curves method is an ideal analysis technique. This method is based on defining the natural frequency and structural damping as a function of the amplitude of the system response when neither external damping providers nor forcing are present. This information provides a valuable description of the system dynamics that may allow one to characterise, quantify, and highlight interactions between active nonlinearities [55]. Figure 2-7 presents an example of free decaying response data from a monopole survey in St Ives used during the research under calm weather conditions. On left, the analysed free decaying response in accelerations terms, and on right, the stiffness and damping backbone curves.

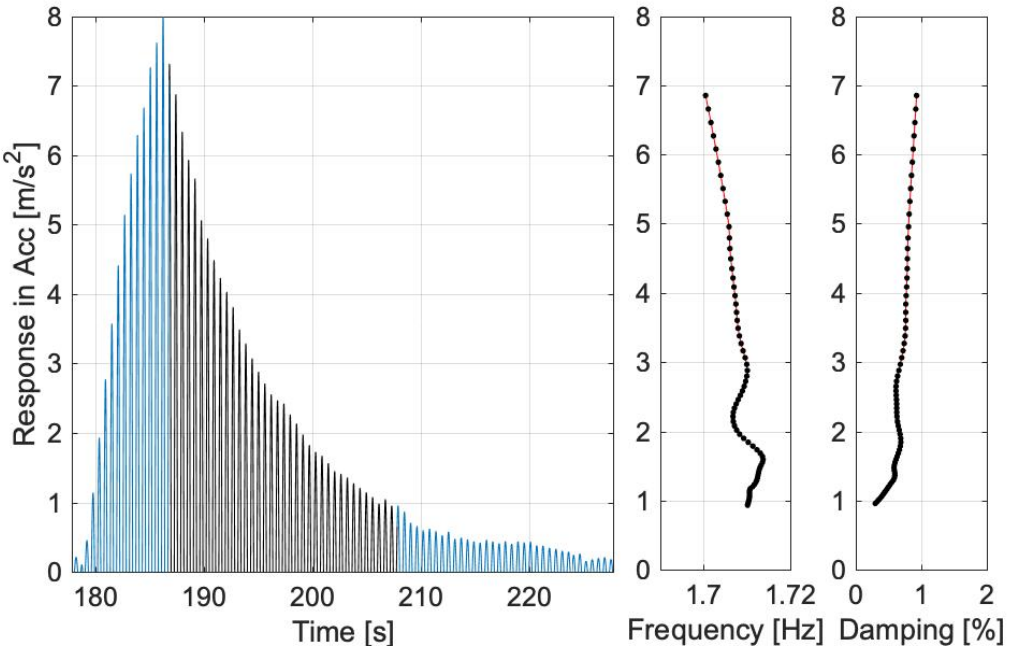

Figure 2-7. Example of backbone curve in St Ives FC. Zero-crossing method [56].

Currently, the lack of information and high uncertainty regarding real structural damping behaviour have led institutions to be very conservative when modelling damping for design purposes. Differences among methods of estimating damping for field/laboratory conditions in the literature provide inconclusive results which induce use of relatively conservative damping values. Simplistic values are used for highly complex parameters, and linear formulations are used to represent proven nonlinear behaviours.

In an industry as changeable as communications, the current practice of not optimising certain damping properties could be preventing the financial improvement of thousands of current structures or better designs from manufacturers. This research examines the nonlinear performance of certain freely decaying responses in monopoles where likely damping sources are limited to soil influences, friction behaviours of different connections (mainly bolted and welded), the impact of loose cabling, or hysteric material damping. The findings from such simple structures could inform further investigations of more complex structures.

2.3.1.2 The impact of soil-foundation in structural damping

Communications structure foundations are typically supported by either isolated pad foundations for each leg of wide lattice towers (see Figure 2-9); spread footing or piled

foundations (which are less common) for monopoles or short structures such as Figure 2-8; and cube blocks of concrete for high guyed masts (see Figure 2-10). When the soil on which an ordinary shallow foundation would rest is of insufficient strength to hold the load from the structure, it may be necessary to use a piled foundation, with the purpose of transferring the load to stiffer materials at a lower level.

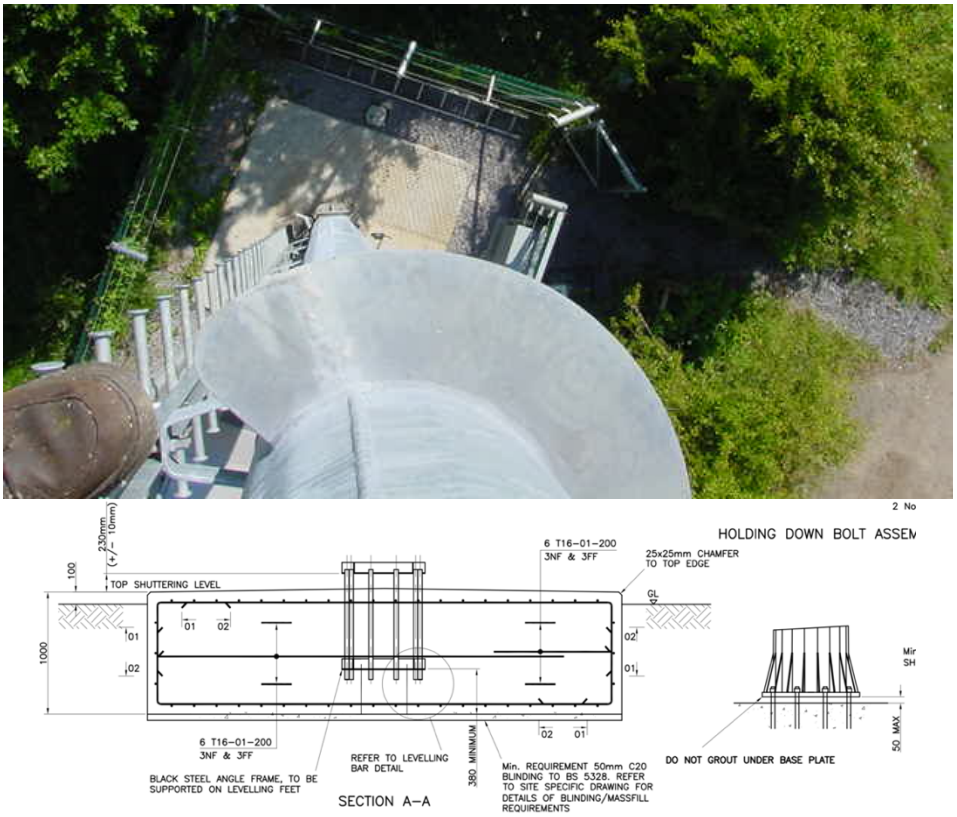

Figure 2-8. Typical footing foundation for monopoles and short lattice towers.

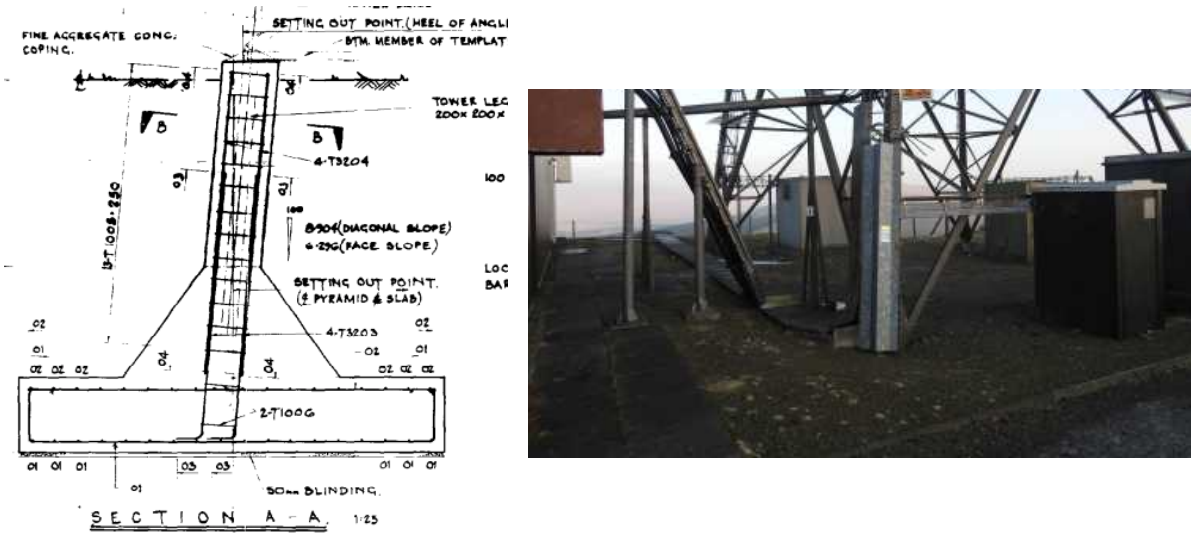

Figure 2-9. Typical pad foundation for high lattice towers.

Figure 2-10. Typical stay anchor-foundation of HGM.

The rigidity of boundary conditions like the foundation-soil system determines another mechanism of energy dissipation of the structure as modelled in Figure 2-11 and Figure 2-12. Desired stiff base conditions, such as rock soils or piled foundations, do not dissipate energy in the same way as soft soils like some types of clays on superficial foundations. In terms of dynamics, the oscillation frequency and manner of its decay depend on the physical parameters of the structure foundation and its soil support. As described in [57], the rigidity of foundation soil makes the combined system less stiff than if the structure were on a fixed base. This decreases the natural period, which in turn generally increases the dynamic response of the tower. According to [58], the lowest natural frequency is the most affected as it involves the highest proportion of soil in the mode shape.

High percentage of the existing studies were based on steady-state foundation vibrations induced by rotating machinery. There, the foundation and soil structure may change ground stiffness, producing settlement of the ground surface or possibly a reduction in strength. This dynamic behaviour is governed by parameters such as the initial void ratio, soil boundary confinement, or intensity of the loading.

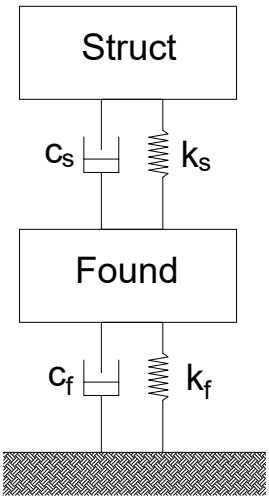

Figure 2-11. Model of foundation and superstructure in communication structures.

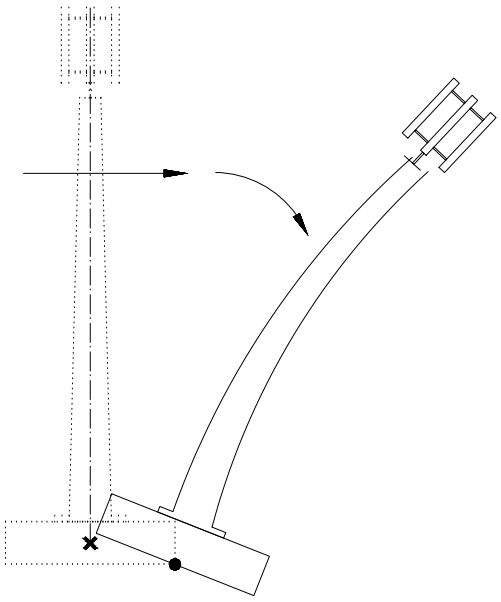

Figure 2-12. Model to represent coupling of horizontal and rocking motions for an embedded foundation.

The soil's contribution to damping can be divided into two components as first introduced in [49]: loss of energy through propagation of waves from the footing and the internal energy loss due to hysteretic and viscous effects. The literature has identified representative damping ratios for each component source:

- Radiation damping, $\zeta_{foun,j}$. This elastic property is associated with the soil material parameter. Stress waves propagate away from the foundation surface in a manner

that depends on the soil layers and the type of soil. The radiation is compounded by different forms of oscillation, rocking and horizontal translation.

- Material damping, $\zeta_{foun,mat}$. This damping is caused by viscous and frictional effects within the soil that result in a non-linear stress-strain curve under numerous cycles of loading applied to a sample soil. The stresses developed by sliding soil particles create an energy loss exhibited by a hysteresis loop in the stress-strain relationship. This relationship can be obtained under either static or dynamic conditions. This factor is a function of strain amplitude, confinement, and water saturation as determined in the literature through empirical formulation.

According to literature on field testing, it is difficult to evaluate radiation and material damping independently and each includes a contribution of foundation damping. Some authors [59] recommend extracting the material damping from each radiation mode and considering how each soil type behaves under specific static and dynamic loading conditions during geotechnics laboratory tests. This study does not separate both sources – instead, it identifies a generic critical equivalent damping for each form of oscillation (i.e., for translation and rotation at the foundation, which will form a generic foundation damping).

Although some damping approaches consider foundation and soil damping source to be important factors when assessing structural damping, these approaches are limited to the new designs and development of buildings, bridges, and rotating machinery. No advanced studies have been conducted in the field of communication structures. This research studies the behaviour of structural damping for three different types of soil-foundations categories in monopoles based on existing geotechnical reports and advanced knowledge of the chosen structures.

2.3.2 Aerodynamic Damping

With the assumption that velocity fluctuations in the approaching flow are completely correlated across the face of the structure [60], aerodynamic damping forces arise from the relative motion between the tower and the wind and depend on the mean wind speed, structure geometry, aerodynamic coefficients (drag factors), and generalised mass corresponding to the chosen mode [61].

Considering aerodynamic and aeroelastic effects, all the procedures defined by ESDU [54] provide the most extensive literature review and the best recommendations for

advanced structural designing. The present research has applied some of those texts and approaches to communications structures. The equation for motion of the equivalent single degree of freedom model using equivalent viscous damping for building may then be expressed as follows:

Eq. 2-14

$$M_j\ddot{X}_j + 2(\zeta_s + \zeta_{aer})_j\sqrt{M_jK_j}\dot{X}_j + K_jX_j = F_j$$

Where F_j is given by the mean generalised modal force and the buffeting generalised modal force terms. For each vibrational mode, the modal aerodynamic damping ratio in communication structures may be expressed as,

Eq. 2-15

$$\zeta_{aer} = \int_{z=0}^{H} \frac{\rho_a\overline{V_z}(z)WC_D(z,f_j)\mu_j(z)^2dz}{4\pi f_j m_H} = \frac{\rho_a\overline{V_H}}{4\pi f_j m_H}\int_{z=0}^{H} WC_D(z,f_j)\mu_j(z)^2\left({}^{z}/_{H}\right)^{\bar{\alpha}}dz$$

However, for tall and slender buildings, the damping for the first bending translational mode can be defined using a simplified equation Eq. 2-16:

Eq. 2-16

$$\zeta_{aer_j} = \frac{\rho_a\overline{V_H}W\overline{C_D}}{4\pi f_j m_H}\cdot\frac{3}{3+\alpha}$$

The variables in Eq. 2-15 - Eq. 2-16 indicate the following:

f_j, is the generalised modal wind force (Hz).

ρ_a, is the air density (approximately 1.29 kg/m3).

V, is the instantaneous wind speed. (V_H hourly mean wind speed, m/s).

z, is the reference height of the structure (m).

C_D, drag coefficients.

m_H, is the mass per height unit of the structure (kg/m).

W, is the width of the structure (m).

μ_j, mode shape of the fundamental mode shape.

α, parameter to correlate the effects of shear flow on the drag forces. Taking values between 0.1 on open water terrains and 0.3 on towns and city centres.

ζ_{aer_j}, modal aerodynamic damping (%).

The induced wind forces acting on a finite-length structure are essentially affected by the turbulence features of the approaching wind flow, the surface roughness of the structure and the flow Reynolds number (Re). Those points are captured by drag coefficients C_D, as Eq. 2-15 and Eq. 2-16. Normally, those factors [62] are found by integrating the measured pressure distributions over the surface of the structure, as suggested in left side of Figure 2-13 where C_p is the wind mean pressure coefficient obtained from incident uniform flow in circular shapes.

Three different regions can be separated, according to the estimation of drag factors, related to the transition from laminar to turbulent flow, and are consequently highly affected by Re, as right side of Figure 2-13. The most important point is the characterization of the sudden reduction in drag factor behaviour inside the transitional zone. This point has a marked influence on the pressure distribution over the rearward surface of the body and consequent estimation of wind forces over the structure. Figure 2-13 shows the typical behaviour of drag factors for different geometries and Re where the trans-critical regimen is defined.

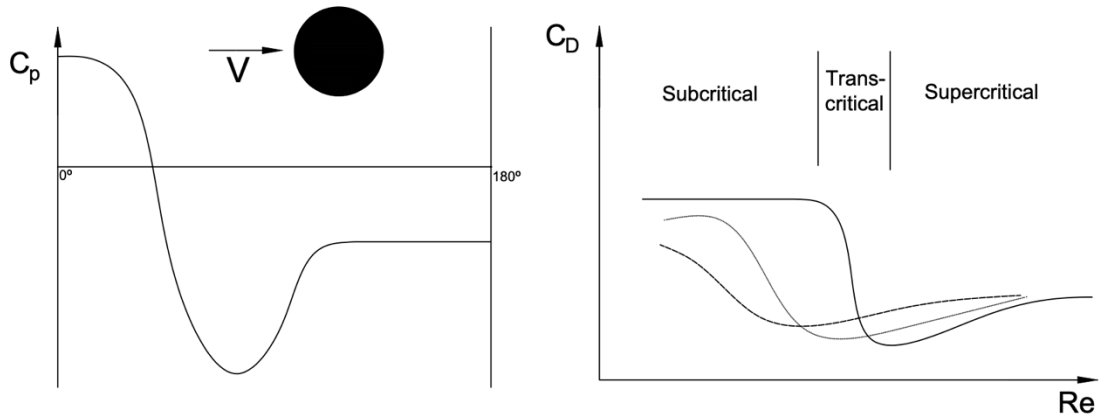

Figure 2-13. (Left) Typical variation of the mean pressure distribution of uniform flow on a circle. (Right) Drag coefficient versus Reynolds number on diverse geometry [62]

The determination of drag/lift factors has become the most challenging problem in wind engineering applied to communications structures due to the large variety of

factors involved. In specific important and critical cases such as challenging antennae, wind tunnel laboratory tests are required. Minor changes in geometry, roughness, or wind flow significantly impact forces. There is no agreement between standards about the recommended drag values which depend on different structures types, geometries, the performance of linear and small attachments, etc…, which leads to a great deal of uncertainty when designing these structures.

Concerns regarding the uncertainty of drag factors affect the structural engineers' modelling at both design and analysis stages. Overestimation of drag factors leads to an increase in design loading. Monopole structures do not achieve remarkable heights, generally placed at ground level and consequently experience high turbulent shear flow. As was shown, the basic wind-force coefficient for estimating overall forces and moments is the overall drag factor, and an appropriate mean flow velocity is needed. Turbulent shear flow can be reasonably approximated as follows:

Eq. 2-17

$$drag\left(=\int_0^h 1/2\,\rho {V_r}^2 C_{Dr} W\,dz\right) = 1/2\,\rho {V_{hc}}^2 C_{Du} W \int_0^h \left({V_z}/{V_{hc}}\right)^2 dz = 1/2\,\rho {V_m}^2 C_{Dm} W h$$

Where C_{Dr} is the local drag factor at each level of the structure, C_{Du}, is the drag factor of the step model recommended for tapered structures and C_{Dm} is a mean value to be used on structures of constant section.

On the other hand, on tall structures such as lattice towers, the drag coefficient is usually based on the shadow area, and an effective value of W equal to the actual width and solidity ratio should be used in the evaluation response.

The implementation of Eq. 2-15 using standardised values of drag values led to high values of aerodynamic damping, and consequently increase dynamic capacity of the structure, which might be beneficial. This has not been verified on the existing literature.

The necessary optimisation of expensive and/or old structures is a compelling reason to avoid a continued practice of overestimating drag factors. This research studies those concerns in short structures to validate existing formulation and values of drag factors.

Aerodynamic damping depends on the response of the structure vibrating in air flow. So, the aerodynamic contribution to damping increase with height. At low heights where turbulences are dominant, structural damping tends to be more important than aerodynamics. However, on tall structures damping can take much higher values under conditions of low-to-moderate reduced wind speeds. Other sources of aerodynamic damping come from alternative restraint conditions like guy vibrations, or aeroelastic effects induced by vortexes at geometries appearing along the structure.

Most structural shapes are aerodynamically bluff, and the airflow separates from the surface to form a wide wake of retarded turbulent air [6]. Those aeroelastic effects can cause self-induced oscillations due to vortex shedding (VS) or galloping where geometric characteristics, oscillation frequency and amplitude of the oscillation determine the energy absorbed by the system. Figure 2-14 compares both types in terms of incident flow and structural capacity. In galloping, for higher wind velocities the oscillation amplitude increases depending on the level of structural damping existence on the structure. Alternatively, VS occurs at relatively-low and well-determined wind velocity and amplitude response is defined by a limited value.

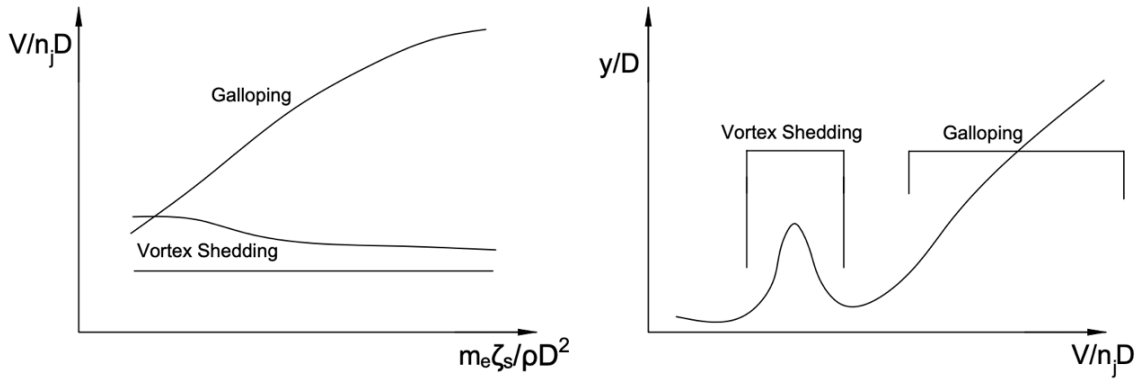

Figure 2-14. Alternative vortex shedding at subcritical Reynolds number. Sketches illustrating vortex and galloping excitation of a square-sectioned cylinder.

2.3.2.1 Aeroelastic issue: Vortex shedding

VS becomes a particularly critical issue in communications structures because of the risk of fast deterioration and fatigue failure. When wind flows about a circular cylindrical structure at medium or high Re [62], vortices are usually shed on alternating sides of the body (Figure 2-15). These asymmetric fluctuations generate regions of low pressure, result in a net lift force which alternates in direction as vortices are shed,

and a drag force which fluctuates in magnitude only i.e. always same sign. When this phenomenon appears at the natural frequency of the structure and exceeds the structural damping, the structure resonates under the shed frequency. This effect can create a long-time constant frequency and amplitude response called “lock-in”.

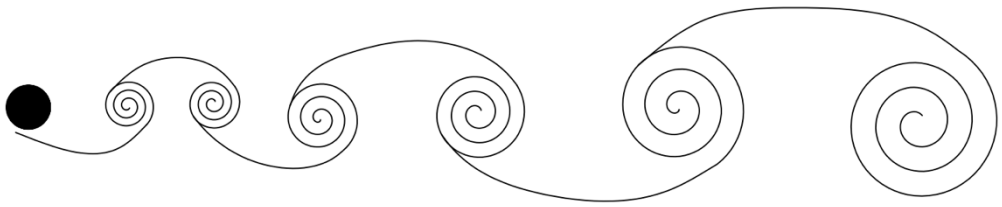

Figure 2-15 Alternate vortex shedding at subcritical Reynolds number.

Lock-in events is able to induce high numbers of cycles at significant amplitude with very relatively low wind speed conditions, which is extremally dangerous in cases of fatigue. The relationship between the flow speed, V_{crit}, and the geometric parameters and natural frequency is defined by Strouhal number, St:

Eq. 2-18

$$V_{crit} = \frac{1}{St} f_n D$$

Where f_n is the natural frequency of the body/structure under vortex shedding, and D is the diameter of the bluff body or the crosswind dimension of the structure under consideration.

As defined in EN1991-1-4: Table E.1 [26], the Strouhal number is assumed to be 0.18 for a circular shape, or between 0.06 and 0.15 for sharp-edged bodies. The behaviour of the Strouhal number in the across-wind response has proven very dependent on Re, as indicated in Figure 2-16, where ε is the equivalent roughness height of cylinder surface, D the cylinder diameter and Re_e the effective Reynolds number, and turbulence properties of the across-flow oscillations proven experimentally by Vickery [63]. On other approach, Krenk and Nielsen [64] introduce turbulence as key parameter in their theoretical lift- oscillator model.

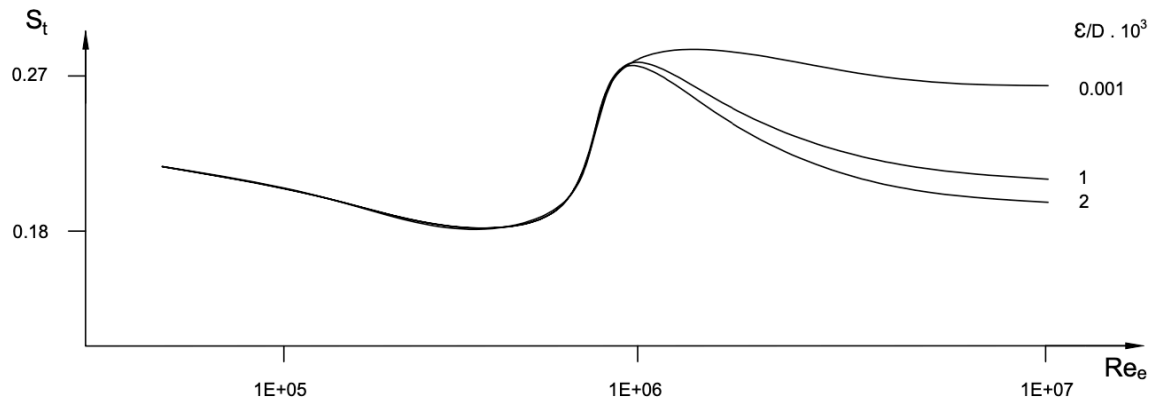

Figure 2-16. Strouhal number behaviour versus Reynolds numbers for cylinder shape [62].

This inclusion has significant implications in shorter structures close to the ground under high turbulence, such as a monopole. At a certain height, mean flow induces stable vortex shedding to generate large amplitudes. Previous models were implemented to estimate likely VS events in high Arqiva structures where critical antennae can create vortices.

The Scruton number assesses the structural resistance or propensity to vortex shedding of a structure. The Scruton number, Sc [65], is a crucial parameter for determining the vortex-induced vibrations of structures. This non-dimensional index is proportional to the structural damping and to the ratio between the vibrating mass and the mass of the air displaced by the structure, and it is defined as follows:

Eq. 2-19

$$S_c = \frac{2\delta_s m_e}{\rho_a D^2}$$

Where:

δ_s is logarithmic decrement of structural damping.

m_e, the effective mass resonance modes.

$$m_e = \frac{m_{T,j}}{\int_o^h \mu_j(z)^2 dz}$$

h, the structural part excited under vortex shedding.

$m_{T,j}$, the total modal mass of the excited vibrational mode under VS as defined below:

$$m_{T,j} = \int_0^L m(z)\,\mu_j(z)^2 dz$$

Where m(z) is the vibrating mass per unit length.

For a cylindrical bluff body, practical experience has indicated that vibration modes with a Scruton number of more than 15 are highly unlikely to exhibit significant VS behaviour. Example of this response on typical communications structure is visualised in Figure 2-17 characterised by high nonlinear behaviour.

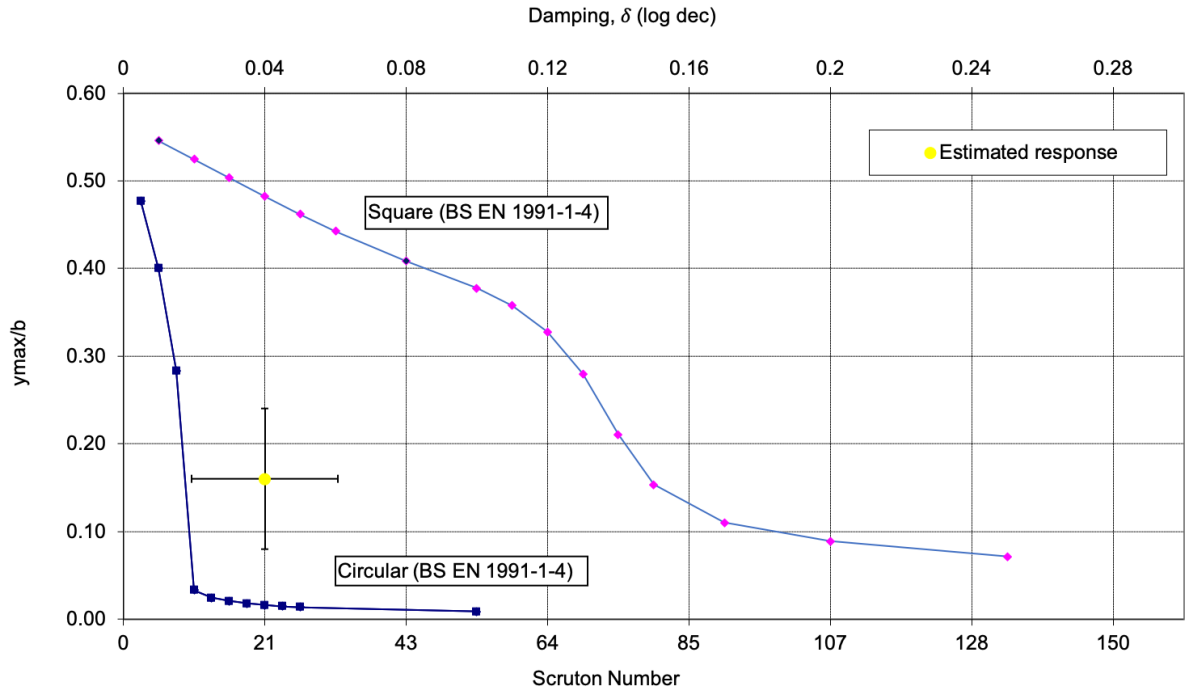

Figure 2-17. Measured response and vibration predictions of circular, square section and intermediate section against Scruton number and damping. Report from Moel-y-Parc assessment shared by COWI.

The forcing induced by lock-in effects in VS, $F_{lock\text{-}in}$, consists of an inertia load proportional to accelerations of the structure and an aerodynamic damping proportional to the velocity of the structure:

Eq. 2-20

$$-m_a\ddot{y}_{cross} - c_a\dot{y}_{cross} = f_{lock-in}$$

Where $\ddot{y}_{cross}$ are the crosswind accelerations. The added mass of air m_a is small and so the acceleration dependent term can be neglected. The second component

indicates that the aerodynamic damping force $c_a\ddot{y}_{cross}$ decreases the effective damping of the vibrations for negative values of c_a.

The definition of aerodynamic damping under VS given by [63] is as follows:

Eq. 2-21

$$\zeta_a = c_a\dot{y}\left(1-\left(C\dot{y}/(bf_e)\right)^2\right) = \frac{\rho D^2}{m_e}K_{a,ref}\left(\gamma_K - \left(\frac{\sigma_{y,ref}}{\gamma_{aL}a_{L,ref}D}\right)^2\right)$$

Where γ_K, γ_{aL} are correlation factors, and $\sigma_{y,ref}$ is the standard deviation of the structural deflection as defined in the literature [66]. Hansen [66] extracted an aerodynamic approach of the form $a\dot{y} - b\dot{y}^3$, in which the first term introduces negative aerodynamic damping and the last, non-linear term produces positive damping to ensure that the response is self-limiting.

2.3.2.2 Aeroelastic issue: Galloping

Galloping [67] is an aeroelastic response mechanism in which fluid-dynamic loading results from the structure velocity, as demonstrated in Figure 2-14. This mechanism is particularly important in light-damped, flexible structures or elements such as street lighting, cables, and stays of both circular and non-circular cross sections. It affects flexible structures such as lattice towers and high guyed masts.

In the case of galloping, variations in wind load are in phase with structure velocity as Eq. 2-22. For an unstable, not self-limiting, response i.e. with effective negative damping, the change in wind load ΔF must be positive in response to positive increment in structure velocity, $\Delta\dot{Q}$:

Eq. 2-22

$$\Delta F/_{\Delta\dot{Q}} > 0$$

For a structure to be unstable (i.e., susceptible to galloping):

Eq. 2-23

$$\zeta_{s,j} - \frac{1}{4\pi f_j M_j}\frac{\Delta F_{Qj}}{\Delta\dot{Q}_j} > 0$$

This dissertation will study two examples of VS on lattice towers in Chapter 8 and galloping events on high guyed mast in Chapter 9, not found previously in the existing literature. They will provide introduction and understanding of these cases in damping terms and analyse the control chances using external adding damping.

2.3.3 Dampers

The implementation of supplemental damping provided by damper devices is an excellent solution to reduce the impact of dynamic excitations like earthquakes or wind loading on current structures. In communications structures under wind loading, dampers have been predominantly used to control undesired and otherwise uncontrollable aeroelastic effects like vortex shedding.

The main factors defining selection and design of an effective damper are the source of excitation, the range of design frequencies, the required efficiency or damping, maintenance requirements, and safety. In communications structures, due to the assumption of a lack of power supply in significant events and the need for exhaustive maintenance, passive dampers are always preferred. These dampers also tend to be less expensive and easier to implement than active versions; for the latter, frequent inspections are necessary to ensure continued functionality [1].

Although there are many damper prototypes, this research studies tuned liquid dampers as part of the structural health monitoring system installed in Moel-y-Parc high guyed mast and hanging chain dampers with which Arqiva has had excellent experiences in the past.

2.3.3.1 Tuned liquid dampers in communications structures

In the existing literature, tuned liquid dampers (TLDs) have been proven to be excellent vibration dissipators and are applicable to several types of structures, from marine vessels to buildings [68, 19]. Their main advantages are low costs, non-restriction to directional loads, and few maintenance requirements such as performance under possible freezing weather conditions.

A TLD relies on shallow liquid sloshing in a rigid tank to reduce the horizontal vibrations induced by dynamic loading like wind. This process creates a set of forces which oppose the current response of the structure. The equation of motion for a structure with a TLD installation can be approximated as follows:

Eq. 2-24

$$M_j\ddot{X}_J + 2\zeta_j\sqrt{M_jK_j}\dot{X}_J + K_jX_j = F_j + F_{TLD}$$

The fundamental natural frequency of liquid sloshing motion depends on the size of the container as Eq. 2-25:

Eq. 2-25

$$f_w = \frac{1}{2\pi}\sqrt{\frac{\pi g}{2a}\tanh\frac{\pi h}{2a}}$$

Of particular interest is these systems' capacity to adapt to geometry restrictions [69] like monopoles: the sloshing ring-annular cylindrical tanks could be as effective as other tank types and with better fitting in monopoles, Figure 2-19.

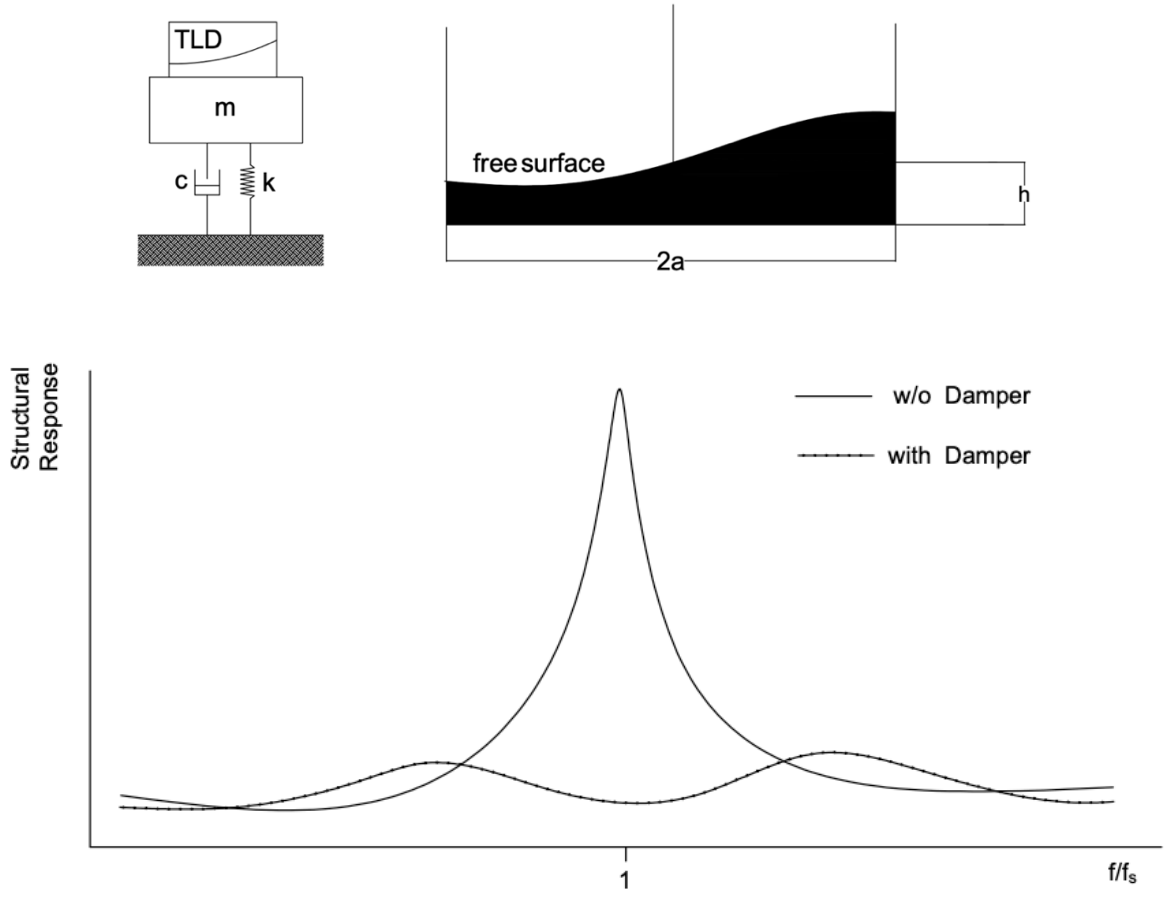

Figure 2-18. Model sketch and typical structural response of a tuned liquid damper (TLD) [19].

In monopoles which tend to have issues of high dynamic vibrations due to buffeting (for the fundamental mode(s)) and VS, TLDs are the most common damping devices on the market. The geometry and high effectiveness of these devices are advantageous when structural capacity is very limited. Required working frequency ranges can easily be obtained for TLDs within space requirements in monopoles such as shown in Figure 2-19.

Figure 2-19. Typical TLD in monopoles. Canada [70].

In high guyed masts, where new generations of wrap antennas tend to have aeroelastic challenging geometries, solutions based on TLD have been very efficient in avoiding responses under a wide range of frequencies.

There are very limited published investigations on the performance of TLD in communications structures. This lack of knowledge impedes implementation and optimization of advance solutions from dynamic point of view based on TLDs. The research presented in Chapter 9 investigates the performance of a large TLD installed in a Moel-y-Parc, (Figure 2-20) to control VS events.

2.3.3.2 Hanging chains dampers in communications structures

As stated in [72], hanging chains dampers (HCD) comprise one or more chains hung from high levels of a vibrating structure. As the structure moves, the amplitude of motion of the free end of the chain increases. Two energy dissipation mechanisms exist in HCD operation: firstly, the energy loss due to the inelastic impact of the chain against the wall of the cylinder; and secondly, the internal friction of the chain links rubbing against each other.

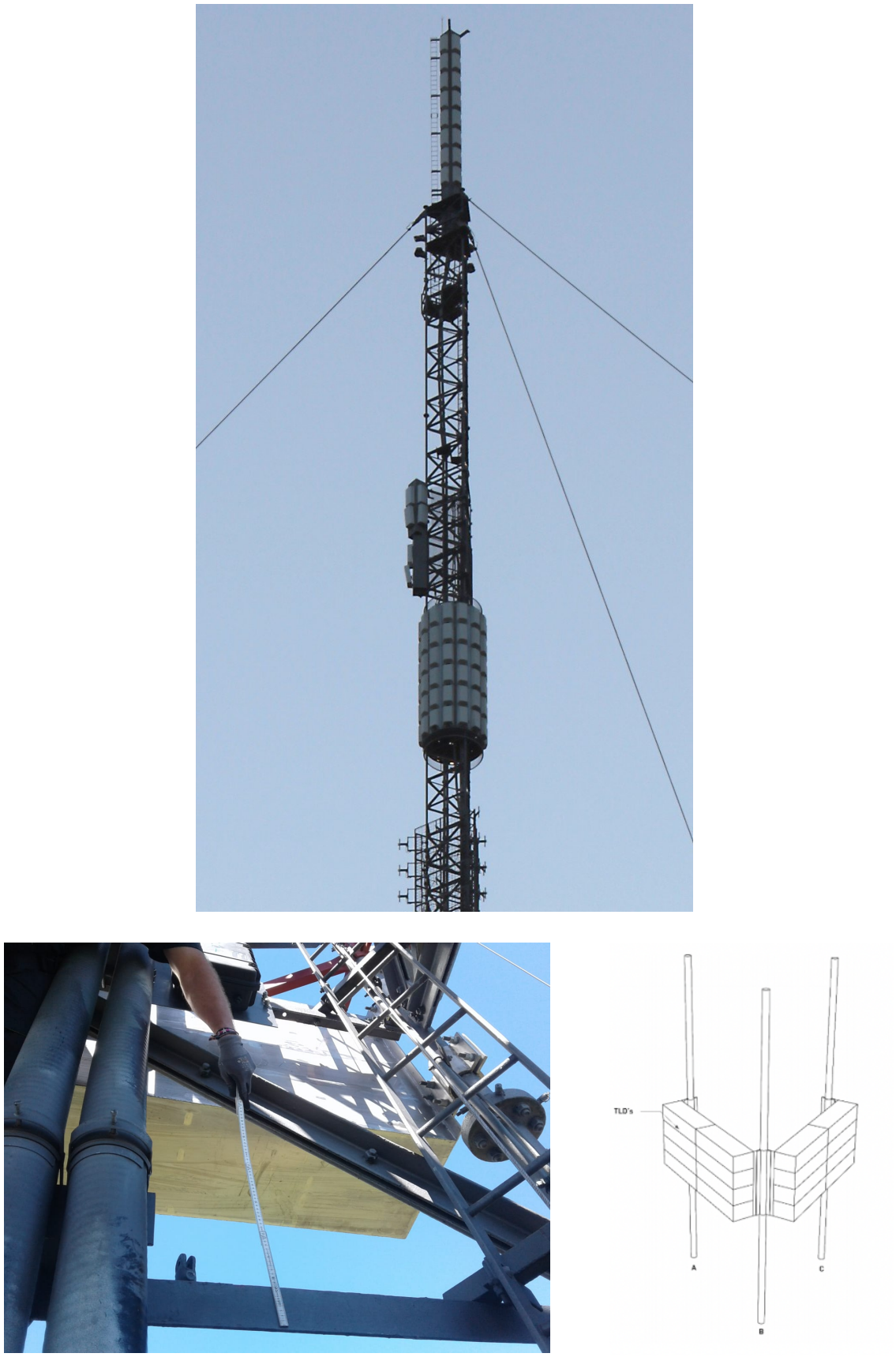

Figure 2-20. Sketch and picture of a TLD installed in Moel-y-Parc [71].

For each vibration event, different configurations of HCD might satisfy damping requirements to control VS events or reduce dynamic response under buffeting. Final designs are determined by pragmatic considerations such as chain size availability and cylinder sizes.

Review of the literature has identified four key design parameters when designing an HCD damper:

- The length of the chain bundle, which determines the natural frequency of the hanging chains.
- The mass of the chain bundle.
- The coefficient of restitution of the tube.
- The gap between the chain bundle and the tube wall, d, relative to the damped vibration amplitude of the structure, x_o.

Figure 2-21 plots the damping performance of an HCD for two different gap ratios, d/xo, of 4.78 and 1.72 versus the frequency ratio between the structure and the chain damper, where d is the existing gap in the HCD and xo the expected response of the structure at that level. The damper will dissipate energy for all frequencies that lie between approximately 1 and 6.5 times the first fundamental natural frequency of the chain. In the past decades, Arqiva has had good experiences in high guyed masts as Winter Hill or Belmont. For example, in Winter Hill several ranges of 1.5 - 3 Hz HCDs were installed to cover structure vibration mode frequencies below 0.5 Hz to avoid VS events with HCM design frequencies at maximum 0.325 Hz, verifying previous approach. Above this design frequency events of VS are not expected, so the solution keeps always in the full impact region.

- At low structure (natural) frequencies the level of damping will be low. The chains will vibrate in the tube such that the chains strike against the tube wall twice per cycle of the structure, but the impact will only occur over a short length at the bottom of the chain.
- The most effective damping occurs between approximately 3.5 and 6.5 times the chain frequency when more impacts per cycle occur and the full length of the chain impacts the tube wall.

- If the structural frequency is more than 6.5 times the chain frequency, the motion of the chain becomes chaotic and it does not strike the tube at all. No damping is added.

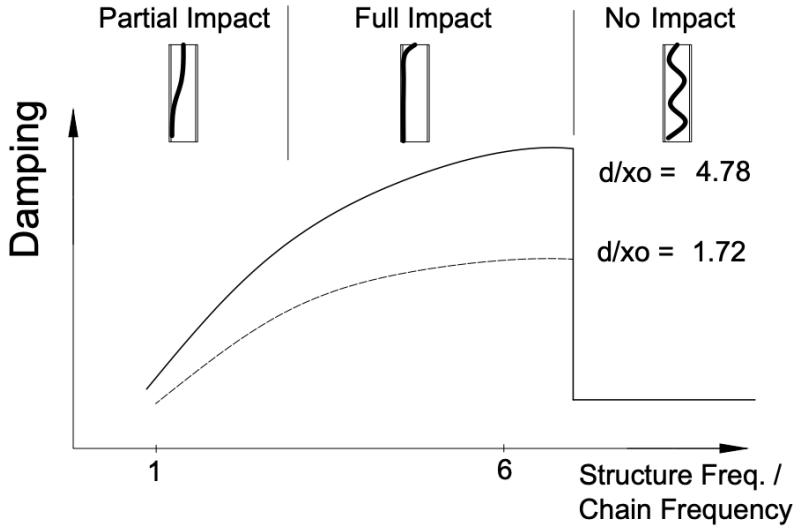

Figure 2-21. Effect of chain bundle frequency versus damping effects .Figure based on Flint and Neill reports extracted from [18].

An “optimum” damper design (i.e., a damper that provides most damping with minimal chain mass) will operate at structural frequencies just below the critical frequency. The level of damping achieved is proportional to the mass of the chain bundle provided. The disadvantages of increasing the mass of chain beyond that required are the practical difficulties of sourcing a heavy chain, fitting a chain group into a sufficiently large bundle, and installing a larger diameter tube as scheme and pictures found in Figure 2-22.

High Lattice Towers in the UK are normally finished by a cylindrical cardioid antenna 200 – 450 mm in diameter, as depicted in Figure 2-23. In the event of clean wind flow, the VS induced from these antennas can excite second and third modes of the whole structure, leading to the previously mentioned “lock-in” effect which might damage the structure and inconvenience nearby neighbourhoods due to movements or cracking sounds. In the last 2 years, some mechanical dampers (DVA-systems, in Figure 2-23) have been a solution to avoid this effect. More than 2 years ago, TMDs based on chain movements sufficiently reduced the response.

Figure 2-22. Damper installation in Brougher Mountain Lattice Tower (COWI). Right. Model of a chain damper [18].

In the future, the equipment required for 5G and further technologies will challenge current designs as they will be more dynamically wind-sensitive. The need of dampers will be essential to solve dynamic issues and develop solutions to keep the integrity of communications structures. Nowadays, there are no available examples and studies of the performance of these types of dampers in communications structures. The research provides an exhaustive summary of the results from exceptional projects and some other interesting projects and recommendations to improve current designs related to the performance of dampers in communications structures.

2.4 Summary

Different approaches exist in the literature to represent contributions of damping in communication structures under wind loading. These methods are highly important to define dynamic augmentation factors within quasi static approaches to analyse structures under buffeting. Damping also takes large importance in assessing structural response under aeroelastic events, the propensity of vortex shedding, and the definition of amplitude responses that can occur under lock-in effects, or the occurrence of galloping events in stays in the presence of low values of structural damping.

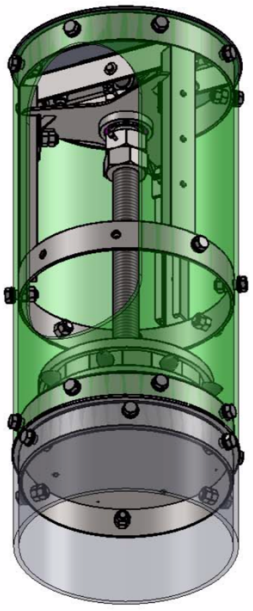

Figure 2-23. Sketch of cardioid antenna and dynamic vibration absorber (DVA) mechanical dampers. Top. Picture of Weymouth Lattice tower. Bottom. Damper installation and scheme (IBK Fibertec).

2.4.1 Structural damping

The typical values recommended by codes are not verified. No studies have validated their suitability and is disagreement among literature sources. In other fields of engineering, structural damping has shown a complex behaviour characterised by an amplitude and frequency dependency, and strong influences of foundation-soil characteristics. Owners, consultants and manufactures are requiring a more reliable definition of structural damping than the current simplistic theories.

2.4.2 Aerodynamic damping

The literature advises that aerodynamic damping in communication structures is determined by geometric characteristics of the structure, the characterization of wind flow and the drag/lift capacity of the structure. However, there are no available studies to support existing formulations. Wind-ambient monitoring and operational modal analyses are essential to characterise reliably the loading/response of communication structures and to reduce the high levels of uncertainties in estimation of aerodynamic damping, an issue that has been neglected in communication structures for decades.

Better knowledge of dynamic behaviour under wind-ambient loading would confirm/improve current formulation with expected consequences in definition of wind forcing following quasi static approaches as well as wind resistances having implications on drag factors, with the final aim of achieving more reliable structural performance prediction.

2.4.3 External additions of damping

Finally, diverse types of mass and liquid dampers have been progressively tried in communications structures for the last decades with satisfactory results. However, due to the ignorance of the subject, vibration control based on adding damping is not a common option in structural engineering. Moreover, there are no academic investigations which could lead to better designs and find further applications. The dearth of publications on these topics must be addressed.

Preface to Chapter 3

For the last decade, expert consultants and manufacturers have expressed serious concerns about the reliability of structural damping values recommended by national codes. Structural damping has been shown to be a key property with high impact on structural capacities on short telecom structures.

The following chapter has been published as “Damping estimation using free decays response in short telecom structures” which was submitted to Journal of Advances in Structural Engineering (ASE). It shows a comparative exercise of structural damping between 16 field surveys on several types of monopoles and the recommendations provided by numerous literatures. Results are consistently obtained by two different acquisition methods and analysed by 2 identification systems.

Chapter 3 Damping Estimation Using Free Decays Response in Short Telecoms Structures

3.1 Introduction

In the progressive research areas of structural dynamic engineering, such as deterioration diagnosis from fatigue, monitoring of vibration in terms of response and loading identification, and response prediction to build adequate structural assessments, numerically modelled vibration modes must agree with real behaviour of structures in terms of stiffness and damping. Due to the complexity of civil-engineering structures in terms of geometry, materials, uses, and so on, the differences between calculated predictions and measured responses may be quite different. Modal structural damping is invariably a parameter that provides more uncertainty during the calculation of structural dynamics and is normally assumed as a proportional damping value for simplicity, chosen from conservative estimations in completed investigations in the literature. Unlike natural frequencies and mode shapes, where the accuracy is high enough to be accepted, structural damping requires further research on each structure typology to provide essential knowledge for increasing the precision of predictions. A need has existed for this development in communications structures because since being pushed by telecoms engineering, more and more structural assessments refuse coming technologies due to a lack of capacity of present structures according to current knowledge, and the sub-optimal approach frequently taken to the evaluation of dynamics.

The first advances in understanding and quantifying structural damping arose from research conducted in nuclear structural buildings [41, 42]. The results of these studies were used extensively in the US and Japan for seismic analysis in the 60s and 70s. During these decades, [8] structural damping was defined as the energy dissipation during vibration due to friction, impact, scraping, and motion of trapped fluid within a joint, also establishing the related material damping due to yielding and heating of energy dissipation of materials or fluid damping to explain viscous drag dissipation

and radiation to the surrounding fluid. Further researches, [43, 44] classified structural damping by materials, stress levels, connection types or soil-foundations influence, firstly applied to communications structures in [45].

The most important mechanisms considered in structural damping are material damping and friction/coulomb damping. In actual slender structures, material damping is based on energy losses due to internal hysteresis in materials that comprise the structure [46]. On the other hand, there is evidence that a high percentage of structural damping is caused by connection friction (Coulomb friction) of the structural response. These friction forces occur when relative motion occurs between adjacent members. In communication towers and masts, these members include the joints between leg bracings and horizontal members of lattice towers and the joints between the foundation and superstructure or between steelwork installed to hold equipment. Those forces are independent of the amplitude, frequency, and velocity of tower motion and constantly oppose the normal motion of the structure. Welded connections tend to reduce the contribution of interfacial damping compared to bolted connections.

A more feasible engineering concept considers structural damping as the energy dissipated calm air without fluid aerodynamic, external passive, or active damping. Since this definition, [46] focused the issue in telecoms structures and claimed that structural damping depends mainly on construction methodologies and is highly independent of frequency and amplitude over the decay time course, essentially relying on the material component to explain the differences between diverse results with foundations which were considered to contribute considerably to overall structural damping.

Later, during the building of the standards and resulting from the high discrepancy in the existing literature, a unique value of structural damping related to conservative estimations of the theretofore analysed results was suggested. In those terms, [24], [31] advise logarithmic decrement values of steel and the nature of structural connections between δ_{St} = 0.015 – 0.06 with the allowance of an augmentation factor dependant on the soil-foundation softness of up to three times the base value. Other standards, such as Eurocode [26], set the total structural damping at δ_{St} = 0.012, dependent on structure type defined by materials, connections and functions but not taking into account the contribution from soil stiffness. On the other hand, in ESDU

[73] higher values of between ζ_{st} = 0.4 – 1 % may be considered. Such values showed high discrepancies, which confirms the need for new agreements based on modern acquisition possibilities, new identification methods and more computing techniques.

As a consequence, an updated theoretical prediction of the response may result in more reliable dynamic models and structural assessments. In such predictions, damping is highly relevant for the definition of the integrity of the structure. It has been demonstrated to be a key factor in the determination of possible aeroelastic effects, such as vortex shedding in across-wind vibration and helps to reduce high responses in resonance frequencies under buffeting along-wind excitation, providing more 'structural capacity'.

The difference between the current state of the structure and the best-optimized design is called structural capacity. An increase in this capacity is used by owners to potentially increase the amount of equipment supported by each structure. Unlike other civil engineering fields, the optimization of the structural design of towers and masts is a goal closely tied to business as well as to requisite safety margins. An increase in total damping, from either a better understanding of the topic or strengthening based on the provision of supplementary damping, can offer a consequent increase in financial profit.

For that reason, both owners and consultants require improved trustworthiness and coherent damping approaches to correctly represent dynamics in their assessments. This chapter provides damping evaluation using full-scale data on short telecom structures in the UK. Structural damping is calculated from free-decaying responses under calm weather conditions. External human excitation using ropes through pull and release is able to obtain different amplitudes of the response without affecting the free-decaying performance. Two acquisition methods, synchronized accelerometers and visual vibration capture systems, were used to extract suitable response data to be analysed by two methods of parameter identification: typical free-decaying curve-fitting (CF) in the time domain applied to re-orientated data on main modal coordinates, and the eigensystem realization algorithm (ERA) using cross-covariance functions generated from the same free-decaying response.

Reliable data for 16 telecoms structures (including two short lattice towers) covering different manufacturers, designs, geometries, foundations, and lumped masses have

been compiled in a database to describe damping-ratio characteristics of short telecoms structures. A summary of such data can build an idea of damping behaviour to increase current knowledge and compare it with current recommendations that appear in the literature.

3.2 Characteristic Response of Short Telecoms Structures

With the purpose of supporting the necessary antennae for different telecoms technologies, such as broadcasting, radio and, in particular, mobile telephones, telecoms structures are characterised as highly wind-sensitive and flexible due to a high degree of slenderness, with natural frequencies often below 2 Hz. This chapter focuses on short structures of below 40 m, mainly designed to cover nearest fields for a variety of mobile customers.

The two most common specific types of the aforementioned structure are shown in Figure 3-1: (1) Monopoles, which are vertical steel cylinders used to hold equipment at the top of the element but rarely along the length of the structure—monopoles have a height range of between 10 and 35 m and are typically around 15 – 20 m tall; and (2) Short steel lattice towers (below 40 m), which look like a smaller version of the tall lattice towers used in broadcasting or the pylons used by the National Grid to transport electric power. Such towers have varied typologies, being triangular or square and tapered or straight, and can be used for different technologies and customers at several levels.

The above structures, with a design life of 25 years, began to be placed at the end of the 1990s, comprising categories of steel between S275J0 and S275JR, with foundations based on concrete blocks. On the one hand, in terms of connections, monopoles tend to have linear welding along their tubular or polygonal sections and a slip-sleeve or flanged joint between tapered shafts. At the base, holding bolts attach the structure to the foundations through a flat flange welded to the first shaft panel. On the other hand, lattice towers use bolted connections between leg elements and foundations and either bolted or welded connections between corresponding bracing or horizontal elements.

Figure 3-1 Left. Example of a monopole. Right. Example of a short lattice tower.

In terms of dynamics, standards agree a response described by a main mode with a typical cantilever bending shape defined by the industrialised geometry which is highly symmetric about different axes. However, all the necessary attachments, such as ancillaries, antennae and steelworks, and linear loadings, such as necessary cabling or ladders, break the symmetry with two primary directions of stiffness, which define the mentioned modes as the singular value decomposition diagram shows in Figure 3-2. This figure identifies modes as the dominant singular value in typical frequency range (for monopoles) between 1.2 and 2 Hz.

Under ambient wind loading, such as during service life, or free-decay vibration after forced excitation, such as the field tests proposed in this chapter, these closely related modes tend to work in a coupled manner, defining an elliptical shape. Such a vibration pattern, in the absence of loading, appears to move from one mode direction apparently due to the asymmetry.

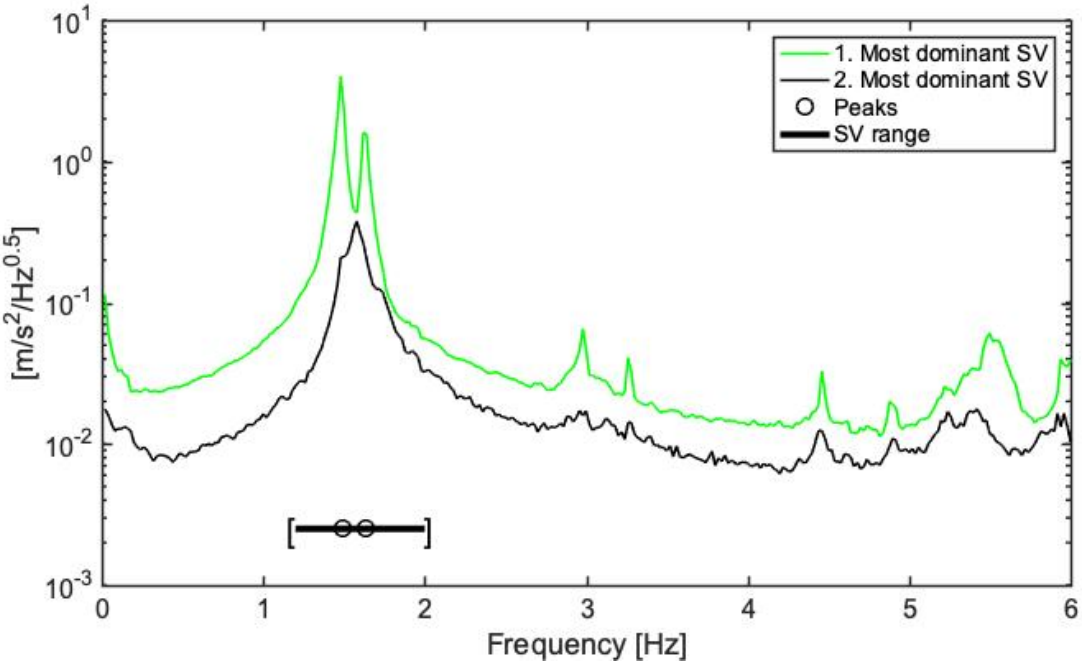

Figure 3-2 Singular value (SV) decomposition of average ambient response data spectra, with corresponding mode frequencies identified by experimental modal analysis (EMA).

Figure 3-3 plots the response of a typical monopole (as in Figure 3-2) during a free-decaying response. The response is captured by two accelerometers positioned orthogonally to each other at the top of the structure in along symmetry axes defined by the location of the external ladder and cabling, and expected to align with vibration modes. The (a) figure shows the free-decay response after an external impulsive force in a particular direction intended to excite both modes, for research purposes. This way, first and second channels can identify the two modes, as shown in the power spectral density in the (b) figure, which also captured second and third pairs of modes. Finally, the main (c) figure shows, in plan view, how both modes combine to define a free-decay response which oscillates in different directions.

This behaviour makes separation of modal response, needed to identify proper modal parameters, via simple free decay estimation more difficult. Given this, to obtain the perfect modal damping the responses must be in agreement in any given modal direction to maximally reduce the amount of energy absorbed by the other mode.

Under present ambient loading conditions, such a state is not achievable, as the turbulent component of buffeting will always include high components of cross-wind response belonging to the undesired mode, unless some aeroelastic event, such as

vortex shedding, induces the resonance and 'lock-in' of the mode—an event whose occurrence is unlikely for the aforementioned main pair of modes.

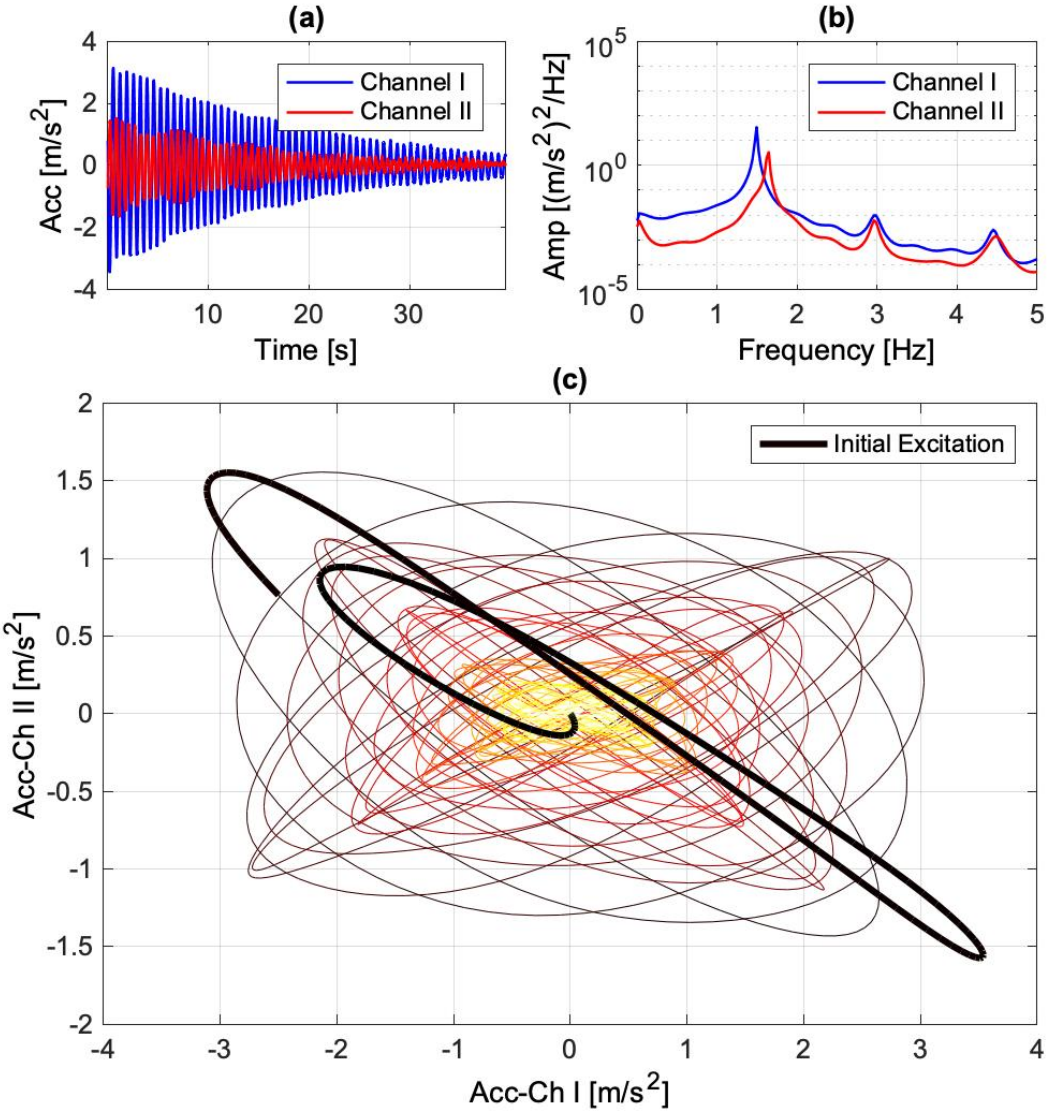

Figure 3-3 Typical free decaying response in monopoles. (a) Free-decaying time line. (b) Power Spectrum Density of free decaying response. (c) Horizontal vibration of monopole under free-decay vibration.

Such bi-modal behaviour is not covered by any of the current standards, which mainly focus on buffeting along-wind excitation in a single mode. To obtain useful results with which to draw comparisons, there is a need for a specific methodology to apply during field data acquisition, subsequent analysis of the responses, and damping estimation.

3.3 Critical Damping Ratio Identification

The exercise uses the excitation called the ‘pull and release’ method. This is based on the application of sharp tugs on a rope attached to a point close to the top of the structure timed to build up a strong (resonant) response before allowing the structure’s vibration to decay freely. This has been shown to be a highly effective method to obtain a desired free-decaying vibration during operational modal analysis (OMA) surveys [74, 75], in which the chances of installing a shaker are very limited due to logistical challenges. Such free vibration tests performed in other civil engineering structures for the identification of modal damping ratios [76] may arise from the application of periodic sinusoidal loads with an excitation frequency coincident with either the structure’s natural frequencies, an impulse force, or imposed displacement. Both excitations are applicable to those structures to obtain responses at different heights. Other advantages of this methodology include the following:

- The resonant response level achieved is similar to the level of response for serviceability design service life estimation under service wind loading.
- The range of main frequencies of the structures of 0.5 – 2.5 Hz is readily achievable by timed rope tugs. The ranges of frequencies encountered are easily achievable by human excitation.
- The influence of the rope after the application of the pull is negligible.

This excitation method encounters some issues in dealing with taller structures, which, despite being more slender than short ones, require stronger forces to be excited due to the amount of distributed mass to mobilise with the pulls, in turn requiring more people with the corresponding synchronization to achieve the desired responses shown in Figure 3-4.

In the absence of wind, obtained decays are suitable to assess structural damping. To agree perfect conditions, only calm weather days were specifically chosen to carry out modal surveys. However, some minor aerodynamic influences might arise from sporadic low gusts or turbulent present as a result of the structure’s movement.

Figure 3-4 Picture of pull application on lattice towers during modal test.

In this work, two methods were used for damping ratio extraction from the free-decay vibration: the curve-fitting (CF) and the eigen realization algorithm (ERA) methods. The principle of the CF method [77] is that the envelope of free-decay vibration curve is an exponential function with a damping ratio-related index. Once the envelope of the decay curve is obtained, the damping ratio can be obtained with CF. This method requires a clean and perfect response to have a good fit along the decay, using the same number of peaks as an optimization method. This would mean a decrease in the reliability of the fitting at key high amplitudes, presumably due to the existence of non-linearity caused by different sources. The principle of the ERA method [78, 79] is to use the decay measurement to estimate the system matrix, then calculate the damping ratio with eigendecomposition of the system matrix. The ERA methods are often used with stabilization diagrams. A stabilization diagram shows the results of different assumed system orders. Only the results which can compose a straight line are reliable.

This procedure was implemented on 16 different structures with different geometry and loading. The following section sets out an example of the acquisition and analysis of a Portasilo monopole.

3.4 Field Test of Kinning Monopole

3.4.1 Introduction of Monopole Structural Details

To illustrate the procedure and results followed on each field survey, this modal analysis was carried out on a Portasilo monopole, one of the most common telecoms structures existing in the UK portfolio. The structure is a monopole comprising S275J0 steel for the main core and plates of 25 mm thick S355J2. There are two sections: a tubular tapered panel between ground level and 14.5 m and a triangular steelwork headframe suitable for the accommodation of mobile antennas. Also, there is an external spine ladder with a Latchways fall arrest system. For loading, three antenna panels are installed in the upper section, with a small plate antenna at 14.3 m and all necessary cables run internally. This structure is joined to the foundation through a flange plate and 12 grade 8.8 M24 bolts, without grouting. Some other details are shown in Table 3-1.

These monopoles are characterized as very flexible structures, with relatively low stiffness and high masses which help to obtain high responses under ambient wind loading and which are also easily excited by sharp human tugs. The high dynamics implications penalise these structures heavily, with one of the highest dynamic amplification factors [31] during static structural assessments, in turn ruling out any spare capacity for additional equipment. In addition, major concerns have been identified at the base level due to fatigue induced during the short service life (less than 10 years from installation).

The new loading requirements with the upcoming wave of 5G technology will test the integrity of thousands of existing structures which are currently close to total capacity. Expensive replacements or strengthening works will be required under current design rules.

In particular, this site (Figure 3-5 and Table 3-1) is situated between Exeter and Barnstaple in Devon, United Kingdom, with a relatively high basic wind speed.

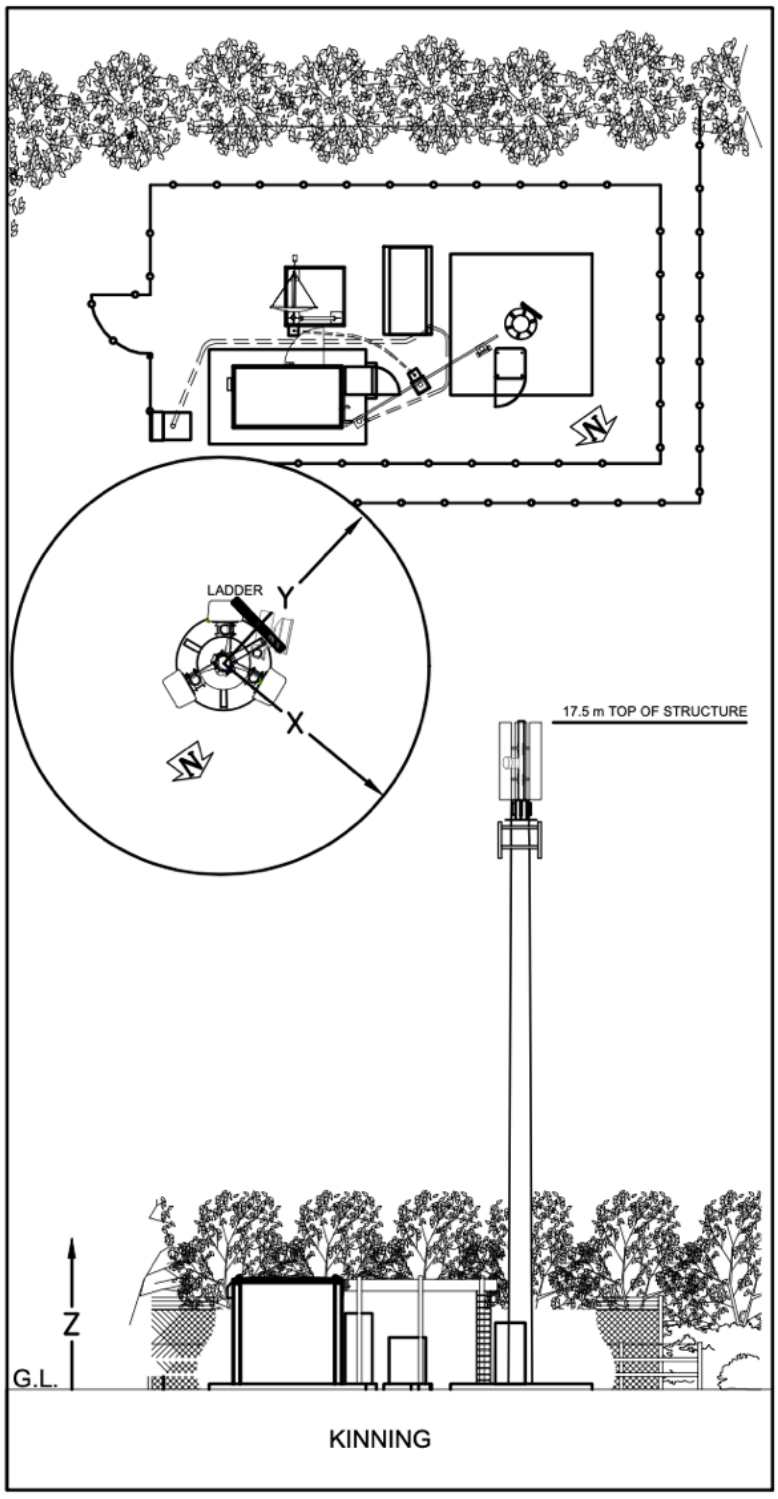

Figure 3-5 Elevation and plan view of surveyed site: Kinning monopole.

Table 3-1 Selected site details.

Site Name	Structure Type	Height	Foundations	Top frame	Cable Location
Kinning	Portasilo	17.5 m	Pad: 3.6 x 3.6 x 0.85 m	Mounting pole	External

3.4.2 Experimental Setup and Response Data

Previous exercises revealed key information that helped during the OMA at Kinning. The structure responds at two main frequencies: f_1 = 1.485 Hz and f_2 = 1.635 Hz. The latter tends to move in the direction of the ladder and the external cabling, having the lower mode orthogonally. With the purpose of exciting both modes as well as possible, two sets of ropes were set up in the aforementioned directions. Furthermore, the orientations of the Opal™ and Video Gauge™ systems were set specifically to capture both vibration excitations during an initial climbing of the structure.

3.4.2.1 APDM OPALs™ system

OPALs™ are wireless inertial measurement units including triaxial accelerometers with a noise floor of ~120 μg/Hz$^{0.5}$. Four OPALs™ (i.e. four triaxial accelerometers) were placed at different level locations as shown in Figure 3-6. Working at a sampling frequency of 128 Hz, these provide the best approach for measuring the mode shape of the structure. These devices are wireless sensors that synchronise over short distances typical for mast measurements, and by keeping one OPAL™ at the top of the monopole and locating the remaining three to other heights on the mast it is possible to identify the vibration-mode shapes very efficiently. Alternatively, the set of four can be left in place to track variation of mode shapes with vibration decay.

3.4.2.2 Video Gauge™ System

The Video Gauge™ system, which is developed by iMETRUM was also used for data acquisition. The Video Gauge™ system uses high-speed and high-resolution cameras to obtain videos of the measured structure, before using a sub-pixel template match algorithm to predict the movement of a certain target. The highest resolution can be 1/500 pixel and the real-world resolution depends on the scale of the targets.

During the measurement, shown in Figure 3-7, two cameras were set up on each main vibration direction of the monopole. To improve the accuracy and robustness of the Video Gauge™ system, artificial bull's eye targets were installed directly below the antenna, which is close to the OPAL™ sensor. The sizes of the bull's eye targets were taken as references to obtain the target movement in real-world coordinates. Only measurements taken during each pull were recorded since the video files are relatively large.

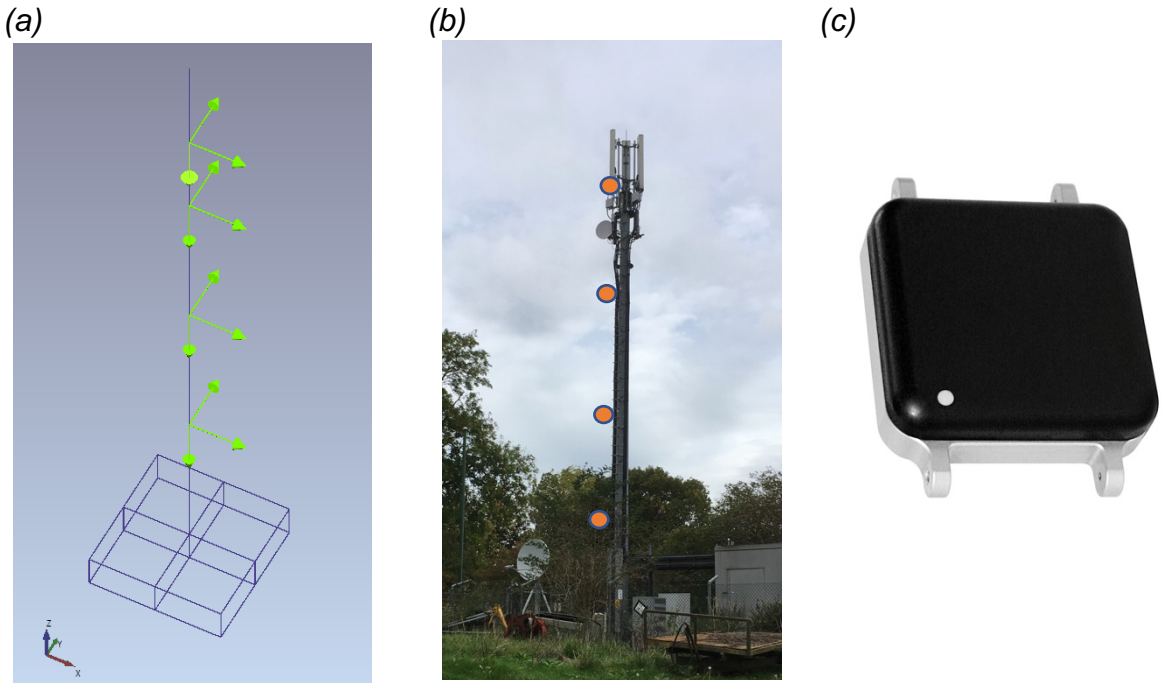

Figure 3-6 (a) Measurements using OPAL™ system. (b) OPAL™ installed in monopole. (c) OPAL™ sensor.

Figure 3-7 Camera setup in Kinning and Bull's-eye Target.

3.4.3 Results of Modal Survey in Kinning

Each response was initially compared across acquisition methods through the integration of the accelerations and the composition of both camera recording channels. The displacements obtained from the two systems were consistent without differences. For the purpose of the analysis, accelerations were taken as the main response unit and a higher percentage of the surveys were carried out with the APDM Opal TM system.

At Kinning, the OMA survey findings can be divided into three types of vibration: free-decay vibration (at 1.49 Hz excitation in the x direction), free-decay vibration (at 1.63 Hz excitation in the y direction) and coupled vibration between *x* and *y*. These vibration data were processed and analysed in the following sections.

Even with the correct direction of pull, data collected from both acquisition systems required slight rotation to find the best decay for each decay analysed. This rotation does not distort results with either method. Under CF, the correlated curve minimises the error between typical viscous-damping decay and processed data to obtain the best fit. The ERA method is used to process the decay vibration data. That method can be combined with stabilization diagrams to show which identified modes are stable. In this work, the PSDs are also plotted with stabilization diagrams as references.

- First mode. Decay vibration (at 1.49 Hz excitation in the x direction)

  The rotated decay vibration, shown in the first plot of Figure 3-8, suggests a suitable decay under the first mode and minimal influence of the secondary mode which oscillates slightly along the decay. During the vibration, energy can be transferred from one direction to the other, and the vibration presents a beat characteristic. Nonetheless, the response obtained in the main excitation mode is well accepted for the CF method, as shown in the second plot of Figure 3-8The discrepancies between real decaying and CF would suggest a nonlinear amplitude-dependence behaviour which should be studied with other methodologies.

  The third plot in Figure 3-8 shows the corresponding stabilization diagrams of rotated data after the application of ERA, which finds both modes. For damping analysis purposes, results in the second mode were neglected as they were meaningless. The similar results of the first six decays shown in Table 3-2 provide a consistent main natural frequency at 1.48 Hz for both methods, and critical damping ratios between 0.47 – 0.75 %, where CF values tend to be slightly lower than ERA.

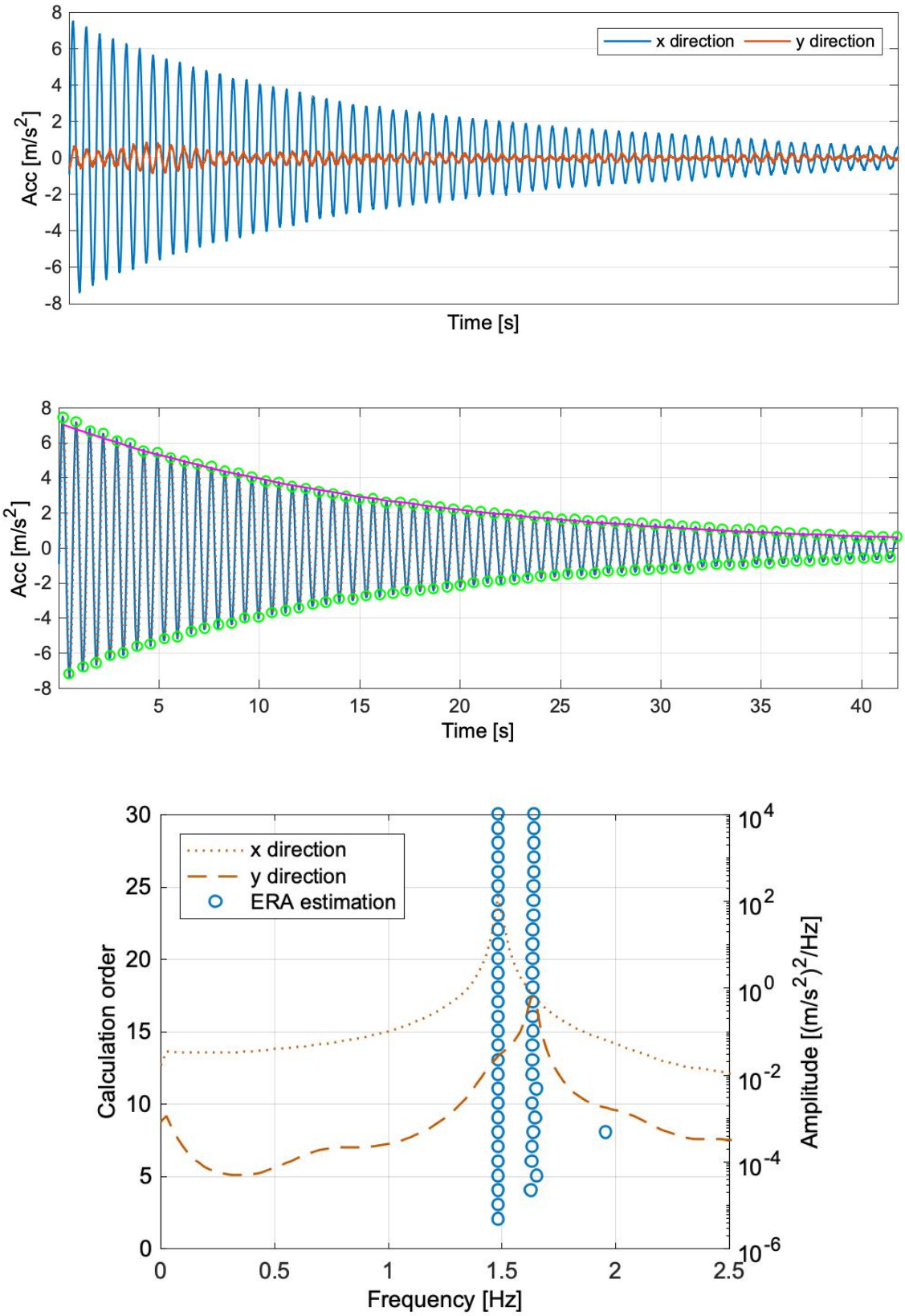

Figure 3-8 Uncoupled decay vibration and coupled decay vibration (at 1.49 Hz excitation in the x direction).

- Second mode. Decay vibration (at 1.63 Hz excitation in the *y* direction)

  Similar to the previous decay, the excitation of the second mode was capable of obtaining clear responses thorough a degree of rotation to decrease the impact of the first mode.

  In these kinds of monopoles, the higher mode is normally related to stiffening elements installed in the structure which break the original symmetry. In Portasilo monopoles, external linear loading, such as the existence of ladders or external cable trays align to the orientation of the mode shape to excite under pulling.

  The third panel in Figure 3-9 shows the corresponding stabilization diagrams of rotated data after the application of ERA, which finds both modes as previously. For damping analysis purposes, the results in the first mode were neglected as they were of inferior quality for the estimation. The results of five similar decays shown in Table 3-2 provide a consistent main natural frequency at 1.63 Hz and critical damping ratios between 0.5 – 0.85 %.

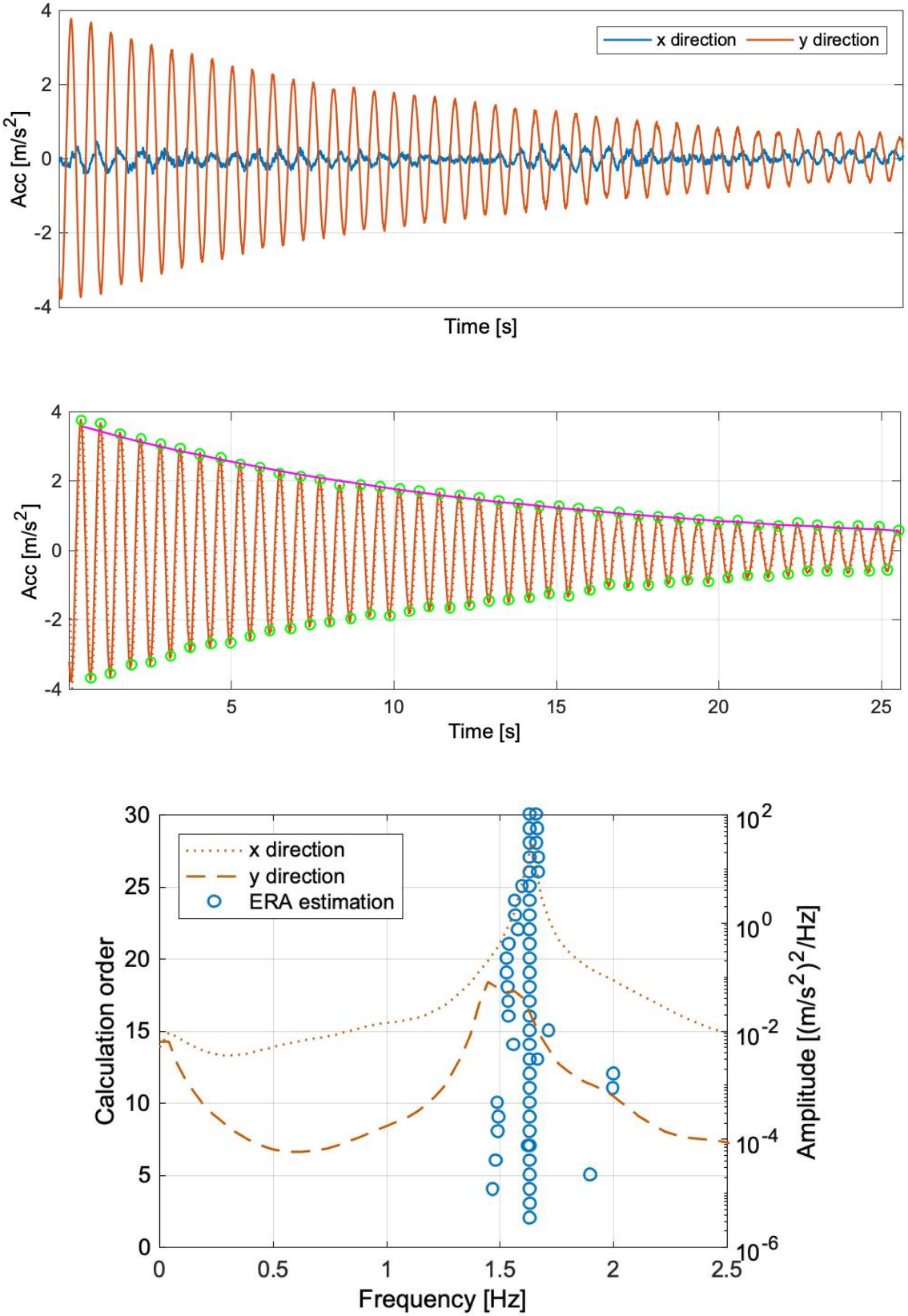

Figure 3-9 Uncoupled decay vibration and coupled decay vibration (at 1.63 Hz excitation in the y direction).

- Coupled modes. Decay vibration.

  Finally, to verify the behaviour of the structure under coupled motion, a few pulls were carried out in the non-main modal directions. This way there is a high influence of both modes along the decay—the rotation of the response does not improve the shape of the decay and consequently both modes form beat features which deteriorate the response to be analysed under CF, as shown in Figure 3-10. The second mode response was not taken for CF analysis as the optimization did not converge.

  The third plot in Figure 3-10 shows the corresponding stabilization diagrams of non-rotated data after the application of ERA, which finds both modes.

  The result of the last entry in Table 3-2 provides sensible values in terms of natural frequencies at 1.4883 – 1.631 Hz for both methods and critical damping ratios validated as 0.61 % on the first mode and 0.45 % on the second mode, which do not match with values obtained previously.

As shown, the coupled scenarios tend to have lower values of modal critical damping than the individual cases due to cleaner decay responses, higher amplitude responses thanks to achieving a higher resonance level, or the transfer of energy dissipation between modes. Responses under the main modes are then a target to be obtained during the OMA survey. Since the OPAL sensor remained on the structure, the whole-time history was obtained as shown in Figure 3-11, where each considered decay (in red) was analysed. On the other hand, the Video Gauge™ system takes time sets for each pull that are later correlated to the APDM Opal ™ system.

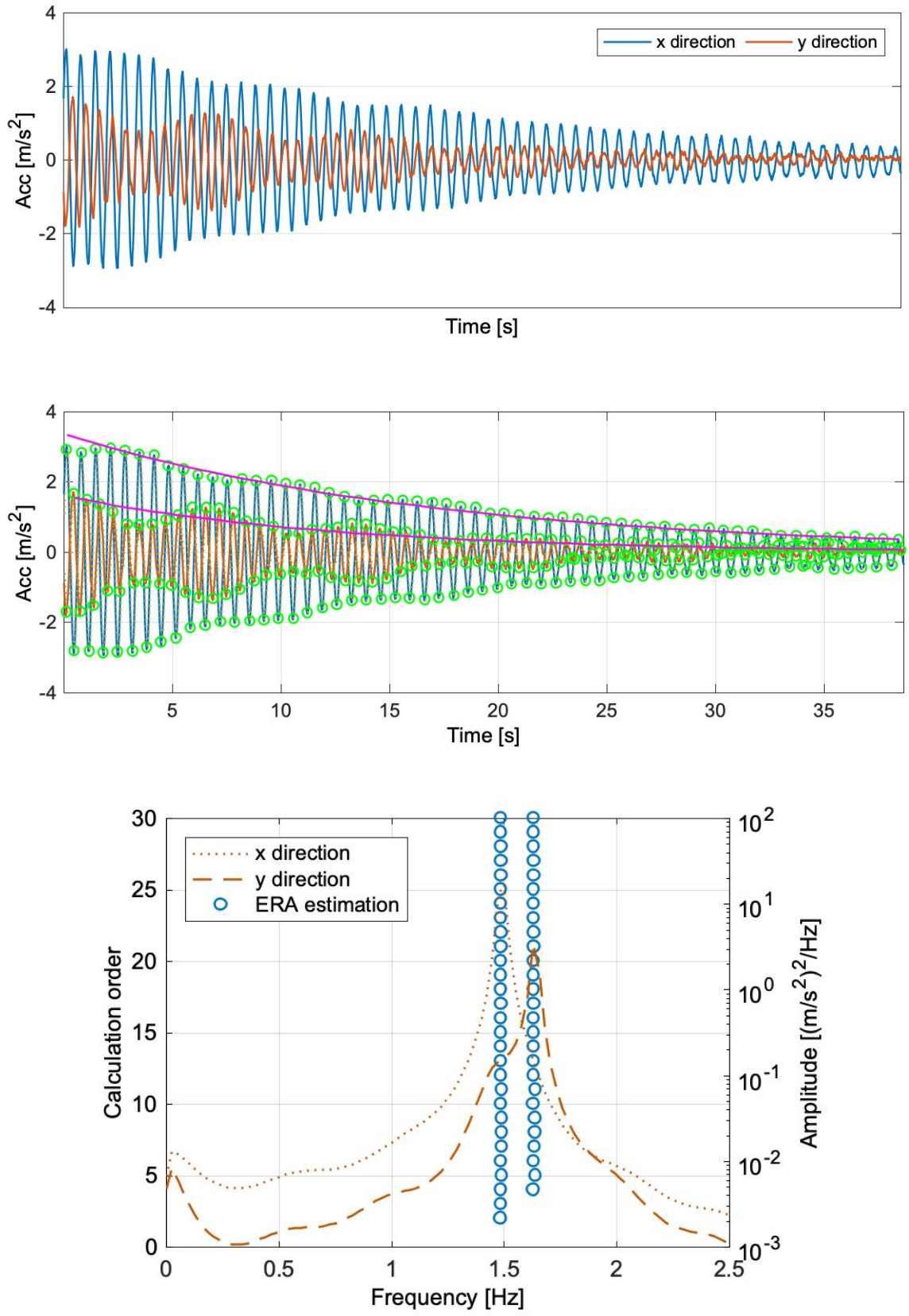

Figure 3-10 Uncoupled decay vibration and coupled decay vibration (excitation in symmetric direction).

As shown in Figure 3-11, different levels of maximum response are achieved due to different levels of resonant forcing. As the exposed methodology calculates the mean damping taken as the most optimised value found along the selected decay, as shown in Figure 3-12, no evidence of amplitude dependency was found in this case. Applying time-dependent damping identification on each decay such as via amplitude-dependency backbone curve methodology [55] would provide instantaneous damping values from which amplitude dependency might be indicated.

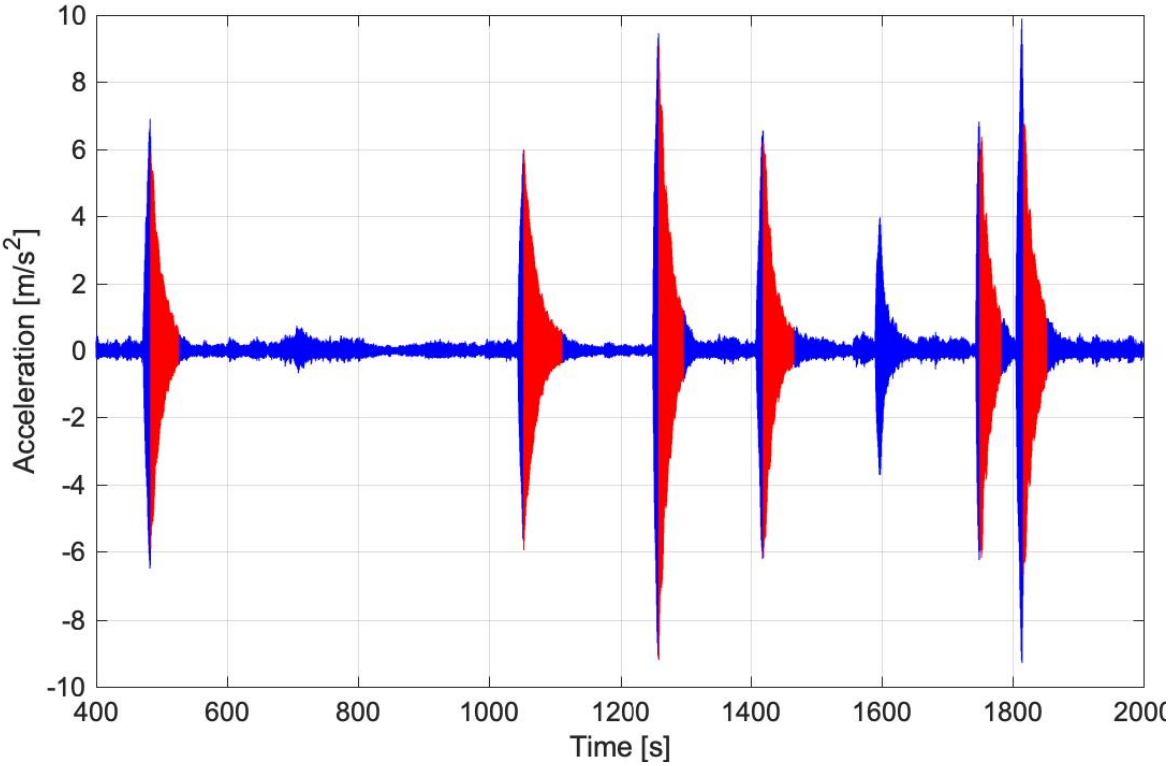

Figure 3-11 Period of time response of the Kinning Survey.

In addition to that, there is a trend among methods in which CF approaches slightly lower values than ERA. This behaviour which depends on the quality of the signal is not confirmed in other surveys. The final results in Table 3-2 suggest similar behaviour between modes with common values of critical damping in a narrow band between 0.5 – 0.8 %. The results between modes do not differ as anticipated, similar values were found. First mode mobilises less amount of structural mechanisms due to the influence of ladder or cables, and consequently, higher damping was expected for the second mode.

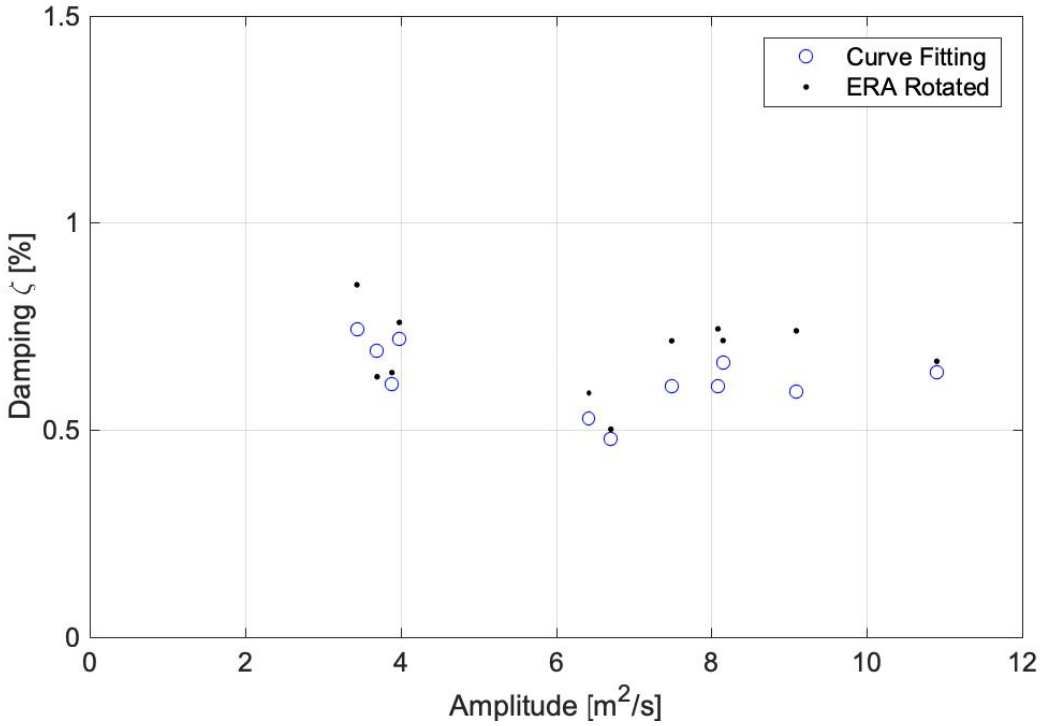

Figure 3-12 Amplitude against Damping in Kinning OMA.

Table 3-2 Results summary of each selected pull of the survey.

Pulls	Ampl. $/^{m}/_{s^2}$	CF. Main Mode during Decay.		ERA			
		f/Hz	$\zeta/\%$	$f_{mode\ 1}$ $/Hz$	$\zeta_{mode\ 1}$ $/\%$	$f_{mode\ 2}$ $/Hz$	$\zeta_{mode\ 2}$ $/\%$
1	7.495	1.495	0.604	1.487	0.714	-	-
2	6.713	1.490	0.478	1.484	0.500	-	-
3	10.90	1.485	0.639	1.480	0.665	-	-
4	8.090	1.489	0.603	1.481	0.743	-	-
5	8.155	1.486	0.661	1.481	0.715	-	-
6	9.098	1.484	0.591	1.480	0.739	-	-
7	3.695	1.634	0.691	-	-	1.631	0.627
8	3.981	1.638	0.718	-	-	1.635	0.759
9	6.425	1.630	0.525	-	-	1.624	0.588
10	3.885	1.630	0.611	-	-	1.629	0.637
11	3.435	1.633	0.742	-	-	1.629	0.850
12	3.133	1.488	0.607	1.486	0.610	1.631	0.452

3.5 Application to Population of Short Communication Structures

The previous procedure was applied to a range of structures between 15 – 20 m in height, although some examples of higher structures are also listed in Table 3-3. Tall structures, generally less stiff than short ones, also tend to have more distributed mass which requires stronger tugs at the main frequencies to achieve considerable responses capable of building good decays.

Table 3-3 summarises the ERA results obtained for each set-up as mean values and the corresponding deviation for natural frequency and modal critical damping applied for both main modes. This way, each site can easily be classified and compared with each other and with respect to recommendations. Figure 3-13 plots results from Table 3-3 enclosing each modal result in a rectangular block using mean values as centre point and deviation as sides. That way, the figure shows how both parameters behaves, natural frequency in x axis and modal critical structural damping in y axis. On some surveys, there was no possibility to obtain clear decays on both modes, and consequently, CF was not applied in such cases. As expected, a similar response based on two main close-related cantilevered modes was identified in all cases with deviations less than 1 % in almost all of them. The existing methodologies approximate this mechanical parameter with a high degree of certainty. In addition, at least one mode for all structures was verified in the wind-sensitive area below 2 Hz, which confirms the pole's status as a dynamically active structure.

As shown in previous Table 3-2, damping estimation is more challenging as the deviation between data from the same site is much higher than between frequencies, with an error margin of 20 % of the mean value. However, there is a clear band of damping values between 0.3 – 1.2 %, which can be assumed to be standardised.

Between the estimation methodologies, ERA and CF, the tendency observed in the Kinning results Table 3-2 is not followed for the full population of surveys. The quality of the response decay is the key factor defining the CF or the cross-correlation function used in ERA, and consequent damping results.

In terms of typology, the exercise covered a few typical short lattice towers, called Euromasts, which have been used extensively in the UK for the last decade. Despite being wider and heavier structures with more connections between leg, bracing and

horizontal members, they have similar dynamic parameters to monopoles. The main frequencies appear in the same range of between 1 – 2 Hz, with damping values of 0.58 – 0.7 %. Several Portasilo structures, similar to Kinning, were used to verify the diversity of the results using several loading, age and boundary-soils conditions. They showed high discrepancies between old installations which exhibited lower frequency levels and very low values of damping (0.2 %) and new versions such as Kinning where levels above 0.5 % are generally obtained. These variations may show some structural improvement in terms of connections or section thickness or proof of deterioration over time, and comparison with results from other structures of the same type could be helpful for structural diagnosis with further research.

On the one hand, all of the above results appeared to be in the ranges provided by ESDU [73], which are based on an extensive literature review of similar steel structures, such as chimneys or tall lattice towers. However, some values exceed this range on both sides: conservatively and non-conservatively.

On the other hand, the recommended value of 0.235 % suggested by Eurocode and British Standards is broadly below the trend obtained during the analysis of damping results, which found values between two to five times higher, including those for the lattice towers. Only the aforementioned old Portasilo and case 8, a Calzavaras-type structure, would be placed close to the design code value. These results support the design code's conservative safety first approach which should ensure that no failures occur but also suggest that there may be benefits for owners and their agents to use more structure-specific values in their design assessments. The impending wave of 5G equipment roll-outs appears to offer an excellent opportunity to assess new and old structures using more representative dynamic terms.

The old considerations provided by the IASS, particularly for bolted steelwork rather than welded, are also within the range of results experienced in this study.

The variability of the results obtained from the full scale tests endorses the need for field test surveys to find essential dynamic parameters, in turn enhancing structural design assessment by decreasing the level of uncertainty. Over time, and by generating a database of values, this could be used to support a change in the current standards or at least allow them to offer more representative guidance without compromising safety.

Table 3-3 Summary of Pull & Release surveys. Results on ERA method including limit deflections by ULS and during forced excitation.

Sites	Structure Type	Age [years]	50 years ULS Deflects [m] / Forced Deflects [m]	ERA							
				μ(f1) [Hz]	σ(f1) [Hz]	μ(ζ1) [%]	σ(ζ1) [%]	μ(f2) [Hz]	σ(f2) [Hz]	μ(ζ2) [%]	σ(ζ2) [%]
Case 1	Monopole. Portasilo Supersline. 14.5m.	18	0.152 / 0.06	1.431	0.004	0.380	0.109	1.589	0.009	0.538	0.279
Case 2	Monopole. Portasilo Supersline. 14.5m.	20	0.153 / 0.05	1.653	0.013	1.152	0.173	1.824	0.007	1.039	0.078
Case 3	Monopole. Portasilo Supersline. 14.5m.	22	0.151 / 0.075	1.660	0.009	0.843	0.051	1.830	0.018	0.574	0.116
Case 4	Monopole. Francis&Lewis. Unknown. 30m	24	0.170 / 0.038	0.990	0.010	1.435	0.284	1.027	0.002	0.913	0.067
Case 5	Monopole. Portasilo Supersline. 14.5m.	18	0.135 / 0.091	1.480	0.028	0.928	0.084	1.632	-	0.531	-
Case 6	Monopole. Francis&Lewis. Unknown. 17m	20	0.160 / 0.120	1.431	-	1.663	-	1.569	0.027	0.373	0.109
Case 7	Monopole. Portasilo Supersline. 14.5m.	18	0.143 / 0.120	1.499	0.011	0.296	0.081	1.641	0.006	0.300	0.111
Case 8	Monopole. Calzavara. 18m.	26	0.08 / 0.045	1.753	0.009	0.465	0.255	1.817	0.005	0.322	0.128
Case 9	Monopole. Francis&Lewis. DM1A.15.5m.	2	Unknown / 0.065	1.979	0.007	1.189	0.326	2.115	0.011	1.180	0.117
Case 10	Monopole. Portasilo Supersline. 14.5m.	19	0.152 / 0.092	1.572	-	1.944	-	1.708	0.003	1.005	0.109
Case 11	Monopole. Portasilo Supersline. 14.5m.	17	0.203 / 0.105	1.264	0.013	1.021	0.266	1.391	0.016	1.002	0.200
Case 12	Monopole. Swann. D1MA. 22.5m	10	0.132 / 0.065	1.218	0.004	1.050	0.215	1.287	0.010	1.146	0.245
Case 13	Monopole. Calzavara. 18m.	23	0.08 / 0.025	1.775	-	1.748	-	1.835	-	0.819	-
Case 14	Monopole. Portasilo Supersline. 14.5m.	19	0.135 / 0.125	1.480	0.010	0.743	0.128	1.627	0.009	0.781	0.361
Case 15	Lattice Tower. Euromast. Sections:EDC. 22.5m.	24	0.362 / 0.155	1.217	0.013	0.985	0.385	1.234	0.005	0.884	0.372
Case 16	Lattice Tower. Euromast. Sections:EDC. 22.5m. Strengthened.	24	0.158 / 0.070	1.587	0.007	0.721	0.229	1.611	0.007	0.652	0.214

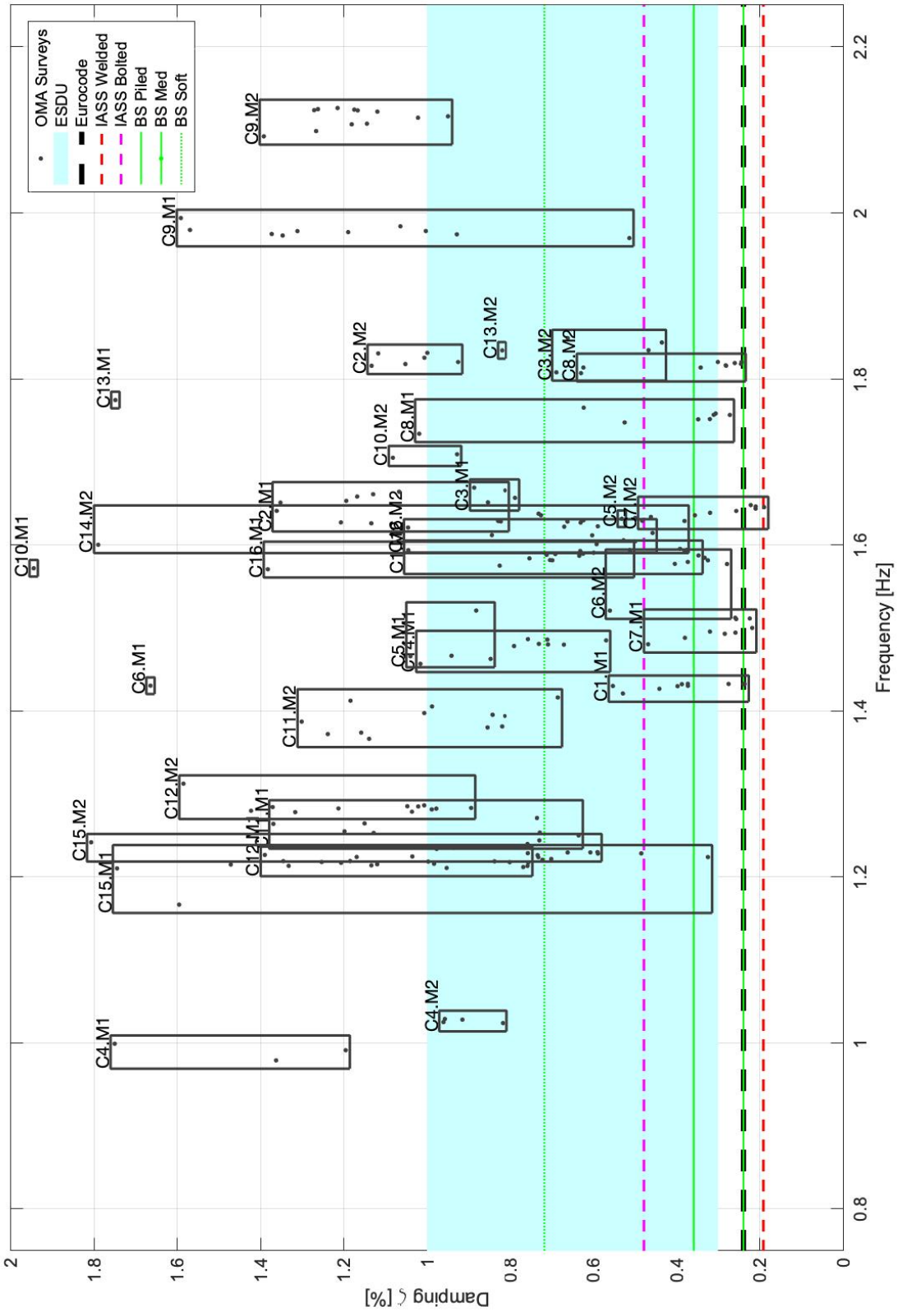

Figure 3-13 Comparison of damping and natural frequency values obtained from Pull & Release surveys (Table 3-3). Each box includes the ERA results of each found mode during 16 OMA surveys. Recommendations given by existing codes are plotted as horizontal lines.

3.6 Conclusions

Short communication structures demand better knowledge of dynamics to properly calculate their structural integrity under dynamic loading, such as seismic or wind loading. By using a simple field test based on human excitation with response acquisition systems to obtain free-decaying responses of two main modes, the key modal parameters (natural frequency and structural damping) can be found, providing essential information for structural engineers.

Curve fitting and eigensystem realization algorithm estimation methods are proven to work satisfactorily for the analysis of the decays. Between methods, small discrepancies were found that explain the differences in quality in the free-decay response. To obtain the best performance of the decay for each mode, it is necessary that each excitation focus on the desired mode. Here, previous knowledge of each structure can be helpful.

After implementing the methodology in 16 cases of field tests, of which 14 were monopoles and 2 were lattice towers, the calculated structural damping values covered a wide range of between 0.3 – 1.2 % despite the similarity of the structures and their similar response frequencies between 1 – 2 Hz. Each survey exhibited a low degree of deviation in frequency terms and a medium level in structural damping terms. The discrepancies found during the estimation of critical damping rely on the initial amplitude of the free decay and the excited mode as the weather conditions remained calm during the acquisition of the data.

The results confirm the concerns of the consultancy sector about the conservative values of damping recommended by the main codes. All the results of the chapter showed superior values to the 0.25 % given by Eurocode and British Standards. The ESDU band is considered an a priori good estimation. However, the best approach will always be to carry out appropriate field test which can provide more reliable results. The knowledge of essential dynamic properties in communications structures is a key parameter with significant cost implications for owners.

Preface to Chapter 4

The previous chapter showed how typical methods based on providing unique values of modal critical damping can vary significantly for the same structure under different levels of amplitude response during field tests. Each measurement of free decay response can provide valuable information of the amplitude dependency of damping which provide essential information to identify structural mechanisms involved in the energy dissipation. The following chapter analyses the existing of this amplitude dependency.

The chapter is a journal paper entitled “Using Resonance Decay Responses to Model the Nonlinear Behaviour of Telecom Monopoles via Backbone Curves” which was presented and submitted to SEM’s IMAC conference in Houston in February 2020. It demonstrates the existence of nonlinearity against amplitude in terms of stiffness and structural damping. Also, it validates the backbone curves method applied on free decaying response on communication structures.

Chapter 4 Using Resonance Decay Responses to Model the Nonlinear Behaviour of Telecoms Monopoles via Backbone Curves

4.1 Introduction

During the last two decades development of mobile/telecoms technologies has meant an increased number of antennas to allow final consumers to be always connected. In addition, the forthcoming implementation of 5G networks will require the use of bigger and heavier antenna-equipment which would compromise the structural integrity of current structures. Between all the existing types in the market, Monopoles are sensitive and vulnerable structures in this sense, since the dynamics induced by the tip-lumped mass increment, the slenderness and increasing loading due to higher wind resistances would dare the current knowledge and more exhaustive analyses of stiffness and damping in fatigue and other matters like vortex shedding will be necessary. Nonlinear behaviour has already been found in the dynamic response of several monopoles under demanding operational conditions.

Nowadays we live in a world of continuous changes, the high degree of innovation makes engineering to keep finding solutions which satisfy the society with reliability and safety. Telecoms could potentially be one of the most continuously changing branch of engineering, new developed networks influence secondary affected fields like masts and towers structural engineering. The new technology requirements oblige either an improvement on the structural designs of already placed buildings or the replacement of high percentage due to new dynamics. In some cases, this second option could put in danger the viability of customer programmes. This conference paper pretends to provide value knowledge of structural non-linear behaviour of monopoles which could help on new designing approaches, especially in terms of fatigue, and be applicable to other civil engineering fields.

Figure 4-1 Left. F&Li monopole. Right. Portasilo monopole.

Monopoles, Figure 4-1, are considered the weakest structure in this matter, the main frequencies of those structure are excited under the spectrum density of wind loading, and the low mass distribution are compatible with high wind resistances to induce high vibrations which act as principal and ultimate limit state. In addition, previous points agree perfect conditions to have resonance under human excitation.

The study will control excitation, response and external factors, avoiding ambient loading with the purpose of obtaining a perfect free response decays either with climber agitation or, better, with the application of sharp tugs on a rope attached to a point close to the top of the structure, timed to build up a strong (resonant) response before letting the structure under free vibration. Accompanying this excitation with portable acceleration acquisition on the structure, two pair of OPAL™ (APDM) in this exercise, it is relatively easy to capture the dynamic behaviour.

Any operational modal analysis (OMA) would provide key main properties important for a dynamic designing, but acquired data can give much more information around some aspects of the structure in terms of stiffness and damping, defining their behaviour related to amplitudes. Those aspects are local defects, connections, influence of soil-foundation conjunction and asymmetries between others. The method

backbone curve [55, 80] is applied to extract the energy dependency of nonlinear normal modal curves and their frequencies from decaying time series.

This chapter shows an estimation of non-linearities in stiffness and damping for different acceleration measurements carried out on a monopole with the application of backbone curve methodologies (Zero Crossing and Wavelets [81]) after a postprocess based on accelerations integration and OMA, extracting displacement decays working modal coordinates.

4.2 Field Tests & Acquisition

In this exercise, the measurements were obtained from a monopole tested in Norwich, United Kingdom. The structure is a monopole comprising S275J0 steel for main core and plates of 25 mm thick S355J2. There are two sections: a tubular tapered panel between ground level and 14.3 m and a triangular steelwork headframe suitable to accommodate mobile antennas. Also, there is an external spine ladder with latchway fall arrest system. For loading, three panels are installed at the upper part, with a small plate antenna at 14.3 m, with all necessary cables run internally. This structure is joined to the foundation thorough a flange plate and 12 Grade 8.8 M24 bolts, without grouting.

The acquisition of the data was carried out using a system of synchronized APDM OPAL™ accelerometers similar to previous Chapter 3 in Figure 3-6. Opals are wireless inertial measurement units including triaxial accelerometers with noise floor ~120 μg/Hz$^{0.5}$. Four OPALs™ (i.e. four triaxial accelerometers) were placed at different level locations as shown in Figure 3-6. Working at 128 Hz sample frequency, these provide the best approach to measure the mode shape of the structure. These devices are wireless sensors that synchronise over short distances typical for mast measurements, and by keeping one OPAL™ at the top pf the monopole and ‘roving’ the remaining three OPALs™ to other height-wise locations on the mast it is possible to identify the vibration mode shapes very efficiently. Alternatively, the set of four can be left in place to track variation of mode shapes with vibration decay. Alternatively, an optical acquisition system based on high-definition cameras focused on dashboard placed at OPALs™ level was set to verify that the displacements calculate are correct. These checks were satisfactory.

The excitation induced by each pull is appreciated on the acceleration time history, Figure 4-2, different amplitudes were achieved after single pulls applying different forces, although to acquire really high amplitudes there is need to apply several pulls at the main frequency of the system until resonance.

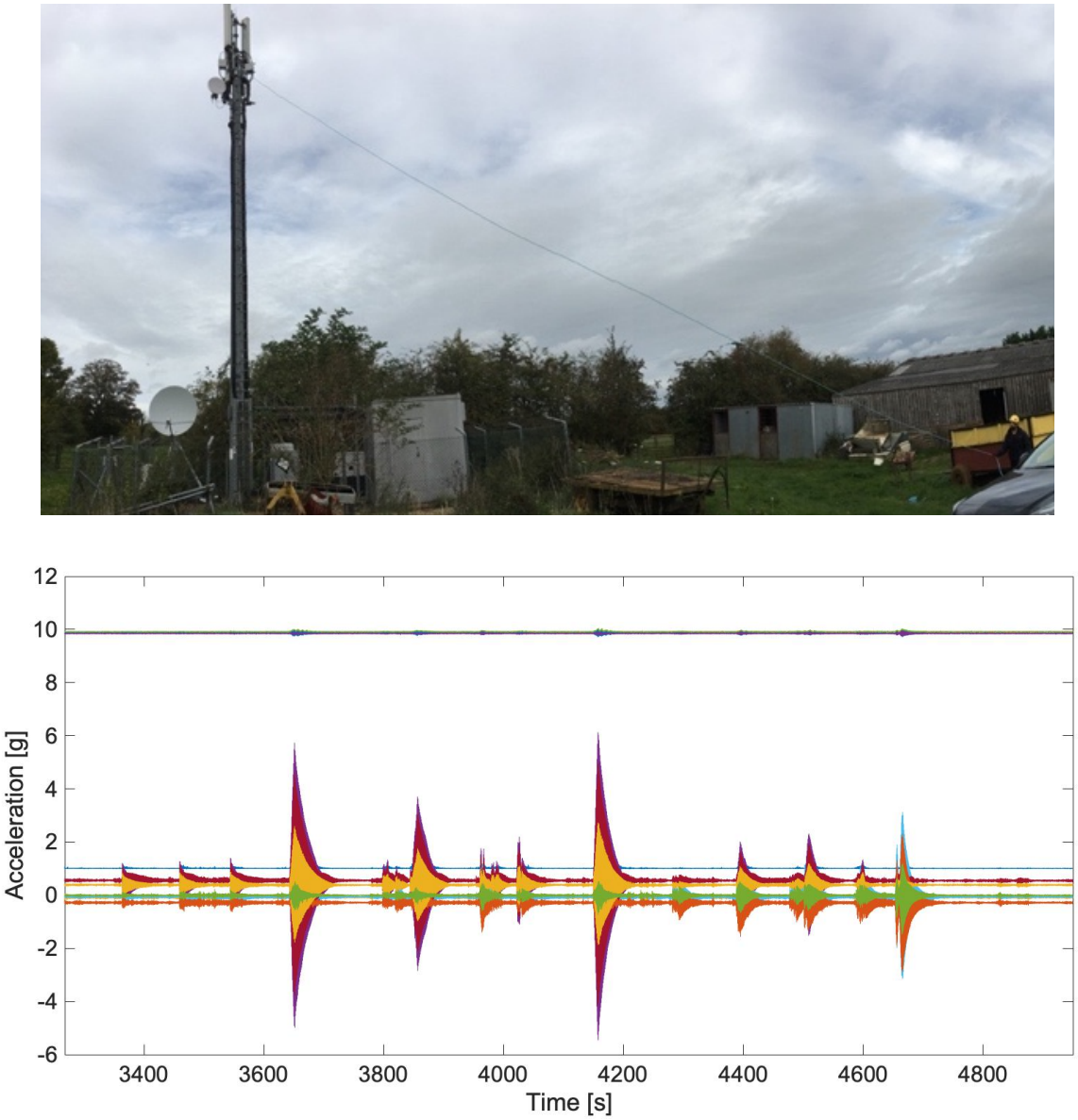

Figure 4-2 Pull test application and acceleration time raw in Norwich.

This type of monopole is characterized by high level of deterioration of inner connections between the shaft column and the flange base. Few failures were identified during last ten years due to quick fatigue events under normal wind buffeting response which modified the current procedure in dealing with those structures i.e. extra conservative factors in terms of tension resistance at base elements and more maintenance and inspections required before new installations. This study reveals as

well that the estimated main frequencies through structural assessments do not satisfy the current ones on site by a large margin of error which can be an evidence of this deterioration or other similar issues. A knowledge of the non-linearities source in the structure will help to understand that conduct.

4.3 Application of Nonlinear SDOF Backbone Procedure

Backbone curve is a method to understand the behaviour on nonlinear systems looking at the shape of the natural frequencies and damping as a function of response when no forcing is present i.e. during a free vibration decay response after an initial forcing or conditions. In this methodology a force pattern at a predefine relevant frequency in the range of the analysed mode is used to harmonically excite the test structure. After achieving the desire response, the forcing is removed and the required decay is recorded. The resonance decay is then analysed by the linear modal space and instantaneous frequency, damping and amplitude envelope is saved.

A SDOF system is created to illustrate the applicability of the backbone procedure introduced by [55, 82] as Figure 4-3. The non-linear simplified system taken this case satisfies:

Eq. 4-1

$$M\underline{\ddot{x}} + C\underline{\dot{x}} + K\underline{x} + f_{nl,1}(x) + f_{nl,2}(\dot{x}) = \underline{0}$$

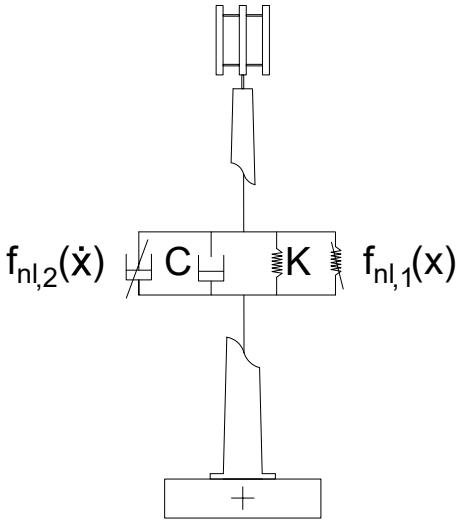

Figure 4-3 Non-Linear simplified model

The experimental backbone curves at very low amplitude are used here to define the properties which defines the underlying linear system (similar to Eq. 2-14) and initial conditions of deflections. Later, they are used to set the stiffness and damping functions that capture the form of the nonlinearity, which needs to be transformed into an analytic expression in the main equation via Harmonic Balance.

This field survey counts on two large resonance responses which are suitable for the analysis covering a good range of displacements as Figure 4-4. As mentioned, any data require post-process to convert accelerations into displacements in modal coordinates.

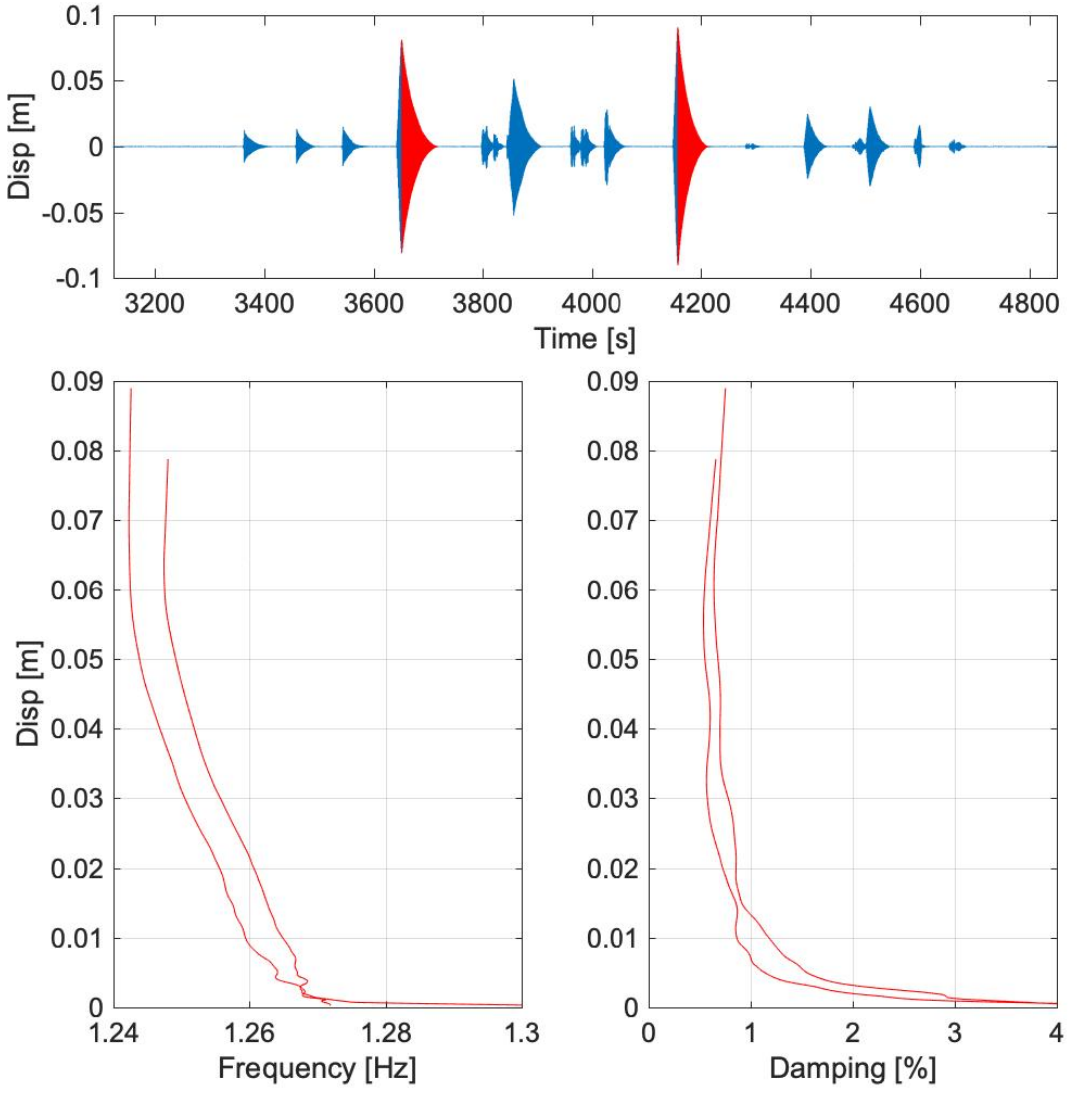

Figure 4-4 Backbone curves from measurements. Upper. Displacements time raw. (Blue: Raw data. Red: Analysed data). Down Left. Frequency behaviour. Down Right. Damping behaviour.

Therefore, those decays are considered large enough to activate the nonlinearity as the backbone procedure obtain on Figure 4-4. The estimated effective stiffness, damping and each respective correlated function are shown on Figure 4-5 and Table 4-1, where sign$(\dot{x})$ could be positive (+) or negative (-) depending on $\dot{x}$:

Table 4-1 Nonlinearities considered in the example SDOF system.

System's nonlinearity	$\boldsymbol{f_{nl,1}(x)}$	$\boldsymbol{f_{nl,2}(\dot{x})}$
Nonlinear stiffness	$k_0\sqrt{x}$	0
Dry friction	0	$c_0\, sign(\dot{x})$

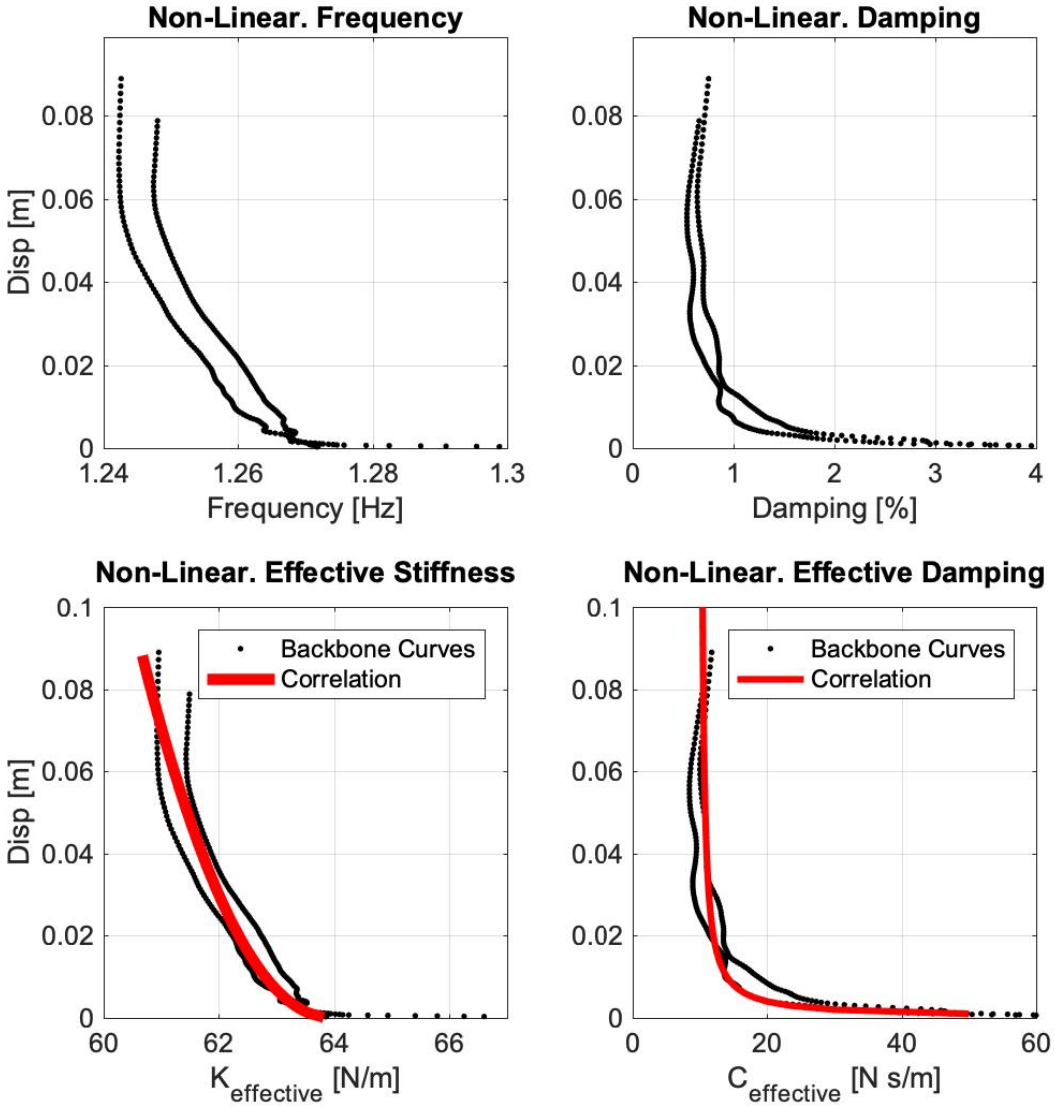

Figure 4-5 Correlated functions of damping and frequency from measured backbone curves.

The non-linearities found in terms of stiffness based on a square root function means a softening performance with the displacements. The approach could be improved as a bilinear function which induce more complexity on the expressions. Chosen function describe a low level of restore stability induced by a reduction inertia forces or help from soils-foundation components.

On the other hand, damping function shows a typical Dry friction or Coulomb-type damping behaviour which is expected from demountable structures and bolts connections based on an interfacial motion as defined on [53]. This source provides high damping at low levels when the movement starts and disappear at high levels where the system behaves nominally linearly. Results agree with current statements of structural damping mainly defined by material and connections components. No evidences of foundation and soils interaction is found which should be specifically analysed with other tools or examples.

Finally, the second plot of Figure 4-6 provides the straight comparison between the typical linear model used for structural assessments (green), and the nonlinear system obtained through the exposed process (magenta) considering the effective stiffness and damping functions calculates in Figure 4-5. It agrees better the free decaying and represents more properly the inherent structural dynamics of the monopole. The discrepancies found at low amplitude are considerably higher than high amplitude were the estimation look appropriated. This way backbone curve methodology is proven as best tool to define the amplitude nonlinear behaviour.

The exercise has been proved as an excellent tool to know advanced detailing of structures abroad standard OMA, which could help to develop tools of deterioration analysis interesting for those type of flexible structures under a high range of loading cycles and likely fatigue issues. A SDOF is capable of achieving an accurate estimation of the backbone curve sufficient to represent with high precision in linear and non-linear terms.

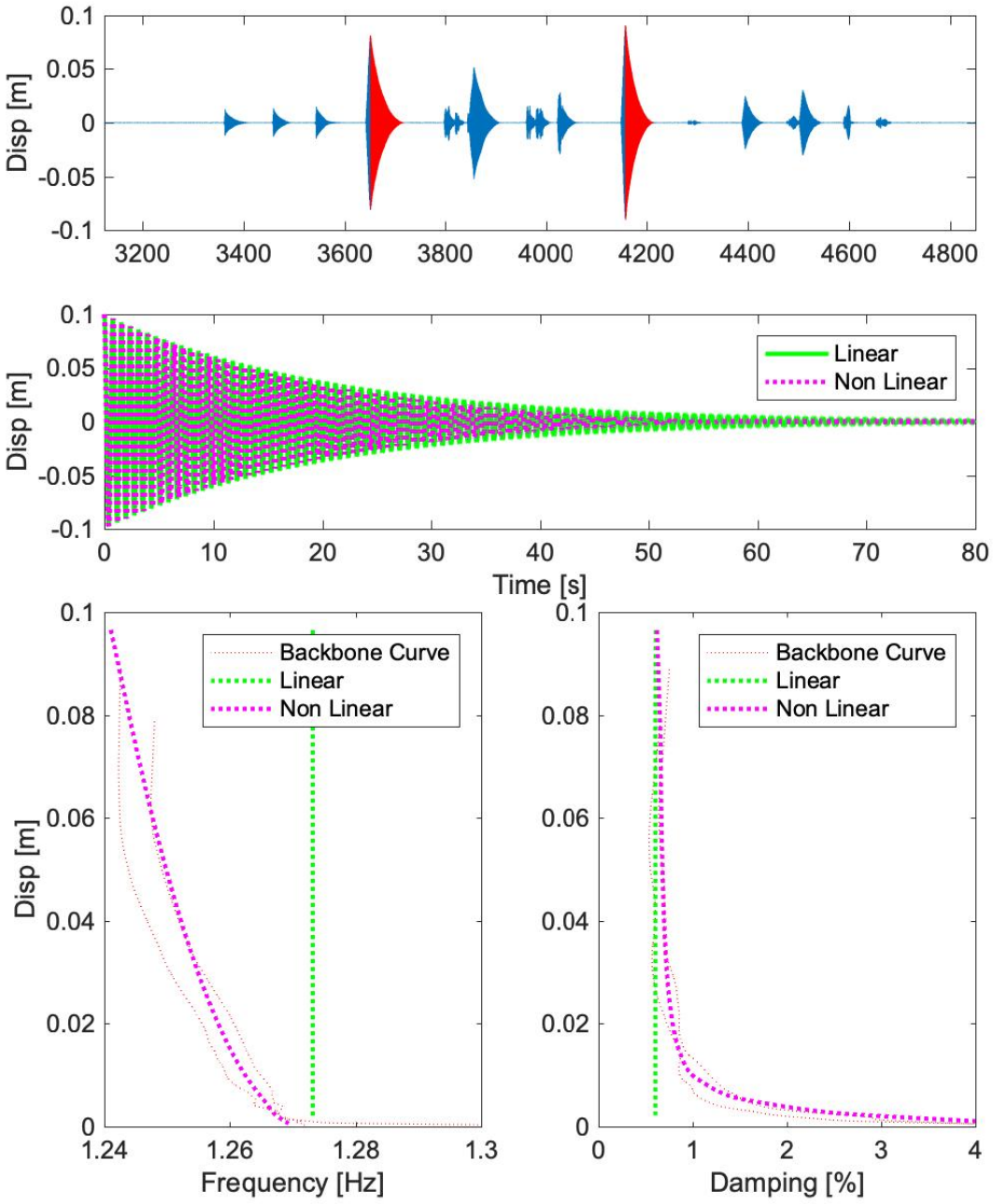

Figure 4-6 Non-linear model fitted to current behaviour of measured backbone curves.

Further exploration in different sites would determine if the behaviour found is standard and applicable to different geometries and boundary conditions.

Preface to Chapter 5

The previous Chapter 3 and Chapter 4 agree some disparity on the results for the same type of structure supporting very similar equipment. Soils and foundations have a capital importance in the definition of structural damping. Authors on diverse structures under seismic loading agree a high dependency of structural damping on typology of foundation and category of soils support of the structure. Some approaches incorporate this concept without large developed experiences in telecommunications structures. The below text confirms this influence based on field tests on three different monopoles using dynamic complex stiffness functions.

The following chapter is a journal paper entitled “Simplified Soils-Structure Damping Interaction on Short Telecommunications Structures” which was submitted to Journal of Structures and Buildings. It demonstrates evidences of foundation-soil interactions under horizontal deflections and wind loading.

Chapter 5 Simplified Soils-Structure Damping Interaction on Short Telecoms Structures

5.1 Introduction

During the last two decades, development of mobile/telecommunications ('telecoms') technologies has resulted in an increased number of antennas, most of them, in suburban environments, installed on rooftops and other locations with limited visual impact. On the other hand, in more rural areas and open spaces with no available building, many short telecoms structures (less than 30m tall) have been deployed to achieve the necessary coverage. The mobile coverage is provided by each mobile competitor individually, which multiplies the number of resources in comparison to broadcasting or digital radio. Hence, in a structure there may be several panels or sectors (antennas) to cover the same area for different providers.

Figure 5-1 shows the most usual two specific types of mobile telecoms structure:

Figure 5-1 Left. Example of Monopole. Right. Example of Short Lattice tower.

(1) Monopoles, which are vertical steel cylinders used to hold equipment at the top of the element but rarely along the length of the structure. These have a height range between 10 and 35 m, typically around 15 – 20 m tall.

(2) Short steel lattice towers, which look like a smaller version of the tall lattice towers used in broadcasting or the pylons used by National Grid to transport electric power. These have varied typologies, being triangular or square, tapered or straight, and could be used for different technologies and customers at several levels.

Logically, those slender structures with very flexible behaviour under horizontal loading tend to be dynamically wind-sensitive. Wind-induced vibrations derive from two mechanisms [4]; the along-wind gust buffeting loading, or the across-wind vortex shedding excitation related to the shape of the structure. Both cases are likely to be ultimate design loadings able to provoke failure of the structure due to fatigue issues which can worsen the structural integrity, deteriorate local connections and decrease service life. Since the development of less expensive acquisition, new challenging structural health monitoring system could assess the dynamic behaviour and control mentioned deterioration.

To manage these dynamic effects, it is vital to define the dynamic properties of the structure, i.e. natural frequencies, typical mode shapes and damping. With respect to damping, the design codes consider the ways the structure absorbs energy during any movement by different means, externally provided by dampers, aerodynamically due to the wind itself, through structural damping arising from distortion of the materials and friction at connections and finally through interaction of foundations radiating energy into the soils.

The previous damping definitions developed during the 1960s and 1970s are no longer appropriate for such slender structures, and new methods can be applied to improve this knowledge. This impetus comes from structure owners who are required to add new antenna payloads to structures already at capacity according to the current standards that prescribe the obsolete damping values.

Furthermore, to improve the structural capacity of existing structures through strengthening or damper installations, it is a requirement to better understand the inherent structural damping and the contribution from combination of soils and

foundations. This contribution arises from energy dissipation in soils due to induced foundation movement, mainly horizontal translation or sliding and rocking.

This chapter outlines the ways in which foundation-soil properties can be described and accounted for in the treatment of damping in the design process. This characterization is founded on the results obtained full-scale dynamic testing of three telecoms structures. Each test is introduced, the observed free vibration behaviour is studied using the SSI complex eigenvalue representation of damping and the result compared to previous experiences with different structure types and standards.

5.2 Background on Soils-Structure Interaction

During the last century SSI has been mainly studied in two fields, the study of dynamic properties of actual buildings using strong-motion records to investigate their seismic design, and the harmonic oscillations induced by machine-generated inertial loading.

A number of authors have provided analytical formulations and several reviews ([83 – 87]). They describe analytical solutions based on integral transform techniques and dynamic finite-element methods using special “wave transmitting” lateral boundaries.

All studies and reviews agree the following key characteristics relevant to SSI, namely:

- the type and shape of the foundation on the interface,
- the embedment of the foundation,
- the nature of the soil profile, deep uniform or layered deposit and
- the mode of vibration and the frequency of excitation.

Design codes avoid detailed consideration of the above characteristics and provide conservative damping values. One of the first proposals in terms of damping according to soil type is for seismic design of pressure vessels [34], setting three different categories as soft soils, for resistant stress $\mathrm{B_p} < 10.5\ \mathrm{MPa}$, medium soils for $10.5\ \mathrm{MPa} < \mathrm{B_p} < 21\ \mathrm{MPa}$ and piled foundation, rock or stiff soils for higher values.

The old British Standard [24] agree the total structural damping δ_S as a multiplication of an optimal modification factor, K_δ, dependent on the foundation-soils interaction which can increase the structural damping logarithmic decrement (log-dec) value δ_S,

using the values of Table 5-1, by up to 3 times from the base value in Table 5-2, as Eq. 5-1. Actually, those assumptions are used in other codes such as [31] for lighting columns. This allowance sets three foundation categories; shallow slab on soft soil which absorbs significant energy during the vibration ($k = 3$), a shallow slab on medium stiff soil ($k = 1.5$), and a rock soil or piled foundation with no damping enhancement ($k = 1$):

Eq. 5-1

$$\delta_S = K_\delta \delta_T$$

Table 5-1 Structural Damping Values. Log Dec. [24].

Structural connections	Surface finish at connections	log-dec, δ_T	Critical damping [%], ζ_T
All welded or all friction grip or fitted bolted	All finishes	0.015	0.239
Welded bracings: bolted flange plate connection to legs	All finishes	0.015	0.239
Welded bracings: black bolted gusset connection to legs	Cleaned, unpainted	0.060	0.955
	Grit-blasted, metal-sprayed	0.045	0.716
	Galvanised	0.030	0.477
Black bolted bracing: bolted flange plate connection to legs	Cleaned, unpainted	0.040	0.637
	Grit-blasted, metal-sprayed	0.030	0.477
	Galvanised	0.020	0.318
Black bolted bracing: black bolted gusset connection to legs	Cleaned, unpainted	0.080	1.273
	Grit-blasted, metal-sprayed	0.060	0.955
	Galvanised	0.040	0.637

Table 5-2 Augmentation Factor. [24].

Type of foundations	Factor, K_δ
Piled foundation or footing on stiff soil or rock	1
Spread footing on medium stiff soil	1.5
Spread footing on soft soil	3

On the other hand, the actual Eurocode [26] only provides typical damping values in the form of logarithmic decrement and shows how this value depends on the structural type, the material and the connections used during the construction similar to Table 5-1, ranging between 0.01 and 0.07 for a steel chimney and stack, and between 0.02 and 0.05 for steel lattice towers, and neglecting any kind of SSI influence. In addition, the Canadian code CSA [23], American code ANSI/TIA-222-G [22] and Australia/New Zealand Standard 1170.2:2011 [25], recommend a wide range of critical structural damping, with 5 – 7 % recommended for seismic loading, but none of those include damping for wind loading analysis.

5.3 Foundations & Soil Conditions

The main purpose of the foundation is to transfer loads from the structure to the soil. Foundations for telecom structures are typically supported by either spread footing or piled foundations (which are less common), made of concrete. Figure 5-2 shows the characteristic foundation used for the portfolio of monopoles in the UK, depending on geometry, depth of embedment and type of soil. When the soil on which an ordinary shallow foundation would rest is of insufficient strength to hold the load coming from the structure, it may be necessary to use a piled foundation, with the purpose of transferring the load to stiffer materials at a lower level. This consideration changes the rigidity of the foundations-soil system compared to previous cases on soft soils and moves close to the ideal of the being founded on rock i.e. a fixed base.

In terms of dynamics, the oscillation frequency and manner of its decay depend on the physical parameters of the structure foundation and its soil support. Following [57], the rigidity of the soils makes the combination system less stiff than if the structure were on a fixed base. This decreases the natural period which in turn tends to result in increased dynamic response of the tower. According to [58], the lowest natural frequency is most affected as it involves the highest proportion of soil in the mode

shape. The combined dynamic parameters of a SSI system govern the nature of its response to any given dynamic excitation. For steady-state vibrations on rotating machinery, the foundation and soil structure may change producing settlement of the surface or possibly a reduction in strength, that is governed by parameters such as the initial void ratio, soil boundary confinement or intensity of the loading. In short telecoms structures, this issue is less important due to low frequency and low loading induced on the foundation.

In terms of damping, the soil contribution can be divided in two components as first introduced in [49]; loss of energy through propagation of waves from the footing and the internal energy loss due to hysteretic and viscous effects. The literature exposes representative damping ratios for each component source, radiation damping, ($\zeta_{foun,j}$) and material damping, ($\zeta_{foun,mat}$) expanded on previous chapters.

Figure 5-2 Left. Sketch typical shallow and deep foundations. Elevation and plan view showing coordinate system. Right. Picture of Portasilo monopole.

In terms of field tests, there are difficulties in trying to evaluate both separately. Normally, several forms of radiation damping for various forms of oscillation are applied to specific footing cases. Some authors e.g. [59] recommend extracting the material damping from each radiation mode considering how each soil type behaves under specific static and dynamic loading conditions during geotechnics lab tests. This study will not separate both sources, instead achieving a generic critical damping for

each form of oscillation i.e. for translation and rotation at the foundation which will form a generic foundation damping.

5.4 SSI Application. Forces and Displacements at Footing-Soil-Interface.

The objective of system identification is to evaluate the influence of foundation-soil interaction on the total 'structural' damping. To give a simple quantification of the effect of soil-structure Interaction (SSI) on service response during strong wind events, modal properties are identified using input-output relationships obtained from direct experimental study. The focus of this chapter is on fundamental-mode vibration period and damping ratios for different foundation-soil conditions which enables simple quantifications of SSI effects, suitable for wind design following specific codes on short telecom structures. On the determination of the dynamic properties, among the extensive literature published about the application of this methodology, almost all agree some important points on the procedure [88] for site tests; the need to work in both time and frequency domain, the importance of the input and output motions used and the quality of the transformation into frequency domain as main points.

Those structures are characterized by a main elliptical movement defined by two very closed modes of vibration. The standards consider this behaviour as the first flexural bending mode which will be relatively simple to achieve, and for practical purposes, it will be used in that approach. Also, to have a better understanding of the issue, the literature creates two different states of the structure, the "Fixed" system where foundation response is non-existent, and the "Soil-Structure-Interaction" system where it exists, i.e. the differences between the input and output motions must reflect the flexibility of all components.

In this exercise, the foundation responses (output) totally depend on the loads generated (input) as a result of the deformation and inertial forces of the structure, represented by u_s as indicated in Figure 5-3. In this chapter, these procedures have been used to evaluate SSI effects from strong motion recordings of three similar structures having different SSI conditions.

The dynamic properties of the mast-foundation-soil system shown in Figure 5-4A are more conveniently written in the form of a mass-spring-dashpot system as shown in Figure 5-4B, in terms of stiffness, k_j, and damping c_j, for each form of oscillation j.

The SSI application finds a mass-spring system where the dynamic complex stiffness functions, $\overline{k_j}$, that appear in Figure 5-4C, are built from the coupling of the "real stiffness", k_j, and the assigned damping, c_j, Figure 5-4B, where the in-phase part represents the stiffness and the imaginary part represents the damping contributed by each form of oscillation.

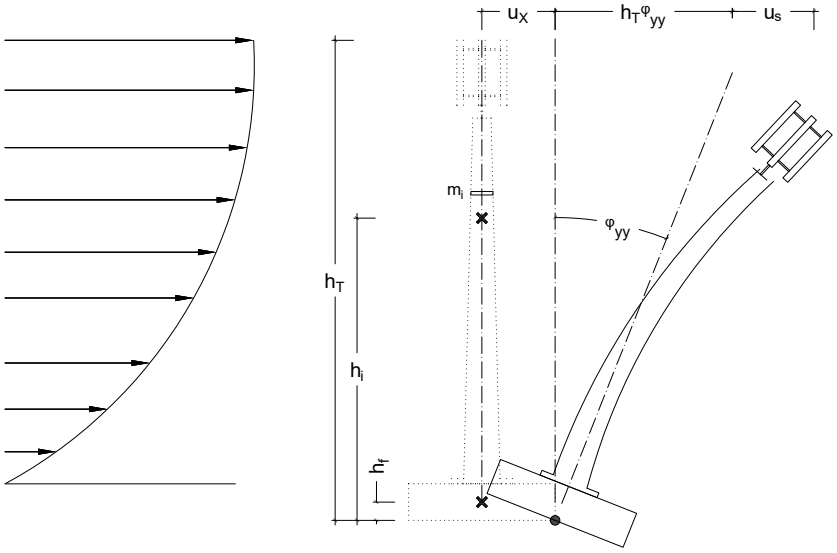

Figure 5-3 Sketch of general monopole structure for analysis of along-wind response.

Some good lessons can be extracted from previous experience. In [89], the formulation of these dynamic complex stiffness functions indicates that hysteretic damping results in frequency-dependent constants of equivalent viscous damping, c_j. Also, radiation damping is significant and increases with the size, depth and embedment of homogeneous deposits supporting the foundation. For the purposes of this research, this radiation damping has been considered as part of a total damping, coming from foundation-soil interaction, as will be described in a later section. In [58] similar methodology is applied to single and multi-storey buildings on an elastic half-space, with the aims to study the behaviour of heavy structures under (building) earthquake response. It was found that the fundamental natural frequency of the building, as well the amplitude of the acceleration input, always decreases because of the dynamic coupling between the building and the soil. However, the effective damping can be either decreased or increased by SSI, depending on the parameters of the system. In addition, the maximum SSI occurs predominantly in the fundamental mode [58] and the interaction for higher modes can be neglected.

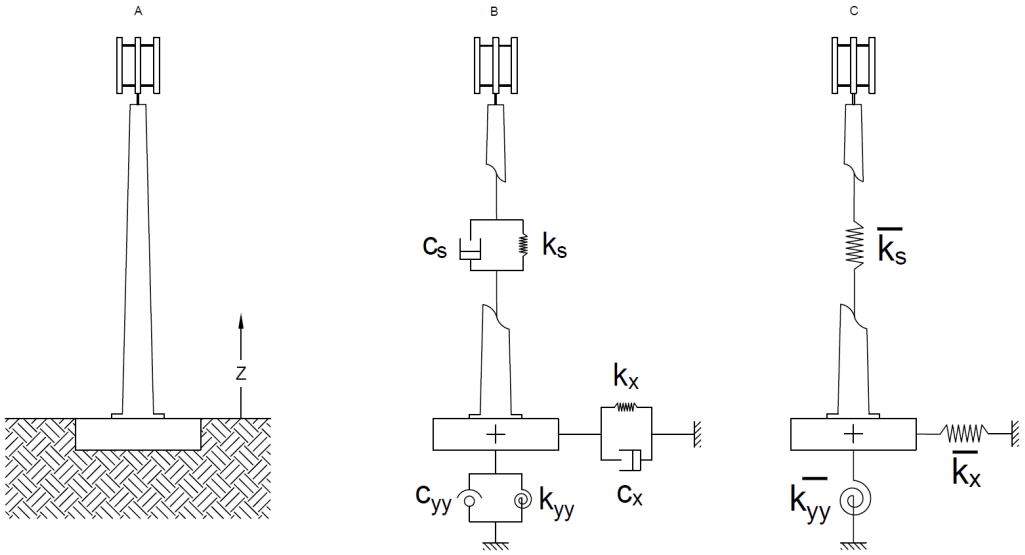

Figure 5-4 Sketches of simplified model. A. Left. Elevation. B. Central. Spring-Dashpot system. C. Right. Proposed SSI spring system for analysis.

In terms of methodology, the dynamic-complex-stiffness-function approach was firstly defined by [47] applied to only one dynamic form of oscillation i.e. translation or rotation. In this case it was found [47] that the results confirm that the equivalent damping ratio will, even in the absence of radiation damping, be somewhat larger than the inherent damping ratio of the structure. Since then, literature was reviewed [47, 90] with the purpose of defining rules to simplify structural dynamic design of buildings, using dimensionless parameters such as: the stiffness ratio between the structure and the soil, the slenderness ratio, or the mass ratio. Due to several geometry/material restrictions, those rules are not applicable to short telecom structures, which are thus the focus of this study. Finally, last researches ([91 – 93]) were based on developing a better physical and mathematical model where the layered ground takes more importance on high structures under wind-loading structures working on similar frequency ranges as this exercise, this study simplifies the issue according to standings carried out by mentioned codes where parameters like SPT help to confirm quality of terrain in terms of stiffness.

According to [47, 59], the dynamic complex stiffness functions, $\overline{k_j}$, is defined in Eq. 5-2.

Eq. 5-2

$$\overline{k_j} = k_j + i\overline{\omega}_j c_j = k_j\left(1 + 2\zeta_{foun,j}i\right)$$

Where $\bar{\omega}$ and $\zeta_{foun,j}$ are the circular frequency on SSI state and critical damping belonging to each form of oscillation (translation and rotation). In previous approaches focused on seismic loading [83, 88], stiffness and damping, $k_j = k_j(a_o, v)$, and $c_j = c_j(a_o, v)$, are developed as functions of a_o, a dimensionless frequency defined by $a_o = {\omega r}/{V_s}$, where V_s is the soil shear wave velocity, r is the foundation radius, and v is the soil Poisson ratio. Those functions can be presented as complex formulation as [84], or plotted in design charts for each form of oscillation–for several form factors, surrounding soil, foundation types and depths, and uniformity soil deposits. This formulation is applicable for heavy excitations over a broad range of frequencies such as in seismic loading and have been heavily used in applications to SSI in buildings. In this study, it is more appropriate to focus on narrow frequency ranges more convenient for ambient loading. Another big difference is the need to include the foundation masses since all previous studies neglected the effect of the base mass on the dynamic properties. Foundation masses are small compared to the superstructure for other civil structures such as buildings whereas for monopoles the masses and dimensions of the foundation cannot be neglected and must be thoroughly considered.

Given the dynamic complex stiffness $\bar{k_j}$, critical damping can be estimated via the ratio of imaginary and real components, Eq. 5-3.

Eq. 5-3

$$\zeta_{foun,j} = \frac{\bar{\omega}_j c_j}{2k_j} = \frac{imag(\bar{k_j})}{2\, real(\bar{k_j})}$$

hence any field test time series must feed into post-processing delivering the complex stiffness, $\bar{k_j}$.

Three different assumptions simplify this process:

- Only horizontal loading is relevant, and results in two forms of oscillation at the base (Figure 5-4C), the horizontal translation in the direction of the loading called sliding, with stiffness $\overline{k_x}$ and rocking, with stiffness $\overline{k_{yy}}$, around a point of rotation located at the interface surface between soil and foundations. To achieve that during the field tests excitation based on pull and release with ropes is applied to

generate a freely decaying response to be studied, as advised [93], both form of oscillation can be perfectly disregarded for a surface footing on homogeneous and non-homogeneous ground on the this range of frequencies without significant loss of accuracy.

- For reliable estimation of the structural damping, any field test has to be carried out under ideal weather conditions to avoid external forcing, since the approach is based on balance of internal forces in free decay.
- The dynamic behaviour of the structure in service will always be dominated by the first (main) vibration mode, with the exception of unusual across-wind cases due to vortex shedding. This allows simplifications i.e. consideration of just a single mode of vibration.

The model shown in Figure 5-3 is thus well suited to identify the key parameters affecting SSI and to study their effects. To identify the foundation part, it is beneficial to divide the total displacement response into its components related to each form of oscillation as:

Eq. 5-4

$$u_T = u_x + h\varphi_{yy} + u_s$$

where u_x is the horizontal displacement of the base, φ_{yy} is the rotation of the base and u_s represents the amplitude of the relative displacement of the structure attached to the rigid base, as Figure 5-3.

The motion equations of the freely decaying system are written for the response of each element of the superstructure, i, applying via Eq. 5-5 for each form of oscillation, j:

Eq. 5-5

$$\sum m_i \left(\ddot{u_x} + h_i\ddot{\varphi_{yy}} + \ddot{u_s}\right) + \sum c_{ij}\dot{u_j} + \sum k_{ij}u_j = 0$$

Separating into forms of oscillation, the following equations are divided into the inertial masses induced by the movement of the monopole and foundation, the dashpot damping and the stiffness of each form of oscillation. In each case, the last two terms

comprise the complex dynamic stiffness whose value can be obtained via measured response and known mass and geometry:

In terms of Horizontal translation,

Eq. 5-6.

$$\int m_i\left(\ddot{u_x} + h_i\ddot{\varphi_{yy}} + \ddot{u_s}\right)dz + c_x\dot{u_x} + k_x u_x = 0;\ \ \overline{k_x}u_x = \int m_i\left(\ddot{u_x} + h_i\ddot{\varphi_{yy}} + \ddot{u_s}\right)dz;\ \ \overline{k_x} = \frac{\int m_i\left(\ddot{u_x} + h_i\ddot{\varphi_{yy}} + \ddot{u_s}\right)dz}{u_x} = \frac{F}{U}$$

In terms if Rocking,

Eq. 5-7.

$$\int m_i h_i\left(\ddot{u_x} + h_i\ddot{\varphi_{yy}} + \ddot{u_s}\right)dz + c_{yy}\dot{\varphi_{yy}} + k_{yy}\varphi_{yy} = 0;\ \ \overline{k_{yy}}\varphi_{yy} = \int m_i h_i\left(\ddot{u_x} + h_i\ddot{\varphi_{yy}} + \ddot{u_s}\right)dz;\ \ \overline{k_{yy}} = \frac{\int m_i h_i\left(\ddot{u_x} + h_i\ddot{\varphi_{yy}} + \ddot{u_s}\right)dz}{\varphi_{yy}} = \frac{M}{\theta}$$

From Eq. 5-6, Eq. 5-7, Figure 5-3 and Figure 5-4, the dynamic stiffnesses of both forms of oscillation in vibration are defined. In the above equations, F, M, U and θ result (from processing free vibration response data) as the time series of the horizontal force, bending moment, translation and rotations. The inertia forces of the monopole in the fundamental mode in free vibration decay, $\left(\ddot{u_x} + h_i\ddot{\varphi_{yy}} + \ddot{u_s}\right)$ excite the combined stiffness and damping forces provided by the foundation at ground level. Other parameters appearing in Figure 5-4 and Figure 5-3 are masses, m_i and heights, h_i.

In order to correlate the motion of the whole structure from just one source of data at a known height of the monopole, $\ddot{u}_{Top}$, the mode shape must be known along the structure, because it is used Eq. 5-8 as the contribution of the inertia forces in the structure, where z is the height from ground level, $\mu_1(z)$ is the main mode shape and $\ddot{u}_{Top}$ is the response of the structure at a selected location.

Eq. 5-8

$$\int \ddot{u}_s \, dz = \int \mu_1(z) \, \ddot{u}_{Top} dz$$

The Eurocode [26] gives recommendations on mode shape, but these may not be relevant for telecoms monopoles and a better and different approach is required. The given (Eurocode) mode shapes for flexural modes of buildings, towers are represented using Eq. 5-9, referring to Figure 5-5 where z is the structural height from ground level and h the total height of the structure:

Eq. 5-9

$$\mu_1(z) = \left(\frac{z}{h}\right)^{\xi}$$

$\xi = 2.0$ for towers and chimneys

$\xi = 2.5$ for lattice towers

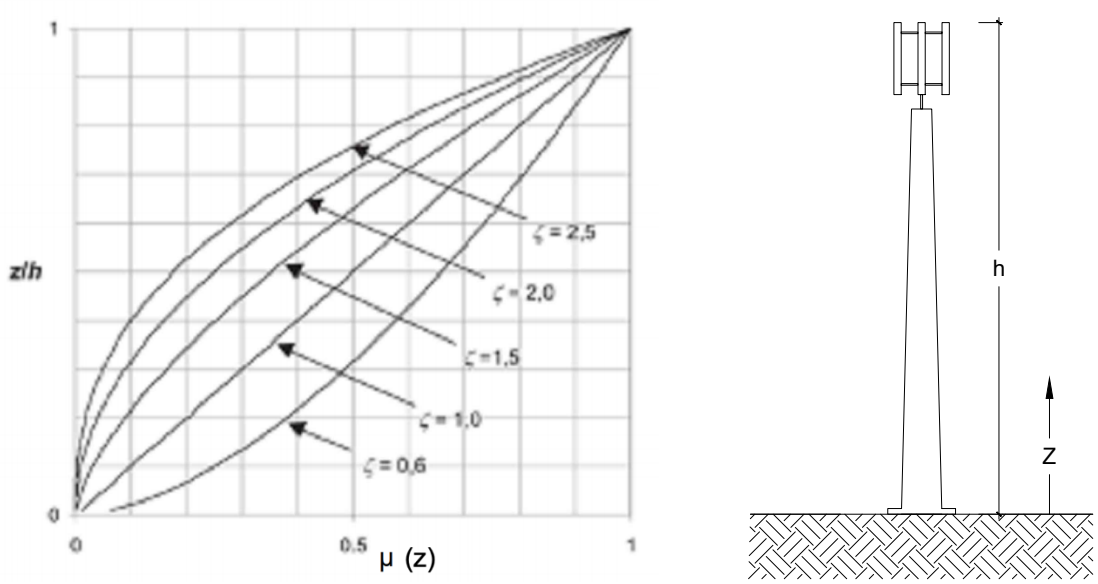

Figure 5-5 Fundamental flexural mode shape for buildings, towers and chimneys cantilevered from the ground. [26].

The free decay vibration signals were used to recover the complex dynamic stiffness by developing frequency response functions (FRFs) from the ratio of the Fourier transform of the measured response [94] output, $\{U, \theta\}$ to the Fourier transform of the forces, $\{F, M\}$ according to Eq. 5-6 and Eq. 5-7. A separate FRF is developed for each form of oscillation as:

In terms of Horizontal translation,

Eq. 5-10

$$\overline{k_x}(\omega) = \frac{F(\omega)}{U(\omega)} = \frac{FRF(F)}{FRF(U)}$$

In terms of Rocking,

Eq. 5-11

$$\overline{k_{yy}}(\omega) = \frac{M(\omega)}{\theta(\omega)} = \frac{FRF(M)}{FRF(\theta)}$$

Once the dynamic stiffness for each form of oscillation as a complex number is obtained, Eq. 5-10, Eq. 5-11, and following Eq. 5-3, the method estimates separately critical damping for each form of oscillation, $\zeta_{foun,x}$ and $\zeta_{foun,yy}$, which, as previously described, will include material damping, $\zeta_{foun,mat}$ where $\zeta_{foun,x}{}'$ and $\zeta_{foun,yy}{}'$ are the radiation damping for each form of oscillation.

Eq. 5-12

$$\zeta_{foun,x} = \zeta_{foun,x}{}' + \zeta_{foun,mat}$$

Eq. 5-13

$$\zeta_{foun,yy} = \zeta_{foun,yy}{}' + \zeta_{foun,mat}$$

The foundation damping ζ_{foun}, is created from both forms of oscillation scaled according to the fictional natural frequencies for each form, ω_x and ω_{yy}.

Eq. 5-14

$$\overline{\omega_x} = \frac{1}{2\pi}\sqrt{\frac{\overline{k_x}}{m_T}}$$

Eq. 5-15

$$\overline{\omega_{yy}} = \frac{\mathrm{h}}{2\pi}\sqrt{\frac{\overline{k_{yy}}}{m_T}}$$

The procedure assumes the only source of the vibration is foundation horizontal translation or rocking, hence:

Eq. 5-16

$$\zeta_{foun} = \left(\frac{\overline{\omega}}{\overline{\omega_x}}\right)^2 \zeta_{foun,x} + \left(\frac{\overline{\omega}}{\overline{\omega_{yy}}}\right)^2 \zeta_{foun,yy}$$

The total critical damping, ζ_{Total}, is then the sum of structural damping, ζ_s, and estimated foundation damping, ζ_{foun}:

Eq. 5-17

$$\zeta_{Total} = \zeta_s + \zeta_{foun}$$

In summary the total critical structural damping is composed of three parts:

(1) contributions of structural damping in the superstructure assuming fixed conditions, $\zeta_s{}'$,

(2) contributions of horizontal translation form, $\zeta_{foun,x}$, and

(3) contributions of rocking form, $\zeta_{foun,yy}$.

Eq. 5-18

$$\zeta_{Total} = \left(\frac{\overline{\omega}}{\omega}\right)^2 \zeta_s{}' + \left(\frac{\overline{\omega}}{\overline{\omega_x}}\right)^2 \zeta_{foun,x} + \left(\frac{\overline{\omega}}{\overline{\omega_{yy}}}\right)^2 \zeta_{foun,yy}$$

5.5 Site Tests & Post-Process of Modal Survey

In order to examine the effect of the soil-foundation properties on total damping on this type of structure, three field tests were undertaken, summarised in Table 5-3. For each structure, there is complete knowledge of geometric and mechanical characteristics of the mass and stiffness of the structure and substructure (foundations), masses of existing antennas given by manufacturer. Soils investigations carried out after geotechnical field tests extracted proportional SPT value helpful to identify the soils category. However, the moisture content of soil which can change between weather conditions (presence of water in the soil profile) of geotechnical field tests and excitation field tests have high importance in the definition of dynamic properties during cyclic loading.

The number of field tests conducted provides an indicative insight into the highly complex mechanism of soils-foundation interaction. Additional field tests under

different weather conditions, and more sophisticated analyses are required to confirm results and induce final changes on codes.

Table 5-3 Field test site details

Site Name	Structure Type	Height	Foundations	Soils Conditions	Foundation Embedment
S1: Marleys Moor	FLi DM1A	17.5 m	Pad: 3.25x3.25x0.85 m	Medium-Soft	No
S2: Norwich Stubb Road	Portasilo	17 m	Pad: 3.6x3.6x0.85 m	Soft	Yes
S3: Chelmsford Office	FLi DM1A	22.5 m	Piled: 3.5x3.5x1 m (8 m)	Soft	No

For the purposes of the research, all the structures conducted were monopoles, similar to Figure 5-3:

- **S1, Marleys Moor** (Figure 5-6A): The structure is a monopole comprising S275J0 steel for main core and plates of 25 mm thick S355J2. There are two sections: a tubular tapered panel between ground level and 14.3 m and a triangular steelwork headframe suitable to accommodate mobile antennas. Also, there is an external spine ladder with latchway fall arrest system. For loading, three panels are installed at the upper part, with a small plate antenna at 14.3 m, with all necessary cables run internally. This structure is joined to the foundation thorough a flange plate and 12 Grade 8.8 M24 bolts, without grouting. The foundation is a concrete block of dimensions 3.25 x 3.25 x 0.85 m. The soil comprises soft clay with rock and concrete deposits, with SPT N-values between 15 - 25.
- **S2, Norwich Stubb Road** (Figure 5-6B): The structure is a 17 m monopole built with four tubular tapered panels made up of a 16-sided pressing of 8 mm thick plate, completed with a 2 m steelwork pole to install the required antennas. In this case, there are six antennas and linear loading based on running cables at both sides of the external ladder. The base of the tower is welded to a baseplate flange with eight gusset plates and the flange is secured to a concrete foundation by eight 36 mm diameter steel rods, that are sunk approximately 700 mm into the concrete foundation. The mast sits on a set of lower M36 nuts above the foundation concrete that are used to level the mast. The foundation is based on a spread

footing of 3.6 x 3.6 x 0.85 m. The exploratory holes for soil investigations show the ground water level at 2.3 m and very soft soils on top of 3 m of superficial deposits and loose sands to a further depth of 8 m, and with a range of SPT N-values between 3 - 20. The site is considered as a spread footing on soft soil as Table 5-3.

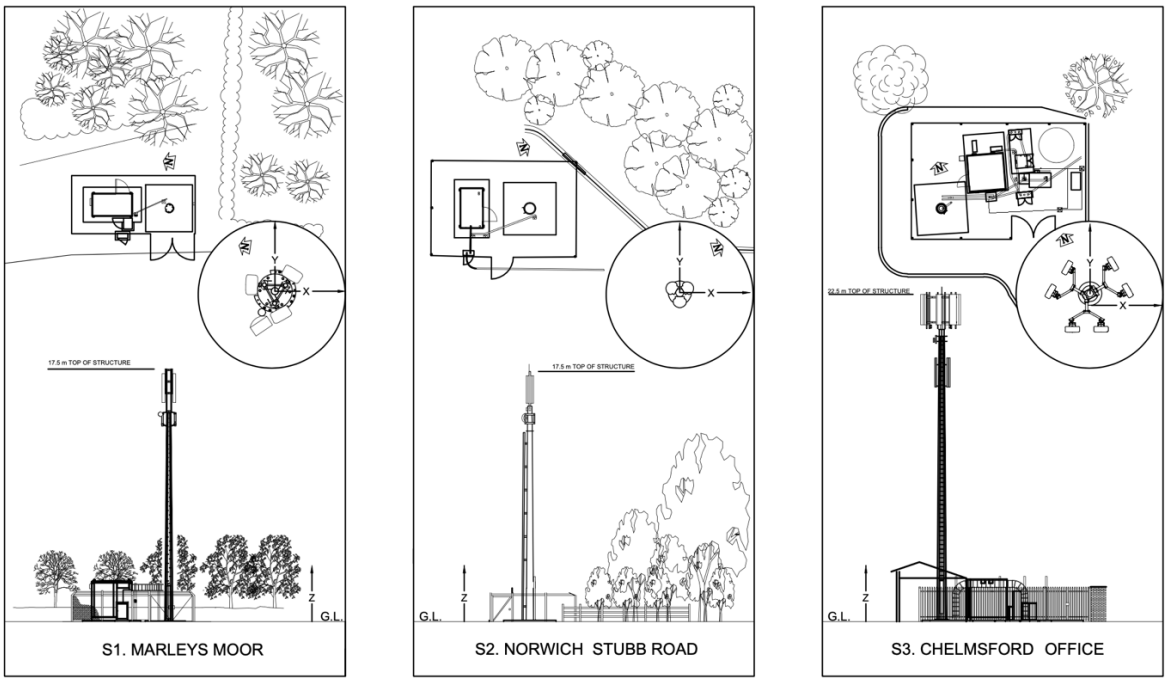

Figure 5-6 Elevation and Plan View of Field Test Sites. A. S1 Marleys Moor. B. S2 Norwich Stubb Road. C. S3 Chelmsford Office.

- **S3, Chelmsford Office** (Figure 5-6C): This monopole is a 22.5 m, a larger version of S1, built with four 16-sided tubular tapered panels between ground level and 19.95 m, and a rocket pole up to 22.5 m. With a similar base to the first example, there are two sets of antenna panels at 21 m and 18.5 m, the cables are run internally and there is a typical climbing ladder. For soil conditions, a ground water seepage was found during the investigation at a depth a 5.9 m, rising to 4.8 m below existing level after 30 minutes. The made ground extends to a depth of 5.9 m generally comprising a very loose, locally clayey, gravelly sand with variable proportions of brick, glass, ceramics and chalk. Glacial sand and gravels were encountered beneath the made ground soil and extend to a depth of 9.8 m below existing level, recording SPT N values between 18 and 21. The foundation comprises a concrete block of 3.5 x 3.5 x 1 m supported by 4 0.3-diameter piles up to 8 m depth.

The field tests used two groups of sensors to record accelerations.

- **National Instruments CompactRIO + Honeywell QA750 system**. This group uses highly sensitive accelerometers recording unidirectional movements on key points around the structure, using a sample frequency of 256 Hz. QA750s are high performance servo-accelerometers measuring to DC (0 Hz) and having noise floor 5-7 μg/Hz$^{0.5}$. Figure 5-7 shows four vertical accelerometers placed at each edge of the foundation to measure foundation rocking, which could determine the rotation deformation form. Two horizontal accelerometers attached to the monopole structure at ground level are used to obtain the horizontal translation, and two accelerometers are used at the top of the structure as a reference for the movement of the superstructure after the pull and release excitation. These last records help to determine dynamic properties of the fixed and SSI systems and the forces at the foundation during the free vibration decay.

Figure 5-7 A. Measurements using QA system. B. QA system in use at Ground Level during Modal Survey.

- **APDM OPALs™ system**. OPALs™ are wireless inertial measurement units including triaxial accelerometers with noise floor ~120 μg/Hz$^{0.5}$. Four OPALs™ (i.e. four triaxial accelerometers) were placed at different level locations as shown in Figure 3-6. Working at 128 Hz sample frequency, these provide the best approach to measure the mode shape of the structure. These devices are wireless sensors that synchronise over short distances typical for mast measurements, and by keeping one OPAL™ at the top pf the monopole and 'roving' the remaining

three OPALs™ to other height-wise locations on the mast it is possible to identify the vibration mode shapes very efficiently. Alternatively, the set of four can be left in place to track variation of mode shapes with vibration decay.

For each field test, the excitation used the 'Pull & Release' method. This is based on the application of sharp tugs on a rope attached to a point close to the top of the structure, timed to build up a strong (resonant) response before letting the structure vibration decay freely. This has been shown to be a highly effective method for this kind of structure, where the chances of installing a shaker are very limited due to logistical challenges. Other advantages are:

- The resonant response level achieved is similar to level of response for design service life estimation under service wind loading.
- The range of frequencies needed around highest SSI response is readily achievable by timed rope tugs. The ranges of searched frequencies are easily achievable by human excitation.
- The influence of the rope after the application of the pull is negligible.

To have different response cases to compare the SSI behaviour under several conditions, different sets of pulls were applied from different directions, aligned with the accelerometer orientation to have the highest response on foundation perpendicular, to each face side. Also, as shown in Figure 5-8, each set of pulls was aimed to induce low, medium, high and very high response of the superstructure, having around 1 - 2 minutes of rest between each pull to capture the whole decay to negligible response levels. To achieve very high response, it was necessary to apply harmonic pulling at certain frequencies.

After the acquisition, post-processing was applied to both data systems (QAs and OPALs™) in time and frequency domain.

A

B

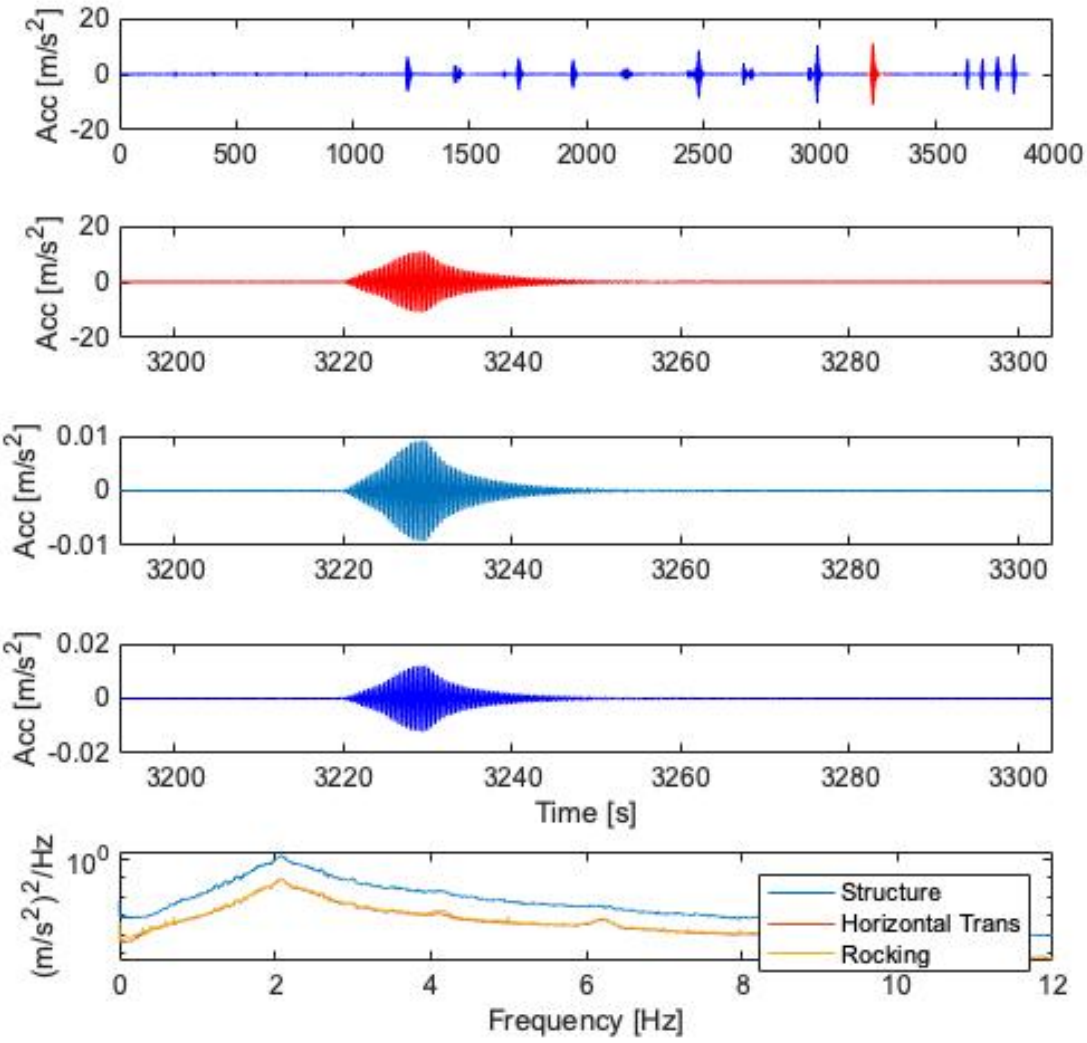

Figure 5-8. A. Picture of a pull application. B. Time Serie of Marleys Moor site test in accelerations. I. Whole time serie. II. Superstructure Response, $\{\ddot{u}_s\}$. III. Horizontal Translation Response, $\{\ddot{U}\}$. IV. Rocking Response, $\{\ddot{\theta}\}$. V. PSD. Whole time series.

On one hand, the time domain processing extracts certain useful parameters to be used during the analysis and prepares time data series to be analysed. Each “Pull” (response after the application of the pull) is isolated and analysed individually, as Figure 5-8. As free viscously damped vibration of a single degree of freedom system can be expressed by the exponential function enveloping the vibration decay:

Eq. 5-19

$$x = x_o e^{(-2\pi f_n \zeta_{Total})}$$

Where, x_o is the initial amplitude, f_n is the natural frequency and ζ_{Total} is the critical damping ratio. The method interpolates each peak of the decay to match with the function. Piecewise rundown curve fitting to the free decay i.e. in successive blocks of a few cycles, allows estimation of the frequency and damping variation throughout the decay. The purpose of measuring those frequencies for the experimental signals is to focus the effectiveness of the analysis on this range instead of analysing the whole frequency spectra. The analysis limits the working range of frequencies between SSI and fixed conditions, it allows comparisons between both states of the structure.

Also, during this process, operational modal analysis (OMA) of the OPAL™ data was used to estimate the mode shapes of each pull direction. The results of the OMA are used to determine actual ξ parameter in Eq. 5-9 for comparison with recommendations.

Finally, over the sets of short time series, Eq. 5-6 and Eq. 5-7 are applied to obtain the pairs of series, $\{U, F\}$ and $\{\theta, M\}$. Applying the Fourier transform, Eq. 5-9 - Eq. 5-10, a script was created in MATLAB to build both dynamic stiffnesses, $\overline{\mathrm{k_x}}$ and $\overline{\mathrm{k_{yy}}}$ leading to damping estimates from each source, $\zeta_{foun,x}$, $\zeta_{foun,yy}$, $\zeta_{foun}$and ζ_{Total}.

5.6 Results after Modal Survey

5.6.1 Mode Shapes on Monopoles

In order to apply and verify the already explained methodology, with both mode shapes, (the superstructure mode shape built from QAs system and the structure one built from OPALs™), must agree each other and be consistent with the vibration modes illustrated in Figure 5-3. In previous, Figure 5-9 presents the flexural mode shapes of the telecom monopole structures, as expected, the shape is similar to

cantilevered structures under perpendicular excitation. The results obtained for each structure are presented below:

Table 5-4 Mode Shape Results of OMA on APDM OPALs TM system

Field Test	$f_{n,FIXED}\ [Hz]$	ξ
S1. Marleys Moor.	2.125	2.052
S2. Norwich Stubb Road.	1.265	1.508
S3. Chelmsford Office	1.32	1.835

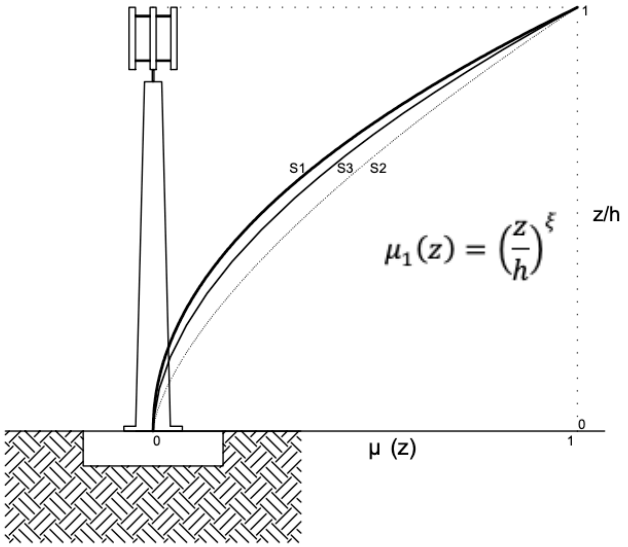

Figure 5-9 Normalized mode shapes for superstructure at fundamental resonant frequency from field tests obtained using OPALs^{TM} system.

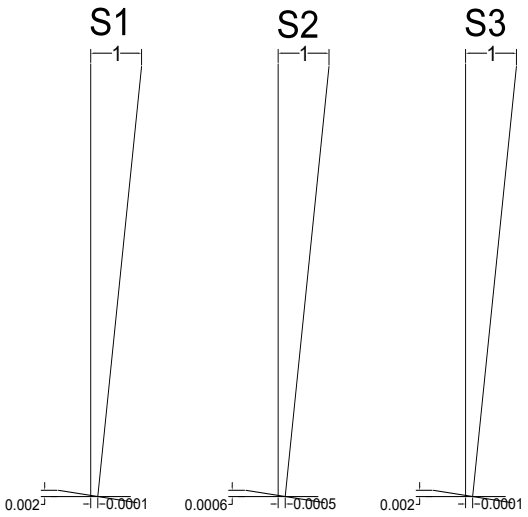

Figure 5-10 Mode shape for foundation obtained using QA System.

Following the results of Table 5-4 to Eq. 5-9, the mode shape model given by Eurocode [26] is seen to be appropriate for these structures, taking exponential parameters between 1.5 and 2. Monopoles tend to have values closer to chimneys rather than lattice towers or buildings.

OPAL™ sensors proved to be an excellent tool to provide a good estimation of the mode shape of the structure for fixed and interactive soil conditions. They were able to demonstrate that the soil-structure interaction does not influence the mode shape of the structure, i.e. the superstructure mode shape does not change during free decay.

In relation to QA system, as expected, the superstructure translation comprises components from each form of oscillation: (1) base translation; (2) tangential motion due to base rocking; and (3) structure translation as illustrated in Figure 5-3.

In Figure 5-10, the mode shape of the superstructure is plotted using three different reference points: the uplift of the foundation on the edge reflects the rocking oscillation, the horizontal translation in the centre of the foundation, all related to the response at the top of the monopole. A review of the mode shape shows the uplift in rocking oscillation is around 0.2 to 0.07 % of the top response, on the other hand, horizontal translation takes 0.1 to 0.05 %.

5.6.2 Frequency Estimation via Rundown & Curve Fitting

Following the procedure described, each free decay was processed applying piecewise curve fitting ‘rundown’ methodology. The results with the aims of achieving the range of working frequencies are shown in Table 5 and the second row of Figure 5-11. The first row shows examples of characteristic free decays of the response for each site surveyed. In the second row, the rundown execution exposes how the frequency varies along the decay. It can be observed that the frequency is not constant, and each example has particularities, but it is well verified, as Table 5, that a frequency reduction of no more than 3 - 5 % is observed at higher amplitude responses. Those frequencies determine the limits of the analysis.

In addition, the curve fitting to the complete decay record can provide averaged values of damping and natural frequency. In Table 5-6, frequency values lie in between the margins limited by the rundown (Table 5), therefore there is an agreement between different methodologies. As third row in Figure 5-11, this method tries to provide a plot

as close as possible to the actual data following by the exponential function (Eq. 5-19); the fitting is good enough to be used for this purpose.

Table 5-5 Range of Frequencies. Rundown Method.

Sites	$f_{n,SSI}\ [Hz]$	$f_{n,FIX}\ [Hz]$
S1, Marleys Moor	2.075	2.125
S2, Norwich Stubb Road	1.24	1.265
S3, Chelmsford Office	1.26	1.32

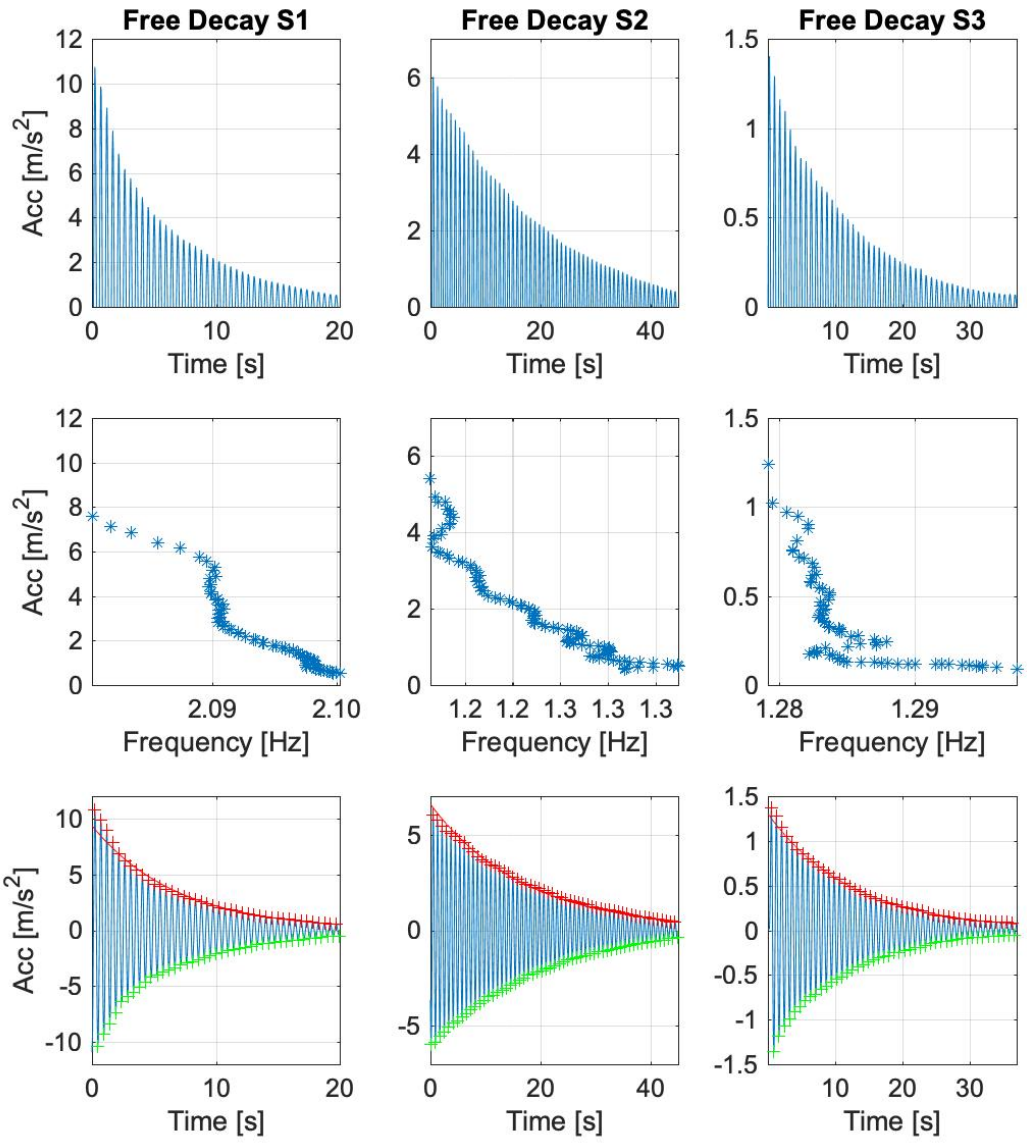

Figure 5-11 Analysis of free decay curve of each tested structure. First Row. Positive response of characteristic response of the superstructure. Second Row. Rundown application. Third row. Curve Fitting application.

Table 5-6 Frequency and Total Damping achieved. Curve Fitting Method.

Sites	$f_n\ [Hz]$	$\zeta_{Total}\ [\%]$
S1, Marleys Moor	2.1	1.2
S2, Norwich Stubb Road	1.255	0.77
S3, Chelmsford Office	1.285	1.1

5.6.3 Foundation Damping Estimation

In terms of foundation damping, application of Eq. 5-14 - Eq. 5-18, yields results shown in Figure 5-12. These charts represent the behaviour of both forms of oscillation (horizontal translation in green dots and the rocking rotation in magenta), and the total foundation damping (in blue), all against the frequency limits defined previously in Table 5-5.

The results reveal that foundation damping contributes between 0.3 % and 0.7 % critical damping to the total damping at resonance level. Those values, as suggested in [47], decrease almost linearly along the frequency range up to the $f_{n,FIXED}$ level where lowest effects of foundation on damping are found. Following the theoretical description, in a “fixed” state, there is no foundation influence, but results advise that some marginal damping value can be found at low amplitudes, that would mean that the fixed conditions are not well obtained on site. In the particular case of S_1, the foundation was not fully embedded and the confinement was not warranted due to a recent excavation to extend the foundation that could explain this effect. Also, as many authors report, the foundation behaviour is mainly defined by the horizontal oscillation which takes up to 90 % of the whole foundation damping and defines the descending slope between states. On the other hand, rocking oscillation is not so important and tends to contribute a uniform damping with constant values between 0 - 20 % of the total.

In terms of soil conditions Figure 5-13 shows that there is no good correlation between soil categories defined by resistant stress (SPT N-values), and the foundation critical damping. All cases achieve a similar range of foundation damping between 0.3 - 0.7 %, which could be applicable to other similar studies. The explanation for these results could come from the boundary and mechanical conditions of the study case. Firstly, the forces, even at high oscillation amplitudes, are not generally large enough to result in high soil and foundation deformation such as occurs with buildings

or larger structures with seismic loading. And finally, the range of amplitudes achieved for frequencies selected (around the resonance level, Table 5-6) are insufficient to activate the friction of soil particles, in this case, the contribution of material damping ($\zeta_{foun,mat}$) would not appear.

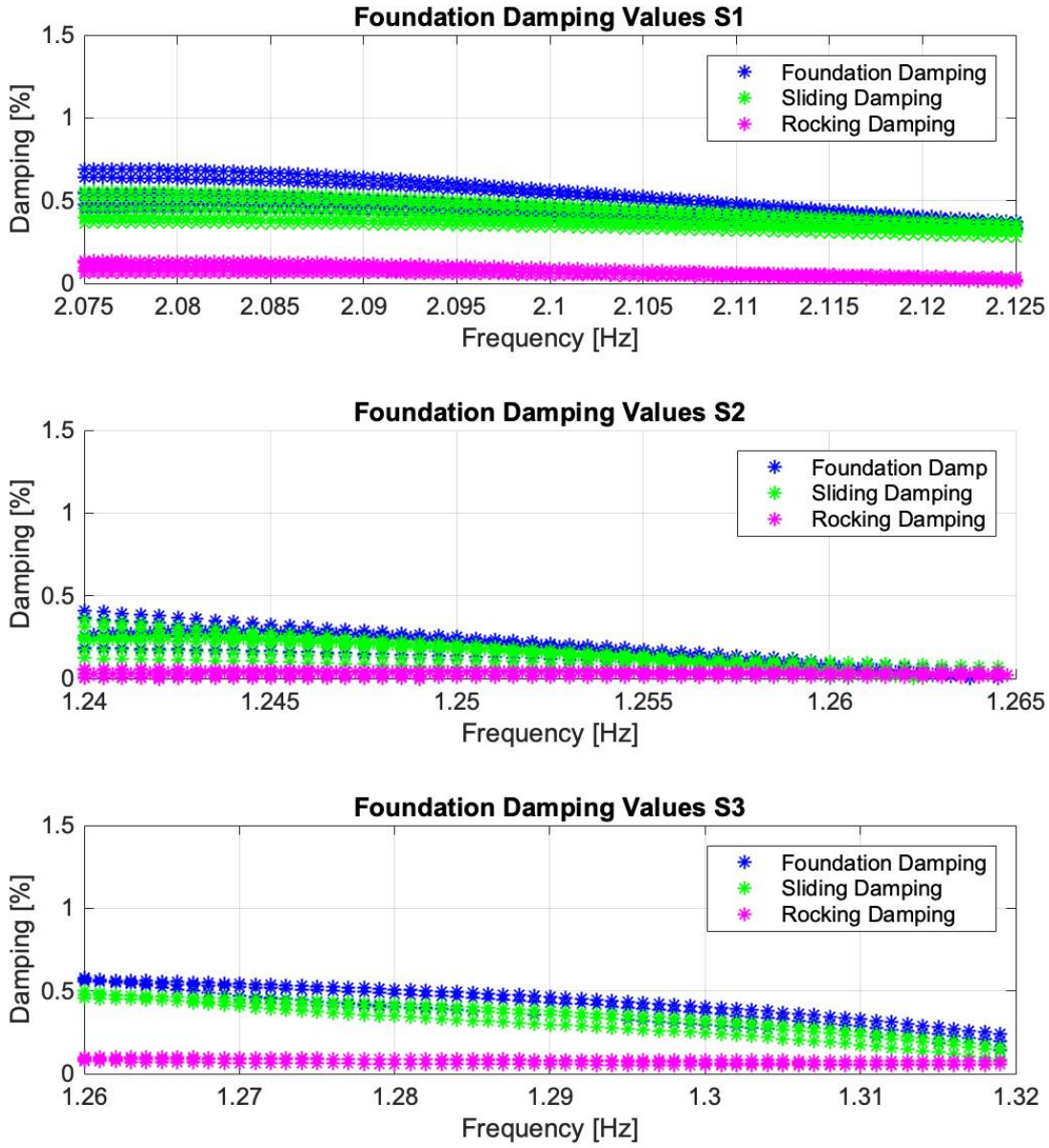

Figure 5-12 Damping values obtained from Field test. A. S1. B. S2. C. S3.

The results at resonance level show that foundation damping, ζ_{foun}, takes values around half of the total critical damping (Table 5-7) and the proportion remains approximately the same for all types as shown in Figure 5-14. The inherent structural damping, ζ_s, can be considered as the difference between ζ_{Total} and ζ_{foun}, taking

different values for each structure, contrary to the constant values in the recommendations.

According to the comparison on the right in Table 5-7 and Figure 5-14 neither the method nor the final values given in the recommendations [24, 31] can be accepted. The foundation damping is not proportional to the structural damping, contrary to the recommendations.

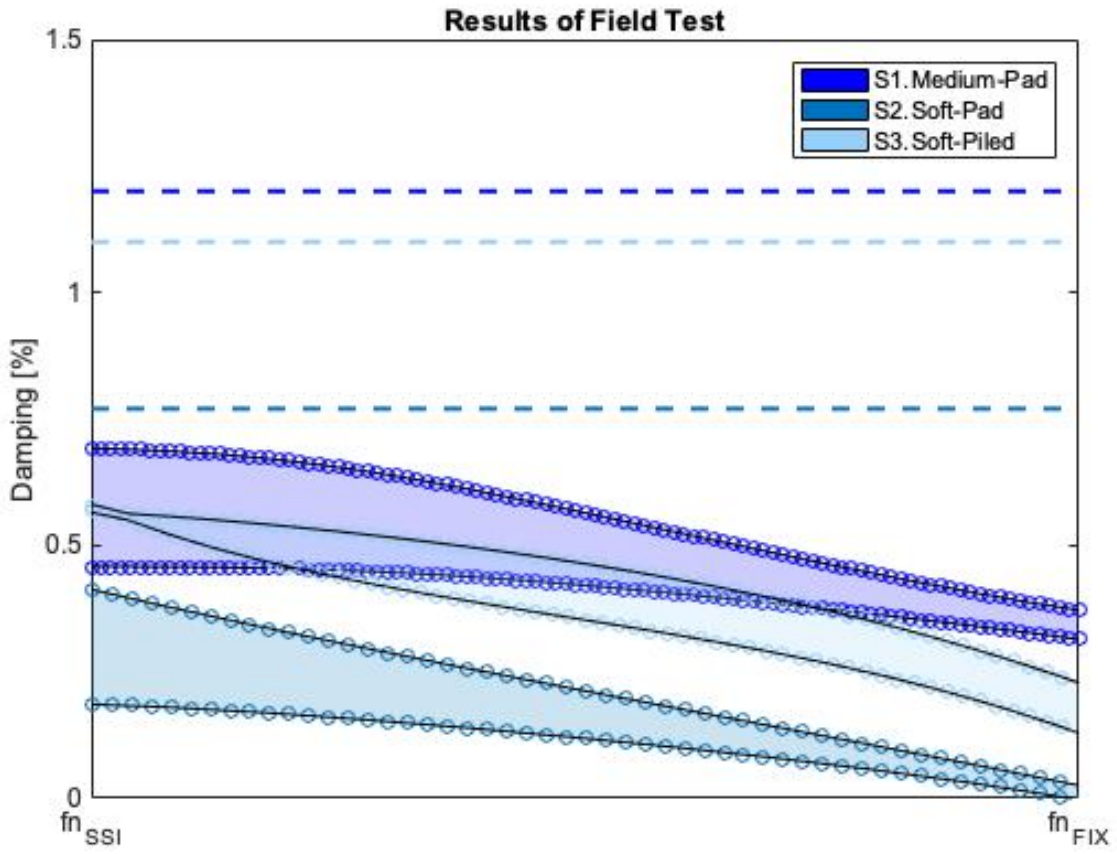

Figure 5-13 Comparison between field tests results

Table 5-7 Comparison between damping results for different sites and estimations. [24], [31].

Sites	Results. S1/S2/S3.			Recommendations [24], [31]		
	ζ_s [%]	ζ_{Total} [%]	ζ_{foun} [%]	ζ_s [%]	ζ_{Total} [%]	ζ_{foun} [%]
S1	0.5-0.75	1.2	0.45-0.7	0.24	0.36	0.12
S2	0.3-0.43	0.77	0.3-0.47	0.24	0.72	0.48
S3	0.5-0.6	1.1	0.5-0.6	0.24	0.24	0

Specifically, for S1, estimates based on recommended approach are quite far from the experimental results. Total, structural and foundation critical damping (dark blue, green and yellow in Figure 5-14) are underestimated severely. For S2, the approach was satisfactory for the foundation but not for the structural damping. The method correctly predicts structural-damping value of this particular kind of monopole simply because it is low. Finally, the case of S1 (piled foundation) shows that the recommendation of zero foundation contribution is incorrect.

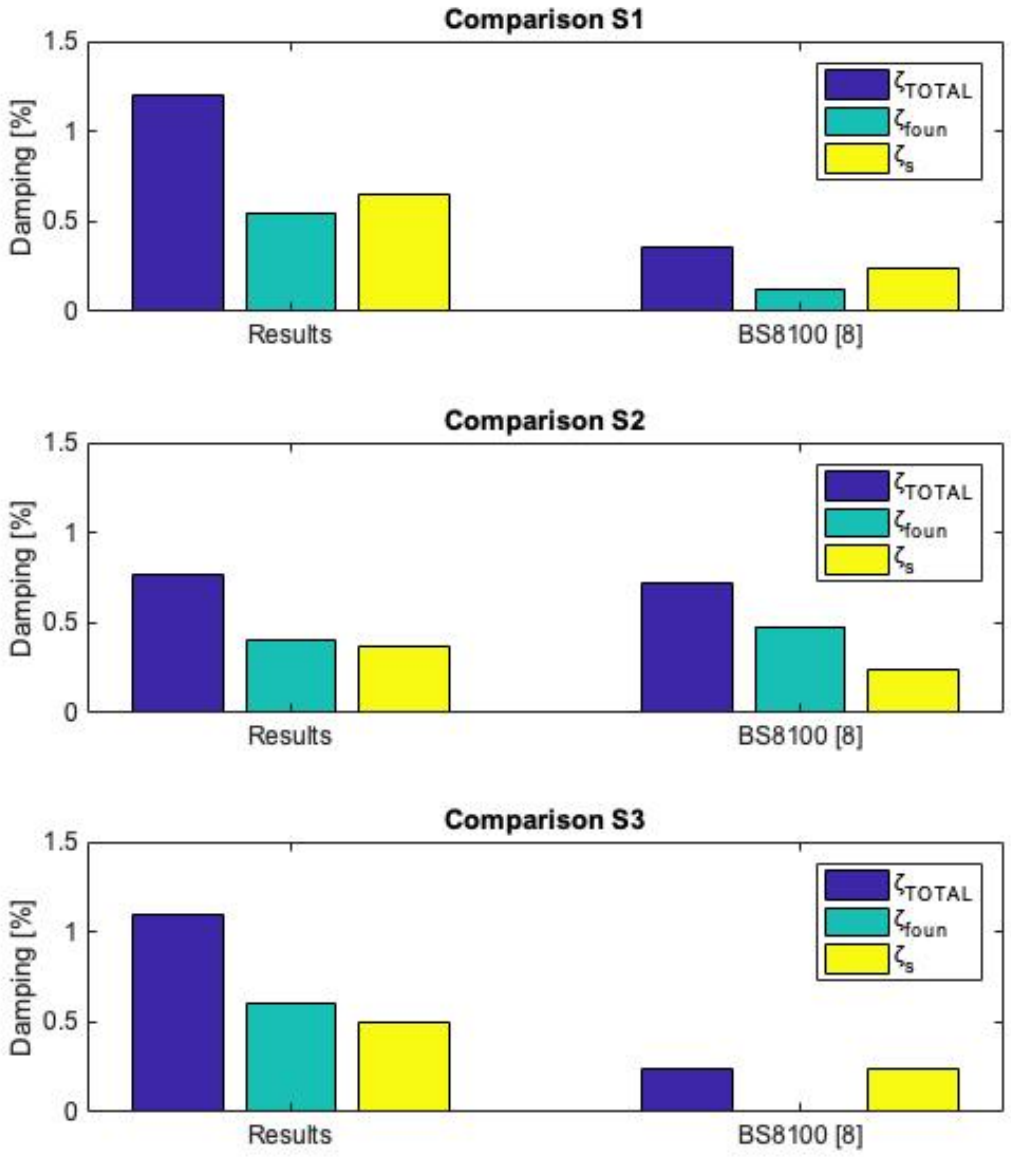

Figure 5-14 Damping values obtained from field test compared to the recommended values given by BS 8100 and BS EN 2006 1-4 at resonance level. [24], [31]. A. S1. B. S2. C. C3.

For total damping, the recommendations [24, 31] which include foundation effects predict very conservative values of total damping. For S1 and S3, the values are 3-4

times lower than the real data, and for S2, the values are correct despite the incorrect method. A new method based on adding damping from each source would have more logic and would represent better the damping behaviour in monopoles. In addition, new and correct structural damping values will improve the assessment.

5.7 Conclusions & Recommendations

This chapter presents a methodology to determine the dynamic Soil-Structure Interaction on short telecom structures, from response data (structure and foundation) obtained during free decay of artificially induced large-amplitude free vibration. The methodology takes advantage of the complexity of the structure, where the study of the first mode is all that is necessary.

The analysis was undertaken by developing a numerical model using MATLAB, at a first level to deal with the response time series, to obtain the range of analysable frequencies and measure global values of damping and secondly a damping estimation for each form of oscillation.

The results show that:

- In terms of mode shape, a recommended exponential factor of $\xi = [1.5 - 2]$ can be taken to represent the main flexural mode of shape in Eq. 5-9
- For all tests carried out, the total structural damping has a foundation component. This component is mainly defined by the horizontal oscillation motions and marginally by rocking motions.
- There is no high correlation between type of soil-foundation and the foundation damping.
- There is a dependency between foundation damping and inherent structural damping of the monopole. They achieve similar values for each monopole analysed.
- The conservative value $\zeta_s = 0.24\ \%$ ($\delta_T = 0.015$) given by codes and literature is too conservative to be applied for a dynamic study on monopoles. It has been shown that damping takes several values depending of the type of structure chosen.

- The augmentation factor K_δ method given in Eq. 5-1 and Table 2-3 has a meaning due to the correlation between both sources of damping but the values taken appeared to be wrong. A single proposed value between $[\mathbf{1.5 - 2.5}]$ could represent it better. Otherwise, an additional component can be used:

$$\zeta_{foun}\,(\%) = [0.3 - 0.7] \text{ i.e.}$$

Eq. 5-20

$$\zeta_{Total}\,(\%) = \zeta_s + \zeta_{foun}\,;\ \ \zeta_{foun}\ \ \in [0.3 - 0.7\ \%]$$

Or

Eq. 5-21

$$\zeta_{Total}\,(\%) = K_\beta * \zeta_s;\ \ K_\beta\ \in [1.5 - 2.5]$$

Finally, the optimization of dynamic structures using new technologies will require specific knowledge which will move away from the current static designs included in standards.

Preface to Chapter 6

As agreed with main national codes, the aerodynamic contributions take high importance in the definition of total damping. However, there are not available investigations or studies which could corroborate those existing approaches. The below text introduces one of the first monitoring systems with structural identification analysis in monopole communications structures to characterise damping in operational wind-ambient conditions.

The following chapter is a journal paper entitled “Ambient vibration testing and operational modal analysis of monopole telecoms structures.” which was submitted to Journal of Civil Structural Health Monitoring (CHSM). It shows a specific acquisition instrumentation system to monitor response and wind loading on telecoms structures, and the implementation and performance of Bayesian OMA as structural identification system with initial investigations of modal properties.

Chapter 6 Ambient Vibration Testing and Operational Modal Analysis of Monopole Telecoms Structures

6.1 Introduction

Due to requirements for new fifth generation of mobile telecoms (5G), structures for mounting antenna equipment at height need to be optimised to sustain the increased loads. The weakest structures in this respect are ‘monopoles’ i.e. slender steel cylindrical structures which reach from 10m to 30m above ground to place equipment at elevated positions for highest possible coverage. The introduction of new technology such as 5G is presently requiring new heavier and larger equipment payloads that change monopole dynamic behaviour under wind loading.

Structural engineers, following recommendations written in national standards, assess main modal properties (MPs) to account for dynamic effects via typical quasi-static wind-loading analysis. The reliability of MPs used in these approaches have been in doubt by consultants during the last decade. Further investigations based on newly acquired full-scale performance data and structural identification methods are required.

With respect to damping, the design codes [24, 26, 31] consider the ways a monopole structure absorbs energy during vibration by different means i.e. externally provided by dampers, aerodynamically due to the wind itself, through structural damping arising from distortion of the materials and friction at connections and finally through interaction of foundations radiating energy into the soils. Effects related to e.g., geometry of the structure, location of the site, soil conditions on site or hold equipment, define dynamic properties that are important during design and review of capabilities during the life of the structure.

Currently, a high percentage of monopole structures are invalidated to support new antennas according to standards i.e. the most modern Eurocode BE EN 1991-1-4: 2005 “Wind Actions” [26], British Standard BS8100: Part 1:1986 [24] and the Institution

of Lighting Engineers (UK) Technical Report Number 7 [31]. This lack of capacity means extra cost for owners and customers who need to agree expensive structural strengthening or tower replacements. This would also involve delay in the total implementation of 5G programmes with additional costs for the end users.

To avoid such delays and extra costs, there is need for further development to improve the current approaches regarding dynamic performance in which the values of structural damping were proved to be very conservative for a high percentage of the structures. Predicting natural frequencies with numerical modal analyses with precise agreement with in-situ values (e.g., less than 10 %) is found to be challenging. This can be attributed to, e.g., lack of knowledge and variability in the effectiveness of foundation-soil to dissipate energy and problems with the aerodynamic-damping formulation using inappropriate drag coefficients working under turbulent wind loading.

There are also concerns around fatigue in ground level connections with a number of failures identified during the previous two decades. Some of these concerns are best addressed by conventional inspection of the inner connection of the base flange, but a better knowledge of dynamics and a continuous record of their evolution can provide a wealth of information capable of addressing many of the key concerns. This impulse comes from structure owners that are required to add new antenna payloads to structures already at capacity according to the current standards that prescribe the obsolete damping values. Several investigations are setting a new perspective in this issue.

In order to obtain in-service performance data, a Structural Health Monitoring (SHM) system was developed that aims at acquiring information about wind loading and response of the structure under a variety of working conditions. This form of detailed non-destructive evaluation was deployed to understand the dynamics of the structure under several loading conditions, remodel structural assessments, evaluate fatigue life and (if required) provide information to design a retrofitted damper. Signals from a mechanical anemometer and two uniaxial horizontal accelerometers were collected using a ground level data logger. The system has been deployed in several structures but this chapter will cover the data obtained during more than two months on a Portasilo Monopole in St Ives; see Figure 6-1.

Figure 6-1 (Left) Picture of St Ives FC Portasilo monopole. SHM system install. Arqiva. (Right) Location of St Ives in South-West of the UK.

This type of monitoring systems will be more feasible in future. New acquisition methodologies [95] based on economically viable equipment coupled with data delivery and analysis would better support decisions on structural management. For this purpose and to improve current approaches, the present chapter introduces modal identification procedures to identify and explain dynamic load/response mechanisms.

This exercise executes the operational modal analysis (OMA) procedure based on innovative Fast Bayesian ambient modal identification method (BAYOMA) [96], [97], which has been applied to other civil structural types such as buildings, bridges and lighthouses [98]. This chapter compares and contrasts the procedures applied to assessing monopole performance using three different lengths of data time frame (T_{fr}). It will set a final decision where to base technical conclusions in terms of dynamic properties like frequencies, damping or mode shapes to apply to other SHM.

Results are verified using a Stochastic Subspace Identification method (SSI, [99]) - well-known and tested in several type of dynamic sensitive structures [100] for the last two decades implemented by ARTeMIS software-. The focus is then the performance of BAYOMA for further developments on communications structures. In the case of the monopole studies, BAYOMA applied to T_{fr} = 10 minutes time frame is shown as most advantageous method because it provides means and variances of all MPs, including mode shapes and the power spectral density matrix of modal forces along the whole range of amplitudes found during the monitoring. This is the background to a project to install SHM system for structural diagnosis of several types of telecom structures in the existing portfolio.

6.2 Structural Health Monitoring System in Short Telecoms Structures

As stated, the main purpose of this SHM exercise was to obtain information on structure response under different wind load cases. Due to the geometry and the slenderness of the structure, it can behave under two different scenarios [4]; along-wind buffeting where response depends on the wind intensity, and vortex shedding at relatively low wind speed driving strong cross-wind response when shedding frequency matches a natural frequency. To define both effects requires knowledge of the wind from the anemometer, and of the structure dynamics (main frequencies, structural and aerodynamic damping and mode shapes) from the accelerometers.

The implemented SHM system (Figure 6-2) had the following components:

- Two monoaxial PCB accelerometers model 393B04, with a sensitivity of 1000 mV/g able to measure between $\pm 5\ \mathrm{g}\ (\pm 49\ \mathrm{m/s^2\ pk})$ placed in a waterproof box to capture response.
- A RM Young mechanical anemometer to capture wind loading in terms of horizontal instantaneous wind speed and direction from North. It produces an AC sine wave signal with frequency proportional to wind speed with 3 cycles per propeller revolution (0.098 m/s per Hz) and FFT of 2-s data blocks is used to capture wind speed up to 100 m/s with operating temperature between -50 and +50 ºC, far beyond the expected range in this application. A threshold minimum frequency corresponding to an instant wind speed of 2 m/s is set to avoid erroneous readings for low wind speeds.
- National Instruments cRIO-9064 with 9234 input module installed in a protected chassis is used as data logger. The system oversamples at 5.120 kHz to capture the anemometer signal. Each block of data acquired is resampled to 128 Hz with FIR filter to avoid aliasing, with 120 dB alias rejection and normalised bandwidth of 0.454.
- Cables run from sensors to logger and requiring proper protection due to extreme outdoor environmental conditions.
- Steel mounting designed to place the anemometer beyond the reach of radio frequency interference due to the antennae installed below. Likewise, attachments

were designed to place the accelerometer at highest horizontal level available in the structure, around at 15 m, as shown in Figure 6-2.

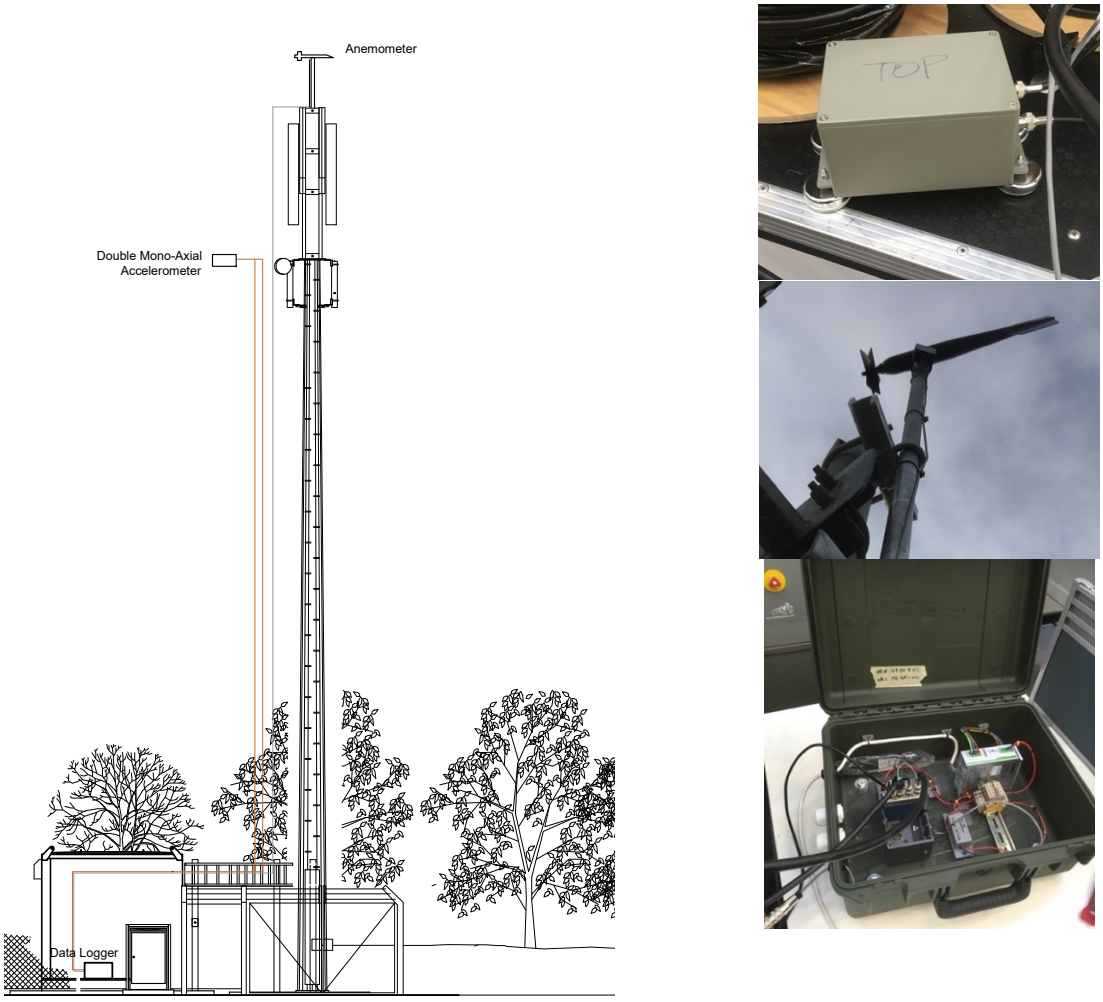

Figure 6-2 SHM system overview. (Left) Elevation sketch of SHM. (Upper right) Response box containing two mono-axial accelerometers. (Centre right) anemometer located on site in St Ives. (Downer right) Logger box.

6.3 SHM Installation in St Ives FC Monopole

6.3.1 Monopole Structural Details

Meeting a requirement for the most effective deployment of the SHM system, the first suggested site in the Arqiva portfolio was a short Portasilo monopole of 14.5 m located at St Ives Football Club, Figure 6-1, in south west UK. This type of monopole is the most usual type in the Arqiva portfolio, being lightweight and flexible. These monopoles were found to have the highest dynamic amplification factors [31] during structural assessments, limiting their capacity for future changes. They have been found to be prone to failure at base level due to fatigue over short lifespans (less than

10 years). St Ives is located in Cornwall, a region with the highest designing basic wind speed in the UK, 23 - 24 m/s. In addition to that, the site is less than 1 kilometre from the sea shore, with theoretical high mean wind speeds and relatively low turbulence with terrain categories I and II. In terms of topography, the site is placed at the top of hill surrounded by residential houses to the north and east and clear fields to the south and west. Consequently, significant orographic influence is expected from those wind directions.

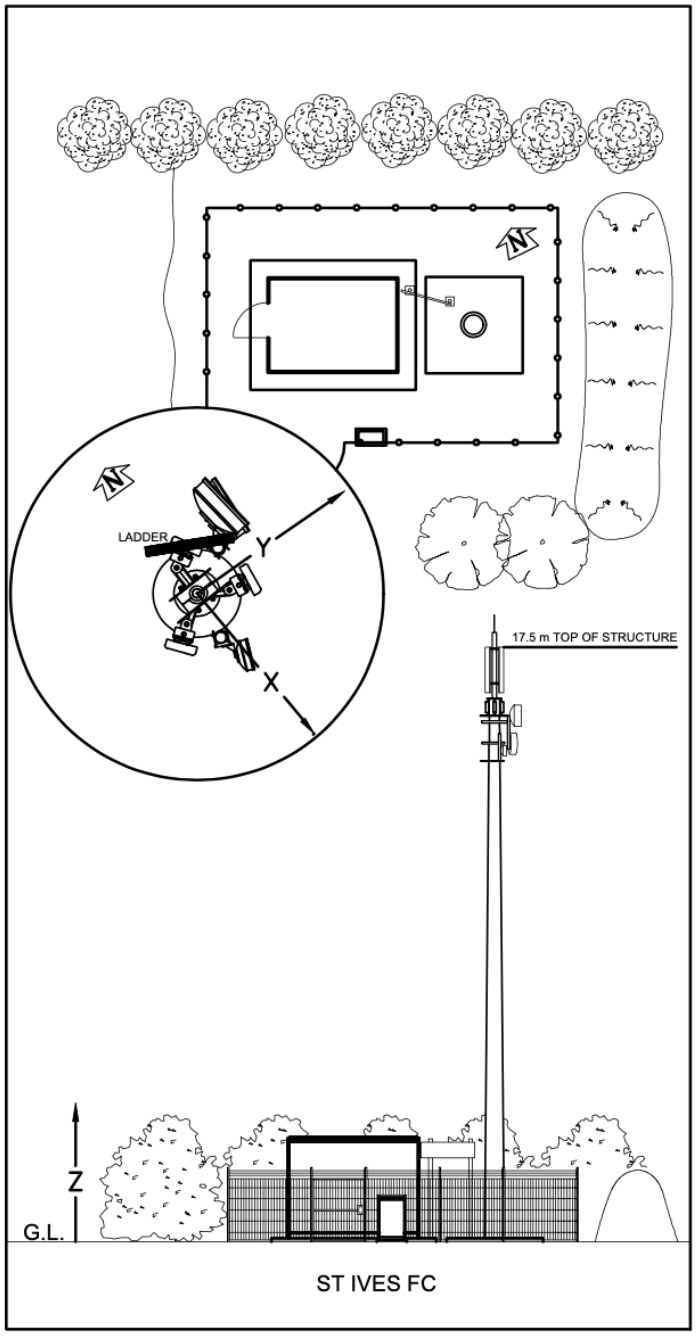

Figure 6-3 Elevation and plan view of monitored site. St Ives FC.

Arqiva provides a complete knowledge of geometric and mechanical characteristics of the mass and stiffness of the structure and substructure (foundations), masses of existing antennas given by manufacturer, and soils investigations carried out after geotechnical field tests. The structure is a monopole comprising S275J0 steel for main core and plates of 25 mm thick S355J2. There are two sections: a tubular tapered panel between ground level and 14.3 m and a triangular steelwork headframe suitable to accommodate mobile antennas. Also, there is an external spine ladder with latchway fall arrest system. For loading, three antenna panels are installed at the upper part, with a small plate antenna at 14.3 m, with all necessary cables run internally. This structure is joined to the foundation thorough a flange plate and 12 Class 8.8 M24 bolts, without grouting. The foundation is a concrete block of dimensions 3.6 x 3.6 x 0.85 m as Table 3-1. The chosen site was proposed for a decommission and replacement under the implementation of 5G.

The equipment was installed in the morning of 22nd of November 2018 and retrieved on 5th of February 2019 by two engineers and two expert climbers, fixing the anemometer with necessary steelwork at 17.5 m and the accelerometers at 14.5 m. No further climbing was allowed to avoid inclusion of non-ambient loading in the monitoring period.

Table 6-1 Selected site details

Site Name	Structure Type	Height	Foundations	Top frame	Cable Location
St Ives FC	Portasilo	17.5 m	Pad: 3.6x3.6x0.85m	Mounting Pole	External

6.3.2 Full-Scale Wind Loading and Response

The 76 days of continuous measurements over the length of the monitoring were divided into consecutive data files of 10-minutes time frame. Each file comprises five channels: acceleration records of both accelerometers, wind speed, wind direction and temperature.

The data extracted were plotted along a time line for the whole monitoring, extracting mean values and gust factors for wind analysis. The time line of wind speed appears in Figure 6-4 showing some high wind speeds, exceeding 40 m/s for a 3-s gust with a

maximum of 48 m/s. Those high values come from a time period with several storm events such as Storm Deirdre between 14th and 15th of December 2018 with large impact based on severe gales and heavy rain in the southwest of the UK, resulting in a wind gust of 35.5 m/s at the Welsh coast. Some other events were caught between the end of January and beginning of February 2019 as shown in Figure 6-4. A wide range of low mid and high wind speeds was also found, providing enough load cases to extract for the analysis, satisfying the purpose of the SHM by capturing a wide range of ambient excitation. The bottom plot in Figure 6-4 shows the structural response recorded by the two accelerometers. There is a good correlation between accelerations and wind speed data, suggesting a clear along-wind response.

In terms of wind directions, the wind rose, Figure 6-5, does not show the typical expected shape in the UK where the strongest winds are predominant from the south-west quadrant. In this location, there are topography aspects which negate the existence of this main directions, having up-hill slope resulting in strongest winds from the north-east direction. In order to examine the nature of the turbulence in the incident wind it is conventional to plot gust wind speed as Figure 6-4. Comparison of mean and peak values in this plot suggests that high intensity of turbulence is found for the range of mean wind speeds.

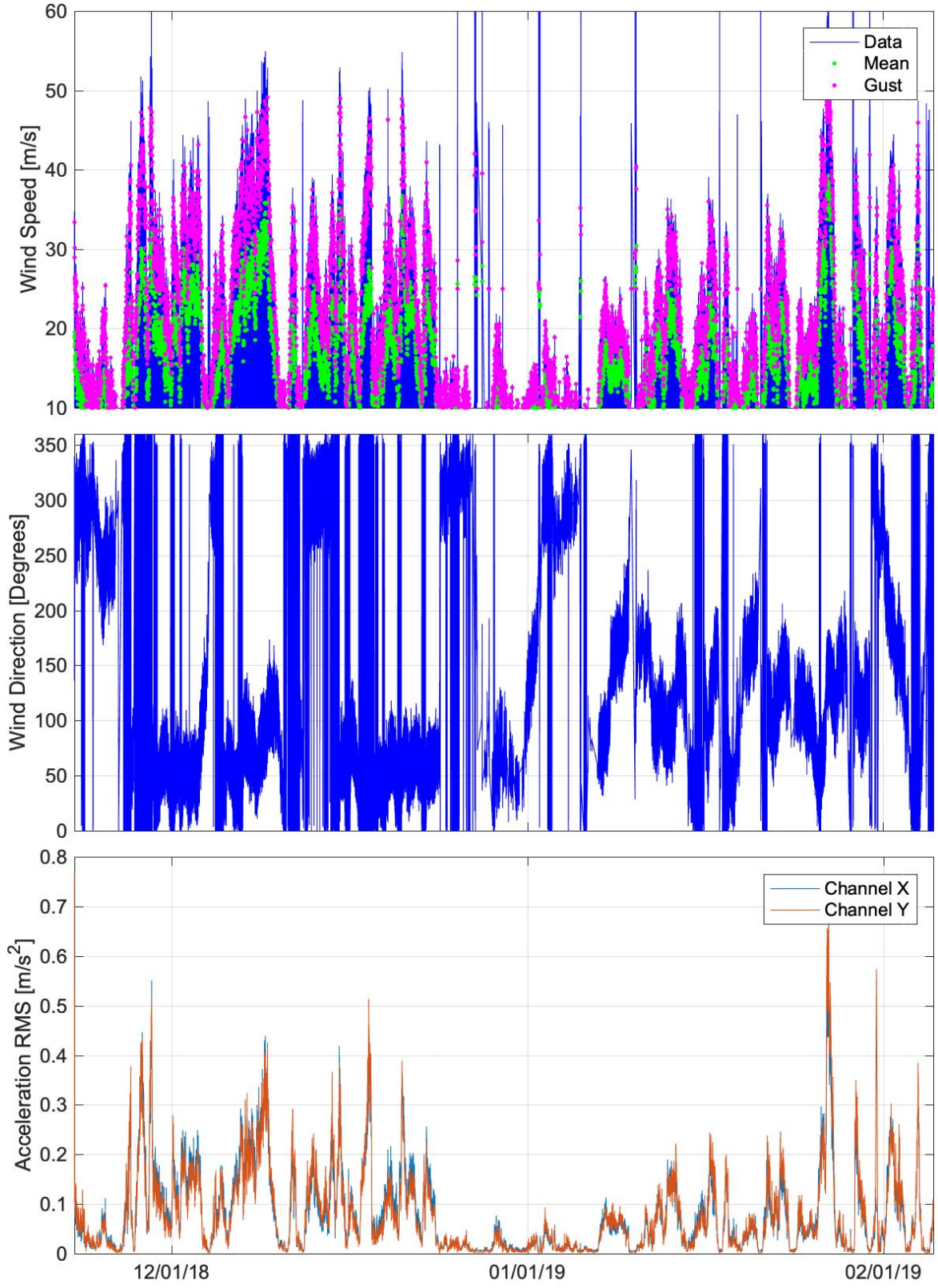

Figure 6-4 Monitoring data in St Ives FC. (Top) Wind speed data. (Raw, mean and gust). (Centre) Wind direction. (Bottom) Response captured by accelerometer.

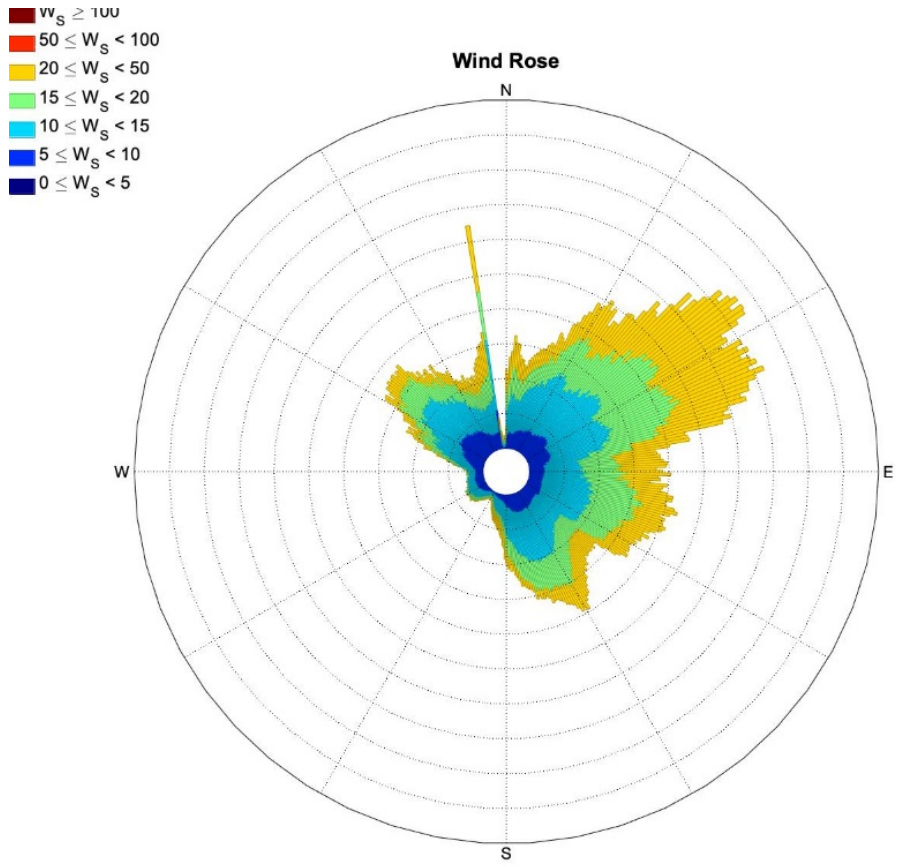

Figure 6-5 Wind rose obtained from anemometer in St Ives.

The results agree with expectations. The anemometer at 17 m is not high enough to avoid high turbulences of wind speed coming from the roughness of the terrain. Current formulations managing dynamic performance due to buffeting apply a gust factor, an approach that works properly for high structures like skyscrapers, high lattice towers or high guyed masts where wind tends to have relatively low turbulence. Monopoles operate in high turbulence environments which dominate the response behaviour.

Figure 6-6 shows the correlation between wind speed and response data. This behaviour is typical for dynamic structural response to turbulent buffeting via along-wind excitation. Figure 6-6 shows no evidence of high responses for wind speed ranges between 6 - 20 m/s, where vortex shedding [101] would appear for second and third pairs of modes in a frequency range between 2 – 5 Hz as Eq. 2-18 using the Strouhal number defined in EN1991-1-4: Table E.1 [26]. The structure responded only under along-wind turbulent buffeting loading.

The data provided by the SHM system were sufficient to characterise the full range of dynamic behaviour under wind loading. The next section will describe the application of several OMA methods, implemented in different software, to understand the evolution of dynamic modal properties at different response levels and varying ambient excitation during the monitoring. Experiences from this exercise would be relevant for similar SHM systems on slender communications structures.

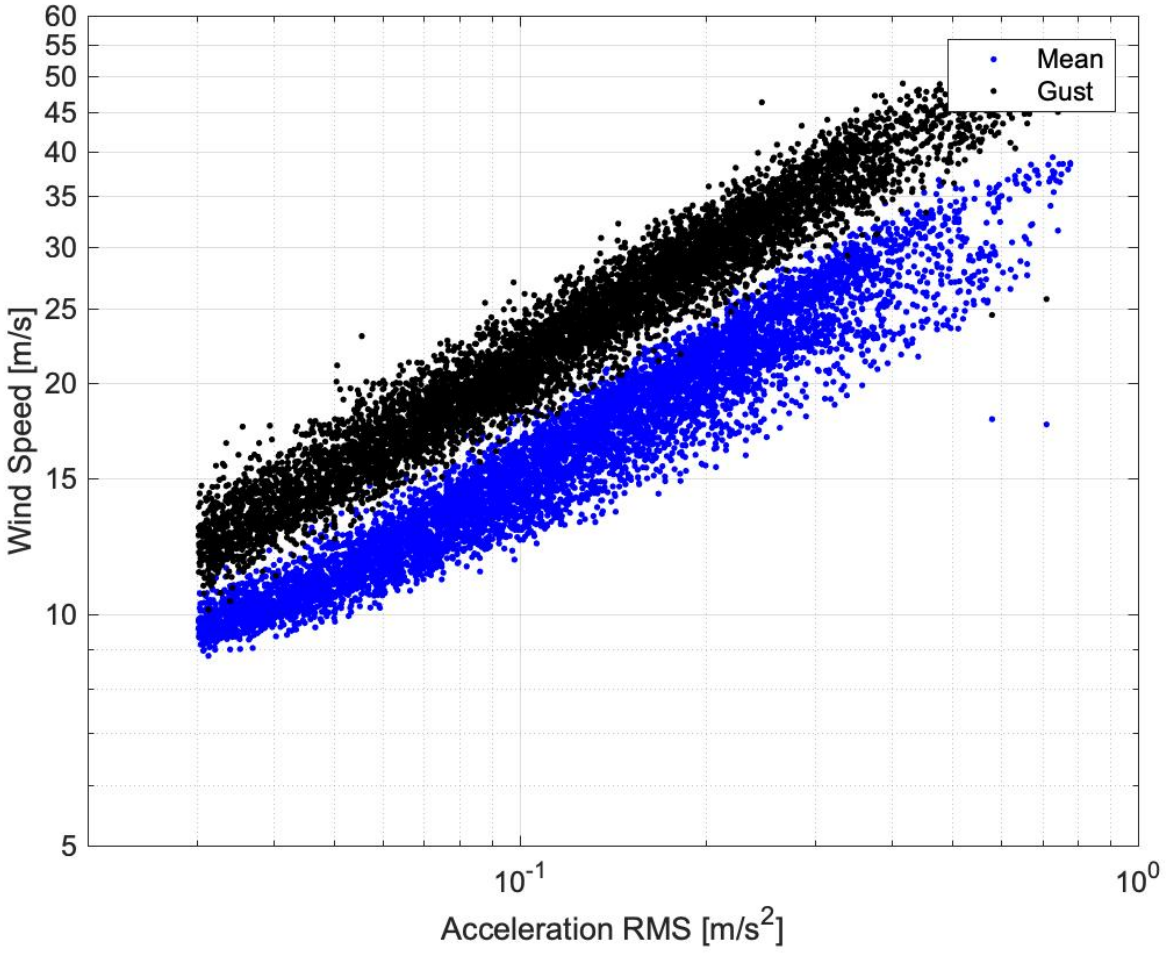

Figure 6-6 Diagram of relationship between RMS and gust and mean wind speed.

6.4 Operational Modal Analysis

The application of operational modal analysis (OMA) is attractive in practice because it avoids the logistical challenges of using mechanical shakers, using service wind-ambient loading.

6.4.1 Power Spectral Densities and their Singular Value Decomposition

The study of frequency domain tools like power spectral densities (PSD) of the response is a common starting point for investigating modal properties via OMA. A frequency band with PSD exhibiting dynamic amplification is a reflection of resonance and hence potential modes, but it does not directly indicate the number of modes. The latter can be investigated via the singular value spectrum, i.e., a plot of singular values of the cross-spectral density matrix. Within a frequency band, the number of lines taking the shape of dynamic amplification indicates the dimension of the subspace spanned by the mode shapes, which is often equal to the number of modes in the band.

The structural response of a monopole under normal buffeting is defined by an oval/elliptical horizontal movement with major axis in the along-wind direction. The circular geometry of the shaft along its height, and the asymmetries found on the structure like the ladders, internal and external feeder cabling and lump-mass ancillaries result in a pair of related modes with close frequencies. These correspond to the main cantilever flexural bending modes as shown on Figure 6-7 extracted from St Ives monitoring. The second and third modes expected between 3 and 6 Hz do not appear clearly on the singular value spectrum; they might be excited under aeroelastic effects or extreme wind event. Some ‘fake’ peaks are found due to analogue of transients (spikes, shifts) from AC equipment which are highly dissipated with high responses.

Bayesian OMA method (BAYOMA) has been implemented to track the MP under ambient loading and yield the ‘most probable’ MP and ‘posterior’ (i.e., given data) variance that measures the identification uncertainty. The posterior variance or uncertainty bound informs about the identification uncertainty given a particular set of data but not the variability of MP over the duration of the time frame. BAYOMA needs to be investigated in an ensemble manner based on the identification results of different data sets.

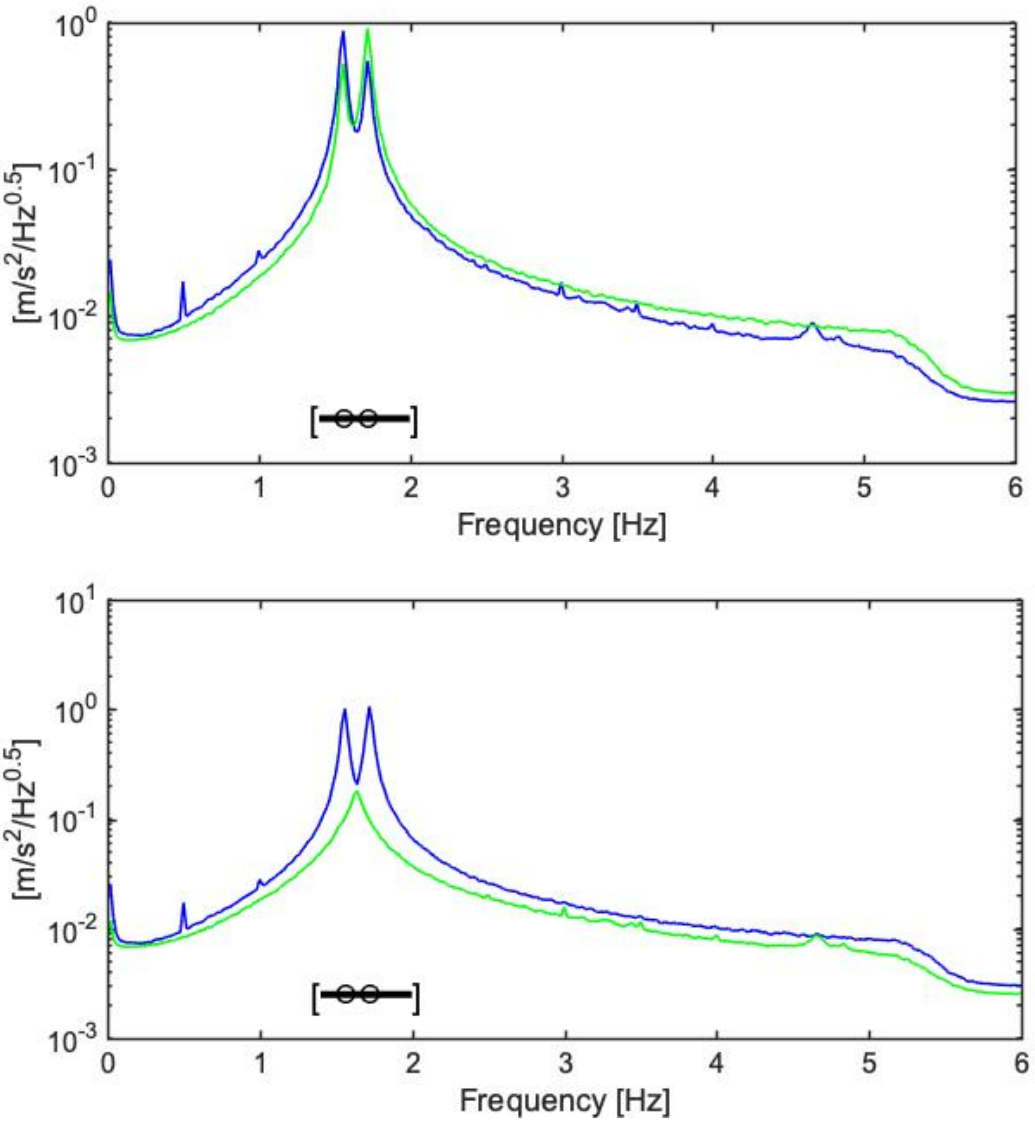

Figure 6-7 Power spectral density and singular value spectrum of ambient response data spectra (blue and green), with corresponding mode frequencies identified by operational modal analysis (OMA) of initial assessments. Error bars indicate frequency bands manually chosen for BAYOMA identification and dots indicate extracted mode frequency (most probable values, MPV).

The main purpose of this kind of monitoring is to provide more knowledge about the ambient loading related to wind in transient and rapid changes, analysing likely high response under buffeting and unlikely high response under vortex shedding. When there is clear time-variation of response signals due to changing modal properties, with impact on stationarity requirements, the T_{fr} of the evaluation window for OMA should trade a balance between identification uncertainty (the longer the better) and modelling error especially with regard to stationarity (the shorter the better). T_{fr} of 10 minutes was found adequate to capture environmental wind variations while obtaining

modal estimates with acceptable quality, and it is a conventional value for mean wind speeds in some codes.

6.4.2 Bayesian OMA

BAYOMA [102, 103] works in the frequency domain through the Fast Fourier Transform (FFT) of ambient vibration time series on a selected frequency band covering the modes of interest. The FFT in the selected band is used directly without windowing or averaging. The FFTs outside the selected band are not used and hence do not affect identification results. Given information from data and modelling assumptions, the uncertain MP have approximately a joint Gaussian distribution. The mean of the Gaussian distribution is the most probable value (MPV), which minimises the negative log of likelihood function (NLLF). The covariance matrix can be calculated as the inverse of Hessian of NLLF at the MPV. Efficient algorithms and computer codes have been developed for the computation of MPV and covariance matrix. Each diagonal entry of the covariance matrix gives the variance (σ^2) of the corresponding property. In this study, the coefficient of variation (c.o.v.), i.e., ratio of standard deviation σ to the MPV, will be reported as a dimensionless measure of identification uncertainty.

BAYOMA involves solving an optimisation problem to obtain the MPV and the algorithm is iterative in nature. It is often more time consuming than explicit identification methods like SSI, especially for close modes. Well-separated modes can typically be handled in a matter of seconds while the computational time for close modes ranges from a few seconds to a few minutes, depending on factors such as the number of modes (the more the longer) and potential modelling error in data (the higher the longer). Recent developments in [104] provide analytical formulas for assessing the identification uncertainty of MP in terms of test configurations, which is of practical relevance in ambient vibration test planning. Some applications of BAYOMA are presented in [105 – 107].

As indicated in Figure 6-7, the MPV of natural frequencies for the first two modes are taken (hand-picked from figure) to be 1.556 Hz and 1.723 Hz. The frequency band whose FFT will be used for identifying the modes are taken to be 1.4 - 2 Hz.

As for other OMA methods that assume time-invariant and stationary models, applying BAYOMA to a single time window does not directly allow one to quantify the variation

of MPs over an extended duration. Currently a simple empirical way to track variation is to apply them to different T_{fr} and track the results accordingly.

6.4.3 Time variation and correlations in MP using BAYOMA

The coloured and possibly time-varying nature of wind speed or human forcing (e.g. due to climbing the mast) changes the spectrum of ambient dynamic loading. Other ambient factors such as temperature and humidity can lead to variation of MPs and collectively result in non-stationary response. The diagnosis of structural issues identified via changes in MPs, and model updating have been a particular problem under investigation in structural dynamics. To implement the method over the whole set of data, the T_{fr} is a key input that affects the estimation of MPs and the relationships among load and response parameters.

To study the MPs behaviour under wind-ambient loading, one requires data that are strongly non-stationary over the duration while being sufficiently stationary within T_{fr}. Long term monitoring is one option to meet both requirements. In the present study, storms with high gust wind speed and buffeting response have been captured by the monitoring data.

Figure 6-8 shows the response of St Ives from 9th to 10th of December of 2018, during passage of Storm Deirdre for three different values of T_{fr}. In first row plot, responses follow wind speed, as was confirmed before on Figure 6-6. Second, third and fourth row plots show estimations of MPs (Natural frequency, modal damping and mode shape orientation) for both modes with error bars representing $\pm 1\,\sigma$ identification uncertainty about MPVs. Both vertical axes are utilised to visualise properly the variation of frequency and mode shape direction for both modes. Using the same frequency range among the plots highlights the differing ‘closeness’ as well as the inherent MP variation.

The centre column shows also estimations of MPs for T_{fr} = 10 minutes segment. Slow decrements of frequency are found in both modes for rising response levels. Damping exhibits higher values due to either amplitude dependency of structural damping or the aerodynamic damping contributions. However, the difference between mode direction changes little (the angles shown in the bottom plot track each other) showing much higher dependency of the geometry factors rather than possible ambient loading characteristics.

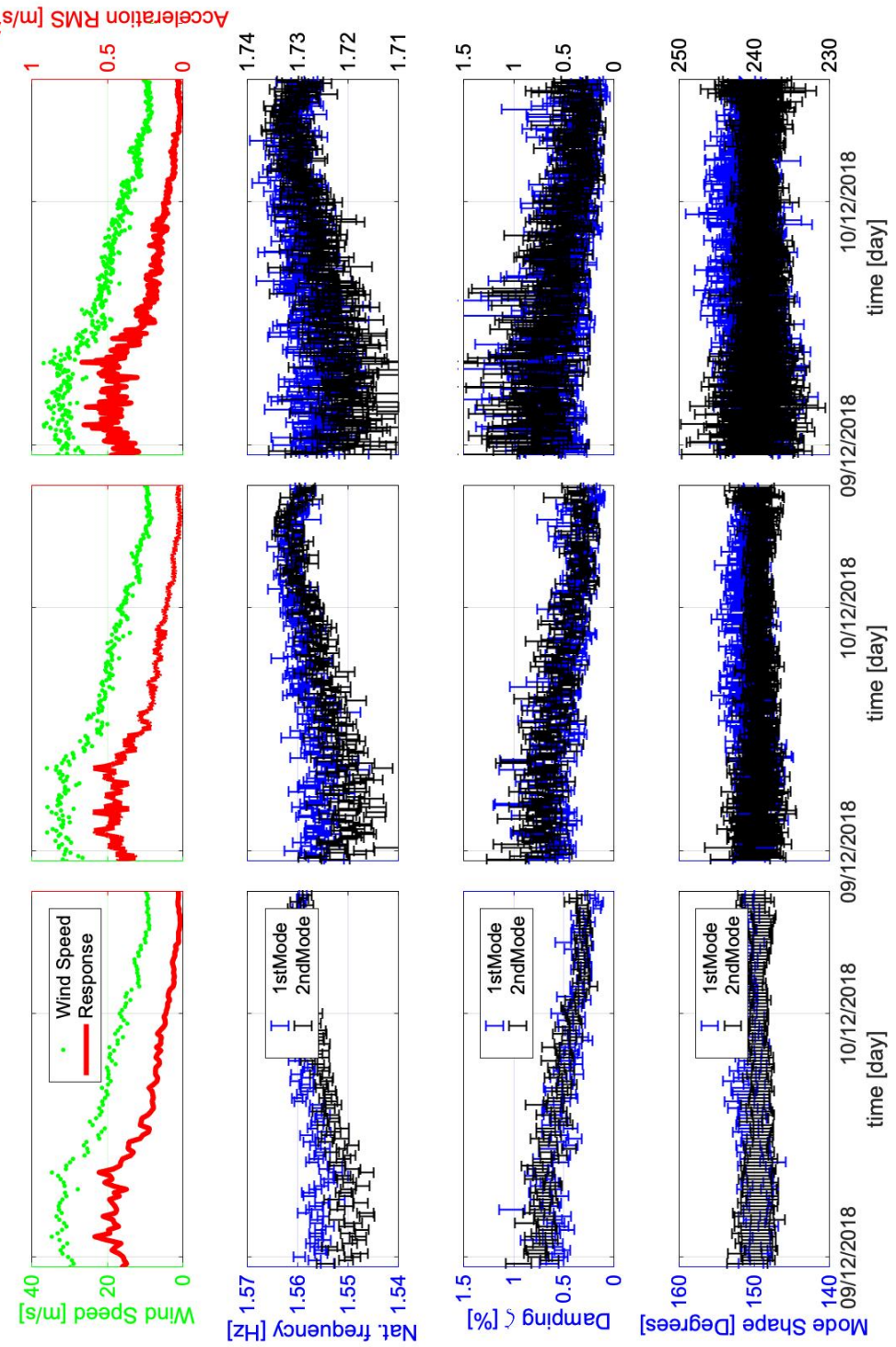

Figure 6-8 Mean wind speed (green line) and response (red line) obtained in St Ives FC during Storm Deirdre, 9-10 Dec 2018. Application of OMA: BAYOMA on response data St Ives FC. (Left to right) Frequency, damping and mode shape (reference angle from accelerometer-Channel X, anticlockwise positive) for first (blue line-bottom axis) and second mode (black line-top axis) shape. Size of error bar reflects 1σ identification uncertainty on estimation. Top side. T_{fr} = 5 min. Centre. T_{fr} = 10 min. Bottom side. T_{fr} = 20 min.

Figure 6-8 also presents BAYOMA analyses applied to data during the same selected period using time segments of T_{fr} = 20 (bottom row) and T_{fr} = 5 min (top row). A coefficient of variation, c.o.v. < 0.2 for damping estimates could be considered as acceptable criteria: T_{fr} = 5-minutes provides c.o.v. > 0.2, while for T_{fr} = 20 min keeps c.o.v. < 0.1. The effect of changing T_{fr} can be seen in the error bounds in the plots. The same slow variations in MPV (with similar clear and consistent trends) are shown for the three segment lengths and clearly the longer segments have reduced variance (which goes approximately with square root of data duration). There appears to be no greater uncertainty where the frequencies (or rather their MPVs) are changing faster with time.

The identification uncertainty associated with an MP estimate from longer duration data T_{fr} = 20 min of merged data would not reveal such variation since it assumes time-invariance over the duration. Similarly, variation of each mode shape MPV in polar coordinates is improved with longer data. One motivation to monitor a structure is to identify factors (such as load variation) that govern the dynamic behaviour in terms of MPs. In this case, shorter T_{fr} can capture the effect of faster changes in loading and so the selection of T_{fr} becomes an important issue. After analysing the previous concerns T_{fr} = 10 minutes is found to agree with good correlated damping, while being able to achieve high percentages of the peak responses of the system. Using T_{fr} = 10 minutes is also consistent with wind engineering practice where it is a standard averaging time for wind speed statistic used in structural engineering.

6.4.4 Frequency & Damping Estimation

The correlation between response data, wind loading and variation of MPs (stiffness and damping) can be seen in Figure 6-9 and Figure 6-10.

In terms of frequency, the trend of both modes shows an amplitude dependency behaviour at high levels of excitation. The restoring forces will exhibit a nonlinear behaviour which might be classified as a softening characteristic [53]. Similar Portasilo monopoles have experienced structural problems due to dynamic behaviour in the last decade, e.g. due to fatigue failures at base inner welded connections. Figure 6-9 shows lower frequencies than calculated in analytical models during dynamic assessments, i.e. Portasilo monopoles tend to be more flexible than estimated by numerical models. This issue might involve a possible deterioration due to the inner

connections, or wrong detailing provided by manufacturer which must be considered to modify and validate current models. Structural diagnosis can be carried out by comparison with other monitoring systems or existing previous data.

The difficulty of estimating damping is commonly recognised. Three main origins of damping include: 1) structural damping, appearing without external loading influence due to material, connections, construction method or foundation; 2) aerodynamic damping induced by the interaction of structure motion with wind; and 3) external damping provided by specific dampers. Currently, a common value of structural damping and a modal aeroelastic approach are given by different literature advising a linear increment of total damping with mean wind speed.

Figure 6-10 shows results reflecting the mentioned linear variation of total damping with response, although existing standards do not take into account the response based on two modes. Structural damping could be extracted from damping values under small excitations with minimum wind influence. At that level, BAYOMA provides high confidence in a constant term of ζ = 0.4 %, onto which amplitude and wind dependent contributions would be added.

Also, Figure 6-10 shows an expected linear aerodynamic component of damping related with levels of mean wind speeds as the Institution of Lighting Engineers (UK) Technical Report Number 7 [31]. However, existing methods of assessing aerodynamic damping do not agree with obtained values. This issue involves the redefinition of wind resistances including drag factors.

Both properties show a disagreement in comparison with recommendations (lower frequency, higher structural damping and lower aerodynamic damping) which compromise current structural assessment with higher dynamic augmentation factor used among the quasi-static procedure suggested by the main Standards. In addition, elements such as the amplitude dependency of natural frequency or the existence of a secondary mode show the crude code approaches to be inappropriate.

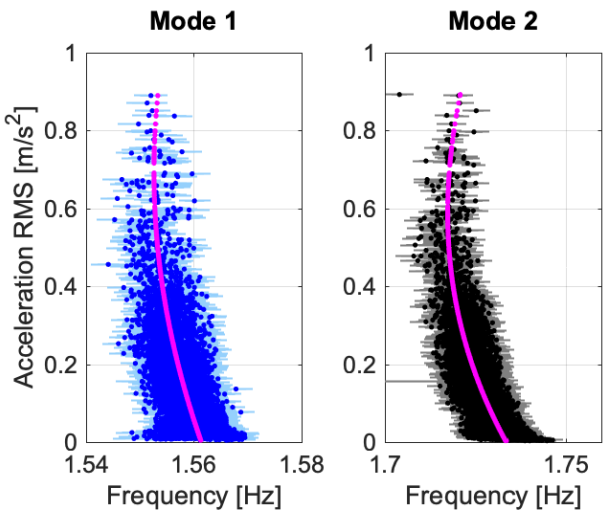

Figure 6-9 Variation of Frequency with Response, BAYOMA.

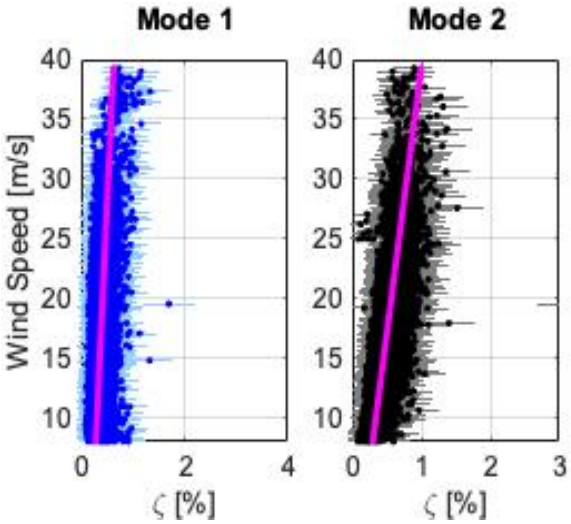

Figure 6-10 Variation of Damping with Response, BAYOMA.

6.4.5 Mode Directionality

The identification of the mode shapes is a challenging issue in symmetric structures. For buildings, structural modes are not generally aligned with structural axis of symmetry due to complexity. Also, previous experiences in flexible lattice towers show strong dependence on (mis-)alignment of the mass and structural features along the height of the structure.

For Monopoles with circular section in plan view, the predominant mode directions are theoretically arbitrary and in reality they are sensitive to asymmetries in stiffness, mass and boundary conditions. Monopoles maintain symmetry along the shaft of the monopole with necessary openings and steelwork introducing minor symmetry disruptions. Variation in steel and base grout stiffness, mechanical fixing between courses (by keying and bolts) or foundation-soils softness may not have significant effect compared to the necessary access steelworks such as ladder and anticlimbing elements that breaks the alignment adding stiffness to some specific directions. This misalignment is even more evident with mass distribution: heavy antennae at different levels and in different directions disturb the symmetry. In addition, feeder cables, normally run internally, can be externally installed and consequently promote a specific orientation for each mode. All these factors result in two close-frequency orthogonal main modes-directions, the lowest frequency mode with less stiffness aligning usually perpendicular to ladder direction.

As shown in Figure 6-1 and Figure 6-8, St Ives Monopole has all the aforementioned ingredients. New monopoles specifically designed to be installed in cities avoid access requirements and shrouded elements which make them to appear totally symmetric. In those cases, hidden panels are not symmetric which induce the differences between modes. However, both modes will appear closer than any other types.

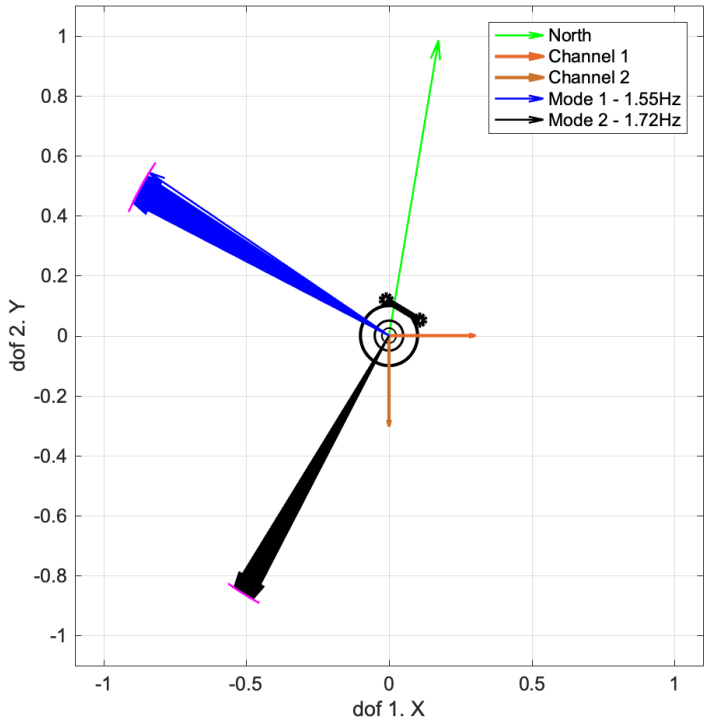

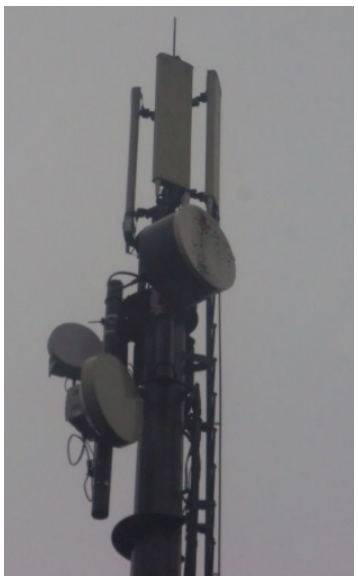

Figure 6-11 Main bending cantilevered modes in St Ives monopole during monitoring. Picture of External cabling and ladder installation.

The St Ives FC mode shapes obtained by BAYOMA are presented in Figure 6-11. The MPVs are illustrated as vectors which are consistent with orientation shown in Figure 6-8. Being vector-valued the dominant identification uncertainty of each mode shape is obtained from the eigenvector (maximum eigenvalue) of its posterior covariance matrix multiplied by the square root of the eigenvalue. This ±1σ uncertainty is shown as (magenta) lines, which are roughly perpendicular to the vector tip and parallel to the coupled mode. The blue (and black) arrows show the most probable mode shape directions from different data sets. Their variability is an aggregate of identification uncertainty (in each data set) and possible variation in the actual mode shape directions (during different data sets). In the present case the variability of the blue arrows is roughly of the same order of magnitude as the identification uncertainty suggested by the magenta arrows. This suggests that the variability over different data sets is not significant. Both modes appear to have a narrow band with low uncertainty which might suggest a non-wind-directional dependency.

6.5 Implementation of Alternative OMA: SSI in ARTeMIS

To provide a supplementary qualitative view of the identified modal properties (e.g., for counter-checking), Stochastic subspace identification (SSI) technique [108, 109] that is common in the literature was also implemented. SSI is based on a time-domain state-space model of successive data. The state matrices are estimated by means of regression, from which the MPs are back-calculated assuming structural dynamics. SSI is attractive in applications as the calculations are explicit, requiring no iterations and being immune from convergence issues. Operating in the time-domain, the unknown excitations and instrument noise are effectively assumed to have constant spectral characteristics from DC up to the Nyquist frequency. As modal properties are back-calculated from estimated versions of state matrices they need not obey structural dynamics, however, which is a source of modelling error. Naturally, the effect on the identified MP depends on how well the state matrices are estimated, which in turn depends on factors such as data length, signal/noise ratio or how well the data agree with structural dynamics.

In this study, SSI was executed on data resampled at 12.8 Hz with order up to 100 poles through ARTeMIS Software. Three common techniques were used, including the unweighted principal component (SSI-UPC), principal component (SSI-

PC) and canonical variate analysis (SSI-CVA). Similar comparison exercises have been presented in [100, 110 – 114] describing two decades of application of OMA to investigate time-variation of MPs of important civil engineering structures.

As part of the SHM, the collected response time series were processed using an OMA procedure coded in MATLAB that fits a state space model to the monopole structure responses driven by ambient excitation [115]. As mentioned from existing experiences, this exercise expects to obtain a non-complex power spectral density with a pair of close modes between 1 - 2 Hz, and second and third pairs between 3 – 6 Hz. This method is applicable to closely spaced modes. Each setup leads to a stabilization diagram such as Figure 6-12. Finally, both most remarkable modes are clearly identified, f_1 = [1.54 - 1.58] Hz and f_2 = [1.7 - 1.75] Hz. Results from SSI under low response are rejected and not taken into the analysis estimation.

6.5.1 Discussion between OMA Identification Systems

The St Ives SHM system provided 76 days of synchronized wind and response data that are helpful to compare how current design static and dynamic approaches predict the behaviour of slender monopole structures. This set of data is probably one of the only studies on monopoles at the present state of the art: such full-scale data with reliable OMA provides essential addition to current knowledge to support advances compared in code provision.

As well as improving the analytical model validation and operational model assessment, the exercise demonstrates the competences and restrictions of the selected techniques for analysing data from future permanent monitoring systems in similar communication structures. For comparison reasons only high response segments above rms 0.580 m/s^2 are presented here. This results in 400 data segments of 10 minutes and correspondingly 400 sets of identification results. Each set of identification results includes, for each modal property, μ = posterior MPV (BAYOMA) or best estimate (SSI) and σ = standard deviation (BAYOMA/SSI) that measures the identification uncertainty. Specific coding was built to link MATLAB and ARTeMIS making the analysis and the collection of the results more feasible.

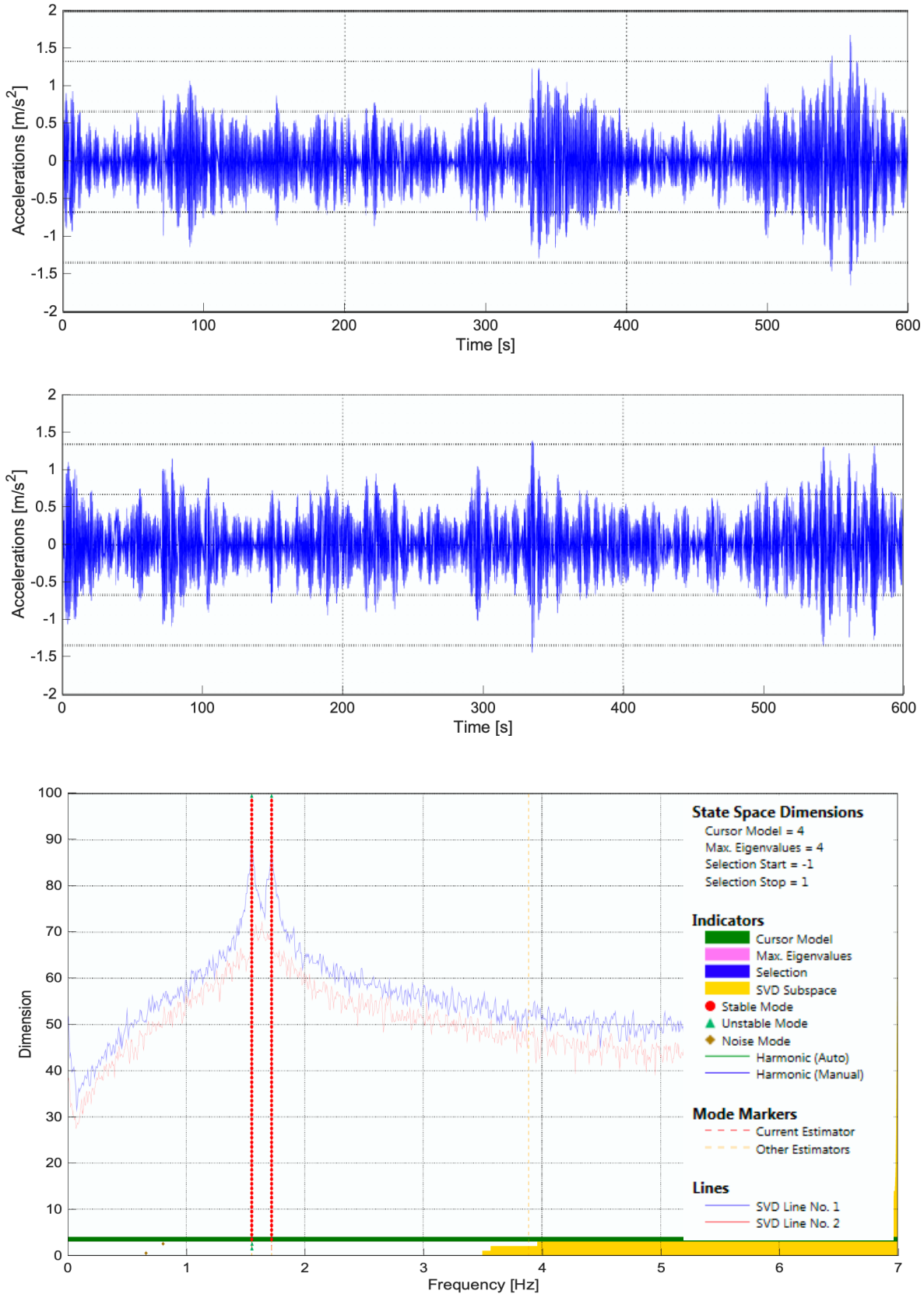

Figure 6-12 Analysed response data and ARTeMIS Stabilization SSI-PC diagrams and PSD applied to selected data in St Ives FC.

Table 6-2 gives a representative picture of the identification results in terms of the average values of μ and σ over the 400 sets of results. The results are plotted in Figure 6-13 with respect to acceleration rms on the vertical axis. Implementation-wise, BAYOMA requires initial guess of natural frequency and selection of frequency band covering the mode(s). SSI requires the choice of Hankel matrix size and order of state-space system. The average values of μ from SSI and BAYOMA are similar for both natural frequencies and damping ratios. The same is not true for σ, however, with values from SSI generally lower than those of BAYOMA. A formal analysis of this difference is out of the scope of this work, as the methods operate on different domains (time vs frequency) and are based on a different set of assumptions (e.g., state-space vs structural modal, white noise in time vs flat PSD on selected band) and effective data bandwidth used (from near DC to Nyquist in SSI vs the resonance band in BAYOMA). As a standard result in classical statistics, if there is no modelling error then the ensemble variability of any unbiased estimator is always greater than the Cramer-Rao bound, which coincides with the variability of the maximum likelihood estimator (MLE). The MLE is numerically equal to the MPV of BAYOMA. Aside, recent work allows the value of σ to be explained in terms of test configurations, in the context of BAYOMA [116].

Table 6-2 Frequency and Damping estimation extracted from ARTeMIS-SSI and BAYOMA identification method. The value of μ (posterior MPV or best estimate) and σ (identification uncertainty) presented here are average values over identification results of 400 data samples to give a representative measure.

	Mode 1				Mode 2			
	$\boldsymbol{\mu(f)/Hz}$	$\boldsymbol{\sigma(f)/Hz}$	$\boldsymbol{\mu(\zeta)/\%}$	$\boldsymbol{\sigma(\zeta)/\%}$	$\boldsymbol{\mu(f)/Hz}$	$\boldsymbol{\sigma(f)/Hz}$	$\boldsymbol{\mu(\zeta)/\%}$	$\boldsymbol{\sigma(\zeta)/\%}$
SSI-PC	1.5543	0.0002	0.9167	0.0127	1.7194	0.0002	0.8090	0.0138
SSI-CVA	1.5538	0.0015	0.9130	0.0791	1.7194	0.0010	0.7677	0.0649
SSI-UPC	1.5538	0.0001	0.9271	0.0085	1.7195	0.0002	0.8101	0.0131
BAYOMA	1.5532	0.0021	0.7423	0.1488	1.7185	0.0023	0.7972	0.1677

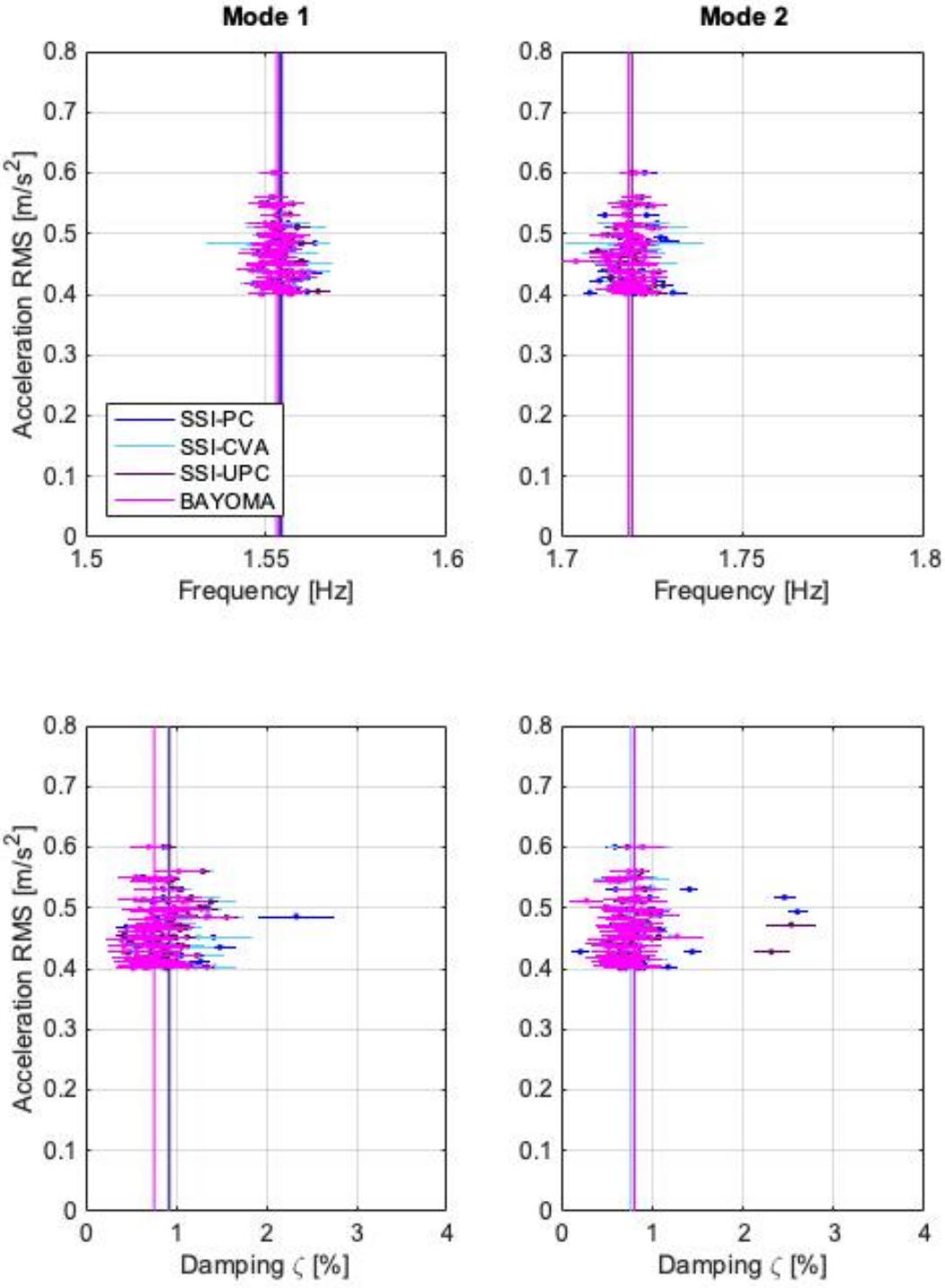

Figure 6-13 MP estimation above RMS 0.580 m/s^2. ARTeMIS-SSI and BAYOMA.

6.6 Conclusions

Under the loading changes demanded by new mobile technologies, better knowledge of dynamics in communications structures is necessary. A Structural Health

Monitoring system has been satisfactorily developed for telecoms monopoles with height ranging 15 - 30 m. This allows the present study to analyse the wind excitation-response relationship, to provide better understanding of structural behaviour in wind-ambient loading and to investigate the evolution of MP with different levels of excitation.

A large dataset of acceleration come from installation on a monopole in St Ives, Cornwall, has been analysed. Modal properties of the first few harmonics along two principal directions have been identified using a Bayesian OMA method (BAYOMA). In addition to the most probable value, the method also provides the identification uncertainty, which is important for downstream investigation of potential relationships. As is conventionally done, structural and statistical wind load properties are assumed to be constant in each short time window for analysis, where a duration of 10 minutes has been found to balance identification uncertainty (the longer the better) and modelling error (the shorter the better).

The performance of modal properties during a wide range of wind events and consequent response amplitude provide important features to study in further structural engineering valuations. Stiffness exhibits a softening nonlinear amplitude dependence behaviour on both main modes. Damping show a clear linear wind-speed dependency, which advice important aerodynamic contributions with similarities with some national codes and shortest value in calm weather at 0.4 % taken as structural damping value.

Consistent with physical intuitions, the fundamental first mode shape directions for monopoles are predominantly aligned according to external elements such as access ladder or cabling. Symmetric geometry does not provide significant evidences, although, external elements defines a specific orientation for each mode of the main cantilevered bending mode shapes.

The monitoring results obtained under BAYOMA, and compared to stochastic subspace identification on standardised software, present opportunities for further studies in terms of understanding dynamic response in monopoles involving codes reformulation, structural diagnosis and model validation.

Preface to Chapter 7

The application of OMA methodologies based on reliable data can now verify the current methods of assessing damping and the validity of the existing quasi static approaches. In addition, the consequences of a new understanding of aerodynamic damping affect the current definition of standardised wind resistances and local drag factors.

The following chapter is a journal paper entitled “Dynamic parameter estimation from operational modal analysis of monopole telecoms structures.” which was submitted to Engineering Structures (ENG-STRUC). It analyses field data from 2 monopoles structures under wind-ambient and human forcing loading. The results conclude how far the current methods of assessing damping are from current behaviour and the straight consequences on estimations of dynamic augmentation factors given by literature.

The concerns given by the paper should change the point of view of several national codes in terms of dynamics in general and damping in particular.

Chapter 7 Dynamic Parameter Estimation from Operational Modal Analysis of Monopole Telecoms Structures

7.1 Introduction

Telecom structures have become increasingly common in the last two decades, occupying rooftops in urban areas while in the form of short lattice towers and monopoles in other more rural locations. Many short (less than 30 m) telecom structures have been deployed in these areas to achieve the necessary coverage. Emerging 5G technology in combination with recent mobile technologies and older ones like radio and broadcasting are challenging the current structural capacity of structures and foundations when evaluated using existing design codes. To meet new requirements, towers must hold new antennas that are roughly three times heavier and two times larger than the current equipment. Furthermore, additional boxes and cabling can potentially amplify the tower loading even more.

Arqiva, the owner of one of the biggest portfolio of telecom structures in the UK, will address this load issue by assuring that structures are designed to avoid serviceability and structural failures. The company has implemented a significant programme to strengthen existing structures and build new installations to satisfy customers and users. As part of this programme, this chapter analyses the most relevant modal properties (MPs) of monopole structures to be examined during structural assessments revising the perspective and veracity of the current codes from dynamics perspective. This knowledge will aid in the review of national standards, improve internal structural action policies, and provide new options for strengthening (such as damper installations) on communications structures with similar characteristics.

Slender structures with very flexible behaviour under horizontal loading tend to be dynamically wind sensitive. Wind-induced vibrations arise from two main mechanisms: along-wind gust buffeting loading and across-wind vortex shedding excitation [4]. Both of these mechanisms can affect the ultimate design loadings and could lead to structural failure due to fatigue issues. Such issues could reduce the structural

reliability and service life, and can rapidly lead to damage in less well engineered connections. To manage and model these dynamic responses, the dynamic properties of the structure (i.e., natural frequencies, typical mode shapes, and damping) must be defined.

Structural assessments must currently follow standards or codes which were themselves built up from previous experiences. These standards comprise a vast set of rules that vary between countries, and these rules, which pertain to dynamics, have not been reviewed since the establishment of the British Standards in the 1980s. Since then, and with more efforts in the last decade, technical experts of Group 4 of the International Association for Shell and Spatial Structures (IASS) have expressed concerns about the implementation of dynamics through the typical augmentation dynamic factors during quasi-static analysis and the necessary and recommended estimation of MPs.

Initial investigations have revealed serious discrepancies between modelled and measured natural frequencies, which shows either, difficulties in modelling connections, especially under poorly detailed, or considerable connection damage may already be present due to fatigue problems. Several recent critical failings have been attributed to this concern as shown in Figure 7-1.

Figure 7-1 Pictures of failed tree monopole in the UK in 2019. Provided by MBNL.

Damping is another particularly important issue. Design codes consider the mechanisms by which a structure absorbs energy during any movement; absorption may occur externally (via dampers), aerodynamically (due to the wind itself), through structural damping (arising from material distortion and friction between connections), and finally, through the foundations radiating energy into the ground. Existing damping

models were developed in the 1960s and 1970s and have limited application to today's slender structures so newer methods must be applied to improve damping knowledge. The use of obsolete damping models or estimation methods may lead to operators being mis-informed about the structure's remaining capacity, so this information is crucial to owners who must add new antenna payloads.

Finally, a better understanding of MPs will improve the feasibility of altering or strengthening structures by adding stiffeners or additional damping mechanisms. Such alterations would reduce the need for total structural replacement and may have significant commercial benefits.

This chapter presents an analysis of the responses of two different monopoles with ambient (wind) loading typical during service life and free decaying response under several conditions, with the purpose of more fully understanding their dynamic behaviour and assessing current recommendations.

For this study, MP analysis was conducted using response data recorded from two different monopoles (Figure 7-2):

Figure 7-2. Left: St Ives FC monopole. Right: Windmill Farm monopole.

- St Ives FC: This 17.5 m Portasilo monopole is considered one of the most flexible structures in the manufacturer's portfolio.
- Windmill Farm: This 17.5 m Calzavara monopole is one of the stiffest available on the market.

To understand the different contributions arising from structural and aerodynamic dissipation, two sets of data were recorded from each monopole. The first was an initial modal survey in which human pull excitation was used in calm weather to obtain free decaying responses; these data were analysed using the backbone curve methodology [55, 117]. The second set consisted of in-operation performance data measured via a structural health monitoring (SHM) system; the recorded ambient wind loading and response data were analysed using fast Bayesian operational modal analysis (BAYOMA) [118, 119].

Each method provides identification and estimation of the main MPs and captures the behaviour of the structure in terms of response, mode shapes, power spectrum density (PSD) of modal forces, frequency, and damping in the presence and absence of wind flow.

As a final purpose of this work, evidence from the analysis of the present results will be used to compare, discuss, and evaluate current codes and their recommendations, exhibiting serious concerns about their suitability.

7.2 Background Formulation

There are many methods to approximate the behaviour of monopoles. Each country provides a set of rules accepted for their design and research [37] has indicated that capacity can notionally be increased by over 20 % by simply using different code formulations. Uncertainty about wind loading, safety factors, or a structure's response leads designers to make conservative decisions, particularly if there is little guidance on some of the important variables for structural assessments, such as dynamic MPs.

Structural engineers generally prefer not to address communication structure dynamics if at all possible. In these structures, the implications of dynamics to the main structural response are large due to ambient excitations in sensitive frequency ranges (along and across wind) and/or the existence of important aerodynamic damping

forces. These concerns are normally covered within structural assessments by a dynamic factor which significantly overestimates mean wind forces.

All dynamics implications in monopoles can be extracted from the dynamic equation of motion with a single degree of freedom model for a slender, line-like structures, as defined in [9] and applied to communications structures in [61, 120]. Let the structure be classically-damped, i.e., its response, x_j, can be written as a sum of modal responses that satisfy their own (uncoupled) equation of motion.

Eq. 7-1

$$\ddot{x}_j(t) + 2\zeta_j\omega_j\dot{x}_j(t) + \omega_j^2 x_j(t) = p_j(t,z)/m_j$$

Here $\omega_j = 2\pi f_j$; f_j is the natural frequency (in Hz) of each mode, ζ_j is the modal damping ratio, m_j and p_j are the modal generalised mass and modal force under the corresponding analysed mode, j.

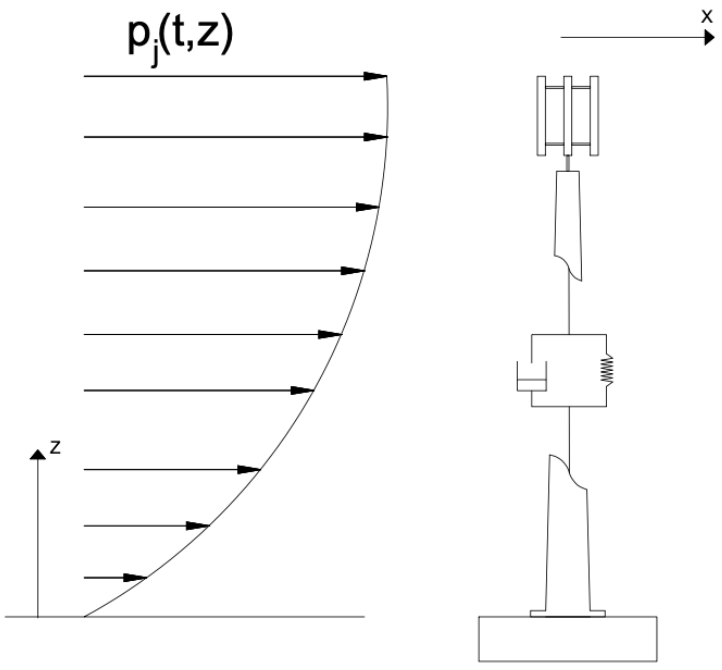

Figure 7-3 Schematic diagram of forces in monopoles as Eq. 7-1.

The force, $p_j(t,z)$, exerted by wind on the structure resolved along the normal direction as represented in Figure 7-3, derives from local pressure dependant as $\frac{1}{2}\rho_a v^2 c_D$, where ρ_a is density of air, v is free stream wind flow and, C_D, drag factor defined by the geometry of the structure. The free stream wind comprises mean and fluctuating

velocity components which produce on a body fluctuating forces which vary with time as:

Eq. 7-2

$$v^2(t,z) = \left(\bar{v}(z) + u(t) - \dot{x}_j(t)\right)^2 + \left(v(t)\right)^2 + \left(w(t)\right)^2$$

$\bar{v_z}$ is the mean hourly local wind speed; $\dot{x}_j(t)$ is the generalised velocity at any point along the oscillating structure; and $u(t)$, $v(t)$, and $w(t)$ are the local instantaneous fluctuating components of wind speed in the mean wind direction, normal to the mean wind direction, and in the vertical direction, respectively. It is assumed that $u(t)$, $v(t)$, $w(t)$, and $\dot{x}_j(t)$ are small with respect to $\bar{v}(z)$. Hence, the second order terms have been neglected (as is conventionally done) and Eq. 7-2 may be approximated up to first order by

Eq. 7-3

$$v^2(t,z) = \left(\bar{v}(z)\right)^2 + 2\bar{v}(z)u(t) - 2\bar{v}(z)\dot{x}_j(t)$$

resulting in the instantaneous generalised force equation for line-like slender structures is given by

Eq. 7-4

$$p_j(t,z) = \int_{z=0}^{H} \frac{1}{2}\rho_a \bar{v}(z)^2\, w(z) C_{D,j}(z)\mu_j(z)dz + \int_{z=0}^{H} \rho_a \bar{v}(z)u(t)\, w(z) C_{D,j}(z)\mu_j(z)dz - \int_{z=0}^{H} \rho_a \bar{v}(z)\dot{x}_j(t)\, w(z) C_{D,j}(z)\mu_j(z)^2 dz$$

Where w is the local width of the structure normal to the mean wind direction at height z; $C_{D,j}(z)$ is the local drag coefficient, dependent on the height and the natural frequency of the mode; $\mu_j(z)$ is the mode shape function, describing the deflected shape of the structure in mode j with the maximum value of unity. The first term is the mean generalised force, and the second is the buffeting generalised force used for static analysis. The third term is a velocity term containing $\dot{x}_j(t)$. The third integral in Eq. 7-4 represents the fluctuating aerodynamic force proportional to the velocity of the structure and opposing the movement and therefore describes the aerodynamic damping.

Additional simplifications related to the approach of wind profile in heights can be introduced as Eq. 7-5:

Eq. 7-5

$$\bar{v}(z) = \overline{V_H}\left({}^{z}/_{H}\right)^{\bar{\alpha}}$$

For each vibrational mode, the modal aerodynamic damping ratio in communication structures may be expressed as

Eq. 7-6

$$\zeta_{aer} = \int_{z=0}^{H} \frac{\rho_a \bar{v}(z) w(z) C_{D,j}(z) \mu_j(z)^2 dz}{4\pi f_j m_j} = \frac{\rho_a \overline{V_H}}{4\pi f_j m_j} \int_{z=0}^{H} w(z) C_{D,j}(z) \mu_j(z)^2 \left({}^{z}/_{H}\right)^{\bar{\alpha}} dz$$

Where ρ_a is the air density, $\overline{V_H}$ is the mean hourly wind speed at the top of the building, H is the height of the structure, z is the height above ground level, f_j is the natural frequency for mode, $w(z)$ is the width of the structure normal to the mean wind direction under consideration, $C_{D,j}(z)$ is the local drag coefficient, and $\bar{\alpha}$ is the power-law exponent for mean hourly wind speed. In the previous Eq. 7-6, two related issues result in significant uncertainty regarding the behaviour of short communication structures. First, at low heights, wind flow contains high levels of turbulence which can alter the estimation of wind forces, $p_j(t,z)$, in Eq. 7-4, and distort the simplification of Eq. 7-5. Second, the same turbulent conditions change the flow regime by modifying the local drag factors, $C_{D,j}(z)$.

Reliable drag coefficient data, C_D, are rarely available but are nonetheless essential for the calculation of mean load effects or mode-generalised force. For slender structures with cross-sectional step changes and for tapered structures like the studied monopoles, C_D assumes different values depending on height. In this case, small variations in drag factor might better represent total behaviour, using different factors for each step, C_{Du}. However, this chapter will assume a mean value, C_{Dm}, applied to total area A, as defined in Eq. 7-7 and defined in the literature [51], to facilitate comparison with values given by existing standards.

Eq. 7-7

$$drag = {}^{1}/_{2}\,\rho \overline{V_H}^{2} \int C_{Du} (v_z/\overline{V_H})^2 dA = {}^{1}/_{2}\,\rho {V_H}^{2} C_{Dm} A$$

Existing literature [51, 73] has confirmed that the use of mean drag factors as Eq. 7-7 for circular cylinders does not lead to the underestimation of main responses, forces, and bending moments under first cantilever bending mode shapes.

The current standards try to provide quasi-static or equivalent static methods of analysis to allow for dynamic behaviour. To do so, dynamic augmentation factors are applied to design wind pressures. These factors are always crude approximations which ignore the dynamics issue and instead use simple formulation for engineering purposes. In the Canadian Standard Association (CSA) [23], the dynamic response to wind is described by the gust factor, which can have values ranging from 2–2.5 depending on the structure type. Alternatively, this code provides an aeroelastic effect and fatigue annex focused on vortex shedding phenomena. The ANSI-TIA-222 standard [22] uses a patch loading method with a 3-s gust as the design wind speed to address the dynamic issues. The Chimney code CICIND [35] also includes dynamics using a gust factor applied to the background and resonant components which depends on natural frequency and damping, including aerodynamic damping.

On the other hand, British Standard BS8100: Part 1:1986 [24] uses a gust wind approach subject to certain conditions i.e. the equivalent static applicability rules, which are not satisfied for most monopoles. In this case, spectral or time history analysis is required. In its Technical Report Number 7 [31], the Institution of Lighting Engineers (UK) applies techniques introduced by Davenport [121] on lighting columns to provide a dynamic augmentation factor, β, that depends on the logarithmic decrement of damping, δ; main natural frequency, n_o; and 10-minute mean wind speed, $V_m(10)$, as depicted in Figure 7-4. This approach has been used extensively by engineers and is considered the best given the lack of a specific code for monopoles. It contains a suitable approximation for dynamic effects based on recommendations of total damping, as defined below:

Eq. 7-8

$$\zeta_{Total} = \zeta_s + \zeta_a$$

Where ζ_s is the structural damping, defined by a unique viscous value that can be increased by a factor up to three times depending on a classification of foundation type and softness of foundational soil. Conversely, aerodynamic damping uses a simplified version of Eq. 7-6, as defined in Eq. 7-9, where $\sum R_{WT}$ and $\sum m_T$ are the wind

resistance (exposed area multiplied by drag) and total mass of the top third of the height of the monopole, respectively.

Eq. 7-9

$$\zeta_a = \frac{1}{2\pi}\frac{\rho \sum R_{WT} V_m}{2.12 n_0 \sum m_T}$$

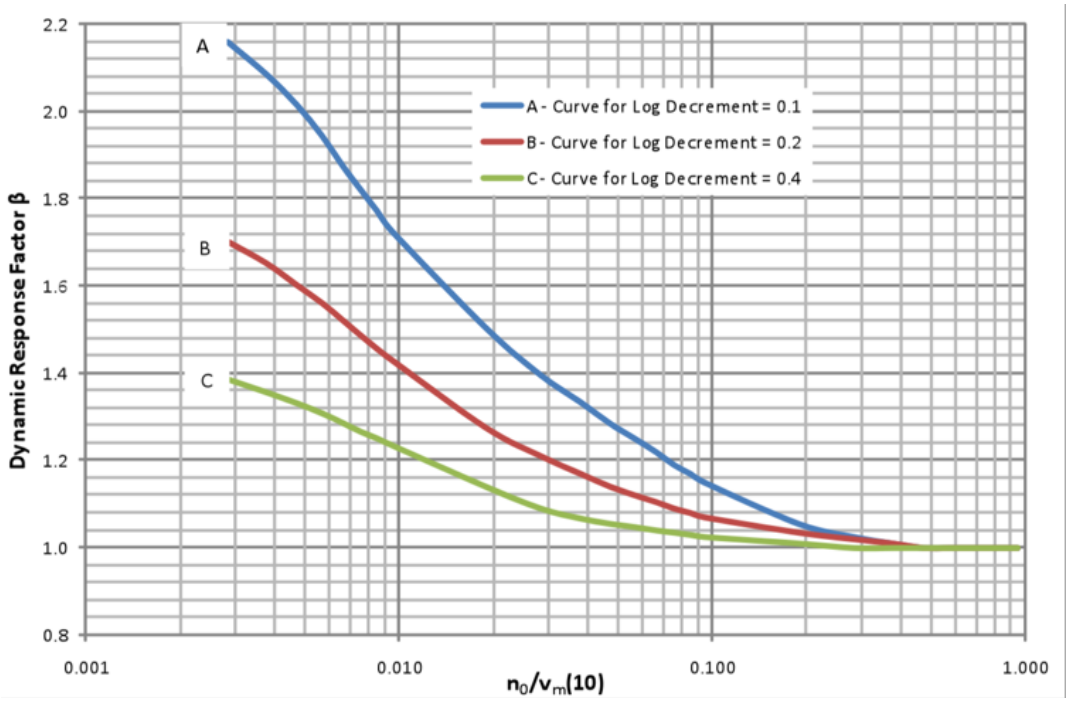

Figure 7-4. Dynamic response factor, β versus Ratio $^{n_0}/_{V_m(10)}$ [31].

In the Eurocode BS EN 1991-1-4: 2005, "Wind Actions" [26], the so-called structural factor $c_s c_d$ includes both the effect of simultaneous occurrence of peak wind pressure on the surface, c_s, of the structure, and the effect of the vibrations of the structure due to turbulence formulated as $c_d = \left(1 + 2k_p I_v(z_s)\sqrt{B^2 + R^2}\right)/\left(1 + 7I_v(z_s)\sqrt{B^2}\right)$, which depends on the resonant response of the structure. k_p is the maximum value of the fluctuating part of the response to its standard deviation, $I_v(z_s)$ is the turbulence intensity at each reference height, B^2 is the background factor, allowing for the lack of full correlation of the pressure on the structure surface. R^2, is the resonance response factor, allowing for turbulence in resonance with the vibration mode, defined essentially by damping estimation as:

Eq. 7-10

$$R^2 = \frac{\pi}{4\,\zeta_{Total}} S_L R_h R_b$$

S_L is function of the wind power spectral density function, R_hR_b is the aerodynamic admittance function of the structure, and ζ_{Total}, damping value obtained through method of assessing damping located in Annex F, dynamic properties of structures, very similar to Eq. 7-8 and Eq. 7-9.

7.3 Monopoles Tested: St Ives FC and Windmill Farm

To characterise MPs on different types of monopoles, the study focused on two dissimilar monopoles. The first, St Ives FC, is a Portasilo monopole that is considered one of the most flexible structures on the market and, based on consultant's reports, the base flange and holding down bolt system on this pole type may have a high susceptibility to fatigue failure. On the other hand, Windmill Farm is a multi-user type Calzavaras monopole and is considered one of the stiffest monopoles in the Arqiva portfolio. Specifications of both monopoles are summarised in Table 7-1. For each structure, the manufacturer has provided comprehensive information on the geometric and mechanical characteristics of the mass, the stiffness of the structure and substructure (foundations) and the masses of existing antennas. Structural details are listed below:

Table 7-1. Monitored site details.

Site Name	Struct Type	Height	Foundations	Top frame	Diameter
A. St Ives FC	Portasilo	17.5 m	Pad: 3.6x3.6x0.85 m	Mounting Pole	~0.4 m
B. Windmill Farm	Calzavara	17.5 m	Pad: 6x6x1.2 m	Delta frame	~0.65 m

- **A. St Ives FC** (Figure 7-5A): The structure comprises S275J0 steel for main core and plates of 25-mm-thick S355J2. There are two sections: a tubular tapered panel between ground level and 14.3 m and a triangular steelwork headframe designed to accommodate mobile antenna panels. There is also an external spine ladder with a latchway fall arrest system. For loading, three panels are installed on the upper section, with a small plate antenna at 14.3 m; all necessary cables run internally. This structure is connected to the foundation via a flange plate and 12 grade 8.8 M24 bolts without grouting. The foundation is a concrete block of dimensions 3.6 x 3.6 x 0.85 m. In terms of wind loading, St Ives is located in Cornwall, a region with one of the highest basic design windspeeds in England:

23 – 24 m/s. Additionally, the site is less than 1 km from the shore, making it very susceptible to high wind speeds and relatively low turbulence.

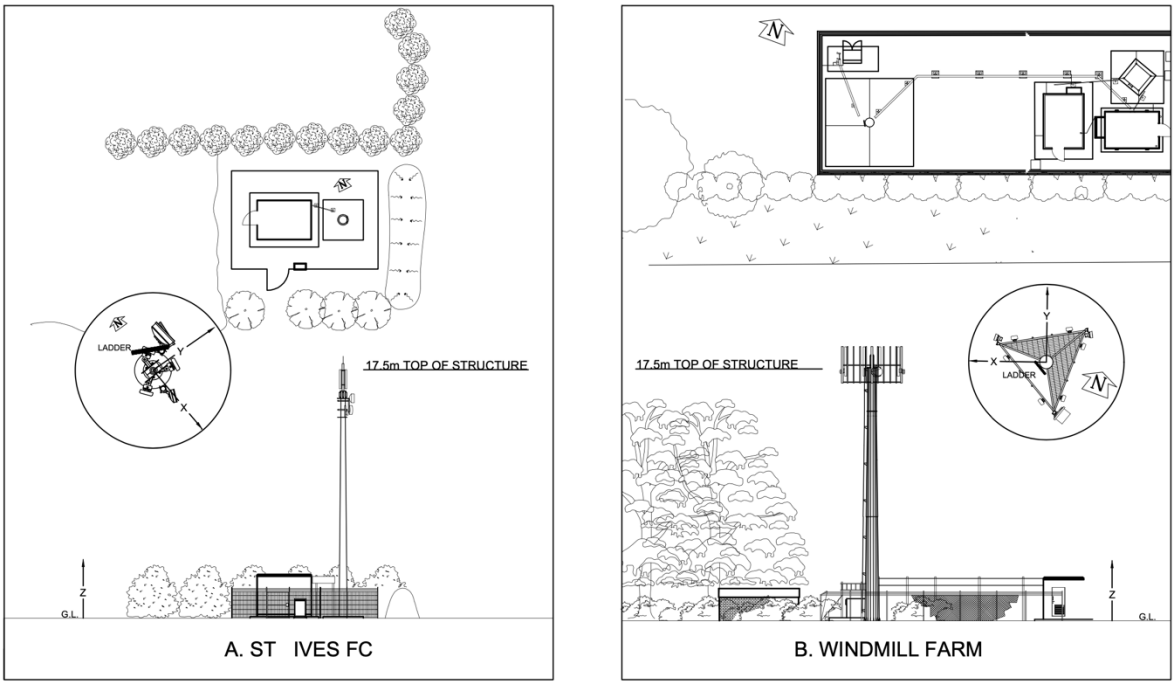

Figure 7-5. Elevation and Plan View of Monitored Sites. A: St Ives FC. B: Windmill Farm.

- **B. Windmill Farm**, (Figure 7-5B): The structure is a 17.5 m monopole built with two tubular tapered panels with 1.6 m overlapping comprising a 16-sided pressing of 10 mm thick plate, completed with a delta frame steelwork equipped with a climber platform to install the required antennas. Currently, there are six 4G panel antenna, two dish antennas, free space to hold twice the current load, and linear loading based on running external cabling. The base of the tower is welded to a baseplate flange with 24 gusset plates, and the flange is secured to a concrete foundation by 24 30-mm-diameter steel rods that are sunk approximately 1000 mm into the concrete foundation. The mast sits on a set of M30 levelling nuts above the foundation concrete. The foundation is based on a spread footing of 6 x 6 x 1.2 m. There are no available reports to categorize the soil or to verify an appropriate bearing capacity. In terms of wind loading, the site is located far from shore in Wiltshire and has a basic design wind speed of 20.3 m/s.

7.4 Dynamic Testing for Condition Assessment, System Identification, and Structural Health Monitoring

The information available on dynamic tests of short telecom structures or monopoles is limited to the research and studies related to structural responses due to wind loading from the current standards [73], which were completed in the late 1980s. New challenges require further knowledge of structural modelling and wind loading and a better understanding of dynamics that will improve further designs and current structural assessments.

Communication structures are designed to withstand the worst wind load cases. Due to their geometry and slenderness, monopoles exhibit behaviour that fits one of two different scenarios [4]: along-wind buffeting, where response depends on the wind speed intensity; and across-wind vortex shedding (VS), where under low wind speed, with little wind turbulence, and certain geometric symmetry, the structure creates vortices that induce movement perpendicular to the wind direction. In large structures, reliable knowledge of wind variations over time and space throughout the structure and of structural response must be captured. In structures below 30 m, such as monopoles, a single representational point is sufficient to collect the desired data.

In line with the exposed damping formulation in Eq. 7-8, this exercise uses two separate sets of data to compare scenarios, in the presence and absence of ambient loading:

For ambient wind concerns, the study requires response data for each monopole during strong wind events, so a SHM system was created to capture operational response and wind data over long periods of time. The continuous recording yields the desired range of loading events in terms of wind speed, direction, and turbulence, from which the acceleration response (magnitude and direction) with MP identification can be correlated to explain the load and response mechanisms.

The SHM system uses two mono-axial PCB accelerometers (model 393B04) and a RM Young mechanical anemometer connected by coaxial cables for synchronized sampling at 128 Hz by a data logger. The logger uses National Instruments hardware placed at ground level and is capable of recording up to 6 months of data limited by memory capacity (Figure 7-6). Each installation of the SHM system required steel

components to place the anemometer with horizontal support close to the top level of the monopole, and a cabin at ground level to hold the logger with a 120 V power supply.

Figure 7-6. Aerodynamic monitoring system. Left: Anemometer installation & Steelwork. Centre: Data logger in Cabin. Right: Monitoring Sketch for St Ives FC.

To analyse the structural behaviour of each monopole without external loading influences, a modal survey was conducted on the date of the SHM installation under calm weather conditions. For each field test, the excitation used the 'human pull excitation' method. This method is based on the application of sharp tugs on a rope attached to a point close to the top of the structure, timed to build a strong (resonant) response before letting the structure vibrations decay freely. 'Pull and Release' [122] has been proven to be a highly effective method for this kind of structure, for which the possibility of installing a shaker is very limited due to logistical challenges. Structural accelerations were recorded using OPALs^{TM} (APDM Opal system) wireless inertial measurement units, which include triaxial accelerometers. OPALs^{TM} were placed at four different level locations indicated in Figure 3-6. With a 128 Hz sample frequency, these devices provide the best approach to measure the mode shapes of each monopole. The responses obtained from the mentioned methodology are free decays which can be readily analysed in the time or frequency domain.

To analyse data obtained during SHM, the fast Bayesian operational modal analysis (BAYOMA) procedure was implemented to identify and monitor the modal properties

over time. In addition to the natural frequencies, damping and mode shapes that are typical targets for modal identification, BAYOMA also identifies the PSD of modal force. This was applied to benchmark the modal wind load PSD from wind tunnel tests with that identified from field data [118].

As defined in previous Chapter 6, BAYOMA [102, 103] operates in the frequency domain using the Fast Fourier transform (FFT) of ambient vibration time series within a selected frequency band for the modes of interest. The FFT is used directly without windowing or averaging. It can be shown that given the data (FFT in selected band) and modelling assumptions, the MPs have approximately a Gaussian distribution. The mean, or most probable value (MPV), of the distribution is analogous to the 'best estimate' produced by conventional (non-Bayesian) methods. The covariance matrix of the distribution reflects the 'identification uncertainty', i.e., remaining uncertainty despite the presence of data. The MPV and covariance are respectively related to the location and curvature of the likelihood function, for which efficient algorithms have been developed previously.

The modal properties that can be identified for each mode include the natural frequency, damping ratio, mode shape, and the PSD of modal forces. All properties are essential to correctly model the response of the monopole. Natural frequency characterises likely amplitude dependence in the structure's stiffness, which is helpful when conducting structural diagnosis during longer monitoring. Critical damping ratio results provide information about energy dissipation methods and facilitate identification of aeroelastic forces. Mode shapes and modal force PSDs help correlate wind forces (from speed and direction) and consequent drag/lift factoring.

The second set of data of free vibration decay responses contains information about the underlying fundamental features of dynamical systems, including properties that are prone to change as a function of the vibration amplitude. Of particular interest are the free vibration records that were recorded when setting the system free after forcing vibration response in a single mode by timed pulling (harmonic forcing) on an attached cable. When the structure is released it undergoes free vibration decaying from the established large amplitude response, which is ideally in a single mode. As long as the amplitude of vibration in the steady state is large enough to trigger structural nonlinearities, the measured decaying response can be used to extract the so-called

backbone curves. Backbone curves store high quality information of the nonlinear structure that can be exploited to estimate the structure MPs. Since preliminary test data revealed changes in the MPs with the vibration amplitude, this exercise applies backbone curve methodology to estimate the current structural behaviour, natural frequencies, and structural damping.

The method previously developed [56] and applied [55] uses zero-crossings and peak amplitudes to calculate the instantaneous frequency and vibration amplitude envelope over the decaying record. These features can be also used to estimate instantaneous damping over time. To do so, responses must be converted into modal coordinates to estimate backbone curves in modal space. The final result is curves of frequency and damping as a function of the vibration amplitude.

To understand the characteristics of investigated MPs with the above methodology, it is necessary to first define the dynamic response of each monopole. The frequency domain is used to identify main modes and their directional mode shapes. Next, a correlation between response magnitude and wind speed loading can confirm which wind scenario is most predominant during each monopole's service life (buffeting vs vortex shedding).

7.4.1 Response Characteristics of Monopoles: Power Spectral Densities and Identified Mode Shapes

The dynamic response of monopoles under wind loading is defined by two coupled modes with a zero-node cantilevered flexural-bending mode shape. Normally, the pair of modes tends to have natural frequency values below 2 Hz, which is inside the wind-sensitive frequency range, and for this reason they define the predominant motions under buffeting along-wind loading. The PSDs in Figure 7-7 specify the pair of close modes contributing to the response at that level. Higher order modes found between 3 – 6 Hz do not appear clearly on St Ives FC spectra, but they might be excited under aeroelastic effects like across-wind vortex shedding or extreme wind events. Also, some 'fake' peaks are found in Windmill Farm PSD due to unknown signal acquisition issues and are identifiable due to their single spectral line.

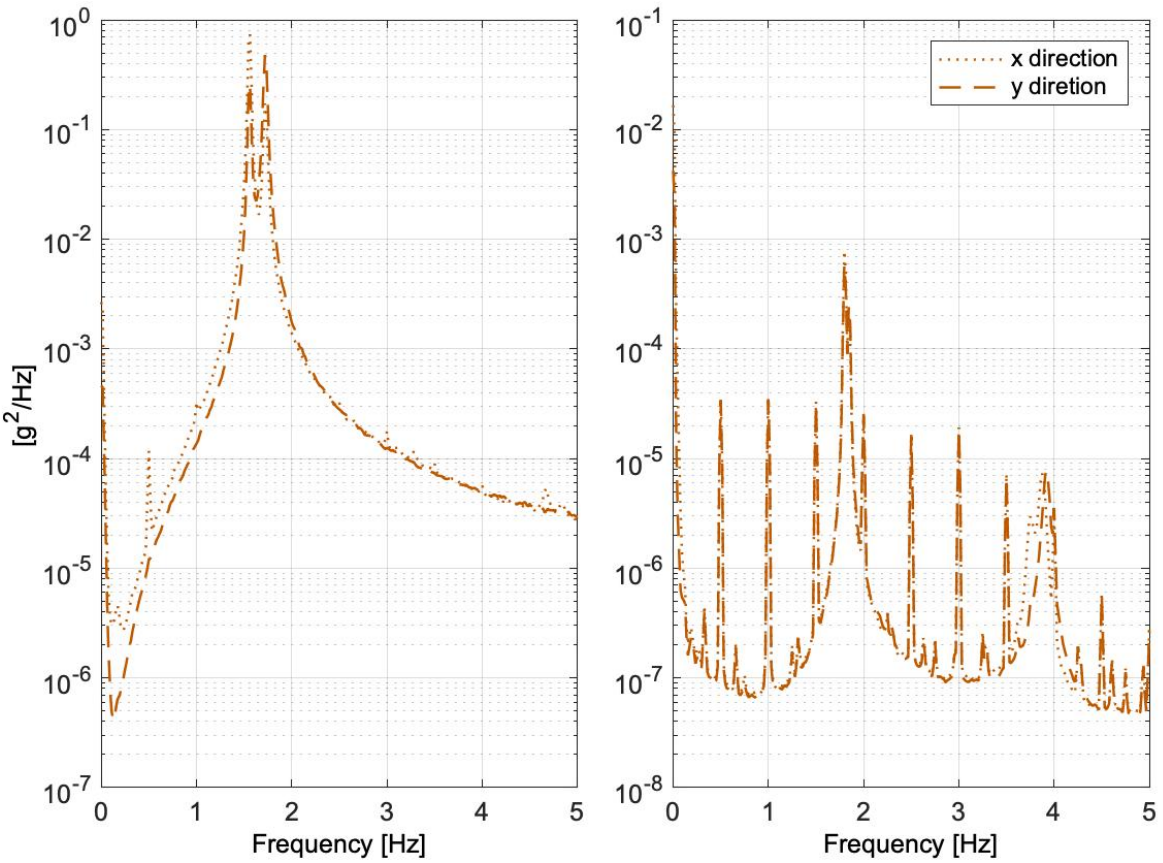

Figure 7-7. Power spectrum density of main degree of freedom in range 0 – 5 Hz. Left: St Ives FC. Right: Windmill Farm.

The typical response of a monopole under horizontal wind buffeting when viewed in plan has an elliptical/oval shape and tends to oscillate between the directions of the pair of modes. Previous investigations have indicated that all the necessary fixed attachments – such as ancillary equipment, antennae and steelworks, and the linear loading such as cabling and ladders – disrupt the high level of symmetry of the industrialised shaft geometry, resulting in two main stiffness directions which define the mentioned modes. The stiffer frequency tends to be aligned with the location of the ladder (Figure 7-8), and the lower (blue-mode) tends to be orthogonal to this direction. In Figure 7-8, ladders are plotted as segments tangential to the circular monopole shaft.

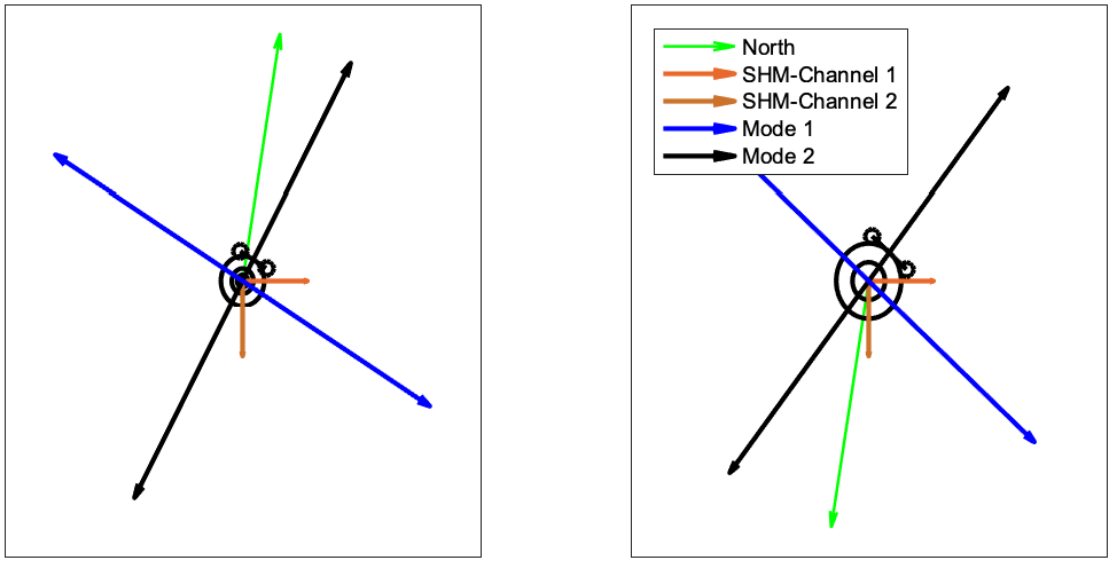

Figure 7-8. Main modal modes identified on St Ives FC (left) and Windmill Farm (right).

7.4.2 Response Characteristics of Monopoles: Ambient Wind Loading

To identify a meaningful correlation between MPs, response, and wind-ambient loading, one must determine how the structural mechanisms arise from fluctuating forces. Monopole structures act under two main response phenomena. The first is buffeting, which is caused by fluctuations in the flow velocity that act directly to produce fluctuating forces on a body in the flow. When a free stream is turbulent, as it is with these short communication structures, consequent forces are more random and have components both along and across the time-mean flow direction.

Alternatively, some forces lead to vortex shedding, which can be dangerous in terms of fatigue failure. The dominant frequency for this phenomenon is defined by the relationship between geometric properties and wind speed through the Strouhal number, which matches a second set of modes between 2 – 4 Hz for relatively low wind speeds below 15 m/s.

Table 7-2 Critical wind speed for vortex shedding of selected structures.

Site Name	Structure Type	Critical wind speed [m/s]	
		1st Pair Modes	2nd Pair Modes
A. St Ives FC	Portasilo	3.8	6.5
B. Windmill Farm	Calzavara	8.5	17.3

Figure 7-9 plots the gust and mean wind speed versus RMS response obtained for the two monopoles using the SHM system. Each point represents the analysis of 10 minutes of data, with mean wind speed in light green and peak 3-s-gust wind speed in dark green. When data are plotted using a logarithmic axis, there is a clear dependency between wind speed and structural response, indicating that the response mechanism is basically buffeting. The higher the wind speed the structure faces, the larger the response. Alternatively, Vortex shedding is characterised by strong resonance responses at clear, low wind speeds (below 18 m/s on main modes). Figure 7-9 presents no evidences of VS.

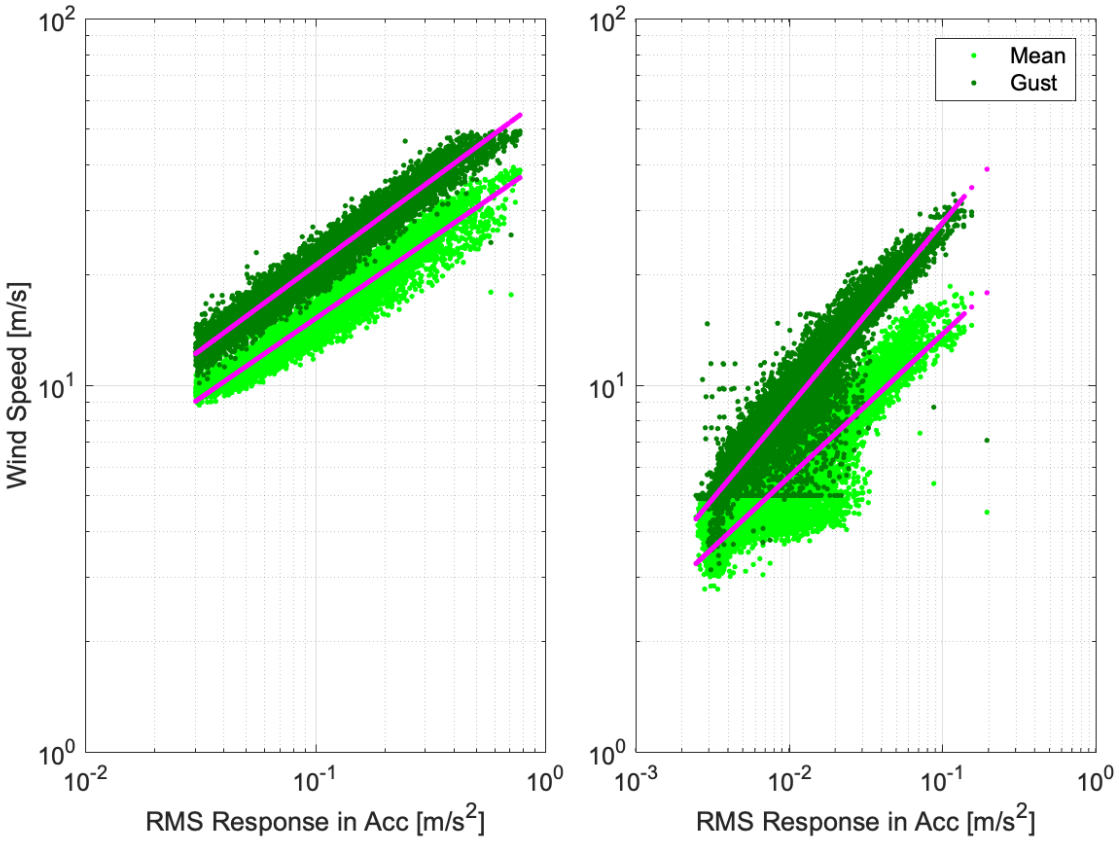

Figure 7-9. Field-identified RMS structural response versus gust and mean wind speed. Buffeting response. Left. St Ives FC. Right: Windmill Farm.

7.4.3 Operational Modal Analysis under Ambient Loading: Fast Bayesian Procedure

OMA is particularly attractive in this SHM because it permits a straight correlation of MPs, response levels and wind speed under investigation in ambient loading. For this study, BAYOMA was chosen to extract the MPs as it implicitly provides in addition the identification uncertainty that can help judge quality of results in a manner consistent with physical and stochastic modelling assumptions.

The length of the time window for the identification must be defined. Long duration recordings reduce uncertainty in modal property estimates, subject to conditions of stationarity [123]. However, capturing MP variability with time (hence consecutive data sets) requires short duration recordings. Previous work has indicated that a duration of 10 minutes is long enough to obtain better than 20 % standard deviation in damping estimates obtained in trial runs on monopole data. Furthermore, following codes, fundamental basic mean wind speed guidelines from the UK National Annex to BS EN 1991-1-4 recommend 10 minutes as a standardised segment, which facilitates comparison of this study's results with existing data.

Over a minimum of two months of data, BAYOMA was implemented on both SHM system installations; this duration was sufficient to capture a representative range of wind events. Figure 7-10 describes the performance of both installations during high wind excitation and subsequently calm weather situations. The wind changes are evident in the upper plot, where mean wind speeds are plotted with the root mean square (RMS) of the response captured by accelerometer channels in red. The correlation is clear, confirming a buffeting response. The loads/responses found during the St Ives FC monitoring are considerably higher than at Windmill Farm due to several very strong wind events during the monitoring time.

For analysis purposes, BAYOMA was focused on the main close wind-sensitive modes (Table 7-3) according to the PSDs presented in Figure 7-7.

Table 7-3. Initial estimate of natural frequency band width for modal; identification in BAYOMA.

St Ives FC	$f_1 = 1.556\ Hz \quad f_2 = 1.723\ Hz \in [1.4 - 2]$
Windmill Farm	$f_1 = 1.81\ Hz \quad f_2 = 1.86\ Hz \in [1.8 - 2]$

The lower plots display the evolution of MPs (natural frequency, critical damping, mode shape direction, and modal PSD forces) for defined modes in Table 7-3. For each property estimation, the size of error bar reflects the standard deviation about the MPV. As expected, damping ratio and modal PSD have much higher uncertainty than the frequency or modal direction.

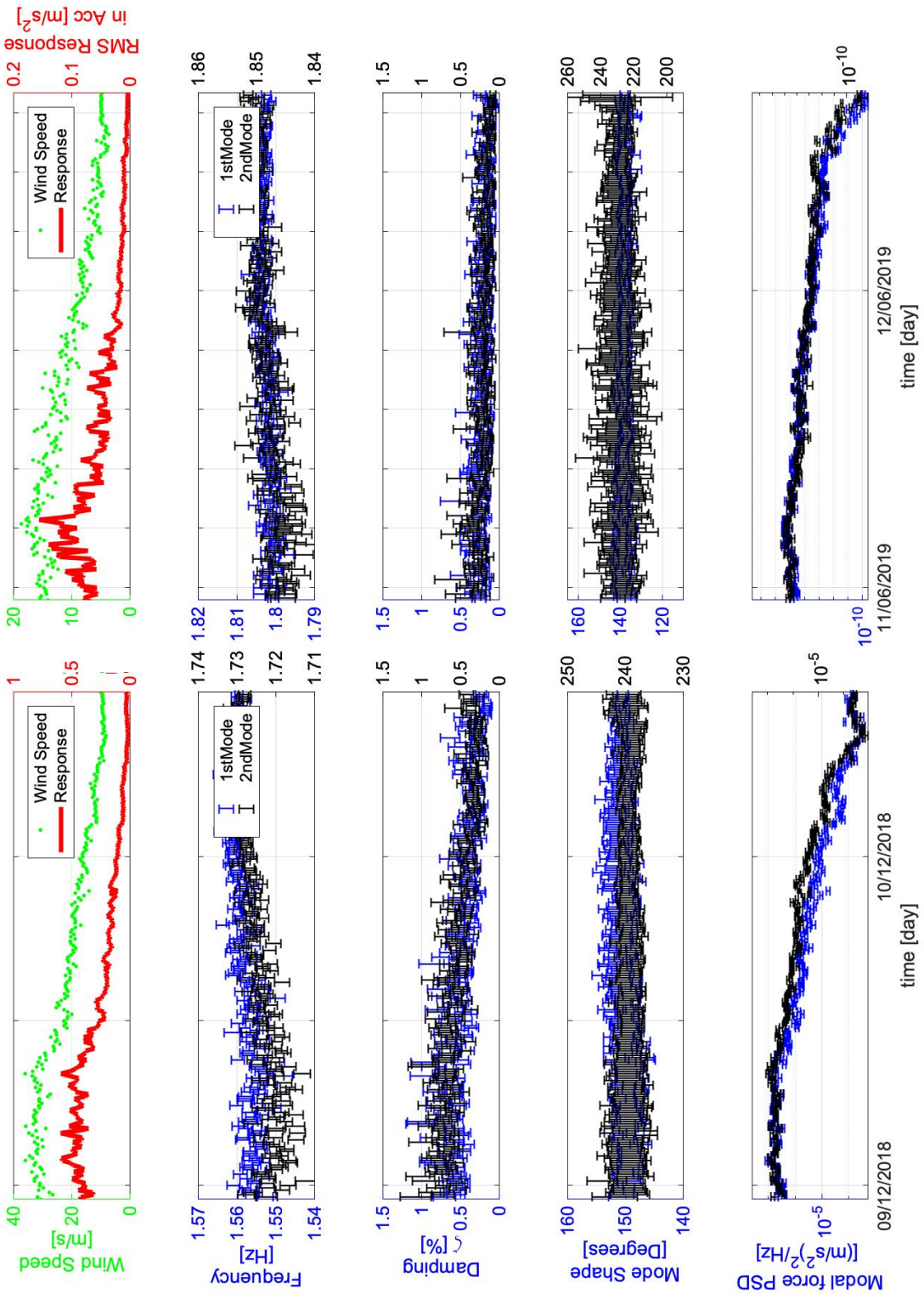

Figure 7-10. Mean wind speed and response obtained at St Ives FC from 9–10th Dec 2018 (bottom) and in Windmill Farm from 11–12th Jun 2019 (top). Application of OMA (left to right): BAYOMA on response data St Ives FC. Shown are frequency, damping and mode shape variation (reference angle from accelerometer-Channel X. Anticlockwise as Figure 7-8) for first (blue line) and second mode (black line) shape. The size of the error bar reflects 1σ identification uncertainty for individual estimate. Time window: 10 minutes.

As observed in other structures, higher response corresponds to a decrease in frequency. Modal PSD forces and damping increase with response, confirming the coexistence of excitation and aerodynamic damping forces with the mean wind speed.

7.4.4 Free Decaying Response: Backbone Curve

To correctly assess the implications of ambient loading on any structure, one needs exhaustive structural knowledge in the absence of any flow influence. Elements of MPs such as structural damping or stiffness can be estimated through response to artificial (human) forcing in the absence of wind loading in calm weather. Those properties tend to have a behaviour exhibiting high amplitude dependency difficult to model. Literature on this subject is very limited and has never been applied to communication structures.

The extraction of backbone curves from free decaying response measured after the 'Pull and Release' exercise provides important information about MPs. A modal survey of each studied structure was conducted. Each response captured by OPALs^{TM} accelerometers was projected to rotated horizontal axis to identify the direction for both modes (see Figure 7-8) in the necessary modal coordinate space. Unfortunately, from the closed-related fundamental pair of modes found in Figure 7-7, only responses for higher mode (f_2 in Table 7-3) were adequate for the analysis; lower-mode (f_1 in Table 7-3) decays tend to couple with higher one, so the desired free decays could not be obtained.

The exercise uses several suitable large amplitude decays which are plotted in Figure 7-11 for both surveys. As anticipated, both surveys yielded different results in terms of amplitudes. Those differences are caused by the necessary mass that was mobilised during each pull. The Windmill Farm monopole is generally much stiffer and heavier (it contains more mass in the crown of the structure with more equipment and platforms). Consequently, even with the target frequency rate and direction, the Windmill Farm pulls were not as efficient as those of St Ives FC.

The backbone curves from several decays define clear modal natural-frequency and damping trends dependent on the response amplitude (accelerations were kept as response units for comparison reasons as Figure 7-10). The trends are consistent for considerable responses. However, the amplitude values at lower one of the studied pair of fundamental modes, f_1, tend to be more inconsistent due to the relative

decrease in the signal-to-noise ratio of the measured response at those lower amplitude levels; this leads to a reduced accuracy sensitivity in the estimation methodology. In terms of frequency, both monopoles exhibit a softening behaviour, with apparent stiffness reducing as vibration amplitude increases, which tended to be cubic or linear in shape. Damping has a linear behaviour that increases with the amplitude with values ranging from 0.3 - 1 %.

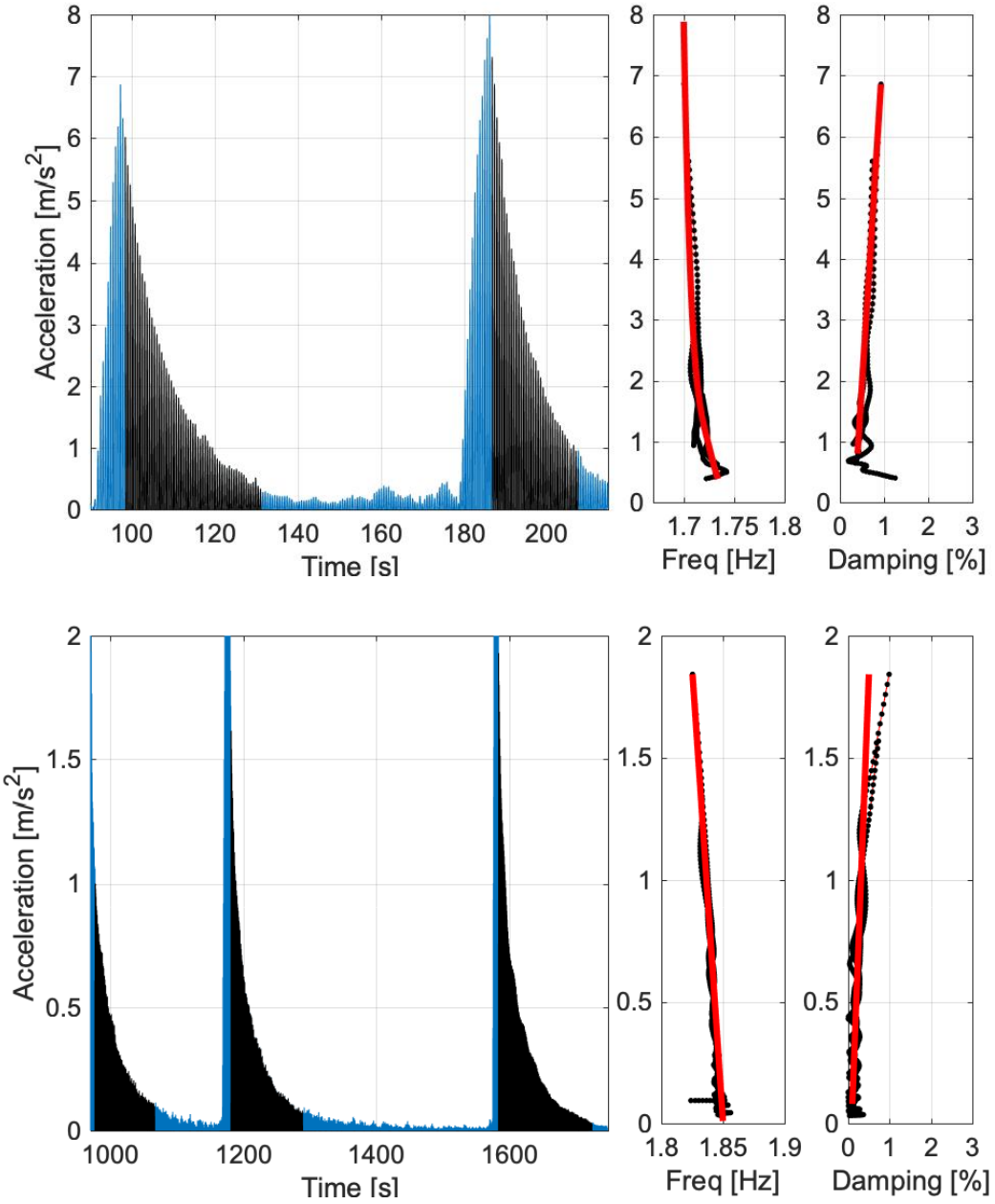

Figure 7-11. Backbone curves extracted from the 'Pull and Release' modal surveys. Top: St Ives FC. Bottom: Windmill Farm. Black: Analysed response. Red: Interpolated curve.

7.5 Field-Identified Modal Properties

This section analyses the behaviour of MPs obtained from free vibration decay and ambient vibration data. First, the modal PSD forces are compared to the wind direction to observe the extent to which each mode is active for different wind directions. Next, the impact of two frequency and damping approaches on amplitude response and wind speed loading is compared for each of the previously described scenarios.

7.5.1 Field-Identified Mode Shape Values versus Modal Forces PSD

Along-wind buffeting excitation expressed by modal PSDs over the structure suggests that, depending on wind direction and speed, different fundamental translational modes might be excited. The modal PSD diagram in Figure 7-10 indicates a continuous co-existence of both modes for each wind load direction case. This behaviour was demonstrated by the monitoring data and confirms the assumptions that both modes are well-excited. The interactions between modes can be studied by examining the correlation of modal force PSDs and mean wind speed and direction (Figure 7-12). In this approach each mode contains different along- and across-geometry sections which can affect drag factors and aerodynamic components. The upper plots of Figure 7-12 represent the existence of modal forces PSD against the wind loading polar distribution for the first and second modes (drawn in blue and black, respectively), compared to the main direction of mode shapes. At both analysed sites, there are no dominant modes in any direction. Larger and minor responses are always formed by both modes, even when wind direction is aligned with mode shape direction.

The lower plots depict modal forces PSD versus mean wind speed. As demonstrated, both modes are excited over the wind speed range, with higher forces taken from higher modes. At Windmill Farm, the lower mode (mode 1), is less consistent than mode 2 which absorbs more energy. The results in Figure 7-12 confirm that the typical response under buffeting in monopoles is based on a pair of modes which are active for all wind speeds and directions. The response depends strictly on the intensity of the loading. The high turbulence of the loading supresses directional influences of the geometry, inducing similar along- and across-wind responses.

7.5.2 Field-Identified Frequency Behaviour

Knowledge of the variation of natural frequency dependent on environmental and structural factors is imperative in structural engineering during structural diagnosis to

anticipate deterioration or to improve linear analysis with further investigations. This section reports a clear frequency dependency on amplitude, in particular, the apparent structural stiffness decreasing with vibration amplitude, especially in the St Ives FC monopole.

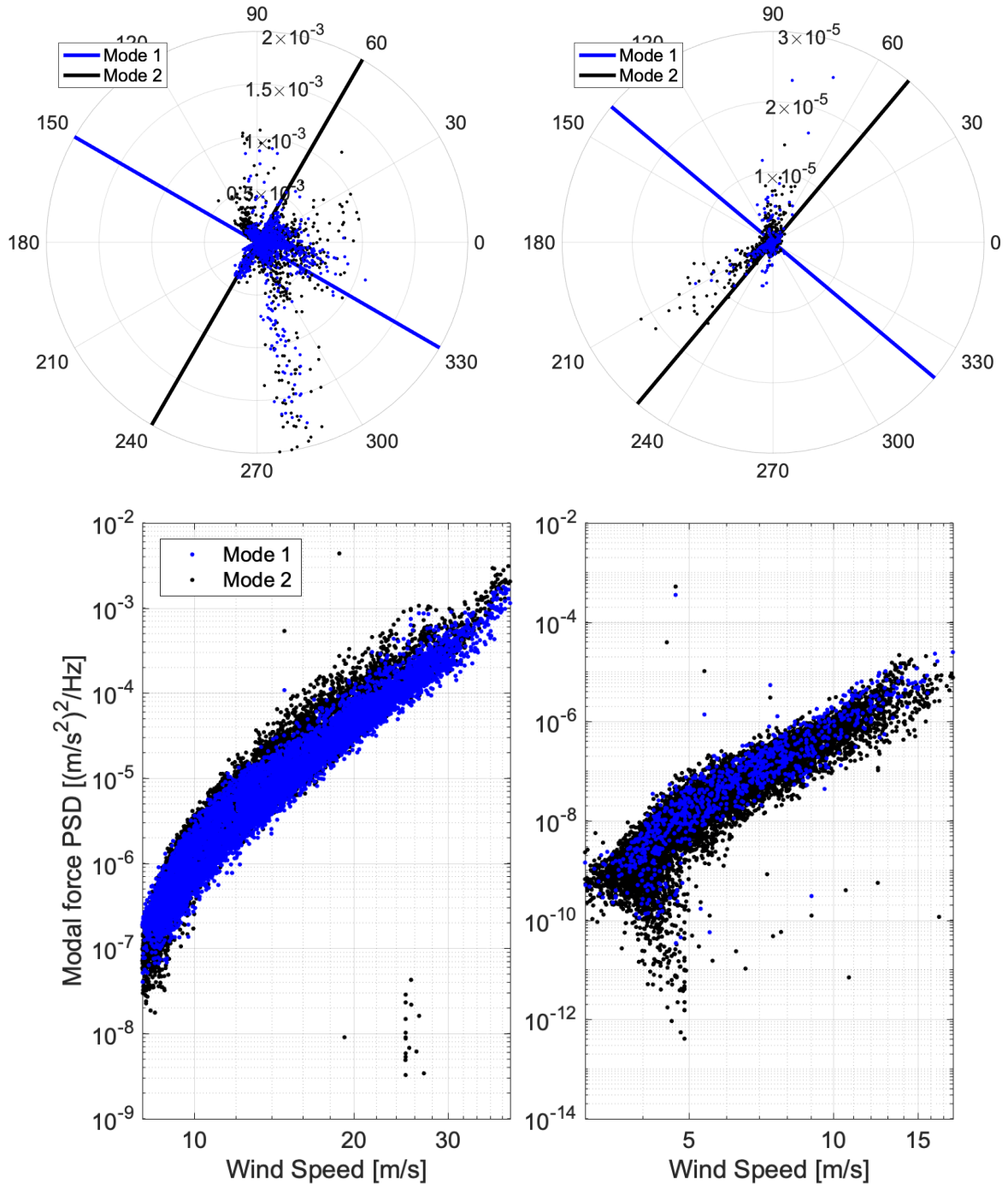

Figure 7-12. Field identified modal force PSD versus wind data. Top: Directional influence. (Radius: Modal force PSD). Bottom: Mean wind speed. Left: St Ives FC. Right: Windmill Farm.

Figure 7-13 plots the MPVs of the two natural frequencies and their uncertainty margins ($\pm 1\ \sigma$) for each mode with a regression line showing amplitude dependence via correlation with RMS accelerations. A cubic regression approach was found to be appropriate in St Ives and linear regression in Windmill Farm.

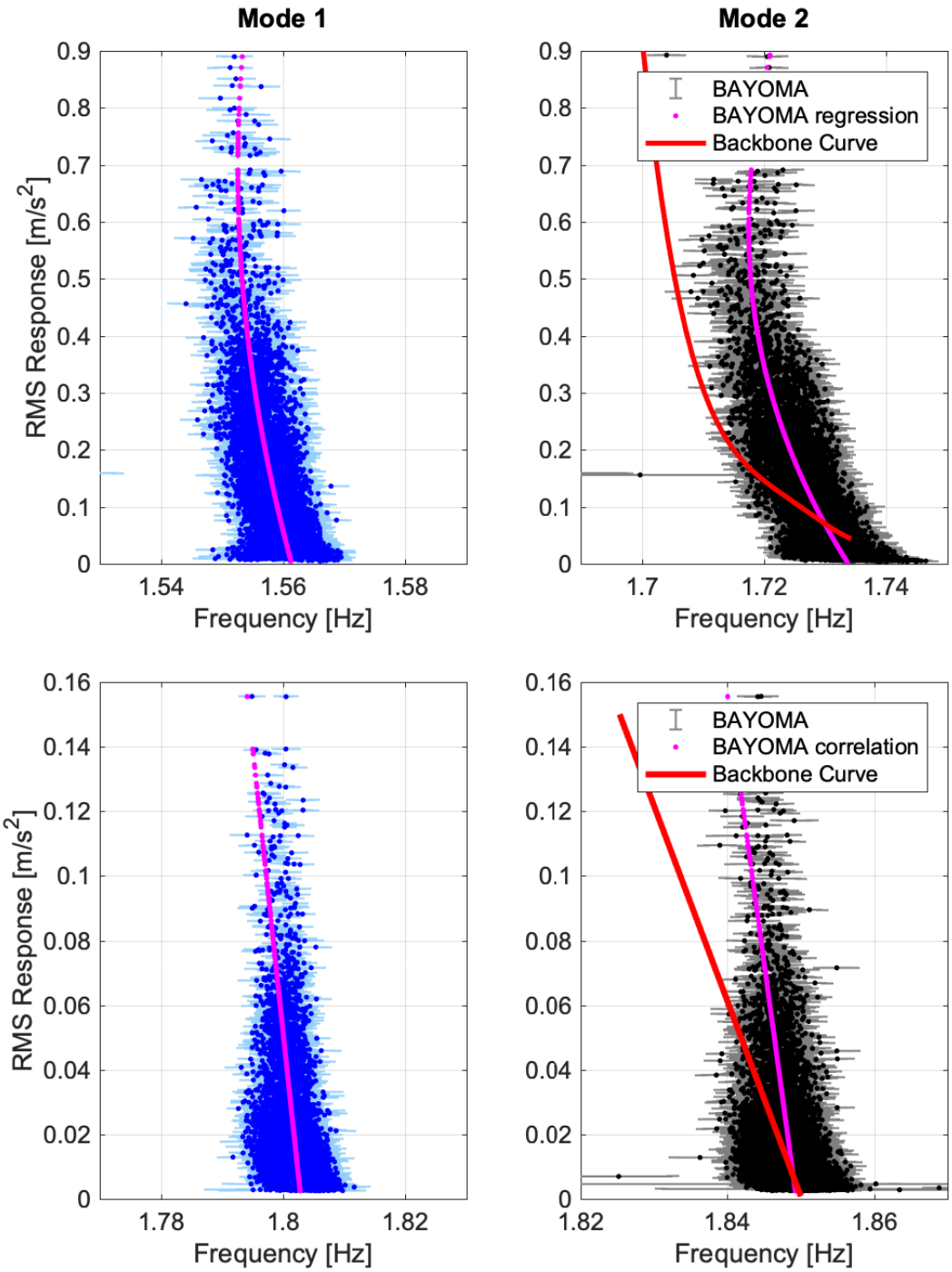

Figure 7-13. Frequency behaviour vs amplitude. Up: St Ives. Down: Windmill Farm.

In addition, the backbone curve bands included in Figure 7-11 have been correlated with RMS response, and are indicated by a red line in the second mode. The

agreement between methods at low levels of vibration is strong. However, at high responses in wind, the structures appear to be stiffer than in free conditions. This finding strongly suggests the existence of aeroelastic stiffness which increases with the amplitude response.

The character of both the BAYOMA estimations and backbone curves suggests a strongly nonlinear softening behaviour caused by several sources, such as foundational soil influence, inherent material stiffness, possible connection bolt friction behaviour, or the previously mentioned aeroelasticity component.

7.5.3 Field-Identified Damping Behaviour

In the absence of dampers, wind-sensitive structures are characterised by two main sources of damping. Structural damping is defined here as damping components in the absence of induced flow. These components generally include material, connections, dry friction, and foundation-soil influences. Structural damping is characterised by the backbone curve analysis in Figure 7-11. Furthermore, the flow which induces ambient oscillations in the structure also serves to reduce oscillations due to aeroelastic damping forces. This component assumes greater importance for slenderer and more dynamically active structures. For tall and slender structures such as high guyed masts, the structural component of damping is sometimes assigned a very small constant and conservative value, relying primarily on the aerodynamic component; this component is derived from several elements such as stays, affected by aeroelastic effects in galloping or vortex shedding. BAYOMA results in Figure 7-10 shows values of total damping which count on both aerodynamic and structural components.

The lack of consensus on an acceptable approach to estimate total damping for short, medium, and tall structures is cause for serious concern in academic and consultancy circles. This estimation has a high financial impact for issues related to the definition of vortex shedding, real capacity of the structure, or strengthening based on dampers. The current understanding of total damping is based on the addition of both components at any amplitude response or wind-ambient loading as showed Eq. 7-8, and the linear wind speed dependency of aerodynamic damping as Eq. 7-9. Both have not been verified for communications structures in the existing literature.

Figure 7-14 plots the field-identified critical damping values at both SHM sites. Blue and black points (for the first and second modes, respectively) represent the MPV with the coefficient of variation (c.o.v., ratio of standard deviation σ to the MPV) margins, and magenta lines corresponding to the linear correlation of the whole set of values for each mode and site.

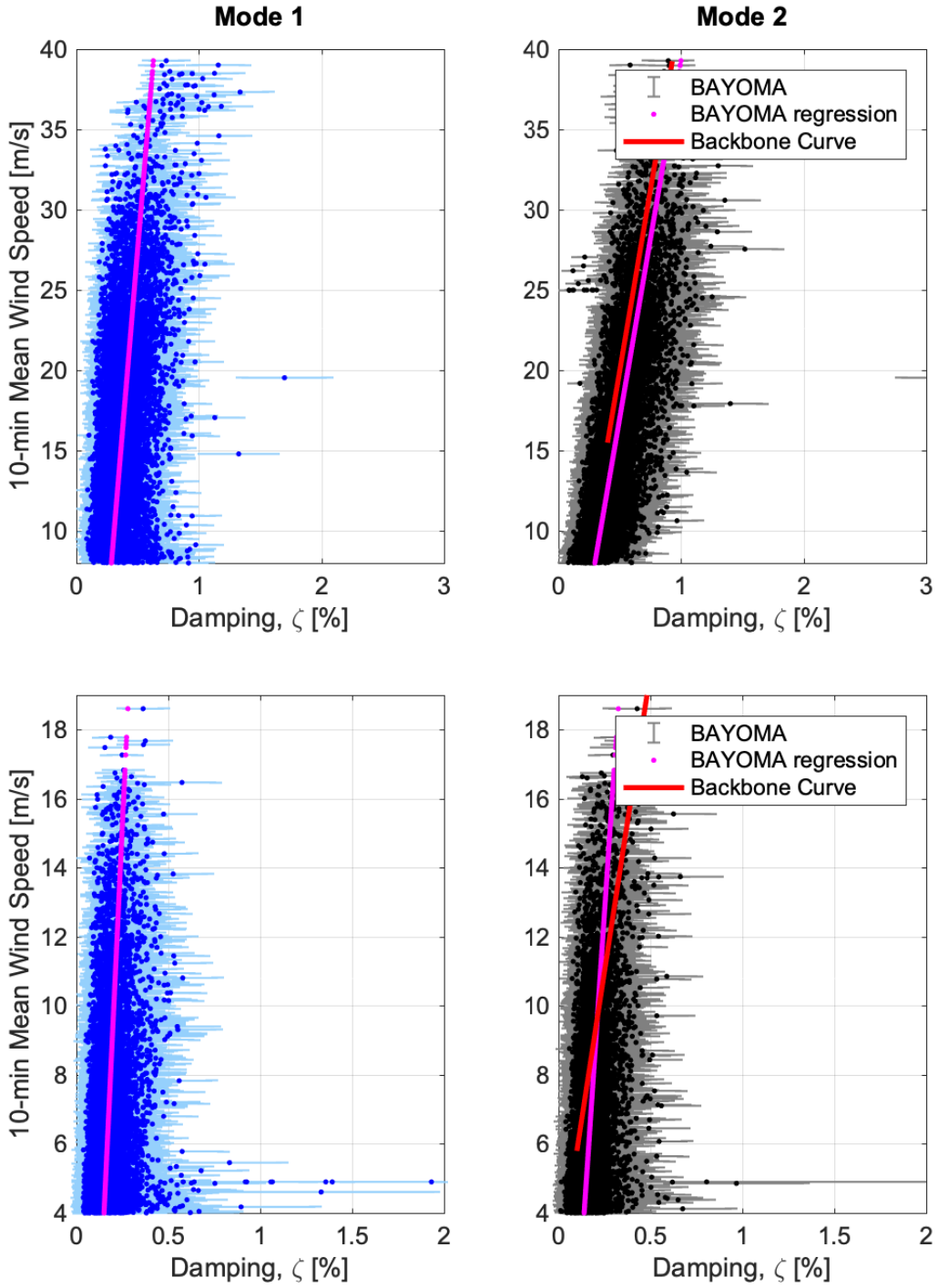

Figure 7-14. Damping amplitude vs mean wind speed. Left: St Ives FC. Right: Windmill Farm.

The plots clearly indicate an increasing linear trend with wind speed that is similar between modes, as well as other amplitude dependencies as suggested in the Eq. 7-7 and Eq. 7-9. However, very low responses and mean wind speeds provide meaningless high-damping results at ground level. These results were removed to avoid distorting high response results.

Figure 7-11 demonstrated that the structural component of total critical damping also has an important amplitude dependency. The red lines in the second mode plots of Figure 7-14 are obtained thorough an amplitude-wind speed correlation as Figure 7-9. The plot thus compares total critical damping and correlated structural damping versus mean wind speed.

Both scenarios, total damping and structural damping, have a very similar linear behaviour. This behaviour suggests that the initial Eq. 7-9 is not satisfied for high amplitude response. The amplitude dependency of structural damping rejects the equivalent-viscous damping value taken by the formulations. In addition, the collaboration between aerodynamic and structural damping is not as effective as suggested by the codes. In its place, the existence of aerodynamic damping negates the total action of structural damping at each level of wind flow, and consequently amplitude response. In other words, the structural damping is only impactful in the total absence of wind flow. In those conditions, the assumption of conservative and constant structural damping might be acceptable, even if it does not fully represent appropriately its current behaviour.

This approach confirms that the slope of the damping shape is defined by wind resistances (area and drag factors), mass distribution, and modal frequency range (see Eq. 7-6 and Eq. 7-9). A reverse exercise could lead to an alternative method to derive values of mean drag factors.

7.6 Discussion: Comparison of Results and Standards

All results shown in previous sections provide enough information to evaluate the existing methods of assessing dynamic properties defined in national standards. This study's results support existing codes in that the main mechanism driving response is turbulent buffeting. However, codes only consider a unique mode to determine the whole response, which is contrary to previous results that confirm behaviour involving

two close modes, that can mean an excessive simplification of the structural response. Simplified static approaches do not consider this matter appropriately, a dynamic modal analysis would address the issue more aptly.

Figure 7-15 compares the results of Figure 7-14 with the method of assessing damping given by the Institution of Lighting Engineers (ILE) in its Technical Report N.7 [31]. Thicker lines represent the results of SHM of main pair of modes (blue and black for first and second modes, respectively) and backbone curves (red), thinner lines depict the damping approach defined by Eq. 7-9 and Eq. 7-10 that applies the obtained natural frequencies in SHM, and the orange line is the damping estimation from the owner's pre-existing structural assessments, based on models not validated by field data. The vertical (purple) line defines the design wind speed from recommended wind map.

In terms of structural damping, the value given by ILE [31], which is similar to Eurocode or British Standard, is close to the levels indicated by the backbone curves at low wind speeds as well as the SHM values for both sites. The aerodynamic damping deviates significantly from the linear correlation from field-identified values and Eq. 7-9.

The differences are caused by (i) the existence of a secondary mode (Mode 2) working alongside the main one (Mode 1) which absorbs part of the response and dampens the structure; (ii) the uncertainty of structural damping mechanism, which has more complex behaviour than the standard constant value; and (iii) the large discrepancies stemming from turbulence drag factoring (Eq. 7-7) that yield damping estimations 2 – 3 times higher than current behaviour observed during service life.

7.6.1 Assessment of Dynamic Response Factor

The previously mentioned discrepancies have serious consequences on the application of quasi-static methodology used by several codes. Low values of damping involve a significant amplification applied to the static response of each structure. Figure 7-16 presents a comparison between previous structural assessments of the ILE in its Technical Report N.7 [31] and the same assessment using the MP results of this chapter. The chart correlates the design mean wind speed, main natural frequency and main damping (in log dec) with the dynamic amplification factor applied to wind-loading pressure; that is, the factor amplifies the peak equivalent static pressure (buffeting loading) to address dynamic oscillations.

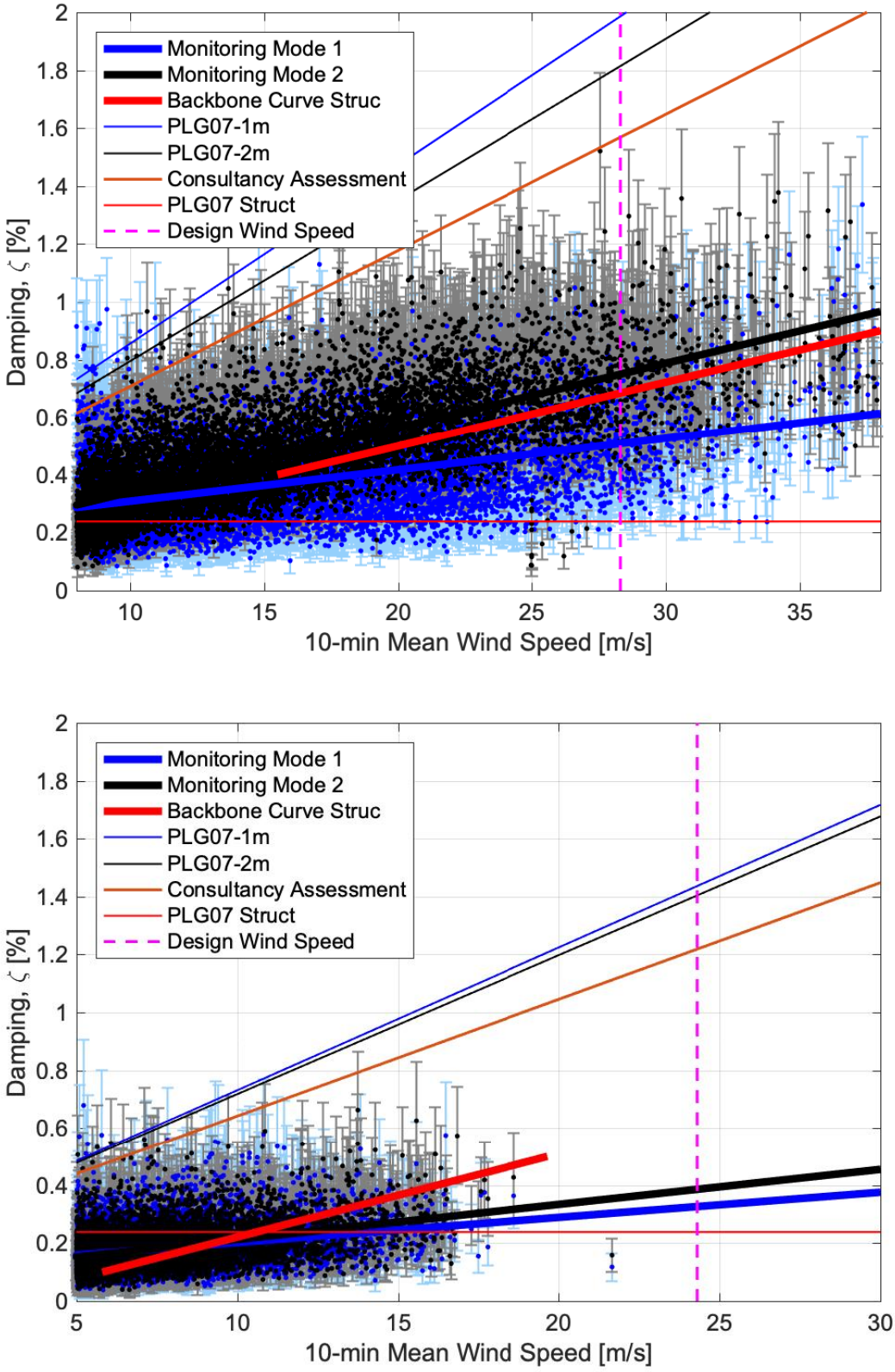

Figure 7-15. Damping assessment. Up: St Ives FC. Down: Windmill Farm.

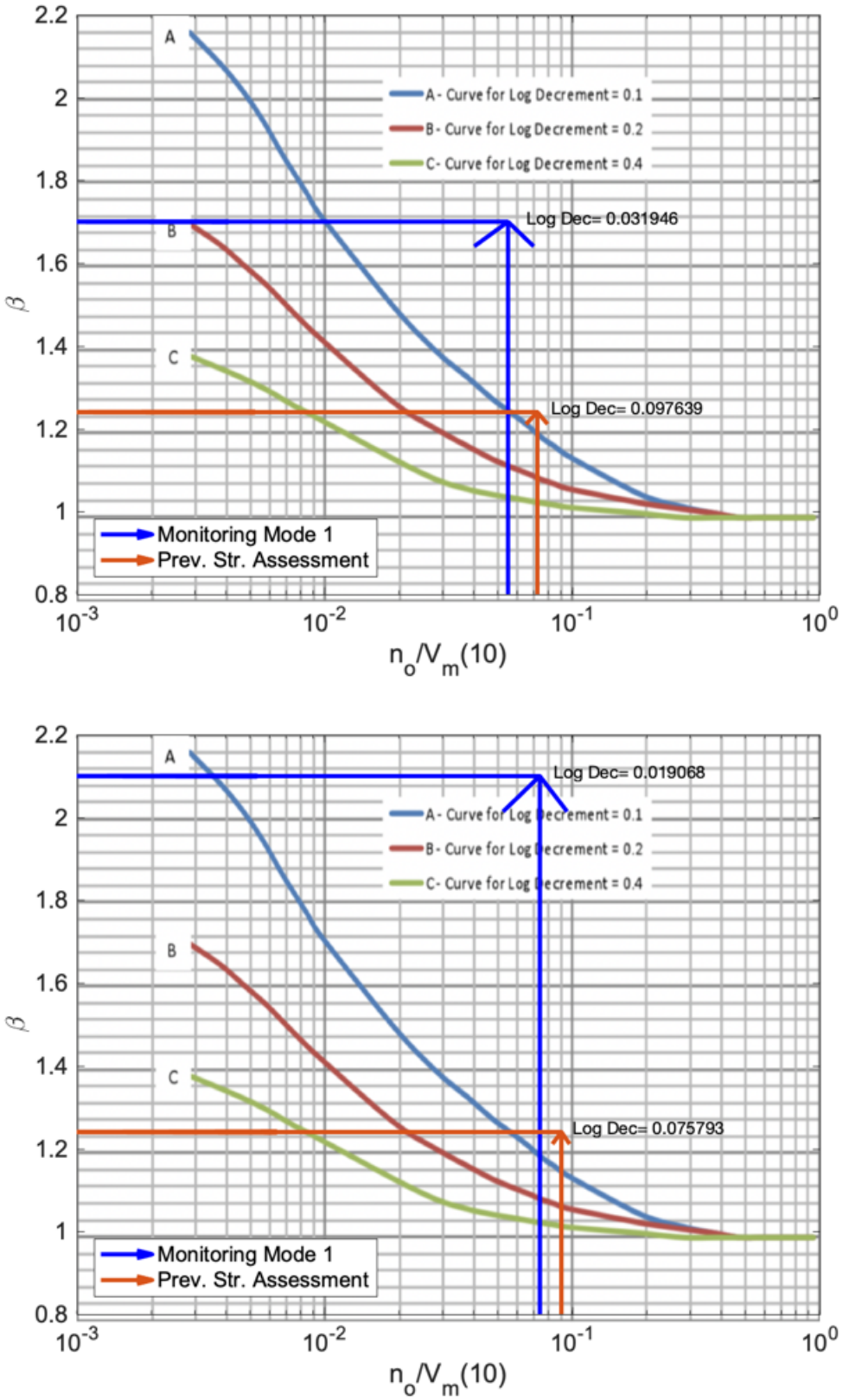

Figure 7-16. Dynamic response assessment on PLG-07. Left: St Ives FC. Right: Windmill Farm.

The small discrepancies found in the identification of main natural frequency are not as important as the new damping results. The new values tend to be in an undefined region above the scale of damping defined by the code. The code also recommends a 'conservative' minimum value of log dec = 0.1, in case the method of assessing damping given in previous Figure 7-15 is not supported by the manufacturer. However, this value appears to be on the nonconservative side following current results.

The new dynamic factors are much larger than previous values: new wind loading pressure is 40 % higher for St Ives and 100 % higher for Windmill Farm. The structures, which are currently close to 100 % capacity i.e. further loading would overstress the structure, are not designed to withstand this large increase in loading. These findings prove the limitations of quasi-static approaches in considerably high dynamic-sensitive structures. Other approaches based on dynamic analyses would address this behaviour much better.

Those concerns are equally applicable to the dynamic factor, c_d, Eurocode [26] in Eq. 7-10. Reduction by a factor of 3 on total damping means increments by (the same) factor of 3 times on the resonance response factor R^2 and consequently, proportional increments are found to c_d. Both quasi static methods were showed to be very sensitive to damping values based on a non-accurate method of assessing damping.

Nonetheless, some benefits can be extracted from previous assessments. The highest discrepancies were found during the estimation of aerodynamic damping. The discrepancy between the total damping slopes of the code estimations (Figure 7-15) and those found in this research indicate a large difference between wind resistances in assessments and real behaviour, consequently leading to high discrepancies in drag factors. A new drag factor that is consistent with aerodynamic results will also change the wind resistance used to calculate main forces (i.e., a change in drag factor will better characterise the dynamic response and will also decrease the static mean forcing, which in some case can be beneficial from a structural perspective).

7.6.2 Drag Coefficient

The variation of the drag coefficient C_D along the structure should be considered when calculating the mean load effect, generalised modal force p_j (Eq. 7-4), or aerodynamic damping (Eq. 7-6). Variation is caused by flow distortion near the ends of a structure,

changes in cross-sectional shape, or variations in wind-speed (shear flow) and turbulence along the structure.

Comparison of the use of mean and local values of C_D for subcritical circular cylinders suggests that for typical cantilever mode shapes, the mean value C_{Dm} should be used. The proposed approximation of uniform drag flow value is appropriate for the Windmill Farm (Figure 7-2) site due to only minor changes in shape along the shaft of the monopole – only the frame appears as a step change. St Ives has a significant change in cross-sectional shape with height, but the variances found in drag factors are ± 20 %, acceptable for comparison purposes.

Figure 7-17 presents the construction of a drag factor corresponding to each mode as a regressed value combining aerodynamic damping, mass distribution, and geometry, which satisfies the initial Eq. 7-9. The obtained values appear to be consistently lower than $C_{Dm,}$ the mean value calculated for structural assessments.

At high wind speeds and in lower turbulence, drag factors tend to takes values around 0.6 or lower. For design wind speeds at 25 - 30 m/s, mean values are well below the standardised value at 0.8. On the other hand, at low wind speed, where turbulence tend to be higher, higher deviation of the result is found with higher mean values of C_{Dm} closer to recommendations.

7.7 Conclusions

This study presents research to validate the approach used to determine dynamic properties of monopole structures. This typical quasi-static approach appears in a range of standards applicable to monopole structures. The developed understanding of MP suggests the need for significant changes to existing formulations, with indirect and direct consequences to structural assessments. Analyses of two very different types of monopole under free decay and ambient response suggest the following:

- Main response under wind buffeting loading is defined by two coupled cantilevered bending modes relatively close in frequency and within a wind sensitive range below 2 Hz. Both mode shapes are identified in plan view with misalignments that modify the inherent structural symmetry, providing more inertia for one direction

than its orthogonal. Typical linear-loading ladders or cable trays are ideal to identify stiffer mode shapes orthogonal to the first mode.

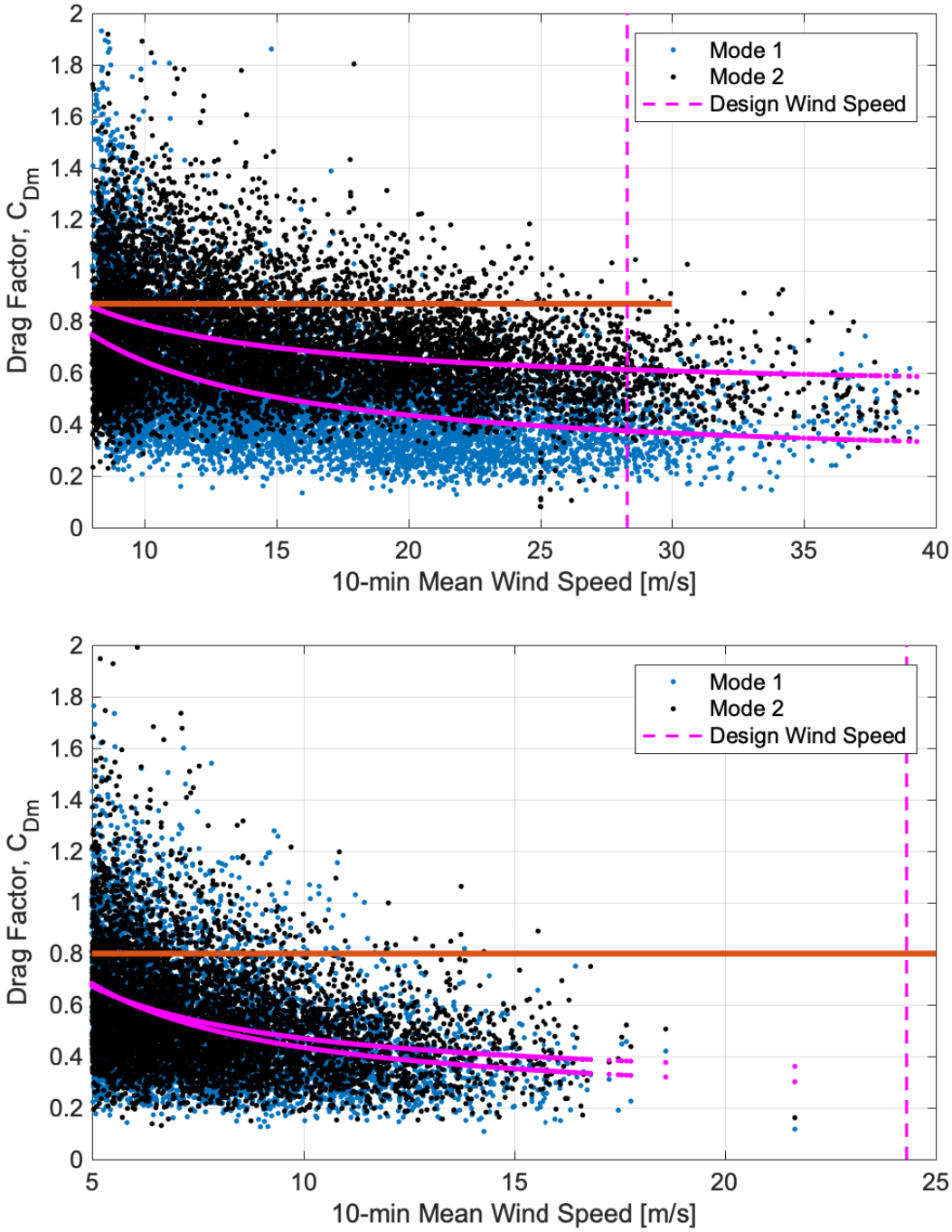

Figure 7-17. Drag factor calculated from field-identified damping. Top: St Ives FC. Bottom: Windmill Farm.

- The understanding of dynamics requires analyses of structural behaviour under two scenarios, with and without wind and its effects. In still-air conditions, the subject was addressed by modal surveys, where manual forcing at resonant

frequency was induced by an attached rope. This method generated high responses and consequent free decay that were analysed using backbone curve methodology. For in-wind behaviour, a structural health monitoring system was specifically designed to capture wind-ambient loading and response. Fast Bayesian modal analysis was implemented to identify MP and their uncertainty over 10-minute response windows. Explained procedure has been demonstrated as an excellent tool to obtain performance of MP under both scenarios, and consequent comparison provides high relevance on the amplitude dependency study.

- The estimation of the modal PSD forces confirms the coupled response for buffeting excitation. The high degree of turbulence of wind ambient loading excites both along- and across-wind components for all ranges of mean incident wind speed and direction. The stiffer mode (aligned with ladder and cabling tray) tends to be more excited for both structures. Localised impulsive pulls can achieve unimodal response decays ideal for backbone curve study.
- In terms of frequency, monopoles exhibit a non-linear softening behaviour; for high responses, first mode (pair) frequencies are lower. Similar behaviour was found in both data sets, although wind flow helps to reduce the stiffness changes achieved under pull excitation.
- Properly estimating and understanding damping is one of the more challenging issues in dynamics. Monopoles essentially rely on two main damping sources: structural and ambient. Both sources are combined to define a linear-amplitude-wind dependency behaviour; this finding is supported by existing codes.
- The damping estimates from this study offer valuable information that can improve current engineering structural assessments. The definition of a viscous-constant value of structural damping was not found to be appropriate, as there is a clear amplitude dependency. However, the highest discrepancies were found during the estimation of the aerodynamic damping: drag factor values are overestimated in turbulent wind flow. In summary, the method of assessing damping provided by codes tends to overestimate total modal damping by a factor of 2 – 3 times current findings, with significant implications for the definition of augmentation factors in quasi-static analysis.

- The drag factor extracted from aerodynamic damping indicates high discrepancies with suggested sectional drag factors taken during structural assessment due to the level of turbulence in short communications structures. The inferred new drag factors and greater dynamic sensitivity challenge the current formulation for checking quasi-static applicability. However, these factors will induce smaller wind forces which may be beneficial from a structural point of view.

In keeping with the advice listed above, a review of the approach to dynamic response in existing codes is necessary. New recommendations must consider the more complex vibrational response, a review of the approach of structural and aerodynamic damping, and drag factors.

Preface to Chapter 8

Damping becomes a crucial property on the definition of dangerous dynamic effects caused by vortex shedding in communications structures. It induces severe and rapid damages which lead to structural collapse when structural damping cannot decrease high responses.

The following chapter presents two exclusive cases of across-wind vortex shedding effects in high lattice towers. The report of such response events and the innovative solutions to provide additional damping in communications structures is unprecedented in the current literature.

Chapter 8 Damping in Lattice Towers under Vortex Shedding

8.1 Introduction

Steel lattice towers (LTs) provide an efficient structural form to support telecommunications and other equipment at heights between 20 and 100 m. Above these levels, stayed masts require less material and can consequently result in lower construction costs (at the expense of larger land requirements and a need to accommodate the stay anchorages). However, there are some examples of taller lattice towers. For example, Crystal Palace, which provides broadcasting services to Greater London, the most populated area in the UK, is 199 m, and also the 152-m Croydon broadcast tower. Both towers were built between 1957 and 1964.

As cantilever structures, the dynamic behaviour of tall lattice towers (defined as being taller than 50 m) are quite well known. The frequency spectrum is defined by two main orthogonal modes associated with the first flexural modes between 0.8 – 2 Hz; taller structures could obtain even lower frequency values.

Second modes are mainly defined by the type of equipment supported by the structure at its top level. Broadcasting antennas often require a cylindrical weather protection shroud, commonly made of fibre reinforced polymers (FRP), that increase the height of the structure by over 10 m. Higher modes are normally not considered because they appear outside the wind action range in buffeting or are unlikely to experience aeroelastic events.

Commonly used software in communication structure analysis does not allow accurate modelling of the attachment of large and bluff ancillaries to the main structure. This failing can significant alter the dynamic response and, consequently, the capacity and integrity of the structure. For example, the software modelling engine models the cylindrical antenna as a wind resistance element with lumped masses located at certain levels on the structure. This assumption, which works properly for small or

medium ancillaries, does not allow for the large modifications in stiffness or aeroelastic across-wind behaviour of the antenna introduced by large attachments. This shortcoming results in unsuitable modelling of lattice tower behaviour. Reliable assessments are essential to properly maintain the structure.

New sites chosen for constructing lattice towers tend to be located close to residential areas, increasing the severity of the consequences in the unfortunate case of a structural failure. Safety factors must be augmented to support such towers' intended design life (typically 50 years). As an added benefit, the surrounding population can help identify and communicate dynamic issues related to significant dynamic responses which can be expressed as unusual noises and visible motions.

The growing communications business requires new solutions and innovations to help maximise the use of each structure. Effective inspections, maintenance, and strengthening plans must be coordinated with structural assessments to identify, as accurately and as early as possible, any issues.

With this information in mind, the proposed monitoring of dynamic response data outlined in this chapter could be a useful tool to identify existing dynamic issues which would not be otherwise captured. This monitoring could help to identify the cause of an issue, design engineering solutions, execute actions, and verify that a solution is successfully implemented. This chapter studies two different cases of lattice towers which have been monitored and subsequently fit with a structural damper.

The first case involves the provision of a tuned mass damper installed over the top of the television broadcast antenna at the Arqiva Salisbury tower, following observations of the antenna shaking and causing significant noise. The second case involves the installation of chain dampers to reduce high responses under buffeting and vortex shedding (VS) at an Arqiva site called Brougher Mountain in the county of Fermanagh, Northern Ireland.

Both solutions relied on gathering a set of response data which resulted in a recommendation to implement a damping device. In addition, this section describes the changes in dynamics due to new model improvements which shifted second modes from 4 - 5 Hz → 2 - 3 Hz, regions where VS tends to be extremely dangerous and provokes fatigue failures.

8.2 Case 1: Salisbury Lattice Tower

8.2.1 Description of Salisbury LT

The Arqiva Salisbury TV and radio broadcast antenna support structure is a 45.6 m tall steel lattice tower (Figure 8-1) built in 1969 to provide TV relay services to the local area. Structures similar to this Arqiva tower comprise a space frame cantilever constructed from a series of panels and with a square base. The panels form a tapered envelope from the ground level to 31 m and a 16 m long parallel portion from 31 m to the top of the structure. The frame elements are connected by bolts and welded gusset plates. The foundations consist of four individual concrete pads (also known as 'pad and chimney' foundations), which are approximately 4 m deep, to anchor the structure into the underlying chalk.

In 2017, the television broadcasting cardioid antenna located at the top of the 45 m lattice tower at Salisbury was replaced by a new cylindrical antenna. This alteration significantly changed the mass of the assembled antenna.

Following this replacement, significant movements were reported by site personnel and neighbours and even captured on video. The reports from surrounding neighbours and inspections can be found in [124].

The evidence indicates that in relatively calm weather, VS events occur and can induce high oscillations in the tower. Initial structural assessment did not capture this aeroelastic event because its frequency analyses provided incorrect natural vibrational modes. The consequent erroneous modelling of the stiffness may have led engineers to execute incorrect structural actions. There is clearly a need to refine or update global stiffness and damping modelling methods with current response data. This validation process has the potential to improve the reliability of structural models, enabling proper capacity predictions in future assessments.

In terms of loading, the structure appears to be relatively congested towards its top, with different types of antennae from several customers. From the base of the tower to a height of 35 m there are mainly phone telecommunication customers, and from 35 m to the top of the structure there are digital radio antennas and a cantilevered UHF 16 Lambda cardioid antenna used to broadcast television service. All antennas

are attached to the structure using mounting steelwork, and every antenna receives its required power and signal via single or multiple feeder cables.

In terms of wind loading, the tower is in Salisbury, Wiltshire, a relatively flat area, which has a relatively low basic wind speed of 20.5 m/s. The site is 30 km from the coast, inside a relatively high turbulence zone with rural and town terrain categories.

The site is at the top of a hill and is surrounded by residential houses to the north and east, with open fields to the south and west. Consequently, orography influence in wind loading is expected from critical wind directions.

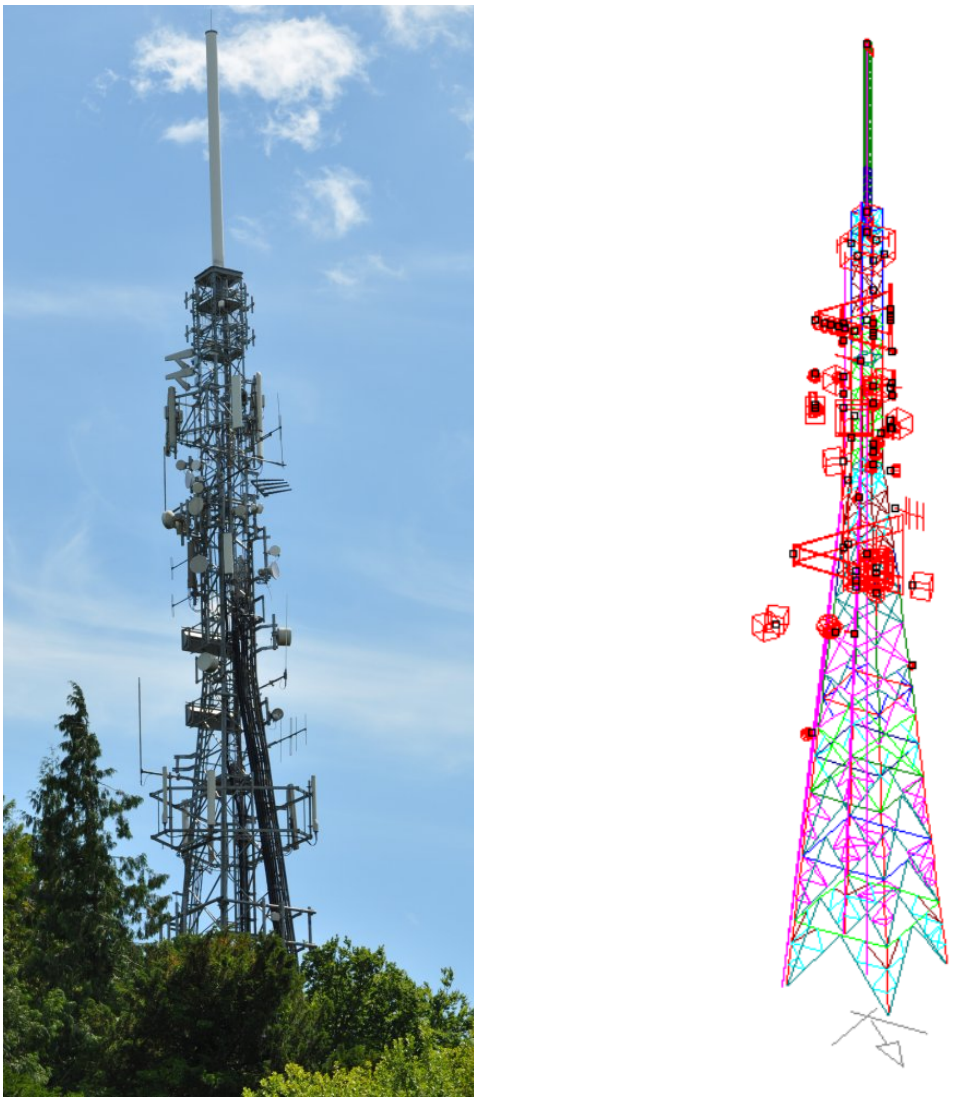

Figure 8-1. Salisbury Lattice Tower. Picture (www.mb21.com). MS-Tower model.

8.2.2 Vortex Shedding in Salisbury Lattice Tower

The VS phenomenon begins following the formation of vortices and large asymmetrical energy loss in the wide wake of a body immersed in the wind flow (see

Figure 8-2.). In low turbulence or with intermediate Re, the flow on the wake of a bluff body is dominated by a periodic train of alternating vortices known as the Kármán vortex street [125]. The separation between vortices depends on the width of the body. These vortices are larger than the boundary layer immediately ahead of the separation point and can produce large-scale and low-frequency fluctuation forces in the fluid flow.

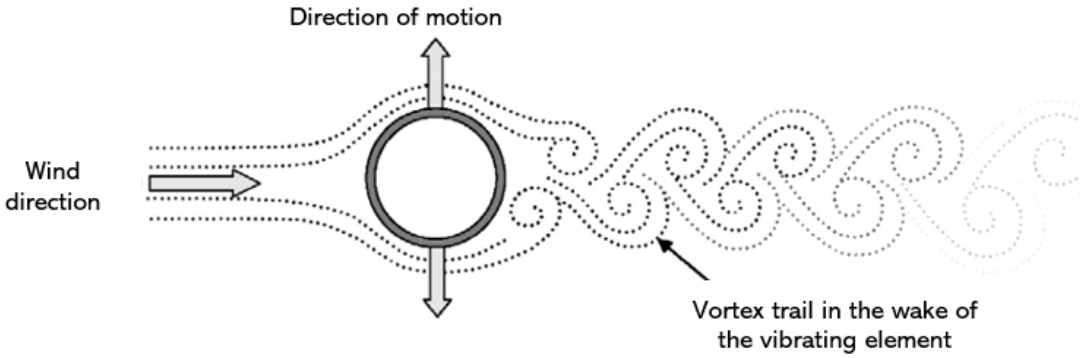

Figure 8-2. Diagram illustrating vortex shedding. ASCE library.

The VS response can be estimated by calculating the Strouhal number, a non-dimensional number which represents the predominant value of alternating frequency of VS as previously introduced in 2.3.2.1. A critical wind velocity is associated with each vibration mode. This velocity is defined as the wind velocity at which the frequency of VS equals the natural frequency of the mode.

The structural resistance or propensity to VS can be estimated by calculating the Scruton Number [65]. For a cylindrical bluff body, practical experience indicates that vibration modes with a Scruton number of more than 15 are highly unlikely to exhibit significant vortex-induced vibrations as expressed on Eq. 2-19 and Figure 2-17.

The effect of VS need not be considered when the critical wind velocity is greater than 1.25 times the characteristic mean wind speed at the level of the bluff body. The effect becomes a relevant and important subject for communication structures in low wind speeds (below 15 m/s) when the appearance of lock-in events might induce fatigue failure.

In lattice towers such as the one at Salisbury, characteristic second and third bending-translational modes can experience VS excitation. First modes tend to be below 2 Hz and VS occurs at relatively low wind speed and does not provide enough energy to

mobilise the corresponding modal masses. Further, fourth pairs of modes are far enough from the dangerous frequency range with a critical wind speed above the typical wind design.

As suggested by the Scruton number definition in 2.3.2.1, structural damping is highly important to the appearance of the aeroelastic event and to defining its response. The addition of damping with damper devices at operative heights is very effective in the dissipation of VS.

In Salisbury, the discussed antenna is a Cardioid RFS Model 16UD-HP400, a 10 m cylinder with 0.4 m diameter, and the radome is constructed from a glass fibre reinforced polymer (GRP) cylindrical shell which provides structural support and rigidity and houses the internal equipment with the corresponding antenna and cables. The overall weight of the assembled equipment, antenna support, and mounting system is approximately 500 kg.

The value of $V_m(z)$ defined by Eurocode at the mid-height of the antenna is 35 m/s, which implies that vibration modes with frequencies of up to 15 Hz must be evaluated. Furthermore, the first natural frequency of the cardioid (on its own) is set as 2.5 Hz and is in the range of the second translational mode of the whole lattice tower, so the main vibrational response of the antenna might lead to excitation of the second mode of the lattice tower. Therefore, the second mode appears to be the highest risk mode in the structure for VS, yielding values of $V_{crit,2}$ = 6.5 m/s and Sc $\approx$ 10, with a high propensity to experience across-wind vibrations.

In July 2019, Arqiva experienced the collapse of a cardioid antenna in a similar lattice tower, Whitehawk Hill, located in Brighton, UK. A significant TV signal in the region was lost. The failure was caused by fatigue of connection elements of the antenna. To assist the investigation of VS response in Salisbury and in other similar structures throughout the UK, Arqiva has implemented a dynamic response monitoring programme with the aim of identifying and providing structural damping solutions where needed.

The following sections summarise the analysis conducted in Salisbury, from the identification of VS issues to the installation of a mechanical TMD damper.

8.2.3 Initial Data Acquisition

To acquire the dynamic responses, a monitoring device was installed on the 45 m lattice broadcast tower at Salisbury. The acquisition system was a battery powered multifunction extended life (MEL) Gulf Coast Data Concepts (GCDC) accelerometer with an integral data logger.

The location for the device would ideally be at the point where the maximum antenna response is anticipated (i.e., at the top of the cantilevered GRP cylinder antenna shroud). However, due to practical, safety, and operational considerations, the best possible location was chosen as the top of the lattice tower, approximately 500 mm below the underside of the GRP shroud. This location in some LTs could match the neutral response level of the mode shape belonging to the second vibrational mode. In that case, the accelerometer would not provide expected results as it might neglect the desired second mode. To mitigate this issue, all monitoring equipment installed had at least two GCDC devices placed approximately 10 vertical metres apart. This study only used the measurements from one device.

Figure 8-3 includes a picture of the final location of the device in Salisbury. The device is located 44 m above ground level (1 m below the cylindrical antenna) and secured using ties and black tape to protect the unit against water ingress.

The accelerometer was set up with sample frequency of 16 Hz, enough to capture the desired frequency range below 5 Hz.

The battery life (the device is powered with two ‘D’ size batteries) should normally be approximately 5 weeks. However, in the first monitoring exercise of this work, the batteries ran out of power and the device stopped working after 2 weeks of recordings, probably due to lower than average ambient temperatures. The length of the recorded data was found to be suitable and sufficient as the data covered a high range of responses (which may indicate a wide range of wind speeds and a mixture of laminar and turbulent flow occurrences).

The first monitoring session took place from 14th March 2019 until 27th March 2019, as displayed in Figure 8-4. The UK Meteorological Office (‘Met Office’) did not report any significant storm events. However, high and turbulent responses suggest that some events occurred during the monitoring. Apart from these events, the Salisbury LT experienced relatively calm weather with ideal conditions for VS events.

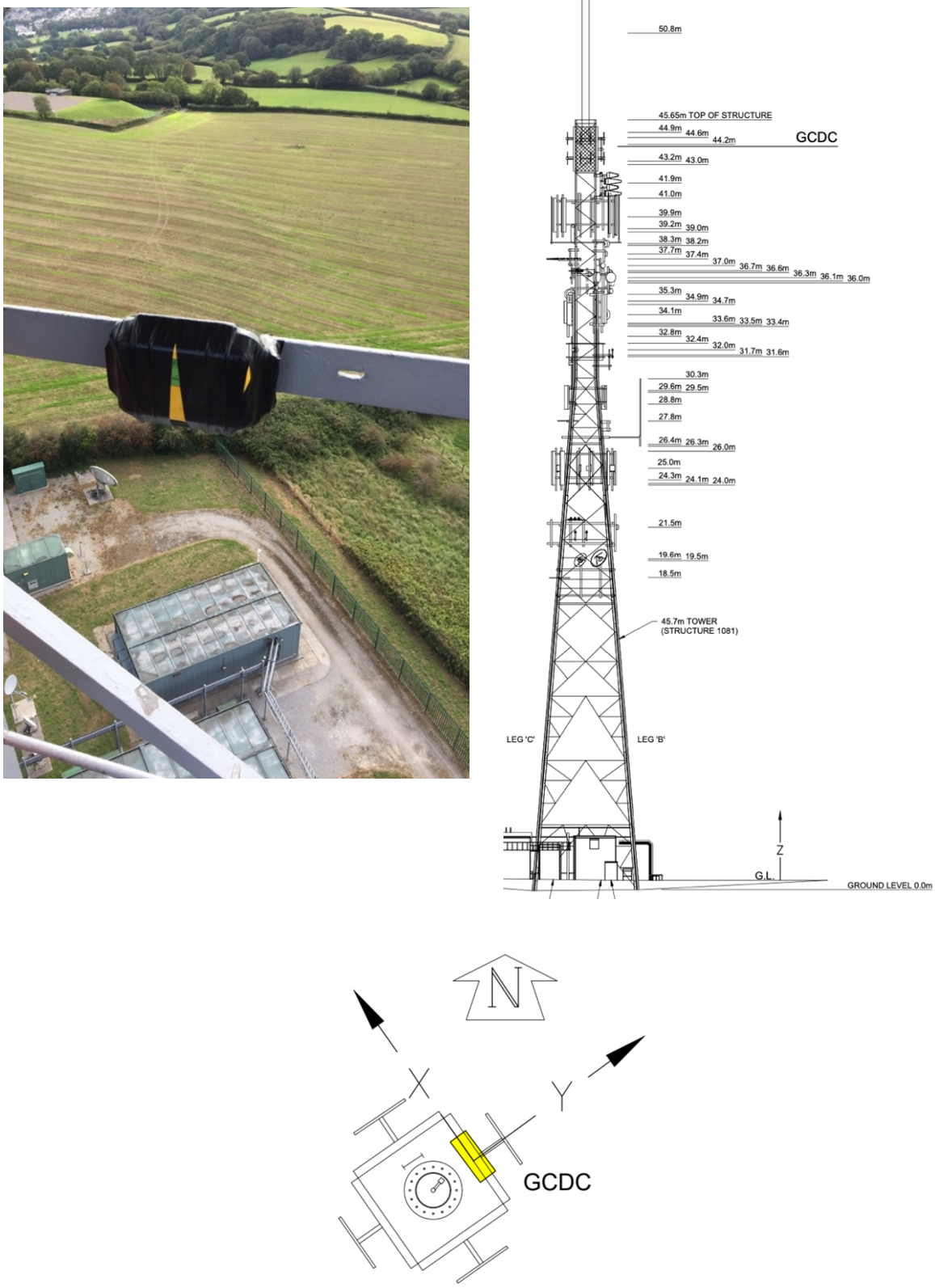

Figure 8-3. Accelerometer GCDC placement. Picture, elevation and plan view.

The fast Fourier transform (FFT) power spectrum density in Figure 8-5 indicates the expected and typical frequency distribution of lattice towers with similar characteristics. A clear first mode at 1.2 Hz dominates the response under along-cross-wind turbulent buffeting. The second mode is located at 2.65 Hz with relatively high power which suggests likely events of VS. The higher third mode occurs at 4.1 Hz.

The identification of the modes helped to better define the stiffness and the mass distribution of the structural model. Both qualities had previously been underestimated. Figure 8-6 plots the modes shapes determined after the optimisation of the Salisbury model done using the MS Tower analysis software. All modes are associated with the main typical cantilevered bending translational modes.

In an attempt to identify each VS event, each suspected response event was separately inspected and analysed. The example of a 15-minute event found on 15th March 2019 is described below. The following evidence was used to identify the VS phenomena:

- Typical VS initiation and lock-in behaviour: A structure experiences high response levels and remains in this state for several minutes (even in the absence of excitation). This so-called ‘lock-in’ effect tends to have a constant response amplitude after reaching the resonance level. The event in Figure 8-7 indicates in red the clear behaviour of a lock-in when the structure suddenly reaches resonance and maintains this behaviour for several minutes until structural damping takes control and decreases the response.
- Wind loading: At the Salisbury LT location, the calculated critical wind speed is very low (6 – 8 m/s is classified as a calm weather condition). The exercise does not count on available wind speed data on site. However, the wind data indications of the UK Meteorological Office and the low turbulence found in response data before and after the event assure the fulfilment of wind conditions. In Figure 8-7, low turbulent behaviour is especially apparent on the Z axis (second time). Behaviour in this direction tends to be more active in turbulent buffeting events.

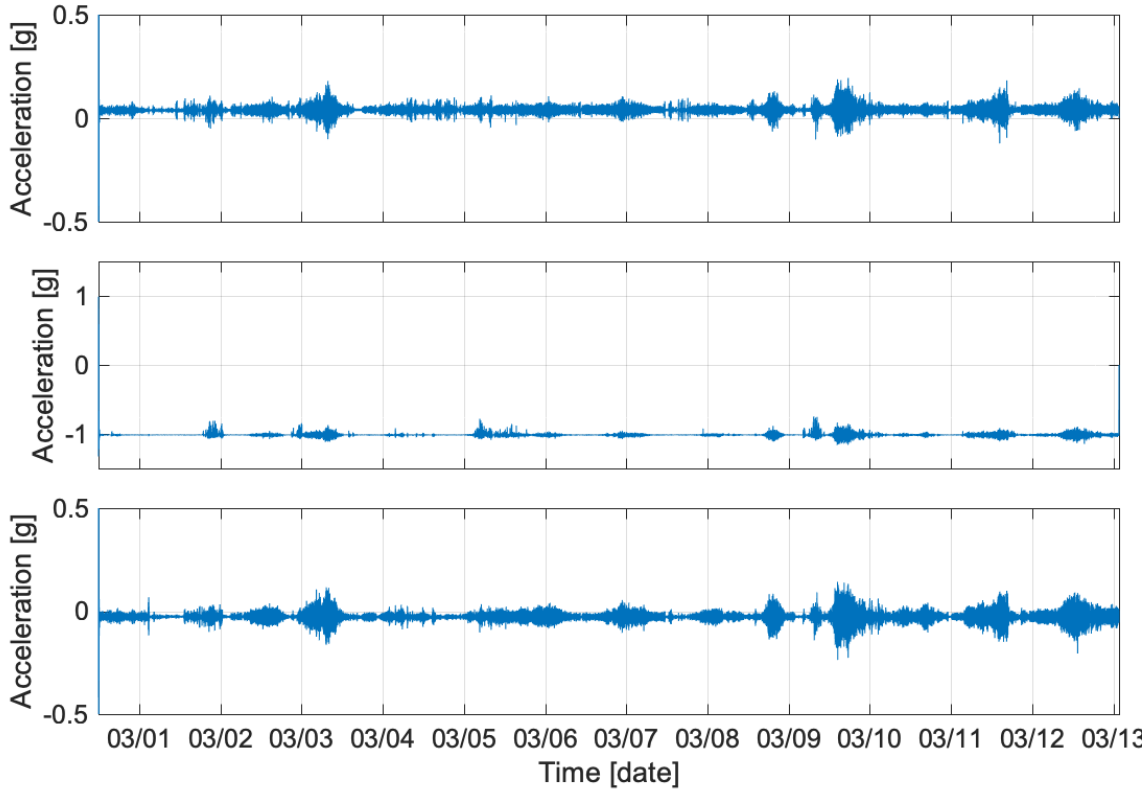

Figure 8-4. Raw time series data from before-damper monitoring. Axes X, Z, and Y are presented in the top, middle, and bottom figures, respectively.

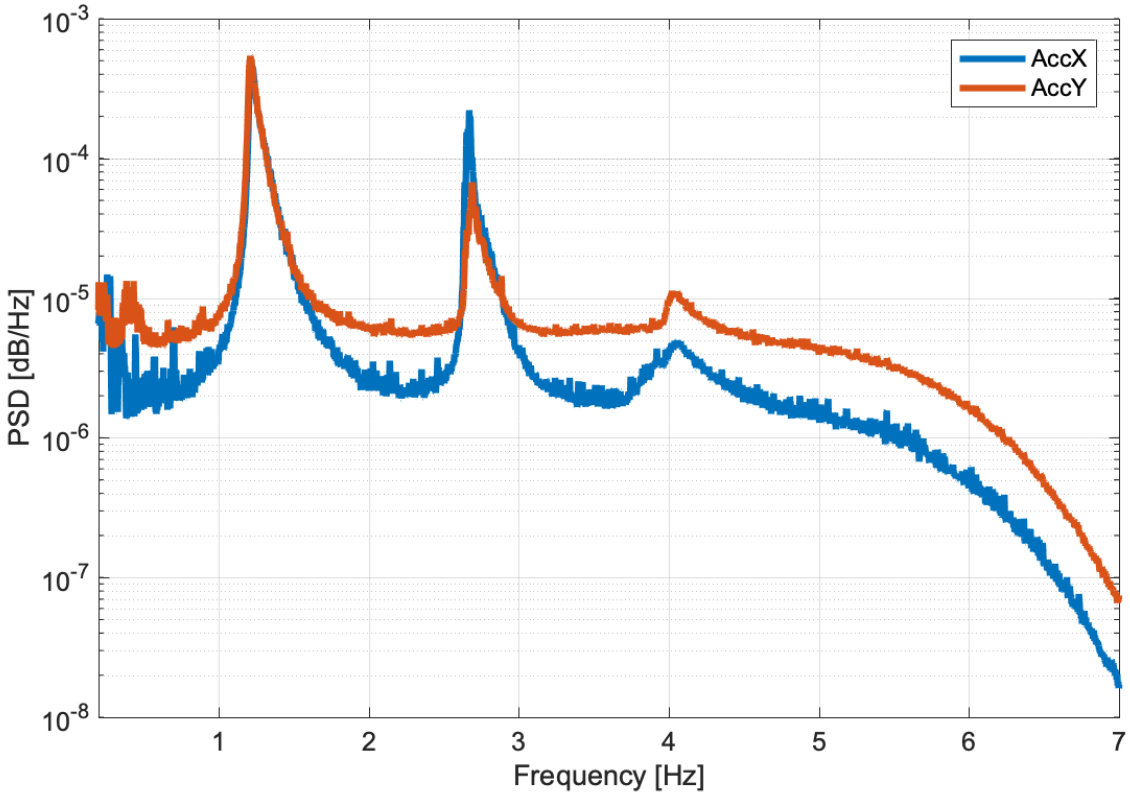

Figure 8-5. Power spectrum density of before-damper monitoring in Salisbury.

- Typical VS response plan geometry: The lock-in effect is characterised by a unidirectional response, as the structure is blocked at a resonance level on one critical mode. The response then tends to have a very flat elliptical shape perpendicular to the wind flow direction (see Figure 8-8). This behaviour is typical and constant in cases of different structure types analysed in the literature.
- Frequency match to model: Finally, a lock-in event must be defined by the critical, n_j, introduced by the calculations of St introduced in 2.3.2.1. Figure 8-6 depicts the corresponding PSD of the VS event, where the second mode assumes much higher power than the first or third compared to Figure 8-5.

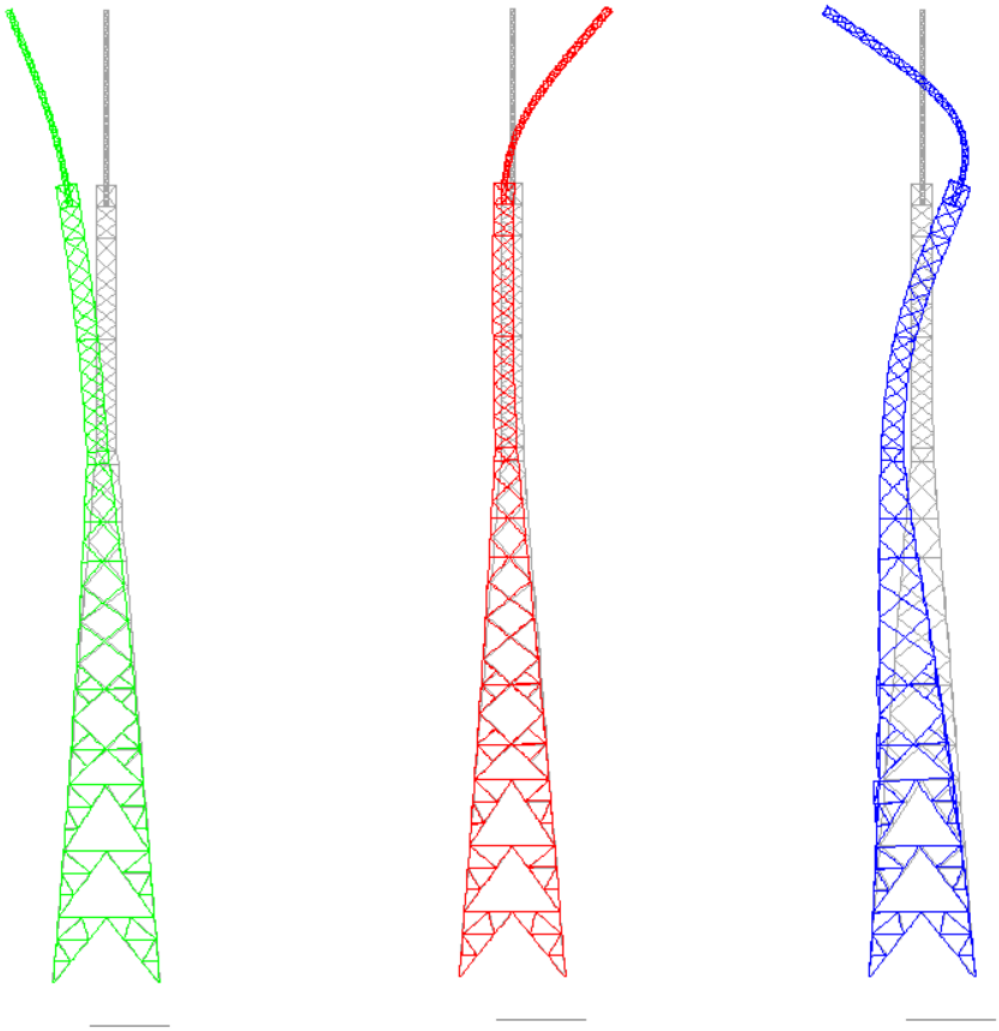

Figure 8-6. Mode shapes of the Salisbury lattice tower before damper installation. First Mode: 1.2 Hz (Green). Second Mode: 2.65 Hz (Red). Third Mode: 4.1 Hz (Blue).

The aforementioned points confirm a clear case of VS. Similar to this case in Figure 8-7, at least 3 to 5 sensitive 5-minute lock-in events were counted per hour on calm days. Some long, continuous events of 2 – 3 hours were also captured. All events act under very different response orientations but at the same resonance frequency of 2.65 Hz. The symmetric section of the antennas makes the response totally dependent on the wind direction.

VS causes fatigue damage to TV broadcasting antenna components inside the cylinder that may adversely affect the quality of television broadcast signals in the surrounding area and may even result in objects detaching and falling to the ground. To prevent these deleterious events, Arqiva agreed that a damper should be installed.

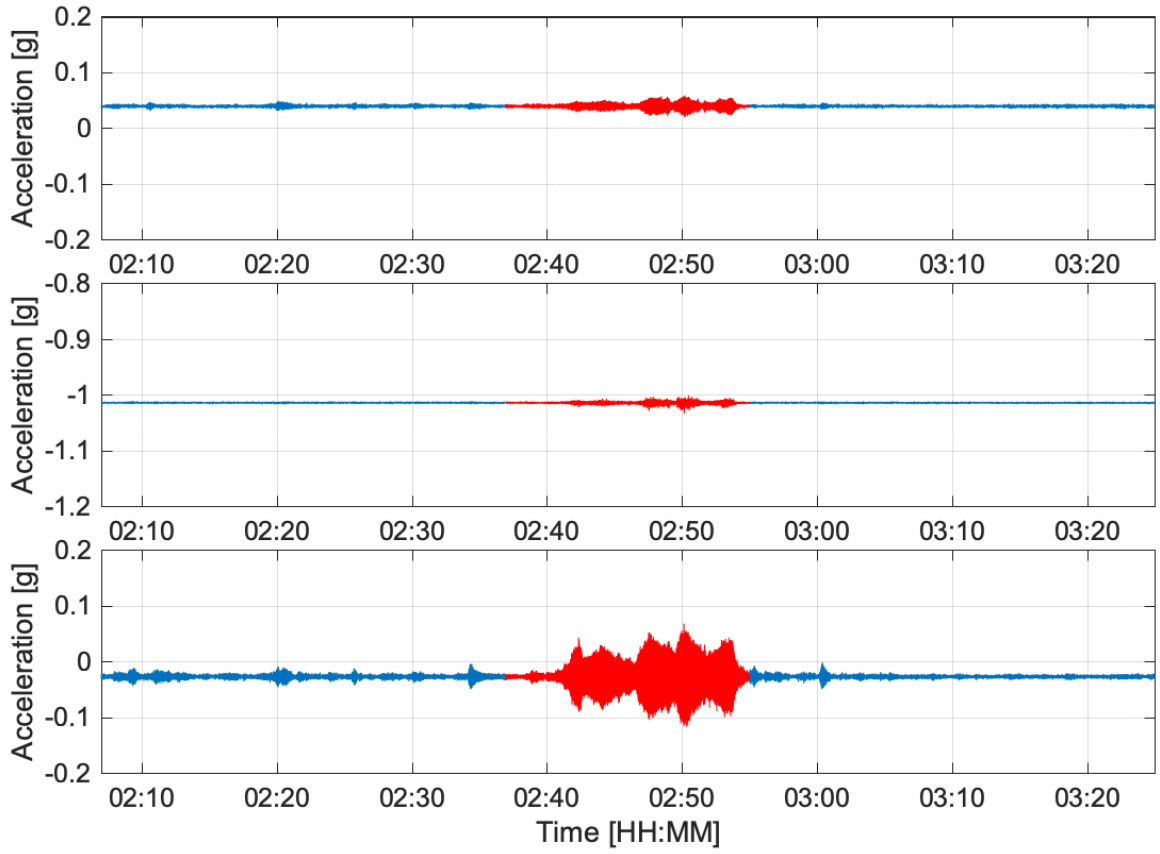

Figure 8-7. Timeline of the VS event at the Salisbury LT on 14th March 2019 from 01:35 – 01:55. Axes X, Z, and Y are presented in the top, middle, and bottom figures, respectively.

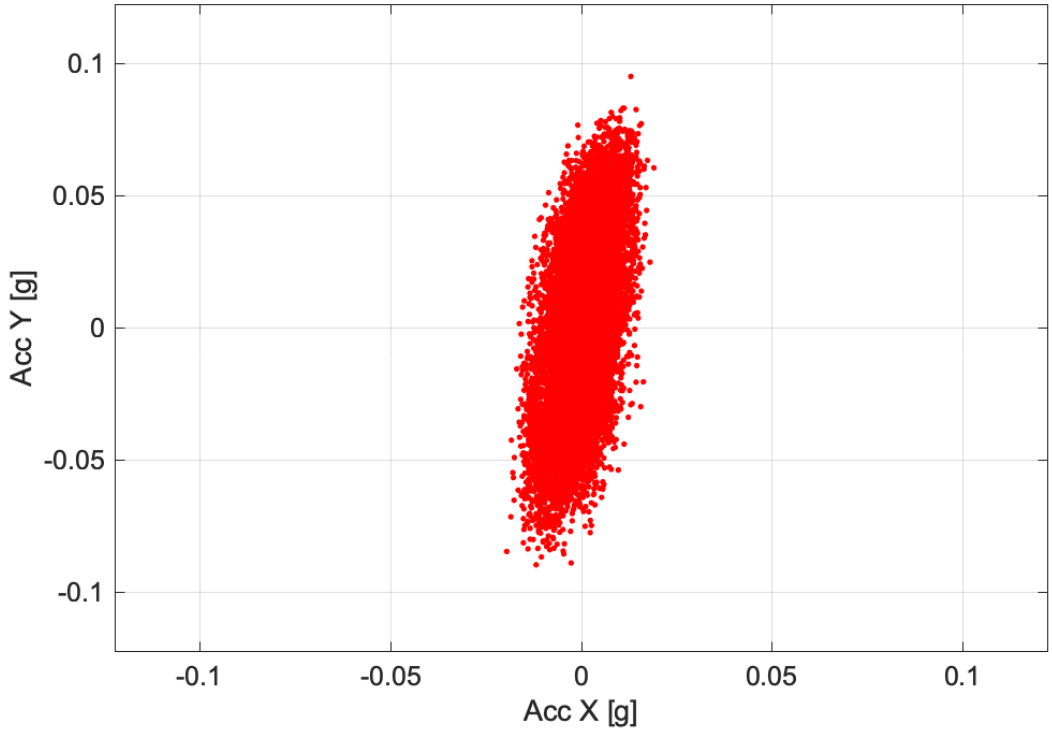

Figure 8-8. Plan view of the VS event at the Salisbury LT on 14th March 2019 from 01:35 – 01:55.

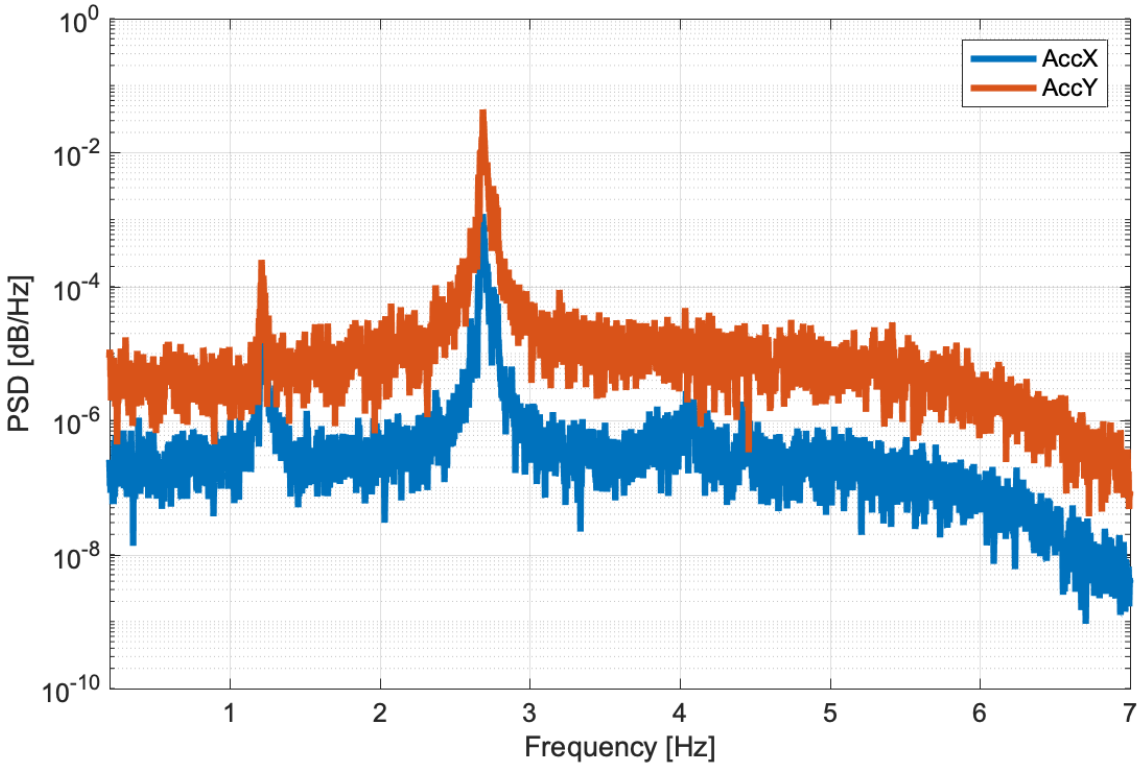

Figure 8-9. Power spectrum density of the VS event at the Salisbury LT on 14th March 2019 from 01:35 – 01:55.

8.2.4 Damper Installation

The damper chosen for the Salisbury site is a dynamic vibration absorber (DVA) damper designed by Professor Michael Wahle from Geilenkirchen, Germany, who has previous experiences with similar issues. The design is based on a suspended pendulum with additional friction from a spring-damper element placed with a variable length lever arm to the joint at the top of the tower. This joint is designed to allow movement in all directions with very small friction effects (Figure 8-10).

The damper features a 'stop-choc' stainless steel element which maintains initial working conditions throughout the device's lifetime without corrosion or temperature dependency. This new element has undergone various laboratory tests to determine its feasibility and to design its mechanical properties. The effective stiffness (storage stiffness) and the effective damping values (loss stiffness) were calculated for all response combinations. Hysteresis curves measured for the resonance conditions of the structure.

Based on the stiffness and mass changes following the installation of the DVA, the optimal tuned properties are $n_{2,\text{crit damped}}$ = 2.65 Hz and $\zeta_{2,\text{crit damped}}$ = 0.25 %; these values were verified by a complete set of directional operational modal analysis (OMA) experiments conducted using a prototype built for that purpose by Prof. Michael Wahle. Free decay fitting confirmed a minimum of 0.2 – 0.4 % of critical damping very near or over the optimal required value of 0.25 %.

The changes in additional mass and damping will redefine the propensity of the cardioid of the antennas to respond to VS, increasing the S_c above the 15 – 20 region with no risk of likely VS (i.e., the geometry will still generate vortices, but the structural capacities of the antennas will hinder any across-wind response).

8.2.5 Post Damper Installation Monitoring

To establish whether the damper was performing as expected, further monitoring was conducted based on the same conditions of previous monitoring. The main objective was to determine if the second mode is still present, which would indicate that VS events may still be occurring.

No additional equipment had been installed or decommissioned from the lattice tower since the previous monitoring event. Any considerable mass changes would alter the results and distort the analysis.

Figure 8-10. Mechanical damper in Salisbury. Picture of Salisbury. 3D damper sketch and Drawing scheme.

The damper was installed and monitoring began on 31st January 2020. Monitoring was completed on 23rd February 2020 (Figure 8-11). The response timelines indicate high responses of the lattice tower, especially in two cases that were associated with two of the strongest storms of 2020 in the UK. The first one, called Ciara, swept across the whole of the UK on 9th February 2020, bringing heavy rain and very strong winds. The strongest gust recorded was 44 m/s at the Needles, Isle of Wight, located just 25 miles from Salisbury. The second storm, Dennis, caused the most significant impacts, causing flooding in parts of South Wales and England. The strongest wind gust of 41 m/s was recorded at Aberdaron, in North West Wales. Apart from these events, the weather was generally quiet, generating ideal conditions to obtain low wind speeds comparable to those of the previous monitoring period.

Figure 8-12, reveals very interesting results in the frequency domain in comparison to those of Figure 8-5. The background response level of the data increased to 200 g^2/Hz, significantly higher than the previously obtained values. This difference can be attributed to the high-response data: the high turbulence of wind loading and the response distort the data. For lower level of response, PSD characteristics at the same levels are generally similar to the previous monitoring data.

In terms of mode behaviour, the main mode appears at the same level with much lower power absorbed, whilst the second and third modes are buried in background response or dissipated by the damper. A more focused examination was needed to identify modes. Figure 8-14 plots the PSD of the clearest second mode response throughout the entire second monitoring session. This mode appears to be located at 2 Hz after the mass was introduced by the DVA. Further, the first and third mode shift to 1.1 and 3.9 Hz. Nevertheless, the data (Figure 8-14) do not indicate considerable responses, and lock-in events are not further generated.

A search for lock-in cases similar to that of Figure 8-7 was conducted but was unsuccessful. On most of the calm days, the second mode was absent, which suggests that the DVA system acts as expected in this frequency range. However, some minor events appear to be related to the third mode resonance. However, due to their associated low amplitudes, these events were not considered an important dynamic issue.

8.2.6 Conclusions

This study was prompted by an observed excessive high frequency response of the existing cardioid antenna in a lattice tower following cardioid antenna replacement as part of a television broadcast re-engineering project.

As a result, a monitoring system was installed and detected clear events of VS at the second vibration mode. The results were analysed and satisfied properties recognised in the literature. This response is dominated by low winds and appeared to fit predictions of Strouhal given by Eurocode. The short response monitoring provided enough evidence to identify VS events. Despite the relatively short duration of the monitoring and the lack of wind data, the results were sufficient to identify VS events, the effect of different wind conditions on the response of tall lattice towers, and the benefits of trustful update to structural models based on acquired data.

A DVA damper system was constructed to absorb vibrations of the cardioid antenna and was tuned according to the frequency range identified by initial monitoring. A further monitoring exercise verified that no furthers VS events were occurring and suggests that the DVA is an effective solution to control VS response.

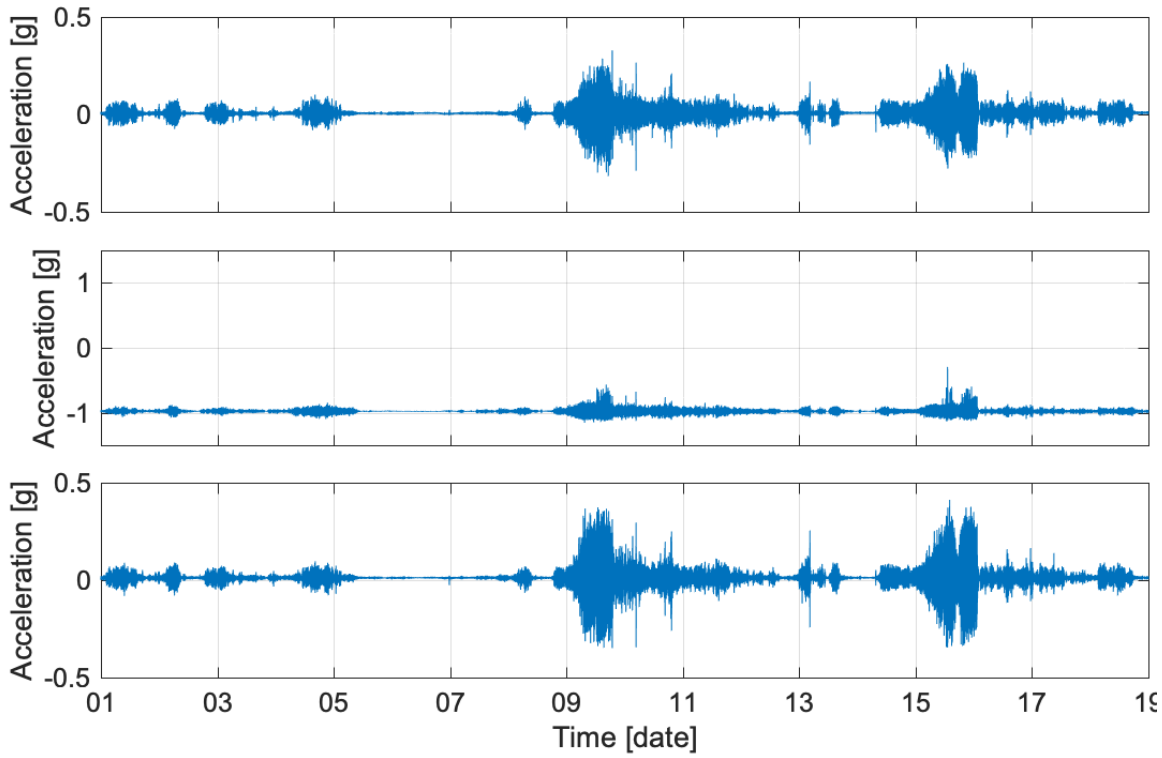

Figure 8-11. Raw time series data from after-damper monitoring in Salisbury. Axes X, Z, and Y are presented in the top, middle, and bottom figures, respectively.

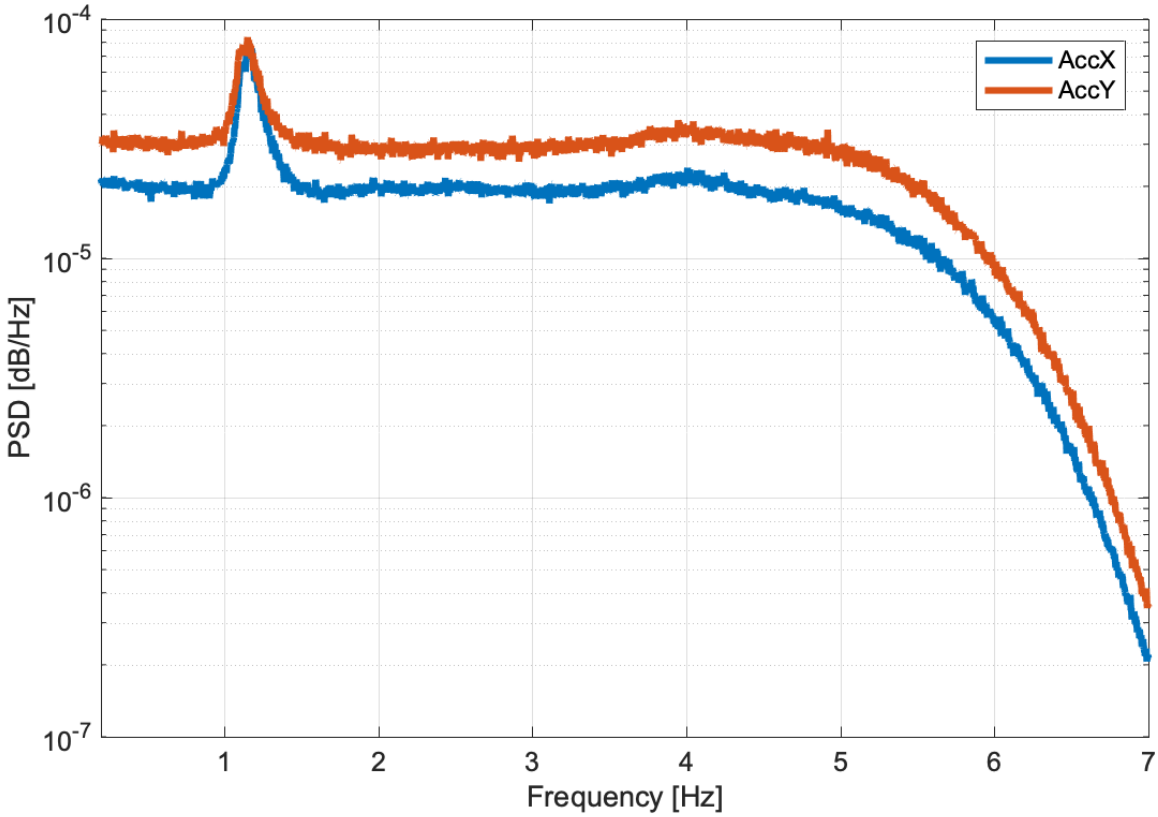

Figure 8-12. Power spectrum density of after-damper monitoring in Salisbury.

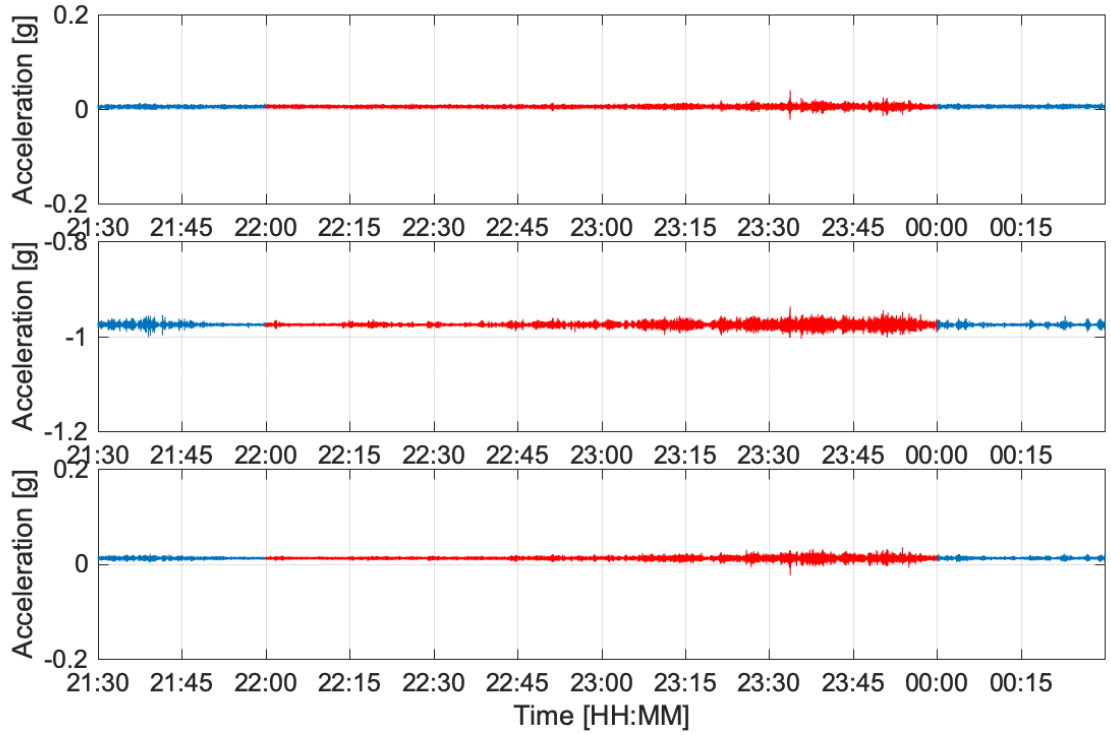

Figure 8-13 Response timeline of calm day after-damper monitoring in Salisbury. Axes X, Z, and Y are presented in the top, middle, and bottom figures, respectively, on 31st January 2020 from 22:00 – 00:00.

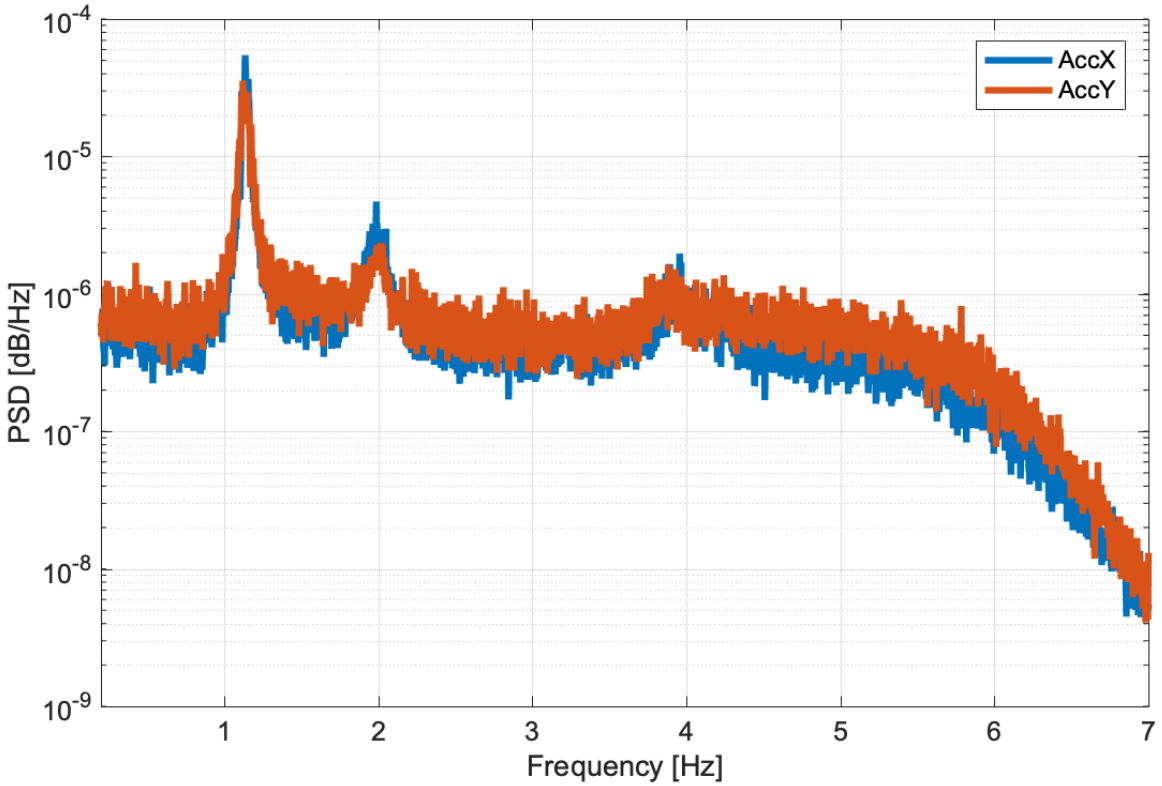

Figure 8-14. Power spectrum density of response data from after-damper monitoring in Salisbury, on 31st January 2020 from 22:00 – 00:00.

8.3 Case 2: Brougher Mountain Lattice Tower

8.3.1 Introduction

In 2010, the Brougher Mountain tower was observed to vibrate excessively, so Arqiva commissioned Flint and Neill (F&N), currently known as COWI, to investigate the likely cause of these vibrations and their structural significance [126].

Consultants COWI have the best structural engineering experience related to communication towers in the UK, have several publications related to national codes writing, and are the main consultant for the most difficult projects in the Arqiva portfolio. Some information, reports, and monitoring data used in this chapter were written by their engineers; this work is proof of the company's invaluable experience obtained in recent decades.

The likely excitation mechanism would be VS from the UHF panels mounted on a cantilever spine on top of the tower. Inspection of the tower after the events yielded

evidence of bolt loosening within the leg joints at the top of the tower (Figure 8-15). All the affected bolts have subsequently been replaced or re-tightened.

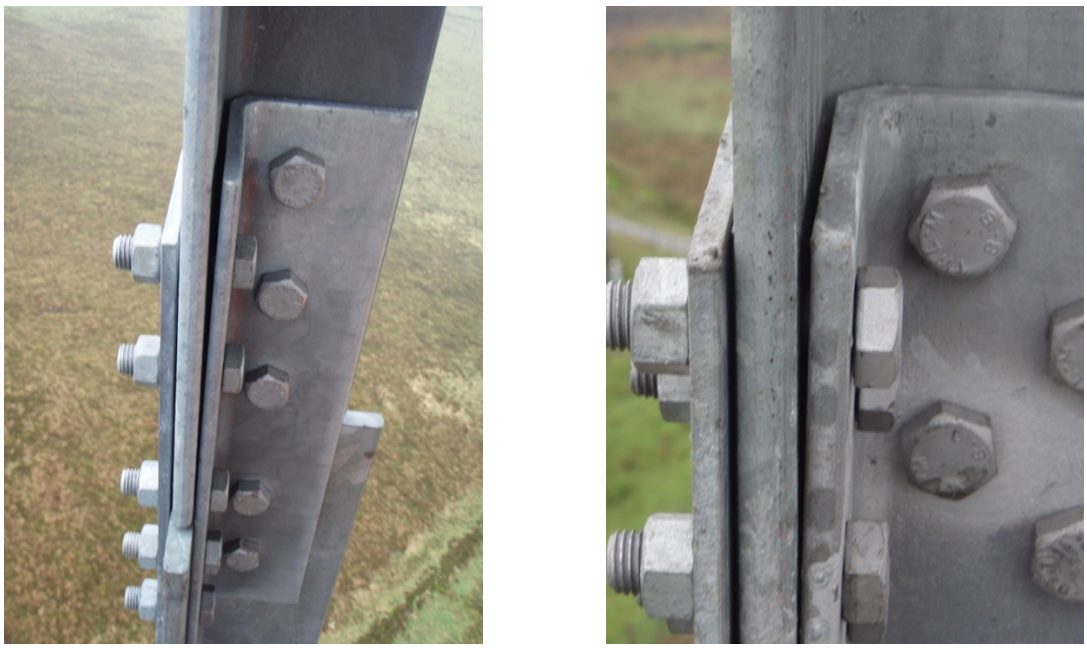

Figure 8-15. Pictures of inspection of leg joints at Brougher Mountain after VS events.

For this reason, an initial investigation focused on the possible crosswind response of the tower and did not include other dynamic responses to wind loading.

Initially, COWI provided an extensive reporting based on the calculation of the crosswind response of the tower to vortex excitation following the procedure described in British Standards [24]. Additionally, and for comparison, the VS response of the tower was also calculated using Approach 2 in Annex E of Eurocode [26]. The conclusions revealed that serious VS-induced damages appear in the first four vibration modes of the UHF antenna. Higher modes tend to be neglected due to the turbulence intensity of high wind speeds and higher structural damping produced by larger relative displacements between structural components. Therefore, low modes may be more susceptible to VS excitation. Full-scale monitoring can provide further quantitative information on the effect of VS, so wind tunnel testing of the existing antenna was commissioned. The addition of damping was recommended as the preferred mitigation method.

Three sets of monitoring data were obtained during different scenarios of structural damping in the following 5 years until 2015 to analyse the response and wind loading of the LT.

This section summarises these data and final consultant concerns to analyse how main modal properties behave under each loading condition, especially across-wind VS and external damping conditions after the installation of hanging chain impact dampers (HCD) tuned according to each threatening mode. For this analysis, structural identification methods such as stochastic subspace identification (SSI) and fast Bayesian OMA (BAYOMA), which are already expertise acquired during the research (Chapter 6 and Chapter 7), reveal interesting points. The reporting provided by Flint and Neill has been included in this research because it contains key information from throughout the duration of the monitoring project. The researcher is grateful to John Rees and Daniel Parry of the COWI team for all their help.

8.3.2 Description of Brougher Mountain LT

Brougher Mountain Tower (Figure 8-16) is a square steel lattice tower located in Northern Ireland. It is 317 m above sea level and is located at latitude 54.42 ° and longitude 7.46 °. The tower's overall height is 64 m, including a 10.5 m tall cantilever spine supporting an array of eight tiers. It has four UHF panels. The face width of the tower is 7.4 m at ground level; this tapers to 1.6 m at the 46 m level and remains constant to the top of the tower at the 53.62 m level.

The depth of the UHF panels is 200 mm and the face width of the cantilever spine on which these UHF panels are mounted is 640 mm. The overall width of the antenna system is therefore 1040 mm measured perpendicular to a spine face or 1470 mm across its diagonal. For simplicity and due to a lack of detailed records on wind directions which would enable a more refined estimate, an average overall bluff body width of 1.25 m extending from 54.60 m to 63.95 m has been adopted for this study.

In terms of wind approach, Brougher Mountain is in a region with high design wind speed in the UK of 26 m/s. Further, the site is located in a rural area with terrain categories I – II. In terms of topography, the site is at the top of hill surrounded by clear farm fields.

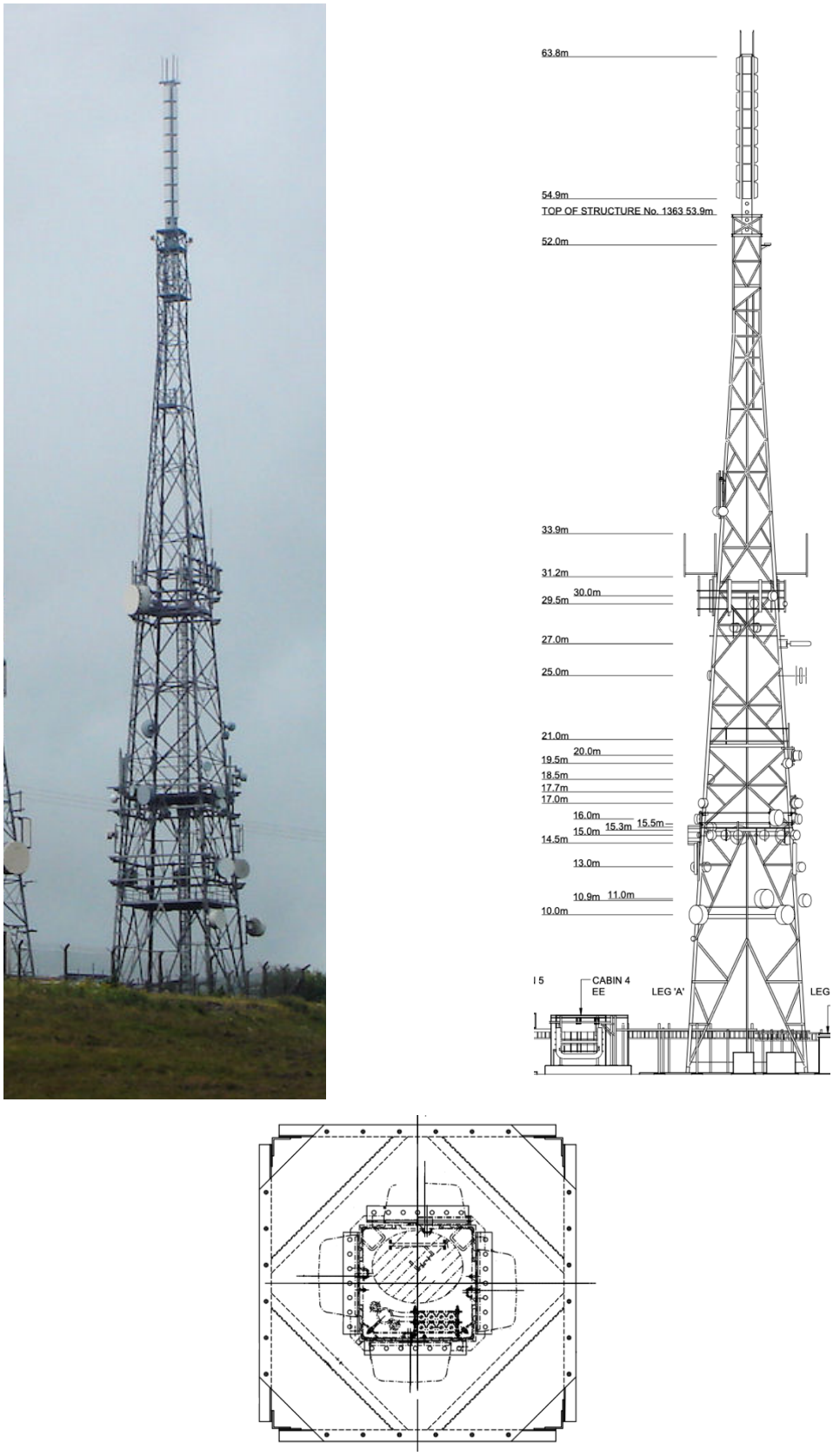

Figure 8-16. Brougher Mountain LT. The left image was obtained from www.mb21.com. The right image is an Arqiva in-house drawing. Downer, the plan view of top spine.

8.3.3 Design Monitoring

8.3.3.1 Introduction

Flint and Neill (F&N) conducted an initial assessment to reduce VS vibrations by installing hanging chain impact dampers. The intended design was sensitive to the undamped amplitude of vibration and the frequency range, so site data were required to achieve correct operation.

To ensure a correct design, the following monitoring was recommended before, during, and after the installation of the damping devices to define the dynamic properties of the tower vibration before proceeding to a detailed design phase and to ensure that the devices worked as expected. Strainstall was appointed to install the specified instrumentation as Flint and Neill's sub-contractor.

The entire exercise adhered to the following timeline:

- 30th Mar 2012. Instrumentation was installed.
- 30th Mar – 9th May 2012. Monitoring 0. Data received from accelerometers were heavily affected by radio frequency interference (RFI). Additionally, power supply issues resulted in the loss of significant quantities of data.
- 27th Sept 2012. New instrumentation was installed; power supply stability and RFI shielding of the sensors were improved.
- 27th Sept 2012 – 13th Nov 2012. Monitoring I. Bare tower conditions without damper actions were measured to define tower dynamic properties.
- Feb – Dec 2013. A damping system was designed for mode 1.
- 5th Dec 2013 – 25th Mar 2014. Monitoring II. A bare tower was monitored in high wind speed conditions to confirm the need for second- or third-mode dampers.
- Jun 2014. A mode 1 damper was installed by NG Rigging.
- 27th Jan – 1st Jun 2015. Monitoring III. The purpose of this monitoring phase was to confirm whether the installed damper adequately suppressed the vibrations previously observed.

The final reports confirmed that responses obtained after the installation would not further deteriorate the structural integrity of the lattice towers. The peak stress range resulting from the last displacements during monitoring III (acceleration peaks of

0.18 g) was estimated to be $\pm$ 15 N/mm^2 and was well-separated from the range of $\pm$ 41 N/mm^2 previously recorded during Monitoring I and II before the installation of the damper.

8.3.3.2 Instrumentation

The instrumentation Flint and Neill specified to be installed on the tower consists of the following components:

- Two pairs of monoaxial accelerometers installed at two different levels (Figure 8-17). Accelerometers a1 and a2 were installed at the 52.6 m level, whilst accelerometers a3 and a4 were both installed at the 47.8 m level. At both these levels, a pair of accelerometers was installed to detect accelerations in orthogonal directions on a horizontal plane. Accelerometers a1 and a3 were aligned perpendicularly to the north and south faces, whilst accelerometers a2 and a4 were aligned perpendicularly to the east and west faces. All accelerometers functioned in the range of $\pm$ 5 g at a sampling rate of 20 Hz.
- A single anemometer was installed at the 52.4 m level. The anemometer was located at the end of a tube which cantilevered approximately 2.5 metres to the south of the structure. The tube was connected to leg C and leg D of the structure by leg clamps. The anemometer works within the horizontal wind speed range of 0 – 60 m/s for wind from any direction (i.e. 0 – 360 ° ETN). Unfortunately, the anemometer was configured by Strainstall to sample wind speeds at 0.167 Hz (i.e., one sample every 6 seconds) rather than at the specified sampling rate of 1 Hz (i.e., one sample every second) required by F&N specification. This limited the useful data that could be extracted from the anemometer to hourly mean wind speed and direction; turbulence could not be properly defined.
- One temperature probe was incorporated into the anemometer.

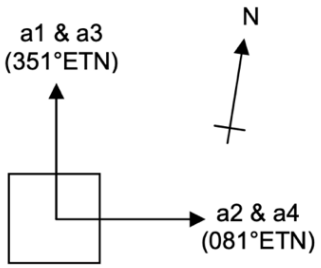

Figure 8-17. Orientation of accelerometers, courtesy of the Flint and Neill reports.

Figure 8-18. Monitoring instrumentation in Brougher Mountain, courtesy of the Strainstall report.

8.3.3.3 Hanging Chain Impact Damper

HCD consists of a tied bundle of chains suspended centrally from a universal joint within a lined steel tube. The universal joint allows the suspended chains to rotate freely about the horizontal axes (see Figure 8-19). Arqiva had previous positive experiences with HCD in the Belmont and Winter Hill masts in the early 1970s.

During a vibration event, the chain will oscillate out of phase with the motion of the structure. If the damper is correctly designed and the vibrations are of sufficient magnitude, the chains will strike the sides of the tube twice per cycle of the structure in a stable manner, thus dissipating energy.

Figure 8-19. A picture of the hanging chain damper at Brougher Mountain, courtesy of Flint & Neill reports.

At Brougher Mountain, the assessed target of damping to supress mode 1 VS was calculated as log dec δ = 0.06 → ζ = 0.95 %. It is assumed that the structure itself provides δ = 0.02, leaving the damper to augment this value by δ = 0.04 → ζ = 0.63 %. The assumed level of structural damping is lower than the codified level of damping provided by a tower with angle legs and bracings and black bolted connections; for example, Eurocode [26] gives δ = 0.05. However, codified values are provided for use in the calculation of along-wind response at ULS. At lower wind speed events such as VS, lower levels of damping are expected as bolted connections do not slip, so little energy is dissipated through friction.

The chain length was set such that the ratio between the fundamental frequency of the Brougher Mountain tower and the hanging chains was 3.5. At this ratio, the entire

length of the chain is expected to make impact with the wall of the tube, thus maximising the dissipation of energy.

The gap between the chain and the tube has been set low so that $d/x_o = 1.72$ for the peak displacement. This gap ratio has been employed so that the damper starts to work at lower magnitude vibrations rather than just the peak displacements identified. Such a gap ratio has suboptimal efficiency; a relatively high chain mass has been used to compensate for the relative damper inefficiency.

Tests previously undertaken on behalf of Arqiva on the chosen tube have indicated that the tube has a coefficient of restitution between 0.20 and 0.25.

Figure 8-20 indicates the range within which the damper installed on Brougher Mountain is expected to achieve two stable impacts per cycle and thus be effective. The peak tip displacement identified in previous monitoring phases was $x_o = 121$ mm; this is the assumed displacement used to achieve $d/x_o = 1.72$. For the design coefficient of restitution, the damper is only effective if the magnitude of vibration is such that $d/x_o < 5.3$. This value corresponds to a cantilever tip displacement of around 40 mm. The damper will be ineffective if the magnitude of vibration is lower than this value.

In situations where the damper is effective, it will reduce the magnitude of vibration. However, by suppressing the magnitude of vibration, x_o declines and the ratio d/x_o increases. This effect will cause the damper to become ineffective, as the chain will no longer strike the sides of the tube. If the forcing mechanism is sustained, the vibrations will increase until the chain starts striking the tube again, and the level of damping will increase. This cycle will repeat until the forcing frequency changes.

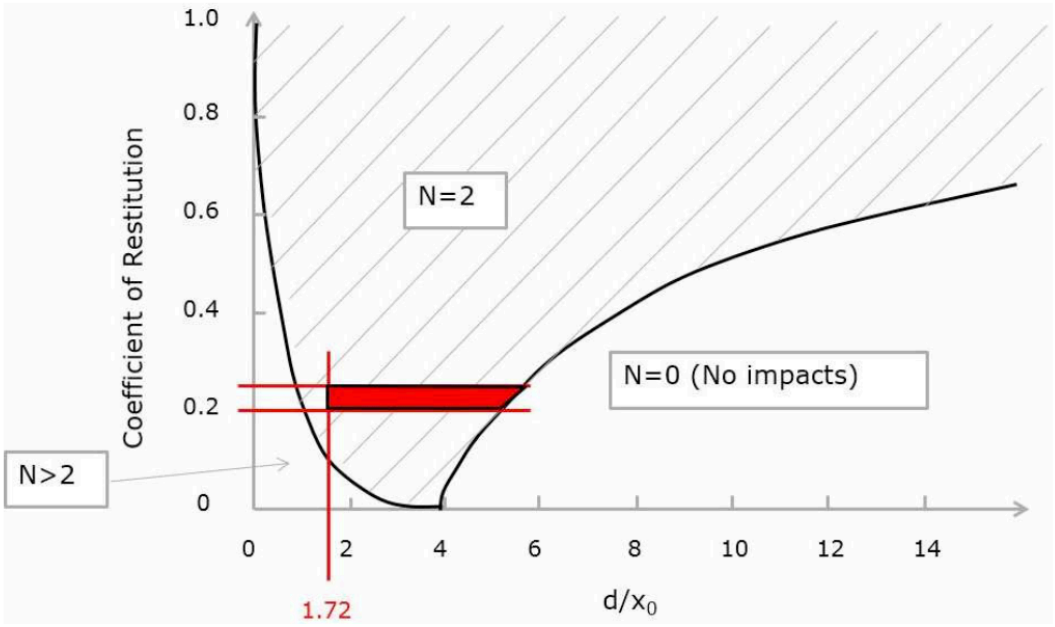

Figure 8-20. Range of stable impacts in Brougher Mountain, courtesy of Flint and Neill. Assessment report of Brougher Mountain.

8.3.3.4 Monitoring 0

These kinds of structures are specifically designed to hold UHF and VHF antennas which provide broadcasting and radio services for the coverage area. These analogue technologies require high power equipment and cabling which radiate dangerous frequency within metres of their location.

For those reasons, climbs up to those height levels have work restrictions that require antennas to be switched off.

During the antenna's service life, RFI can affect severely any acquisition device like the proposed accelerometer. The initial instrumentation installed on the tower between 30th Mar 2012 and 10th May 2012 recorded strange behaviour which suggested RFI. Additionally, there were power supply issues with the data logger which resulted in the loss of significant quantities of data. Those issues are enhanced proportionally to the exposed cabling in heavy weather conditions.

As indicated by the example in Figure 8-21, the insufficient-quality data obtained could not determine properties for the damper detailed design phase. The data collected from this period were discarded. Strainstall investigated methods to improve RFI shielding for the sensors and enhance power supply stability.

Those experiences will be very useful for further installations, such as those detailed in the next chapter where a sophisticated monitoring system is applied to the higher power antennas in high guyed masts.

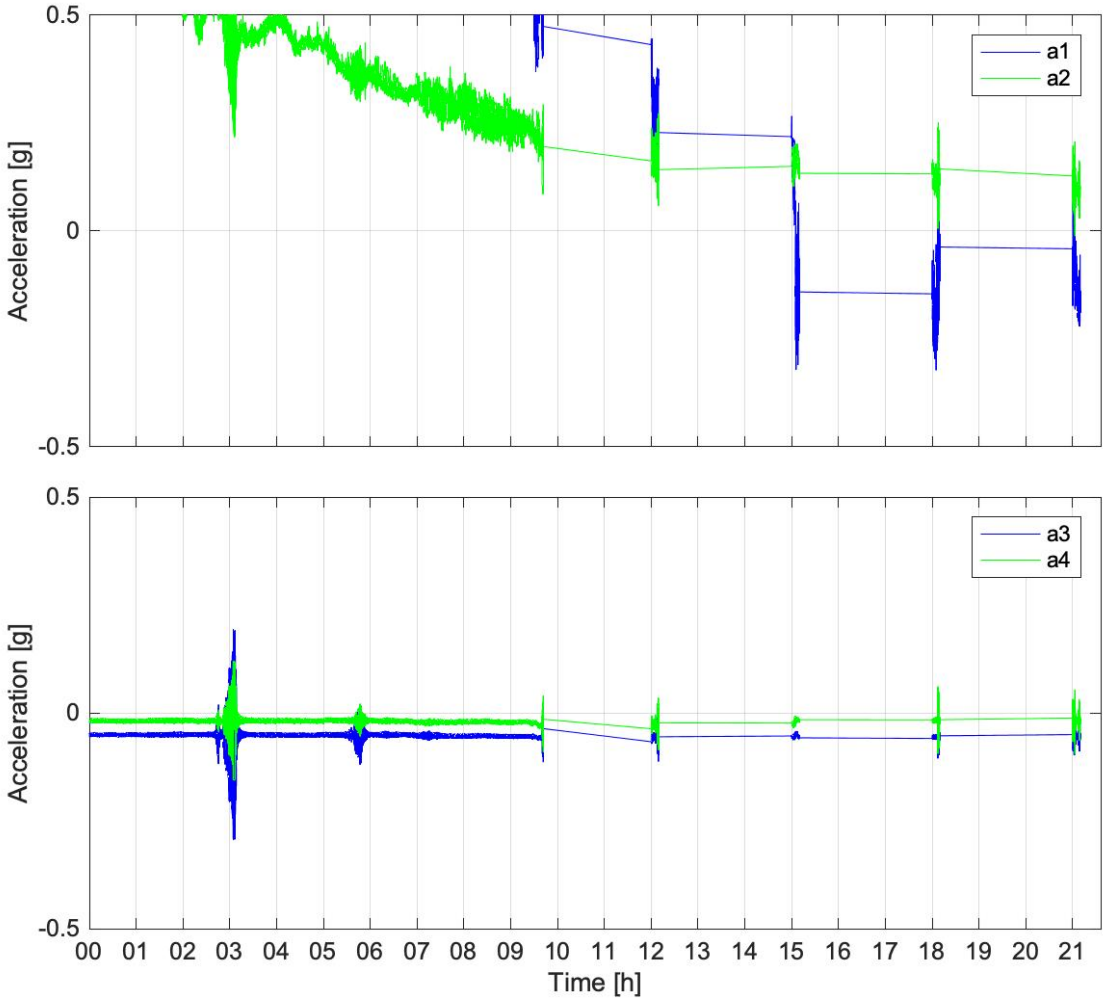

Figure 8-21. The response timeline of accelerometers on 20th Apr 2012.

8.3.3.5 Monitoring I

The purpose of this first of batch of data was to identify the dynamic properties of the lattice towers under high vibrational events observed by inspections, verify the analytical model, and provide enough data to design and install a damper to absorb vibrations.

The instrumentation collected data during the period from 00:00 on 27th September 2012 to 18:00 on 13th November 2012. The exception is a period between approximately 05:00 on 18th October 2012 and 09:00 on 23rd October 2012 not recorded for acquisition equipment issues. In total, approximately 998 hours of data

were collected out of a potential total of 1,026 hours (97% of potential data). Figure 8-22 shows the response timeline of day with high responses.

In terms of loading, wind speeds did not reach values higher than 20 m/s; the collected data were sufficient to assess the structure under across-wind response for VS under mode 1. However, the data would not have captured responses of likely second or third modes. Longer monitoring under winter conditions was still required.

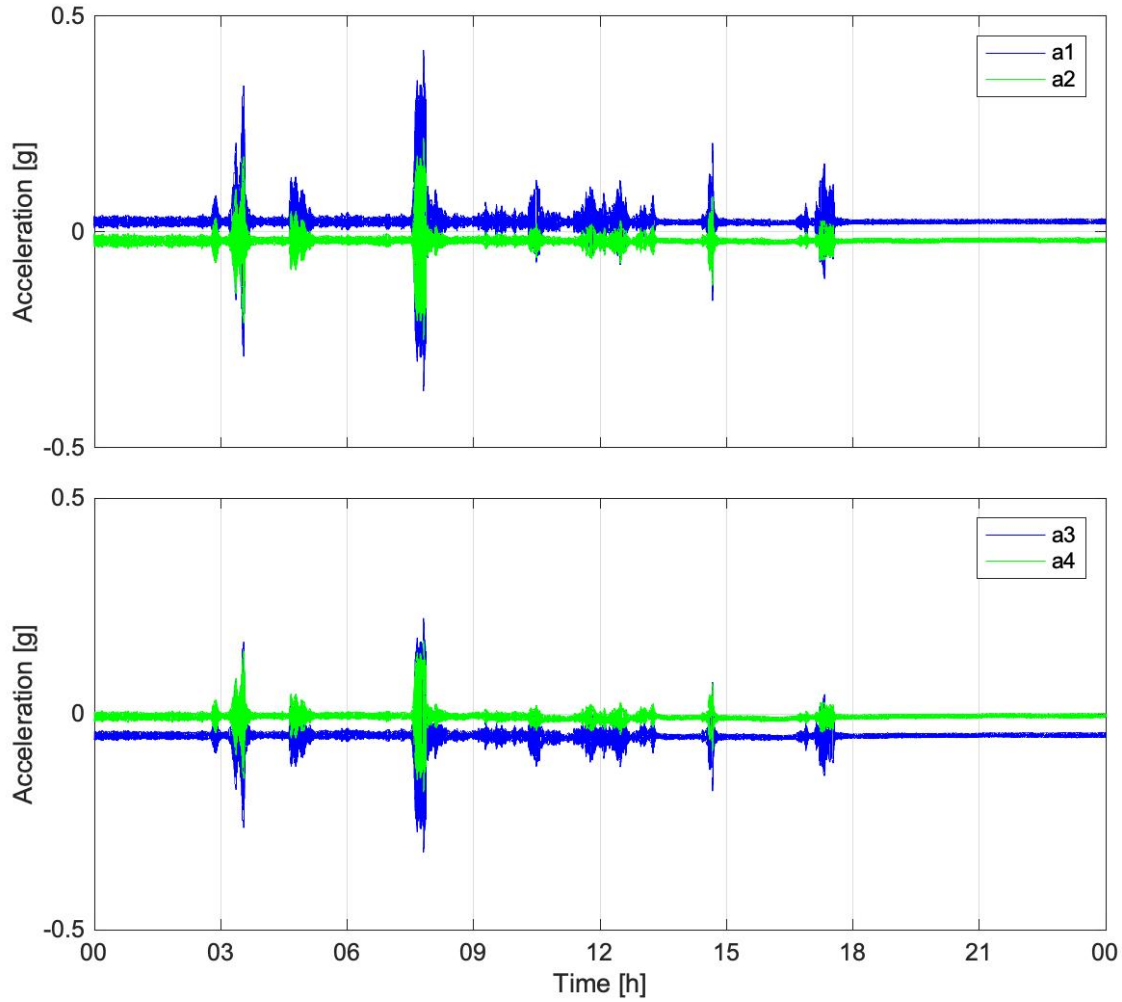

Figure 8-22. The response timeline of accelerometers on 12th Oct 2012.

8.3.3.6 Monitoring II

This monitoring period was intended to augment the information covered by Monitoring I by detecting mean wind speeds over 20 m/s. This data would confirm further cross-wind responses in different modes and buffeting responses of mode 1.

The instrumentation collected data from the period from 00:00 on 5th December 2013 to 12:00 on 25th March 2014, similar to depicted in Figure 8-23. The data recorded

between these two dates is generally complete. Every 7 days there is a 10-min period at approximately 00:45 for which data are not collected. Additionally, approximately 56 hours of anemometer data have null values; this lost data are distributed over twelve days in total. The total monitoring period was 2,652 hours long; the accelerometer data are 99.9% complete whilst the anemometer data record are 97.8 % complete.

The monitoring data satisfied all requirements and led to the decision to install a hanging chain damper. The same installation used in the previous monitoring periods has been used to verify the efficacy of the damper.

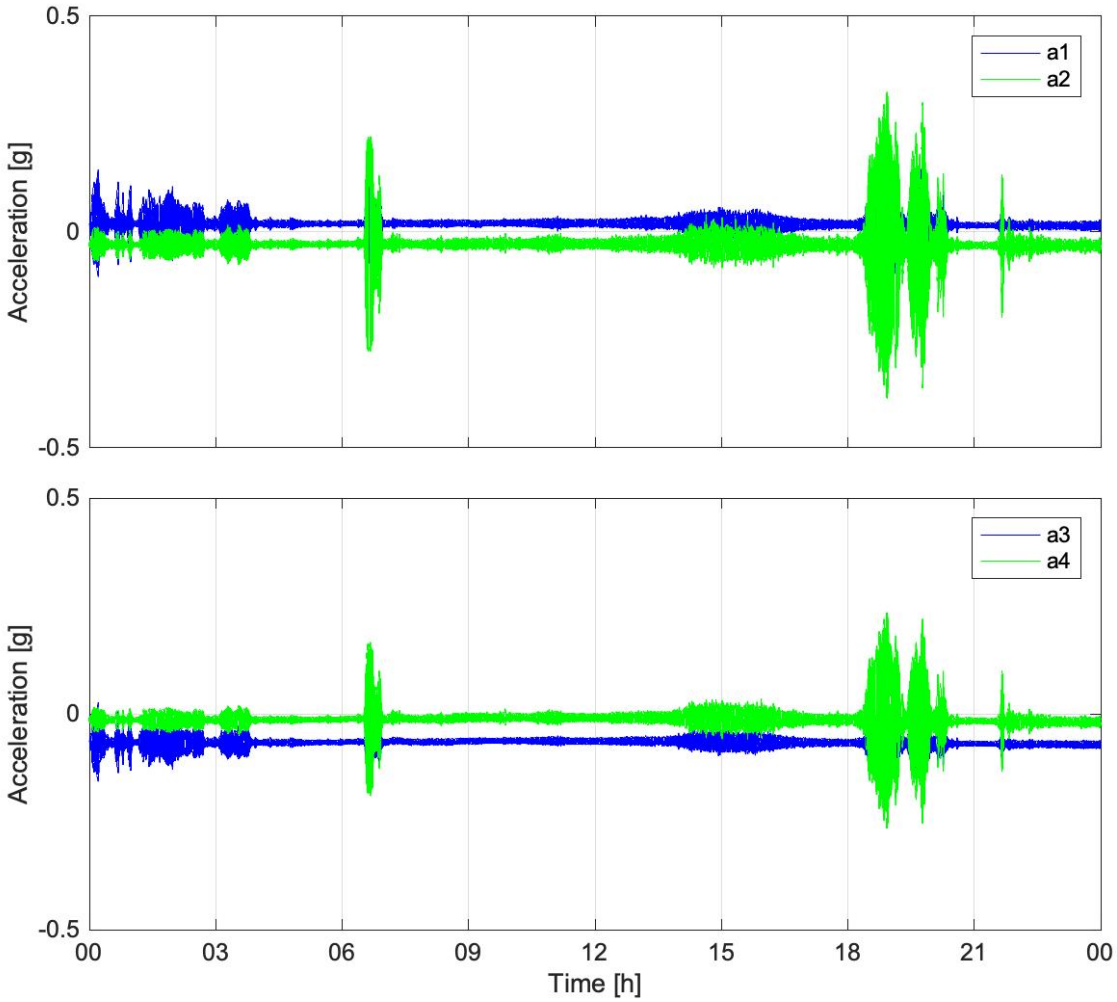

Figure 8-23. Accelerations response on Monitoring II on 14th Jan 2014.

8.3.3.7 Monitoring III

The purpose of this data was to verify how the designed damper behaved during a VS event such as those found in the previous data.

The monitoring system was restarted on 27th January 2015 and was in operation until 1st June 2015 (i.e., 126 days of data were collected). Strainstall was commissioned by Arqiva to provide six weeks of data (i.e., 1,008 hours of data across 42 separate days). Much data were lost from power supply issues which prevented further analyses.

Initially, monthly statistics files were received for the entire monitoring period. From these, the 42 days that contained the most 10-minutes periods with wind speeds in the range of 6 – 10 m/s were identified. Previous monitoring phases identified that wind speeds in this range were the most likely to result in mode 1 VS vibrations. Figure 8-24 and Figure 8-25 depict response and the wind rose timelines of one of those days. As expected, no excessively high responses were found under low wind speeds.

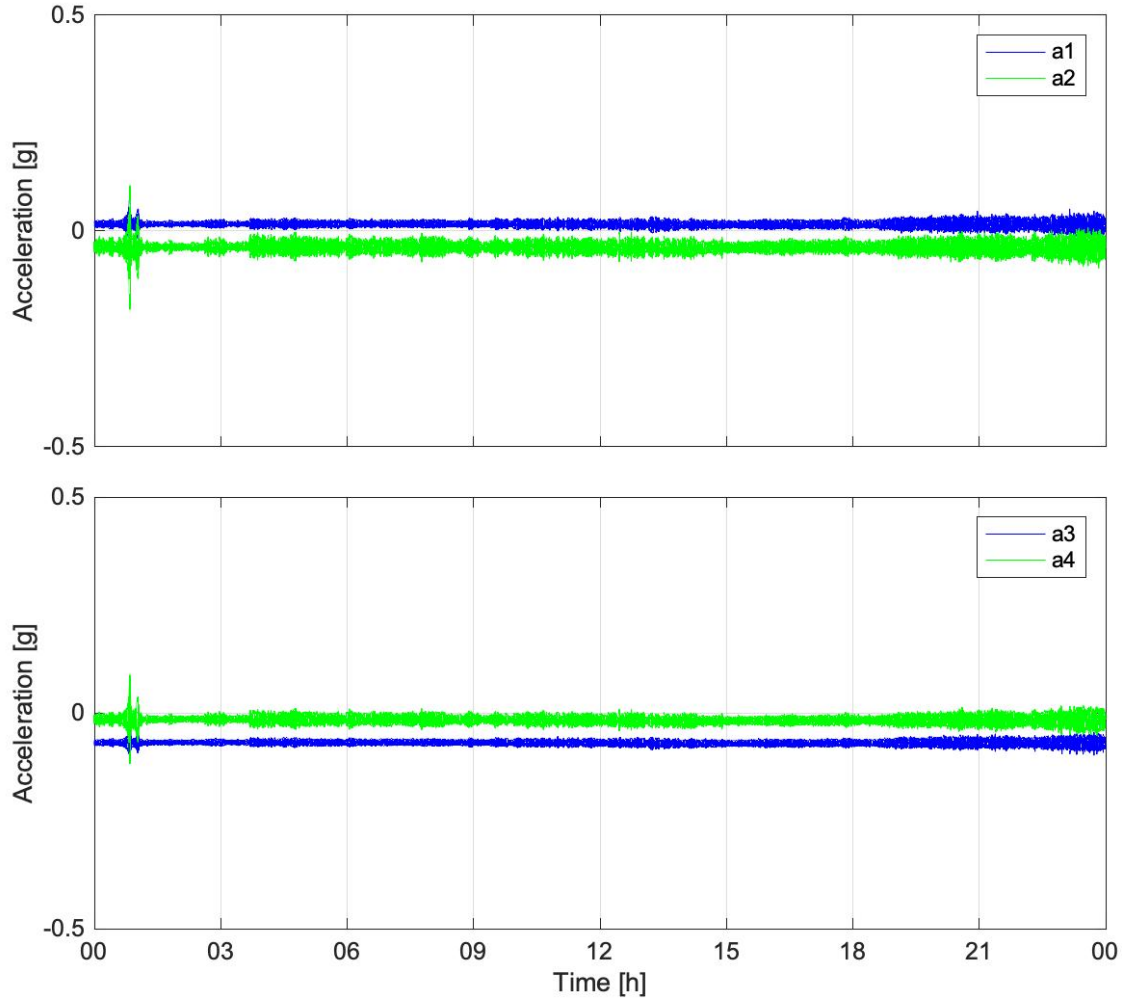

Figure 8-24. Accelerations response on Monitoring III on 16th Feb 2015.

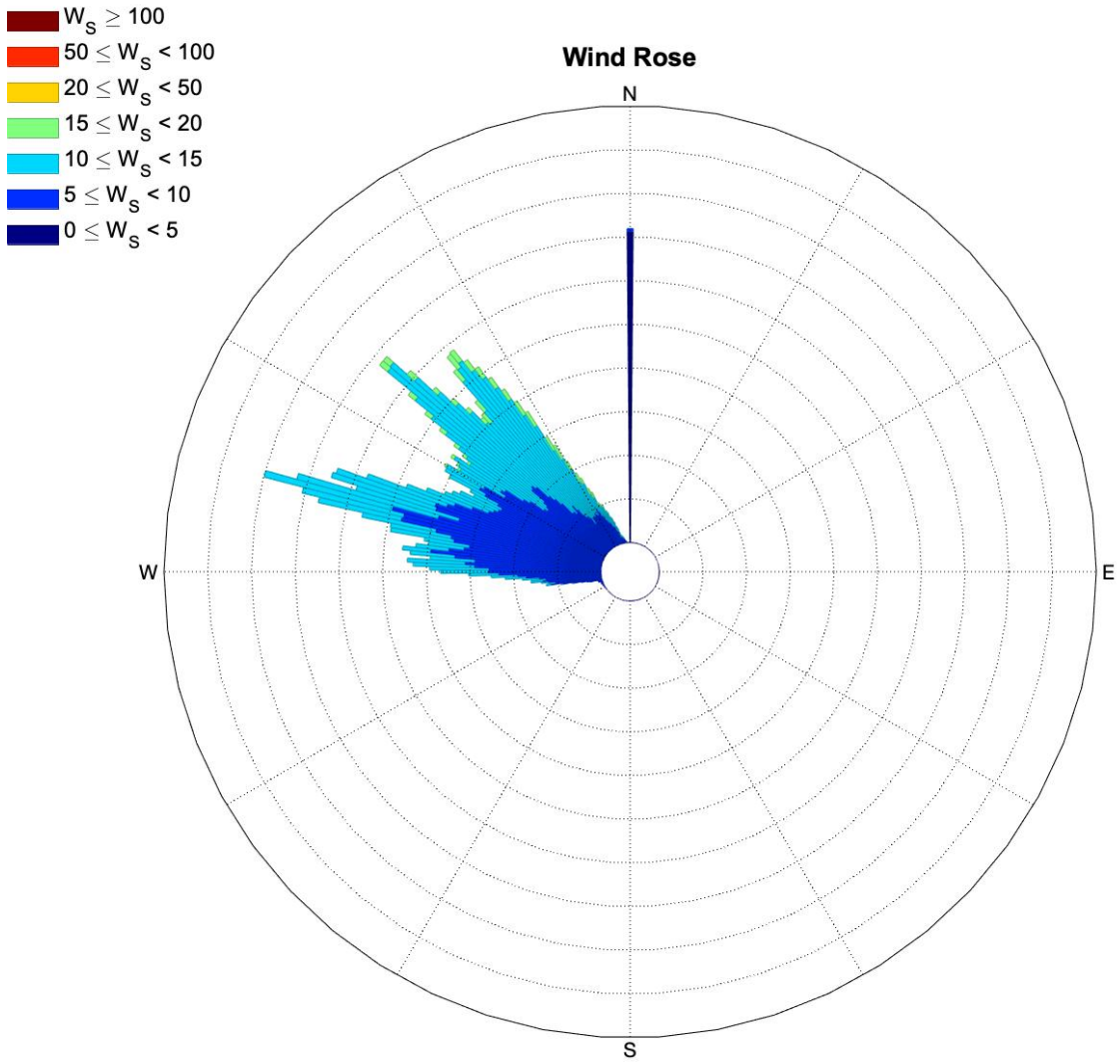

Figure 8-25 Wind rose on Monitoring III on 16th Feb 2015.

8.3.4 Analysis of monitoring in Brougher Mountain

8.3.4.1 Comparison to Predicted Frequencies

The frequency spectrum plot in Figure 8-26 depicts tall, narrow peaks at main natural frequencies of the structure. Those peaks are clear at 1.28 Hz which corresponds with the main mode of vibration. Secondary peaks are evident at 3.2 Hz (second mode) and a group of modes appears at 5 Hz (third mode).

The first mode defines the main behaviour of along-wind vibration from high turbulent buffeting response; moreover, it governs the main across-wind response observed during VS events. On the other hand, second modes could potentially be partially excited by buffeting but do not achieve sustained resonance because the energy content of the wind gust spectrum at these frequencies is low. Only across-wind events

should be considered as VS critical wind speeds are below the design wind speed for buffeting excitation.

As demonstrated by previous examples, response data become an important tool to verify the predicted modes during initial dynamic assessment (Flint and Neill conducted the assessment relevant to this work). High discrepancies are found in Table 8-1, which describes the differences between current results and those previously modelled.

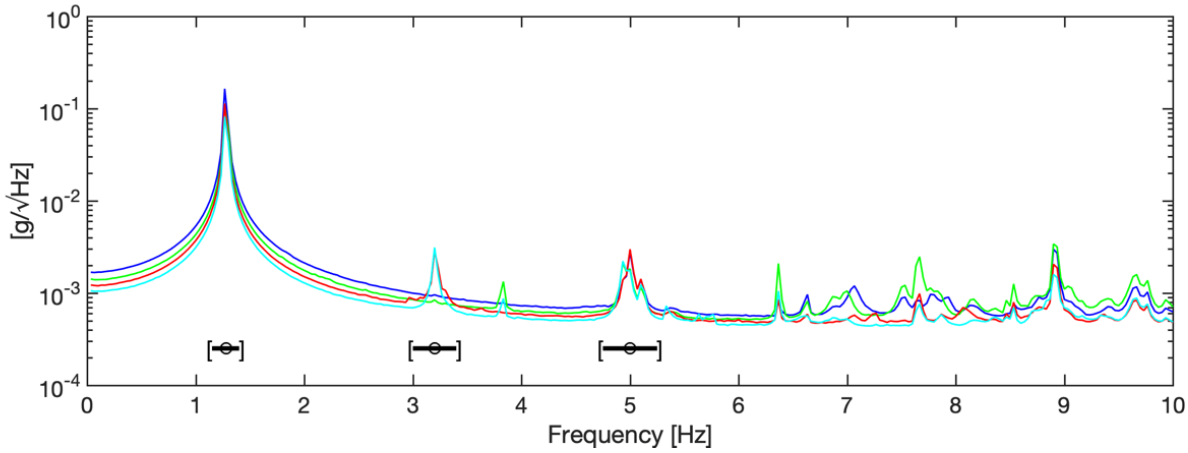

Figure 8-26. Power spectral density at Brougher Mountain from Monitoring I.

Table 8-1. Comparison to predicted frequencies, courtesy of Flint and Neill reports.

Mode	Observed frequency [Hz]	Predicted frequency [Hz]	% difference [%]
1	1.28	1.29	0.8
2	3.2	3.86	20.6
3	5	6.54	30.8
4	-	9.95	-

8.3.4.2 Responses against wind speed

After the reception of the data referred by COWI, the research implements a MATLAB script for postprocessing. The script analyses all data of each monitoring set and reports mean, RMS, and peak responses and power spectrum density or wind speed characteristics.

To facilitate the posterior OMA, a time window of 10 minutes is the optimal time segment to obtain reliable modal properties and to capture main events of wind loading as previous Chapter 6 and Chapter 7.

First, to inspect the global behaviour of the structure, Figure 8-27 presents the correlation between instant wind speed and the corresponding response at both monitored levels. The lower level readings (a3 & a4) are in blue and the upper level readings (a1 & a2) are in black for each introduced monitoring phase.

All plots indicate a response with mean wind speed which shows the behaviour of the structure under turbulent buffeting. This along-wind behaviour is proportional to the level of gust wind loading present and is characterised by high levels of turbulence and aerodynamic damping which collaborate to achieve resonance levels, mainly under the first mode at 1.2 Hz. The highest wind speeds must correspond to larger storm events that occurred during each monitoring session. This buffeting behaviour is plotted in red line for mean wind speed higher than 10 m/s with similar behaviour between monitoring phases.

A notable element of the plots is the highest responses found between 6 – 8 m/s at both high levels. These responses likely correspond to events of VS with high cross-wind response. Further, no similar peaks are found at higher mean wind speeds, negating the existence of VS events in other modes, as objective of Monitoring II.

In the third plot, obtained from Monitoring III, the VS peak is also present but does not have values over RMS 0.1 g. These data are the first indicator that the performance of the hanging chain damper does not prevent the existence of VS events as the Salisbury mechanical damper does, but instead controls the response.

Monitoring III has three times fewer responses than before damper installation under same events, which should substantially reduce the oscillations and the risks of fatigue issues.

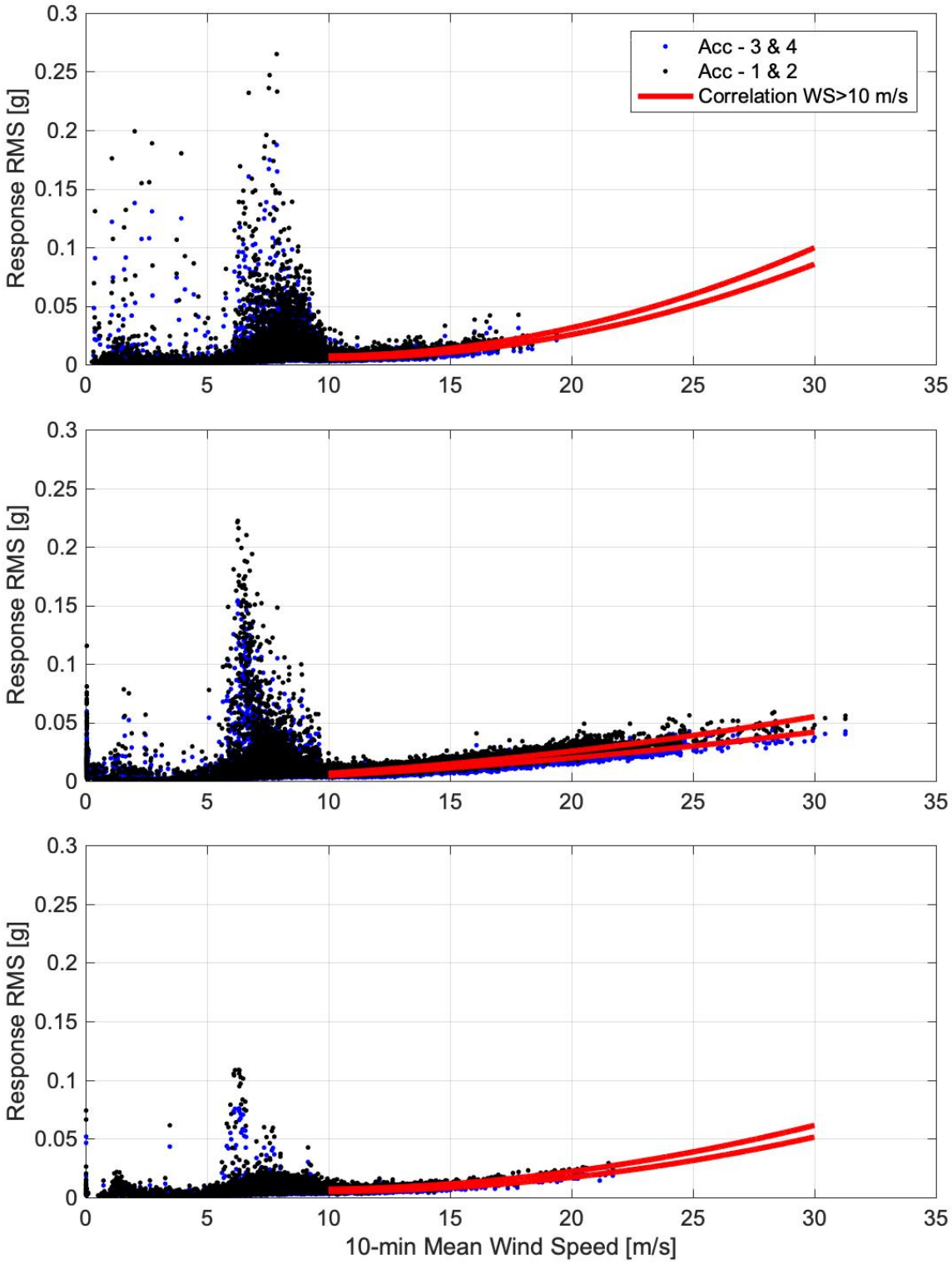

Figure 8-27. Response against 10-min mean wind speed at Brougher Mountain (Monitoring I, II & III are presented in the top, middle, and bottom plots, respectively).

8.3.4.3 Vortex shedding in Brougher Mountain LT

The response is induced after vortexes are created by the incident flow in the bluff spine antenna of 10 m. The plan shape (see Figure 8-28) is a sharp-edged body which should have a Strouhal number between 0.2 and 0.15; these values are given by the codes for cylinder or square examples. Following the formulation introduced in 2.3.2.1, an approximation of the critical wind speed can be found in Table 8-2:

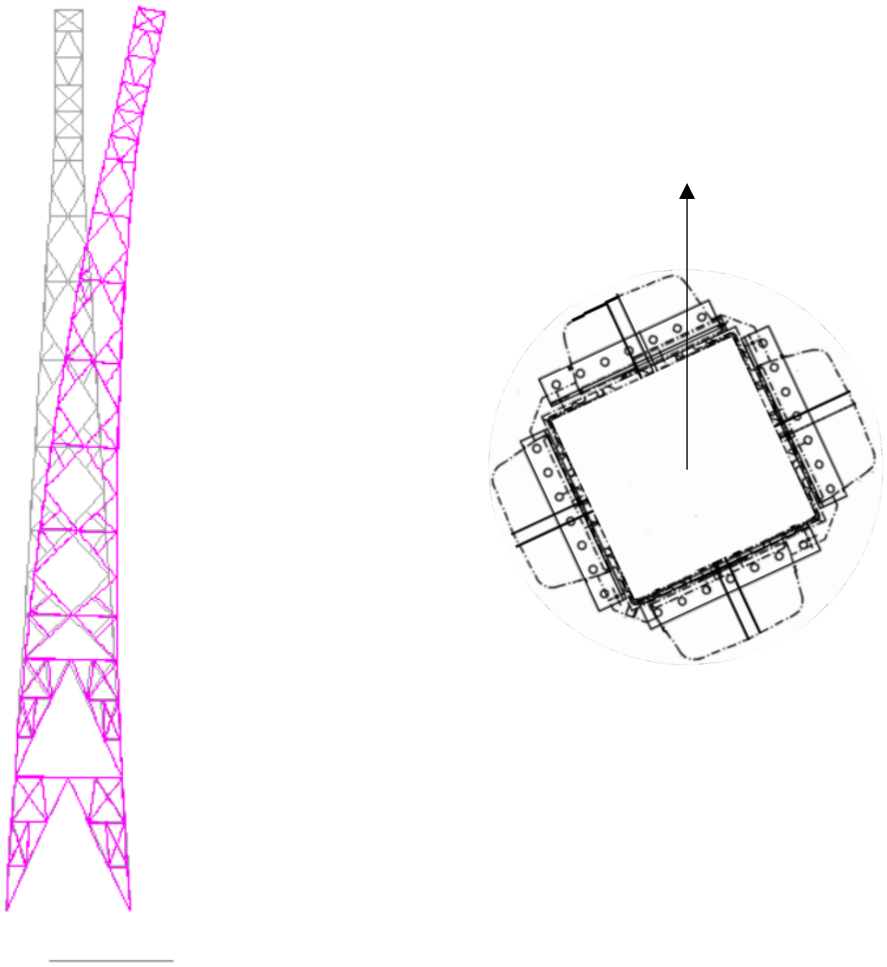

Figure 8-28. First mode shape in Brougher Mountain at 1.28Hz and the plan view of top spine

Table 8-2. Critical hourly mean wind speed for observed modes.

Mode	Obs. Frequency [Hz]	V_{cr} Circular [m/s] (face/corner)	V_{cr} Square [m/s] (face/corner)
1	1.28	7.11 / 9.95	10.67 / 14.9
2	3.2	17.78 / 24.89	26.67 / 37.33
3	5	27.78 / 38.98	41.67 / 58.33
4	7	38.97 / 54.44	58.33 / 81.67

Similar to Salisbury LT, VS events in this case are identified by several criteria:

- The presence of lock-in response, suddenly high response events, acc > 0.1 g, from a relatively calm position.
- The vibration of the event is a resonance level of the first mode of vibration at 1.2 Hz as indicated in the second plot of Figure 8-28.

The response is characterised by an elliptical shape, perpendicularly orientated to the mean wind speed before and during the event and the wind speed has values between 6 – 8 m/s.

The following Figure 8-29, Figure 8-30, Figure 8-31 and Figure 8-32 show two typical cases found during Monitoring I (before damper installation) and Monitoring III (after damper installation). Each case is based on two main figures. The first plots the raw response data from two monitored levels, highlighting the lock-in response, the power spectrum density of the selected data, and the corresponding wind speed and direction data. The second figure approaches the horizontal accelerations at each level compared to the mean direction of wind loading during the event.

In the first example, the lock-in event is not constant and is somewhat dependent on the wind speed. The response achieves high values around 0.5 g.

The response plots in Figure 8-31 indicate a limited response at 0.17 g which is controlled by the impacts of the hanging chain damper; due to the damper, response drops suddenly before beginning to increase again. A saw tooth pattern is evident until the structural damping of the lattice tower controls the system and eliminates the response. This behaviour proves that an initial displacement matched with the d/x_o design parameter is required to activate the damper.

Comparing Figure 8-29 and Figure 8-31, the damper does not fully prevent VS events. It only controls the response to prevent the system from exceeding certain dangerous values determined by fatigue calculations.

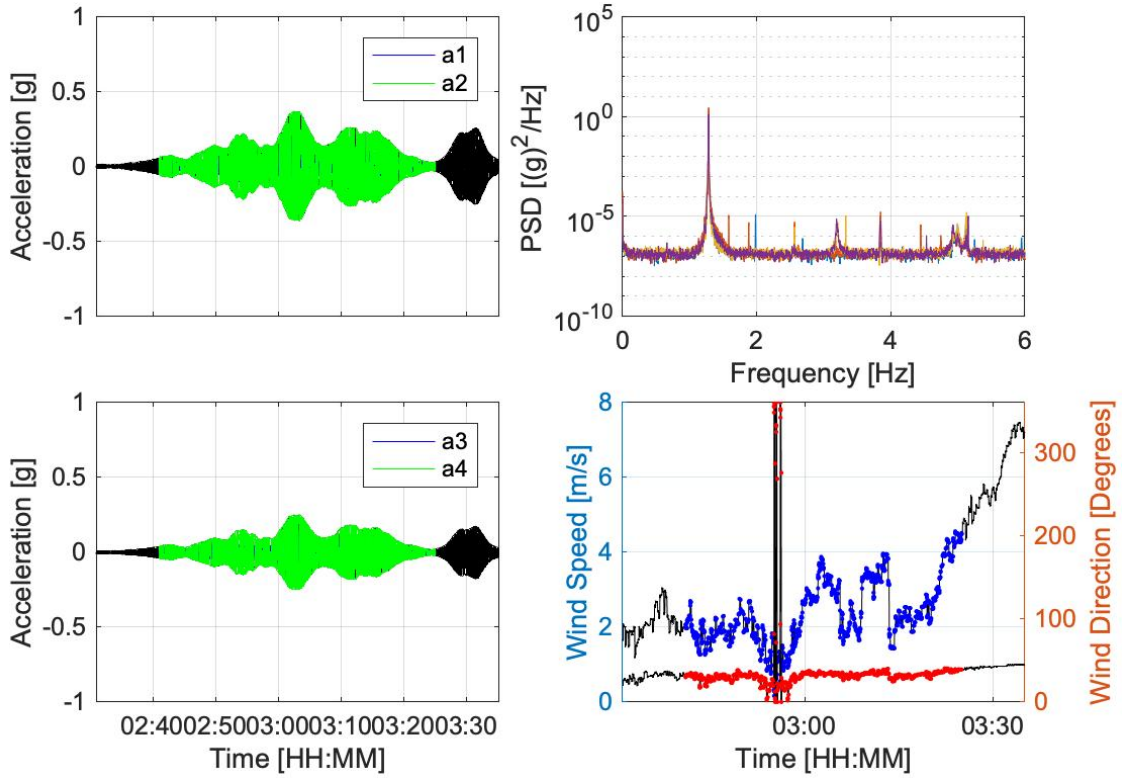

Figure 8-29. Raw data of VS event at Brougher Mountain from Monitoring I. Left: Identified lock-in response in green. Right: PSD during lock-in response and Wind data (instant wind speed and orientation).

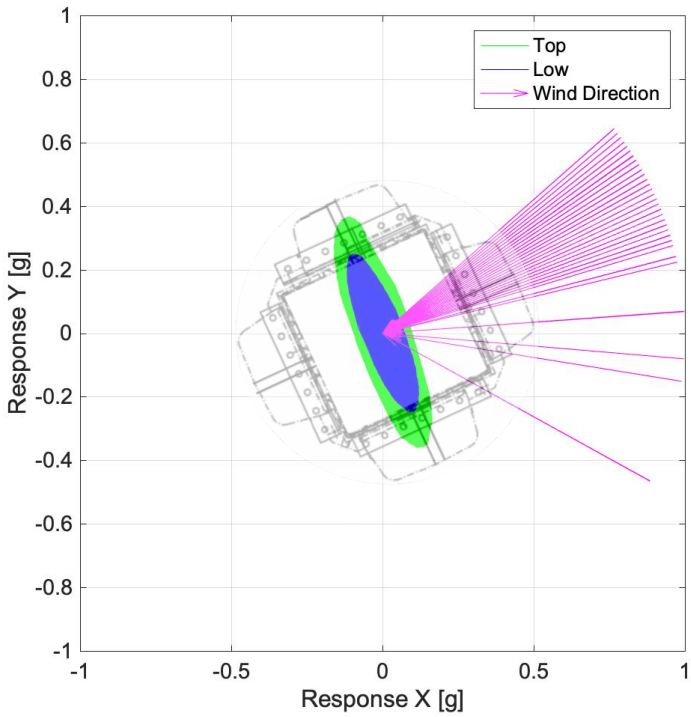

Figure 8-30. Plan view of VS behaviour at Brougher Mountain from Monitoring I.

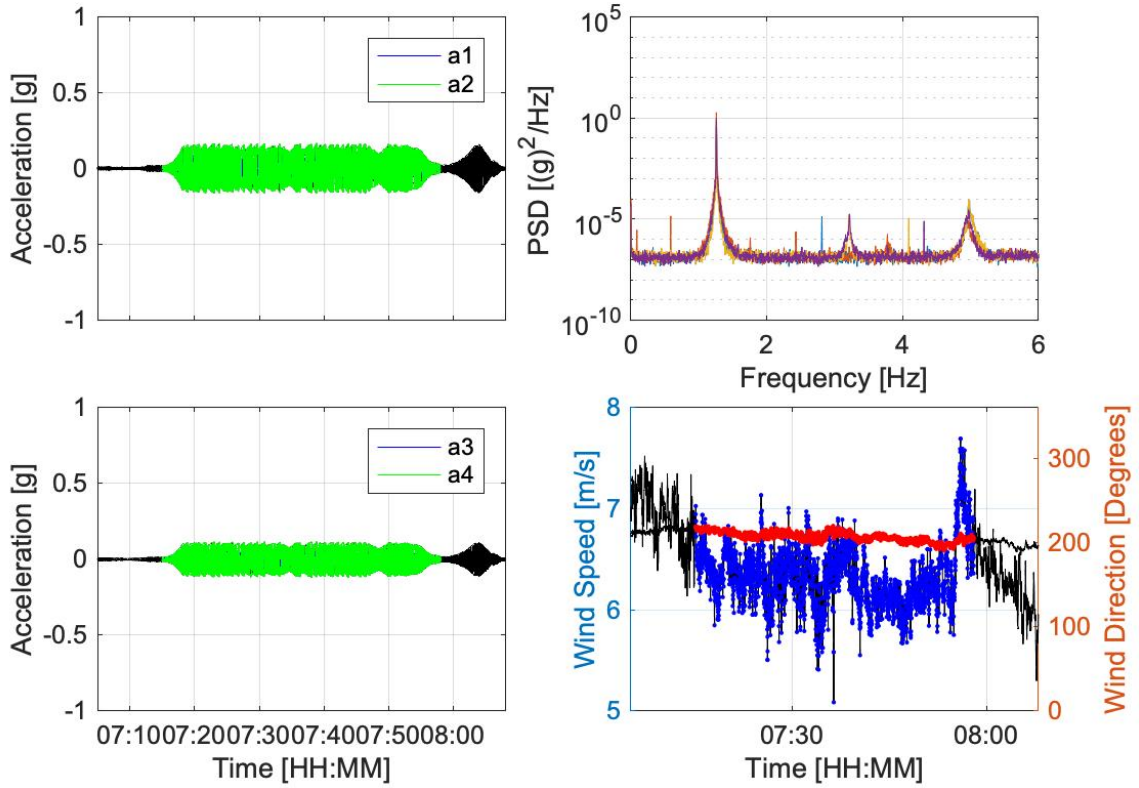

Figure 8-31. Raw data of VS event at Brougher Mountain from Monitoring III. Left: Identified lock-in response in green. Right: PSD during lock-in response and Wind data (instant wind speed and orientation).

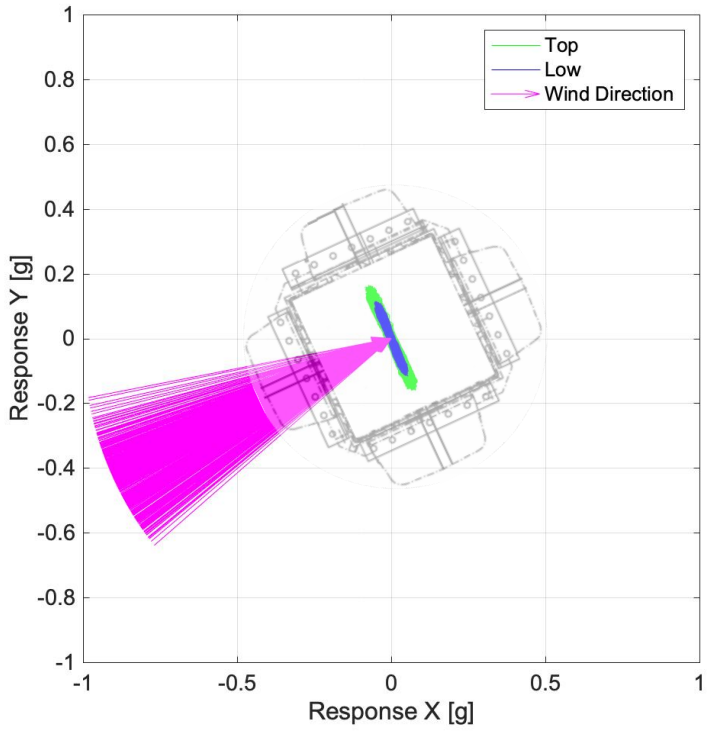

Figure 8-32. Plan view of VS behaviour at Brougher Mountain from Monitoring III.

8.3.4.4 Operational Modal Analysis: SSI and Fast Bayesian Method

To compare the dynamic properties before and after the installation of the damper, the natural frequency and modal critical damping of main three modes were extracted using two alternative system identification procedures: the stochastic subspace identification (SSI), which was chosen due its numerical robustness and lack of a need for user interaction, and fast Bayesian method (BAYOMA), which was chosen due to the already verified estimation of deviations of each property. Both methods were implemented using MATLAB scripts for time segments of 10 minutes, very similar to the previous explained exercise on Chapter 6, where both methodologies are well introduced

Figure 8-33 and Figure 8-34 plot the performance of both methodologies in terms of main frequency and corresponding modal critical damping matched with the level of the response acquired by accelerometers and the wind loading. The values provided by BAYOMA are shown in blue with estimated deviation and the mode values of SSI for the initial 10 poles are represented by black dots.

There was a significant decrease in the main vibrational mode frequencies between modes. Before damper installation (Figure 8-33) the base level was found to be 1.28 Hz. However, the lumped mass decreased that value to 1.25 Hz (Figure 8-34).

With the correct alignment of results, key behaviours of the structure can be extrapolated and a strong analysis of before-after data can improve one's knowledge of the structure. Figure 8-35 plots the dynamic properties obtained by the BAYOMA method for Monitoring II (in blue) and Monitoring III (in black) against gust and mean wind speed.

The frequency decrease induced by the existence of the damper was confirmed. Both shapes tend to represent a linear and constant behaviour which is broken before the damper by the slight decrement of stiffness provided by VS events, which are less important after the damper installation.

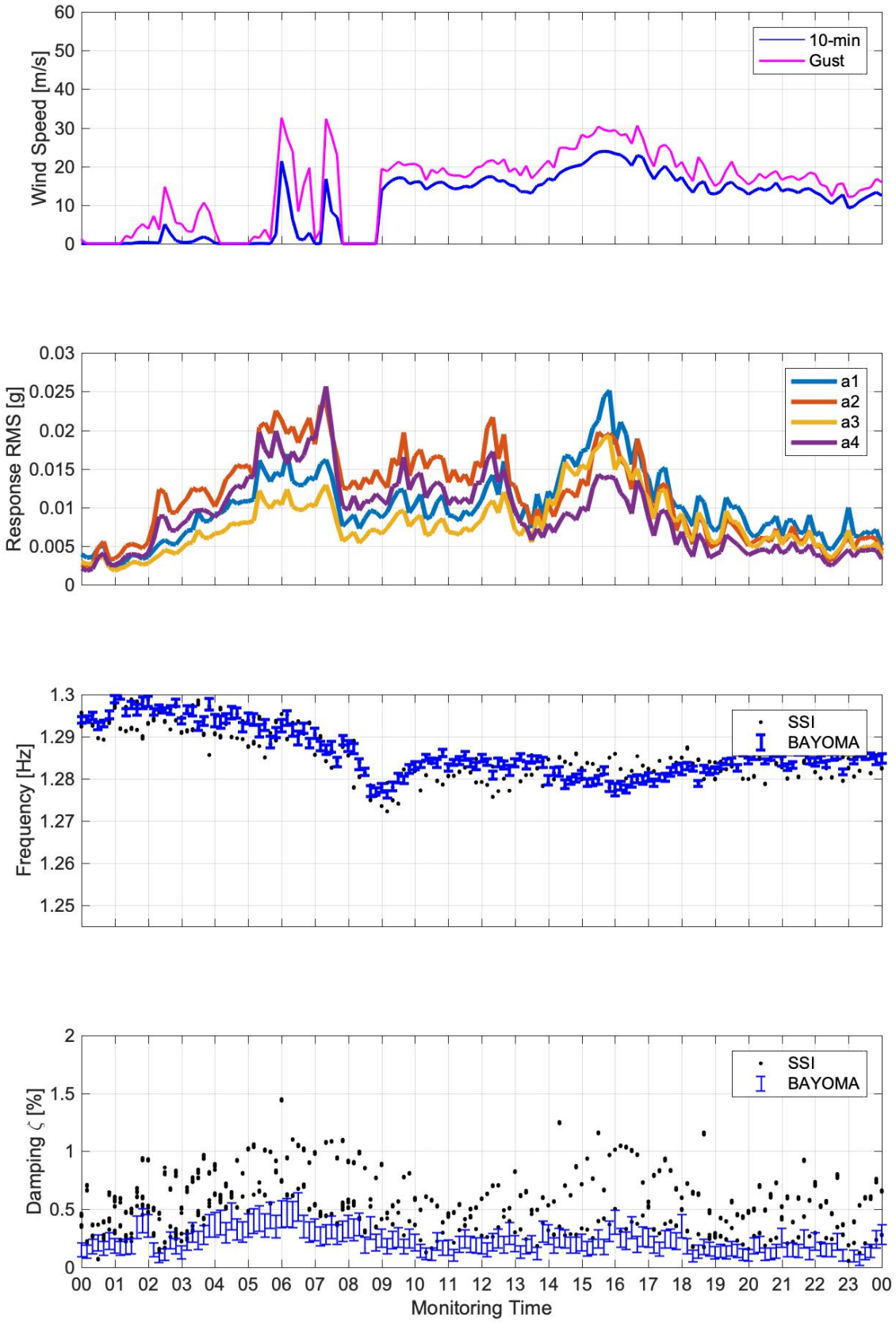

Figure 8-33. Operational modal analysis example from Monitoring II. Application of SSI & BAYOMA. Date: 20/02/2014.

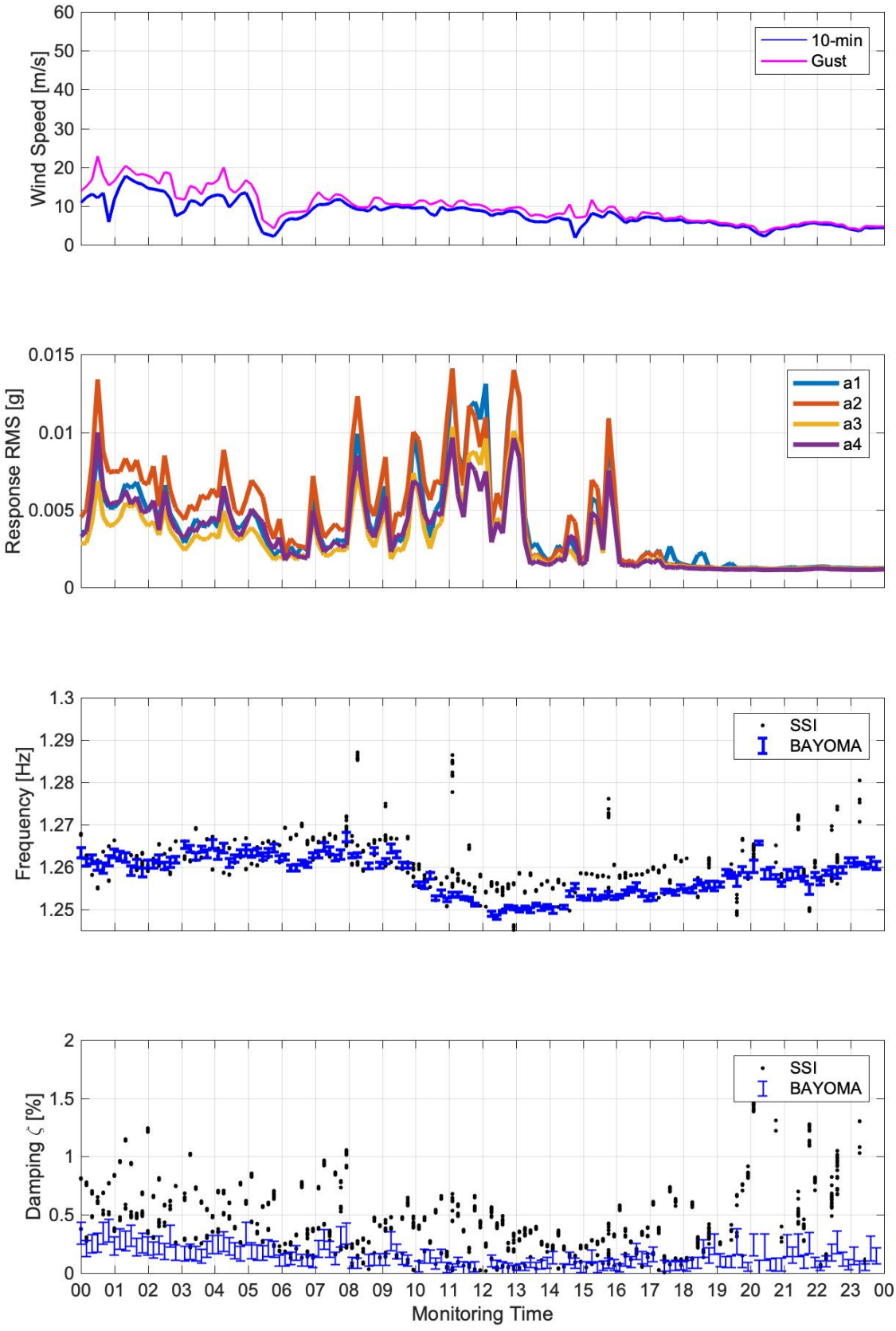

Figure 8-34. Operational modal analysis example from Monitoring III. Application of SSI & BAYOMA. Date: 02/01/2015.

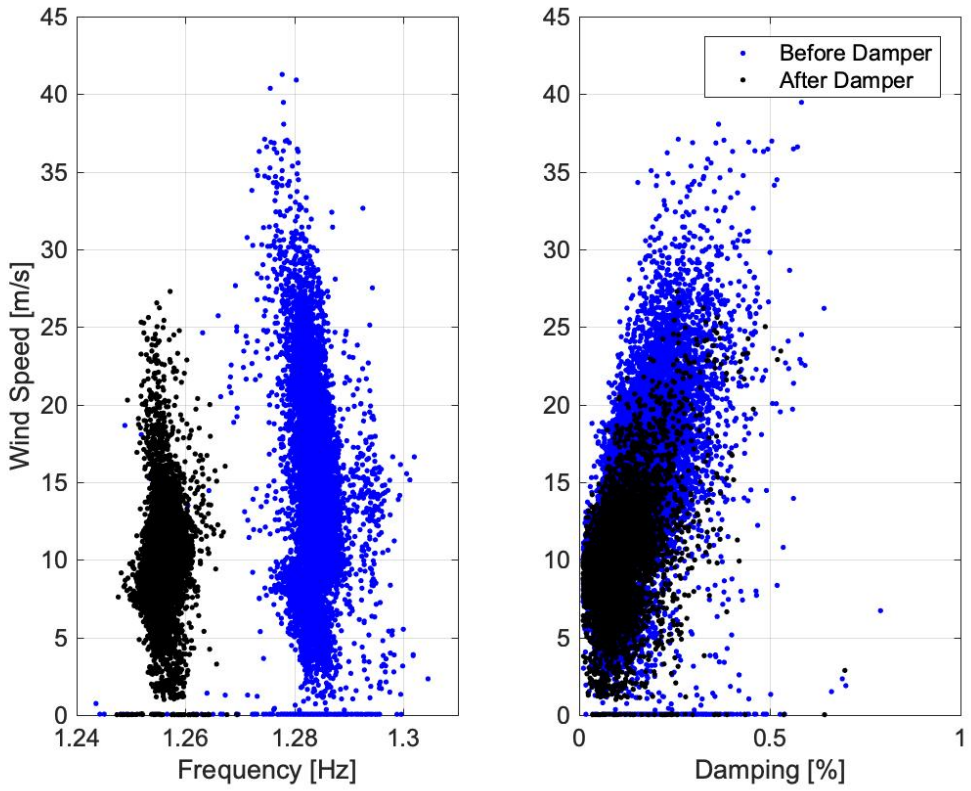

Figure 8-35. BAYOMA results from Monitoring II and III, before and after damper installation.

On the other hand, damping does not yield excessive differences between scenarios. This is because the hanging damper is only activated under certain conditions of resonance of mode 1 at levels of response above 0.14 g. At least, as found in the previous monopole exercises, the component of aerodynamic damping or an amplitude dependency can be well correlated with a linear approach. Similar behaviour was found using alternative SSI.

Those methodologies were well-tested in the previous Chapter 6 where turbulent buffeting was the dominant phenomena and 10-minute frames were sufficient to properly detect storm events with good estimations of damping and its behaviour with respect to amplitude. Overall, the methodologies provided strong estimations with low uncertainty. However, they are not able to analyse VS events if the duration is lower than the selected time frame.

For this reason, a focused exercise was implemented in both methodologies using a much shorter time window of 1 minute for events found during each monitoring. Some concerns were identified:

- BAYOMA is not able to converge upon a solution for short segments where there are increases in the response coming from the negative damping induced by VS until the high level of lock-in events.

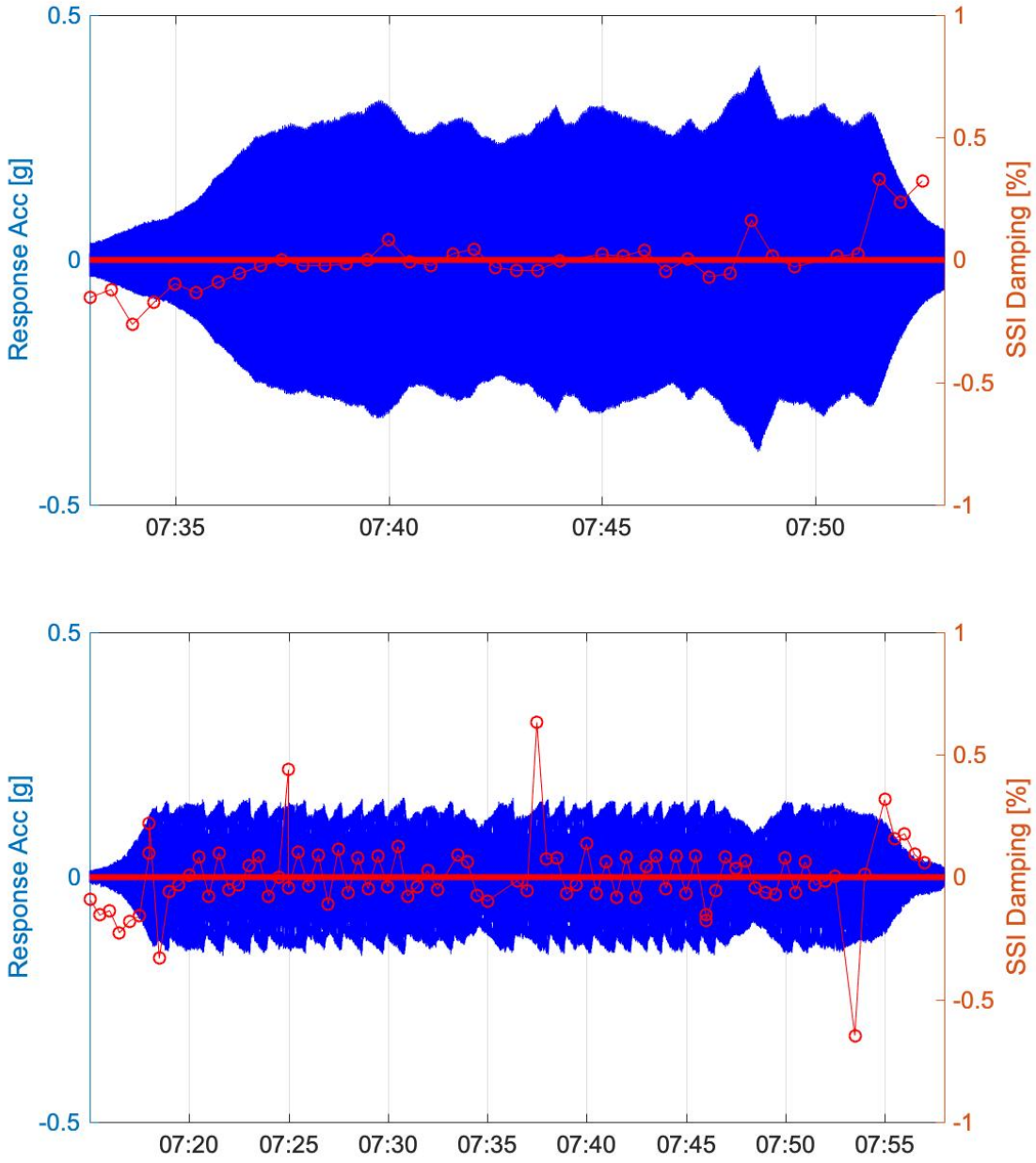

Figure 8-36. SSI damping under lock-in response during VS events before and after hanging chain damper installation.

- SSI provides good instantaneous estimations of damping, as indicated in Figure 8-36, which corresponds to previously analysed events from Figure 8-29 and Figure 8-31. Undamped lock-in events with high negative damping raise the response up to a certain limit where the system stays stable in a very harmonic,

undamped response until the vortices are dissipated and the structural damping regains control of the situation, eliciting a free decaying response that can offer information about real structural damping. However, with appropriate segment division, SSI is able to detect the impacts of the damper, yielding a saw tooth behaviour similar to the measured response of damping.

With adequate formulation, both methods can facilitate the identification of any event, detecting dangerous events or increasing the existing knowledge of structural modelling or structural diagnosis during long-term monitoring projects.

8.3.5 Conclusions

This study was initiated because of an observed excessive low frequency response of Brougher Mountain lattice tower that was caused by VS on the spine antenna installed at the top of the structure.

Flint and Neill commissioned a three-stage monitoring project to analyse the VS issue and to identify possible actions to reduce vibrations. They determined that the issue is essentially defined by the resonance of the first vibrational mode and high responses above 0.2 g.

A hanging chain damper was constructed to reduce vibrations during VS events. The installed damper did not increase the inherent structural damping of the lattice tower or avoid further VS events. Instead, the damper controls the response, keeping it under an acceptable range of responses where fatigue does not cause damage to the structure.

An operational modal analysis of the acquired data indicated some advantages and disadvantages during the data interpretation. An analysis of the before and after status of dynamic properties was conducted, and some significant changes were detected. Shorter time segments are required to study the structure during sporadic VS events.

8.4 Summary

The present chapter describes two specific projects where high vibrations under VS induced structural risks in the medium-sized lattice towers at Salisbury and Brougher Mountain. The main points of this work are as follows:

- Both projects started when high oscillation events were detected during regular inspections and reported by local residents. This information concerned structural engineers in Arqiva because of the relatively calm weather conditions, as fatigue may have caused structural failure.
- Both issues were caused by the vortices created after a low-turbulent wind flow in the large bluff antennas which crowned each structure. The phenomena induced the resonance of the structure under specific modes (the second mode at Salisbury and the first mode at Brougher Mountain) for period of time ranging from several minutes to hours at an almost constant response called the lock-in effect.
- Although no local wind data were available for Salisbury, other measurements confirmed that in both cases, mean wind speeds below 10 m/s caused the issue. These findings were consistent with the recommended Strouhall number for circular and square plan sections.
- The different sets of monitoring data obtained exposed discrepancies between existing models and reality. Similar monitoring exercises would provide essential recursive feedback to update theoretical analyses and determine better approaches to represent either loading or response, as more innovate tools can be used. The lattice towers studied in this work have a typical spectrum density based on a main mode below 2 Hz that dictates the turbulent buffeting and secondary modes below 6 Hz which can be excited by across-wind events.
- The behaviour of the different dampers suggests that very different mechanisms can supress high responses. The Salisbury DVA removed any response under the desired second mode, whereas the Brougher Mountain hanging chains only functioned at certain response levels to control fatigue failure. The performances of both systems were explained and compared in a before and after analysis.

An operational modal analysis provided an understanding of the dynamic behaviour of the structure for along-wind buffeting, but long time frames neglect minor VS events. Smaller time segments might be required.

Preface to Chapter 9

The following chapter addresses one of the most important projects of data acquisition and analysis in communication structures currently in the world. The Structural Health Monitoring (SHM) of the 230m High Guyed Mast (HGM) at Moel-y-Parc demonstrates advances in the method of data acquisition under extremely aggressive environmental conditions and the analysis provides essential knowledge of dynamic behaviour to validate existing analytical models. The monitoring assists evaluation of the performance of a tuned liquid damper (TLD) and enables identification and analysis of other dynamic events including stay galloping.

A paper on the data acquisition system has been published by Dr. K. Y. Koo and PhD candidate Jimenez Capilla entitled “Innovative Sensing solution and SHM for Moel-y-Parc Telecommunication high guyed mast” in Institution of Civil Engineering journal presented at International Conference on Smart Infrastructure and Construction (ICSIC), Cambridge, UK, July 2019.

The technical findings were presented in International Association of Spatial Structures (IASS) bi-annual conference in Winchester, UK, September 2019 delivered by Jimenez Capilla and Dr. K. Y. Koo.

Chapter 9 Structural Health Monitoring at Moel-y-Parc

9.1 Introduction

HGMs are considered one of the most complex and challenging structures for engineers to design. There is need to understand their non-linear behaviour, the effects of large deformations and to appreciate their in-wind dynamic sensitivity. Any design shortcomings can certainly lead to structural failure – there is some history of such catastrophes ranging from short-term collapse due to significant vibrations, such as Teutoberger HGM [127] in Germany, to heavy aerodynamic effects due to icing of the stays such as at Emley Moor in the UK. Other collapses have been experienced due to the failure of fatigue-sensitive connections. Requirements for new technologies demand ever greater structural optimization which in turn necessitates improved understanding of dynamic behaviour.

One of the most structurally challenging projects in the last decade on high guyed structures has been the “700 MHz Clearance” project. It is based on the re-allocation of broadcasting frequencies in the UK to leave free space for new mobile technologies without any disruption to broadcasting services during the transition. It required new antenna equipment with different geometries for many current broadcasting structures, and consequently has entailed an amazing effort to achieve the necessary structural works on the main Arqiva portfolio.

This chapter is based on the analysis of Moel-y-Parc, a 230 m high guyed mast (Figure 9-1) which now supports some of this new broadcast equipment, and which was highlighted as being potentially dynamically sensitive - essentially vulnerable to high across-wind responses induced by vortex shedding (VS) around the new antenna geometry. To mitigate this risk, unusual Tuned Liquid Dampers (TLD) were designed and installed to limit or stop such effects.

The absence of earlier full scale monitoring i.e. a total reliance on consultant’s computational modelling of the dynamic response, and the atypical damper solution obliged Arqiva, as owner of the structure, to monitor the performance of the structure

for a reasonable period after the changes to verify that the structure was behaving as predicted and not at undue risk. A structural health monitoring (SHM) system was required from the summer of 2018, the time of the damper installation, for a duration of two years. The responsibility for the monitoring was placed on the author, offering a great opportunity to enhance the existing knowledge of dynamic behaviour and damping properties associated with this type of structure, using the experience and the guidance of FSDL as part of the University of Exeter, during the creation and the assessment of the SHM.

After more than 18 months of recordings, no significant evidence of VS has been observed. However, significant responses relating to galloping effects on sets of stays and other typical buffeting along-wind effects were witnessed, albeit not reaching high deflections or exceeding the acceleration limits defined by expert consultants as likely to cause damage.

The results of structural identification methods applied to SHM response data provide good insight into the performance of dynamic properties of the structure as structural/aerodynamic damping, or the performance of the TLD.

This chapter will focus on the design of the SHM, as innovative state-of-art system not existence in the literature, main results in terms of dynamic properties found with attention to the influences of the TLD, and validation of modelling and assessments of current wind and structural engineers.

Figure 9-1 Picture of Moel-y-Parc. Jimenez Capilla.

9.2 Description of the Structure and Site

Moel-y-Parc station was built in 1962 with the requirement to achieve at least 750 ft (229 m) to enable UHF coverage of coastal resorts from Conway to Prestatyn, given the special orography near to the shore. The radiation pattern was approximately semi-circular, 25 kW being radiated from south-east to northwest with reduced power north and east so as to cover the Welsh areas but avoiding overlap with English areas already served. In addition, it provides supplementary service to Cheshire, Manchester and Lancaster counties, areas of strong importance due to high population.

Moel-y-Parc HGM (MYP), the large violet triangle Southern-West from Liverpool in Figure 9-2, is the main broadcasting station in the area coloured in dark blue, linking with other nearby relay stations (small triangles) to amplify the coverage in the field. The supplementary coverage area is indicated in light blue.

Apart from the UHF equipment focused on Television Broadcasting, MYP holds antennas from several customers with a range of frequencies. Presently, a VHF Digital Radio antenna is installed at 188 m, with other capacity below 150 m taken by the telecoms sector, with customers such as EE, Airwave Solutions, 3TM and CTIL using a variety of equipment like sector panels, dishes or dipoles, as well as the corresponding cabling and feeders for each antenna running internally.

The mast is of lattice construction, triangular in plan, with four stayed levels. The lower sections between ground and the 3rd stay level at 171.7 m have a face width of 2.6 m, reducing to 1.9 m for the top section up to the 4th stay level. Finally, the total height of 240 m is achieved with a cantilever spine antenna of 12 m based on a square lattice frame of approximately 1 m width.

The mast is designed to be stiffer at lower levels with larger leg sizes and more complex steelwork configuration to avoid buckling failure. Legs at ground and lower levels are solid round rods of 146 mm unlike the 4th level that uses 95.2 mm rods, and equal angles are used for primary and secondary bracing. All members are made of mild steel, although further strengthening has used steel with higher grade. Additionally, the connections are mainly bolted – leg joints are flanged with bolts working in tension, the bracing connections use bolts in shear / bearing.

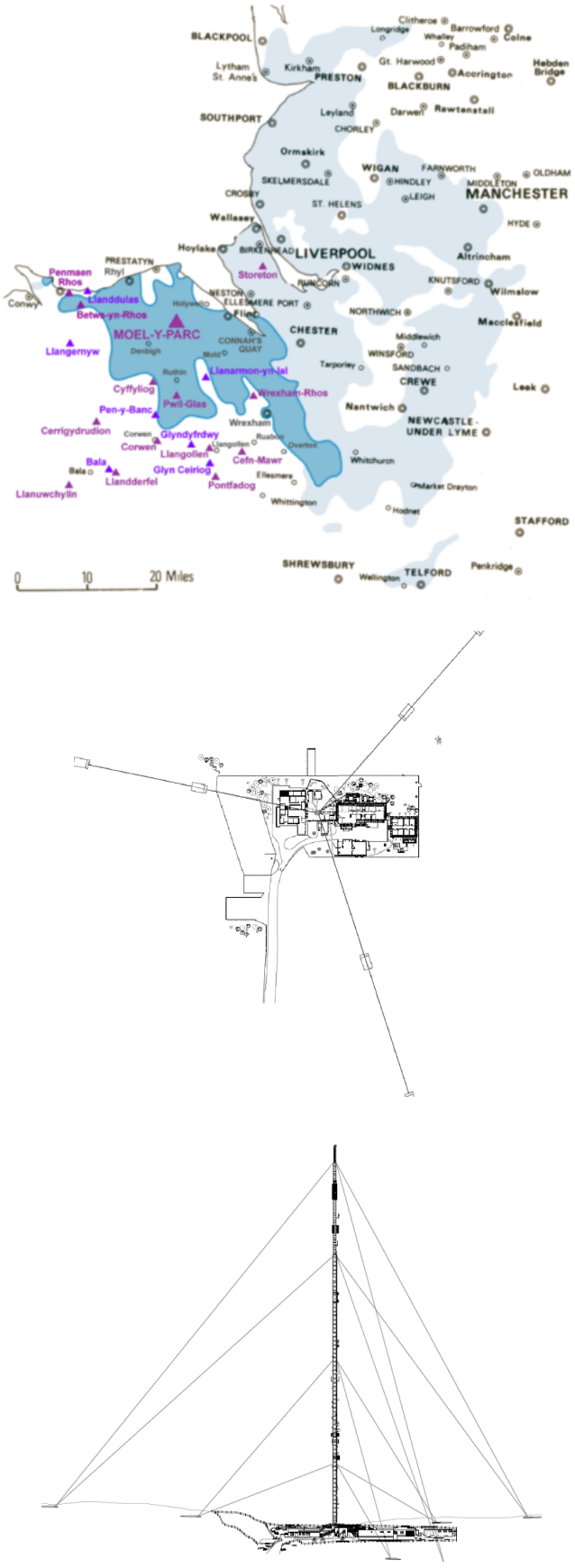

Figure 9-2 Moel-y-Parc HGM. A) Coverage. B) Site Plan. C) Elevation.

The mast is held at four stay levels with three stay lanes at each level (12 stays in total) with orientation 92°, 212° and 332° East of North. Due to the orography, each stay has its own configuration of diameter, initial tension, and geometry which is defined to provide enough tension at each joint level. Finally, the stays are attached to concrete foundation blocks in pairs as the figure above.

The standard loading design is defined by the buffeting gust wind speed coming from south-west which is heavily amplified by the orography of the location. Also, due to the characteristics of the antenna, an aeroelastic effect around the mast could induce large movements which could risk the structural integrity of the mast. Arqiva's consultants engaged for their specialist expertise identified that VS could excite modes of vibration around 0.62 Hz and the "lock in" effect under this VS issue could induce a peak horizontal acceleration of 0.49 g at antenna levels. The dynamic effect added to the existing static loading and the possibility of fatigue failure would present a significant risk to the safety of any person around the antennas, as well as risking the ability to continue broadcasting.

To mitigate these VS vibrations, a tuned liquid damper was designed and installed, aiming to achieve 10 % damping, which would assure acceptable behaviour of the mast.

9.3 700 MHz programme. Requirements and Structural Assessments.

In November 2014, Ofcom and the British Government announced that the 700 MHz band, currently occupied by a number of digital terrestrial television (DTT) services, is to be cleared for use for mobile data by 2020. For Arqiva this meant upgrading and replacing 35 - 40 main station antennas along with approximately 300 antennas at relay sites. All reconfigurations and replacement antennas were carefully planned with the aim of keeping all existing services on-air throughout the programme. From the structural point of view, these conditions (new geometries and new installations with no service interruption) are very challenging for different reasons. First, the existing HGM portfolio was mainly built during 60s and 70s when it was not only designed for totally different loading using old standards and methodologies, but its design life was not foreseen as extending beyond 50 years. Second, new geometries and masses change the drag factors and dynamics of each structure, leading to greater wind

sensitivity with higher stresses. Finally, to maintain services, in some cases new bluff antennas are required close to current antennas for short time periods, forming a large bluff core which can be more susceptible to aeroelastic effects such as VS.

The 700MHz project at Moel-y-Parc proposed that the aperture between 205 and 215 m, already occupied by an old antenna, was adjoined to the coming new antenna between 198 and 205 m creating a 17 m long bluff cylinder of approximately 3 m diameter at the top span of the mast. The concurrent antennas were only present for a temporary time of 6 weeks between transformation – for the final configuration only the new antenna remains.

The consultancy assessment, applying the Approach 2 methodology given by BS EN 1991-1-4 Annex E, indicated significant VS effects. With the neglection of the turbulence at such level which could only help to supress VS, the appropriate critical wind speeds are approximately 10 m/s.

As a reminder of the shortcomings with these semi-empirical approaches, Approach 1, based on the work of Ruscheweygh [128], predicts response correctly or underestimates the response, On the other hand, Approach 2 based on the work of Vivkery & Basu [129], predicts correctly or overestimates it. Neither is consistently reliable.

The approach for this project advised that two modes of vibration were present where there was a reasonable risk of propensity to VS and an expectation that the associated wind conditions may occur for up to 13 % of the year. Those two vibration modes were found to have Scruton Numbers below the limit of 15. The first one, with a Scruton No. 9.2, occurred at a natural frequency of 0.602 Hz and a second one, with a Scruton No. of 10, at a natural frequency of 0.632 Hz. The critical wind speeds associated with those modes are 10 m/s and 10.5 m/s respectively. In this range, a phenomenon called 'lock-in' may occur. Therefore, VS may occur between factors of 0.222 and 0.267 of the characteristic wind speed.

The conclusions from these assessments were that VS induced vibrations could result in fatigue failure within the period that the temporary two-antenna configuration was installed, and that vibrations of a lower magnitude could also continue with just the final new antenna in position. To negate and control VS effects, a relatively small increase in the damping of the structure was recommended via the installation of a

tuned mass damper (TMD) or tuned liquid damper (TLD) on the mast column between the top of the new antennas and the top stay level. This would increase the Scruton numbers avoiding VS. Two sloshing TLD dampers designed by Prof. M. Irvine were installed at 216 m Figure 9-3.

In addition, further strengthening was recommended, consisting of the following:

- Replacement of the existing upper stay landing link in the 4 stay linkage.
- Replacement of the existing upper stay landing link in the 1 stay linkage

The need for a SHM system was identified with the purpose of investigating the existence of VS and to verify if the TLD was providing sufficient damping to suppress the initial response after lock-in effects.

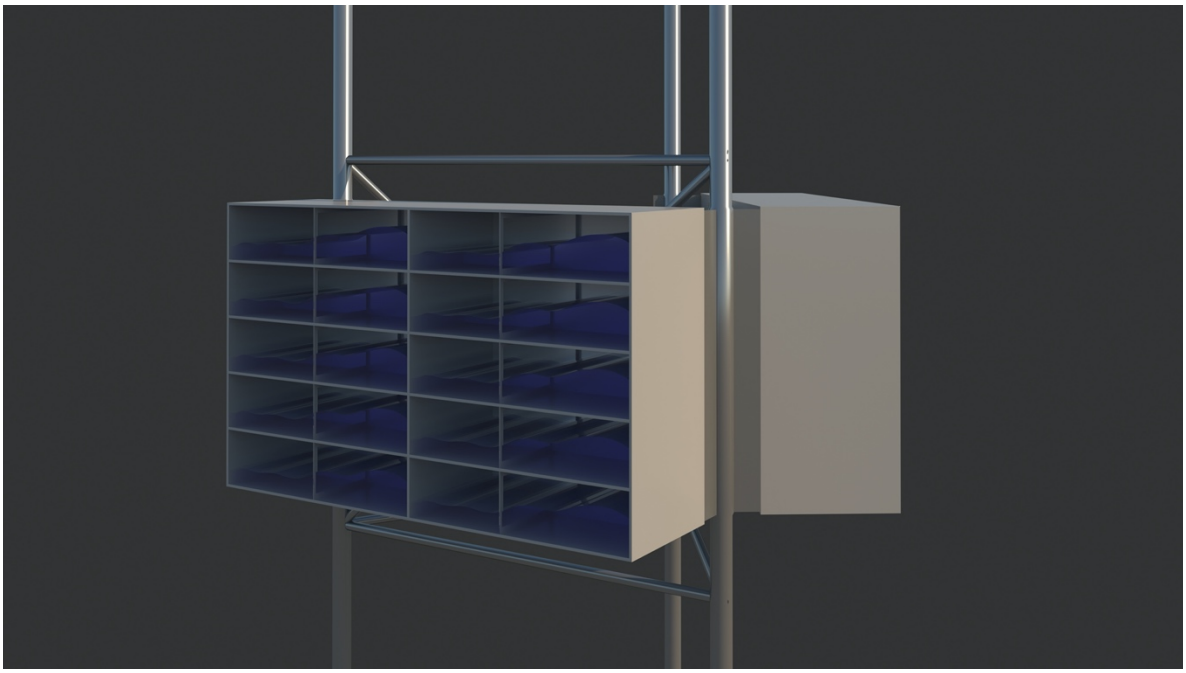

Figure 9-3 Sketch of TLD in Moel-y-Parc.

9.4 State of Art Acquisition System

A SHM system was designed to record mast vibrations to assure its structural integrity, verifying that the mast behaves as expected, with the TLD effective in controlling excessive movement in all weather conditions. For that, the system was based on 5 biaxial acceleration measurement boxes placed at key levels as shown in Table 9-1.

In addition, in order to correlate different amplitudes of the response with wind conditions, an anemometer was added to the system. Originally designed to be placed at the top of the mast, due to complications during initial installation, it was finally moved to a platform level at 225 m, just below the 4th stay level, as indicated in Figure 9-5.

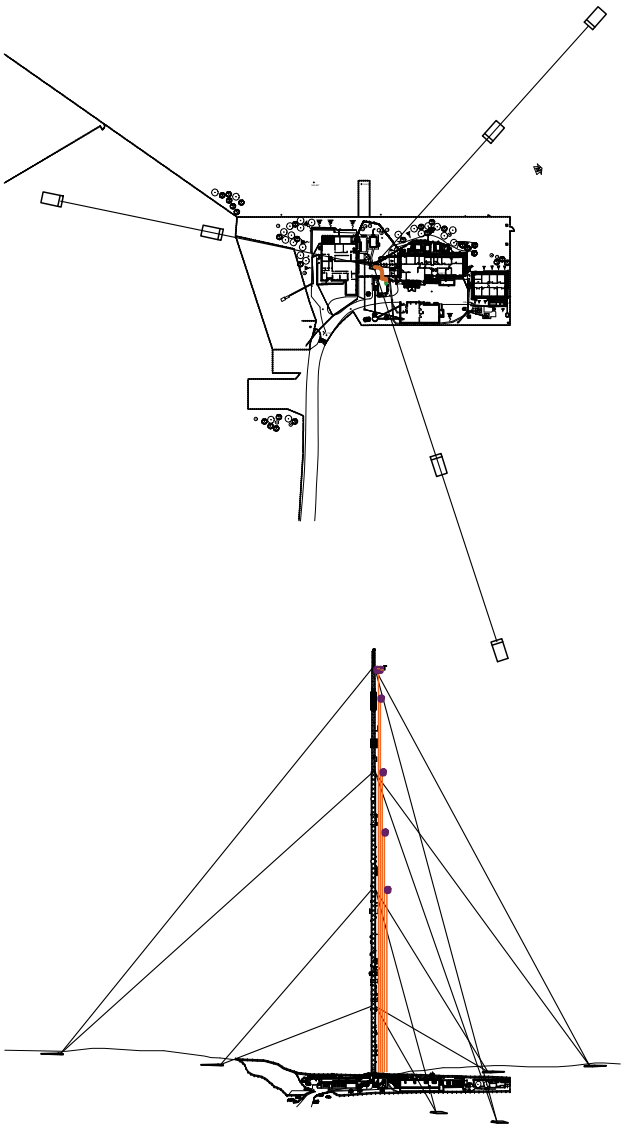

Figure 9-4 Scheme of MYP-SHM. Plan view and Elevation.

Designing and installing the instrumentation on the mast was found to be extremely challenging due to potential radio frequency interference (RFI) from the high powered antennas on the signal cables of a conventional centralised Data Acquisition (DAQ) system. In order to minimise such RFI, the sensor output voltage needs to be acquired at the sensor location suggesting a distributed DAQ system. However, the distributed

DAQ which was acquired introduced a synchronisation problem between the six sensor nodes.

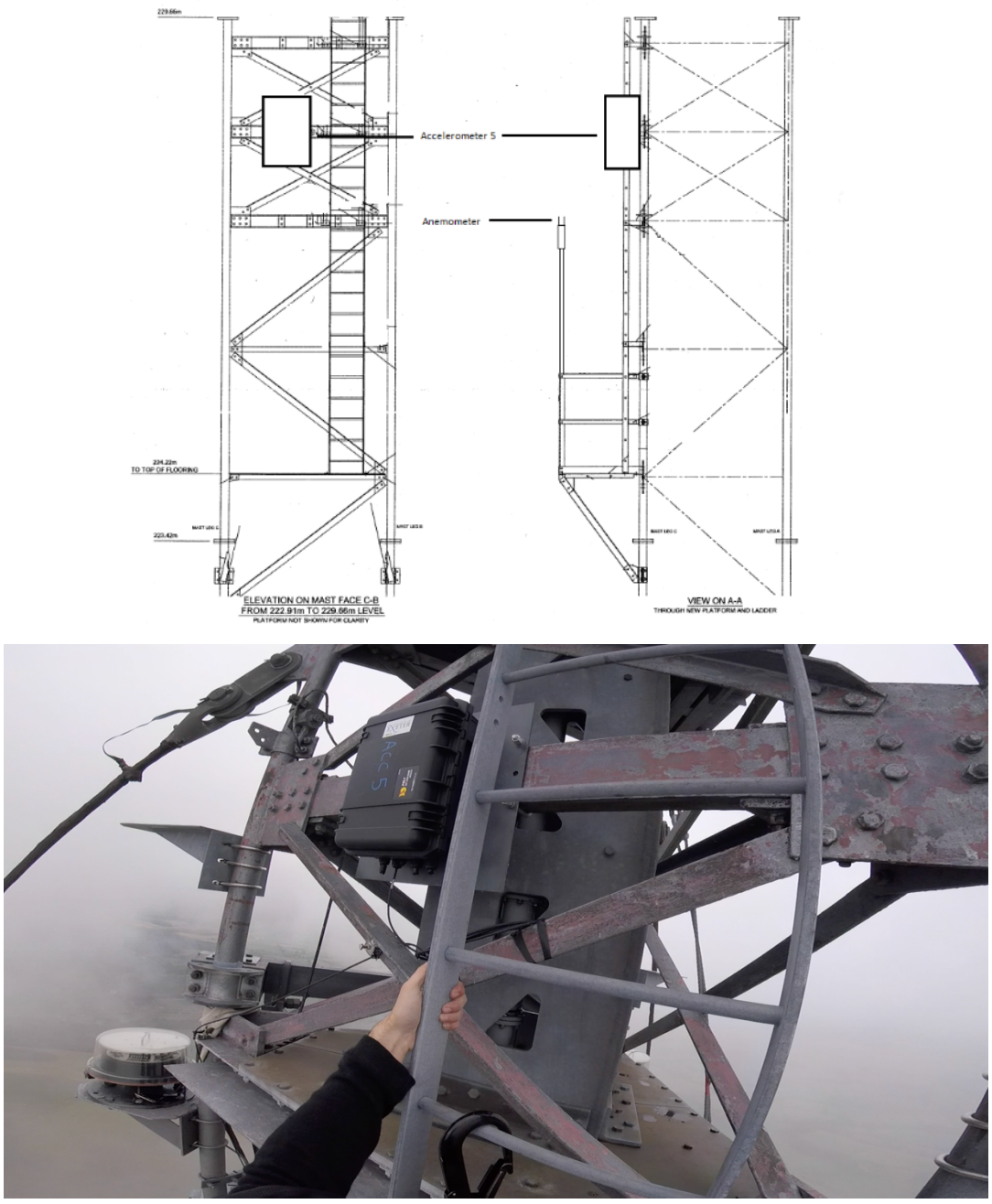

Figure 9-5 Installed position of accelerometer box (ACC5) and anemometer. Picture of accelerometer box (ACC5).

The previous SHM experience in Brougher Mountain, explained in Chapter 8, offered a valuable lesson in dealing with the RFI issue. To address this, the GPS-based time-synchronisation method for wireless sensors [130] was used. In each accelerometer or anemometer box, measured data are accurately time-stamped by the time information provided by a GPS module and then resampled for time-synchronised

measurements. For immunity from RFI on the data-transfer from the DAQ boxes to the base station on the ground, a fibre-optic media converter was used in each DAQ box for establishing an Ethernet connection to the base station. The base station was connected to Internet connection via a 4G mobile router. A 110 V main power cable was installed along the length of the mast to provide a permanent power to the six boxes.

Colibrys VS1002A MEMS accelerometers are used, two per box, for biaxial horizontal acceleration measurement. The VS1002A is a good-performance accelerometer with a noise floor = 7 μg/Hz$^{0.5}$ and a moderate cost of £ 180 as of 2018. The anemometer is a RM Young 85004 ultrasonic anemometer, having a RX-232 interface for measured output. Figure 9-7 shows the sensors.

Table 9-1 SHM component locations.

Sensor	Abbr.	Position
Anemometer	WND1	Platform level, 225m
5th Accelerometer	ACC5	Forth stay level, 230m
4th Accelerometer	ACC4	TLD level, 215m
3th Accelerometer	ACC3	Third stay level, 172m
2nd Accelerometer	ACC2	Mid-span of second section, 140m
1st Accelerometer	ACC1	Second Stay Level, 108m

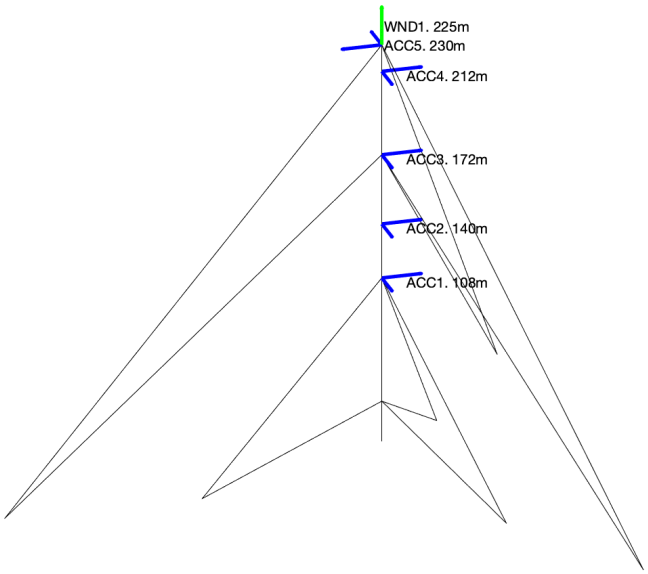

Figure 9-6 Moel-y-Parc SHM Response Scheme.

Figure 9-7 (Left) RM Young 85004 ultrasonic anemometer and (right) Colibrys VS1002A MEMS accelerometer.

The sensor node in each acceleration DAQ box comprised a Raspberry Pi stacked with, 1) an Arduino Mega2560 compatible custom-made board (GPS/OCXO/ Arduino Mega2560 board (GOM)) having GPS-based time-stamping capability, 2) an Analogue-to-Digital conversion custom-made board (ADC board) controlled by the GOM board, and 3) a 2.8” touch-screen TFT display. Two VS1002A sensors placed in the DAQ box perpendicular to each other were connected to the ADC board using a 24-bit 4 channel simultaneous ADC Texas Instrument ADS1274 chip. The GOM board has a GPS module FGPMMOPA6H feeding the accurate time information to the Arduino Mega2560 MCU. The acquired data and corresponding timestamps were sent to UART RX pin of the Raspberry Pi 3 which has a Python script performing the resampling technique [131] with re-sampled data stored in the Raspberry Pi SD memory card. The Adafruit PiTFT screen was used as a console monitor for the Raspberry Pi 3 to show the status of DAQ operation with optional real-time graphs of time-history or power spectral density. The Raspberry Pi 3 ethernet ports were connected to Fibre-option Media Converter for data transfer from the SD memory card to the HDD of the base station. The base station has a set of Python scripts to upload the data files into a secure ftp server at Exeter, executed every two hours.

The sensor node in the anemometer DAQ box was built using a Raspberry Pi and a custom-made GPS module board directly feeding the time-information to the Raspberry Pi. A Python script on the Raspberry Pi was used to parse UART outputs from the anemometer and to store data on to the SD memory card.

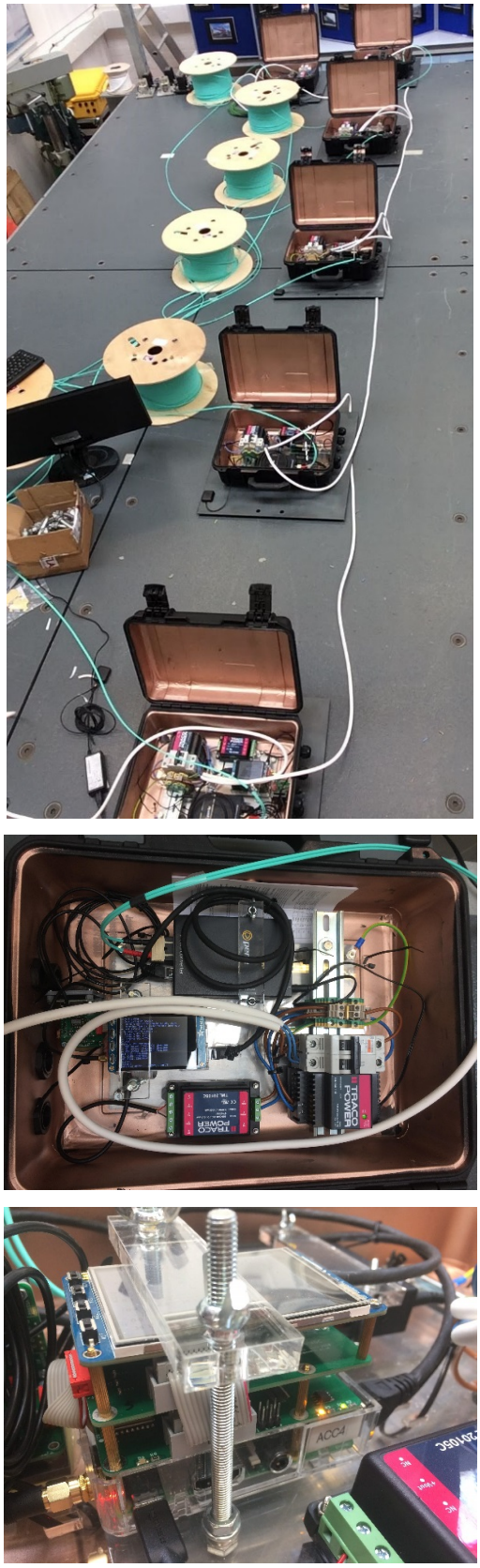

Figure 9-8 SHM HW System: (top) testing of the boxes, (middle) accelerometer boxes, and (bottom) GOM node.

9.5 SHM Programme

The 700 MHz-related works at MYP were planned to be carried out during the summer and fall of 2018. The SHM-MYP project was assigned to and accepted by the author and FSDL between January and April of 2018.

That meant extremely tight deadlines to complete the creation and the installation of the monitoring before the installation of the TLD. COWI as expert consultancy recommended obtaining sample data before any works to allow optimal tracking and to enable comparison between changes.

This mission proved impossible to achieve, but the author managed to obtain some data using a set of GCDC accelerometers for 2 months and a temporary box based on similar technology to the final system around two months before the final installation. This way, the strengthening works of the structure, the installation of the TLD, the installation of the new broadcasting antenna and the removal of the old one, were captured and taken into account during the analysis.

Finally, as Table 9-2, the final set of long-term monitoring was set up on 2nd August of 2018, and has been constantly recording until January of 2020, the final application date for research purposes.

Table 9-2 Timescales of the SHM-Moel-y-Parc.

2018/04/01	Initial Works Date
2018/04/17	GCDC. Initial Recoding Date
2018/05/16	Temporary Box. Initial Recoding Date
2018/05/30	Installation of TLD
2018/07/24	GCDC. Final Recoding Date
2018/08/01	Temporary Box. Final Recoding Date
2018/08/02	SHM-MYP. Initial Recording Date
2018/09/20	Final Works Date
2020/01/25	SHM-MYP. Final Recoding Date

9.6 Data Recording and Implemented Techniques

After the reception of files remotely, scripts using MATLAB analyse the data to extract the desired results. This way, there are different data back-ups, the logger saves each file on a local hard disk and the server also retains the package of files.

Those scripts summarise files in the right order and report results in terms of loading or mean/RMS responses hourly and daily to readily identify significant events or responses which might put the structure under risk, and to help highlight issues worth studying. Each report counts on a PSD-spectrum diagram belonging to a time domain for each period.

An operational modal analysis (OMA) of each set of hourly data was undertaken using the covariance stochastic subspace identification (SSI) and fast Bayesian methods to identify modal properties (MPs), mainly natural frequency and damping. Both methods were well introduced and utilised during previous chapters. A 10-minute time window has been implemented initially to capture RMS responses and characteristic loading parameters (wind speed and direction), and afterwards for MP diagnosis. From previous exercises, this time frame is a good estimator of mean wind speed to identify wind events, and was to obtain better than 20% standard deviation in damping estimates obtained in trial runs on monopole data.

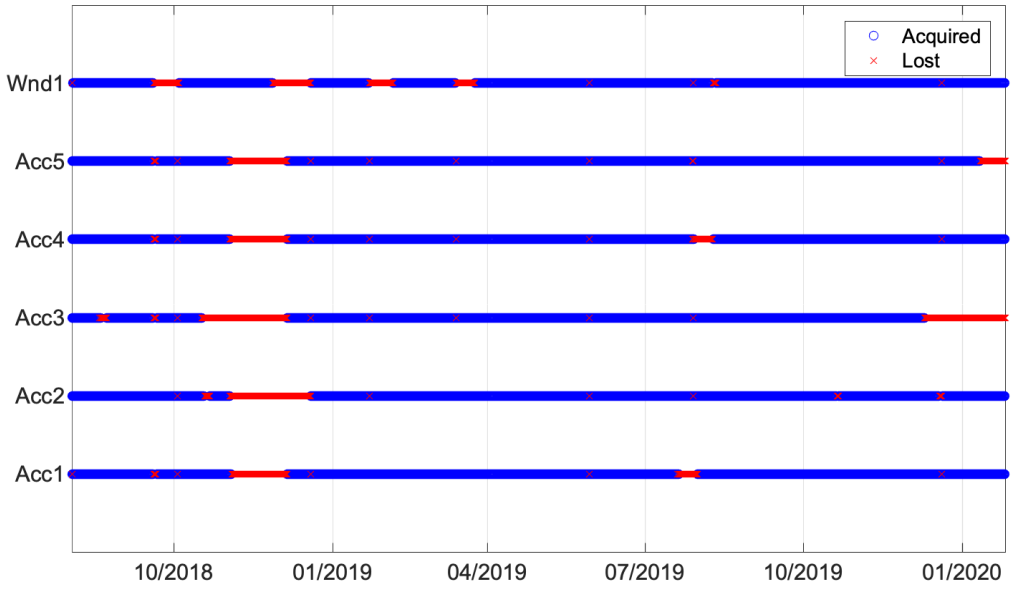

Figure 9-9 Data acquisition diagram during SHM in Moel-y-Parc.

Finally, horizontal amplitude-deflection plots of Acc 5 and Acc 4 are made for visual inspection to identify high responses where the structure works under resonance and tends to create standard figures or shapes which can be related to aeroelastic effects like VS.

As mentioned, the proposed monitoring system was very innovative in addressing the extreme weather and RFI conditions, but has been shown to be stable over time. Just a few minor breaks causing data loss were found over the duration of the project mainly due to issues related to 4G connections and GPS connection losses possibly due to icing or water ingress to the boxes.

9.7 Moel-y-Parc Structural Health Monitoring Results

9.7.1 Loading in Moel-y-Parc

In terms of wind loading during the monitoring, the anemometer provided reasonably reliable data close to the top stay level, TLD and new equipment. Figure 9-10 and Figure 9-11 show the wind data compiled during the monitoring period.

The data time lines indicate a wide range of wind speeds between calm conditions and gust wind speed of 50 m/s, passing thorough critical VS wind speed at 10 m/s.

The wind rose represents the typical wind direction distribution in the United Kingdom where most and higher winds tend to blow from the south to south-west. The location of the anemometer close to the mast introduces drag influences in the data for wind from the south-east quarter, due to shielding from the mast body. The issue does not essentially alter the main data from the monitoring which was used to correlate local intensity to verify VS conditions.

During the last two thirds of 2018, the main contractor proceeded with all works covered by the project to install new antenna equipment. This included the strengthening works, the damper installation and the installation of the SHM system.

These works and further climbing carried out during the length of the monitoring may have introduced some abnormal loading e.g. from materials lifting operations.

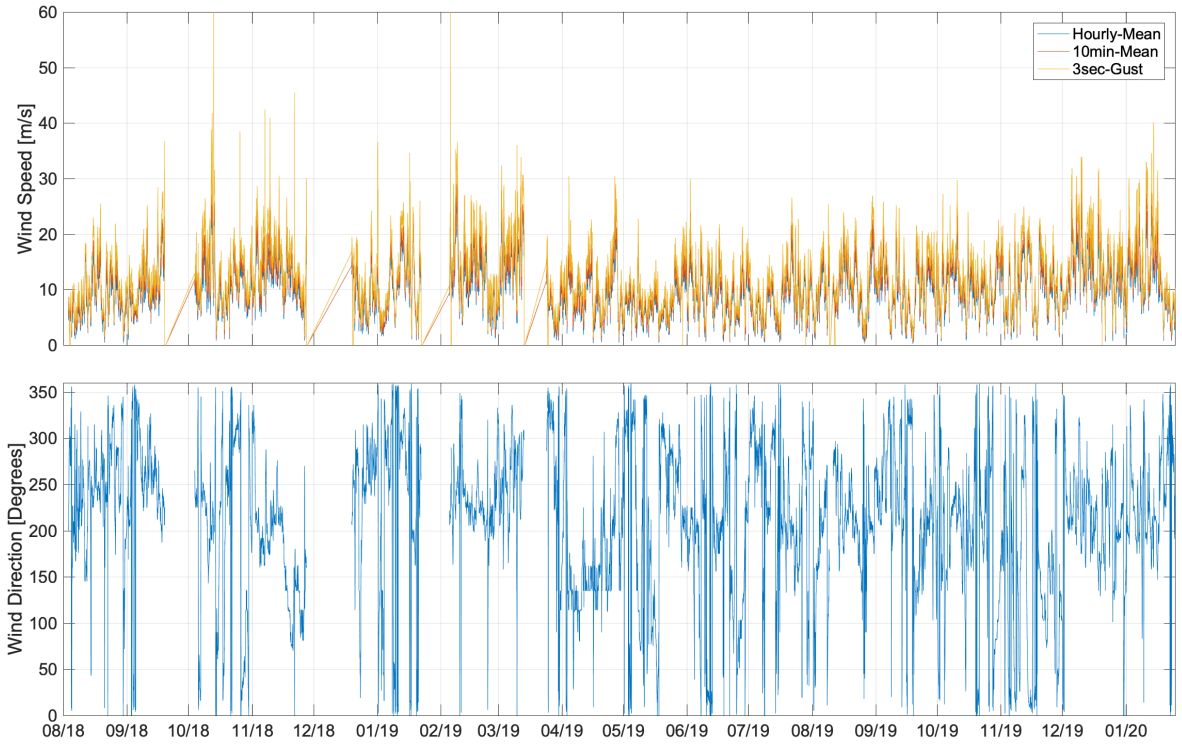

Figure 9-10 Wind loading in SHM-MYP. Wind speed & direction.

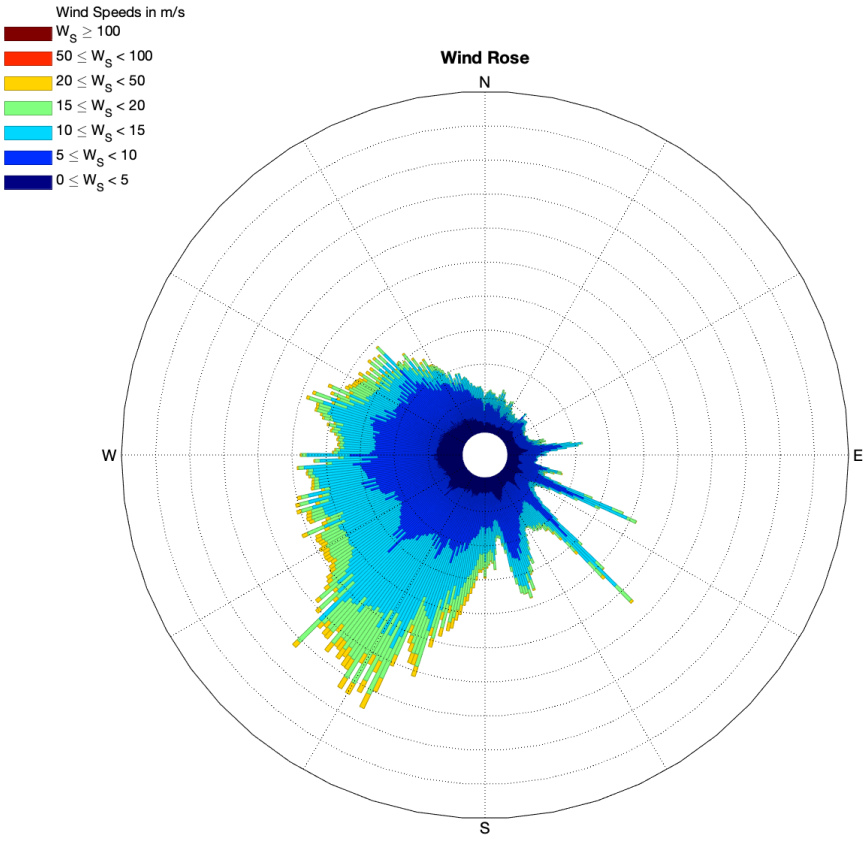

Figure 9-11 Wind loading in SHM-MYP. Wind rose.

9.7.2 Response in Moel-y-Parc

The different load case configurations given by the initial finite element assessments confirmed that the most dangerous modes appear between 0.58 - 0.62 Hz with generalised modal mass higher than 12000 kg and modal displacement of 0.7 m. In addition, the consultant estimated peak acceleration at new antenna and TLD level would be 0.48 g which might induce unacceptable stress in legs of 90 N/mm^2 and 52 N/mm^2 in bracing members.

In terms of the structural behaviour, the mast showed a very complex dynamic response with a crowded frequency range with more than 25 modes in the initial 5 Hz. Figure 9-12 and Figure 9-13 plot the typical power spectrum density (PSD) of two sets of data obtained during SHM. The first shows the frequency domain behaviour over a very calm period without significant response. The response is defined by a complex PSD with several modes below 5 Hz working at a similar level. Most of them are either inherent structural modes or individual stay modes which induce vibrations into the mast. On the other hand, the second plot belongs to higher response events. Two peak modes appear more relevant than others as the structure tends to resonance under a main mode.

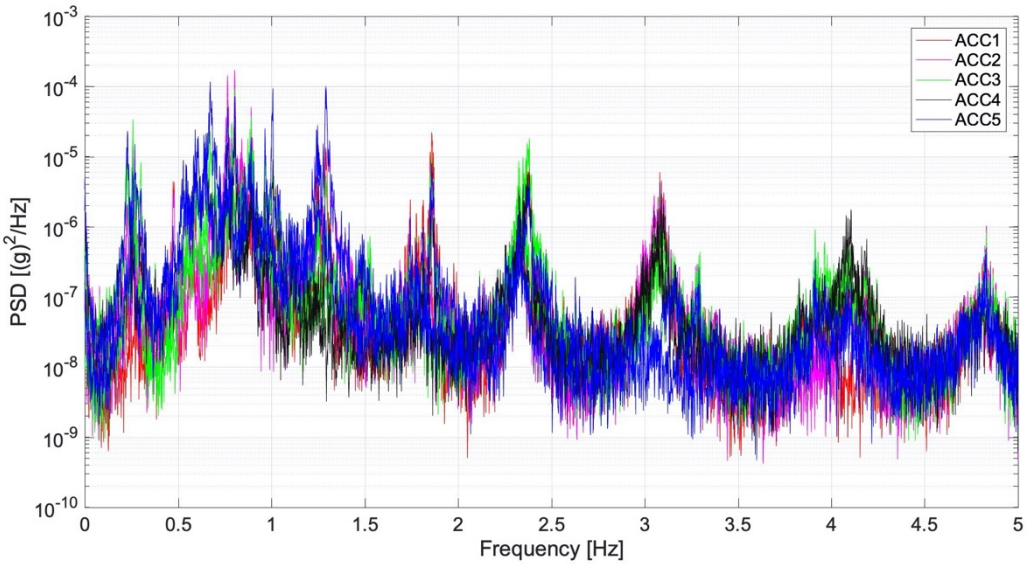

Figure 9-12 Typical power spectrum density of HGM Moel-y-Parc. (Low response).

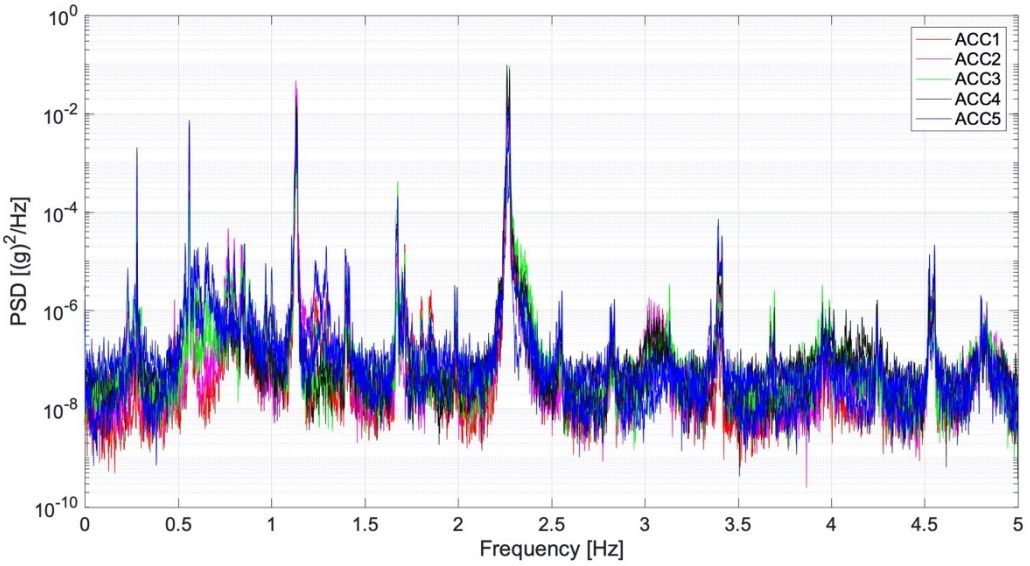

Figure 9-13 Typical power spectrum density of HGM Moel-y-Parc. (High response).

The raw data from the initial GCDC time did not catch any remarkable events to show due to the very high noise floor of the accelerometer. The temporary system in Figure 9-14 indicated a high-response event matched with the week of the damper installation during summer 2018 with no high wind speeds recorded by local weather station.

During the operation of the SHM system in Figure 9-15, the limit acceleration was not exceeded, and there is no evidence of VS behaviour. However, few relatively high responses events were found from the beginning of summer of 2019. One issue that has been found appears to be related to galloping events in several stay sets; it will be investigated in further sections.

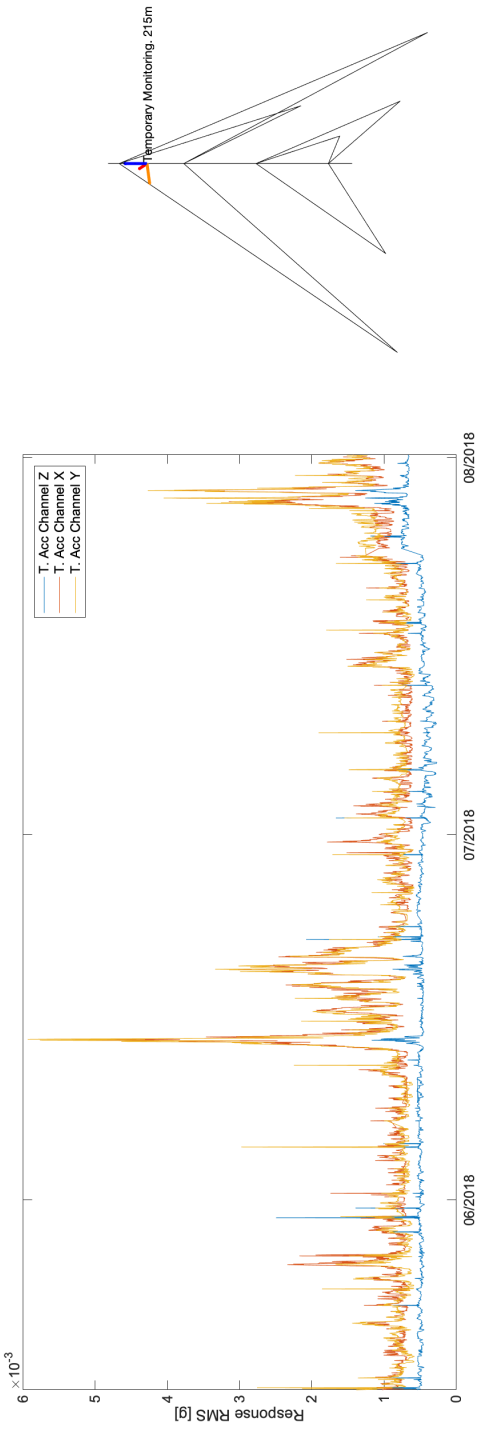

Figure 9-14 Response of temporary system. Moel-y-Parc.

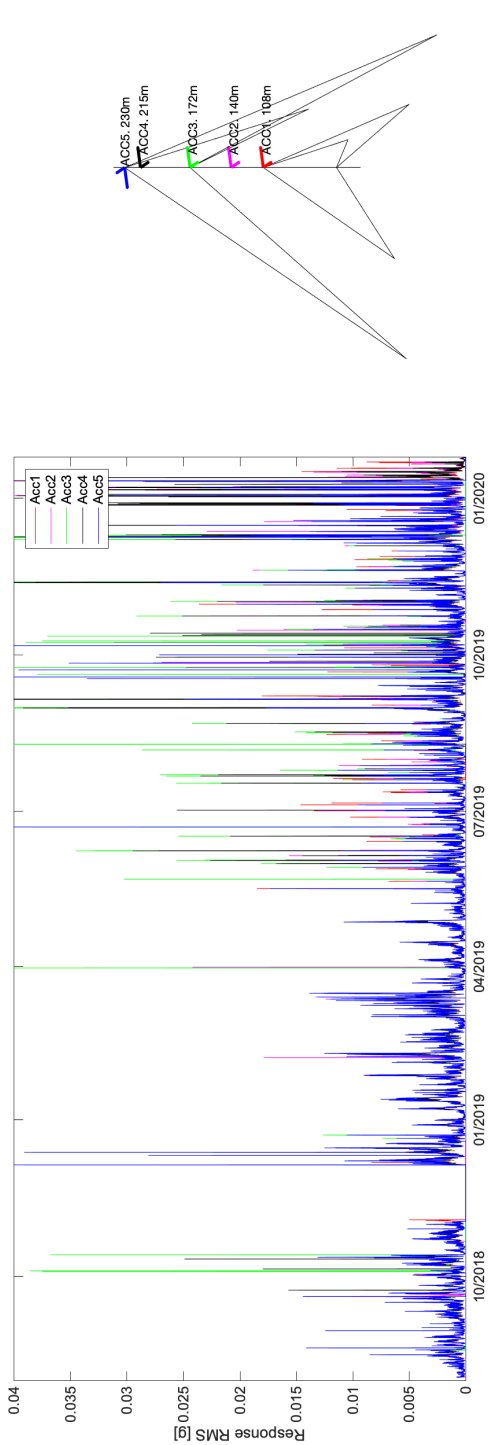

Figure 9-15 Response of structural health monitoring. Moel-y-Parc.

9.8 SHM-MYP Analysis

Apart from analysing the response behaviour of the HGM in correlation with wind data, an operational modal analysis (OMA) was applied to the large amount of the data captured by each accelerometer. The purpose was to identify main MPs that represent the behaviour of the structure, and in particular to see if the TLD was effective at the design frequency. In addition to that, with a simple correlation with RMS response at each stay level on the mast and wind speed/direction, the research provides a better understanding of the complex dynamic behaviour, structural/aerodynamic damping of the structure, performance of the TLD, influences of the stays, etc…

For the first 10 months of SHM the structure behaved under buffeting with response correlated with mean wind speed and along wind direction. Some strong wind storms were experienced by the structure with a peak wind gust of 45 m/s but with little influence from dynamics and acceptable responses. From June of 2019 significant events occurred suddenly at night time and in relatively calm weather. Those events excited two specific modes and correlated with low steady wind speeds between 7 - 15 m/s, which suggests a possible aeroelastic events such as VS.

Figure 9-16 plots the response for each level accelerometer box against the wind data at 225 m. it does not provide the wind loading on the HGM as more than one level of wind data is required to build the instantaneous wind profile. However, it gives clues from the approaching angle of the wind loading. On the left side, the response is compared to the mean wind speed. Two elements are identified; the linear increasing tendency from 0 to 35 m/s shows the buffeting along wind response; and higher response events between 7 and 25 m/s suggest another cause. The right side shows wind direction correlation which classifies all the previous high wind events into very close critical orientation at 200 and 330 degrees. The investigation below confirms those events as aeroelastic galloping events in at least 3 stays of the mast for several wind conditions.

There was very limited clear evidence of VS events during the monitoring period, which may be due to incorrect estimation of the Scruton number and incident wind loading or the action of the TLD which acts to quickly suppress across-wind responses. The SHM provides enough information to study several points related to dynamic behaviour in high HGM.

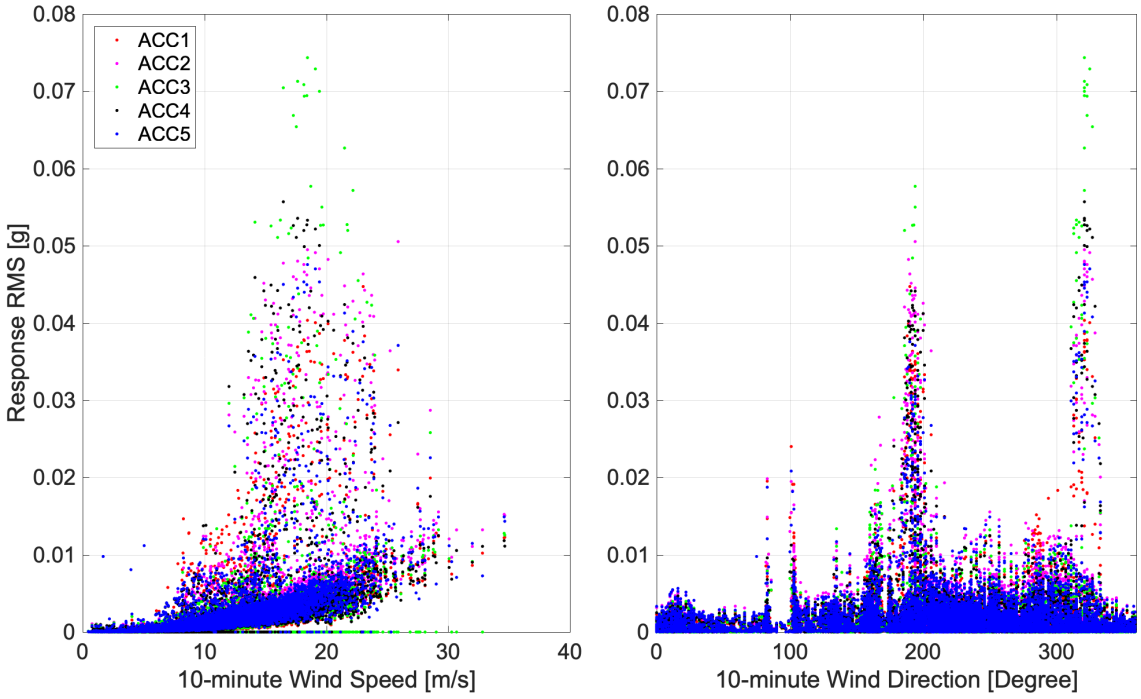

Figure 9-16 Response against wind loading diagram. (Left) 10-min Wind speed. (Right) 10-min Wind directions.

The application of operational modal analysis (OMA) is a useful tool for ambient loading as no input loading/forces are necessary for the estimation of MPs, essential to verify if the structure is behaving as expected in structural assessments.

As a first approach the implemented method was that already used in previous chapters i.e. stochastic subspace identification (SSI) for the whole set of data, and for the most interesting events, BAYOMA and ARTeMIS software were also used. For computing time consuming reasons, the initially selected time frame was defined as 10 minutes, and reduced to 5 min to focus on specific cases. These time segments were proven to be suitable in representing individual stationary conditions for wind loading/response. SSI was used for the initial identification exercise where 25 modes were found in the first 2.5 Hz.

This frequency range tracked over the full SHM period is depicted as the PSD in Figure 9-13. This provides performance of the MPs for any response event. Since the beginning of summer 2019, the mentioned strong response events appeared for relatively normal wind conditions.

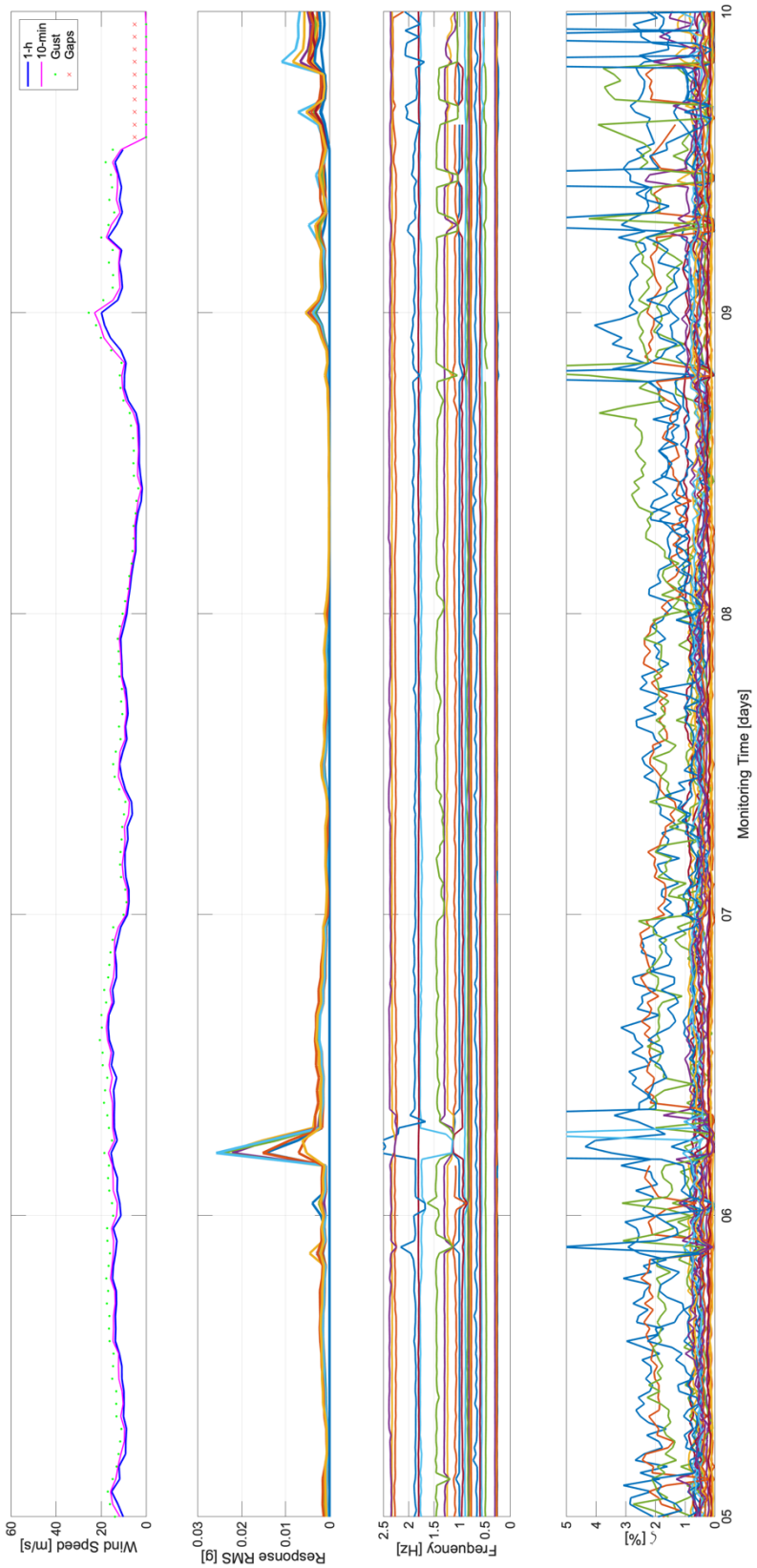

Figure 9-17 Operational Modal Analysis SSI applied to SHM in Moel-y-Parc in August 2019.

Figure 9-17 shows MP tracking using the SHM for few days of August 2019. In the upper plot, the wind information received from the anemometer is analysed obtaining mean and gust values. No evidences of storms were captured with mean wind speeds all below 20 m/s. However, the second plot referring to RMS of the response captured by accelerometers found several high and atypical peaks not found during previous months. Those events belong to the high response events discovered also in Figure 9-16. Third and fourth plots draw the performance of the identified modes in frequency and damping terms. During events the analysis captures strong variations of MPs where some modes disappear under the excited mode in resonance similar to that introduced Figure 9-13.

9.8.1 Issue Found: Galloping Events

From June of 2019 the monitoring started to record relatively high responses (Figure 9-15) during events with certain key frequencies. The duration of those occurrences was between 1 and 10 hours.

All of the them had a figure-of-8-shape behaviour in plan view as shown in Figure 9-18 which plots in blue the response of the Acc4 at damper height and in red the response captured by Acc 5. The response expected was either a chaotic response due to turbulent buffeting or a flat elliptical shape demonstrating VS. However, this kind of shape appearing in Figure 9-18 appears to be built by two resonance frequencies which indicates it is most likely to be an issue related to the stays.

This case was discussed during the International Association of Spatial Structures Group 4 conference in Winchester, UK during September of 2019. Experts agreed that this behaviour could be explained by excessive stays movements which excite the structure this way. In addition to that, Prof Macdonald from University of Bristol agreed that those two frequencies can be created by one main frequency of any stay which induce forces at f_{stay} and $f_{stay}/2$ into the mast. All this feedback helped to instruct periodic surveys to quickly identify that stay motion.

The following reference confirmed the existence of the galloping events, [132]. Galloping is the vibration of slender elements in a direction almost perpendicular to the induced wind direction, and able to increase with increasing wind speed. The shape of the structure and wind turbulence are key factors for the occurrence.

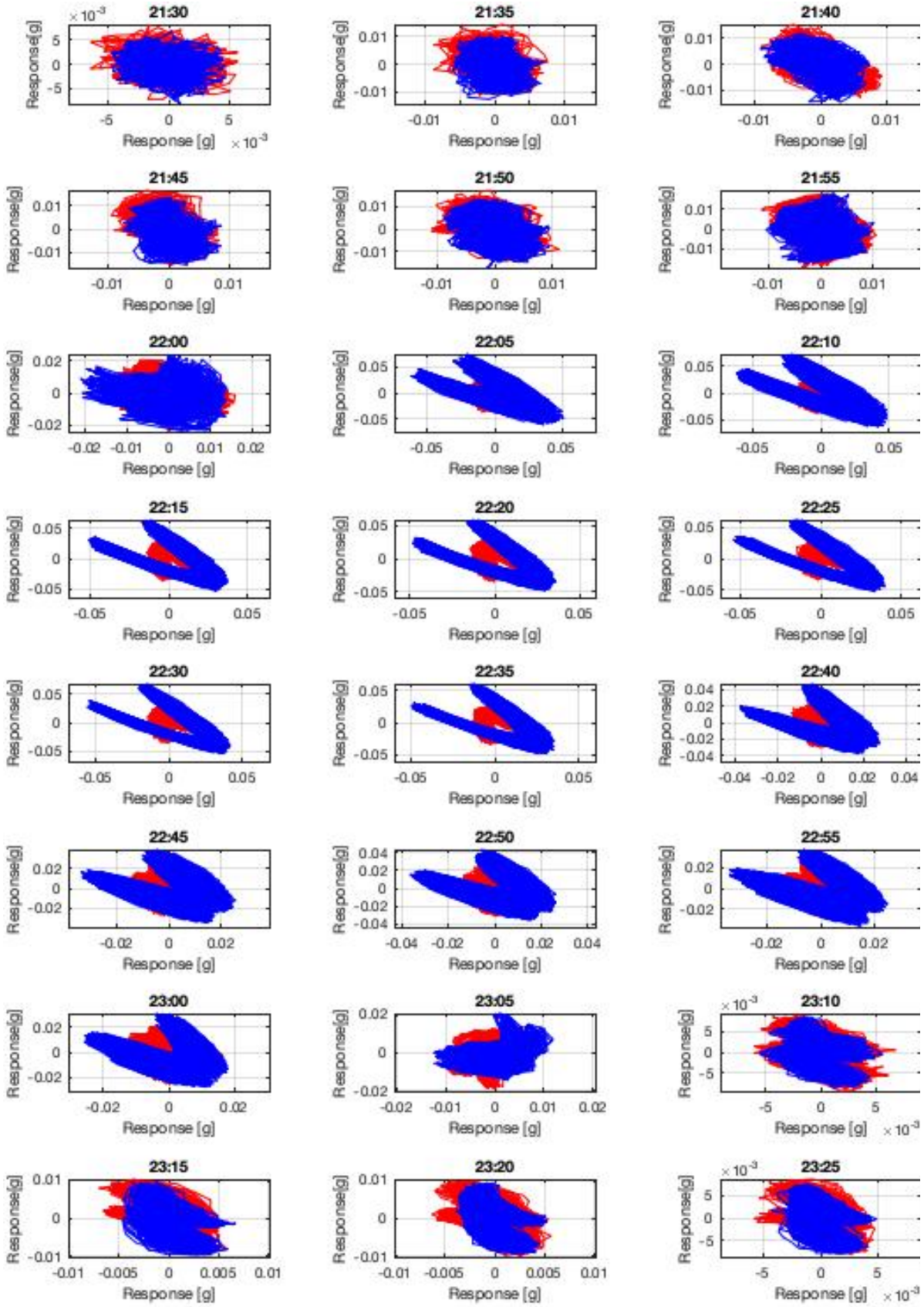

Figure 9-18 Response plan view. Blue line Acc4. Red line Acc5. Event: 1st July 2019.

The responses captured do not exceed the limits of acceleration and stresses set by expert consultants, but specific analysis would confirm if any additional action like galloping stay dampers are required.

For research purposes, in this dissertation only the event described in Figure 9-19 is analysed. Other like events tend to have a very similar behaviour with similar 8 shapes, but frequencies tend to be slightly different as other stays with different length and tension induce the galloping responses.

In this case, at 21:30 of 1st of July of 2019 the response of the mast at the upper levels (captured by Acc 4 and Acc 5) increased from 0 to 0.1 g over half an hour, stayed relatively constant for 40 min then started decreasing as the acceleration time line in Figure 9-19. The below PSD and spectrum show that all accelerometers captured this behaviour which is essentially defined by 2 main coupled modes, 1.2 and 2.3 Hz. This bi-modal response generates an ∞ or 8 shape perpendicular to the galloping stay.

Both mode shapes, plotted in Figure 9-21, have a complex non-cantilever behaviour with high responses at the middle of the structure at the third stay level corresponding with the stay under galloping.

In terms of loading, the wind speed conditions in Figure 9-20 were calm and constant, bearing from 320 degrees and staying close to 10 m/s, with no specific dramatic changes or influences from the structure.

Finally, Figure 9-22 correlates geometry of the structure, location of the damper, orientation of the stays and responses under the galloping event and wind details, all data obtained from the SHM system which confirm that stays of 3rd or 4th level at 332° had a galloping event. After identifying the cause of the response, the SHM provides enough information to identify further cases in any of the stays from the analysis of time response, mode shape distribution and resonant frequencies.

It is notable that this behaviour is not optimal for the performance of the TLD. The asymmetry of the water tanks does not help to provide a good length for sloshing in a perpendicular direction and the vibrational modes encountered are out of the frequency range for which the damper was designed.

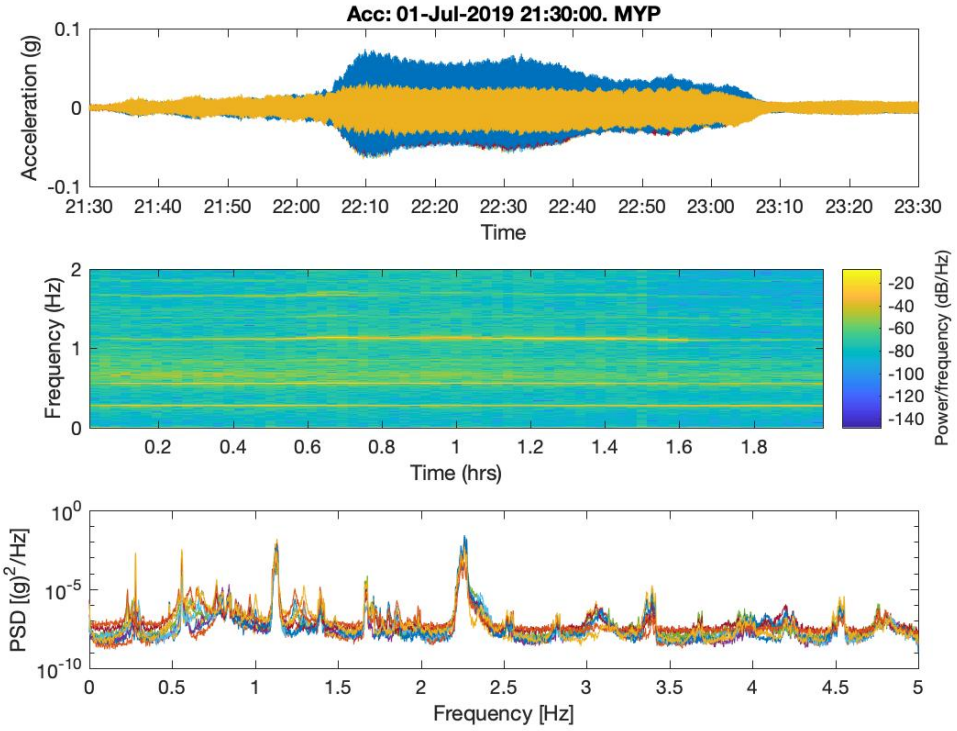

Figure 9-19 Response timeline and frequency spectrum on galloping event found on 1st of July of 2019 at Moel-y-Parc.

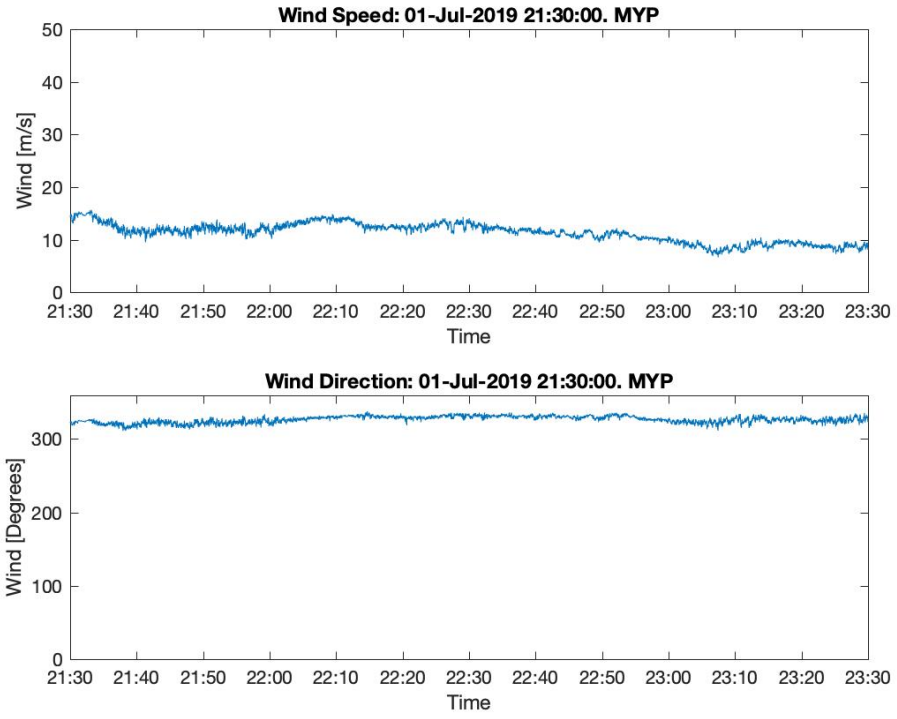

Figure 9-20 Wind loading data of galloping issue found on 1st of July of 2019 at Moel-y-Parc.

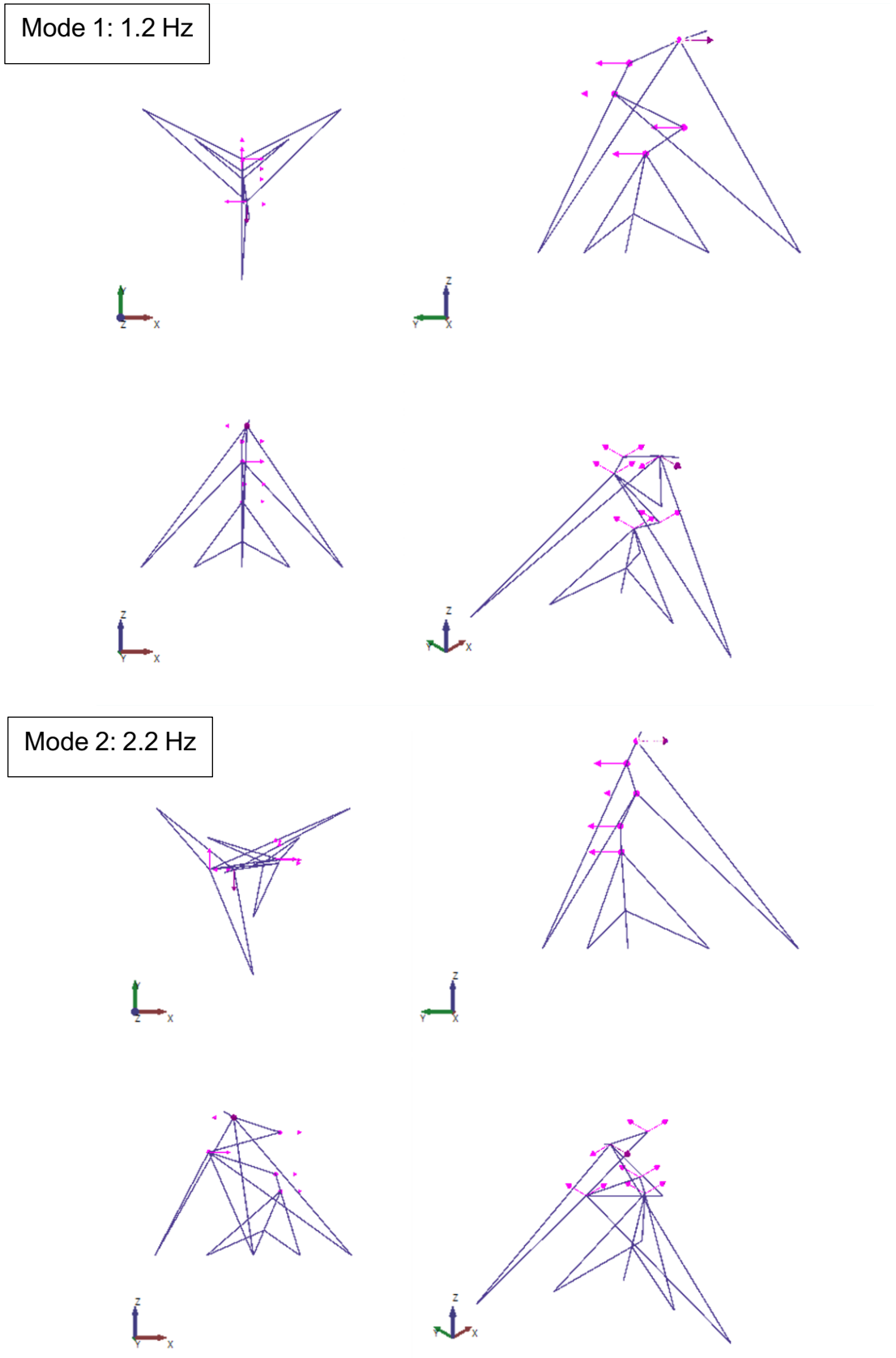

Figure 9-21 Mode shapes excited during galloping event on 1st of July of 2019 at Moel-y-Parc. Mode 1: 1.2 Hz. Mode 2: 2.2 Hz. ARTeMIS.

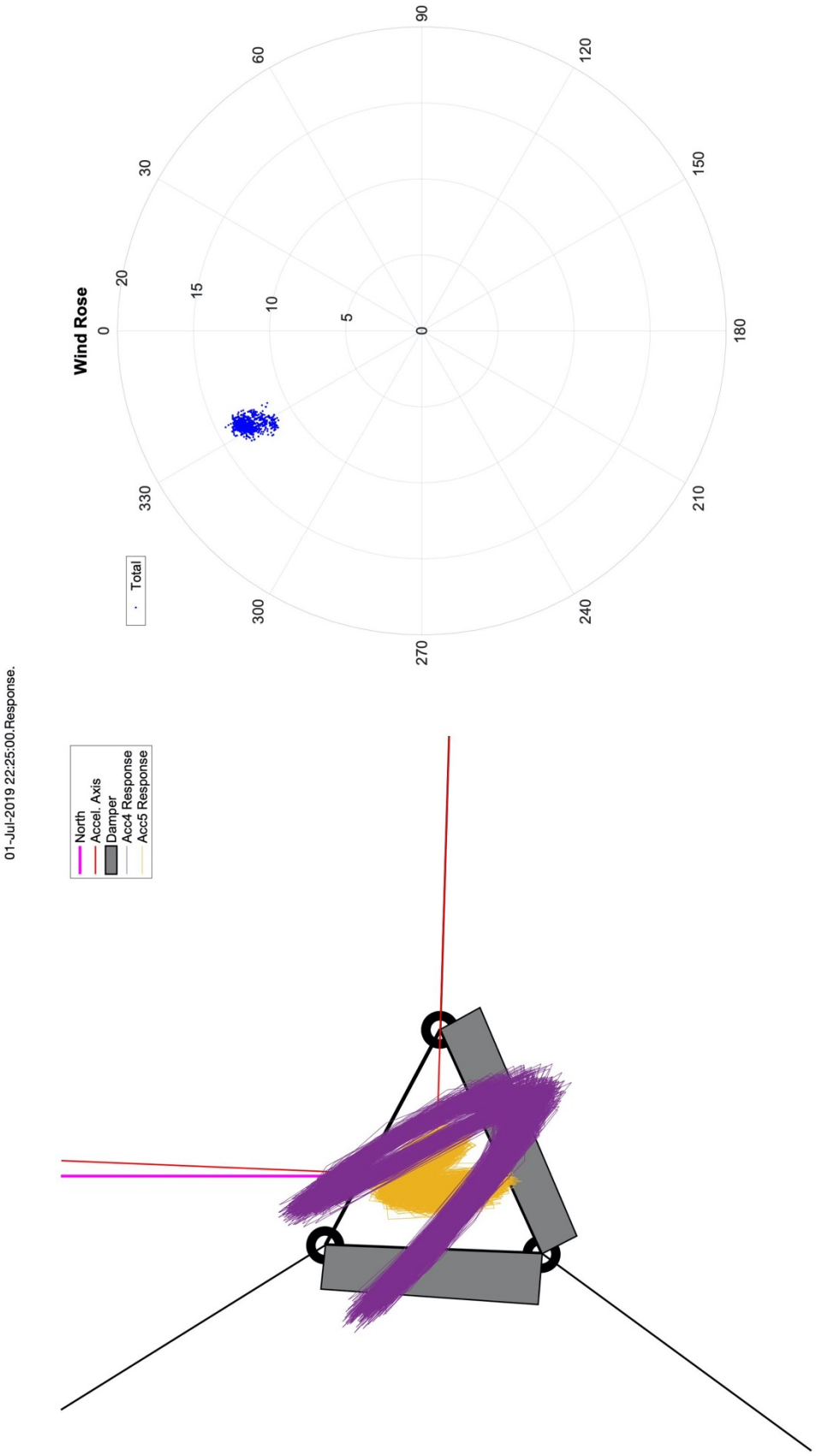

Figure 9-22 20-minutes plan view response and wind rose of Galloping issue found on 1st of July of 2019 at Moel-y-Parc.

9.8.2 Verification of Experimental and Analytical Results

As with other SHM systems in civil engineering, the collection of response data under ambient loading and the application of identification methods is an excellent tool to verify the current stiffness and damping of structures.

It can not only give information for structural diagnosis, but the data can confirm initial stiffness design and allow meaningful updating of engineering models which enhances any further analysis in terms of reliability. In communication structures where the requirements of loading are diverse and change so often, reliable mode prediction is a critical issue, all the more important the more dynamic the structure is, and essential to help evaluate fatigue in older structures.

For example, following Figure 9-23 shows the FEM model used during the initial assessments confirmed the VS critical mode at 0.6 Hz. The model was built from complete historical structural records covering the material properties, member section sizes, masses, loading, etc… Although, these properties are well documented, the behaviour of materials, connections and other elements can change over time. The OMA in SHM found the same actually occurred at 0.68 Hz. As previous chapters, real stiffness provides essential information to validate analytical and FEM models. Further dynamic assessments can rely on these findings to provide more reliable answer in the future. It is worth noting that only two modes were initially assessed as likely to be excited by VS. Real data appear as an essential tool to verify structural engineering work and reduce risks in making decisions.

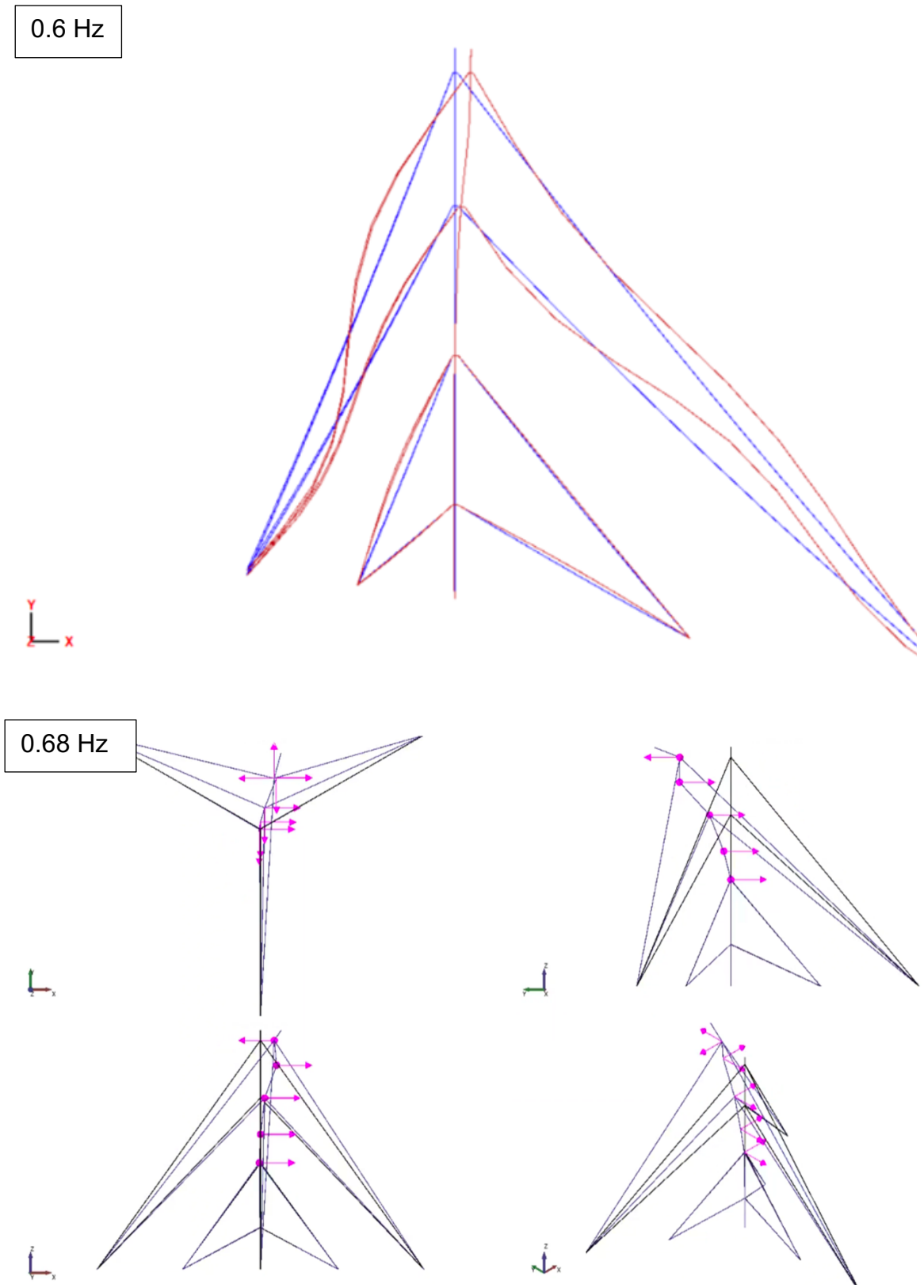

Figure 9-23 Model verification exercise. (Top) Mode estimated by pervious structural assessment. 0.6 Hz. COWI. (Down) Full view of Critical mode identified on SHM analysis. 0.68 Hz. ARTeMIS.

9.8.3 Behaviour of the Tuned Liquid Damper

To review and investigate possible VS events, a graphic view of the plan shapes was plotted in time frames of 10 min. The lock in response must create a flat and elliptical shape working under a main frequency, as previous experiences at Salisbury and Brougher Mountain, obtaining relatively high responses for long periods of time.

Until now, these checks have not provided evidence of VS events at Moel-y-Parc, and consequently it has not been possible to fully validate the installed TLD.

Furthermore, in the previous section and Figure 9-23 it was found that the analogous mode is stiffer than the TLD design mode which could influence the effectiveness of the sloshing, not achieving the optimal performance.

However, the OMA carried out provided a good approach of modes and their damping behaviour as Figure 9-17. Most of the modes tend to have a very low value of damping around 0.6 - 1 %, but the mentioned mode at 0.68 Hz (Figure 9-23) takes higher values around 2 - 2.5 % as Figure 9-24 which shows the behaviour of frequency and response against damping. At resonance levels and high responses, damping values approach around 1.8 %. As a reminder, the specification for the TLD quantified at least 3 % of critical damping obtained when damper motions are appreciable.

At the second harmonic of the frequency design of the TLD ($2\ f_{TLD}$ = 1.1 - 1.2 Hz), there are few modes with higher damping values around 3 %. This fact also might demonstrate that TLD works correctly on the specified range of frequencies. However, the values of damping of those modes are subject a high uncertainty due to the influence of the stay, which may or may not contribute to the total critical damping.

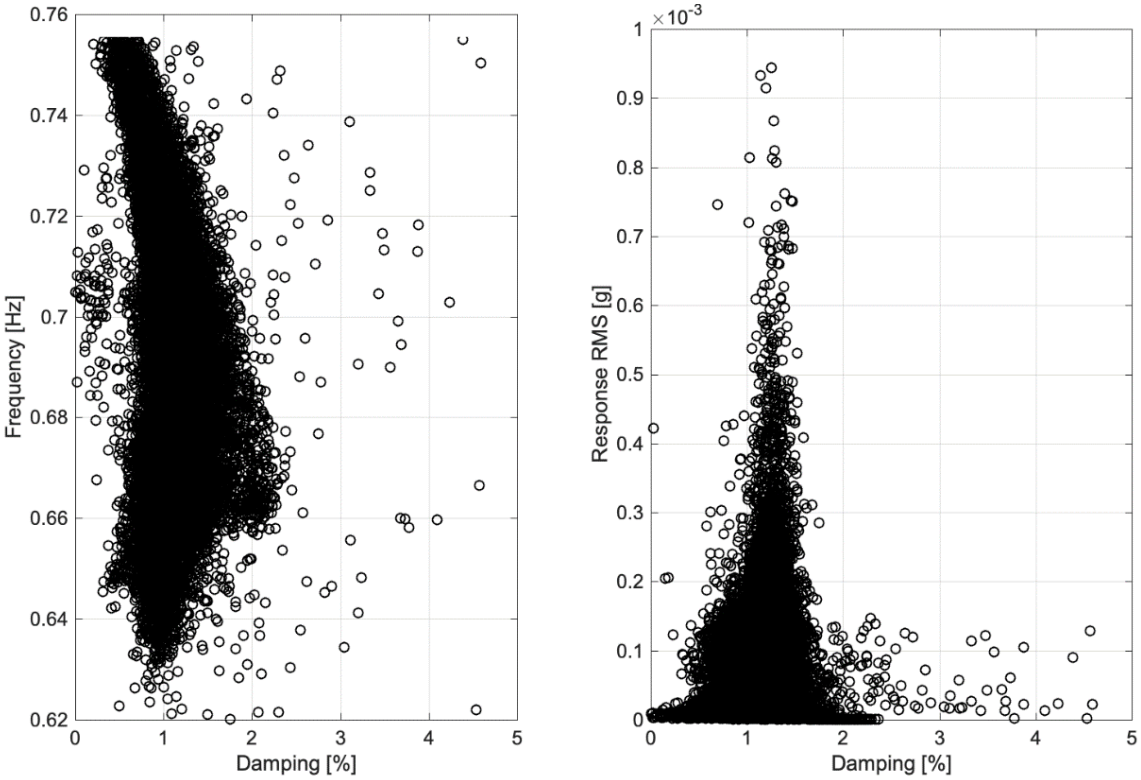

Figure 9-24 Damping behaviour of mode at 0.6 Hz.

9.9 Summary

The present chapter described a unique project based on the monitoring of Moel-y-Parc structure for 18 months. The main points are:

- The design of the SHM relied on an innovative technology system based on digital acquisition due to the need to avoid RFI and to operate in all weather conditions.
- The project provides some of the most extensive measurements and results for HGM ever undertaken. Earlier projects have been thwarted by the weather and RFI conditions and none of them were accessible on previous literature.
- The SHM showed important discrepancies between models and reality. Exercises like this are essential as recursive feedback to update theoretical analyses and find better approaches to represent either loading or response as more innovative tools and techniques become available. This has potentially greater importance in communications structures where more structural capacity allows greater financial profit from further equipment installations.

- The present chapter shows a very complex frequency behaviour with more than 25 active closed-related modes in the first 3 Hz. Ambient wind loading is able to excite the structure causing resonances under buffeting, galloping and VS. The OMA carried out confirmed the modal properties, with low values of critical damping at 0.5 % for a high percentage of the modes. This value is closer to the structural damping values proposed by [21], so it can be concluded that higher responses are required under each mode to trigger aerodynamic contributions on total damping which in high winds should be considerably greater than structural damping.
- The behaviour of the TLD could not be totally validated as there was no evidence of VS events during any load cases related to the 700 MHz project. The problematic mode believed to be susceptible to VS occurred at a 0.68 Hz. This may indicate that the damper is still performing reasonably well, even if not optimally. In the absence of specific before-damper response data, highly tuned damper might be inaccurate. i.e. dampers with a reasonable wide frequency range are preferable.

Finally, specific events of galloping were captured which induced bimodal resonance into the mast, under stable wind conditions. Albeit not exceeding acceptable limits in terms of accelerations or stresses, it is an important issue which will help in the understanding of galloping in stay design.

Chapter 10 Summary and Conclusions

10.1 Summary of Study

The research described in this thesis was undertaken to investigate the damping behaviour of different communications structures subjected to wind loading. The main aim of this work was to validate existing modelling approaches of dynamic properties and enhance knowledge of structural dynamics that has not been updated since codes were first established in 70 - 80s. The study was conducted by implementing practical engineering projects on monopoles, short and high lattice towers, and high guyed masts.

The primary objective of the monopole phase of this study was to characterise the structural damping behaviour of short communications structures. Experts in structural engineering consulting currently doubt the validity of national codes for routine design applications in damping terms. There was need for a validation of the recommended values of equivalent viscous models of structural damping provided in the literature. Modal surveys of 16 monopole structures were conducted to compile a summary of structural damping according to the physical properties and geometric configuration of each short communications structure.

A time-variant methodology was also applied to free response decays which proved the non-linear, amplitude-dependent behaviour of modal properties, natural frequency, and damping for main pairs of modes that define the response of the structure.

Dynamic analyses were performed on the same decays using a frequency domain analysis model in similar ‘Pull and Release’ modal surveys to investigate the influence of the soil-foundation source on structural damping. Three different combinations of soils and foundations were tested and analysed using the complex dynamic stiffnesses methodology. This methodology was applied to the relative response between the top of structures and the sizes of foundations defined under two relative forms of oscillation: the horizontal translation of the base and the rotation of the base.

The second phase of the study of short structures utilised ambient response data captured by specially created monitoring systems to assess aerodynamic damping.

Initially, an innovative investigation was conducted to assess the implementation and performance of different structural identification methodologies in measuring the responses of different monopoles. The results are applicable to several types of structural health monitoring systems in communications structures and support the estimation of modal properties and structural diagnosis.

As a final stage of the monopole studies, ambient response data and structural free decaying response of two different monopoles were analysed to carry out an exhaustive comparison with existing methods of assessing damping and to develop a more comprehensive understanding of monopole dynamics.

The lattice-tower phase of the study had two aims. The first was to identify and conduct a dynamic analysis on severe vortex-shedding aeroelastic events that occur on bluff-body broadcasting antennae in high steel structures. The second was to analyse solutions based on adding external damping to mitigate or dissipate such dangerous across-wind responses.

Response data were obtained before and after damping solutions were implemented in two different case studies: Salisbury, where a mechanical dynamic vibration absorber (DVA) damper was used to control cross-wind vibration in the second vibrational mode of the lattice tower, and Brougher Mountain, where hanging chain impact dampers were used to keep responses of the first frequency mode below safety limits.

Finally, in the high-guyed-masts phase, the research addressed the important structural health monitoring system installed in the 270-m Moel-y-Parc transmitting structure. The primary objective was to first identify the existence of likely aeroelastic vortex shedding issues and then assess how tuned liquid dampers could mitigate this issue.

Using the system described in the previous paragraph, eighteen months of loading and response data obtained from several levels of the structure helped to analyse dynamics responses and assess the structural integrity of such complex structure.

10.2 Conclusions

The following conclusions are drawn based on the results obtained from different structures tested during the research and are classified as follows:

10.2.1 Comments on Approaches to Damping in Monopoles

Both consultancy experts and the results from this study emphasise the need to change the conventional quasi-static analysis methods to incorporate more realistic methods of assessing dynamic properties, especially damping terms. Further, the coming wave of 5G-technology equipment that must be added to current infrastructure will exceed the current structural limits of thousands of short communications structures, complicating the dynamics implications.

In this context, damping appears to be a key dynamic property which determines the level of response and the capacity of energy dissipation of a structure. However, due to the lack of investigations of damping in slender structures under ambient loading and the high level of uncertainty at damping estimation, damping has been an issue neglected for decades since the building of the national standards.

Better understanding of damping is now required to improve structural integrity assessments from a dynamics perspective. Further, this understanding will allow structural engineers to implement solutions that employ damping to prevent undesired responses and to lower risks of fatigue-related failures.

10.2.1.1 Structural damping

This section covers conclusions exposed on Chapters 3, 4, and 5.

1. Field tests were based on human excitation, and response acquisition systems were used to obtain free-decaying responses. In calm weather conditions and with adequate modal direction, this method provides modal structural damping. Curve fitting and eigensystem realisation algorithm estimation methods are proven means of analysing the decays. Acceptable discrepancies between methods validate the damping estimates.
2. This methodology was applied in 16 field test cases (14 monopoles and 2 lattice towers). The calculated structural damping values ranged significantly, from 0.3 - 1.2 % of critical damping, despite the similarity of the structures and their response frequencies (between 1 - 2 Hz).

3. The results confirm the consultancy sector's concerns about the conservative values of structural damping recommended by the main codes. All the results of the study indicated values higher than the 0.25 % of Eurocode and British Standards. The ESDU band is considered a sufficient a priori estimation. However, the best approach will always be to conduct appropriate field test which can provide more reliable results.
4. Backbone curve methodology studies were also applied to free decays to understand non-linear systems. The shapes of the natural frequency and damping curves were examined as a function of amplitude response when no forcing was present. The stiffness non-linearities were based on a square root function and indicate a softening behaviour in amplitude dependence. The approach could be improved with a bilinear function which would complicate the expressions. On the other hand, the damping function exhibits a typical dry friction or Coulomb-type damping behaviour, as is expected from demountable structures and bolt connections based on an interfacial motion. The application of such methodology has proven as an excellent tool to analyse proposed free decays proposing clues for further researches.
5. To analyse the implications of dynamic soil-structure interaction using the same free decaying response, response data from structure and foundation levels were obtained to identify complex stiffness for each form of oscillation: horizontal translation and rocking.
6. In all the tests done for this research, the total structural damping has a foundation component. This component is mainly defined by the horizontal oscillation motions and marginally by rocking motions. It is not based on a high correlation between the type of soil-foundation and foundation damping. On the other hand, there is a dependency between foundation damping and inherent structural damping of the monopole. Both types of damping had similar values for each monopole analysed.
7. The soils-foundations augmentation factor applied to structural damping method in the British Standards is valid due to the correlation between both sources of damping, but the provided values appear to be wrong. A single proposed value between [1.5 - 2.5] could represent this factor better. Otherwise, an additional component of damping between [0.3 - 0.7 %] could be incorporated.

10.2.1.2 Aerodynamic and global damping

This section covers conclusions from Chapters 6 and 7.

1. To obtain data specific to service response and ambient loading, a structural health monitoring system was built. This study investigated the implementation of two different operational modal analysis techniques. The classical stochastic subspace identification method provided by ARTeMIS and the fast Bayesian (BAYOMA) method were evaluated for this purpose; neither methods have been previously utilised in analyses of communication structure response data. The BAYOMA method provides full statistical quantification of modal properties values which are particularly important for structures with close frequencies whose modes have almost identical horizontal mode shapes. Time windows of 10 minutes were adequate to limit uncertainty and identify events in high winds. The results present opportunities for structural diagnosis and model validation.
2. The main response in monopoles is essentially defined by turbulent buffeting wind loading which excites two coupled cantilevered bending modes that are relatively close in frequency and within a wind-sensitive range below 2 Hz. Both mode shapes were clearly identified with misalignments that modify the inherent structural symmetry, providing more inertia for one direction than its orthogonal. Typical linear-loading ladders or cable trays are ideal to identify stiffer mode shapes orthogonal to the first mode.
3. The estimation of the modal PSD forces confirms the coupled response for buffeting excitation. The high degree of turbulence of wind ambient loading excites both along- and across-components of all ranges of mean incident wind speed and direction. The properties of modal PSD forces also indicate that the stiffer mode of the pair absorbs slightly higher forces to be more dominant for both structures. Localised impulsive pulls can elicit unimodal response decays ideal for backbone curve study.
4. In terms of frequency, monopoles exhibit a non-linear softening behaviour under ambient loading that is similar to the behaviour measured during the structural damping study. The amplitude differences between calm and windy scenario, which are more evident at high responses, suggest a reduction of stiffness in the presence of wind flow.

5. Monopoles rely on two main damping sources: structural and aerodynamic. Both sources are combined to define a linear-amplitude-wind-dependency behaviour; this finding is supported by existing codes.

6. Despite relying on the already-verified wrong definition of equivalent viscous value of structural damping which takes mean values and avoids a clear amplitude dependency, the highest discrepancies were found during the estimation of the aerodynamic damping: drag factor values are overestimated in turbulent wind flow. In summary, the method of assessing damping provided by codes tends to overestimate total modal damping by a factor of 2 - 3 times the current findings, with large implications for the definition of augmentation factors in quasi-static analysis. This result proves the insufficiency of conventional analysis methods in high-dynamic, sensitive structures.

7. The drag factor extracted from aerodynamic damping indicates high discrepancies with suggested sectional drag factors taken during structural assessment due to the level of turbulence in short communications structures. The inferred new drag factors and greater dynamic sensitivity challenge the current formulation for checking quasi-static applicability. However, these factors will induce smaller wind forces which may be beneficial from a structural point of view.

10.2.2 Performance of External Dampers to Dissipate Vortex Shedding in High Lattice Towers

The main cause of collapse in communications structures is, by far, fatigue failures induced by high vibrations. Vortex shedding, characterised by long resonant responses under low wind speed conditions, can easily yield high numbers of cycles and fatigue deterioration.

Structural damping appears to be a key property to control the occurrence of potentially damaging events and to define the amplitude of their responses. Systems that add damping are a strong alternative to typical solutions that employ changes in shape, such as aerodynamic spoilers.

Damping solutions like those discussed in Chapter 8 will be more feasible once the field achieves a better understanding of the dynamic behaviour of stiffness and inherent damping with respect to response effects from different wind loading

conditions in slender structures. Main concerns of mentioned chapter are summarised below:

1. The responses in both studied cases were caused by the vortices created in low-turbulent wind flow through large bluff antennas which crowned each structure. The phenomenon induced the resonance of the structure in specific modes: the second mode, 2.65 Hz, in Salisbury and the first mode, 1.2 Hz, in Brougher Mountain for period of time, during the monitoring, ranging from several minutes to hours at an almost constant response called the lock-in effect. Each mode with a critical wind speed below 15 m/s is susceptible to repeated excitation under vortex shedding and must be considered in structural assessments. The resonant response of vortex shedding is characterised by an elliptical shape, perpendicularly orientated to the mean wind speed before and during the event.
2. The approach of using Strouhal numbers for typical structural sections were found adequate for the estimation of the critical wind speeds. A better understanding of global structural damping is necessary for a better estimation of Scruton values and will lead to a better approach of the propensity of such events.
3. The application of structural identification methods to identify and report vortex shedding events was successful. The methodology managed to identify both peak resonance responses and the creation and development of lock-in response through the estimation of negative and constant damping values. Refining time windows may improve the identification approach.
4. A mechanical DVA damper installed in Salisbury successfully prevented any large amplitude responses under the design frequency range. The friction of ‘stop-choc’ elements massively increases the structural modal damping of the second mode, stopping any resonant events. Conversely, the hanging chain impact dampers installed at Brougher Mountain require a level of response after the event is initiated, that is, the damper is triggered by certain responses. Consequently, vortex shedding is present but is kept within safe levels of vibration where fatigue does not occur.
5. Both examples were proven to work satisfactorily. The effectiveness depended on high levels of tuning during design stages and reliable models validated with precise response data obtained from acquisition systems.

10.2.3 Comments on Moel-y-Parc Structural Health Monitoring Project

The peculiarity of the monitoring system in Moel-y-Parc generates stimulating challenges for some fields of engineering. The practical requirements based on extreme weather conditions, the location into the structure, and a heavy radio-frequency environment required to the development of a state-of-the-art technology system based on digital data acquisition. The project provided some of the most extensive measurements and results for high guyed masts ever recorded and published.

1. Moel-y-Parc has a response formed by more than 25 active, closely-related modes at low frequencies, starting from 3 Hz. This complex frequency behaviour is defined by typical bending and torsional modes of the structure and the vibrations induced by each set of stays. This typical frequency behaviour in high guyed masts is not found in any other civil engineering infrastructure under ambient loading. Buffeting, vortex shedding, and galloping are main wind events applied to high guyed masts.
2. The operational modal analysis, correlated with wind loading data, was applied to each mode and suggests low values of structural damping.
3. The behaviour of the tuned liquid damper could not be fully validated as there was no evidence of vortex shedding events during any load cases related to the 700 MHz project. The forewarned occurrence of a potentially dangerous mode appears to be at a slightly higher frequency for which higher damping than other modes was found. This may indicate that the damper is still performing reasonably well, if not optimally. In the absence of specific before-damper response data, a highly tuned damper would be inappropriate (i.e., dampers with a reasonable wide frequency range are preferable).
4. Galloping events caused the highest responses during monitoring. They excited the structure into two couple modes which resonated the mast for between 1 and 10 hours under specific low wind speeds in certain dangerous directions. Although measured values did not exceed acceptable limits of acceleration or stress, this important issue will help further the understanding of galloping in stay design in the future.

10.2.4 Recommendations for Further Research

There are several features of the work conducted in this study which might benefit from further investigation. The ease of acquiring data is increasing as technology costs rapidly decrease, and computer hardware and software enable the application of different estimation techniques. Despite the high level of detail provided on damping in this dissertation, the following subjects need further exploration:

1. The results for structural damping in monopoles included some tentative provisions about the origins and causes of the amplitude dependency. The results from the backbone curve analysis in Chapter 4 indicated likely dry-friction behaviour. However, the dearth of existing knowledge about nonlinear identification in steel civil structures limits the potential of these results. Specific laboratory tests that consider fatigue deterioration would connect these damping findings with other sources and yield a more comprehensive model of structural damping in communications structures.
2. The considerable impacts of soils-foundations systems in structural damping were confirmed in Chapter 5. However, the field tests and the methodology of this work are not sufficient to capture the heterogeneous complexity of ground conditions. Further parametric studies are required to identify appropriate levels of damping depending on structure type, including other structures as high lattice towers. These studies should maintain an ambient loading focus and avoid different seismic approaches.
3. The study indicated that existing conventional quasi-static analyses massively underestimate dynamics responses and properties. Comprehensive design guidelines related to dynamic analyses are required, including a new method of assessing damping based on the present study and a review of the drag factors in short structure conditions.
4. The results from the dampers studied in Chapters 8 and 9 indicated a great margin for structural improvement in terms of dynamics. Until now, existing examples always focused on controlling aeroelastic events such as vortex shedding and galloping. The advent of 5G technology requires actions under gust buffeting. Investigations into damper prototypes for short telecoms structures will be immensely beneficial in the sector.

5. Although it was not considered in the present study, aerodynamic damping provided by stays of guyed masts in combination with wind and ice loading is a subject of considerable importance in fully understanding the mechanisms of damping in high guyed masts and galloping events.

REFERENCES

[1] M. Madugula, “Dynamic response of lattice towers and guyed masts,” 2001.

[2] T. Kijewski and A. Kareem, “Estimation and Modeling of Damping and Engineering Auxiliary Damping Systems in Civil Engineering Structures: An Overview.”

[3] B. W. Smith, *Communication structures*. Thomas Telford, 2007.

[4] ESDU, “ESDU 77032: Fluctuating loads and dynamic response of bodies and structures in fluid flows - background information.” pp. 1–22, 2007.

[5] A. G. Davenport, “Gust Loading Factors,” *J. Struct. Div.*, vol. 93, no. 3, pp. 11–34, 1967.

[6] C. Scruton and A. R. Flint, “Wind-Excited Oscillations of Structures.,” *ICE Proc.*, vol. 27, no. 4, pp. 673–702, 1964.

[7] C. Lu, Y. Ou, X. Ma, and M. Je, “Structural analysis of lattice steel transmission Tower: A review,” *J Steel Struct Constr*, vol. 2, no. 2, 2016.

[8] R. D. Blevins, Blevins, and R. D., “Flow-induced vibration,” *vnr*, 1977.

[9] ESDU, “ESDU 83009: Damping of structures. Part 1: tall buildings.,” no. September 1983, 2012.

[10] K. Suda, N. Satake, J. Ono, and A. Sasaki, “Damping properties of buildings in Japan,” *J. Wind Eng. Ind. Aerodyn.*, vol. 59, no. 2–3, pp. 383–392, Mar. 1996.

[11] N. Satake and H. Yokota, “Evaluation of vibration properties of high-rise steel buildings using data of vibration tests and earthquake observations,” *J. Wind Eng. Ind. Aerodyn.*, vol. 59, no. 2–3, pp. 265–282, Mar. 1996.

[12] B. R. Ellis, “Full-scale measurements of the dynamic characteristics of buildings in the UK,” *J. Wind Eng. Ind. Aerodyn.*, vol. 59, no. 2–3, pp. 365–382, Mar. 1996.

[13] M. Celebi, “Comparison of damping in buildings under low-amplitude and strong motions,” *J. Wind Eng. Ind. Aerodyn.*, vol. 59, no. 2–3, pp. 309–323, Mar. 1996.

[14] G. C. Hart, “Random damping in buildings,” *J. Wind Eng. Ind. Aerodyn.*, vol. 59, no. 2–3, pp. 233–246, Mar. 1996.

[15] J. M. W. Brownjohn, “Estimation of damping in suspension bridges,” *Proc. Inst. Civ. Eng. - Struct. Build.*, vol. 104, no. 4, pp. 401–415, Nov. 1994.

[16] A. Dua, “Dynamic Analysis of Overhead Transmission Line under Turbulent Wind Loading,” *Electron. J. Struct. Eng.*, vol. 15, no. 1, 2015.

[17] M. J. Glanville, K. C. S. Kwok, and R. O. Denoon, “Full-scale damping measurements of structures in Australia,” *J. Wind Eng. Ind. Aerodyn.*, vol. 59, no. 2–3, pp. 349–364, Mar. 1996.

[18] W. H. Reed, “Hanging-Chain Impact Dampers: A Simple Method for Damping Tall Flexible Structures.”

[19] Y. Fujino, L. Sun, B. M. Pacheco, and P. Chaiseri, “Tuned Liquid Damper (TLD) for Suppressing Horizontal Motion of Structures,” *J. Eng. Mech.*, vol. 118, no. 10, pp. 2017–2030, Oct. 1992.

[20] A. K. Chopra, *Dynamics of Structures*. Upper saddle River, New Jersey: Prantice Hall, 2001.

[21] WG4. IASS International Assocition for Shell And Spatial Structures, “Recommendations for guyed masts.” Madrid, p. 112, 1981.

[22] TIA Standard, “ANSI-TIA-222-G-2005: Structural standard for antenna supporting structures and antennas.” 2006.

[23] CSA Group, “CAN/CSA-S37-18: Antennas, towers, and antenna- supporting structures.” 2018.

[24] British Standards Institution, “Lattice towers and masts — Part 1 : Code of practice for loading,” vol. 3, no. 1. 1986.

[25] Standards Australia, “Australian/New Zeland Standard. AS/NZS 1170.2,” vol. 6, no. 2. p. 103, 2011.

[26] E. Commission, “BS EN 1991-1-4:2005 General actions— Wind actions,” vol. 3, 1991.

[27] E. Commission, “EN 1993-3-1:2006. Eurocode 3 : design of steel structures. Part 3-1: Towers, masts and chimneys : towers and masts.” BSI, p. 79, 2010.

[28] British Standards Institution, “PD 6688-1-4:2015 Background information to the National Annex to BS EN 1991-1-4 and additional guidance.” 2015.

[29] British Standards Institution, “BS 6399-2: Loading for building-Part 2. Code of Practice for wind loads.” 1997.

[30] B. S. Institution, “BSI CP 3: Code of Basic Data for the Design of Buildings. Chapter V Loading -Part 2 Wind Loads.” 1972.

[31] The Institution of Lighting Engineers, “PLG07: High Masts for lighting and CCTV.” 2013.

[32] E. Commission, “EN 40-3-1:2013 - Lighting columns. Design and verification. Specification for characteristic loads.” 2013.

[33] T. H. Agency, “BD 94/07: Design of minor strucutres. Design manual for roads and bridges, Vol 2. Highway structures: Design (sub-structures and special strucutres).” 2007.

[34] D. R. Moss, “Pressure vessel design manual,” *Pressure Vessel Design Manual*. pp. 455–458, 2004.

[35] CICIND, “Model code for steel chimneys,” vol. 44, no. August. pp. 0–22, 2002.

[36] H. Ruscheweyh and G. Sedlacek, “Crosswind vibrations of steel stacks. - critical comparison between some recently proposed codes -,” *J. Wind Eng. Ind. Aerodyn.*, vol. 30, no. 1, pp. 173–183, 1988.

[37] E. Lum, P. Fatt, P. Eng, E. Jeyananda, and C. Ahnantakrishnan, “Dynamic analysis of telecommunication monopole under wind loads,” 2007.

[38] L. C. Pagnini, “Model reliability and propagation of frequency and damping uncertainties in the dynamic along-wind response of structures,” *J. Wind Eng. Ind. Aerodyn.*, vol. 59, no. 2–3, pp. 211–231, Mar. 1996.

[39] C. A. Blandon and M. J. N. Priestley, “Equivalent viscous damping equations for direct displacement based design,” *Journal of Earthquake Engineering*, vol. 9, no. SPEC. ISS. 2. pp. 257–278, 2005.

[40] C. F. Beards, “The vibrations of systems having one degree of freedom,” in *Engineering Vibration Analysis with Application to Control Systems*, Elsevier, 1995, pp. 10–87.

[41] J. L. Alford and G. W. Housner, “Spectrum Analysis of Strong Motion Earthquakes,” 1953.

[42] J. D. Stevenson, “Structural damping values as a function of dynamic response stress and deformation levels,” *Nucl. Eng. Des.*, vol. 60, no. 2, pp. 211–237, 1980.

[43] N. M. Newmark, “Seismic design criteria for nuclear reactor facilities,” *Proc. 4th World Conf.*, 1969.

[44] N. M. Newmark, “Earthquake response analysis of reactor structures,” *Nucl. Eng. Des.*, vol. 20, no. 2, pp. 303–322, Jul. 1972.

[45] D. G. Clow, “Steel masts and towers in the British post office,” *Post Off. Electr. Eng. J.*, 1974.

[46] C. Scruton and A. R. Flint, “Wind-excited oscillations of structures,” *Proc. Inst. Civ. Eng.*, vol. 27, no. 4, pp. 673–702, Apr. 1964.

[47] Wolf John, “Dynamic soil-structure interaction,” *Elsevier Sci.*, no. 484, 1985.

[48] M. Novak and L. El Hifnawy, “Effect of soil-structure interaction on damping of structures,” *Earthq. Eng. Struct. Dyn.*, vol. 11, no. 5, pp. 595–621, 1983.

[49] F. . Whitman, R.V; Richart, “Design porocedures for dynamically loaded foundations.” 1967.

[50] B. J. Lazan, “Damping mechanisms and phenomenology in materials,” in *Applied Mechanics*, Springer Berlin Heidelberg, 1966, pp. 493–501.

[51] ESDU, “ESDU: 88019. Calculation methods for along-wind loading. Part 3. Response of buildings and plate-like structures to atmospheric turbulence.,” 2007.

[52] A. P. Jeary, “Establishing non-linear damping characteristics of structures from non-stationary response time-histories,” 1992.

[53] K. Worden, “Nonlinearity in structural dynamics: detection, identification and modelling,” 2019.

[54] ESDU, *Damping of structures. Part 1: tall buildings*, vol. ESDU, 8300. ESDU, 1983, pp. 1–35.

[55] J. M. Londoño, J. E. Cooper, and S. A. Neild, “Identification of systems containing nonlinear stiffnesses using backbone curves,” *Mech. Syst. Signal Process.*, vol. 84, pp. 116–135, 2017.

[56] J. M. Londoño, S. A. Neild, and J. E. Cooper, “Identification of backbone curves of nonlinear systems from resonance decay responses,” *J. Sound Vib.*, vol. 348, pp. 224–238, Jul. 2015.

[57] N. D. P. Barltrop, A. J. Adams, and M. G. Hallam, *Dynamics of fixed marine structures*. Butterworth-Heinemann, 1991.

[58] P. C. Jennings and J. Bielak, “Dynamics of building-soil interaction,” vol. 63, no. 1, pp. 9–48, 1973.

[59] M. J. Givens, “Dynamic soil-structure interaction of instrumented buildings and test structures,” 2013.

[60] P.W. Bearman, *Aerodynamic loads on building and structure*. 1980.

[61] J. D. Holmes, “Along-wind response of lattice towers—II. Aerodynamic damping and deflections,” *Eng. Struct.*, vol. 18, no. 7, pp. 483–488, Jul. 1996.

[62] ESDU, “ESDU 96030: Response of structures to vortex shedding,” no. December 1996, pp. 1–83, 1998.

[63] B. J. Vickery and R. I. Basu, “Acrross-wind vibrations of structures of circular cross-section. Part I. Development of a mathematical model for two-dimensional conditions,” *J. Wind Eng. Ind. Aerodyn. Elsevier Sci. Publ. B.V*, vol. 12, pp. 49–73, 1983.

[64] S. Krenk and S. R. K. Nielsen, “Energy balanced double oscillator model for vortex-induced vibrations,” *J. Eng. Mech.*, vol. 125, no. 3, pp. 263–271, Mar. 1999.

[65] C. Scruton, “An introduction to wind effects on structures,” 1981.

[66] S. O. Hansen, “Vortex-induced vibrations of structures,” *Struct. Eng. world Congr.*, pp. 2–7, 2007.

[67] ESDU, “ESDU 91010: Response of structures to galloping excitation - Background and approximate estimation.” ESDU International, pp. 1–25.

[68] I. Jo, T. Kaneko, S. Nagatsu, C. Takahashi, and M. Kimura, “Development of highway light pole with resistance to wind vortex-induced oscillations.”

[69] S. H. Jeon, M. W. Seo, Y. U. Cho, W. G. Park, and W. B. Jeong, “Sloshing characteristics of an annular cylindrical tuned liquid damper for spar-type floating offshore wind turbine,” *Struct. Eng. Mech.*, vol. 47, no. 3, pp. 331–343, 2013.

[70] J. Wahba, “Dynamic & Fatigue Design as per CSA S37-18,” *IASS*, 2019.

[71] J. A. Jimenez Capilla and K. Y. Koo, “Structural Health Monitoring (SHM) for Moel-Y-Parc telecommunication high guyed mast,” *IASS*, 2019.

[72] L. L. Koss and W. H. Melbourne, “Chain dampers for control of wind-induced vibration of tower and mast structures,” *Eng. Struct.*, vol. 17, no. 9, pp. 622–625, 1995.

[73] ESDU, “ESDU 87035: Calculation methods for along wind loading Part 2: response of line-like structures to atmospheric turbulence,” no. February, 2012.

[74] W. He and W. P. Xie, “Characterization of stationary and walking people on vertical dynamic properties of a lively lightweight bridge,” *Struct. Control Heal. Monit.*, vol. 25, no. 3, p. e2123, Mar. 2018.

[75] F. Weber and H. Distl, “Amplitude and frequency independent cable damping of Sutong Bridge and Russky Bridge by magnetorheological dampers,” *Struct. Control Heal. Monit.*, vol. 22, no. 2, pp. 237–254, Feb. 2015.

[76] F. Magalhães, Á. Cunha, and E. Caetano, “Damping estimation using free decays and ambient vibration tests,” *Mech. Syst. Signal Process.*, vol. 24, no. 5, pp. 1274–1290, 2010.

[77] W. C. Ray and J. Penzien, “Dynamics of structures,” *Comput. Struct.*, 1995.

[78] J. N. Juang and R. S. Pappa, “An eigensystem realization algorithm for modal parameter identification and model reduction,” *J. Guid. Control. Dyn.*, vol. 8, no. 5, pp. 620–627, 1985.

[79] D. Giraldo, O. Yoshida, S. J. Dyke, and L. Giacosa, “Control-oriented system identification using ERA,” *Struct. Control Heal. Monit.*, vol. 11, no. 4, pp. 311–326, Oct. 2004.

[80] A. Cammarano, T. L. Hill, S. A. Neild, and D. J. Wagg, “Bifurcations of backbone curves for systems of coupled nonlinear two mass oscillator,” *Nonlinear Dyn.*, vol. 77, no. 1–2, pp. 311–320, Jul. 2014.

[81] J. R. Wright, J. E. Cooper, and M. J. Desforges, “Normal-mode force appropiation-Theory and Application,” *Mech. Syst. Signal Process.*, vol. 13, no. 2, pp. 217–240, Mar. 1999.

[82] J. M. Londono, S. A. Neild, and J. E. Cooper, “Systems with bilinear stiffness: Extraction of backbone curves and identification,” 2016, pp. 307–313.

[83] A. Pais and E. Kausel, “Approximate formulas for dynamic stiffnesses of rigid foundations,” *Soil Dyn. Earthq. Eng.*, vol. 7, no. 4, pp. 213–227, Oct. 1988.

[84] G. Gazetas, “Formulas and charts for impedances of surface and embedded foundations,” *J. Geotech. Eng.*, vol. 117, no. 9, pp. 1363–1381, 1991.

[85] A. S. Veletsos and J. W. Meek, “Dynamic behaviour of building-foundation systems,” *Earthq. Eng. Struct. Dyn.*, vol. 3, no. 2, pp. 121–138, 1974.

[86] J. H. Rainer, “Simplified analysis of dynamic structure-ground interaction,” *Can. J. Civ. Eng.*, vol. 2, no. 3, pp. 345–356, 1975.

[87] B. R. Ellis, “Significance of dynamic soil-structure interaction in tall buildings.,” *Proc. Inst. Civ. Eng.*, vol. 81, no. pt 2, pp. 221–242, 1986.

[88] J. P. Stewart and G. L. Fenves, “System identification for evaluating soil-structure interaction effects in buildings from strong motion recordings,” *Earthquake Engineering and Structural Dynamics*, vol. 27, no. 8. John Wiley & Sons, Ltd., pp. 869–885, 1998.

[89] M. Novak and L. El Hifnawy, “Structural response to wind with soil-structure interaction,” *J. Wind Eng. Ind. Aerodyn.*, vol. 28, no. 1–3, pp. 329–338, Aug. 1988.

[90] A. Maravas, G. Mylonakis, and D. L. Karabalis, “Simplified discrete systems for dynamic analysis of structures on footings and piles,” *Soil Dyn. Earthq. Eng.*, vol. 61–62, no. May, pp. 29–39, 2014.

[91] L. Andersen and J. Clausen, “Impedance of surface footings on layered ground,” *Comput. Struct.*, vol. 86, no. 1–2, pp. 72–87, Jan. 2008.

[92] Y. Yong, R. Zhang, and J. Yu, “Motion of foundation on a layered soil medium — I. Impedance characteristics,” *Soil Dyn. Earthq. Eng.*, vol. 16, no. 5, pp. 295–306, Jan. 1997.

[93] L. Andersen, “Assessment of lumped-parameter models for rigid footings,” *Comput. Struct.*, vol. 88, no. 23–24, pp. 1333–1347, Dec. 2010.

[94] E. Safak, “Detection and identification of soil-structure interaction in buildings from vibration recordings,” *J. Struct. Eng.*, vol. 121, no. MAY, pp. 899–906, 1995.

[95] K. Y. Koo, J. A. J. Capilla, and J. M. W. Brownjohn, “Innovative Sensing Solution and SHM for Moel-Y-Parc Telecommunication High Guyed Mast,” in *International Conference on Smart Infrastructure and Construction 2019 (ICSIC)*, 2019, pp. 589–594.

[96] S. K. Au, “Fast Bayesian ambient modal identification in the frequency domain, Part I : Posterior most probable value,” *Mech. Syst. Signal Process.*, vol. 26, pp. 60–75, Jan. 2012.

[97] S. K. Au, “Fast Bayesian ambient modal identification in the frequency domain, Part II: Posterior uncertainty,” *Mech. Syst. Signal Process.*, vol. 26, pp. 76–90, Jan. 2012.

[98] J. M. W. Brownjohn, S. K. Au, B. Li, and J. Bassitt, “Optimised ambient vibration testing of long span bridges,” in *EURODYN 2017*, 2017, p. 10.

[99] P. Van Overschee, B. De Moor, W. Dehandschutter, and J. Swevers, “A subspace algorithm for the identification of discrete time frequency domain power spectra,” *Automatica*, vol. 33, no. 12. pp. 2147–2157, 1997.

[100] J. M. W. Brownjohn, F. Magalhaes, E. Caetano, and A. Cunha, “Ambient vibration re-testing and operational modal analysis of the Humber Bridge,” *Eng. Struct.*, vol. 32, no. 8, pp. 2003–2018, 2010.

[101] A. V Belver, K. Y. Koo, A. L. Ibán, J. M. W. Brownjohn, and C. Goddard, “Enhanced Vortex Shedding in a 183 m Industrial Chimney,” *Adv. Struct. Eng.*, pp. 1–19, 2014.

[102] S.-K. Au, “Fast Bayesian ambient modal identification in the frequency domain, Part I: Posterior most probable value,” *Mech. Syst. Signal Process.*, vol. 26, pp. 60–75, Jan. 2012.

[103] S. K. Au, “Operational modal analysis: Modeling, Bayesian inference, uncertainty laws,” 2018.

[104] S. K. Au, J. M. W. Brownjohn, and J. E. Mottershead, “Quantifying and managing uncertainty in operational modal analysis,” *Mech. Syst. Signal Process.*, vol. 102, pp. 139–157, Mar. 2018.

[105] P. Liu, P. Y. Lian, and W. G. Yang, “Horizontal resonance of a 13 story building under external machine vibrations,” *Int. J. Struct. Stab. Dyn.*, vol. 18, no. 1, Jan. 2018.

[106] H. Pan, Z. Xie, A. Xu, and L. Zhang, “Wind effects on Shenzhen Zhuoyue Century Center: Field measurement and wind tunnel test,” *Struct. Des. Tall Spec. Build.*, vol. 26, no. 13, Sep. 2017.

[107] H. F. Lam, F. L. Zhang, Y. C. Ni, and J. Hu, “Operational modal identification of a boat-shaped building by a Bayesian approach,” *Eng. Struct.*, vol. 138, pp. 381–393, May 2017.

[108] B. Peeters and G. De Roeck, “Stochastic system identification for operational modal analysis: A review,” *J. Dyn. Syst. Meas. Control*, vol. 123, no. 4, pp. 659–667, 2001.

[109] P. Mellinger, M. Döhler, and L. Mevel, “Variance estimation of modal parameters from output-only and input/output subspace-based system identification,” *J. Sound Vib.*, vol. 379, pp. 1–27, Sep. 2016.

[110] F. Magalhães, E. Caetano, and Á. Cunha, “Challenges in the Application of Stochastic Modal Identification Methods to a Cable-Stayed Bridge,” *J. Bridg. Eng.*, vol. 12, no. 6, pp. 746–754, Nov. 2007.

[111] F. Magalhães, E. Caetano, Á. Cunha, O. Flamand, and G. Grillaud, “Ambient and free vibration tests of the Millau Viaduct: Evaluation of alternative processing strategies,” 2012.

[112] M. Diaferio, D. Foti, M. Mongelli, N. I. Giannoccaro, and P. Andersen, “Operational modal analysis of a historic tower in Bari,” in *Conference Proceedings of the Society for Experimental Mechanics Series*, 2011, vol. 4, pp. 335–342.

[113] S. Tuhta Ondokuz, M. Üniversitesi, S. Tuhta, and F. Günday, “Application of OMA on the benchscale aluminium brridge using micro tremor data,” 2019.

[114] D. Foti, S. Ivorra, and D. Bru, “Dynamic identification of a pedestrian bridge using operational modal analysis,” *Proc. Elev. Int. Conf. Comput. Struct. Technol.*, 2012.

[115] B. L. de M. Peter van Overschee, *Subspace Identification for Linear Systems: Theory*. 1996.

[116] J. M. W. Brownjohn, S. K. Au, L. Binbin, and A. Raby, “Understanding and managing identification uncertainty of close modes in operational modal analysis,” 2020.

[117] J. M. Londoño, S. A. Neild, and J. E. Cooper, “Identification of backbone curves of nonlinear systems from resonance decay responses,” *J. Sound Vib.*, vol. 348, pp. 224–238, Jul. 2015.

[118] S. K. Au, M. Asce, and P. To, “Full-Scale validation of dynamic wind load on a super-tall building under strong wind,” 2012.

[119] S. K. Au, “Fast Bayesian ambient modal identification in the frequency domain, Part I: Posterior most probable value,” *Mech. Syst. Signal Process.*, vol. 26, no. 1, pp. 60–75, Jan. 2012.

[120] J. D. Holmes, “Along-wind towers: part I- expressions for factors response of lattice derivation of gust response,” *CSIRO*, 1993.

[121] A. G. Davenport, “New Approaches To the Design of Structures Against Wind Action,” Feb. 1968.

[122] J. H. Rainer and G. Pernica, “Determination of dynamic properties of nonlinear structures using thepull-release test,” *Can. Acoust.*, pp. 177–178, 1994.

[123] S. K. Au, “Uncertainty law in ambient modal identification - Part I: Theory,” *Mech. Syst. Signal Process.*, vol. 48, no. 1–2, pp. 15–33, Oct. 2014.

[124] Arqiva, “Multimedia resource: Video recorded from site survey in Salisbury: https://universityofexeteruk-my.sharepoint.com/:f:/r/personal/jj379_exeter_ac_uk/Documents/Dissertation/Vortex_Salisbury?csf=1&web=1&e=QyTCQ8.” 2018.

[125] ESDU, “ESDU 71012: Fluid forces on non-streamline bodies – background notes and description of the flow phenomena,” *Eng. Sci. Data Unit*, no. May, pp. 1–27, 1971.

[126] Arqiva, “Multimedia resources: Video recorded from site survey in Brougher Mountain: https://universityofexeteruk-my.sharepoint.com/:f:/r/personal/jj379_exeter_ac_uk/Documents/Dissertation/Vortex_BrougherMountain?csf=1&web=1&e=opvZdS.” 2014.

[127] P. Campbell, *Learning from Construction Failures: Applied Forensic Engineering*. 2001.

[128] H. Ruscheweyh, M. Hortmanns, and C. Schnakenberg, “Vortex-excited vibrations and galloping of slender elements,” *J. Wind Eng. Ind. Aerodyn.*, vol. 65, no. 1–3, pp. 347–352, Dec. 1996.

[129] B. J. Vickery and R. Basu, “Simplified approaches to the evaluation of the across-wind response of chimneys,” *J. Wind Eng. Ind. Aerodyn.*, vol. 14, no. 1–3, pp. 153–166, 1983.

[130] K. Y. Koo, D. Hester, and S. Kim, “Time synchronization for wireless sensors using low-cost GPS module and arduino,” *Front. Built Environ.*, vol. 4, p. 82, Jan. 2019.

[131] R. E. Kim *et al.*, “Development of a long-term, multimetric Structural Health Monitoring system for a historic steel truss swing bridge,” *NSEL Rep. Ser.*, vol. 022, no. May, p. 338, 2015.

[132] Arqiva, “Multimedia resources: Videos recorded from site survey. Galloping Event in Moel-y-Parc: https://universityofexeteruk-my.sharepoint.com/:f:/r/personal/jj379_exeter_ac_uk/Documents/Dissertation/Galloping_Moel-y-Parc?csf=1&web=1&e=za4K4y.” 2019.

APPENDIX A: Campaign of Field Surveys

A.1 Additional Data for Surveys to Analyse Structural Damping from Free Decaying Response.

The acquisition of acceleration data of field tests on wide range of structures provide time and frequency domain responses to obtain frequency and damping estimations used during the research.

A number of Case Surveys are presented and detailed in this Appendix for which these data have been measured.

CASE No 1	SITE: Manor Farm	29/06/2017

MONOPOLE

SITE DETAILS

Structural Type: Monopole

Model: Super Slimline

Manufacturer: Portasilo

Height: 14.5 m

Base Width: 0.9 m

SURVEY COMMENTS

Excitation:

Pull & Release method.

Human forces.

Acquisition:

Pair of OPALs^{TM} accelerometers at different locations.

TIME DOMAIN RESPONSE

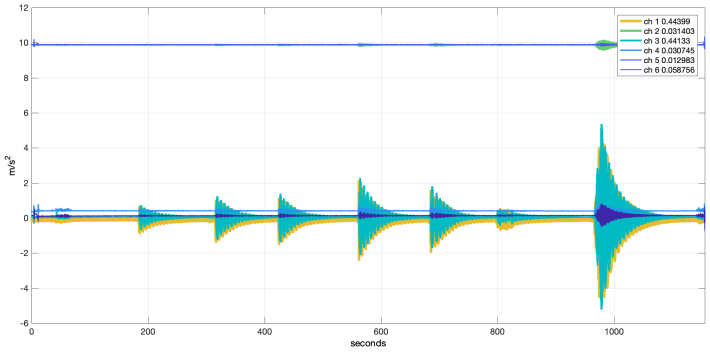

FREQUENCY DOMAIN RESPONSE

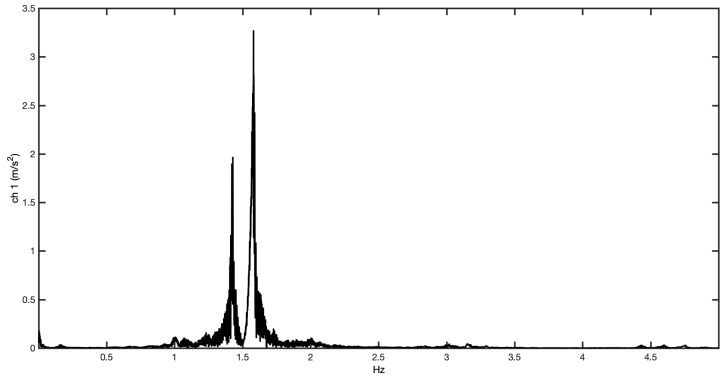

CASE No 2	SITE: Donnington Trust	29/06/2017

SKETCH OF MONOPOLE

SITE DETAILS

Structural Type: Monopole

Model: Super Slimline

Manufacturer: Portasilo

Height: 14.5 m

Base Width: 0.9 m

SURVEY COMMENTS

Excitation:

Pull & Release method.

Human forces.

Acquisition:

Pair of OPALs^{TM} accelerometers at different locations.

TIME DOMAIN RESPONSE

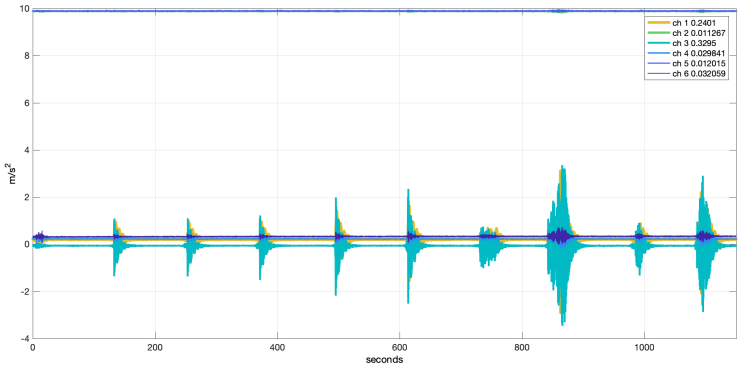

FREQUENCY DOMAIN RESPONSE

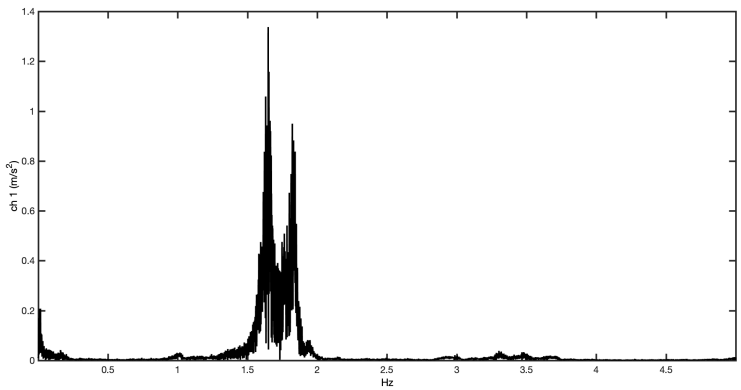

CASE No 3	SITE: Marleys Moor	04/10/2017

MONOPOLE

SITE DETAILS

Structural Type: Monopole

Model: Super Slimline

Manufacturer: Portasilo

Height: 14.5 m

Base Width: 0.9 m

SURVEY COMMENTS

Tower under decommission process.

Excitation:

Pull & Release method.

Human forces.

Acquisition:

Pair of OPALs^{TM} accelerometers at different locations.

TIME DOMAIN RESPONSE

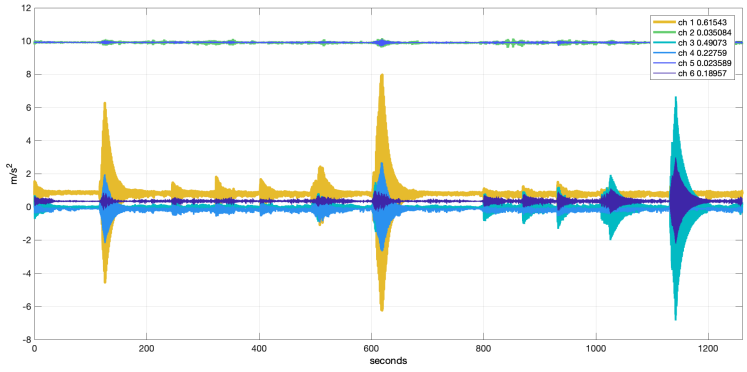

FREQUENCY DOMAIN RESPONSE

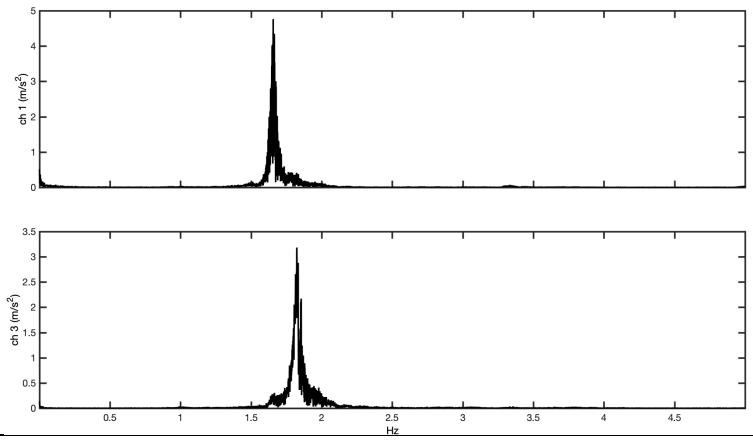

CASE No 4	SITE: Mizens Farm	10/10/2017

MONOPOLE

SITE DETAILS

Structural Type: Monopole

Model: Unknown

Manufacturer: Francis and Lewis

Height: 30 m

Base Width: 1.5 m

SURVEY COMMENTS

Excitation:

Pull & Release method.

Human forces.

Acquisition:

Pair of OPALs^{TM} accelerometers at different locations.

TIME DOMAIN RESPONSE

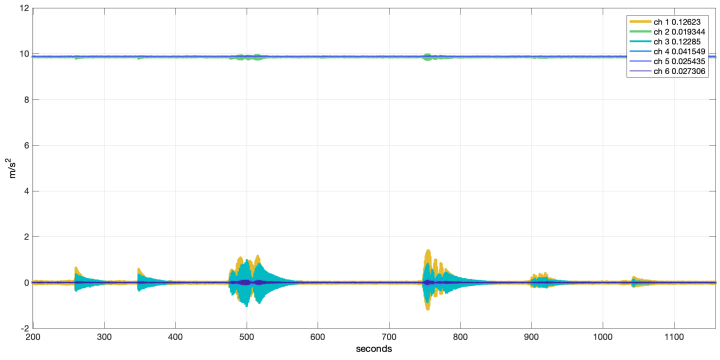

FREQUENCY DOMAIN RESPONSE

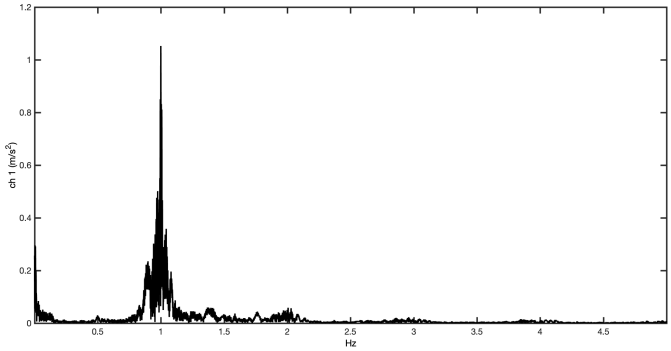

CASE No 5	SITE: Quarry Farm	10/10/2017

MONOPOLE

SITE DETAILS

Structural Type: Monopole

Model: Super Slimline

Manufacturer: Portasilo

Height: 15 m

Base Width: 0.9 m

SURVEY COMMENTS

Excitation:

Pull & Release method.

Human forces.

Acquisition:

Pair of OPALs^{TM} accelerometers at different locations.

TIME DOMAIN RESPONSE

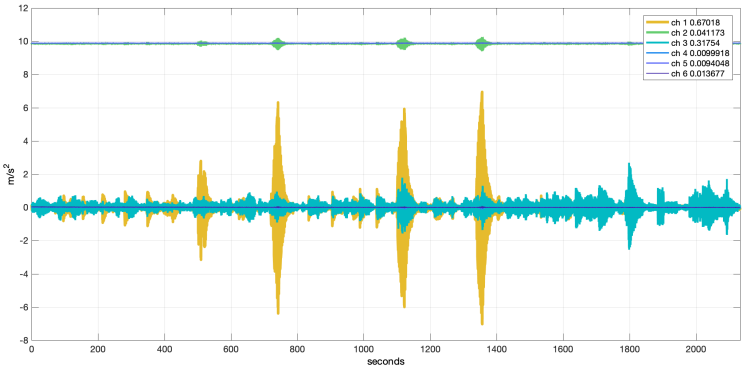

FREQUENCY DOMAIN RESPONSE

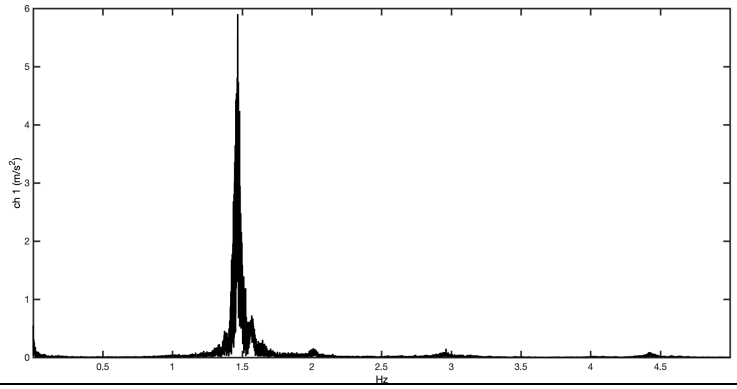

CASE No 6	SITE: East Stratton	01/12/2017

MONOPOLE

SITE DETAILS

Structural Type: Monopole

Model: Unkwown

Manufacturer: Francis & Lewis

Height: 15.4 m

Base Width: 1 m

SURVEY COMMENTS

Excitation:

Pull & Release method.

Human forces.

Acquisition:

Pair of OPALs^{TM} accelerometers at different locations.

TIME DOMAIN RESPONSE

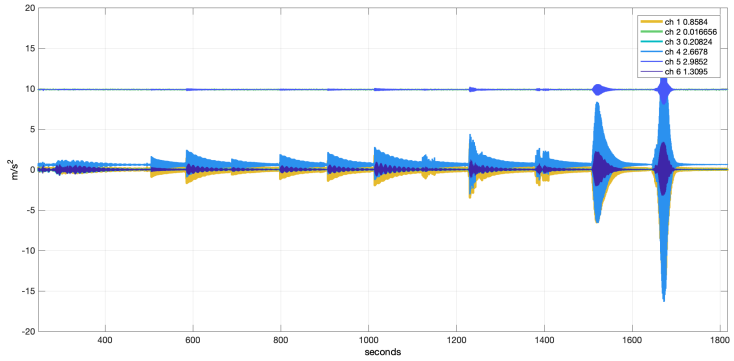

FREQUENCY DOMAIN RESPONSE

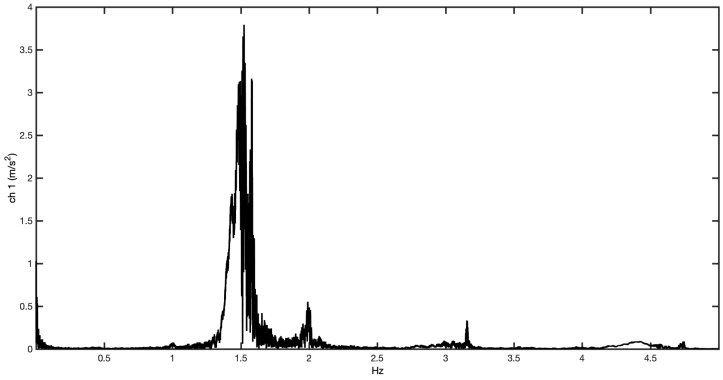

CASE No 7	SITE: Kinning I	13/03/2018

MONOPOLE

SITE DETAILS

Structural Type: Monopole

Model: Super Slimline

Manufacturer: Portasilo

Height: 15 m

Base Width: 0.9 m

SURVEY COMMENTS

Investigation for Students group

Excitation:

Pull & Release method.

Human forces.

Acquisition:

10 OPALs^{TM} accelerometers at different locations.

TIME DOMAIN RESPONSE

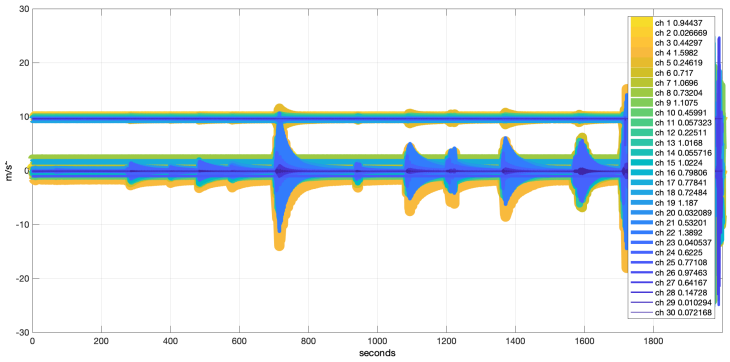

FREQUENCY DOMAIN RESPONSE

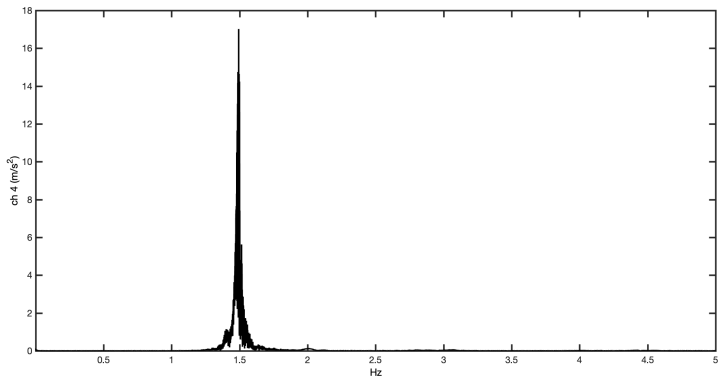

CASE No 8	SITE: Brindle Wood Farm	13/03/2018

MONOPOLE

SITE DETAILS

Structural Type: Monopole

Model: Unknown

Manufacturer: Calzavara

Height: 18 m

Base Width: 1.3 m

SURVEY COMMENTS

Investigation for Students group

Excitation:

Pull & Release method.

Human forces.

Acquisition:

10 OPALs^{TM} accelerometers at different locations.

TIME DOMAIN RESPONSE

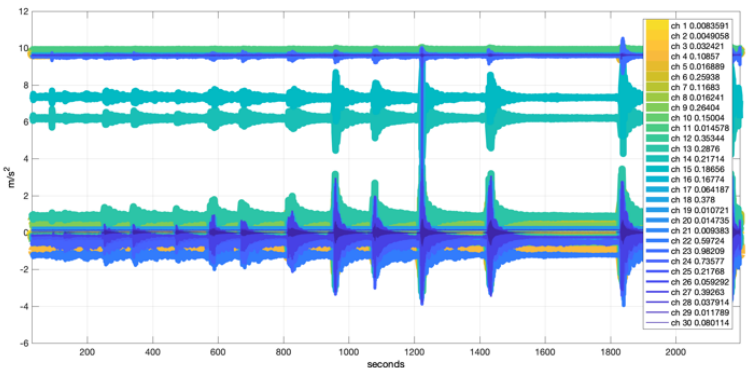

FREQUENCY DOMAIN RESPONSE

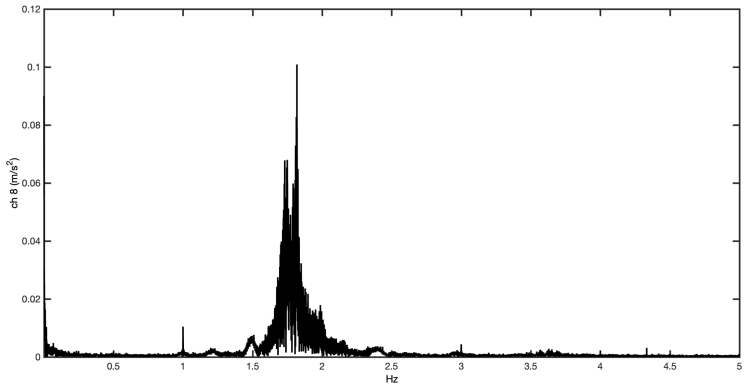

CASE No 9	SITE: Marleys Moor II	03/05/2018

MONOPOLE

SITE DETAILS

Type: Monopole

Model: DM1A

Manufacturer: Francis & Lewis

Height: 15 m

Base Width: 1 m

SURVEY COMMENTS

Foundation survey.

Excitation:

Pull & Release method.

Human forces.

Acquisition:

4 OPALs^{TM} accelerometers at different locations.

TIME DOMAIN RESPONSE

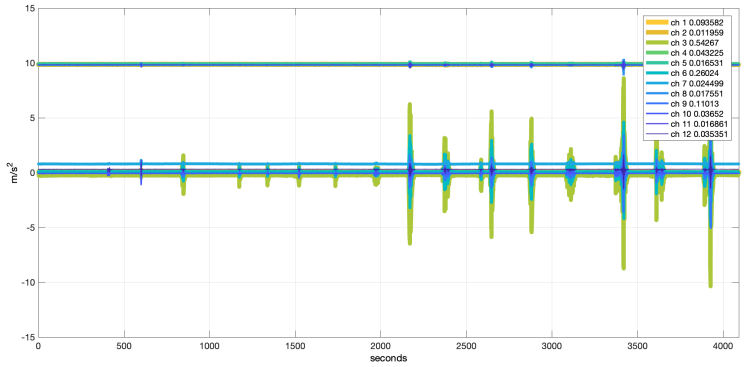

FREQUENCY DOMAIN RESPONSE

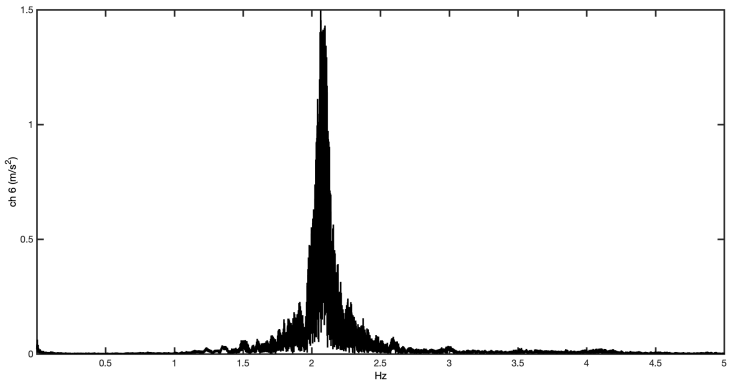

CASE No 10	SITE: St Ives FC	22/11/2018

MONOPOLE

SITE DETAILS

Structural Type: Monopole

Model: Super Slimline

Manufacturer: Portasilo

Height: 15 m

Base Width: 0.9 m

SURVEY COMMENTS

Aerodynamic monitoring installation.

Excitation:

Pull & Release method.

Human forces.

Acquisition:

4 OPALs^{TM} accelerometers at

TIME DOMAIN RESPONSE

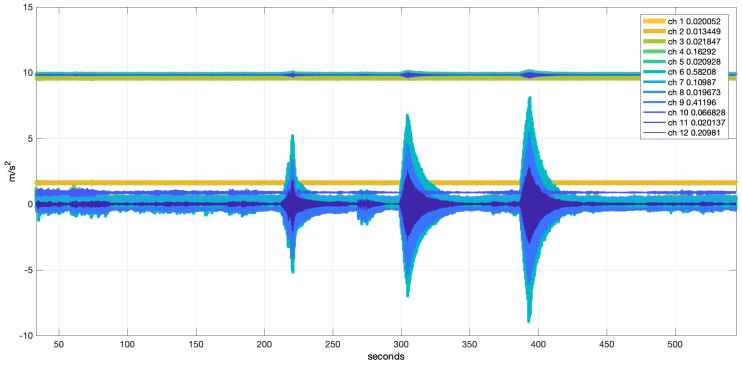

FREQUENCY DOMAIN RESPONSE

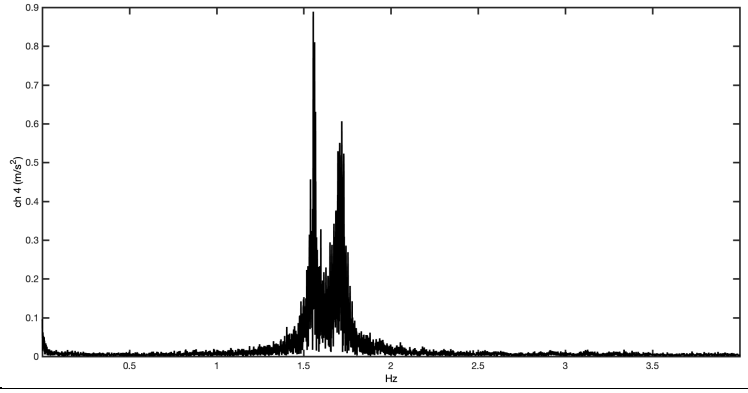

CASE No 11	SITE: Norwich Stubb Office	06/12/2018

MONOPOLE

SITE DETAILS

Structural Type: Monopole

Model: Super Slimline

Manufacturer: Portasilo

Height: 15 m

Base Width: 0.9 m

SURVEY COMMENTS

Foundation survey.

Excitation:

Pull & Release method.

Human forces.

Acquisition:

4 OPALs^{TM} accelerometers at

TIME DOMAIN RESPONSE

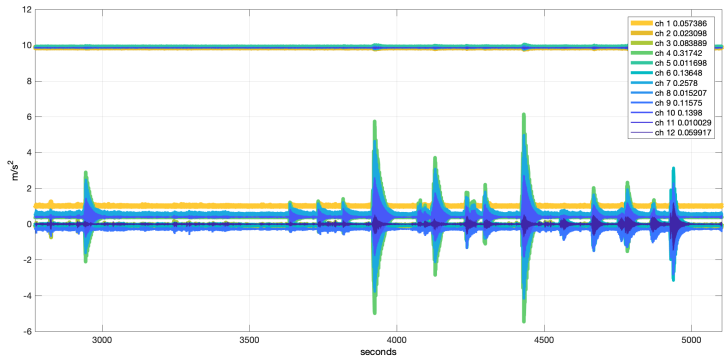

FREQUENCY DOMAIN RESPONSE

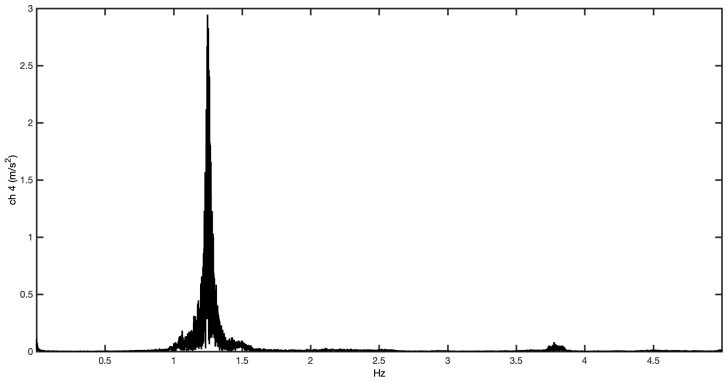

CASE No 12	SITE: Chelmsford Office	06/12/2018

MONOPOLE

SITE DETAILS

Type: Monopole

Model: Unknown

Manufacturer: Swann Ltd

Height: 22.5 m

Base Width: 1 m

SURVEY COMMENTS

Foundation survey.

Excitation:

Pull & Release method.

Human forces.

Acquisition:

4 OPALs^{TM} accelerometers at

TIME DOMAIN RESPONSE

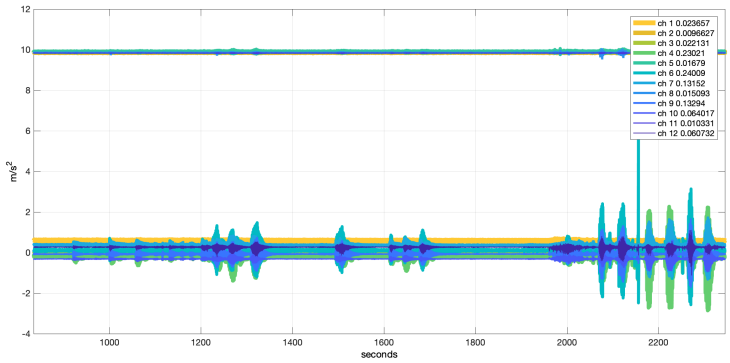

FREQUENCY DOMAIN RESPONSE

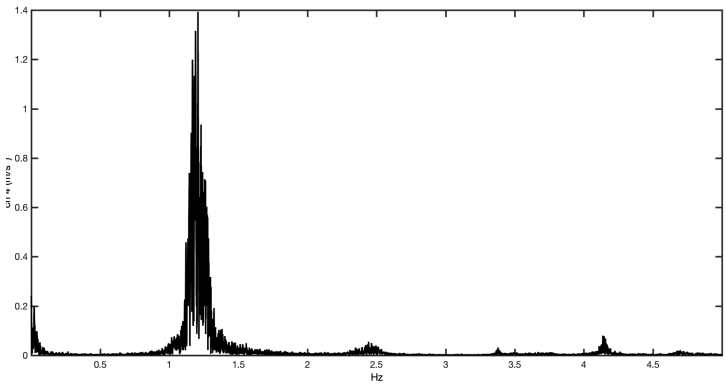

CASE No 13	SITE: Windmill Farm	09/05/2019

MONOPOLE

SITE DETAILS

Structural Type: Monopole

Model: Unknown

Manufacturer: Calzavara

Height: 18 m

Base Width: 1.3 m

SURVEY COMMENTS

Aerodynamic Installation

Excitation:

Pull & Release method.

Human forces.

Acquisition:

4 OPALs^{TM} accelerometers at different locations.

TIME DOMAIN RESPONSE

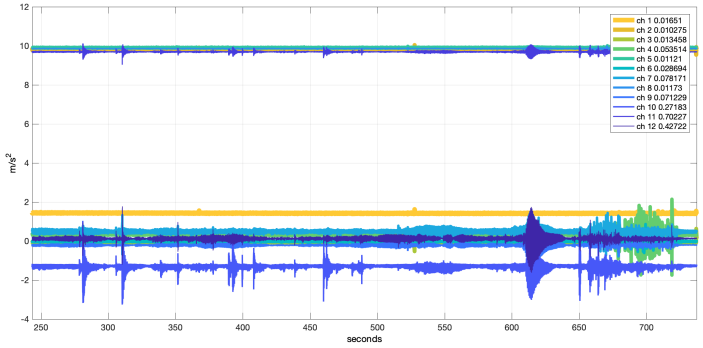

FREQUENCY DOMAIN RESPONSE

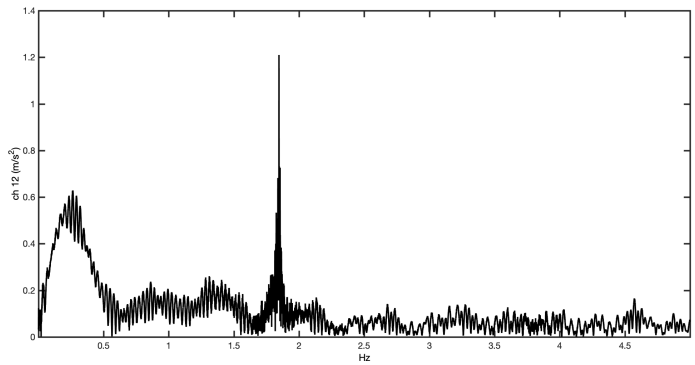

CASE No 14	SITE: Kinning II	27/06/2019

MONOPOLE

SITE DETAILS

Structural Type: Monopole

Model: Super Slimline

Manufacturer: Portasilo

Height: 15 m

Base Width: 0.9 m

SURVEY COMMENTS

Survey to verify backbone integration with cameras.

Excitation:

Pull & Release method.

Human forces.

Acquisition:

4 OPALs^{TM} accelerometers at different locations.

TIME DOMAIN RESPONSE

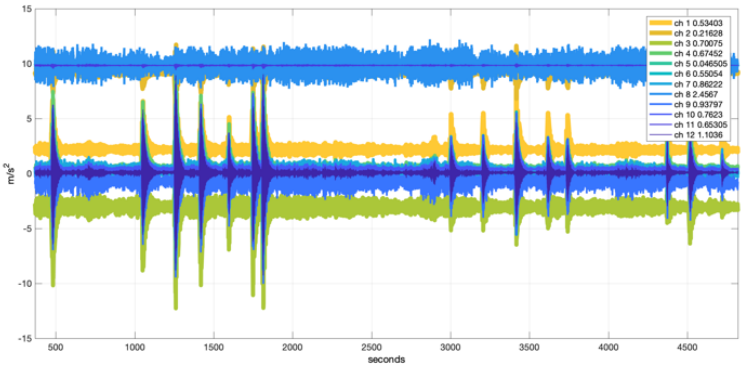

FREQUENCY DOMAIN RESPONSE

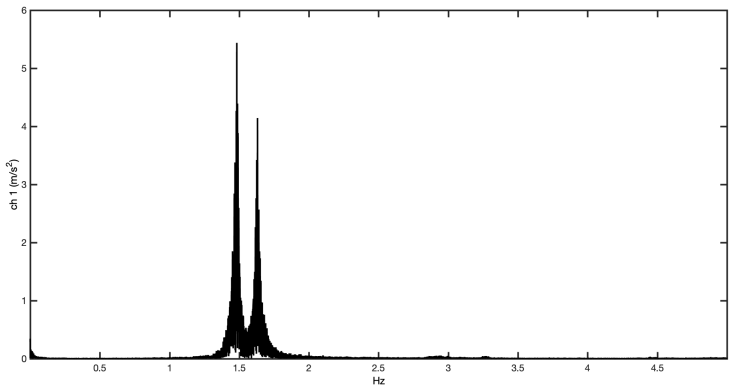

CASE No 15	SITE: Manor Farm	30/10/2018

SHORT LATTICE TOWER

SITE DETAILS

Type: Lattice Tower

Model: EDC

Manufacturer: Euromast

Height: 22.5 m

Base Width: 1.1 m

SURVEY COMMENTS

Excitation:

Pull & Release method.

Human forces.

Acquisition:

4 OPALs^{TM} accelerometers

TIME DOMAIN RESPONSE

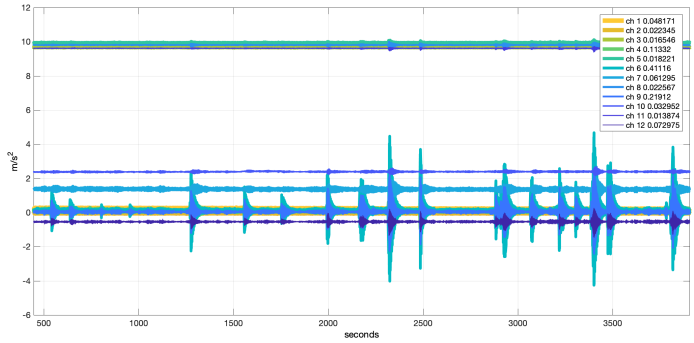

FREQUENCY DOMAIN RESPONSE

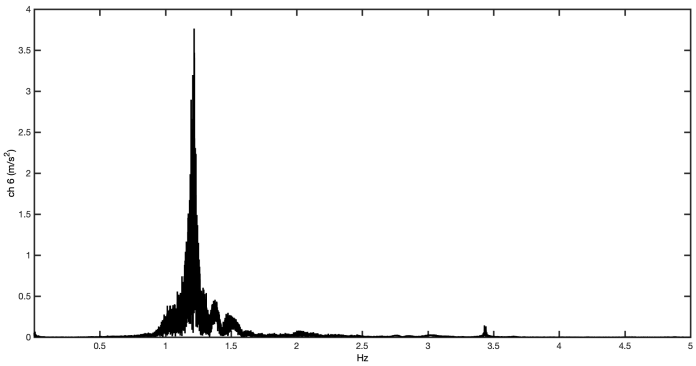

CASE No 16	SITE: Kandy Homestead	30/10/2018

SHORT LATTICE TOWER

SITE DETAILS

Type: Lattice Tower

Model: EDC (Strengthening-leg platting)

Manufacturer: Euromast

Height: 22.5 m

Base Width: 1.1 m

SURVEY COMMENTS

Excitation:

Pull & Release method.

Human forces.

Acquisition:

4 OPALs^{TM} accelerometers

TIME DOMAIN RESPONSE

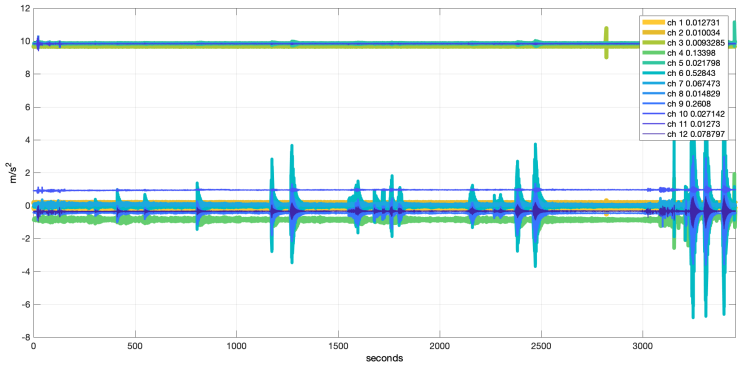

FREQUENCY DOMAIN RESPONSE

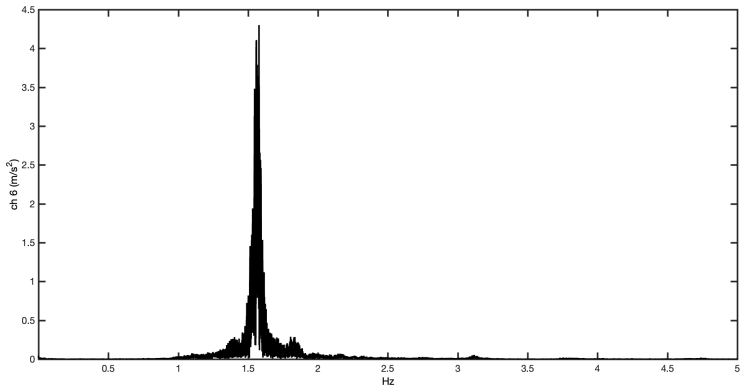

CASE No 17	SITE: Church Farm	18/05/2018

SHORT LATTICE TOWER

SITE DETAILS

Type: Lattice tower

Model: ED

Manufacturer: Euromast

Height: 15 m

Base Width: 1.1 m

SURVEY COMMENTS

Excitation:

Pull & Release method.

Human forces.

Acquisition:

4 OPALs^{TM} accelerometers

TIME DOMAIN RESPONSE

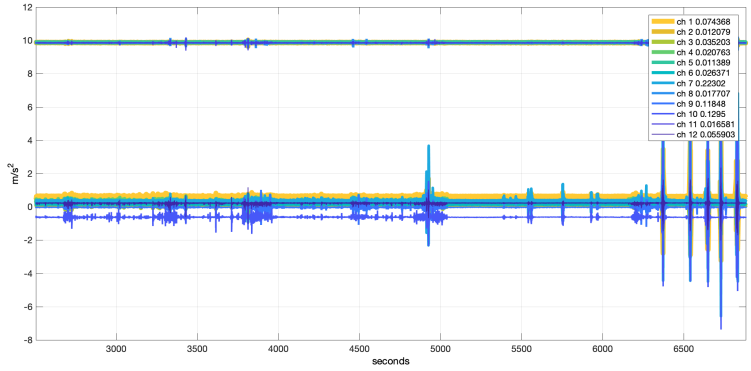

FREQUENCY DOMAIN RESPONSE

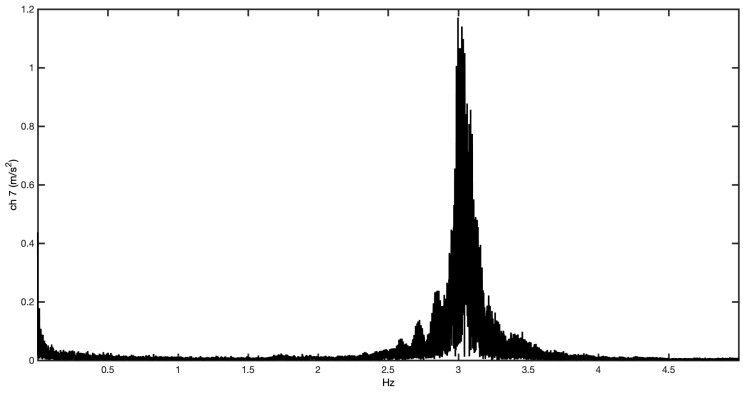

CASE No 18	SITE: Bath	26/07/2018

LATTICE TOWER

SITE DETAILS

Type: Lattice tower

Model: 150

Manufacturer: Cornubian

Height: 45 m

Base Width: 6 m

SURVEY COMMENTS

Excitation:

Human forces. Using climber excitation

Acquisition:

4 OPALs^{TM} accelerometers

TIME DOMAIN RESPONSE

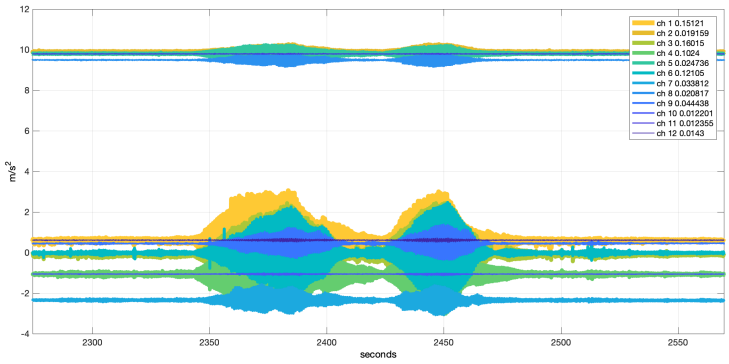

FREQUENCY DOMAIN RESPONSE

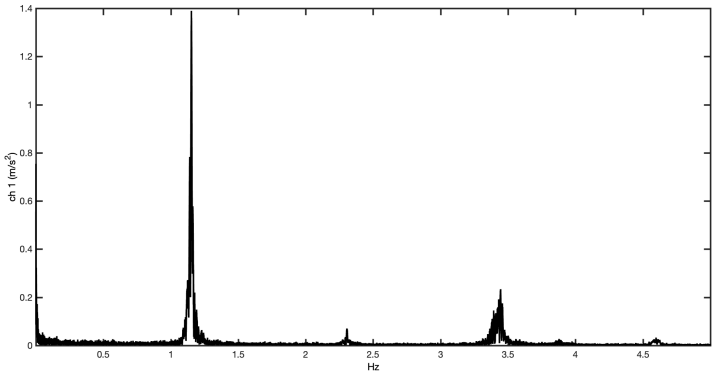

CASE No 19	SITE: Cambret Hill	17/10/2017

LATTICE TOWER

SITE DETAILS

Type: Lattice tower

Model: SSPT

Manufacturer: Alan Dick

Height: 45 m

Base Width: 5 m

SURVEY COMMENTS

Excitation:

Human forces. Using climber excitation

Acquisition:

4 OPALs^{TM} accelerometers

TIME DOMAIN RESPONSE

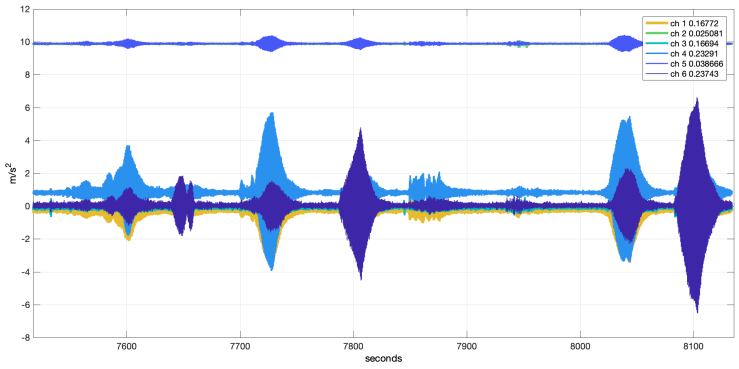

FREQUENCY DOMAIN RESPONSE

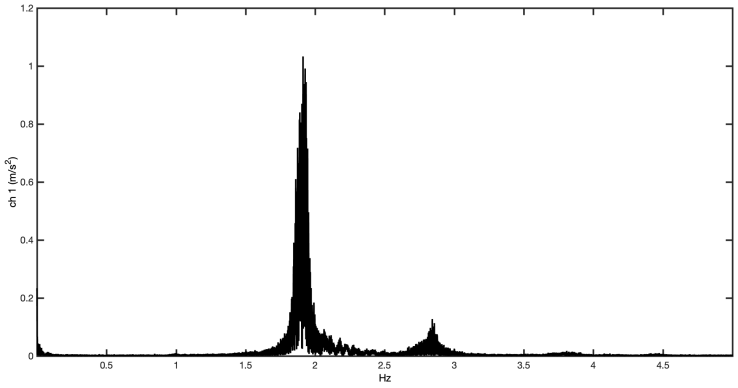

CASE No 20	SITE: Reigate	04/05/2018

LATTICE TOWER

SITE DETAILS

Type: Lattice tower

Model: 500

Manufacturer: Balfour Beatty

Height: 60 m

Base Width: 7.4 m

SURVEY COMMENTS

Excitation:

Human forces. Using climber excitation

Acquisition:

4 OPALs^{TM} accelerometers

TIME DOMAIN RESPONSE

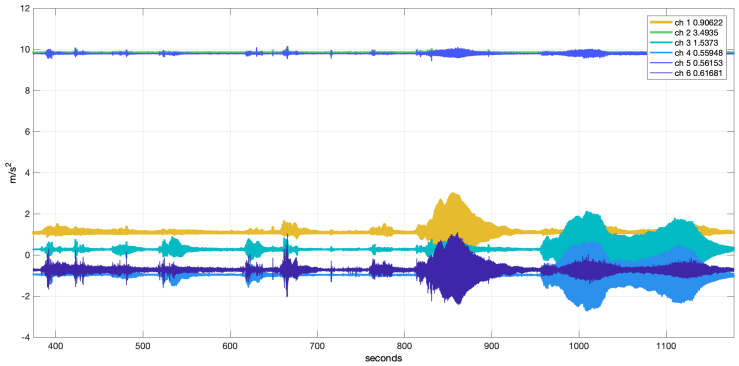

FREQUENCY DOMAIN RESPONSE

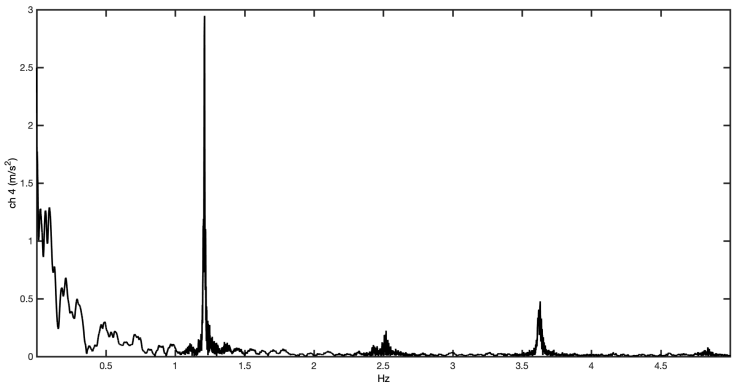

CASE No 21	SITE: Plympton	17/09/2019

LATTICE TOWER

SITE DETAILS

Type: Lattice Tower

Model: C1556

Manufacturer: Eve

Height: 45.7 m

Base Width: 6 m

SURVEY COMMENTS

Excitation:

Human forces. Using climber excitation

Acquisition:

4 OPALs^{TM} accelerometers

TIME DOMAIN RESPONSE

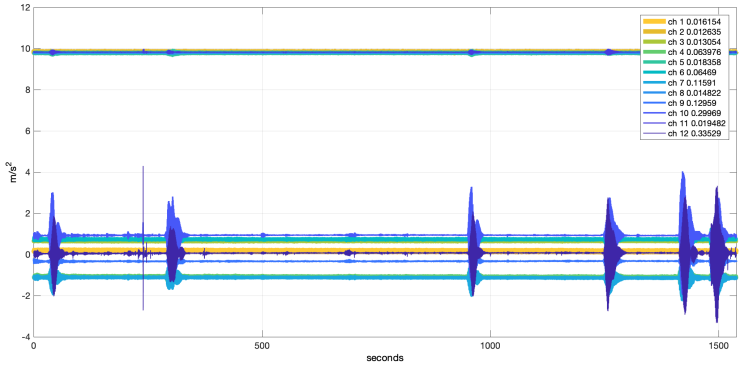

FREQUENCY DOMAIN RESPONSE

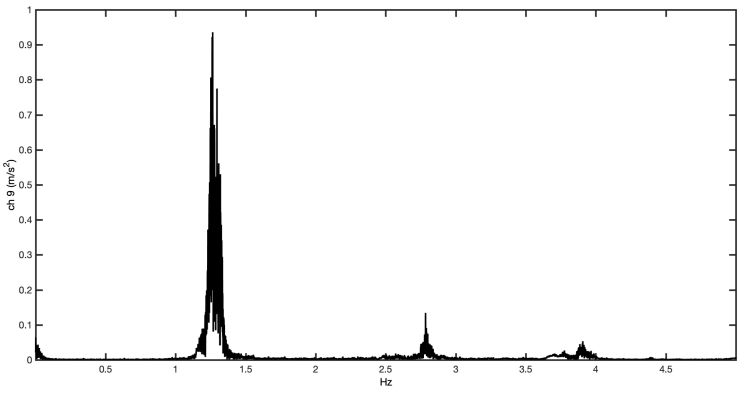

APPENDIX B: Structural Health Monitoring in St Ives FC

B.1 Time Line Response Obtained During SHM in St Ives FC

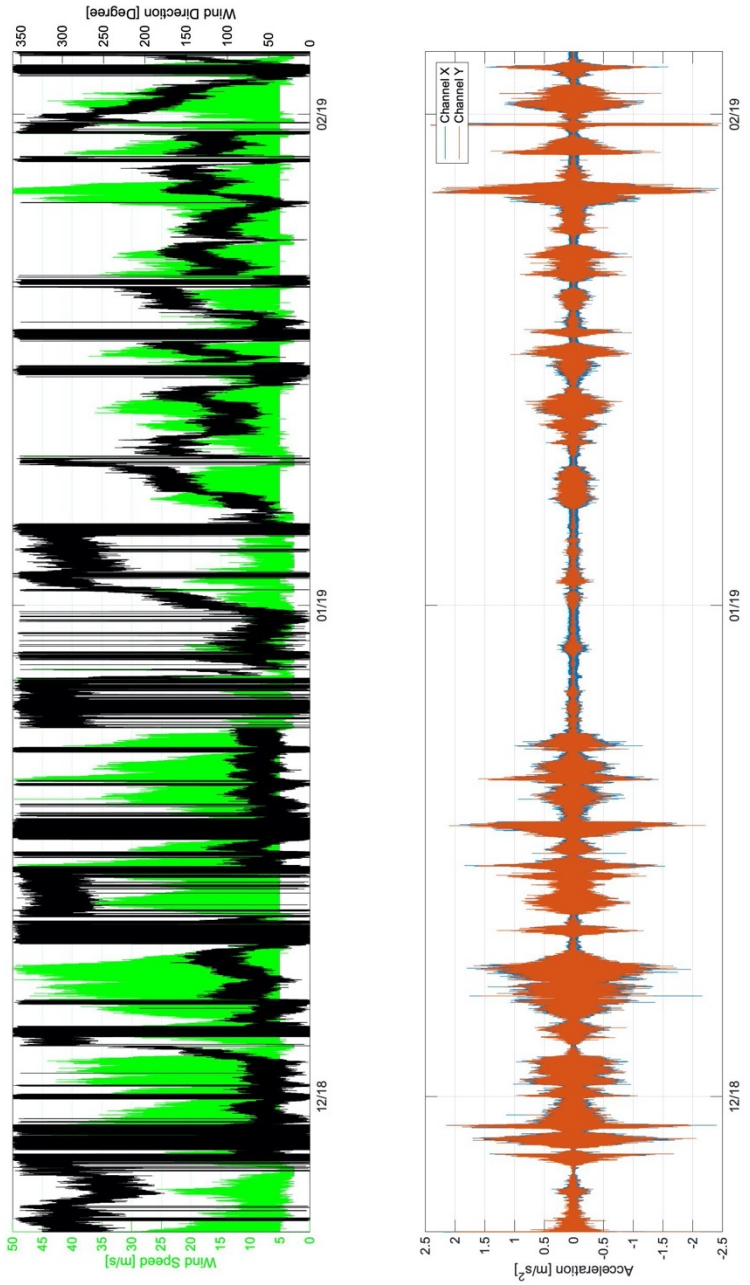

Figure B-1 Timeline raw data in St Ives FC. Time Line. Upper: Wind data. Downer: Horizontal acceleration channels.

B.2 Wind Study in SHM in St Ives FC.

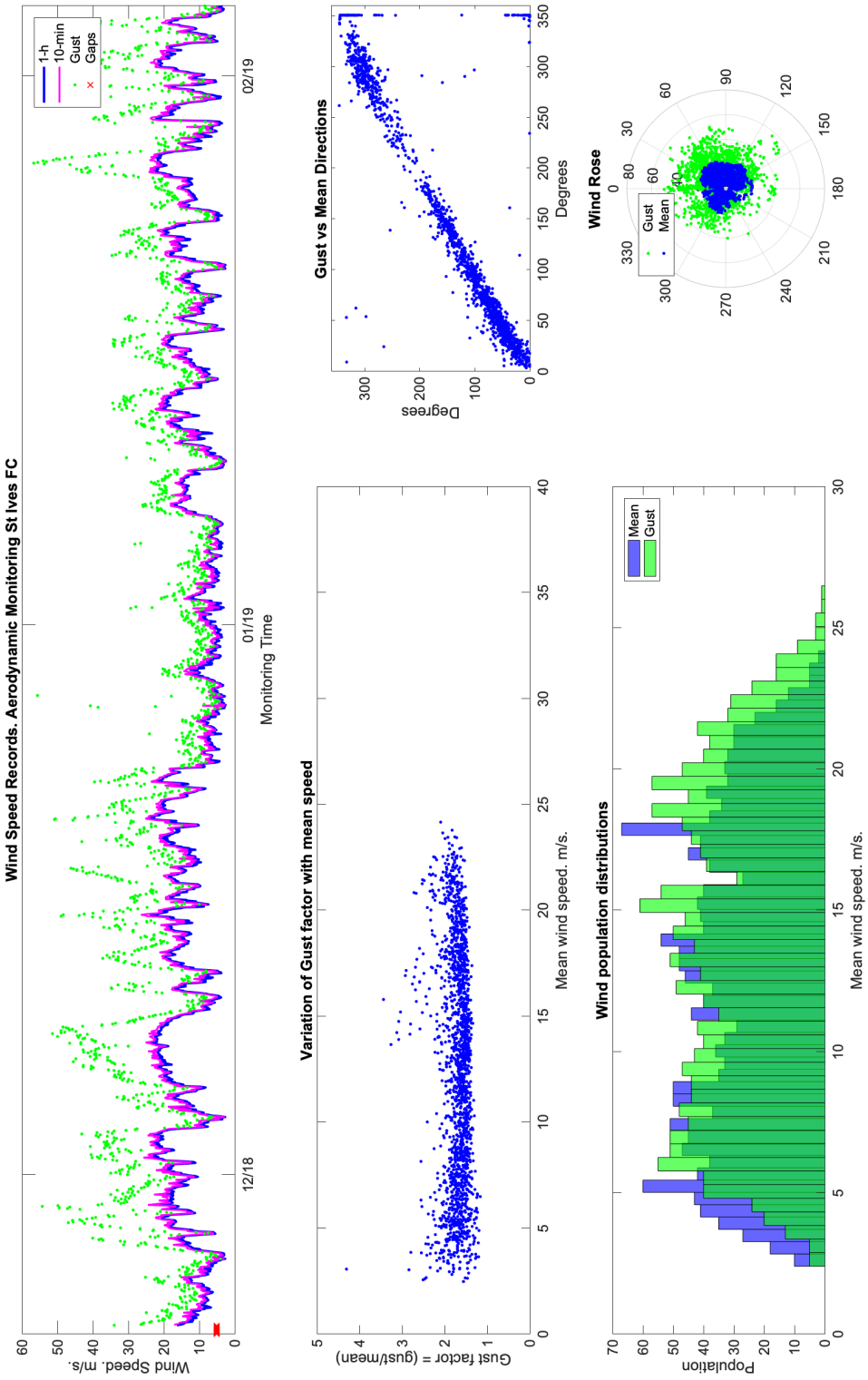

Figure B-2 Wind Study of SHM in St Ives FC.

B.3 Operational Modal Analysis in SHM in St Ives FC. Total and Monthly

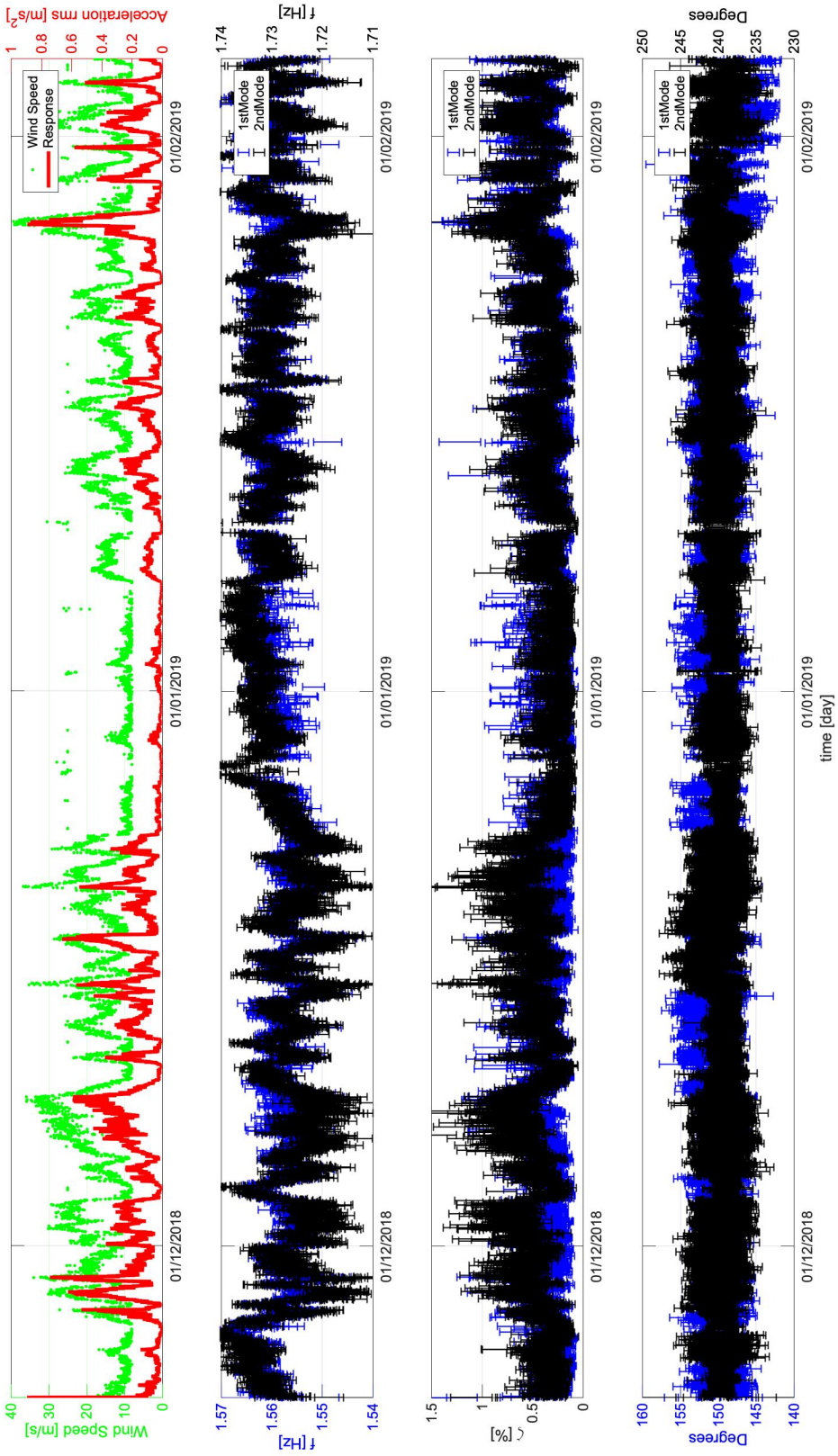

Figure B-3 Operational Modal Analysis BAYOMA applied to St Ives FC. Total.

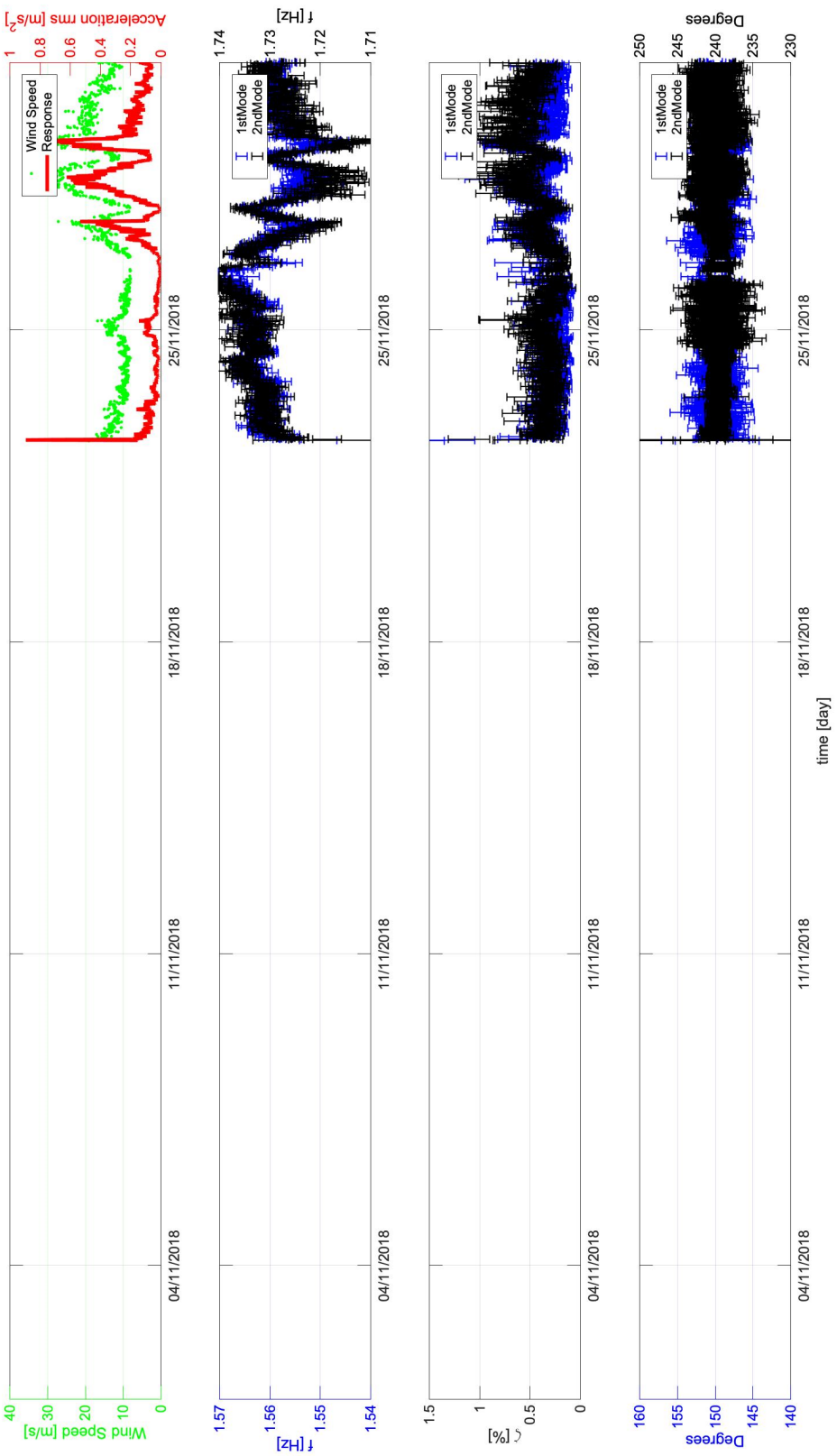

Figure B-4 Operational Modal Analysis BAYOMA applied to St Ives FC. November 2018.

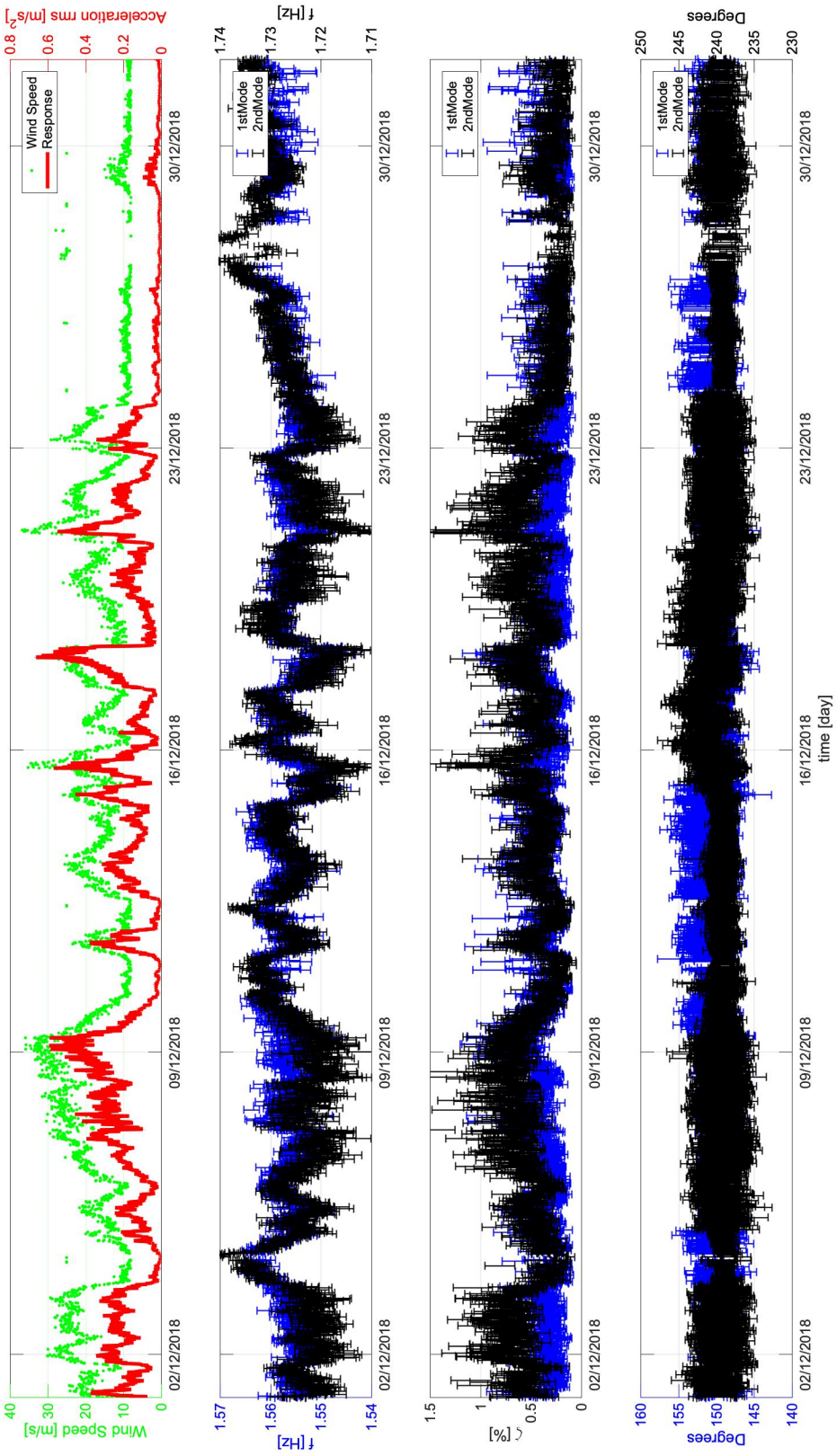

Figure B-5 Operational Modal Analysis BAYOMA applied to St Ives FC. December 2018.

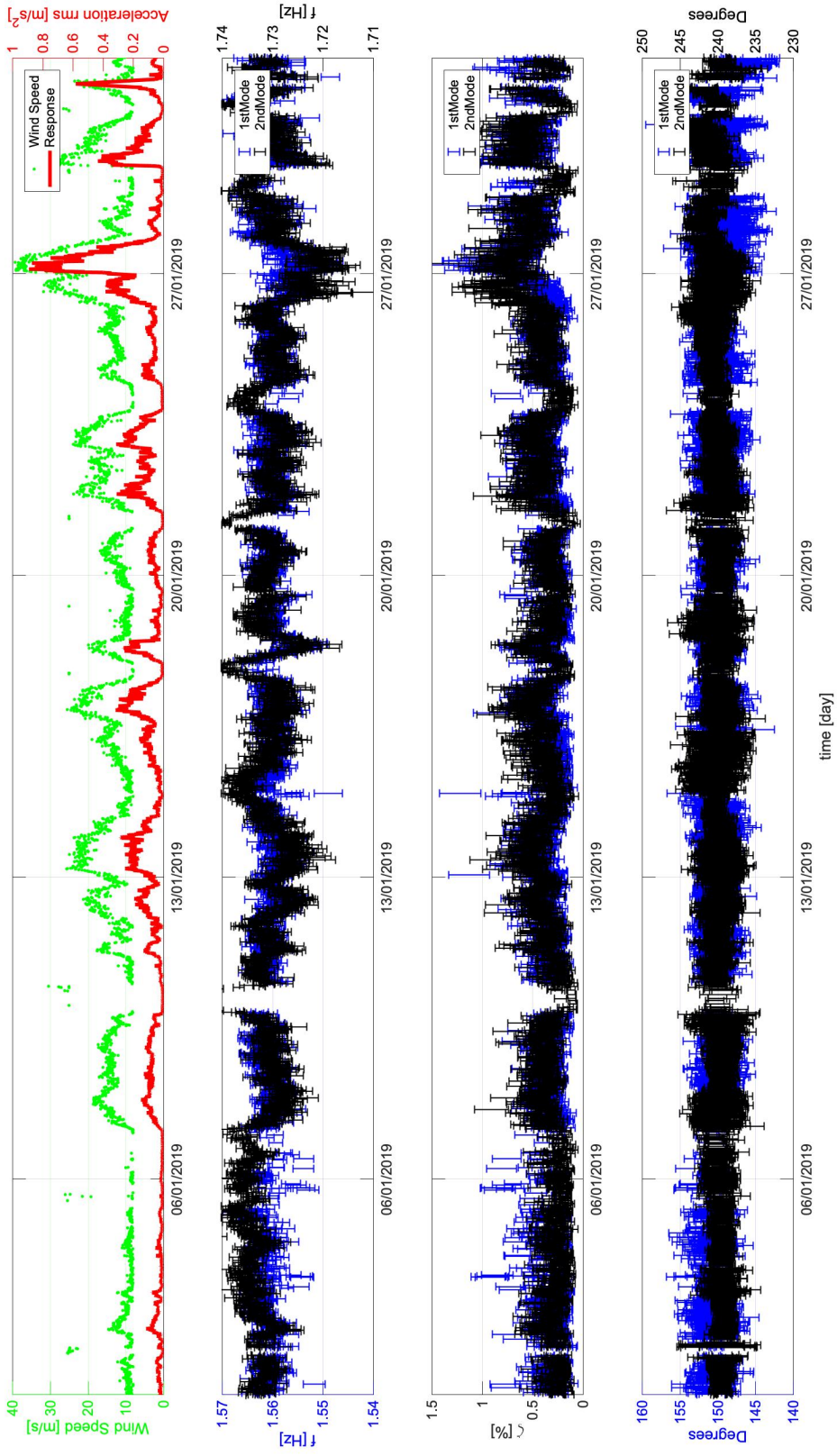

Figure B-6 Operational Modal Analysis BAYOMA applied to St Ives FC. January 2019.

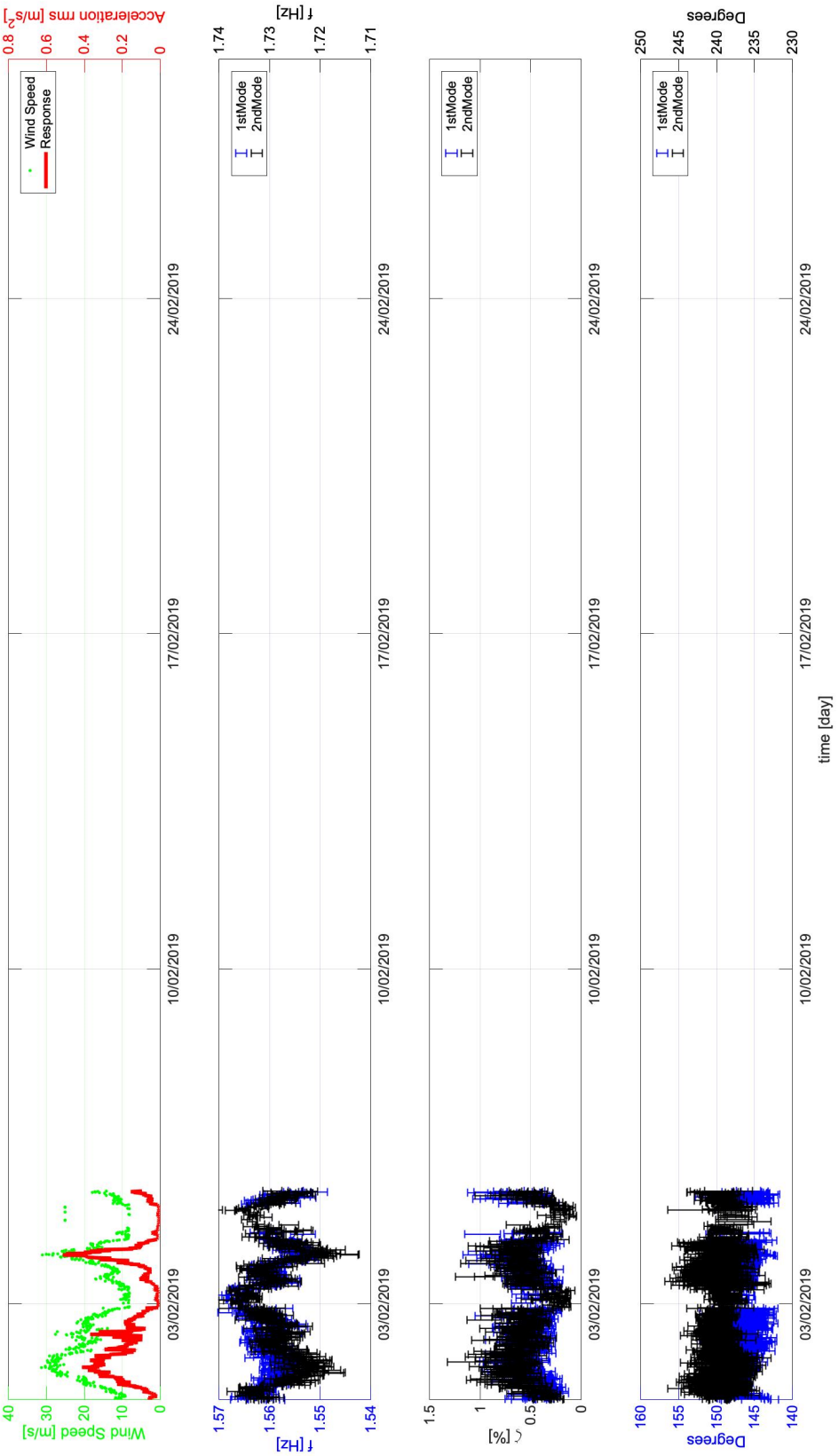

Figure B-7 Operational Modal Analysis BAYOMA applied to St Ives FC. February 2019.

APPENDIX C: Structural Health Monitoring in Windmill Farm

C.1 Time Line Response Obtained during SHM in Windmill Farm

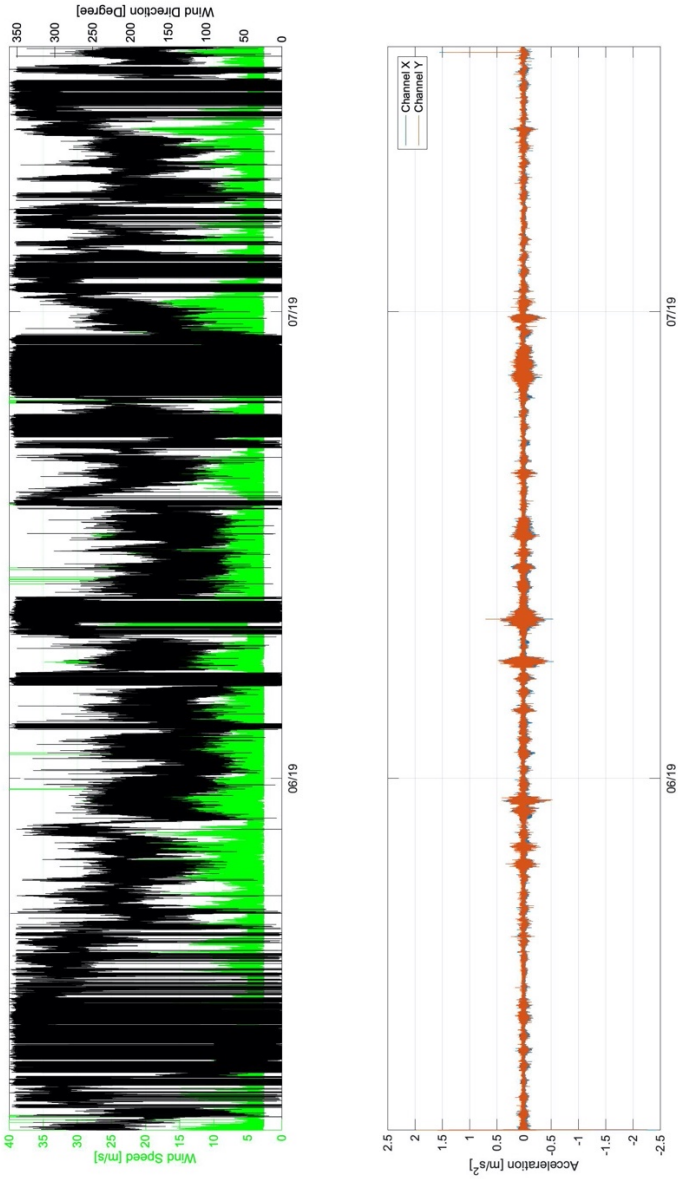

Figure C-1 Timeline raw data in Windmill Farm. Time Line. Upper: Wind data. Downer: Horizontal acceleration channels.

C.2 Wind Study in SHM in Windmill Farm

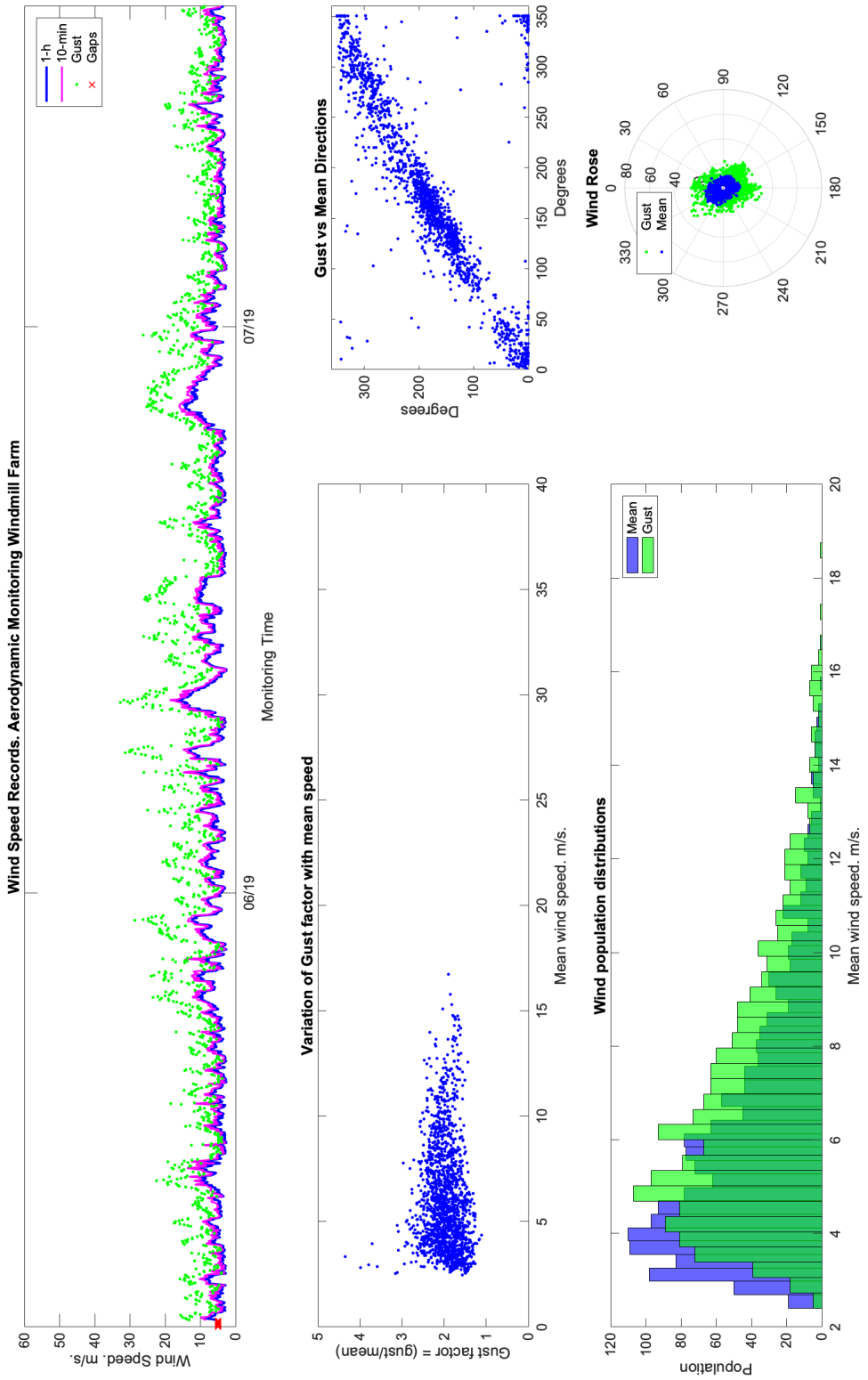

Figure C-2 Wind Study of SHM in St Ives FC.

C.3 Operational Modal Analysis in SHM in Windmill F. Total and Monthly

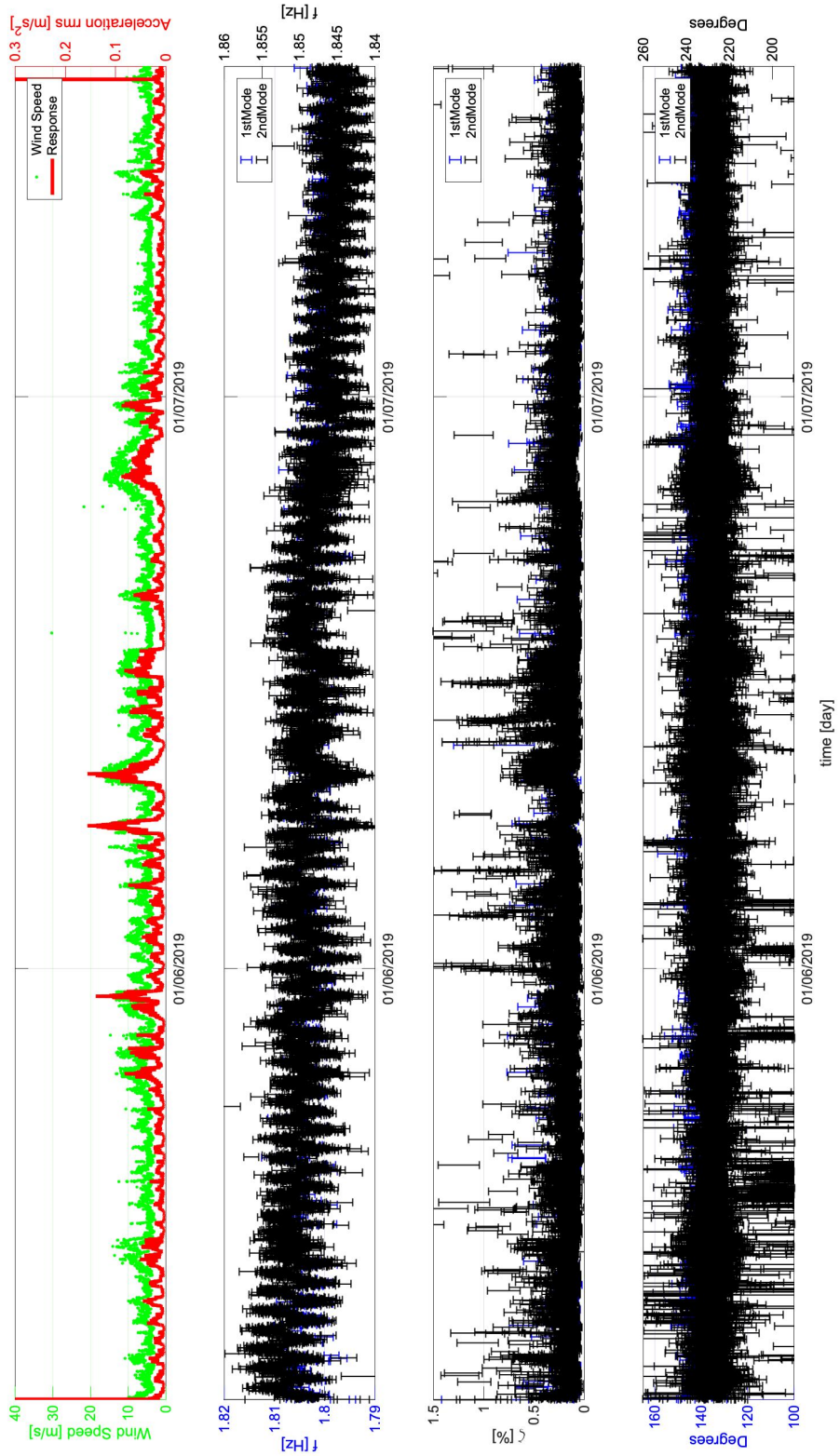

Figure C-3 Operational Modal Analysis BAYOMA applied to Windmill Hill. Total.

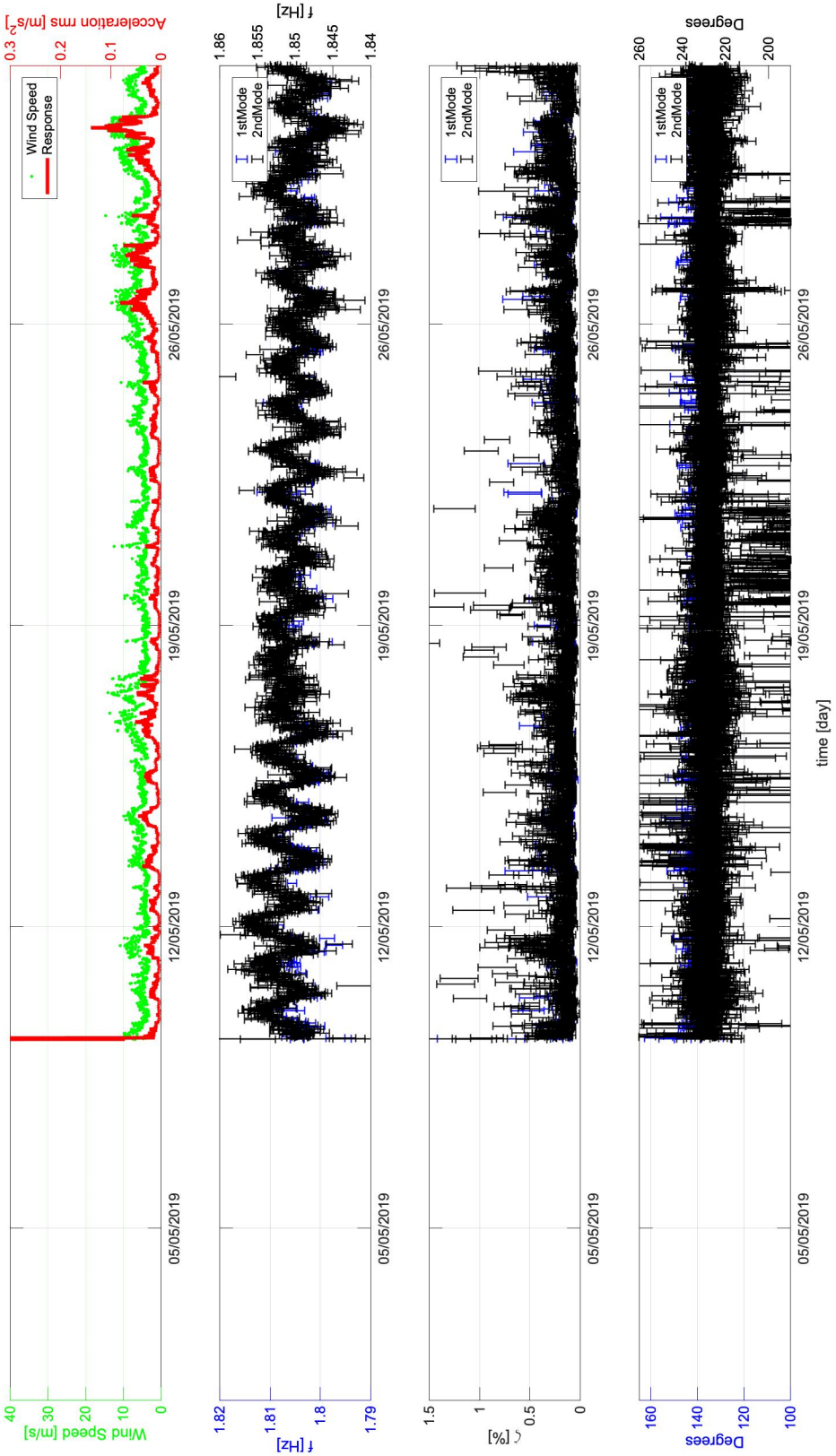

Figure C-4 Operational Modal Analysis BAYOMA applied to Windmill Hill. May 2019.

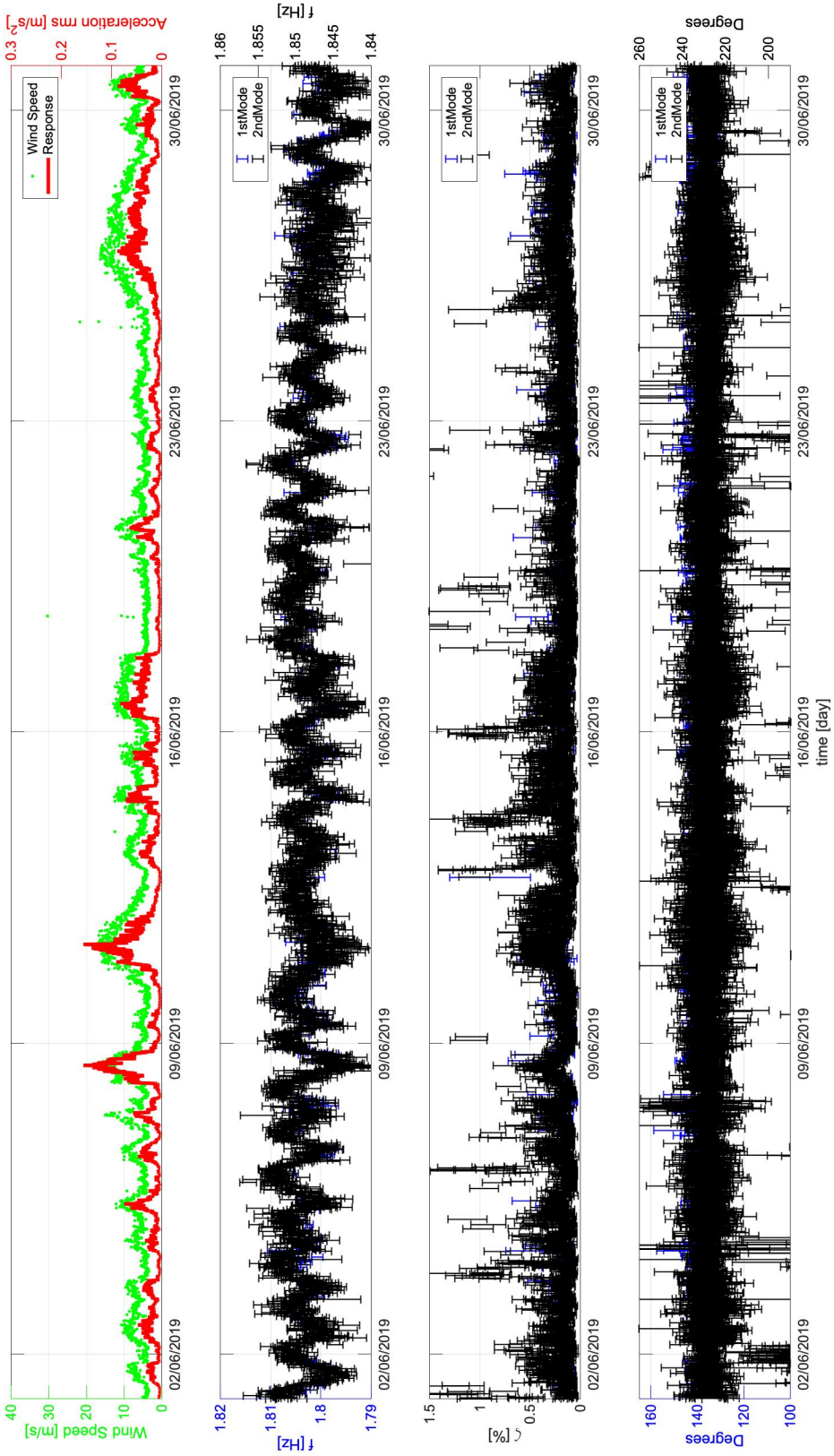

Figure C-5 Operational Modal Analysis BAYOMA applied to Windmill Hill. June 2019.

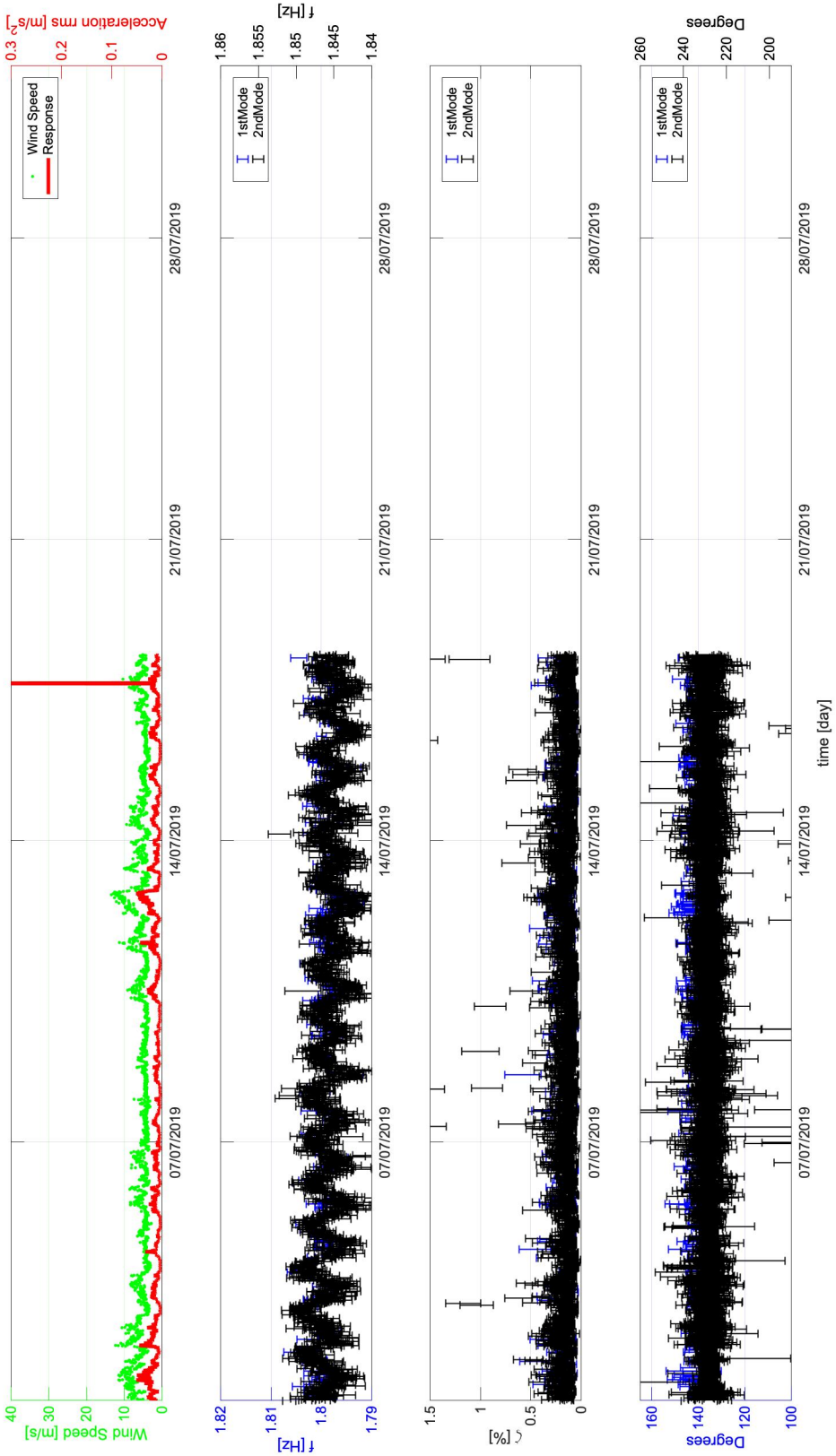

Figure C-6 Operational Modal Analysis BAYOMA applied to Windmill Hill. July 2019.

APPENDIX D: Structural Health Monitoring in Moel-y-Parc HGM

D.1 Time Line Response and Operational Modal Analysis Obtained during Temporary Monitoring in Moel-y-Parc.

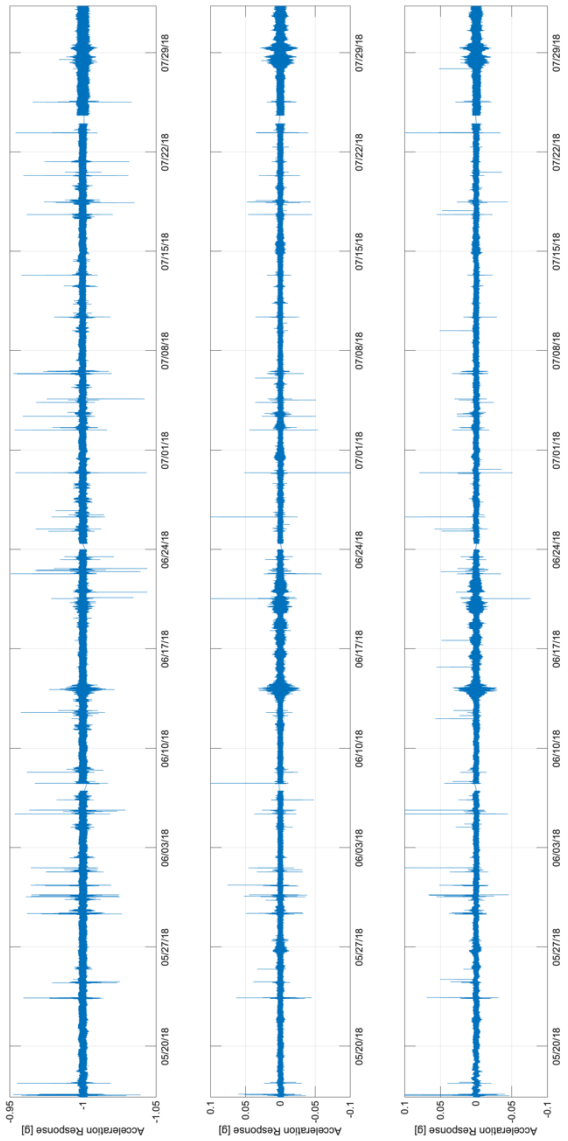

Figure D-1 Operational Modal Analysis applied to Temporary Monitoring in Moel-y-Parc. Time Line. Upper: Vertical channel. Centre and downer: Horizontal channels.

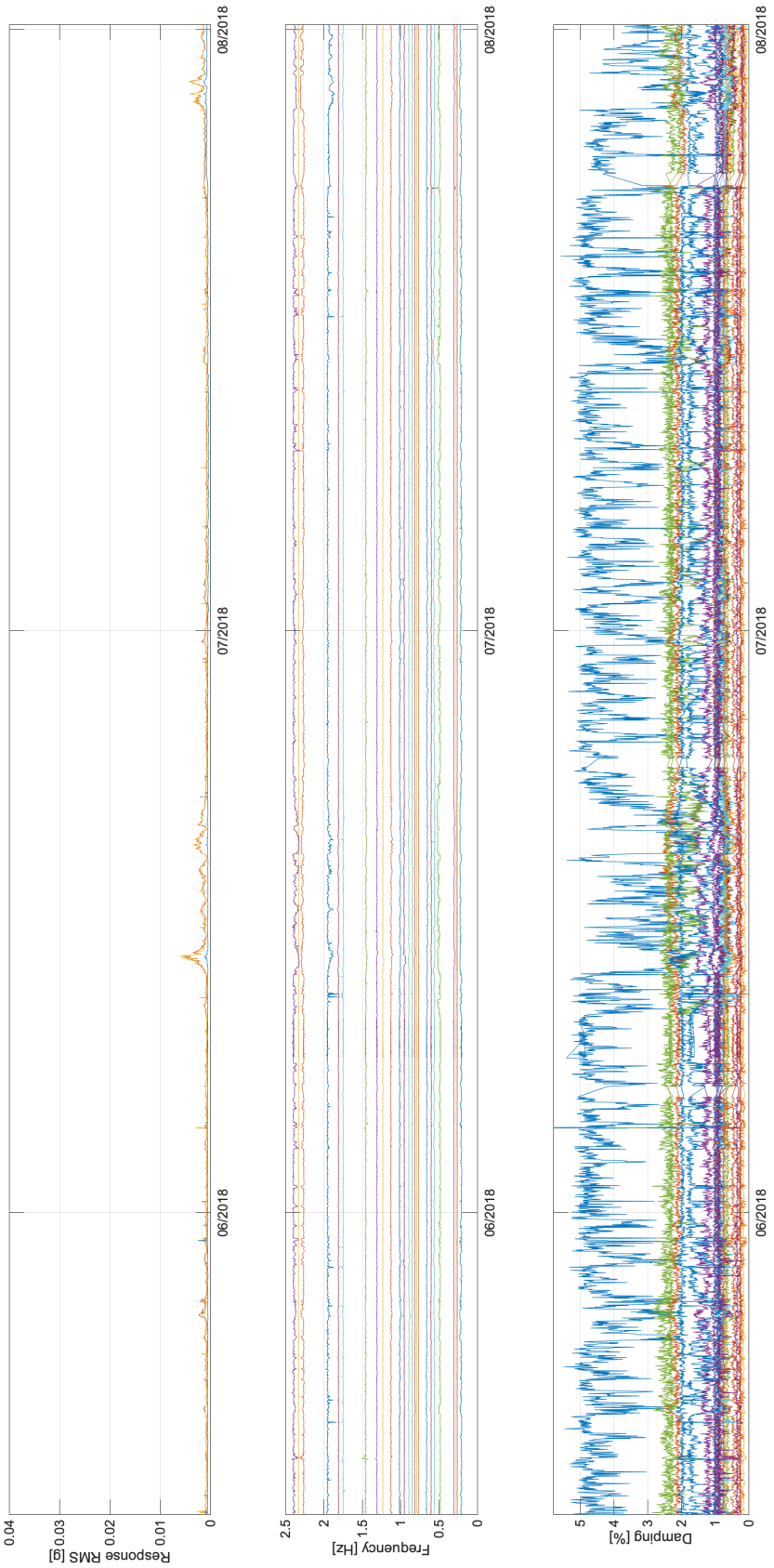

Figure D-2 Operational Modal Analysis applied to Temporary Monitoring in Moel-y-Parc. OMA Results. (Top to bottom) Response, frequency and damping.

D.2 Wind Loading, Response and Operational Modal Analysis in SHM in Moel-y-Parc. Total and Monthly Responses.

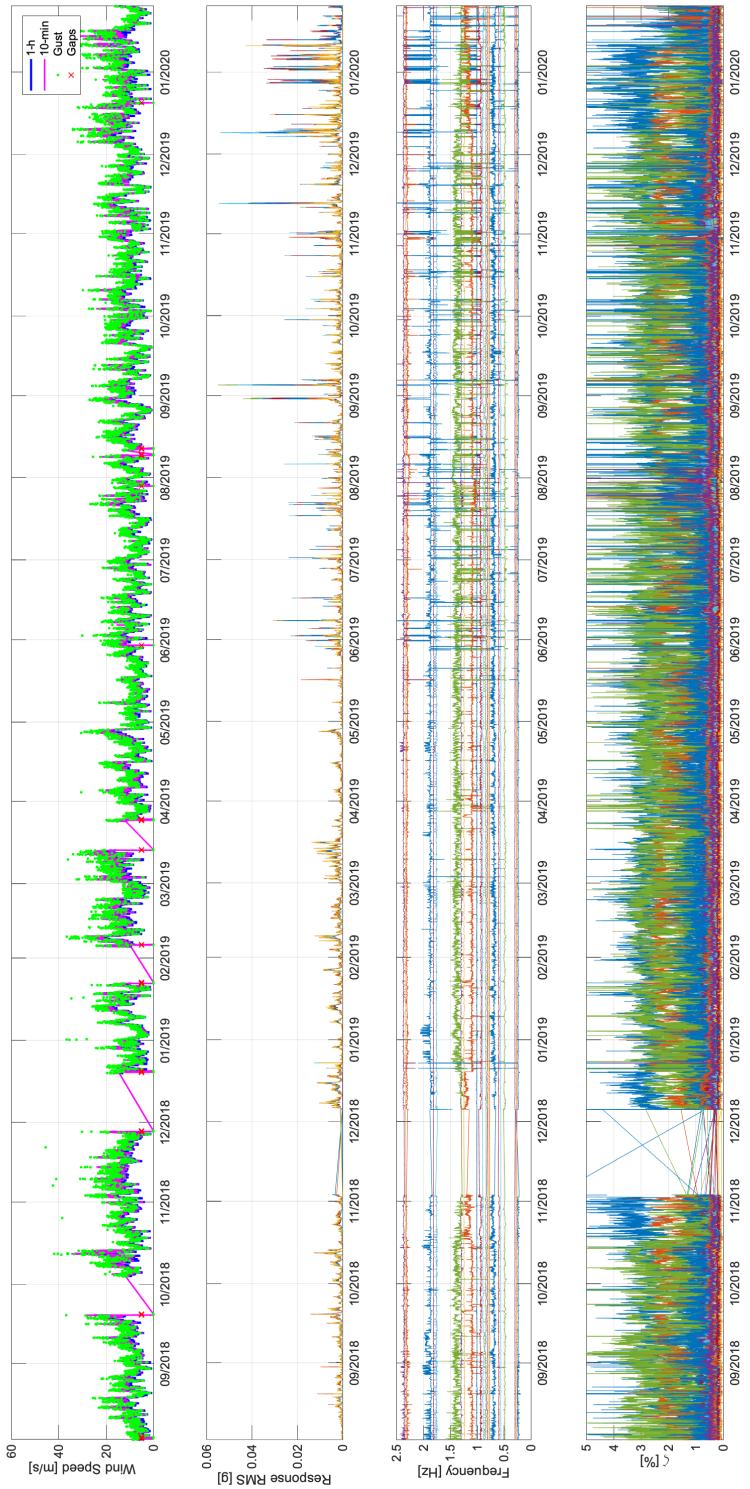

Figure D-3 Operational Modal Analysis SSI applied to Moel-y-Parc.

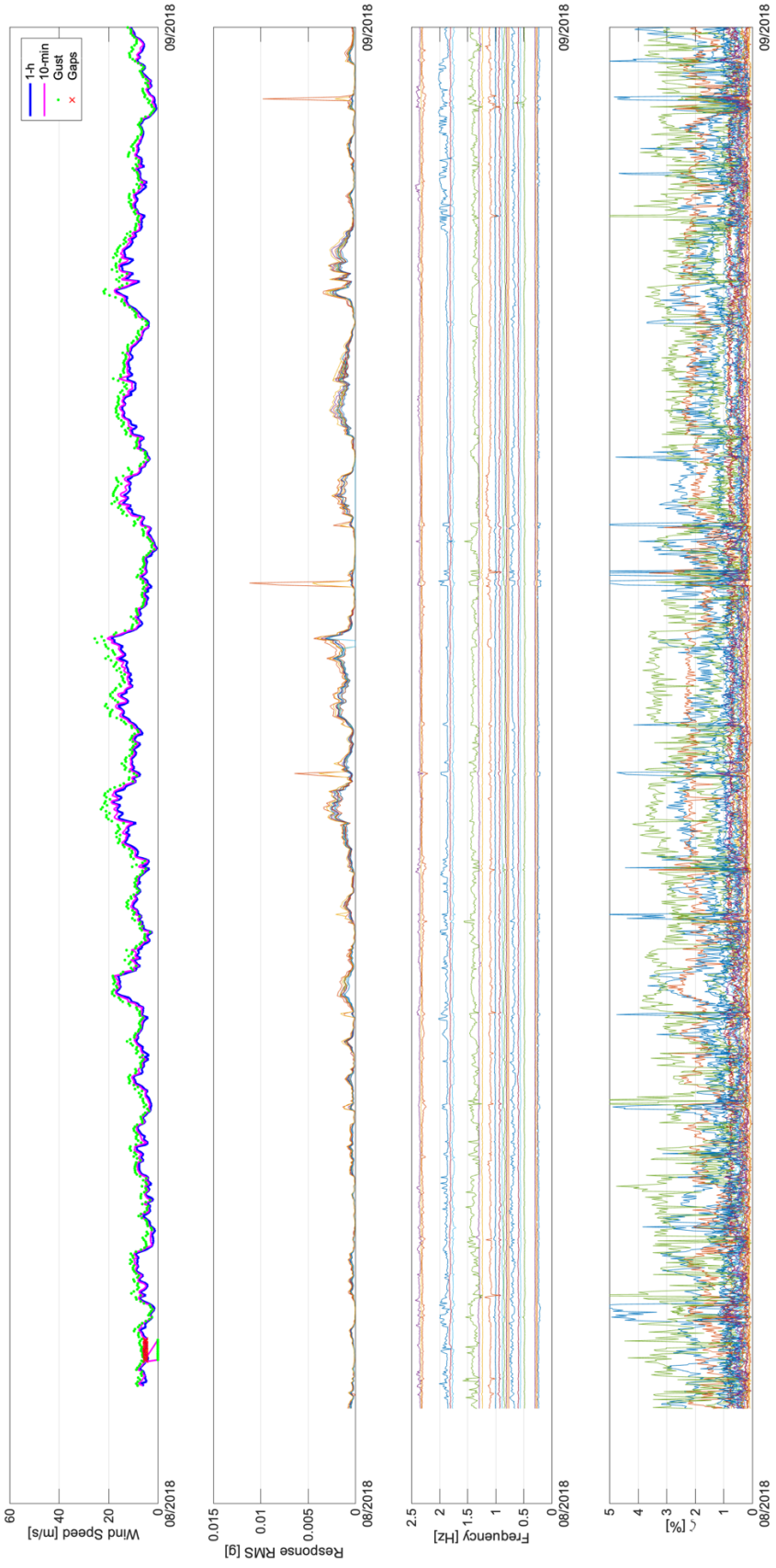

Figure D-4 Operational Modal Analysis SSI applied to Moel-y-Parc. August 2018.

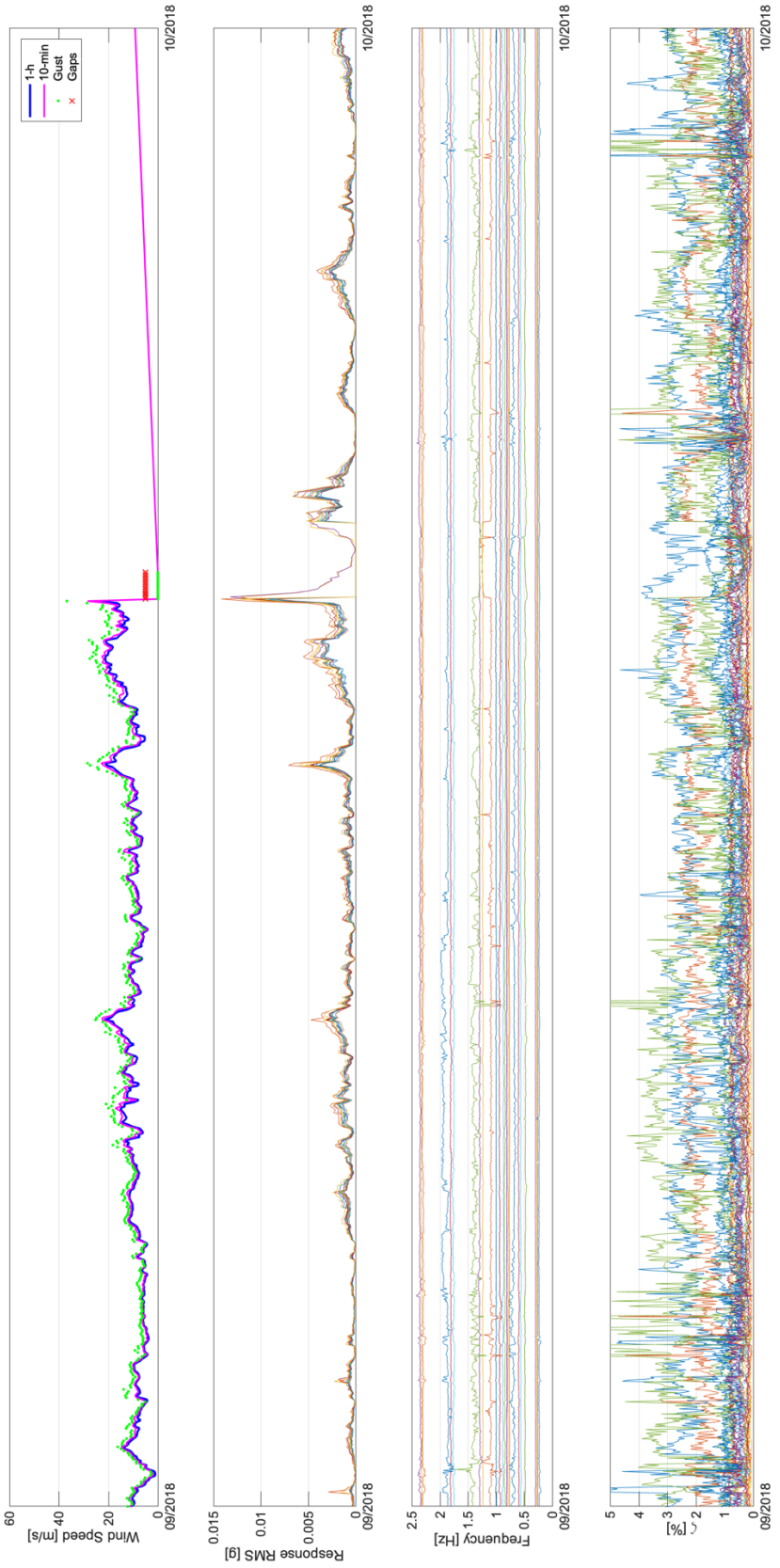

Figure D-5 Operational Modal Analysis SSI applied to Moel-y-Parc. September 2018.

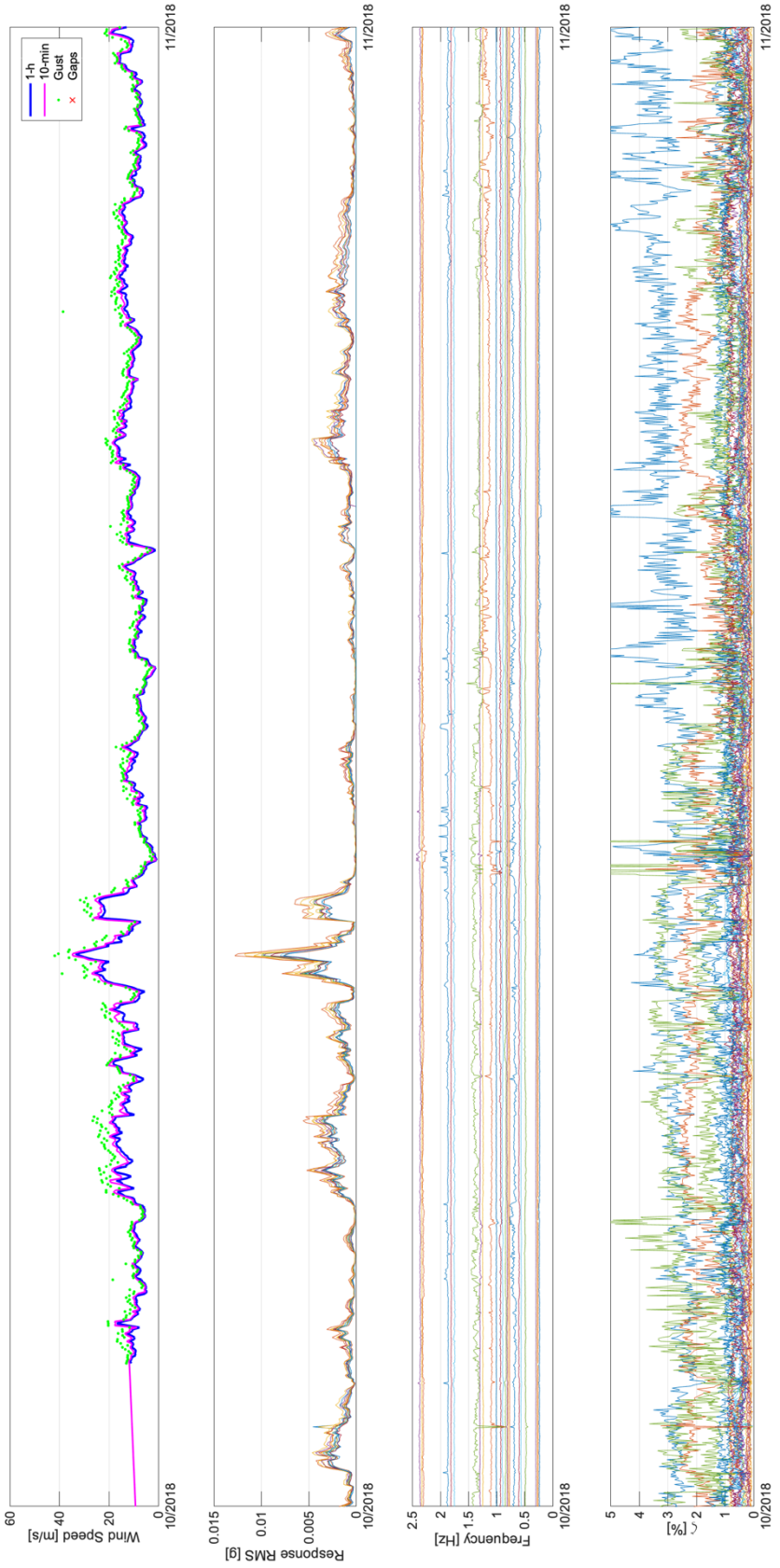

Figure D-6 Operational Modal Analysis SSI applied to Moel-y-Parc. October 2018.

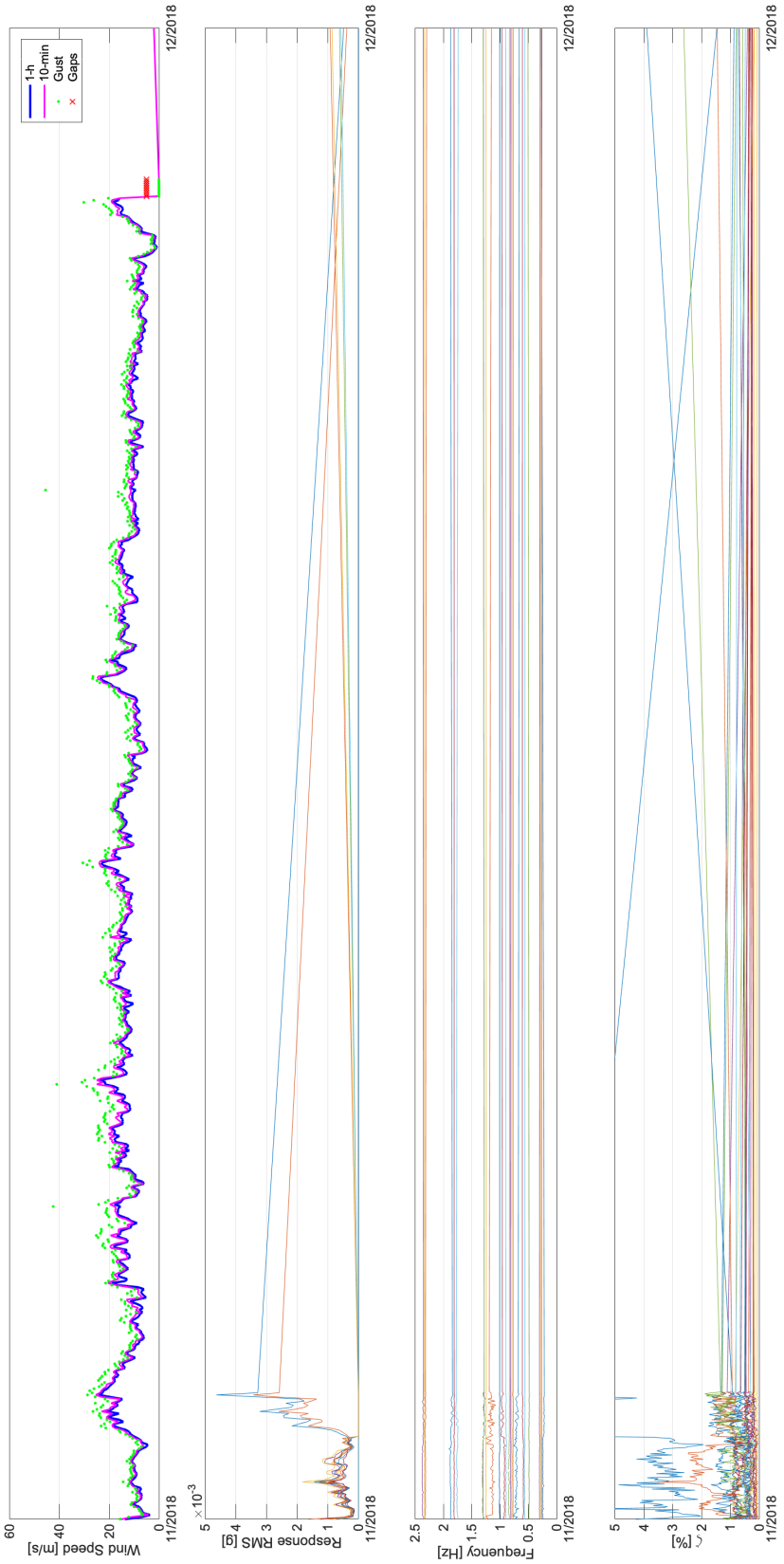

Figure D-7 Operational Modal Analysis SSI applied to Moel-y-Parc. November 2018.

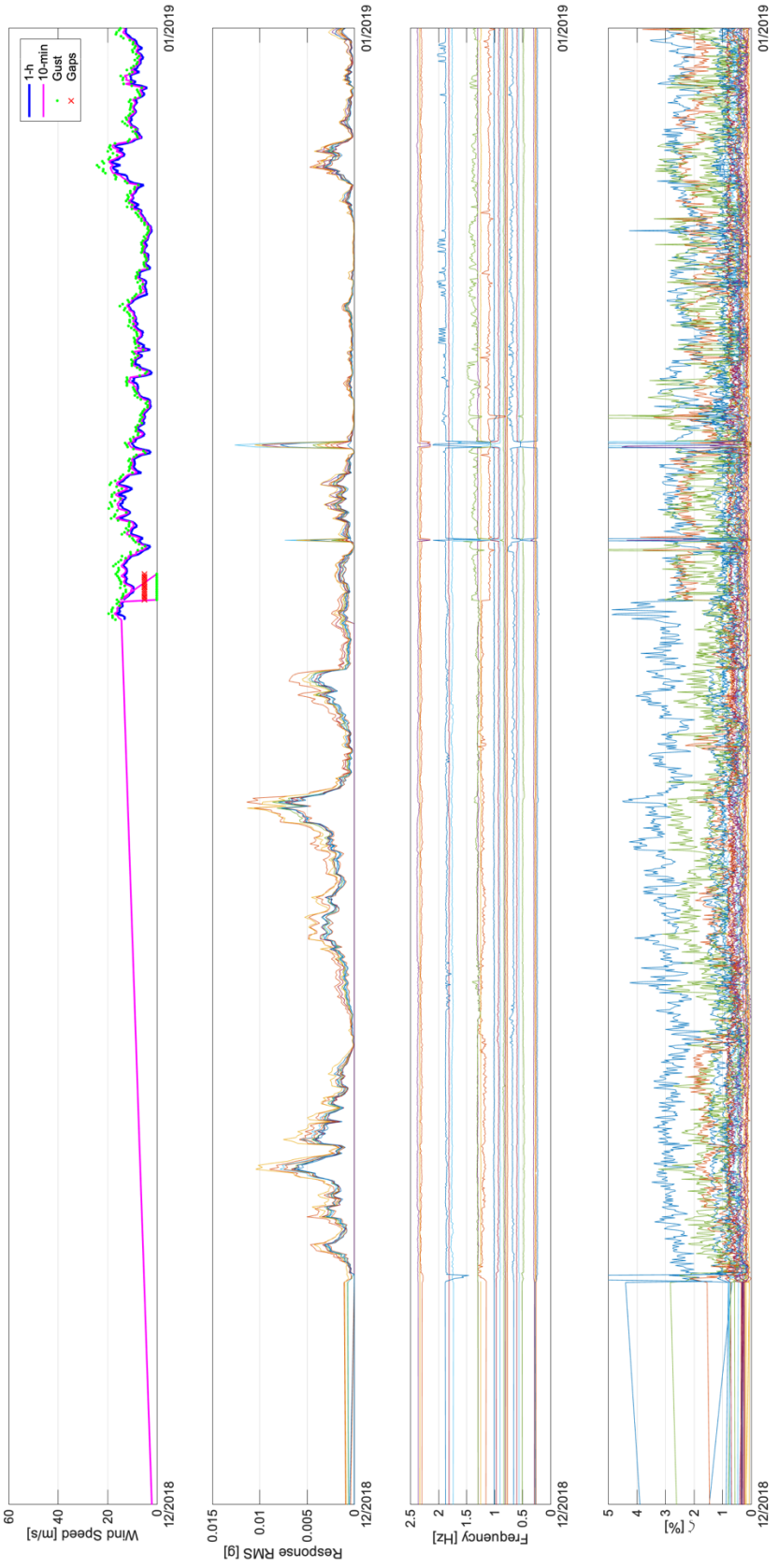

Figure D-8 Operational Modal Analysis SSI applied to Moel-y-Parc. December 2018.

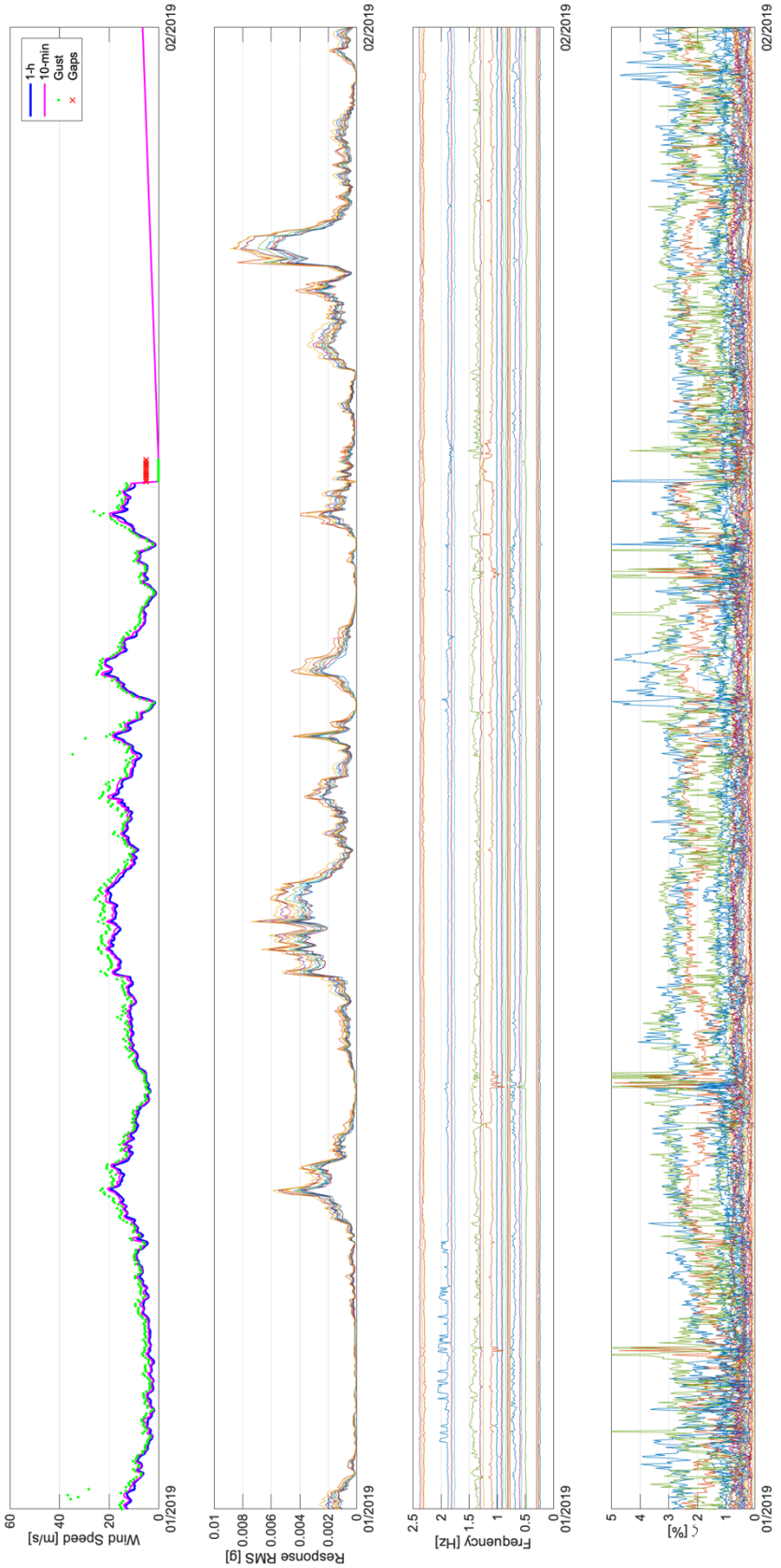

Figure D-9 Operational Modal Analysis SSI applied to Moel-y-Parc. January 2019.

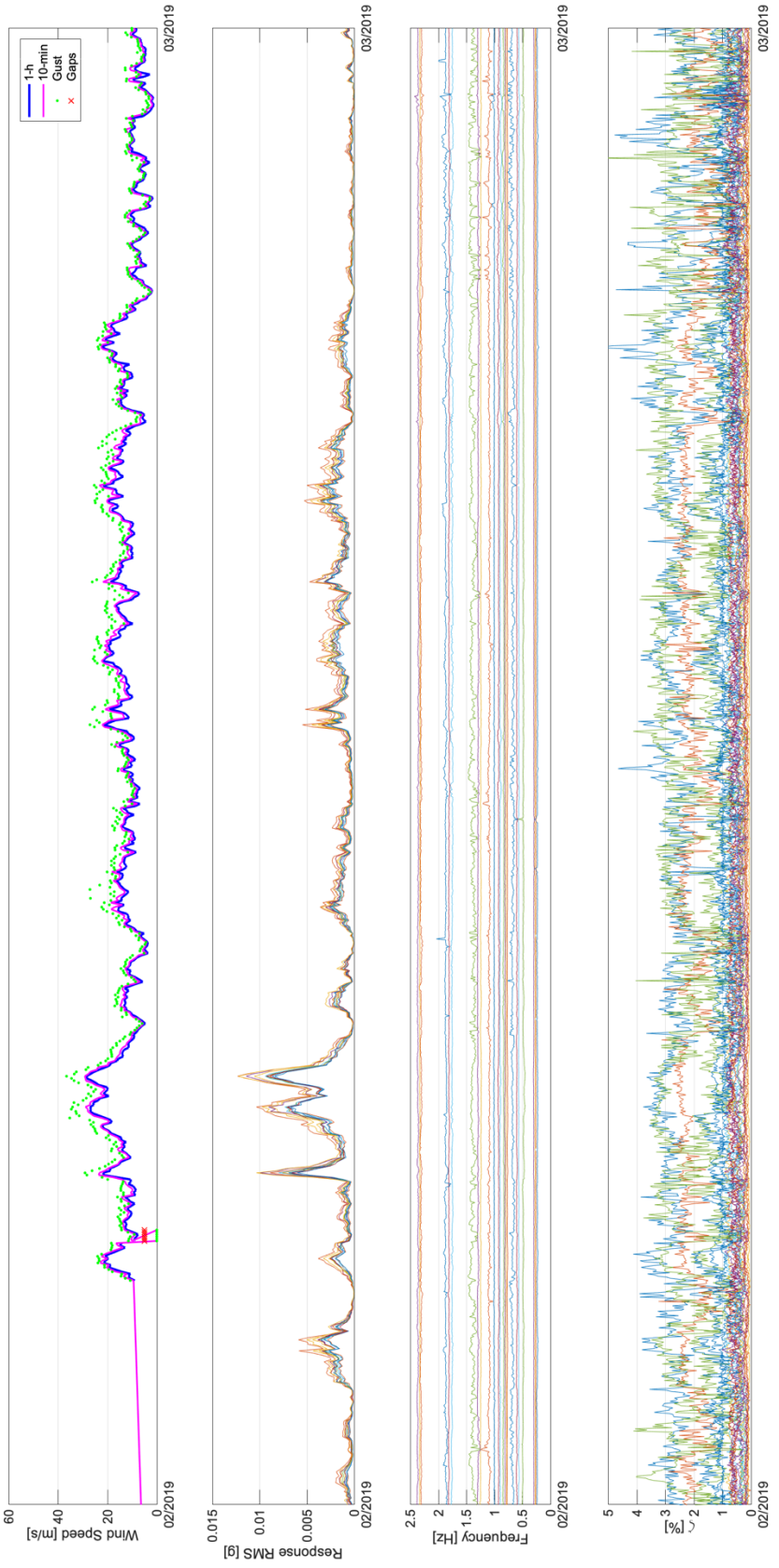

Figure D-10 Operational Modal Analysis SSI applied to Moel-y-Parc. February 2019.

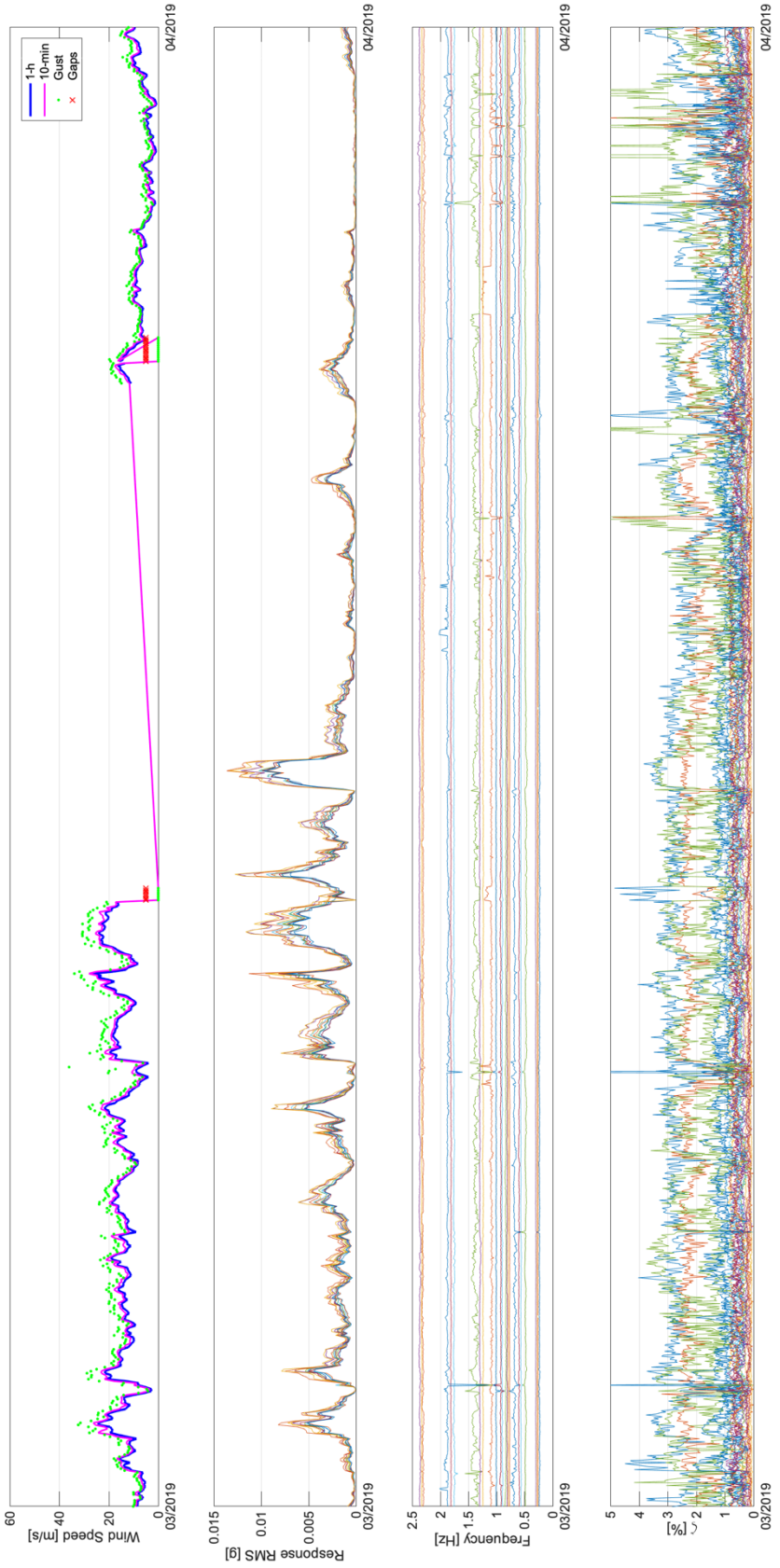

Figure D-11 Operational Modal Analysis SSI applied to Moel-y-Parc. March 2019.

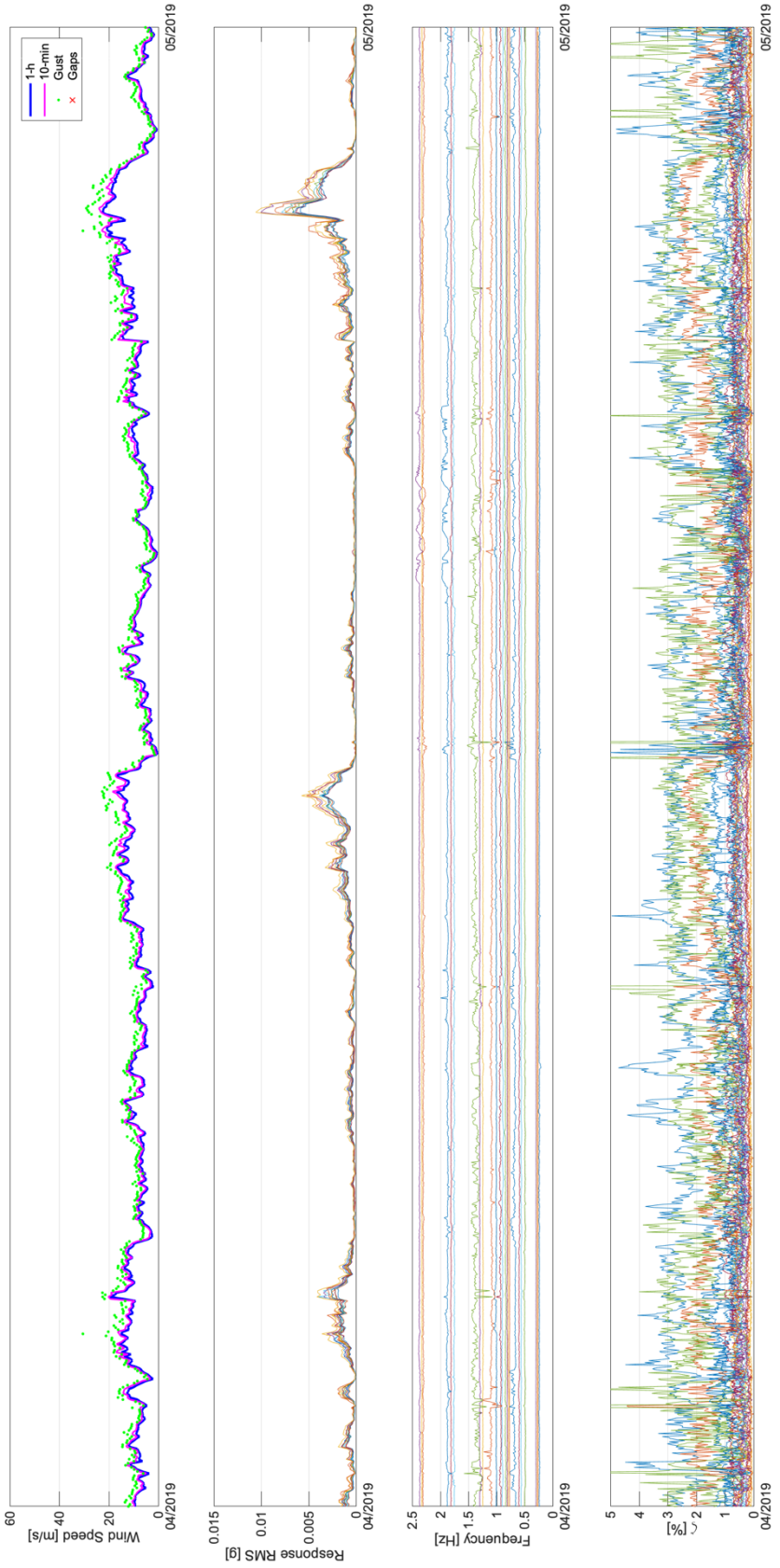

Figure D-12 Operational Modal Analysis SSI applied to Moel-y-Parc. April 2019.

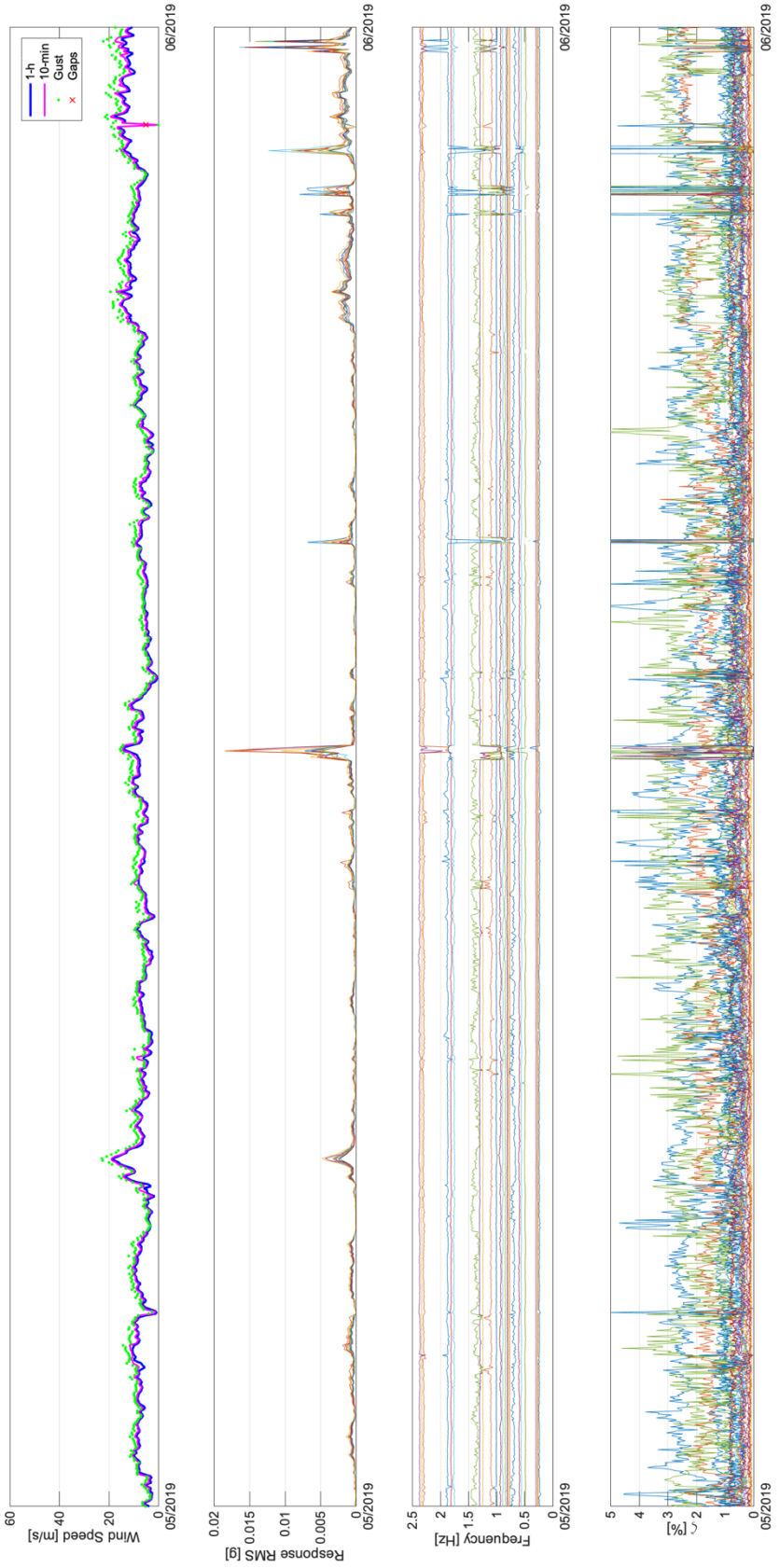

Figure D-13 Operational Modal Analysis SSI applied to Moel-y-Parc. May 2019.

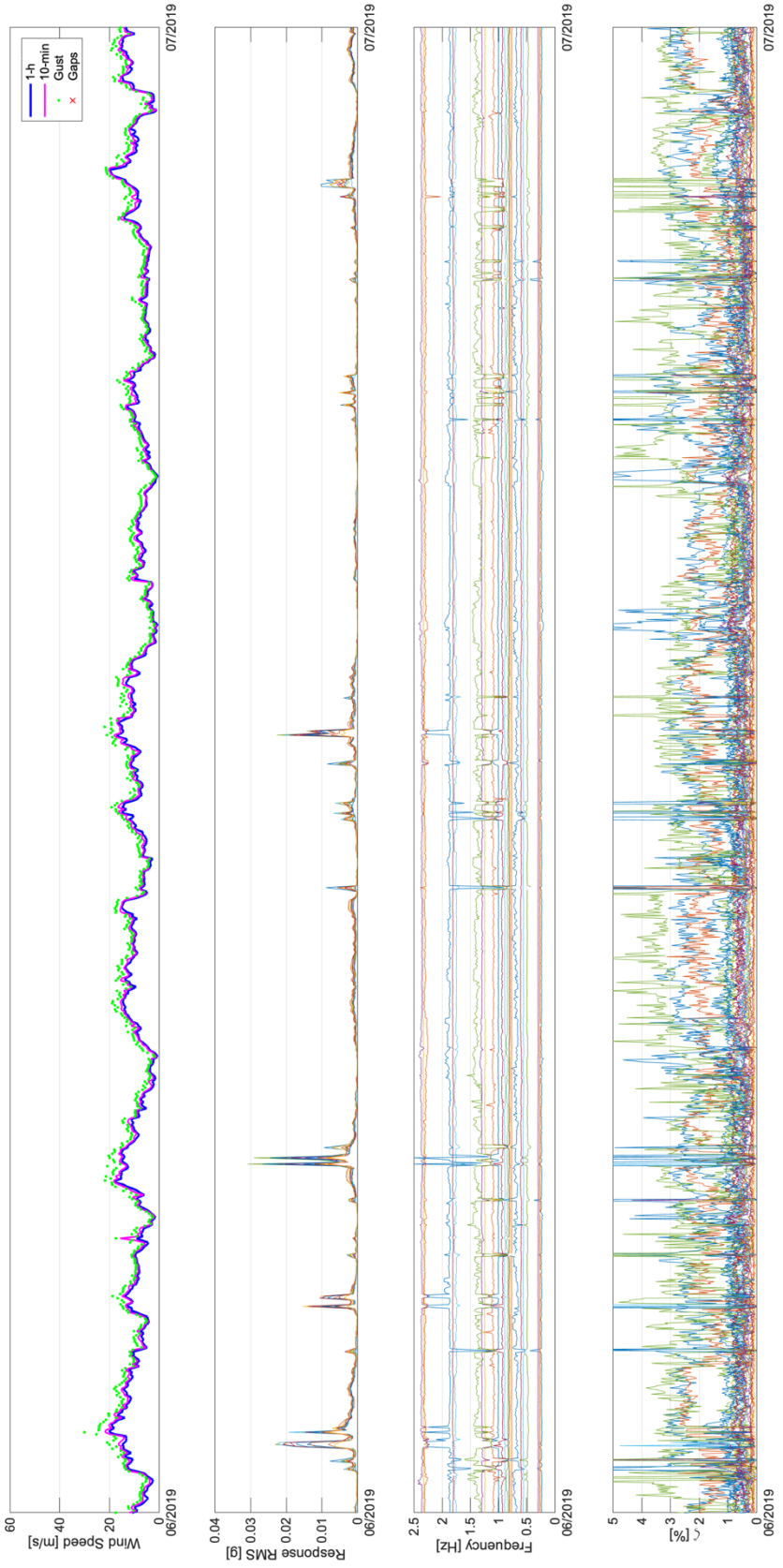

Figure D-14 Operational Modal Analysis SSI applied to Moel-y-Parc. June 2019.

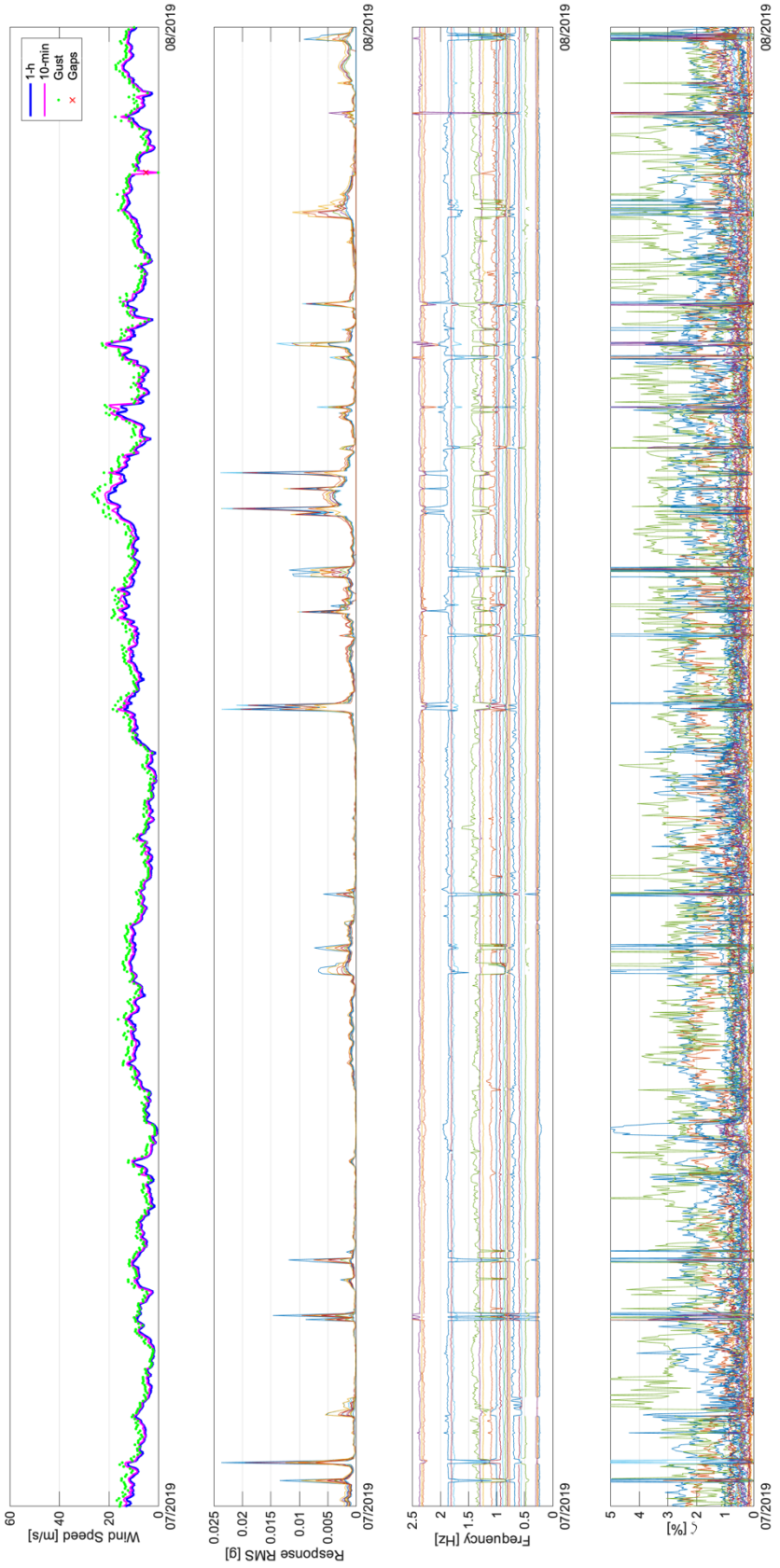

Figure D-15 Operational Modal Analysis SSI applied to Moel-y-Parc. July 2019.

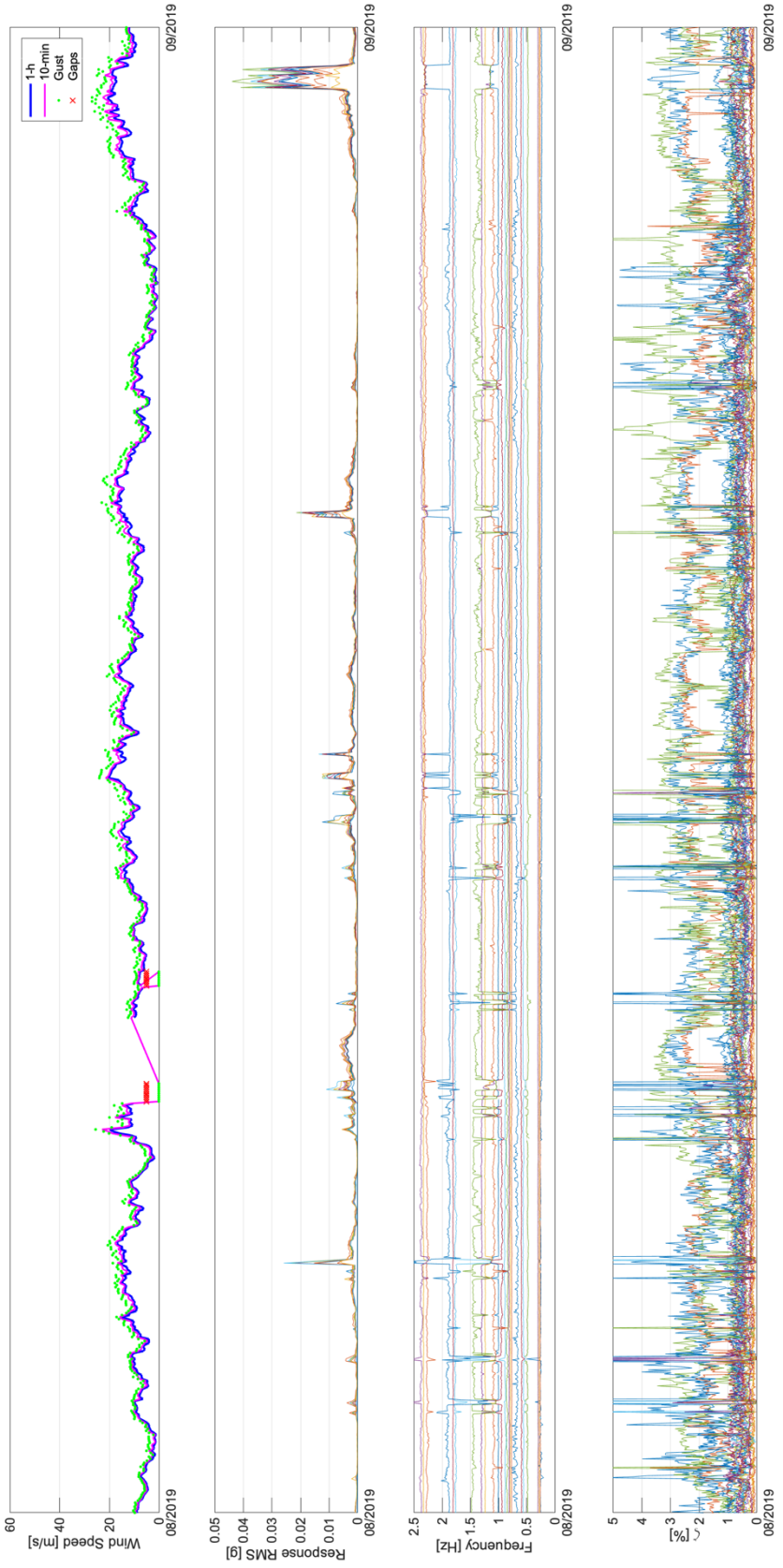

Figure D-16 Operational Modal Analysis SSI applied to Moel-y-Parc. August 2019.

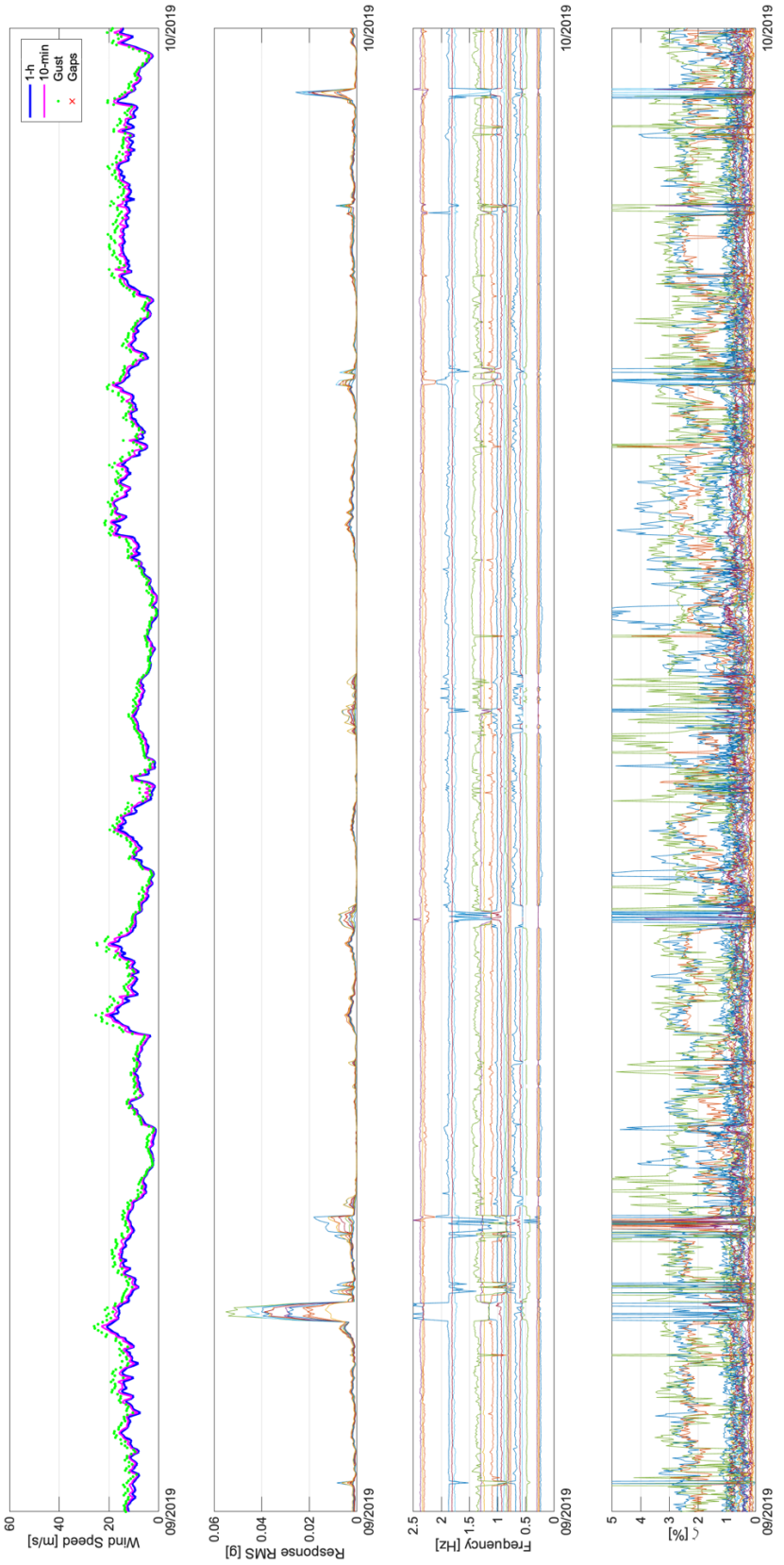

Figure D-17 Operational Modal Analysis SSI applied to Moel-y-Parc. September 2019.

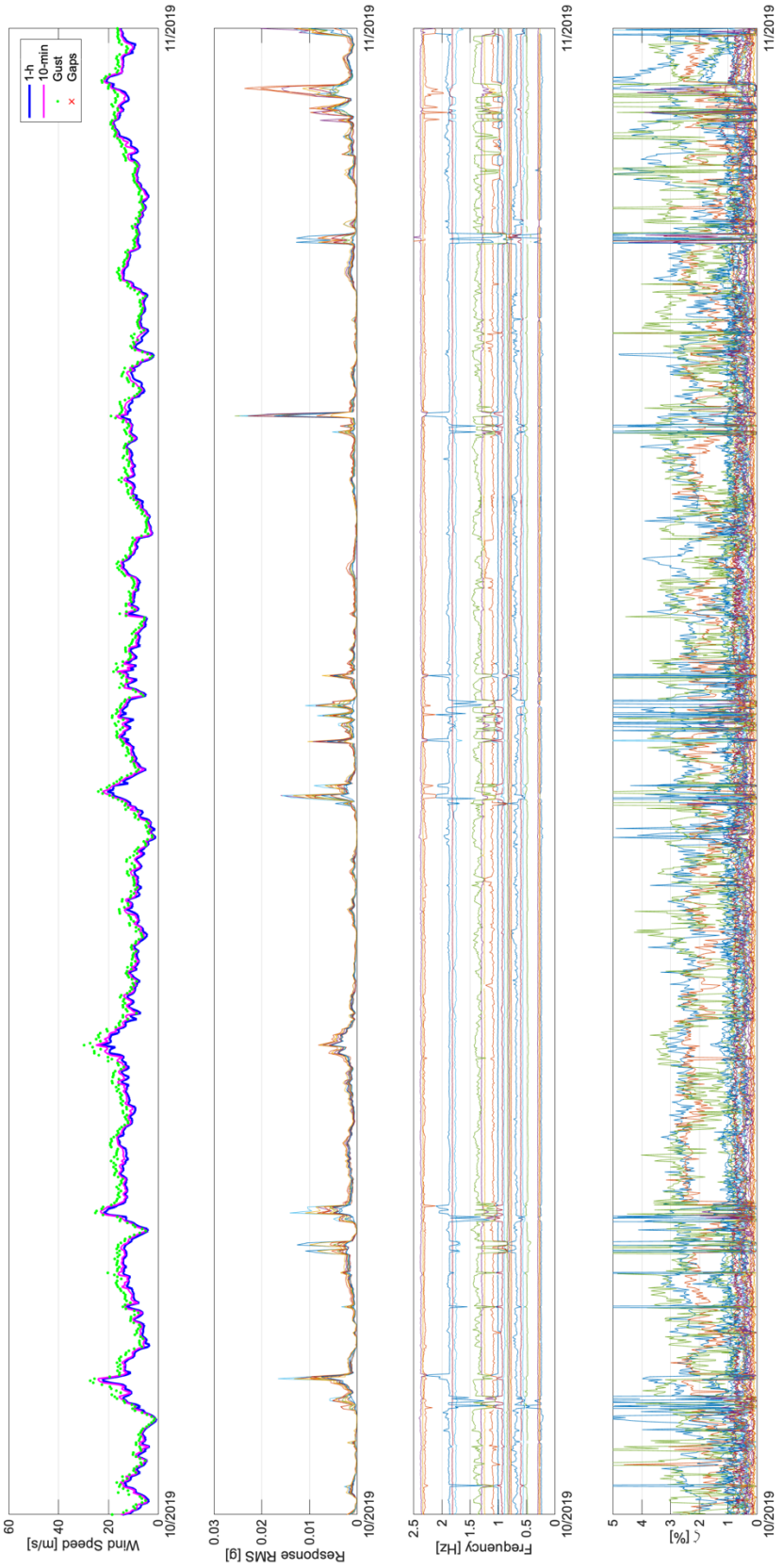

Figure D-18 Operational Modal Analysis SSI applied to Moel-y-Parc. October 2019.

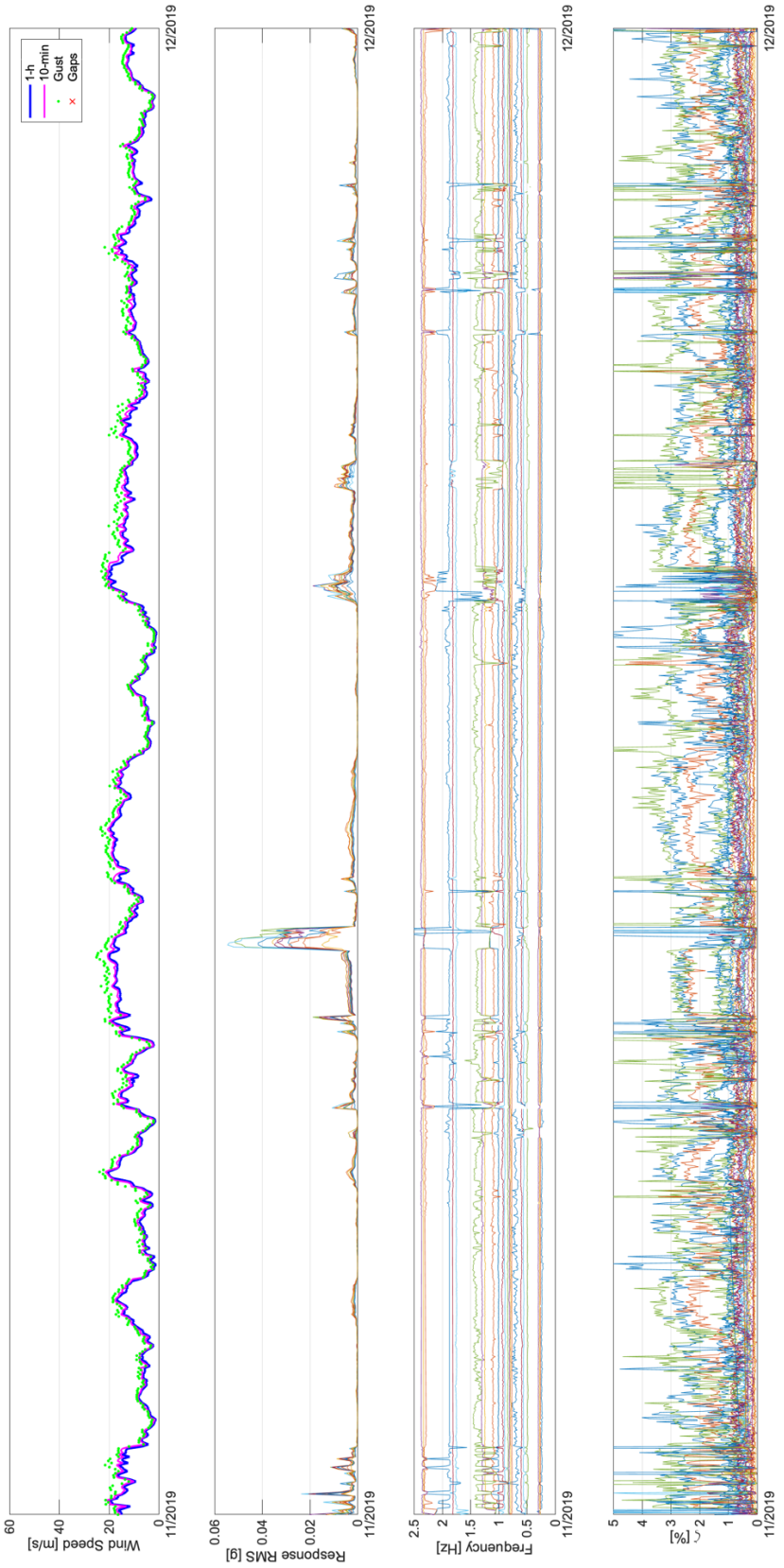

Figure D-19 Operational Modal Analysis SSI applied to Moel-y-Parc. November 2019.

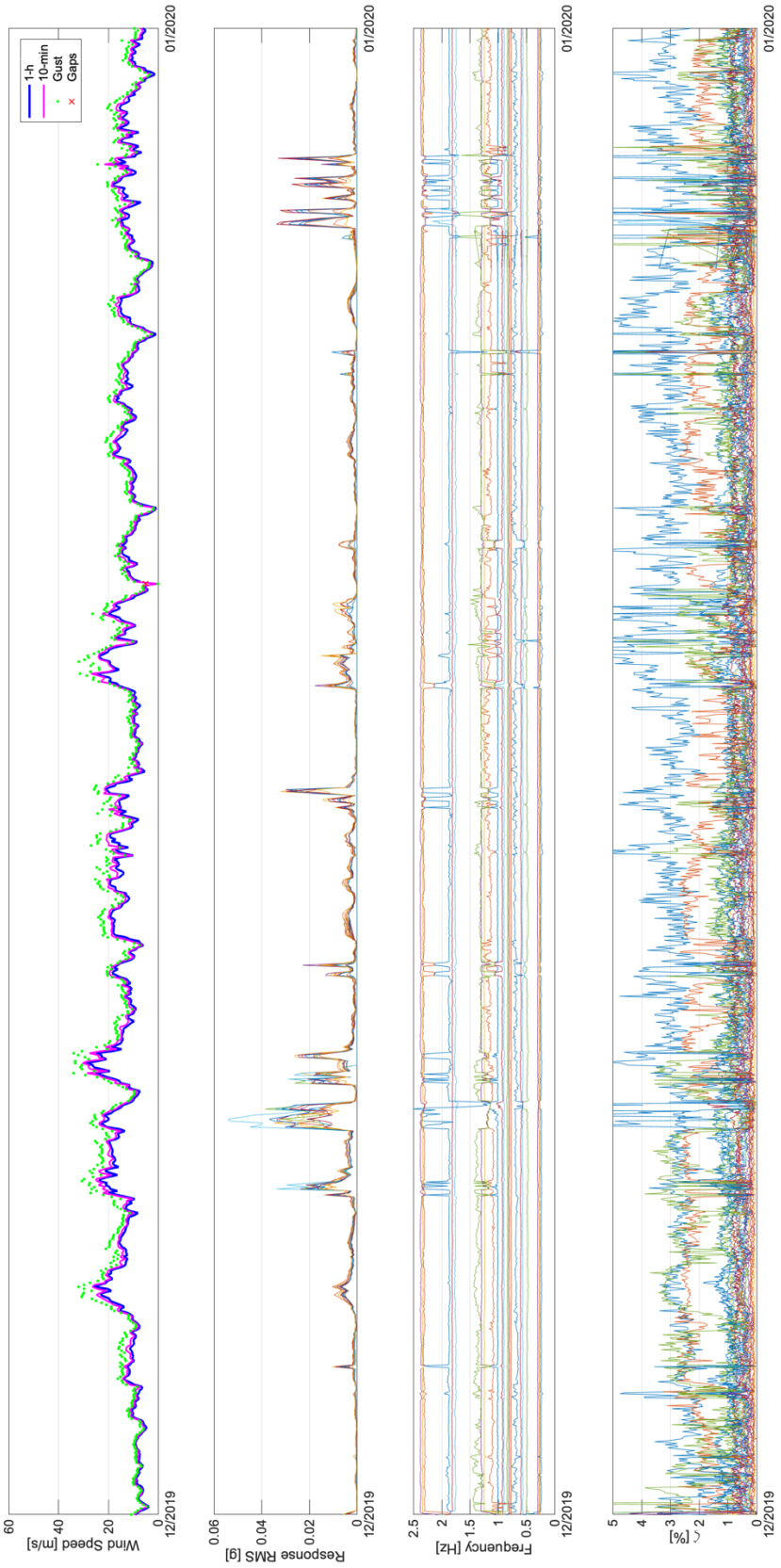

Figure D-20 Operational Modal Analysis SSI applied to Moel-y-Parc. December 2019.

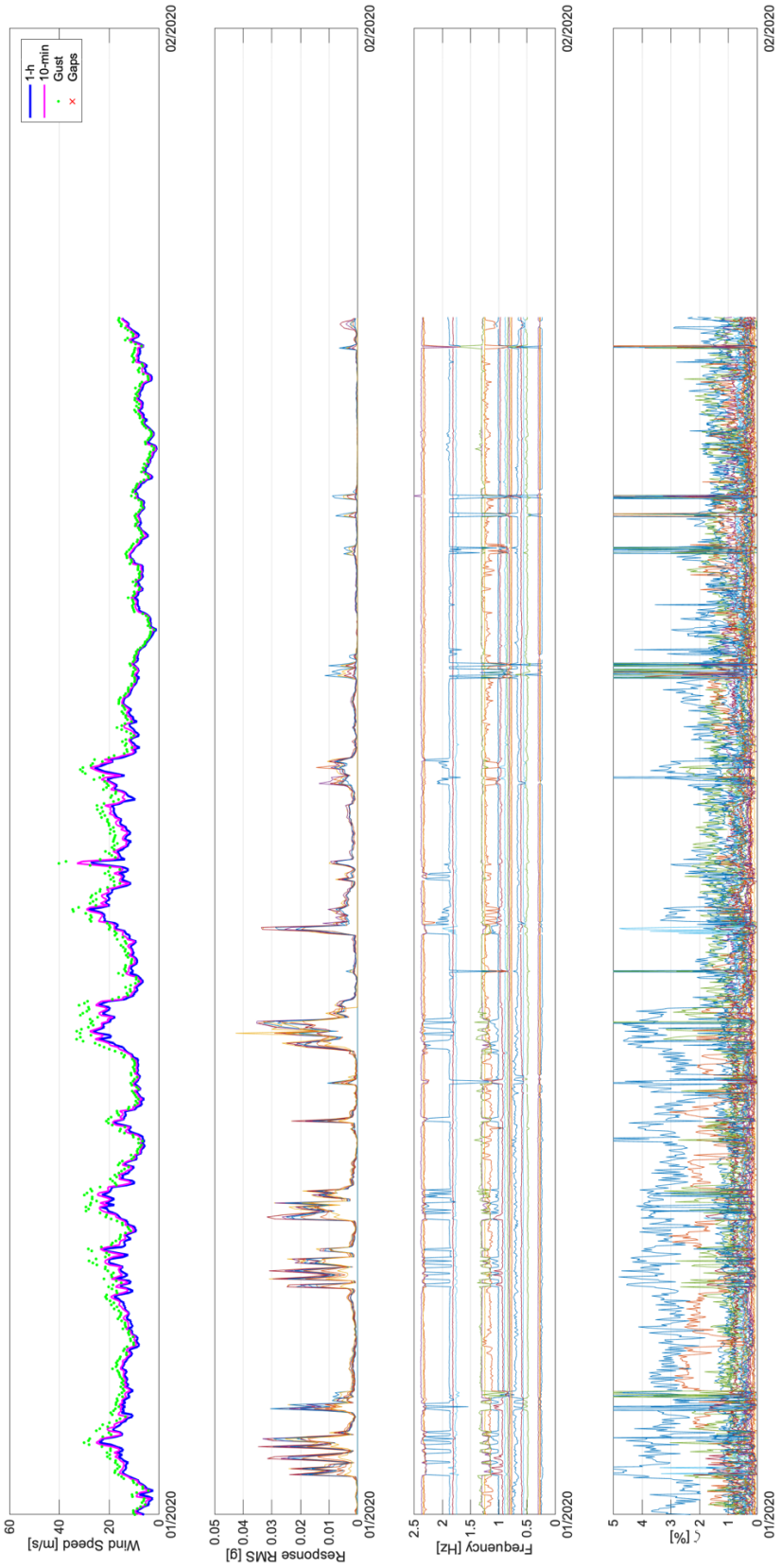

Figure D-21 Operational Modal Analysis SSI applied to Moel-y-Parc. January 2020.